

InSAR Data Accuracy for California Groundwater Basins CGPS Data Comparative Analysis January 2015 to September 2019

Final Report
March 23, 2020

Prepared for:
California Department of Water Resources
Contract No. 4600011239
Task Order No. 37

Prepared by:
Towill, Inc.
Project No. 14750-0137

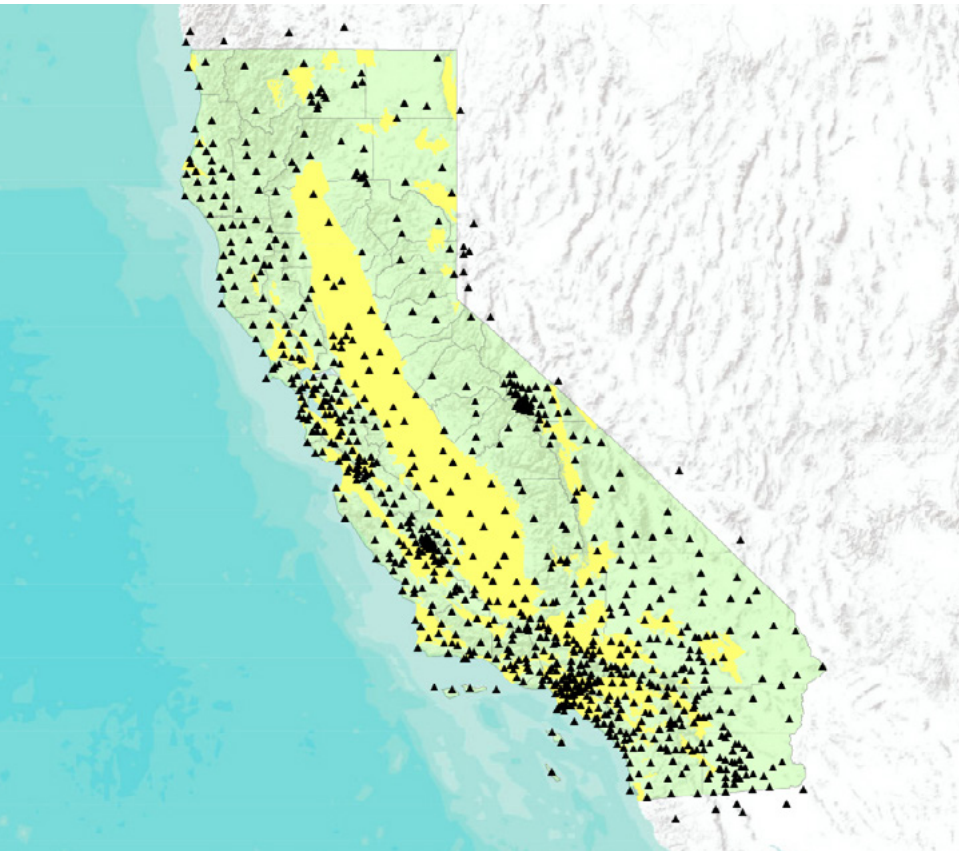


Photo Credit: European Space Agency



Photo Credit: UNAVCO



CONTENTS

| | |
|---|-----------|
| 1. EXECUTIVE SUMMARY..... | 3 |
| 2. BACKGROUND..... | 5 |
| 2.1 SUMMARY OF SCOPE OF WORK AND PURPOSE..... | 5 |
| 2.2 POINTS OF CONTACT..... | 5 |
| 3. CONTINUOUS GLOBAL POSITIONING SYSTEMS (CGPS) TIME-SERIES DATA | 5 |
| 4. INSAR TIME-SERIES SOURCE DATA | 6 |
| 5. COMPARATIVE DATA ANALYSIS | 9 |
| 6. CONCLUSIONS..... | 10 |
| 7. OPPORTUNITIES FOR INSAR-CGPS STUDY ENHANCEMENTS | 11 |

LIST OF FIGURES

- Figure 1 – Distribution of CGPS Stations Used for Comparative Analysis
Figure 2 – CGPS Stations Selected for the InSAR Data Calibration Process
Figure 3 – Example of Graphic Data Presentation from Appendix B

| | |
|--|---|
| APPENDIX A: COMPARATIVE ANALYSIS – TABULAR SUMMARY | A |
| APPENDIX B: COMPARATIVE ANALYSIS – GRAPHICAL SUMMARY | B |
| APPENDIX C: “CGPS DATA ACQUISITION AND ANALYSIS”, TOWILL REPORT DATED FEBRUARY 2019 | C |
| APPENDIX D: “INSAR LAND SURVEYING AND MAPPING SERVICES IN SUPPORT DWR’S SGMA PROGRAM”, TRE ALTAMIRA REPORT DATED MARCH 2020 | D |

SURVEYOR'S CERTIFICATION STATEMENT

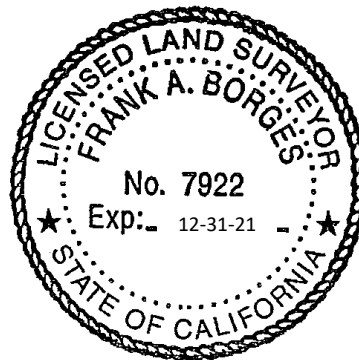
I hereby certify that this report was prepared by me or under my direction, and its contents represent an accurate assessment of the results shown.

Frank Borges, PLS, CA, No. 7922
Associate Principal

Signature: _____



Date: 3/23/2020



1. Executive Summary

Towill, Inc. and TRE Altamira, Inc., performed a study analyzing change in ground elevations across California for the period January 1, 2015 through September 19, 2019. The study compares measurements of vertical displacement in ground surface using two sets of time-series data, one set derived from a state-wide network of continuously operating global positioning system (CGPS) base stations, and another set based on interferometric synthetic aperture radar (InSAR) data collected by the European Space Agency's (ESA) Sentinel remote sensing satellites. The objective of this study is to demonstrate through quantitative analysis the accuracy of vertical ground surface deformation models derived from InSAR datasets through comparison to CGPS datasets whose accuracy and reliability are well established.

This work was performed under contract with the California Department of Water Resources (DWR) as part of DWR's technical assistance program supporting the Sustainable Groundwater Management Act (SGMA), by providing important relevant data to local Groundwater Sustainability Agencies working towards Groundwater Sustainability Plan development and implementation.

This study utilizes data from a network of CGPS stations installed across California by government agencies and scientific academic entities. The specific time-series datasets used in this study were acquired from two separate university-governed consortiums, UNAVCO and SOPAC, which are devoted to researching, analyzing, and archiving high-precision geodetic data. Motion in latitude, longitude, and ellipsoidal height of 878 CGPS stations fixed to the ground were analyzed for each day of the study period. Three hundred ninety-one (391) of these CGPS stations were selected for incorporation into this study based on data completeness in relation to the study period and geographic proximity to the groundwater basins which comprise the study area.

InSAR derived time-series data used in this study were collected by ESA's Sentinel 1A and 1B satellites. The Sentinel-1 mission is comprised of two polar-orbiting satellites which use C-band synthetic aperture radar (SAR) imaging collecting data that supports interferometric methods of detecting and measuring deformation of the earth's surface. The Sentinel datasets were selected for this study based upon: 1) their comprehensive geographic coverage of California; 2) the two satellites have opposite polar orbits, providing both ascending and descending Line of Site (LOS), which allows change in vertical displacement to be isolated from horizontal motion; and 3) Sentinel-1 mission data is made available to users without direct cost.

The objective of this study is to validate the accuracy of the InSAR data through quantitative analysis by comparing to CGPS data where the two time-series datasets align in time and space. TRE Altamira (www.tre-altamira.com) was responsible for acquiring and processing the InSAR data and Towill (www.towill.com) was responsible for acquiring and processing the CGPS data and performing the comparative analysis of the two datasets. Technical details describing how CGPS data were incorporated into the study were presented originally in the report titled CGPS Data Acquisition and Analysis, prepared by Towill, Inc. and dated February 2019, and expanded further in this report. Technical details describing how the InSAR data were processed and incorporated into the study are contained in the report titled InSAR Land Surveying and Mapping Services in Support of the DWR SGMA Program, prepared by TRE Altamira, Inc. and dated March 2020. These reports are attached as Appendices C and D, respectively. The methods and results of the comparative analysis are presented in the present report.

Towill aligned calendar dates for the InSAR and CGPS time-series data using a seven-day interval, plus the first day of each month, for the study period January 1, 2015 through September 19, 2019. The two datasets were also aligned geographically by selecting for analysis only those CGPS stations that are located within 100 meters of an InSAR measurement point. Using these techniques, 181 stations were analyzed as validation points using two quantitative measures: 1) the absolute difference in vertical displacement between the two datasets was

calculated and used to develop a root mean square error (RMSE) value for each station separately and as a consolidated state-wide dataset; and 2) the correlation coefficient was calculated between the two datasets. The comparative analysis demonstrates very small absolute differences in the measurement of vertical displacement between the two datasets. RMSE values for individual stations range from 20.97mm to 1.45mm. The consolidated state-wide RMSE value is 7.91mm. Also, the data demonstrates a high degree of positive correlation between the two time-series datasets. Thirty-five stations (19% of total) have a correlation of 0.9 or higher and the consolidated state-wide mean correlation value is 0.70.

The quantitative analysis performed by comparing the CGPS and InSAR time-series data provides strong evidence that the InSAR data accurately models change in ground elevation. InSAR has several important advantages over CGPS for modeling change in ground elevations. First, the individual InSAR measurement points (MP) are far denser than CGPS measurements. For example, this study utilized 391 CGPS measurement stations compared to more than 185 million InSAR Measurement Points (MP) within the same study area. Secondly, there are several California groundwater basins which do not contain any CGPS stations and other areas where they are very sparse. InSAR datasets are effective in filling these gaps.

Accuracy Statement

The National Standard for Spatial Data Accuracy (NSSDA), developed by the Federal Geographic Data Committee (Document Number FGDC-STD-007.3-1998), offers a well-defined statistic and testing methodology for positional accuracy of geospatial data derived from various surveying methods, including satellite remote sensing. The NSSDA is based on comparison of data from the tested dataset to values from an independent source of higher accuracy. For this study, variation in vertical displacement of California's ground surface over time, as measured from interferometric synthetic aperture radar (InSAR) satellites, was statistically compared to available ground-based continuous global positioning systems (CGPS) data.

Tested: 16 mm vertical accuracy at 95% confidence level.

As tested by the processes described, this analysis provides statistical evidence that InSAR data accurately measured vertical displacement in California's ground surface to within 16 mm (value conservatively rounded up from 15.50 mm) for the period January 1, 2015 through September 19, 2019. This statement of accuracy is based on the assumptions that the number, distribution, and characteristics of CGPS check point locations provide a representative sample of the entire study area and of the entire InSAR dataset, and that the CGPS data constitutes an independent source of higher accuracy. This statement of accuracy applies to the state-wide dataset and may vary for regional or localized area subsets.

2. Background

2.1 Summary of Scope of Work and Purpose

California Department of Water Resources in June 2018 issued Towill, Inc. Task Order No. 26 under Contract No. 4600011239 as part of DWR’s technical assistance role under the Sustainable Groundwater Management Act (SGMA). Under Task Order No. 26, changes over time in ground surface elevations were measured using satellite-based interferometric synthetic aperture radar (InSAR) and compared to time-series data recorded by ground-based, continuously operating Global Positioning System (CGPS) stations located throughout many of the groundwater basins in the state. Task Order 26 was completed, and a Final Report covering the study period January 1, 2015 to June 1, 2018 was published on May 28, 2019.

A second contract, Task Order No. 37, was issued to Towill, Inc. to extend the study period through September 2019. Several new groundwater basins were added to the study area under Task Order No. 37 and as a result, both the InSAR and CGPS datasets were reprocessed for the complete study period January 1, 2015 through September 19, 2019. This report describes the methods and results of the InSAR-CGPS Data Comparative Analysis – January 2015 to September 2019.

2.2 Points of Contact

Questions regarding this report should be addressed to:

| Contractor’s Project Manager | Contractor's Contract Manager |
|---|---|
| Frank Borges, PLS 2300 Clayton Road, Suite 1200 Concord, California 94520-2176 Phone: (925) 682-6976 ext. 1036 Frank.Borges@towill.com | Brian Young 2300 Clayton Road, Suite 1200 Concord, California 94520-2176 Phone: (925) 682-6976 ext. 1041 Brian.Young@towill.com |

3. Continuous Global Positioning Systems (CGPS) Time-Series Data

Towill analyzed time-series data for 878 CGPS stations distributed throughout California. These data were acquired from online archives maintained by the University NAVSTAR Consortium (UNAVCO) and the Scripps Orbit and Permanent Array Center (SOPAC). General details and an overview of CGPS time-series data processing are documented in Towill’s report ***CGPS Data Acquisition and Analysis*** dated February 2019 (see Appendix C).

Several important updates to CGPS data processing were implemented for the January 1, 2015 to September 19, 2019 study period as listed below:

- UNAVCO time-series dataset “cwu.igs.csv” was downloaded on October 22, 2019 and used for the January 2015 through September 2019 study period.
- SOPAC time-series dataset “WNAM_Clean_TrendNeuTimeSeries_sopac_20200207.tar” was downloaded on February 7, 2020 and used for the January 2015 through September 2019 study period.

- CGPS time-series null values up to 15 consecutive days were replaced with calculated values estimated through linear interpolation.
- Three SOPAC stations (CHOW, TEHA, MULN), located in an area of high subsidence, are included in the January 2015 to September 2019 study with modification. Each of these stations has a similar unexplained data spike where the height of each of these station drops approximately 100mm in a two-day period starting April 19, 2016. Time-series data for these three stations were included for the period following the unexplained data spike.

Towill's subconsultant, TRE Altamira, who performed the collection and analysis of the InSAR data for this project, selected 232 CGPS points for calibrating the InSAR datasets. The InSAR data calibration process performs a plane removal function which removes possible errors based on satellite orbital inaccuracies. The calibration process also helps "fix" the elevation of the InSAR image frame reference points (RP) necessary for seismically active areas such as California. Technical details on the InSAR data calibration process are described in TRE Altamira's report *InSAR Land Surveying and Mapping Services in Support of DWR's SGMA Program* dated March 2020 (see Appendix D).

Towill's objective for validation points was to identify CGPS stations which meet the following criteria:

1. Located within a groundwater basin included in the SGMA study area
2. Located within 100 meters of an InSAR synthetic Measurement Point (sMP)
3. Not used by TRE Altamira for the InSAR data calibration process

Geographic Information System (ArcGIS) software was used to identify 160 CGPS points meeting the above criteria; however, all of these are located south of Sacramento. The density of CGPS stations north of Sacramento is sparse and a decision was made to use those available for the InSAR data calibration process. Further evaluation of TRE's report clarified that the calibration methodology involves stabilizing local InSAR reference points to the absolute CGPS time-series reference system; this methodology does not constrain the InSAR dataset to match the individual CGPS time-series data. Based upon this more complete understanding of the calibration method, a decision was made to include in the InSAR-CGPS validation process stations in northern California which were also used for calibration. This compromise provides 10 additional validation points.

Figure 1 shows the distribution of the CGPS stations used as validation points for comparative analysis of the InSAR data. Figure 2 shows the distribution of CGPS stations used by TRE Altamira as InSAR calibration points.

4. InSAR Time-Series Source Data

Details regarding the InSAR time-series data used by Towill for this study are described in TRE Altamira's report *InSAR Land Surveying and Mapping Services in Support of DWR's SGMA Program* (Appendix D). The state-wide InSAR dataset used by Towill for performing the comparative analysis used synthetic Measurement Points (sMP) developed by TRE. Synthetic Measurement Points (sMP) were calculated by averaging all InSAR Measurement Point (MP) values within a 100-meter grid. The larger MP dataset contains more than 185 million individual measurement which were consolidated into 4.6 million sMPs based on a 100-meter grid.

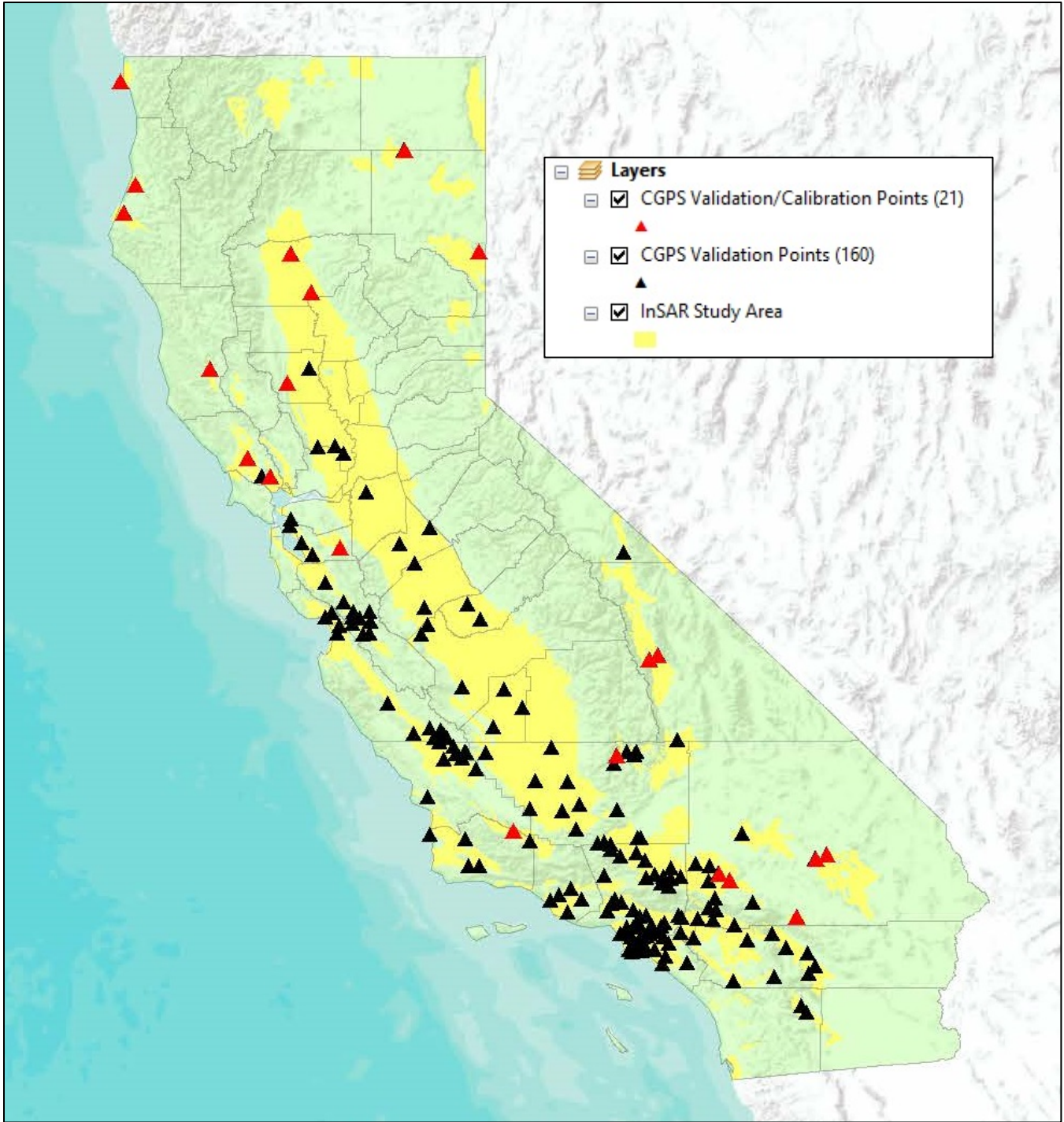


Figure 1 – Distribution of CGPS Stations used for Comparative Analysis

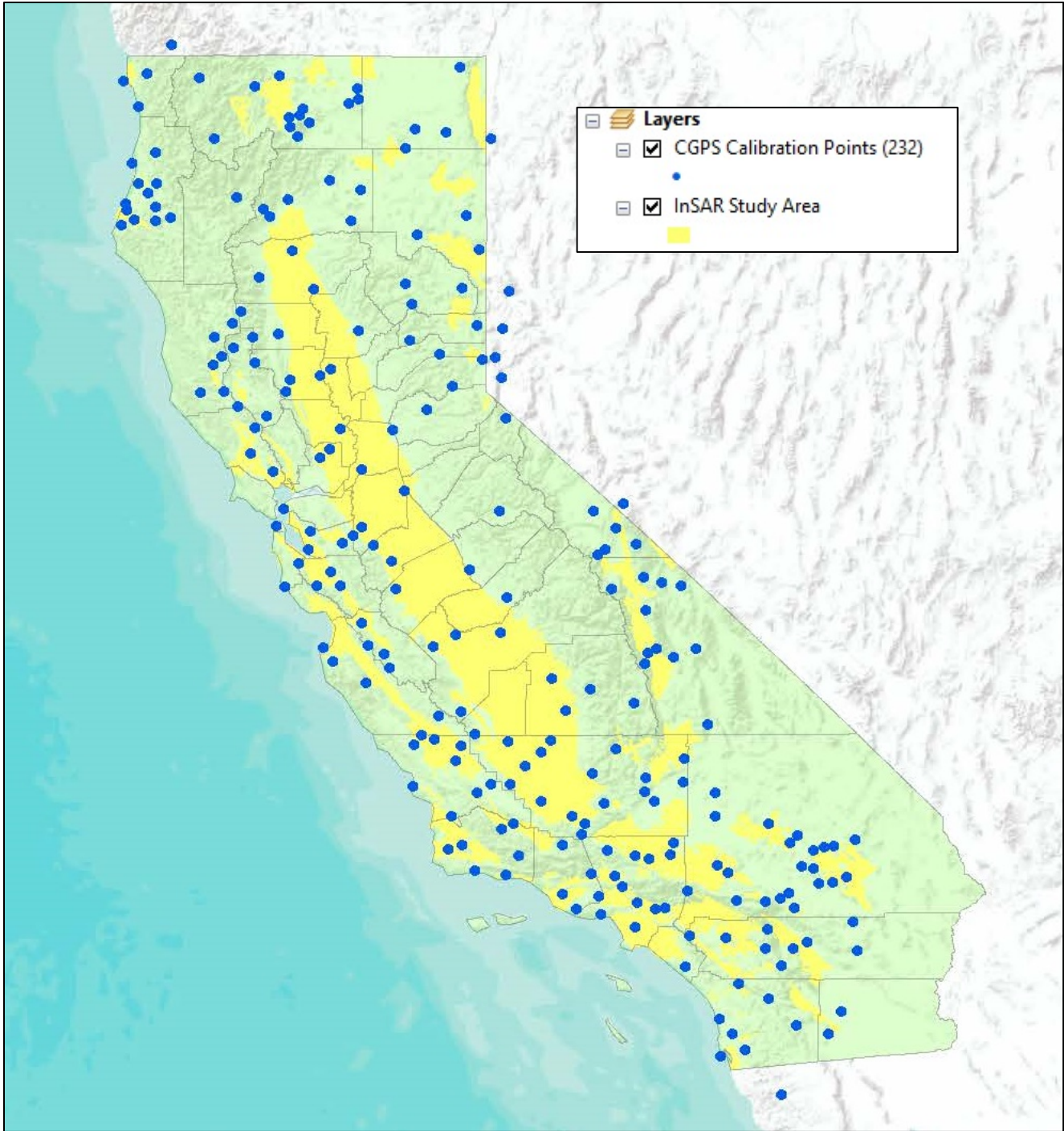


Figure 2 – CGPS Stations Selected for the InSAR Data Calibration Process

5. Comparative Data Analysis

The methods and procedures used to perform the InSAR-CGPS comparative data analysis are described below:

1. InSAR data were downloaded from TRE’s web-portal “TREMps”; ten shapefiles named “CALIFORNIA_DWR_1_VERT” through “CALIFORNIA_DWR_10_VERT” representing the Variable Start Date dataset (01 January 2015 through September 19, 2019) were used in this study.
2. ArcGIS was used to select which CGPS station were located inside the SGMA InSAR study area and are within 100 meters of an InSAR sMP.
3. CGPS time-series data (daily) were reduced in frequency to align with the specific dates of the Variable Period InSAR dataset. Start dates for InSAR sMP range from 01 January 2015 through 19 September 2019. Data values for all InSAR sMP start no later than 13 June 2015.
4. Python and its Pandas library for data analysis and manipulation were used to create a dataframe for each CGPS-InSAR data station in the comparative analysis. The absolute difference in vertical motion between the CGPS station and InSAR sMP were compared and used to develop a Root Mean Square Error (RMSE) for each station and the consolidated state-wide dataset and the correlation coefficient was calculated comparing the two time-series datasets. Formulas for each are presented below:

$$NSSDA\ RMSE = RMSE_z = \text{sqrt} \left[\sum (Z_{data\ i} - Z_{check\ i})^2 / n \right]$$

$$Correlation\ Coefficient\ (X, Y) = \frac{\sum (x - \bar{x})(y - \bar{y})}{\sqrt{\sum (x - \bar{x})^2 \sum (y - \bar{y})^2}}$$

5. The statistical results of the InSAR-CGPS comparative data analysis are presented in tabular form in Appendix A and graphic form in Appendix B. An example of the charts found in Appendix B is shown in Figure 3.

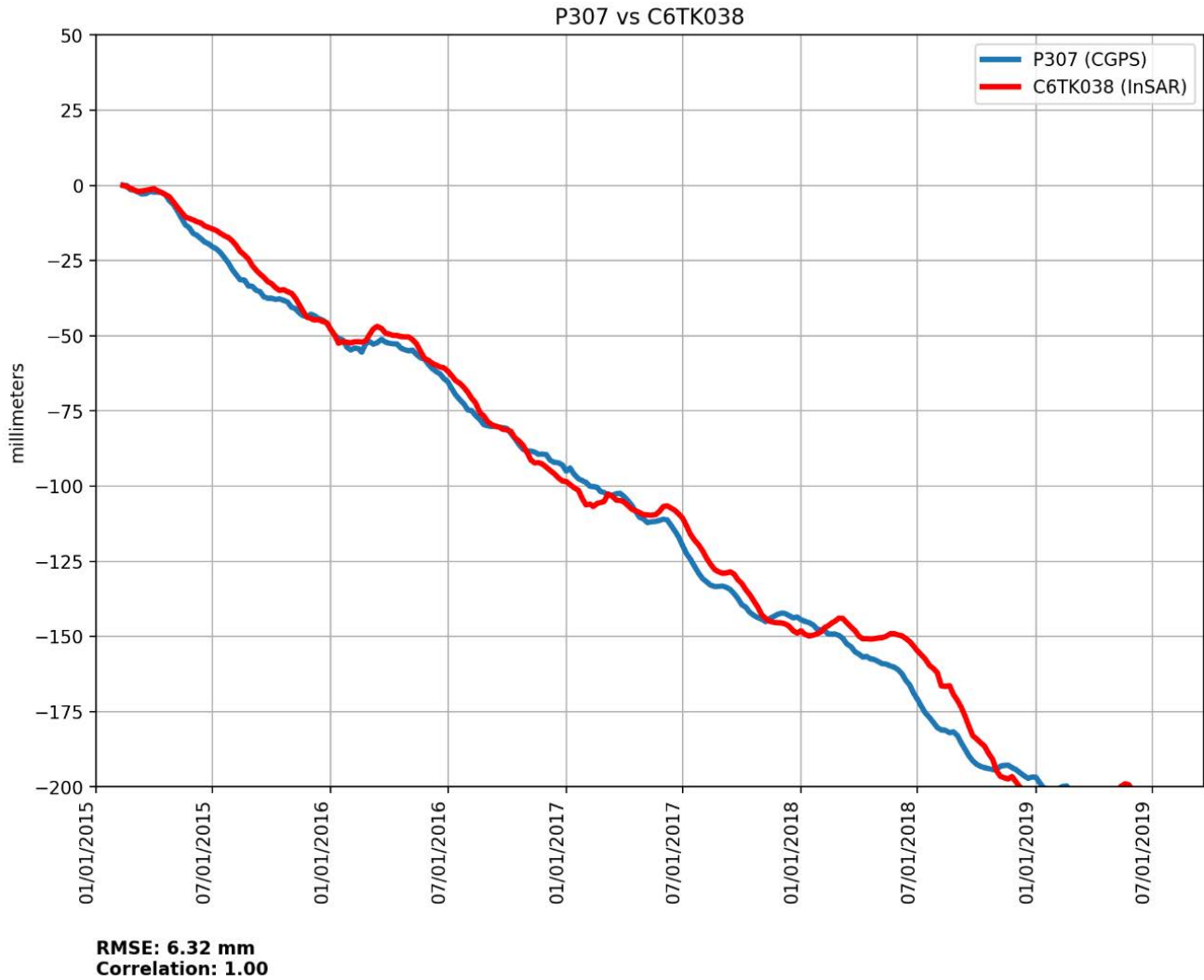


Figure 3 – Example of Graphic Data Presentation from Appendix B

6. Conclusions

The comparative analysis demonstrates very small absolute differences in the measurement of vertical displacement between the two datasets. RMSE values for individual stations range from 20.97mm to 1.45mm. The consolidated state-wide RMSE value is 7.91mm. Also, the data demonstrates a high degree of positive correlation between the two time-series datasets. Thirty-five stations (19% of total) have a correlation of 0.9 or higher and the consolidated state-wide mean correlation value is 0.70.

The quantitative analysis performed by comparing the CGPS and InSAR time-series data provides strong evidence that the InSAR data accurately models change in ground elevation to an accuracy tested to be 16mm at 95% confidence.

7. Opportunities for InSAR-CGPS Study Enhancements

Listed below are several considerations which were identified in the course of conducting this study. Each item is outside the scope of the present study, but should be considered as opportunities for enhancing future studies of a similar type:

- Distribution of CGPS stations is not uniform across the SMGA study boundary and some basins have no CGPS stations in proximity. DWR should consider sponsoring new CGPS stations in areas of high interest.
- The InSAR dataset is based on highly coherent Measurement Points (MP) and these values are used to interpolate vertical displacement through areas of less coherence. Additional analysis should be performed to identify areas of greatest interpolation and weighting data reliability.
- CGPS stations are not equally reliable and have individual error budgets. Additional effort may be devoted to modeling differences among CGPS stations and weighting their influence accordingly.

APPENDIX A

| StatID | System | CGPS-InSAR | Distance (M) | Correlation | RMSE (MM) |
|--------|--------|-----------------|--------------|-------------|-----------|
| ALPP | UNAVCO | ALPP vs B3SH1D2 | 44.53 | 0.856 | 3.75 |
| ALTH | SOPAC | ALTH vs C5RG8YG | 53.82 | 0.574 | 7.71 |
| ARM1 | UNAVCO | ARM1 vs BAPXNOO | 20.78 | 0.991 | 8.33 |
| ARM2 | UNAVCO | ARM2 vs BAPXNOO | 30.74 | 0.992 | 7.93 |
| AVRY | UNAVCO | AVRY vs AX9AUGL | 52.20 | 0.684 | 4.40 |
| AZRY | UNAVCO | AZRY vs AG6VHIS | 24.72 | 0.788 | 4.96 |
| BBRY | UNAVCO | BBRY vs AT15GBN | 31.08 | 0.858 | 2.03 |
| BFLD | SOPAC | BFLD vs BEMFYCX | 33.73 | 0.872 | 8.80 |
| BFSH | SOPAC | BFSH vs BHVQCWK | 52.62 | 0.297 | 16.02 |
| BGIS | UNAVCO | BGIS vs AO1ODTQ | 19.99 | 0.751 | 4.62 |
| BKMS | UNAVCO | BKMS vs ANY3S8O | 57.58 | -0.036 | 6.74 |
| BKR1 | SOPAC | BKR1 vs B9GOPKO | 45.81 | 0.990 | 5.18 |
| BLSA | SOPAC | BLSA vs AKYCBSI | 61.23 | 0.570 | 13.26 |
| BRAN | UNAVCO | BRAN vs AS1RA53 | 48.11 | 0.794 | 3.77 |
| BSRY | UNAVCO | BSRY vs B5IZL0Z | 49.07 | 0.888 | 6.19 |
| BUEG | UNAVCO | BUEG vs AZWK56H | 60.47 | 0.296 | 16.63 |
| CCCS | SOPAC | CCCS vs AM4M3UQ | 43.14 | 0.407 | 6.79 |
| CHOW | SOPAC | CHOW vs C9C1VXP | 41.63 | 0.998 | 6.62 |
| CIT1 | UNAVCO | CIT1 vs AR5LVKR | 45.39 | 0.786 | 2.91 |
| CLAR | UNAVCO | CLAR vs AQNQVPO | 49.81 | 0.865 | 3.46 |
| CMOD | SOPAC | CMOD vs CJKL6UT | 50.84 | 0.415 | 12.57 |
| CRCN | SOPAC | CRCN vs BRI8M90 | 49.05 | 0.999 | 7.18 |
| CRFP | UNAVCO | CRFP vs APDB2XX | 38.77 | 0.108 | 13.11 |
| CRHS | UNAVCO | CRHS vs ALEF0YI | 39.05 | -0.367 | 20.97 |
| CSCI | UNAVCO | CSCI vs ARQG14M | 58.09 | 0.758 | 4.60 |
| CSDH | UNAVCO | CSDH vs AM3F8DK | 70.92 | 0.832 | 4.16 |
| CSN1 | UNAVCO | CSN1 vs ATB07Y5 | 15.12 | 0.823 | 8.97 |
| CTDM | UNAVCO | CTDM vs AY4USJ3 | 99.19 | -0.094 | 9.59 |
| CTMS | UNAVCO | CTMS vs AQX9UAW | 49.90 | 0.837 | 2.43 |
| CUHS | UNAVCO | CUHS vs B5Z28JQ | 33.39 | 0.974 | 18.56 |
| CVHS | UNAVCO | CVHS vs AQ5AFTU | 50.16 | 0.854 | 6.15 |
| DVPB | UNAVCO | DVPB vs AW8ZE2U | 52.87 | 0.481 | 11.56 |
| DYH2 | UNAVCO | DYH2 vs ANIMIHN | 55.73 | 0.551 | 7.46 |
| EBMD | SOPAC | EBMD vs CMRHTQG | 13.34 | 0.920 | 2.96 |
| ELSC | UNAVCO | ELSC vs AP6RAJ7 | 32.87 | 0.932 | 4.66 |
| ELTN | UNAVCO | ELTN vs B1KOYHF | 60.21 | 0.252 | 7.65 |
| EWPP | UNAVCO | EWPP vs AQK6A7I | 53.09 | 0.700 | 3.06 |
| FOXG | UNAVCO | FOXG vs B24XP6F | 30.66 | 0.958 | 2.30 |
| FVPK | SOPAC | FVPK vs AIFUFWK | 26.19 | 0.355 | 7.25 |
| GHRP | UNAVCO | GHRP vs ASE9EFY | 25.56 | 0.521 | 4.29 |
| HBCO | UNAVCO | HBCO vs AKO7YBZ | 32.22 | 0.785 | 2.75 |
| HOGS | UNAVCO | HOGS vs BMYIE9S | 33.86 | 0.751 | 6.89 |
| HOLP | UNAVCO | HOLP vs AN93KS7 | 63.70 | 0.772 | 6.03 |
| IDQG | UNAVCO | IDQG vs AKDI6U4 | 56.90 | 0.457 | 6.39 |
| ISLK | UNAVCO | ISLK vs BJ7D1BD | 63.20 | 0.786 | 11.59 |
| JLN5 | SOPAC | JLN5 vs BN2OF9K | 14.46 | 0.525 | 5.77 |

| StatID | System | CGPS-InSAR | Distance (M) | Correlation | RMSE (MM) |
|--------|--------|-----------------|--------------|-------------|-----------|
| JNHG | UNAVCO | JNHG vs AWW7ALU | 50.53 | 0.738 | 3.82 |
| KBRC | UNAVCO | KBRC vs AVYV00H | 65.18 | 0.748 | 6.14 |
| LAPC | UNAVCO | LAPC vs ARZDJIO | 45.34 | 0.553 | 10.49 |
| LBC1 | UNAVCO | LBC1 vs ALKDD3M | 50.65 | 0.434 | 13.02 |
| LBC2 | UNAVCO | LBC2 vs AKTKUUQ | 31.98 | 0.904 | 2.45 |
| LBCH | UNAVCO | LBCH vs AKQLOT4 | 54.79 | 0.922 | 2.81 |
| LEMA | SOPAC | LEMA vs BURJ09Z | 52.69 | 0.997 | 8.16 |
| LINJ | UNAVCO | LINJ vs B0TB0UO | 20.59 | 0.505 | 5.50 |
| LL01 | UNAVCO | LL01 vs AXKM2HP | 58.15 | 0.767 | 2.85 |
| LLAS | UNAVCO | LLAS vs AZEP6MY | 51.97 | 0.373 | 10.20 |
| LORS | UNAVCO | LORS vs AR385ES | 50.83 | 0.681 | 2.67 |
| LOWS | UNAVCO | LOWS vs BM8WR6I | 63.46 | 0.489 | 6.17 |
| LPHS | UNAVCO | LPHS vs AP4YZW1 | 20.14 | 0.609 | 4.34 |
| LRRG | UNAVCO | LRRG vs AYC006P | 47.05 | 0.718 | 2.52 |
| LUTZ | SOPAC | LUTZ vs CD20DX5 | 24.94 | 0.846 | 6.18 |
| MASW | UNAVCO | MASW vs BMBVXB3 | 76.99 | 0.362 | 15.87 |
| MILK | UNAVCO | MILK vs AR5LVKS | 58.61 | 0.824 | 6.45 |
| MPWD | UNAVCO | MPWD vs AU2ZL50 | 59.87 | 0.825 | 8.82 |
| MTA1 | UNAVCO | MTA1 vs APO0V1U | 47.17 | 0.771 | 3.96 |
| MULN | SOPAC | MULN vs BZSIRYU | 12.10 | 0.990 | 10.54 |
| NOCO | UNAVCO | NOCO vs AN6PURR | 89.37 | 0.849 | 2.09 |
| NOPK | UNAVCO | NOPK vs AOA0G60 | 20.10 | 0.769 | 3.35 |
| OVLS | UNAVCO | OVLS vs AUNTR4S | 44.90 | 0.781 | 4.81 |
| OXYC | UNAVCO | OXYC vs AR08Z2S | 37.91 | 0.658 | 8.42 |
| P058 | UNAVCO | P058 vs E70YGIK | 40.61 | 0.913 | 2.88 |
| P093 | UNAVCO | P093 vs C0JBBM8 | 38.17 | 0.956 | 1.45 |
| P151 | UNAVCO | P151 vs DW86H7N | 51.61 | 0.949 | 2.17 |
| P161 | UNAVCO | P161 vs E2N6L42 | 37.90 | 0.818 | 6.35 |
| P190 | UNAVCO | P190 vs DCZ5UXO | 77.07 | 0.850 | 4.89 |
| P197 | UNAVCO | P197 vs CY1JFZ1 | 46.09 | 0.829 | 2.59 |
| P198 | UNAVCO | P198 vs CUX0IQX | 98.31 | 0.826 | 5.85 |
| P199 | UNAVCO | P199 vs CV0L4G7 | 84.53 | 0.976 | 2.23 |
| P208 | UNAVCO | P208 vs DAJN5ME | 54.04 | 0.883 | 9.05 |
| P210 | UNAVCO | P210 vs C4EMOMO | 95.22 | 0.878 | 3.08 |
| P211 | UNAVCO | P211 vs C5JPLE5 | 93.74 | 0.751 | 8.53 |
| P212 | UNAVCO | P212 vs C732WJF | 49.22 | 0.829 | 3.66 |
| P214 | UNAVCO | P214 vs C7T9Z7A | 58.29 | 0.644 | 6.71 |
| P217 | UNAVCO | P217 vs C9P5E9I | 72.46 | 0.588 | 7.53 |
| P228 | UNAVCO | P228 vs CIUE3RR | 50.41 | 0.292 | 14.28 |
| P233 | UNAVCO | P233 vs C43WVYA | 44.55 | 0.610 | 9.30 |
| P236 | UNAVCO | P236 vs C60DQFF | 31.07 | 0.724 | 4.50 |
| P239 | UNAVCO | P239 vs C732WR5 | 48.89 | 0.069 | 15.28 |
| P240 | UNAVCO | P240 vs C7WUL07 | 94.94 | 0.196 | 7.68 |
| P242 | UNAVCO | P242 vs C6XQ0D6 | 96.43 | 0.923 | 6.15 |
| P243 | UNAVCO | P243 vs C69WO99 | 33.42 | 0.788 | 5.68 |
| P244 | UNAVCO | P244 vs C7ZTR5O | 74.63 | 0.552 | 7.92 |

| StatID | System | CGPS-InSAR | Distance (M) | Correlation | RMSE (MM) |
|--------|--------|-----------------|--------------|-------------|-----------|
| P251 | UNAVCO | P251 vs C4BNIV5 | 57.30 | 0.585 | 11.17 |
| P265 | UNAVCO | P265 vs CZWTFVU | 77.35 | 0.450 | 5.82 |
| P273 | UNAVCO | P273 vs CSACME6 | 41.98 | 0.799 | 5.65 |
| P291 | UNAVCO | P291 vs BNZF9NY | 17.40 | 0.649 | 12.06 |
| P300 | UNAVCO | P300 vs BV0GIOI | 72.75 | 0.785 | 9.91 |
| P301 | UNAVCO | P301 vs C482XNB | 20.63 | 0.913 | 4.86 |
| P303 | UNAVCO | P303 vs C8SEKMW | 56.67 | 0.997 | 5.53 |
| P306 | UNAVCO | P306 vs CMDSVXQ | 95.69 | 0.709 | 5.64 |
| P307 | UNAVCO | P307 vs C6TK038 | 60.43 | 0.997 | 6.32 |
| P344 | UNAVCO | P344 vs DPM11WQ | 56.43 | 0.432 | 14.41 |
| P345 | UNAVCO | P345 vs DVWV784 | 58.58 | 0.919 | 3.89 |
| P347 | UNAVCO | P347 vs ECNZBXE | 26.46 | 0.944 | 8.96 |
| P467 | UNAVCO | P467 vs BZW3EYJ | 33.30 | 0.922 | 2.06 |
| P470 | UNAVCO | P470 vs AX54T2A | 39.30 | 0.800 | 5.12 |
| P477 | UNAVCO | P477 vs AFIGQE1 | 37.19 | 0.947 | 2.71 |
| P486 | UNAVCO | P486 vs AB1PPLF | 14.00 | 0.884 | 3.72 |
| P491 | UNAVCO | P491 vs AGU3FDZ | 51.28 | 0.688 | 2.39 |
| P513 | UNAVCO | P513 vs B5BUBAH | 51.79 | 0.216 | 13.50 |
| P530 | UNAVCO | P530 vs BIICSJJ | 16.10 | 0.772 | 2.96 |
| P531 | UNAVCO | P531 vs BLL3FOT | 55.89 | 0.624 | 5.85 |
| P532 | UNAVCO | P532 vs BIOB4QJ | 19.64 | 0.646 | 9.32 |
| P533 | UNAVCO | P533 vs BKRX6HR | 44.46 | 0.733 | 4.86 |
| P538 | UNAVCO | P538 vs BGU80OZ | 54.35 | 0.154 | 10.81 |
| P541 | UNAVCO | P541 vs BJMUA06 | 71.37 | 0.908 | 7.24 |
| P547 | UNAVCO | P547 vs BO75X13 | 53.45 | 0.774 | 8.13 |
| P552 | UNAVCO | P552 vs BJNPFZ | 45.14 | 0.325 | 9.51 |
| P556 | UNAVCO | P556 vs B2TCGRU | 30.41 | 0.843 | 2.20 |
| P560 | UNAVCO | P560 vs B3RA69A | 59.04 | 0.778 | 2.70 |
| P563 | UNAVCO | P563 vs BEQ0JQD | 39.05 | 0.912 | 6.54 |
| P565 | UNAVCO | P565 vs BKOY18O | 20.36 | 0.986 | 7.80 |
| P570 | UNAVCO | P570 vs BJAC7HI | 49.05 | 0.813 | 6.34 |
| P577 | UNAVCO | P577 vs AU8XY90 | 19.87 | 0.707 | 5.98 |
| P578 | UNAVCO | P578 vs BJS76AC | 39.78 | 0.772 | 7.84 |
| P581 | UNAVCO | P581 vs AY0ORWA | 16.44 | 0.856 | 1.91 |
| P582 | UNAVCO | P582 vs B0AULI1 | 18.63 | 0.616 | 3.79 |
| P584 | UNAVCO | P584 vs AMO9FFS | 23.78 | 0.589 | 10.35 |
| P586 | UNAVCO | P586 vs AYHCX52 | 56.18 | 0.682 | 2.61 |
| P603 | UNAVCO | P603 vs B1TMI6T | 25.84 | 0.881 | 4.88 |
| P612 | UNAVCO | P612 vs AS2Y607 | 58.33 | 0.433 | 6.94 |
| P651 | UNAVCO | P651 vs CI4SJ06 | 34.34 | 0.916 | 2.19 |
| P782 | UNAVCO | P782 vs BJS76AW | 30.10 | 0.792 | 8.52 |
| P799 | UNAVCO | P799 vs ANBHB3X | 24.30 | 0.707 | 9.14 |
| P800 | UNAVCO | P800 vs AP1EDZR | 25.21 | 0.251 | 11.69 |
| P808 | UNAVCO | P808 vs B407O9Z | 42.45 | 0.200 | 10.65 |
| P809 | UNAVCO | P809 vs BKOY18O | 21.49 | 0.983 | 7.67 |
| PBPP | UNAVCO | PBPP vs AXZHWJZ | 33.29 | 0.876 | 5.40 |

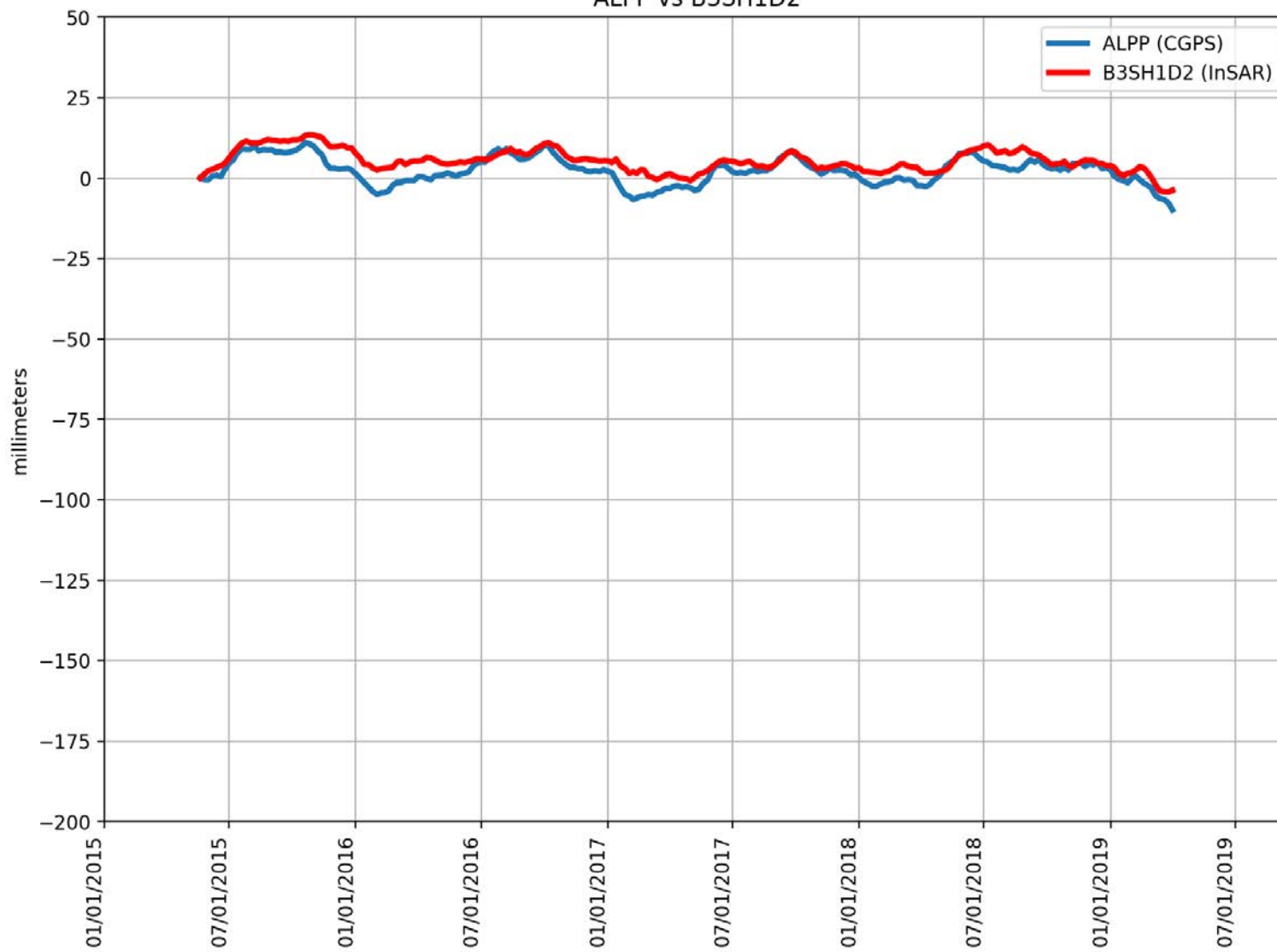
| StatID | System | CGPS-InSAR | Distance (M) | Correlation | RMSE (MM) |
|--------|--------|-----------------|--------------|-------------|-----------|
| PKRD | UNAVCO | PKRD vs APYQNY6 | 48.31 | 0.686 | 5.93 |
| PSAP | UNAVCO | PSAP vs ALBFW58 | 65.87 | 0.578 | 5.81 |
| PTSG | UNAVCO | PTSG vs ENOHYKD | 50.75 | 0.888 | 3.46 |
| QCY2 | UNAVCO | QCY2 vs BSD74MZ | 30.86 | 0.672 | 4.09 |
| RAGG | UNAVCO | RAGG vs B17014A | 59.98 | 0.858 | 2.01 |
| RNCH | UNAVCO | RNCH vs BNKJFMG | 33.77 | 0.499 | 14.32 |
| RSTP | UNAVCO | RSTP vs B4QER6P | 33.28 | 0.859 | 2.15 |
| RTHS | UNAVCO | RTHS vs AQA1X1H | 56.01 | 0.816 | 2.85 |
| SACY | SOPAC | SACY vs AJXFGDJ | 12.44 | 0.846 | 8.06 |
| SCIA | UNAVCO | SCIA vs AZSZLGN | 53.84 | 0.923 | 1.85 |
| SHN5 | SOPAC | SHN5 vs BJF3MWL | 50.36 | -0.061 | 19.68 |
| SHP5 | SOPAC | SHP5 vs BBYL4UV | 52.52 | 0.459 | 7.19 |
| SLHG | UNAVCO | SLHG vs A9T279R | 15.99 | 0.654 | 4.44 |
| SNHS | SOPAC | SNHS vs ANBHBD6 | 37.73 | 0.685 | 6.90 |
| SRB1 | SOPAC | SRB1 vs CNUSFO7 | 22.68 | 0.953 | 2.61 |
| SYNG | UNAVCO | SYNG vs AZSZJMY | 71.85 | 0.946 | 6.23 |
| TAFT | SOPAC | TAFT vs B9WRENH | 44.92 | 0.688 | 13.54 |
| TEHA | SOPAC | TEHA vs B9NTX9P | 65.61 | 0.259 | 5.60 |
| TMAP | UNAVCO | TMAP vs AI1K2LE | 66.53 | 0.152 | 16.93 |
| TORP | UNAVCO | TORP vs AKXQVZB | 63.87 | 0.811 | 2.84 |
| TOWG | UNAVCO | TOWG vs BLVT9SQ | 45.33 | 0.962 | 8.04 |
| TPOG | UNAVCO | TPOG vs B4SSHKX | 39.68 | 0.876 | 2.28 |
| TRLK | SOPAC | TRLK vs CGD33M4 | 29.24 | 0.344 | 7.88 |
| TWMS | UNAVCO | TWMS vs AO4NK59 | 61.57 | 0.638 | 4.42 |
| UCD1 | SOPAC | UCD1 vs D00ZH9A | 53.82 | 0.461 | 9.19 |
| USC2 | UNAVCO | USC2 vs AP07ITY | 35.82 | 0.758 | 3.98 |
| VCST | UNAVCO | VCST vs B4AXGKU | 47.08 | 0.958 | 4.27 |
| VINZ | SOPAC | VINZ vs B6C5SCV | 39.20 | 0.530 | 7.14 |
| VNCO | UNAVCO | VNCO vs ATPW1L3 | 40.91 | 0.965 | 14.85 |
| VNCX | UNAVCO | VNCX vs AU17ALC | 50.95 | 0.717 | 8.30 |
| VNPS | UNAVCO | VNPS vs AXVBV6O | 46.69 | 0.656 | 2.88 |
| WCHS | UNAVCO | WCHS vs APS6WIH | 46.61 | 0.876 | 6.16 |
| WHC1 | UNAVCO | WHC1 vs AOA0GDR | 46.47 | 0.738 | 7.37 |
| WHFG | UNAVCO | WHFG vs BJSSN6C | 48.14 | 0.841 | 5.57 |
| WHYT | SOPAC | WHYT vs AINL2YT | 67.95 | 0.507 | 4.29 |
| WIN2 | UNAVCO | WIN2 vs CJSBSXY | 56.65 | 0.712 | 8.42 |
| WINT | UNAVCO | WINT vs CJSBSXY | 60.25 | 0.569 | 8.51 |
| WMAP | UNAVCO | WMAP vs ATF699A | 75.57 | 0.814 | 6.16 |
| WNRA | UNAVCO | WNRA vs APFOSPJ | 50.05 | 0.688 | 19.81 |
| WORG | UNAVCO | WORG vs BJTE2UT | 44.45 | 0.571 | 11.54 |
| WRHS | UNAVCO | WRHS vs ANVQ1LE | 47.39 | 0.790 | 2.85 |
| WWMT | UNAVCO | WWMT vs ANTXRZJ | 65.17 | 0.387 | 10.61 |
| ZOA1 | SOPAC | ZOA1 vs CHROX84 | 40.50 | 0.886 | 3.85 |

Consolidated State-Wide Mean Values**47.05****0.694****7.91**

APPENDIX B

Appendix B

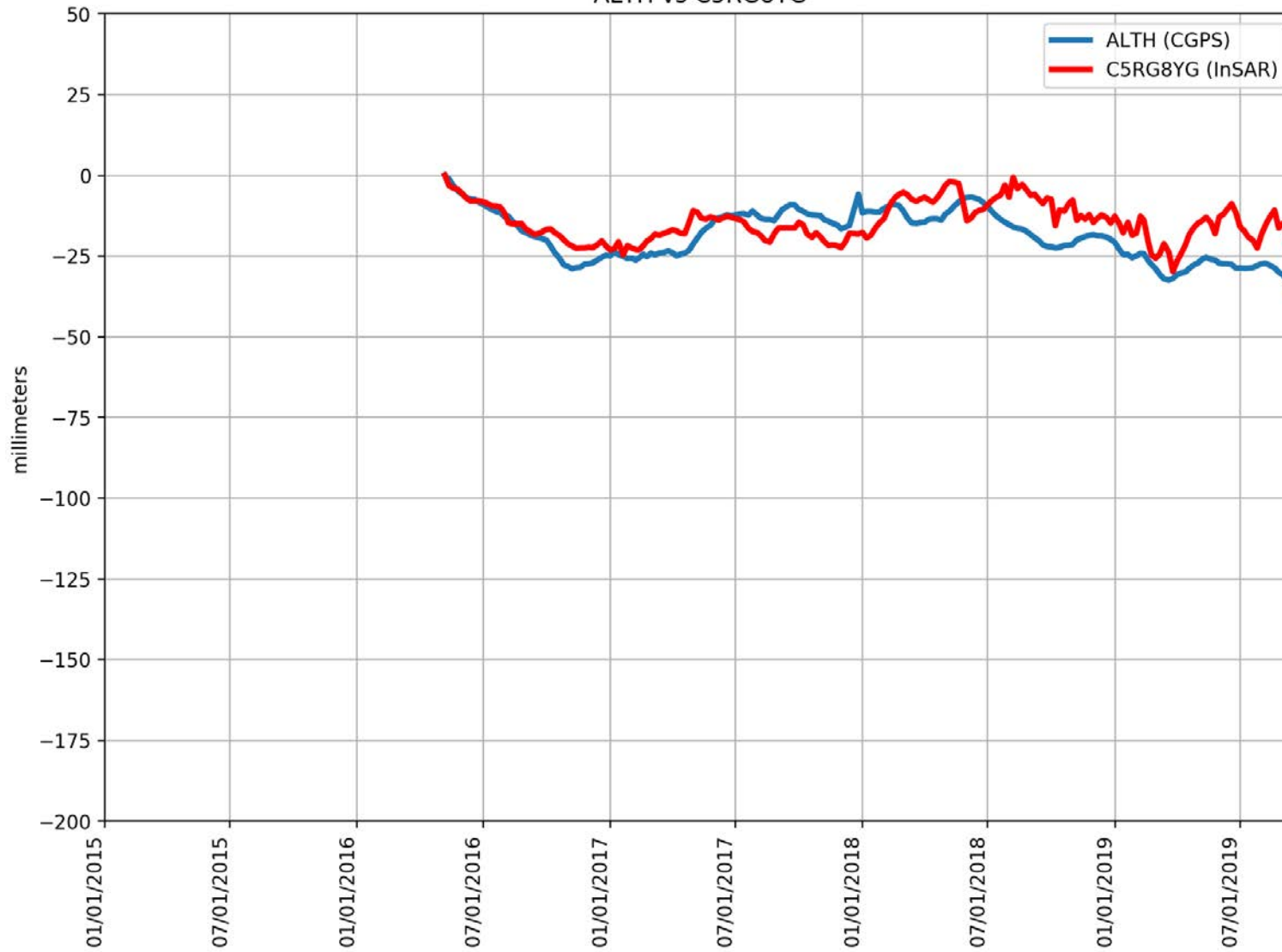
ALPP vs B3SH1D2



RMSE: 3.75 mm
Correlation: 0.86

Appendix B

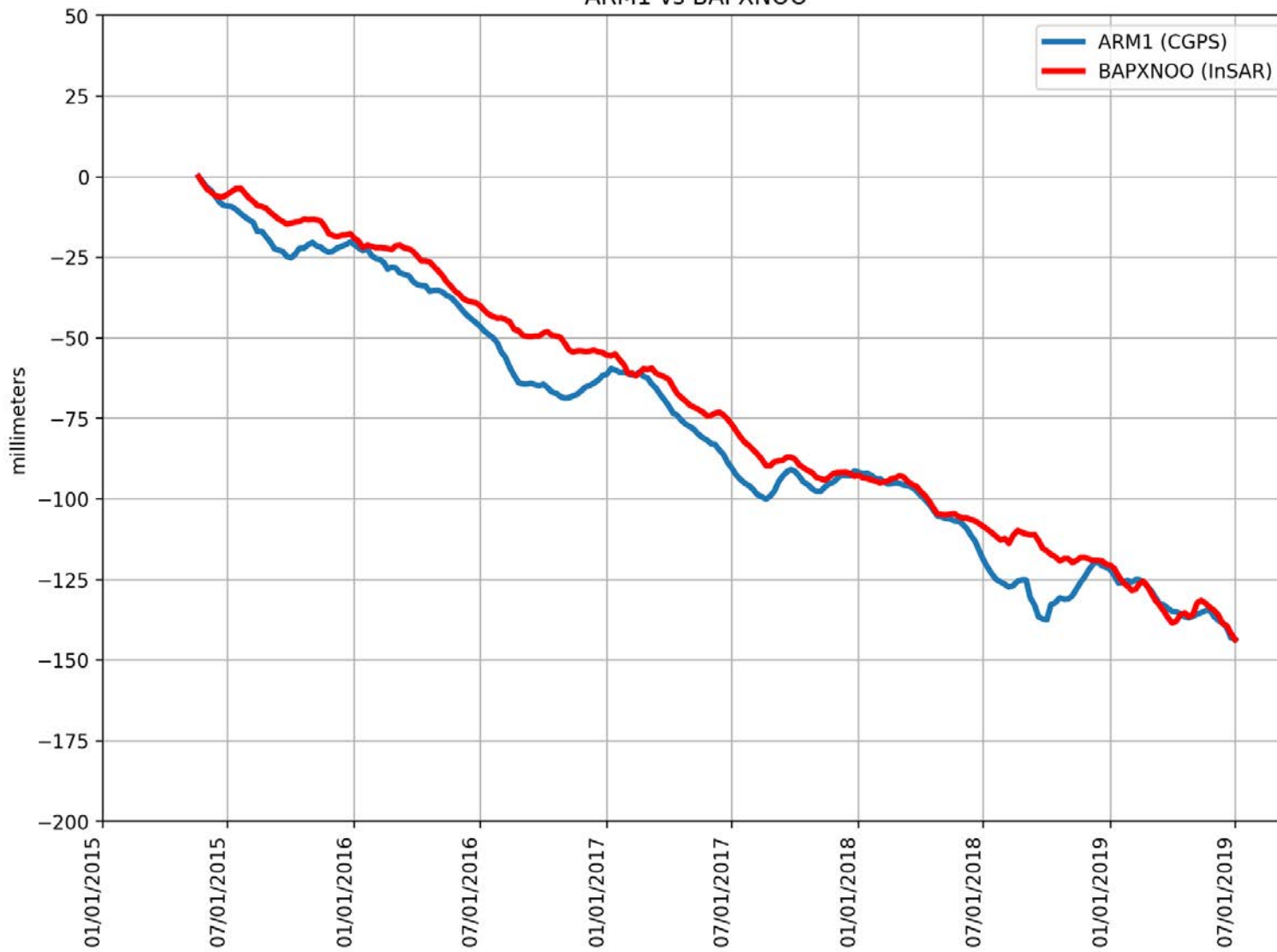
ALTH vs C5RG8YG



RMSE: 7.71 mm
Correlation: 0.57

Appendix B

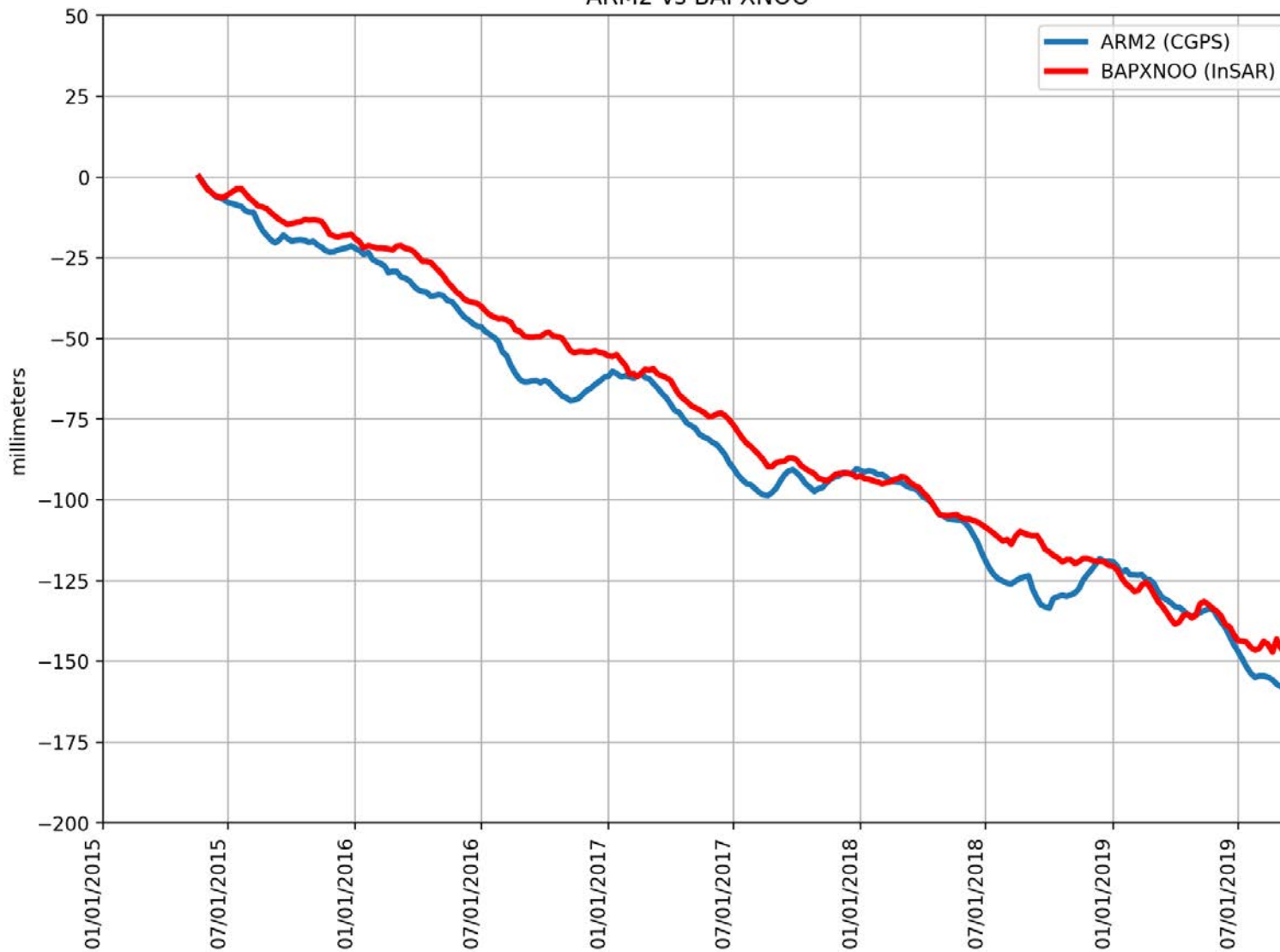
ARM1 vs BAPXNOO



RMSE: 8.33 mm
Correlation: 0.99

Appendix B

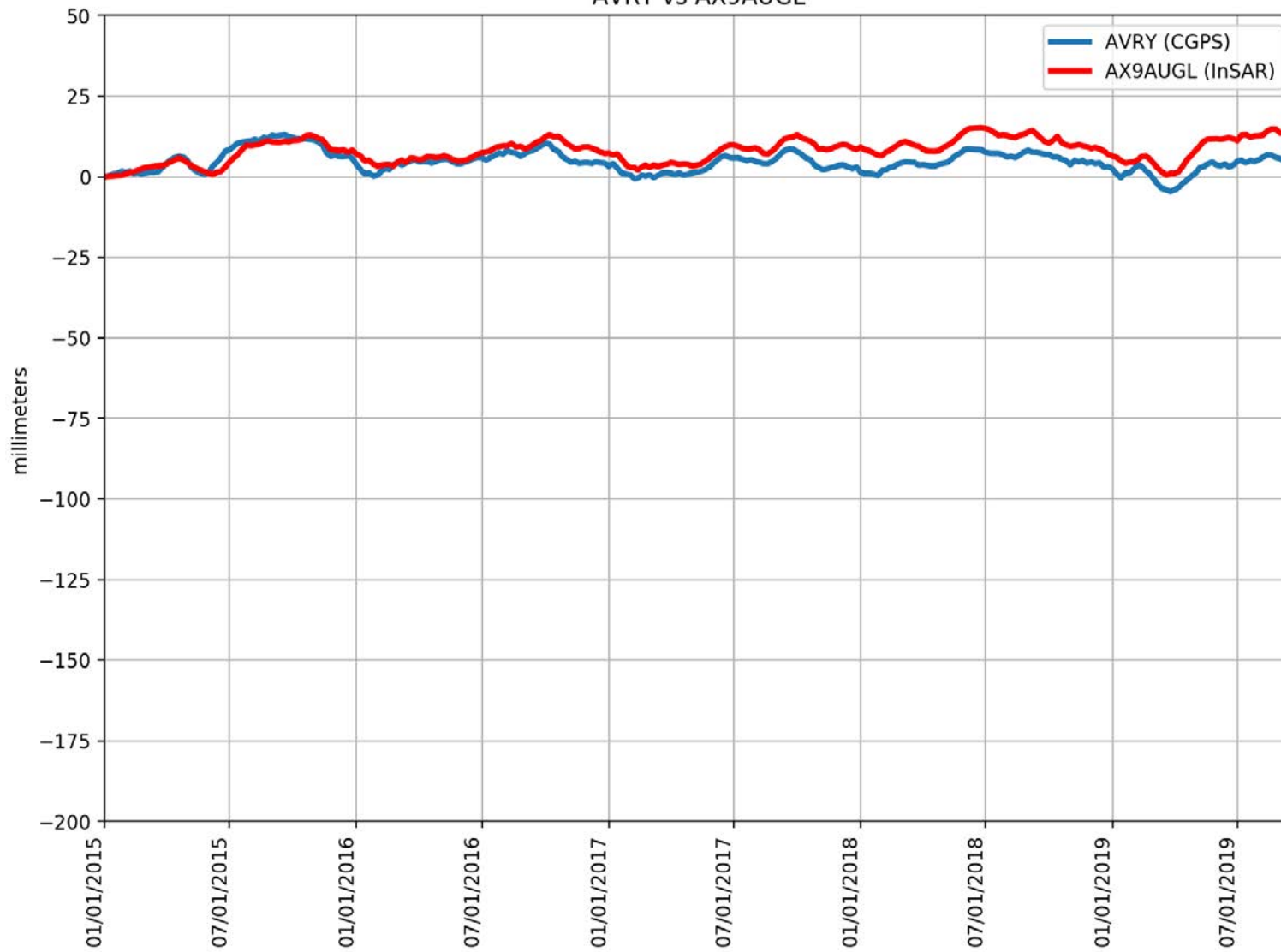
ARM2 vs BAPXNOO



RMSE: 7.93 mm
Correlation: 0.99

Appendix B

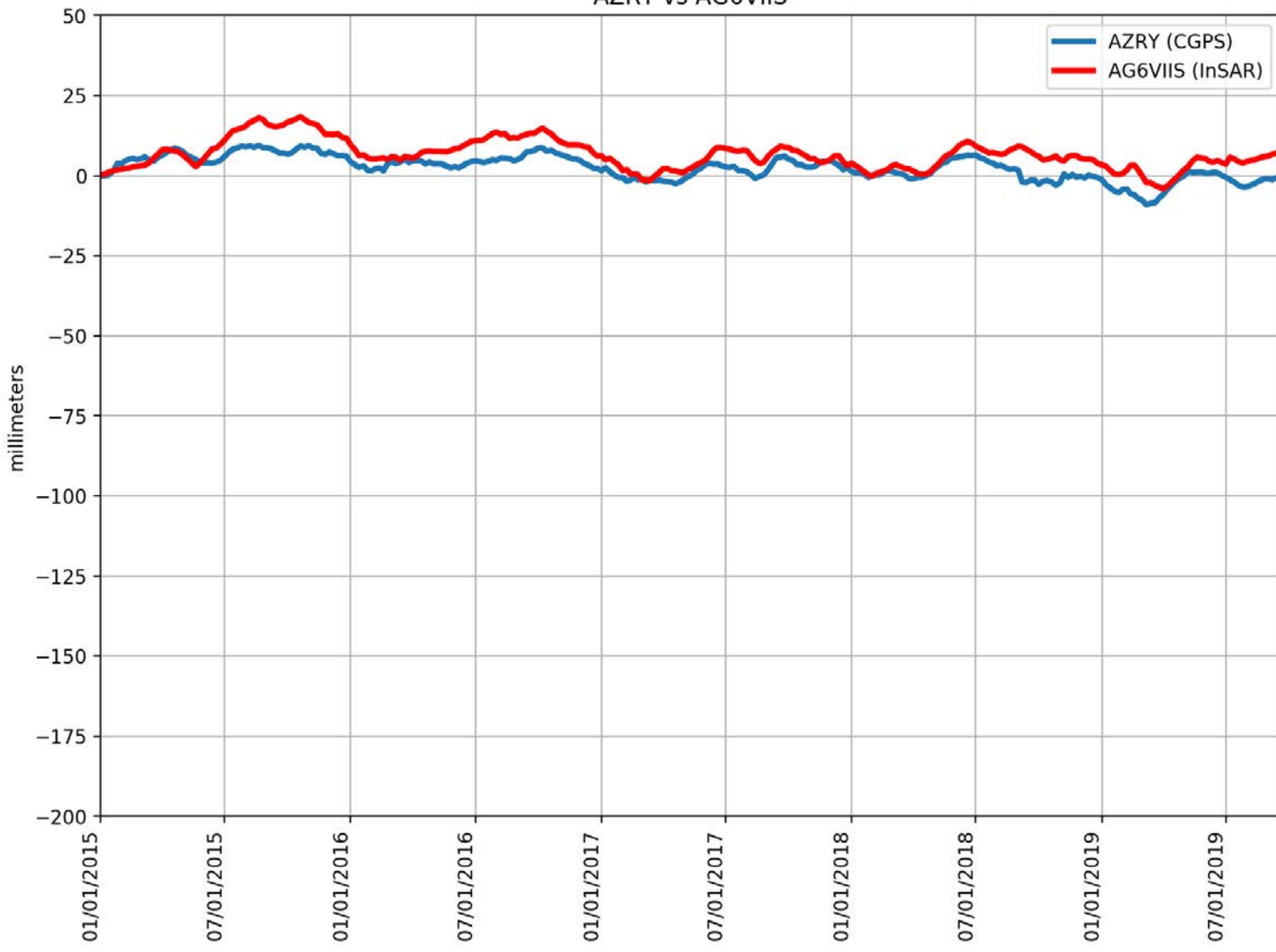
AVRY vs AX9AUGL



RMSE: 4.40 mm
Correlation: 0.68

Appendix B

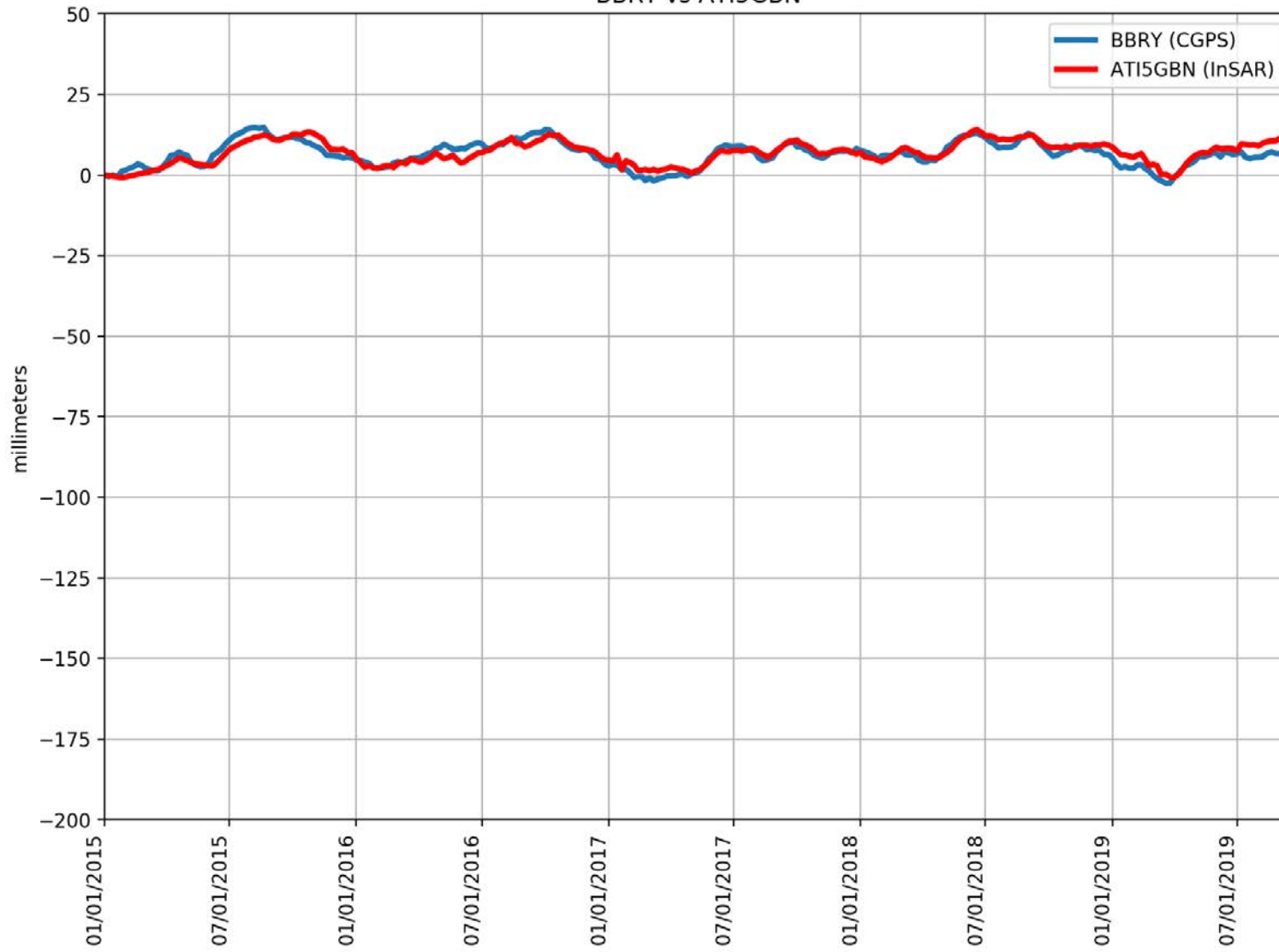
AZRY vs AG6VIIS



RMSE: 4.96 mm
Correlation: 0.79

Appendix B

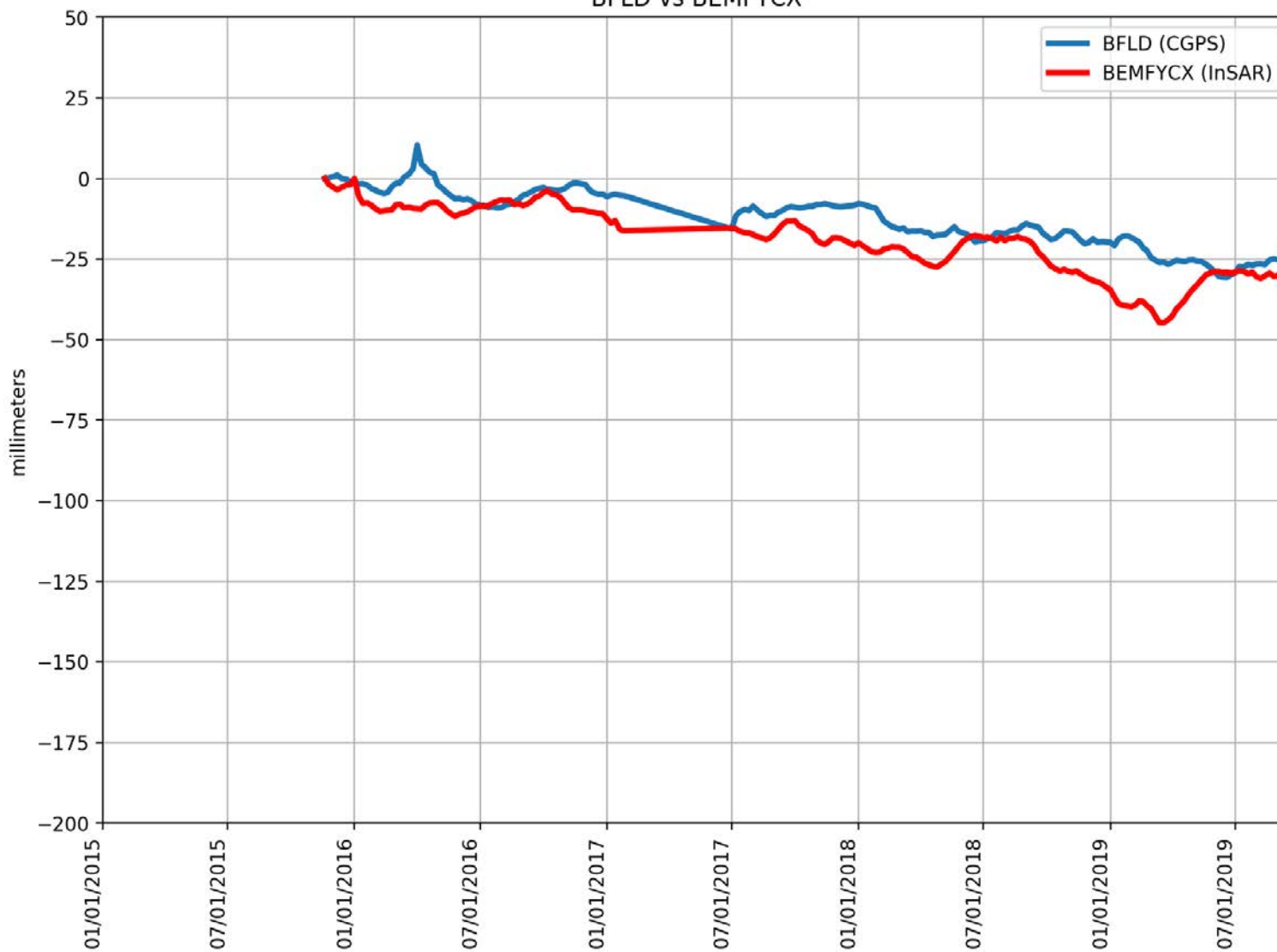
BBRY vs ATI5GBN



RMSE: 2.03 mm
Correlation: 0.86

Appendix B

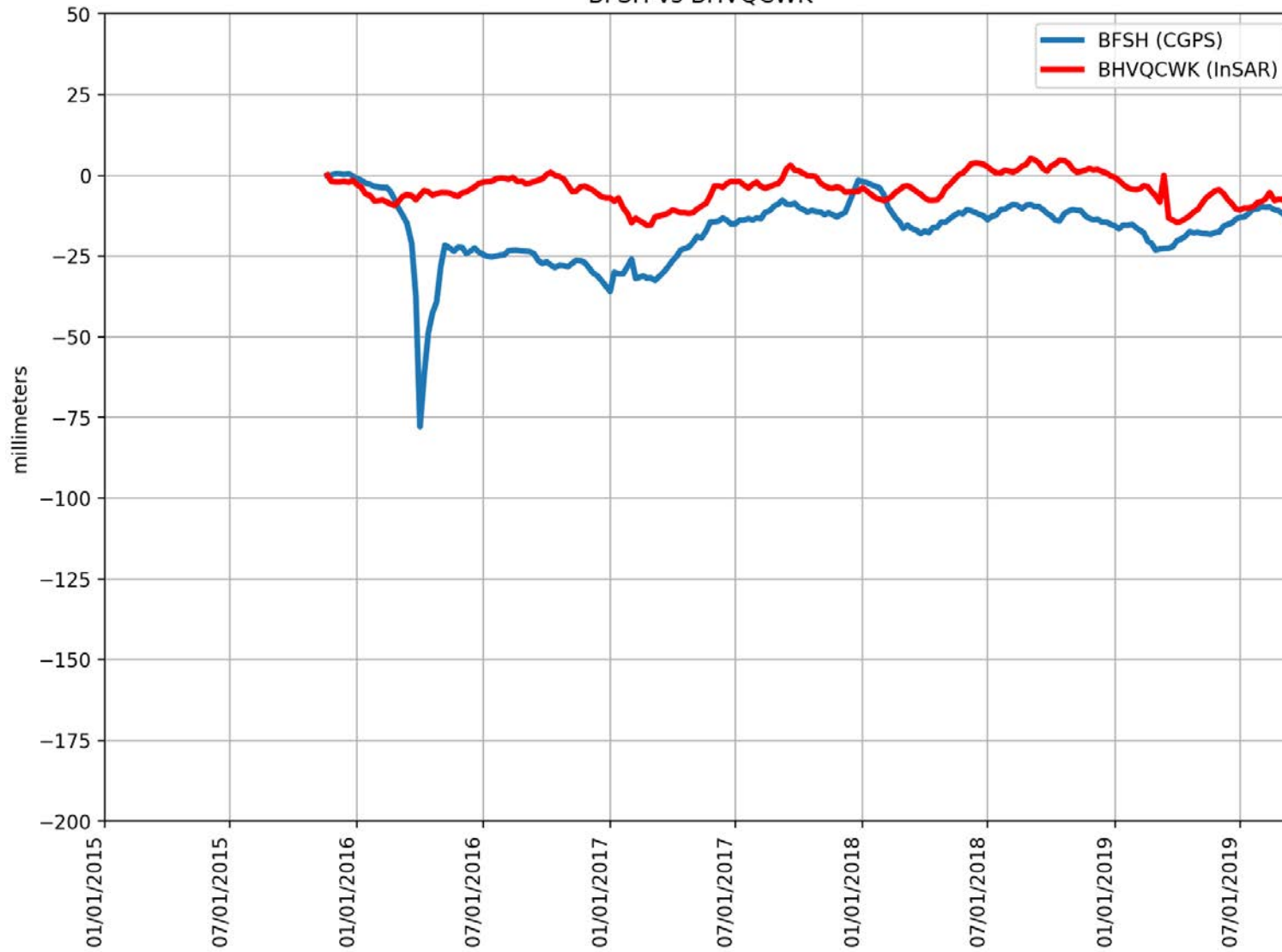
BFLD vs BEMFYCX



RMSE: 8.80 mm
Correlation: 0.87

Appendix B

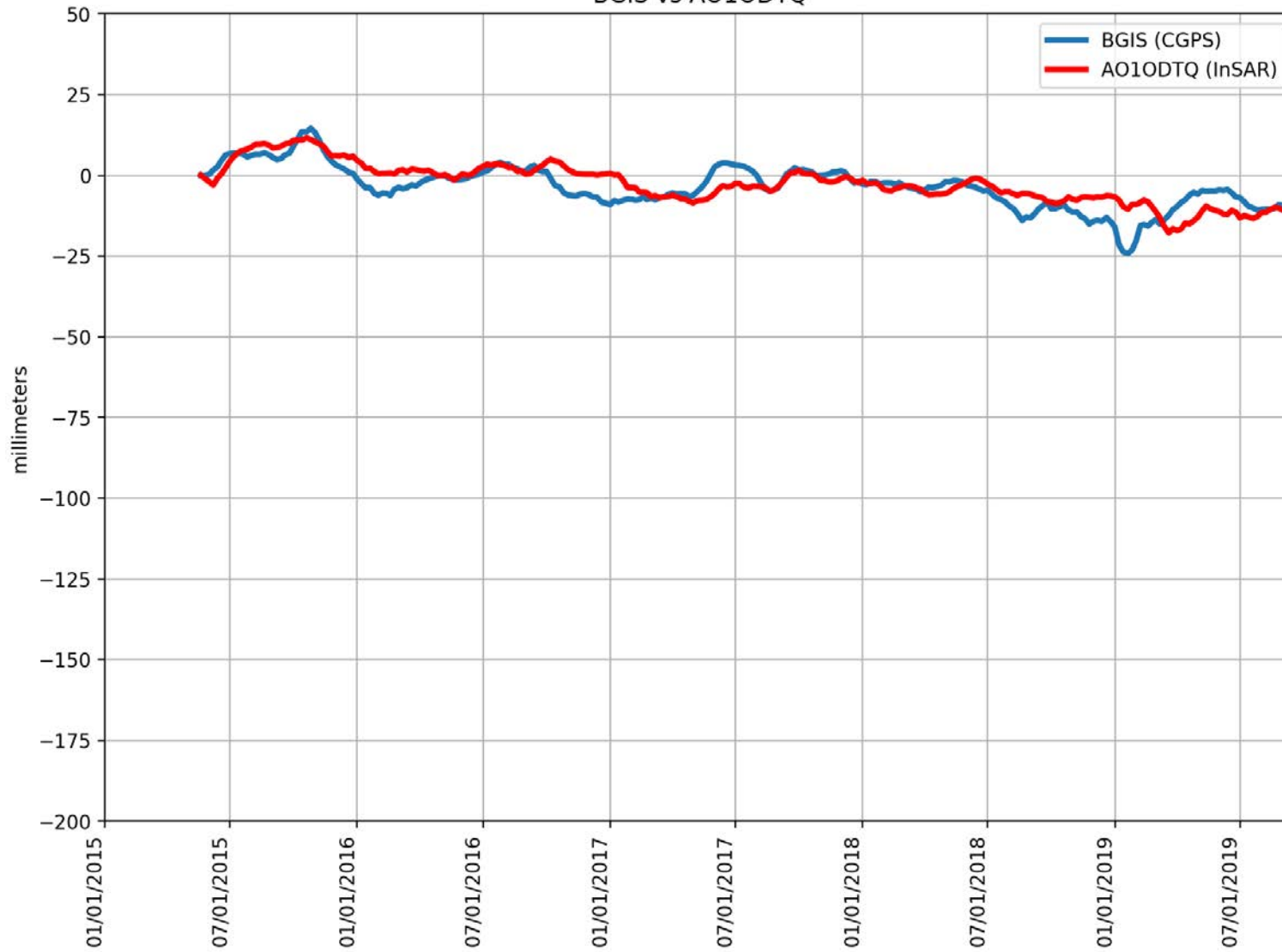
BFSH vs BHVQCWK



RMSE: 16.02 mm
Correlation: 0.30

Appendix B

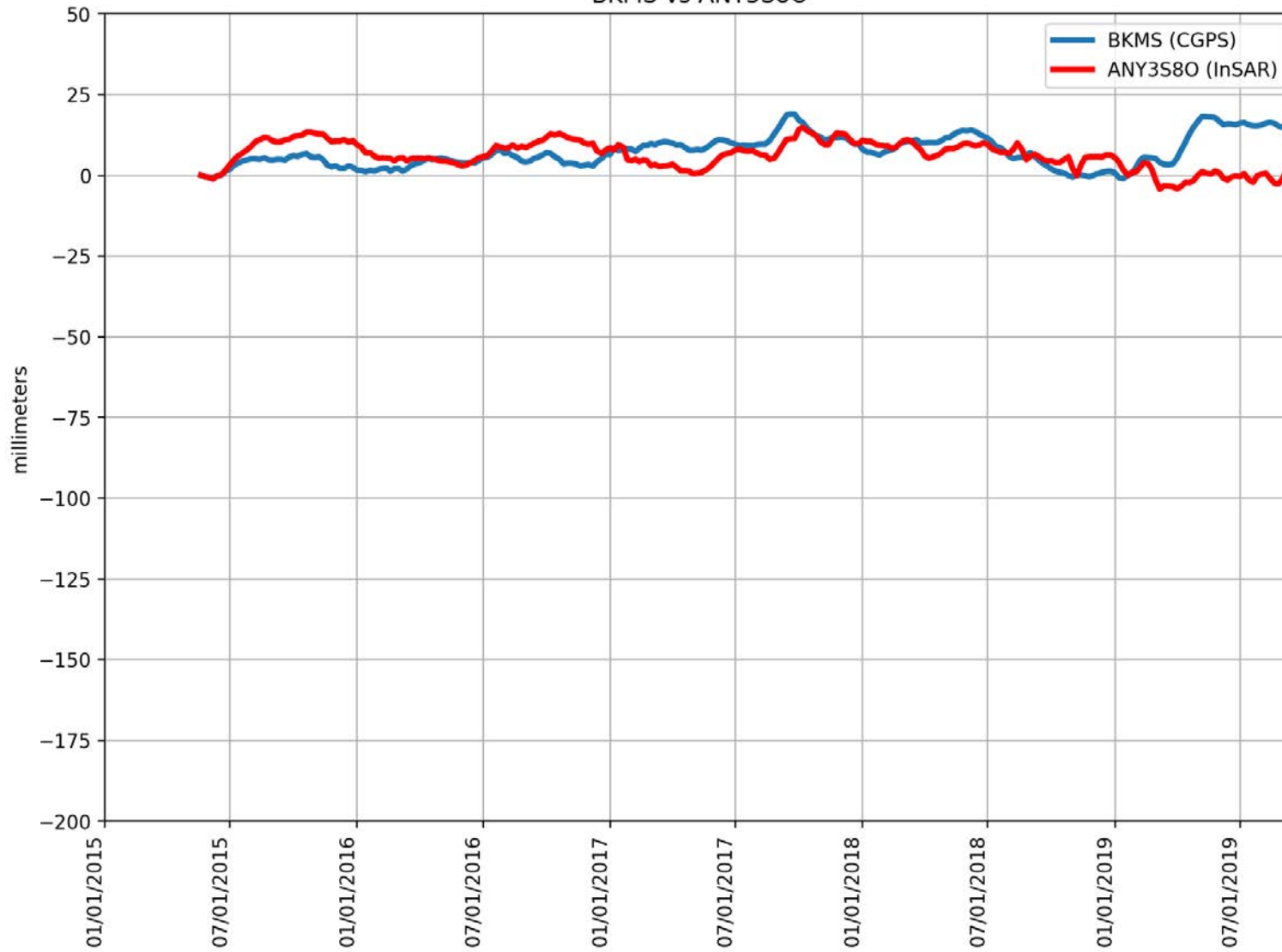
BGIS vs AO10DTQ



RMSE: 4.62 mm
Correlation: 0.75

Appendix B

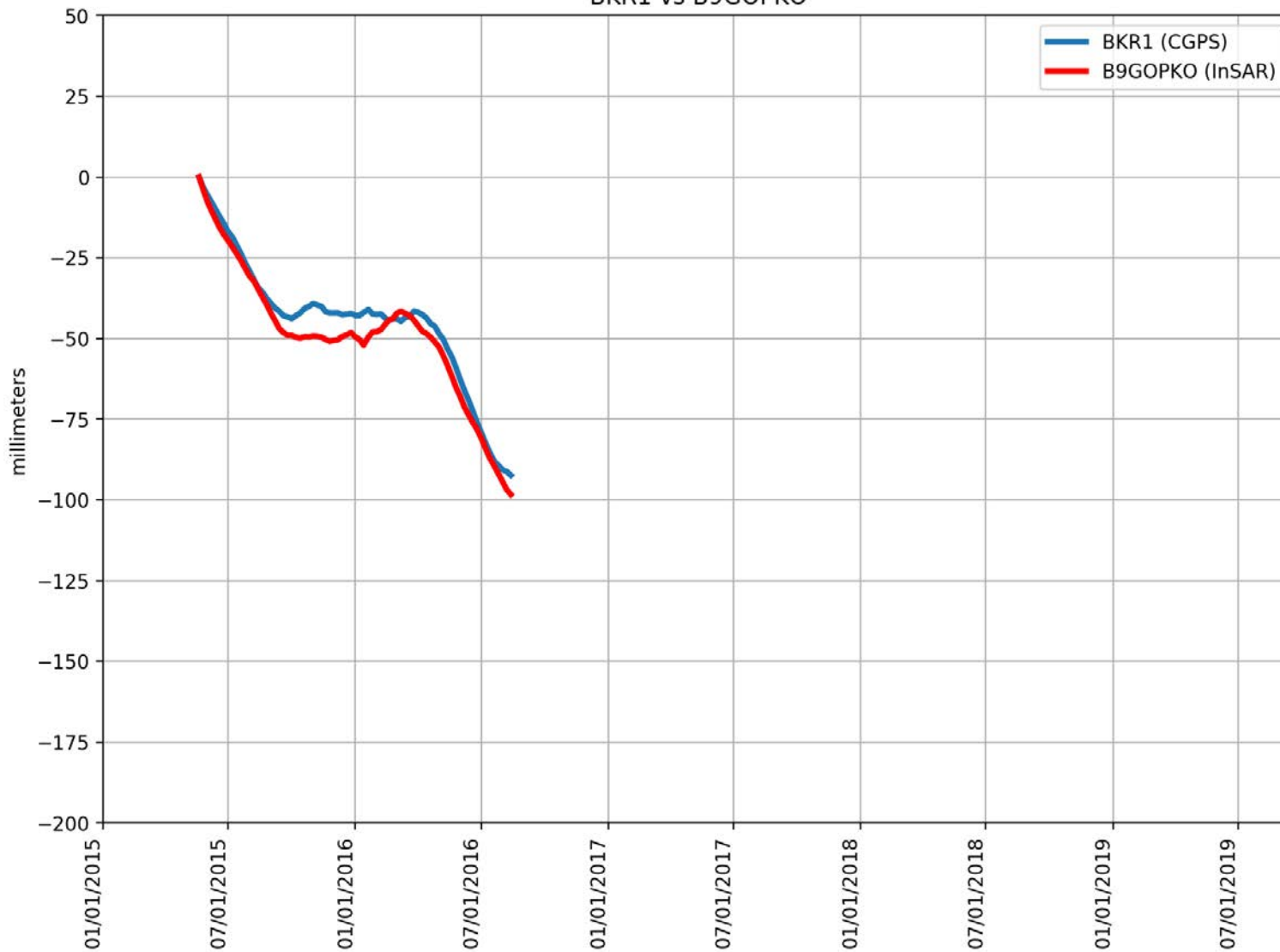
BKMS vs ANY3S80



RMSE: 6.74 mm
Correlation: -0.04

Appendix B

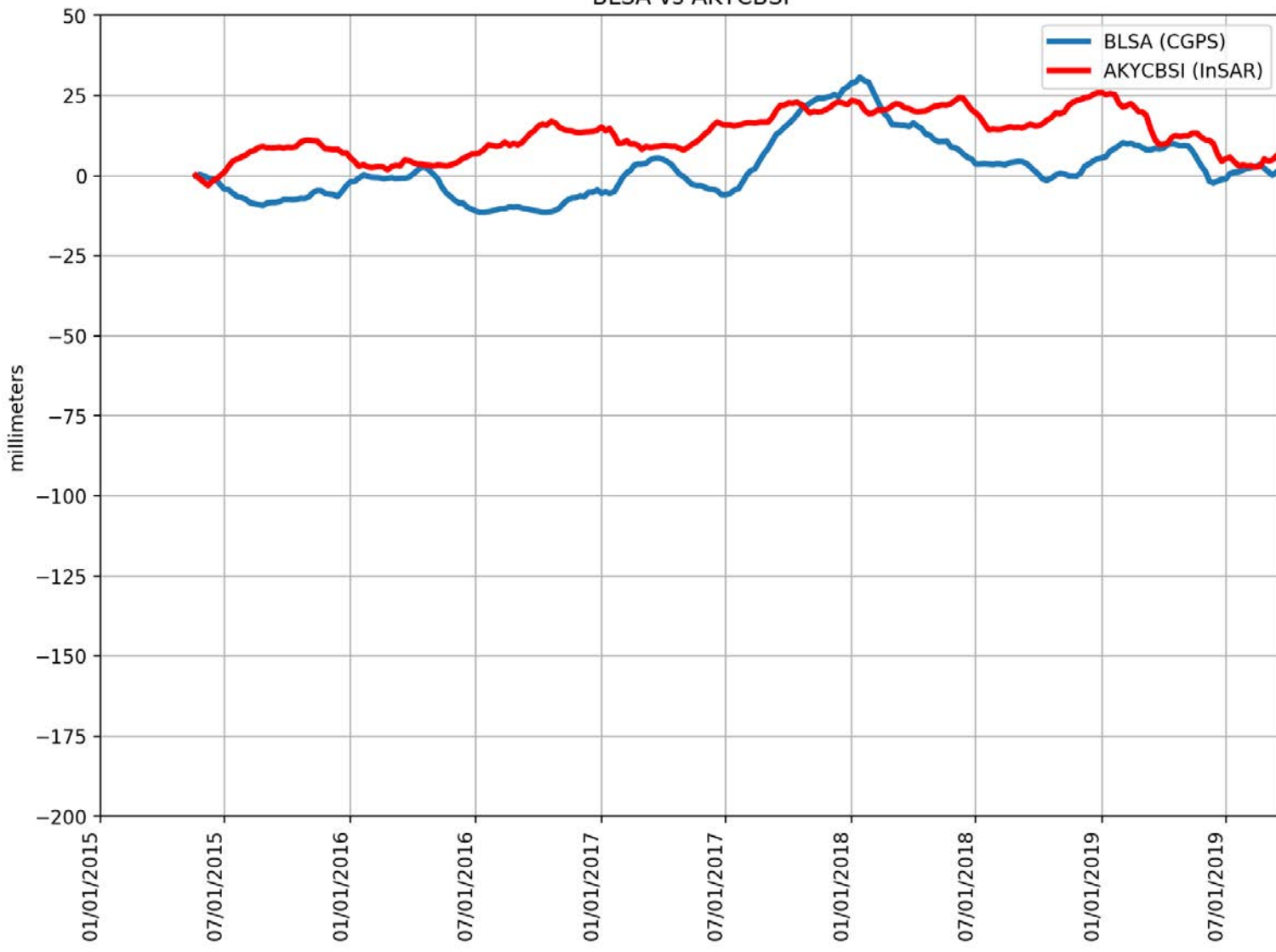
BKR1 vs B9GOPKO



RMSE: 5.18 mm
Correlation: 0.99

Appendix B

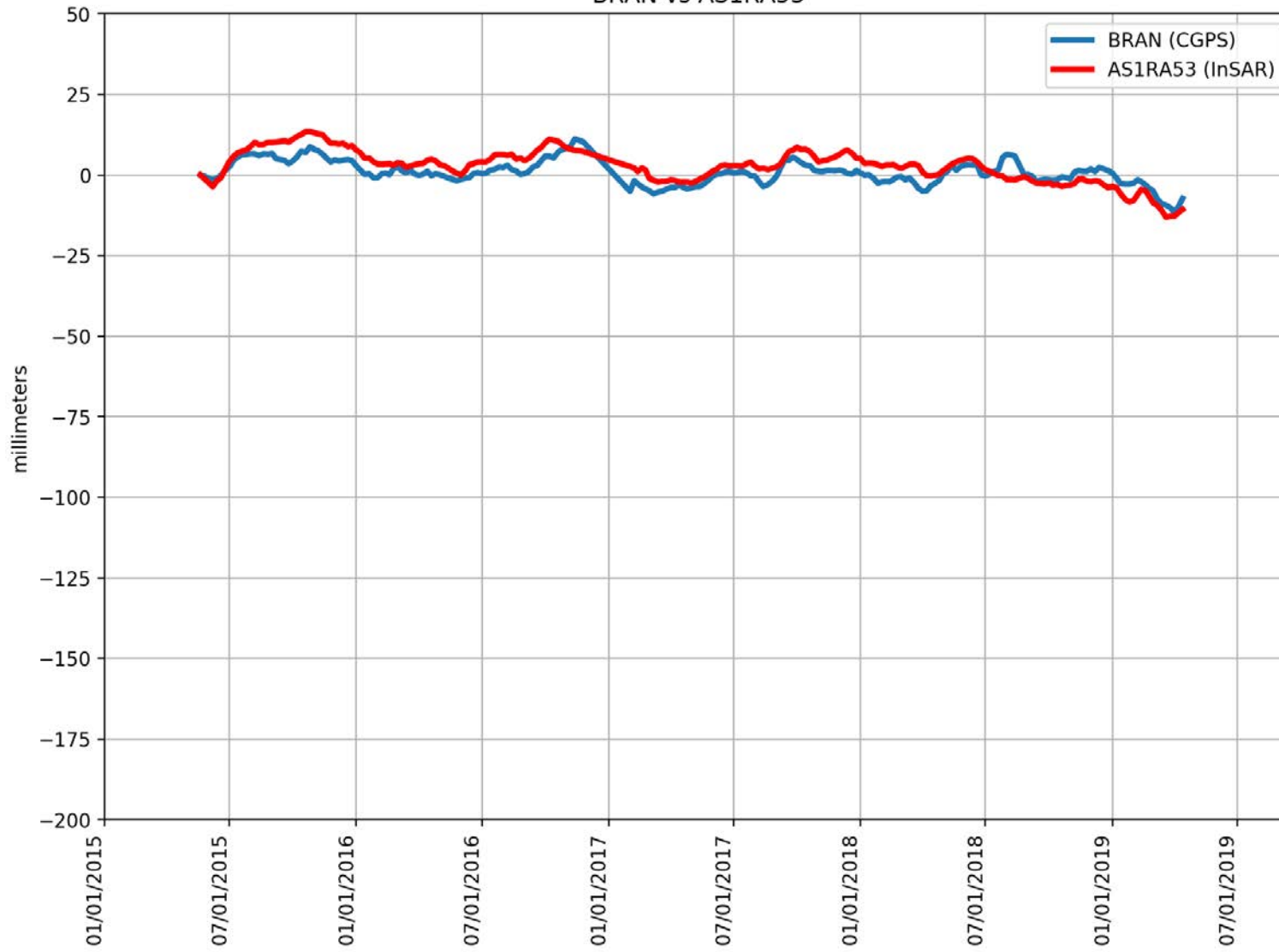
BLSA vs AKYCBSI



RMSE: 13.26 mm
Correlation: 0.57

Appendix B

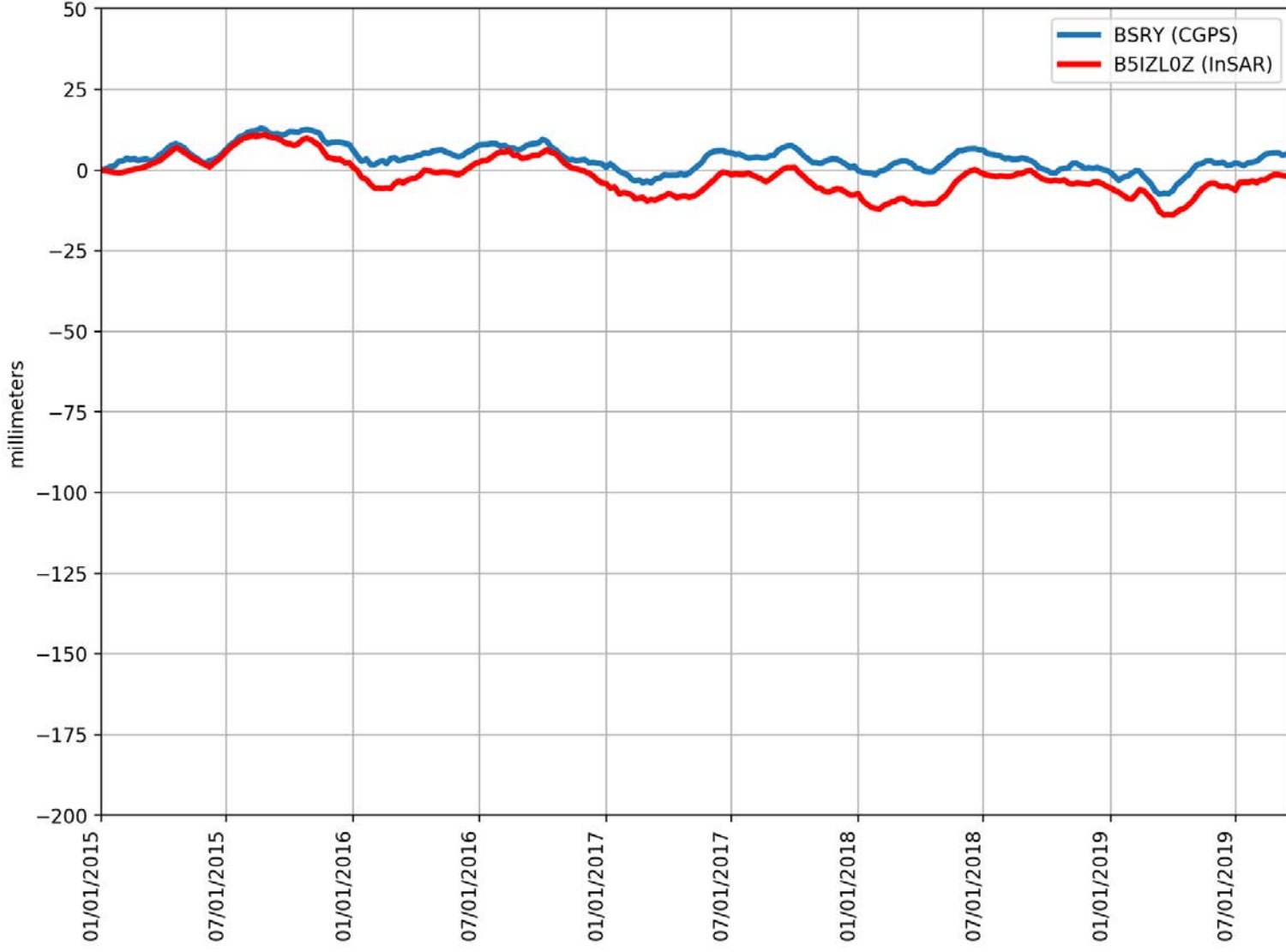
BRAN vs AS1RA53



RMSE: 3.77 mm
Correlation: 0.79

Appendix B

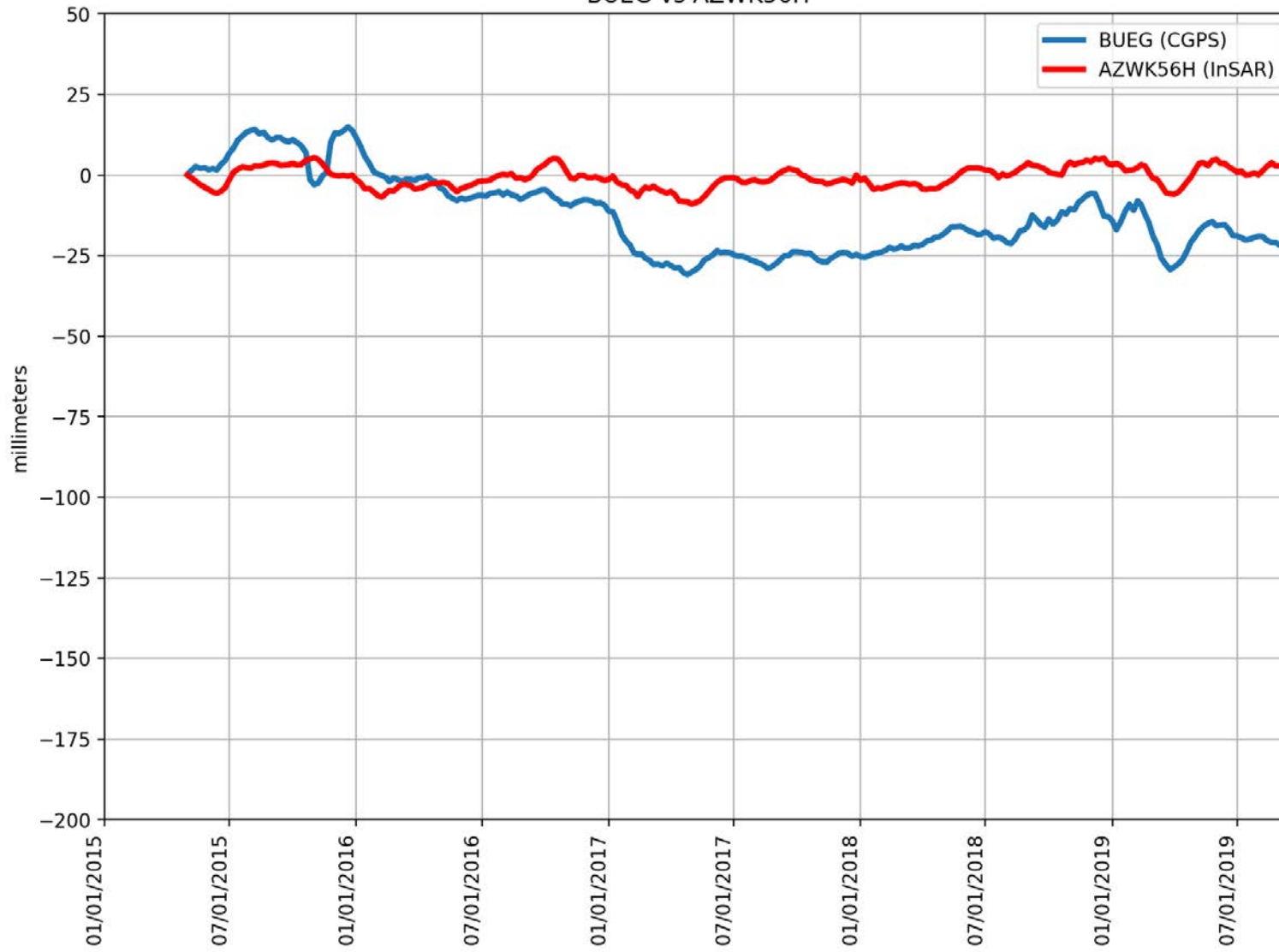
BSRY vs B5IZL0Z



RMSE: 6.19 mm
Correlation: 0.89

Appendix B

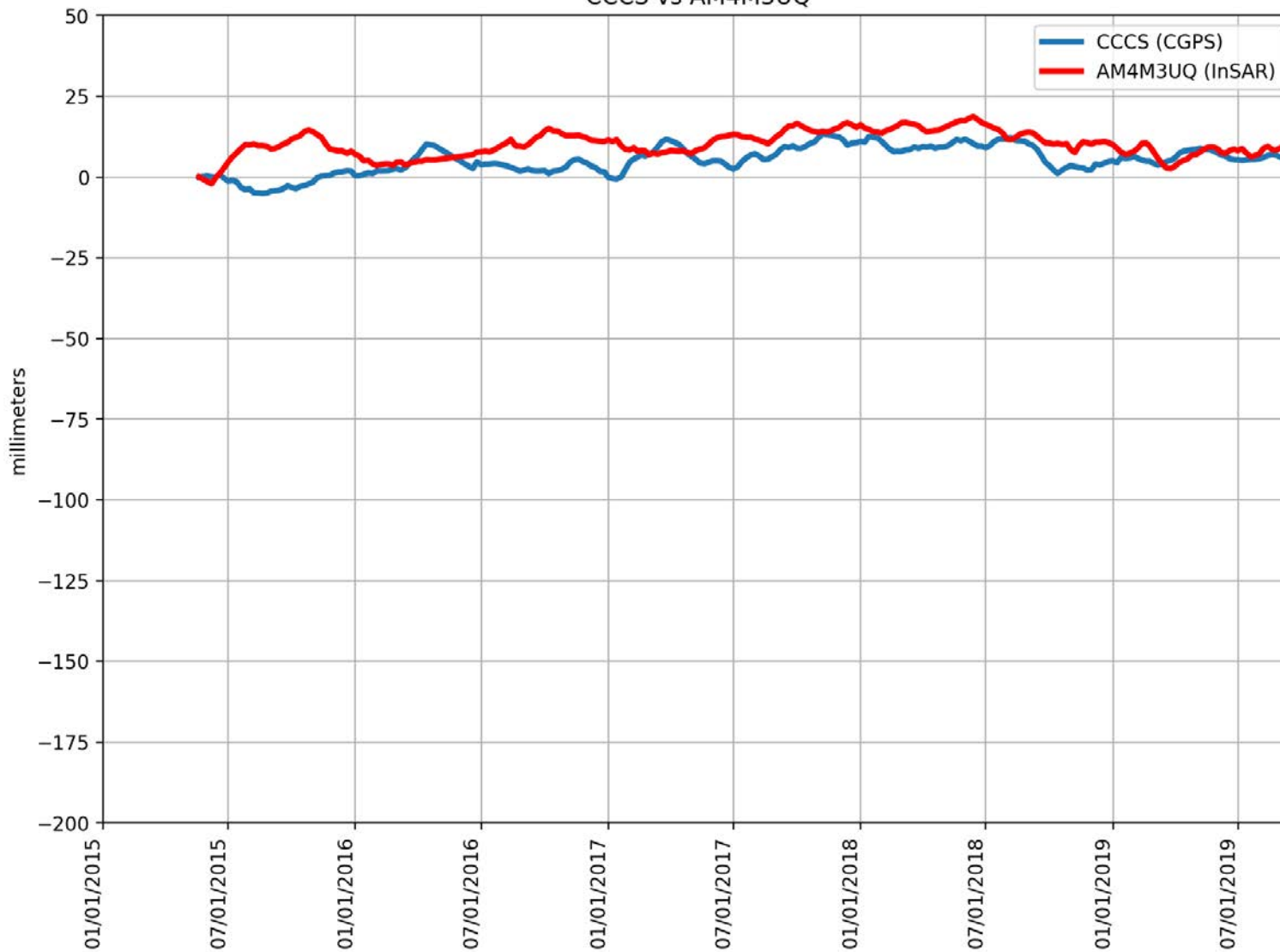
BUEG vs AZWK56H



RMSE: 16.63 mm
Correlation: 0.30

Appendix B

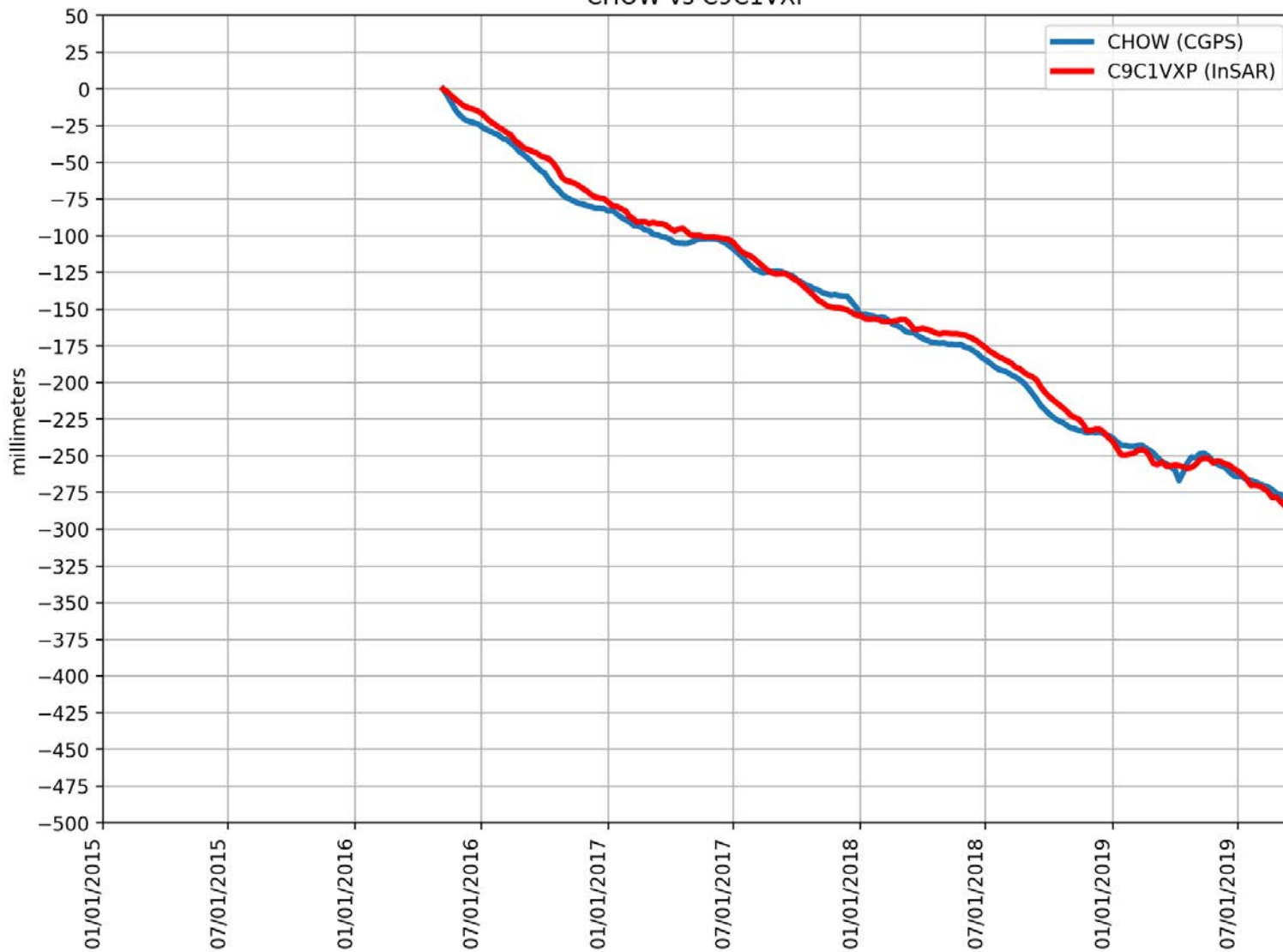
CCCS vs AM4M3UQ



RMSE: 6.79 mm
Correlation: 0.41

Appendix B

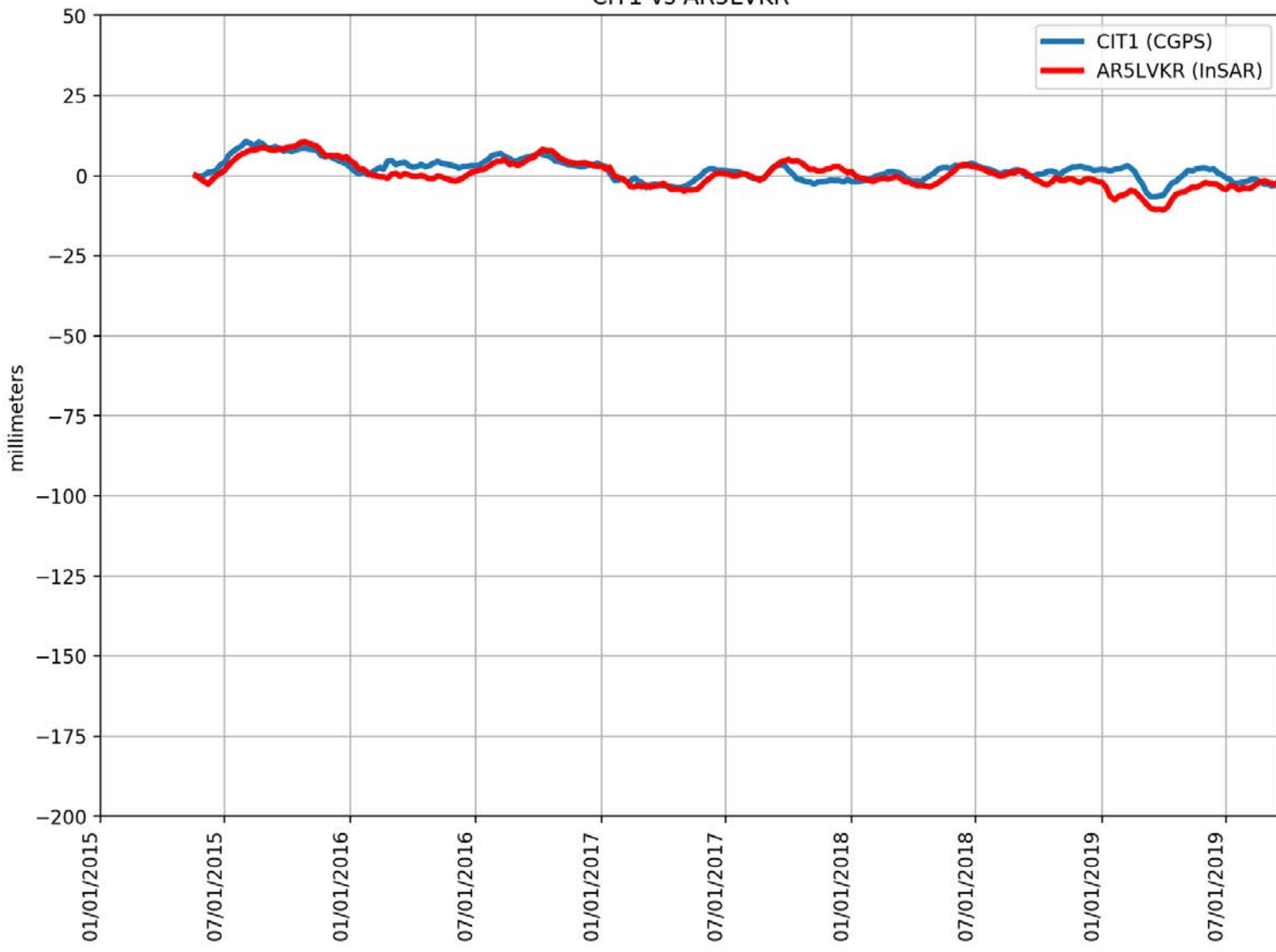
CHOW vs C9C1VXP



RMSE: 6.62 mm
Correlation: 1.00

Appendix B

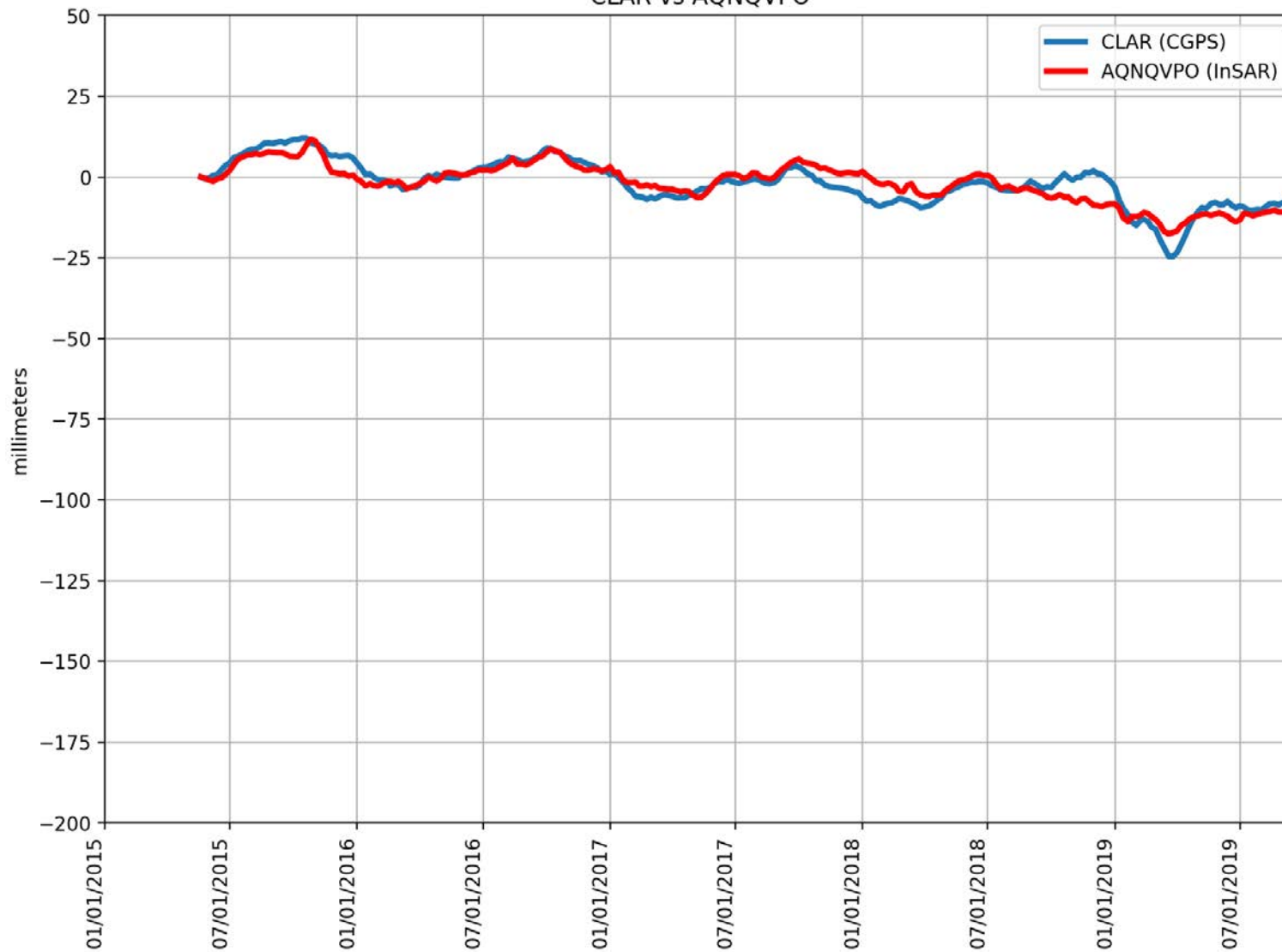
CIT1 vs AR5LVKR



RMSE: 2.91 mm
Correlation: 0.79

Appendix B

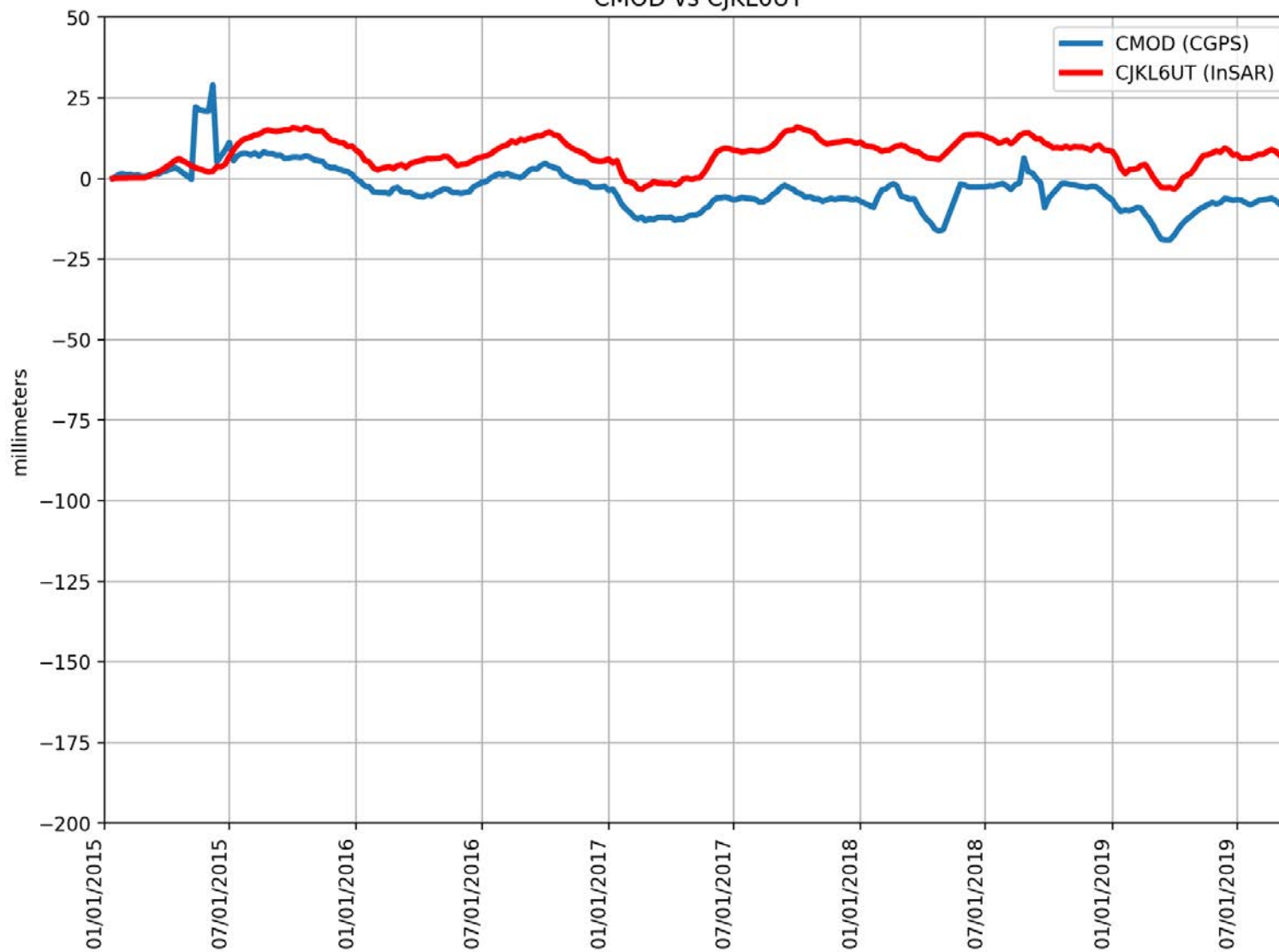
CLAR vs AQNQVPO



RMSE: 3.46 mm
Correlation: 0.87

Appendix B

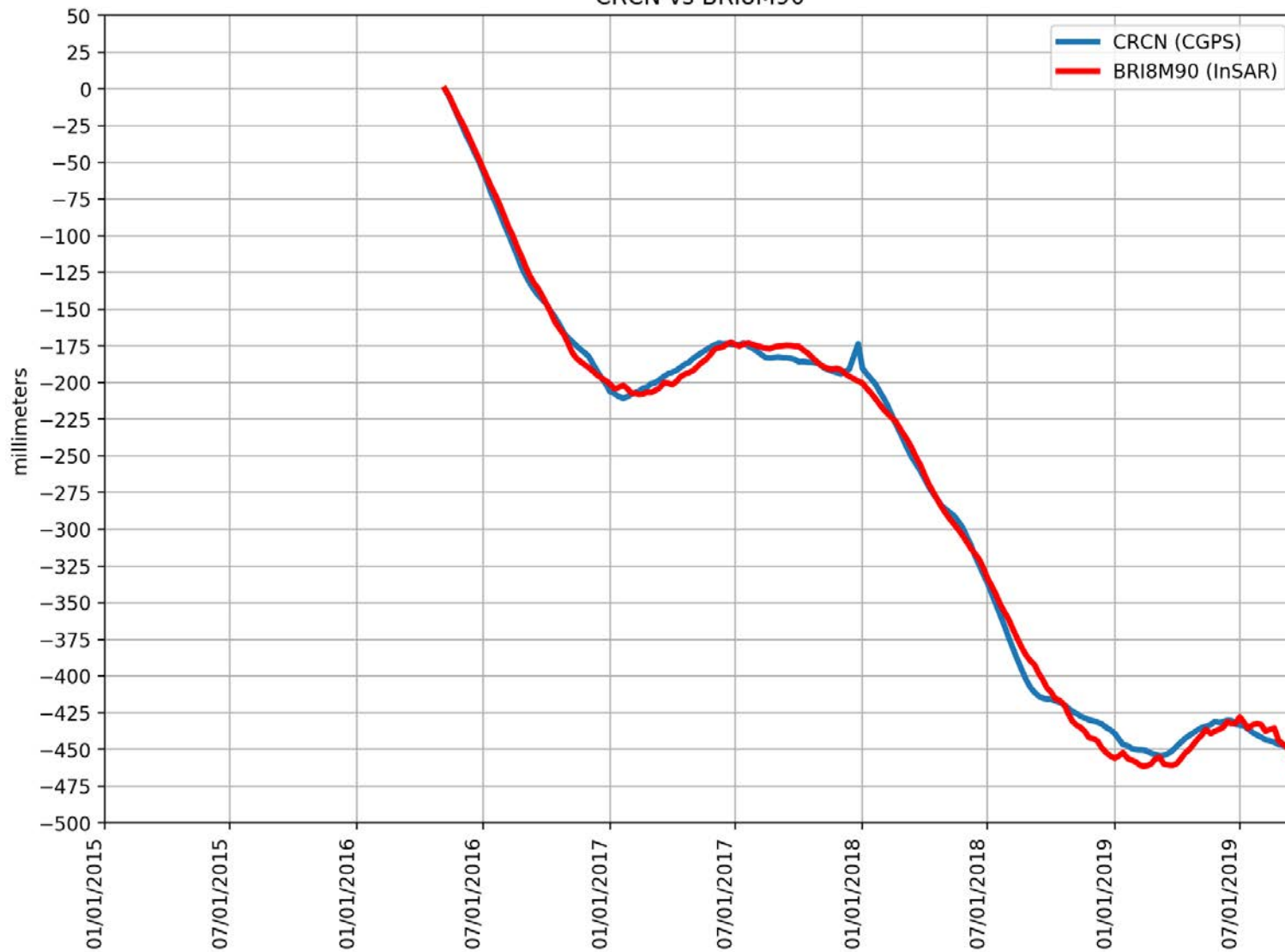
CMOD vs CJKL6UT



RMSE: 12.57 mm
Correlation: 0.42

Appendix B

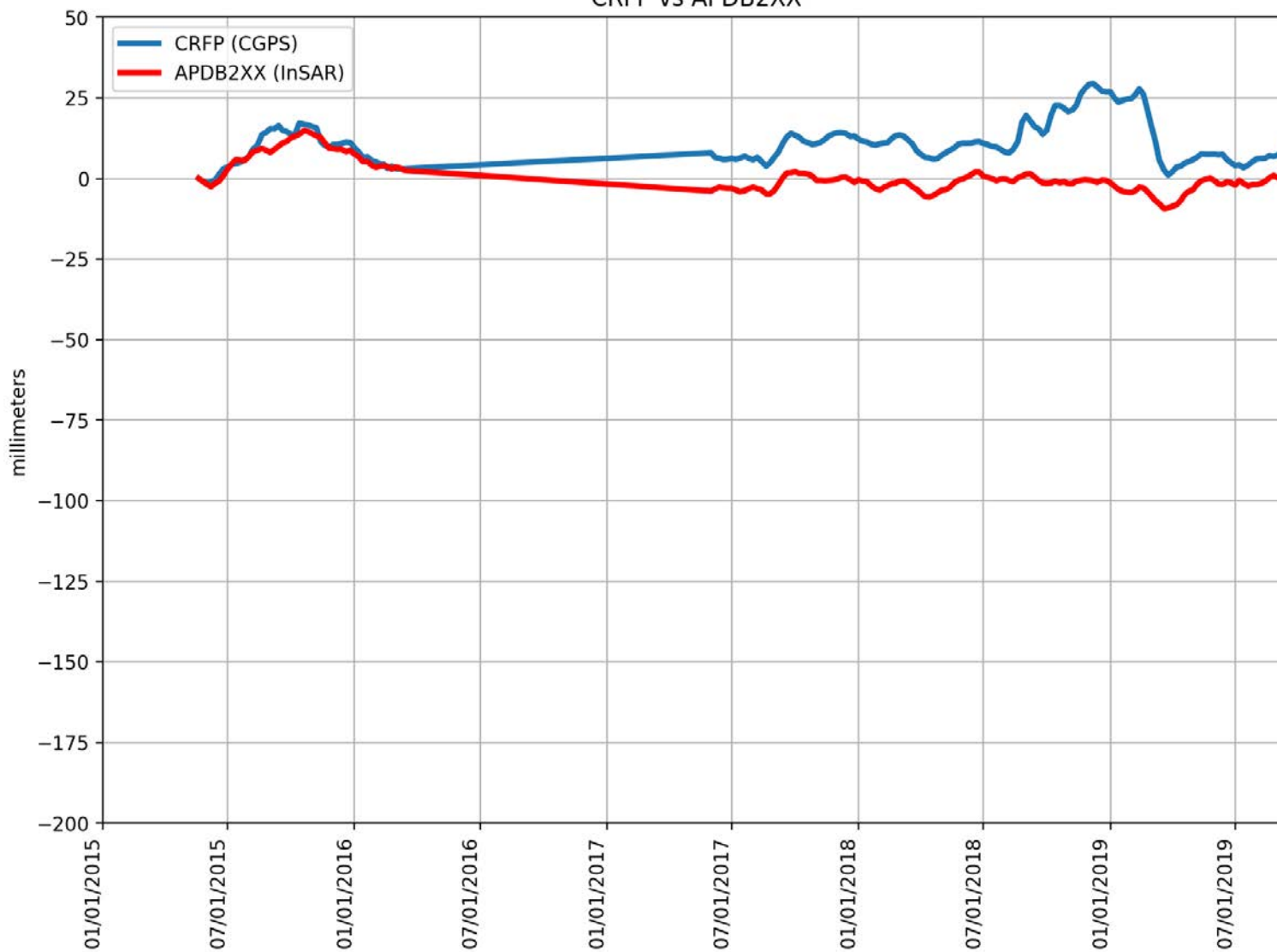
CRCN vs BRI8M90



RMSE: 7.18 mm
Correlation: 1.00

Appendix B

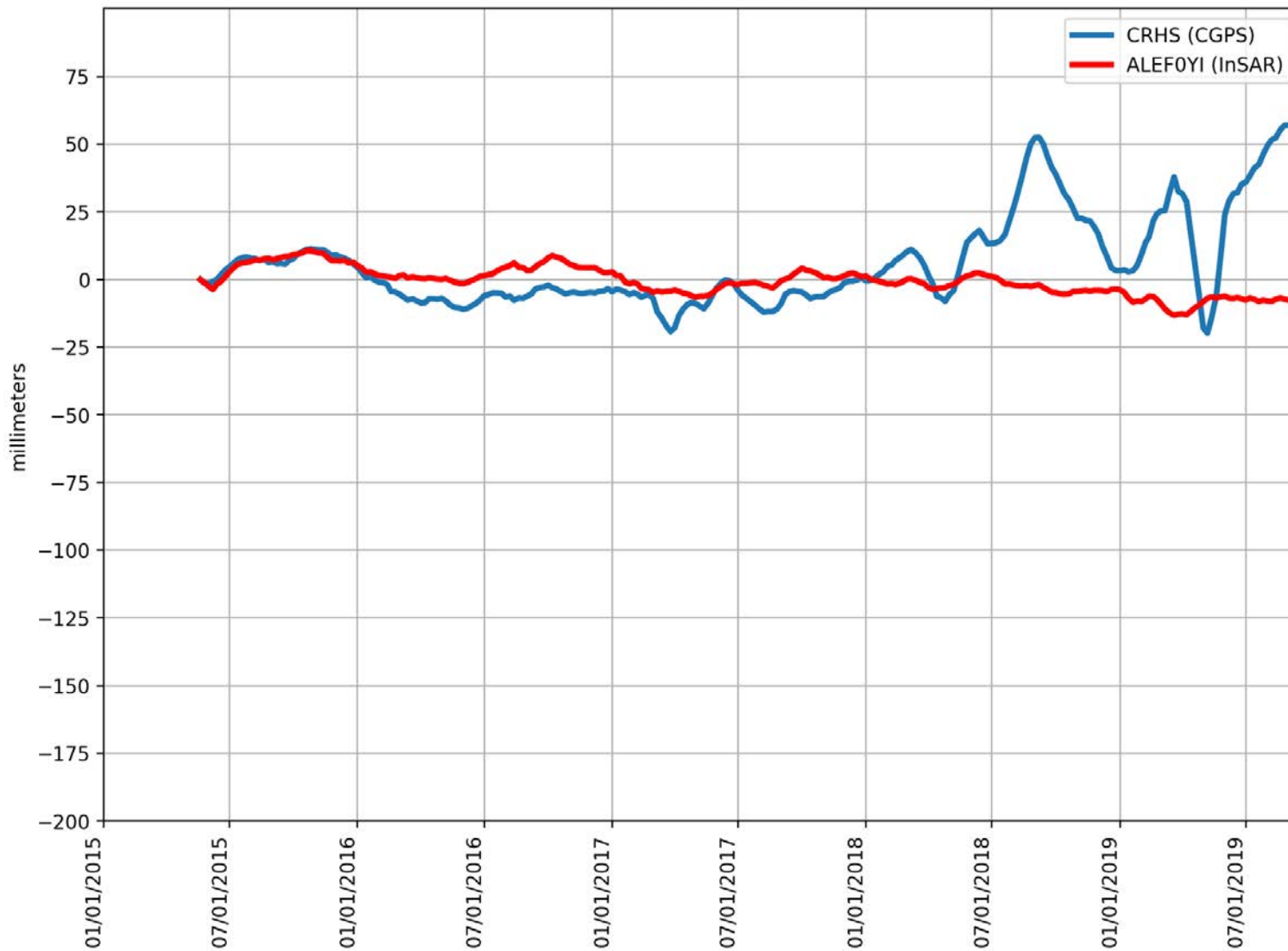
CRFP vs APDB2XX



RMSE: 13.11 mm
Correlation: 0.11

Appendix B

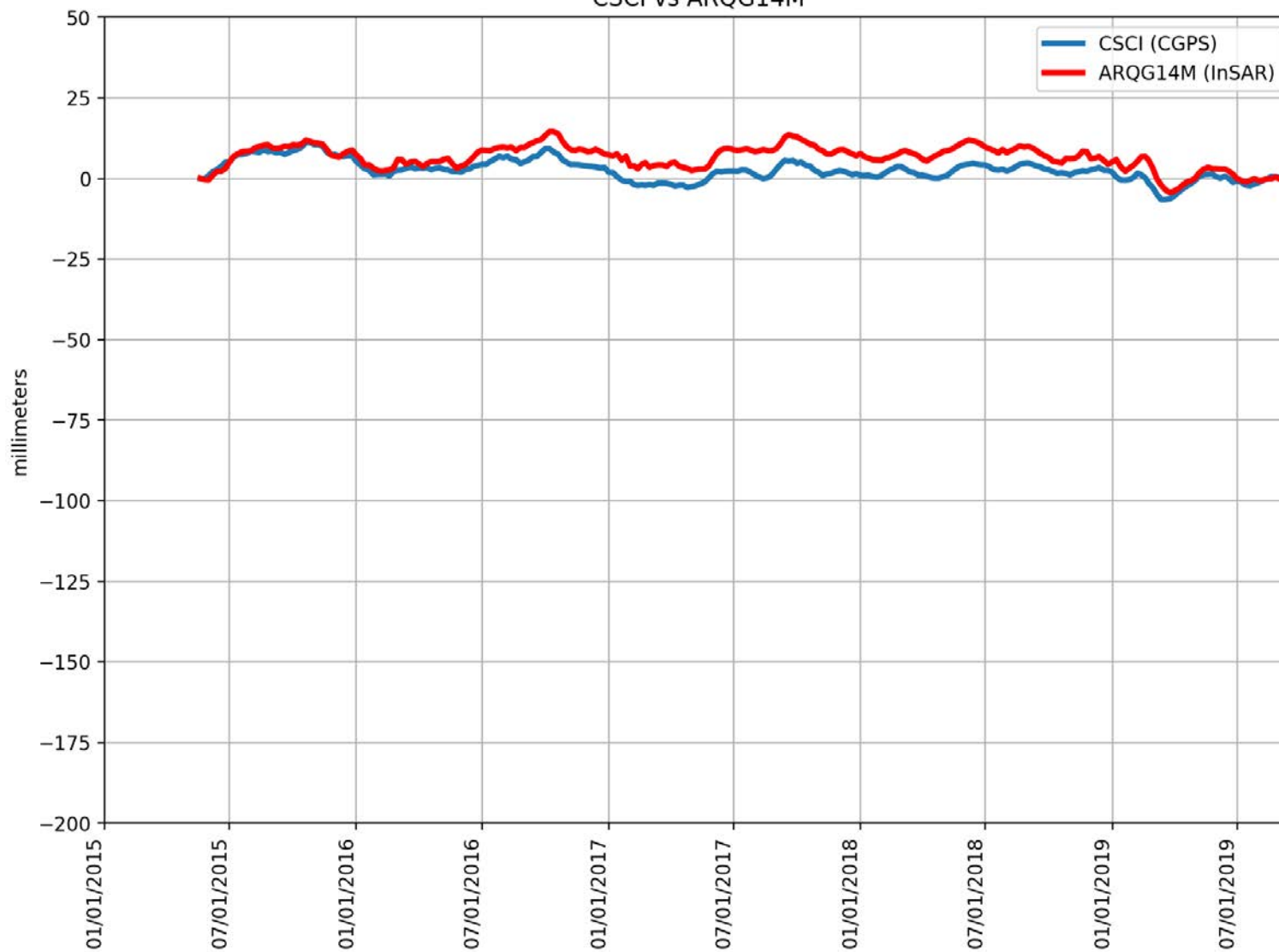
CRHS vs ALEFOYI



RMSE: 20.97 mm
Correlation: -0.37

Appendix B

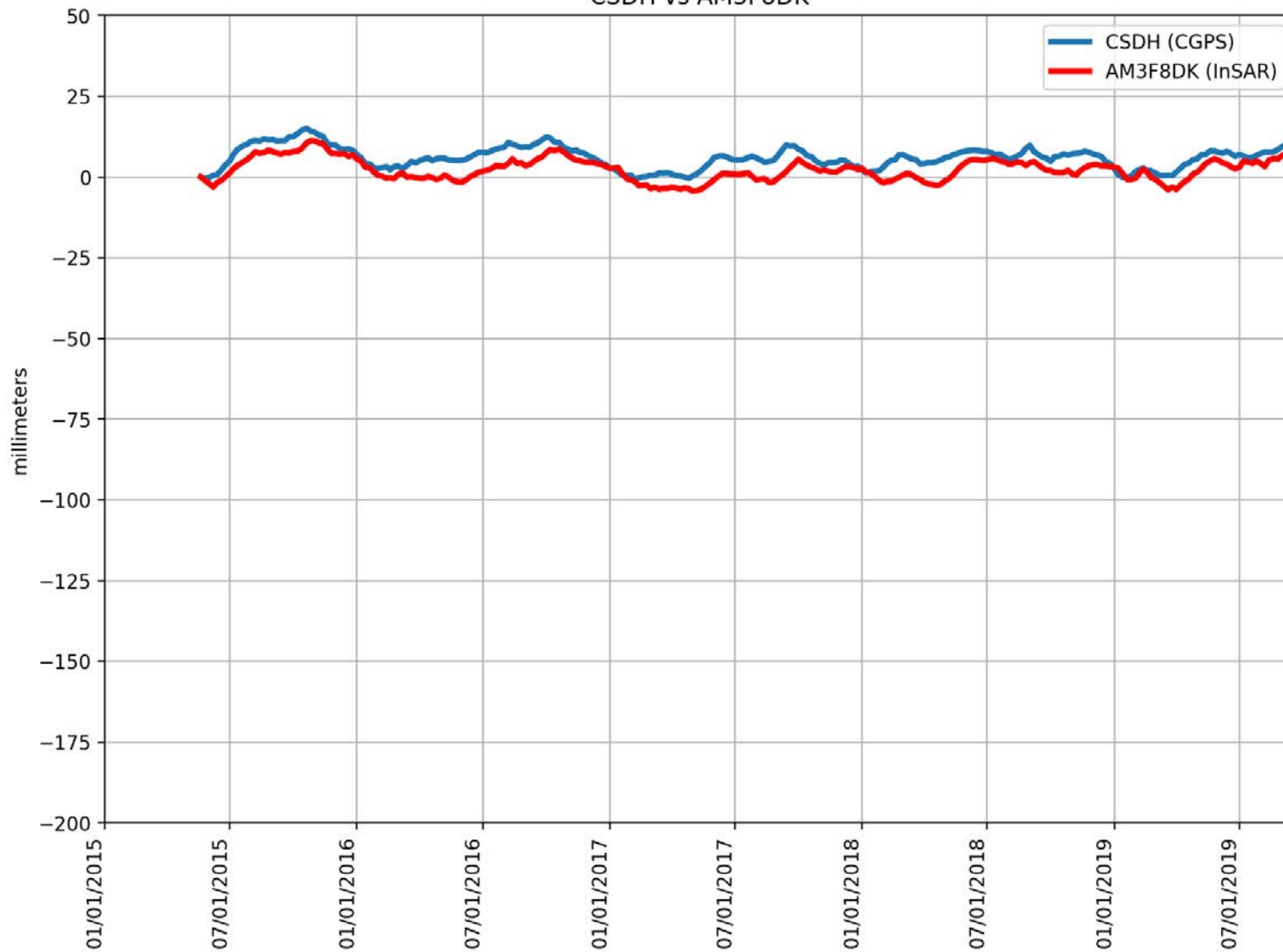
CSCI vs ARQG14M



RMSE: 4.60 mm
Correlation: 0.76

Appendix B

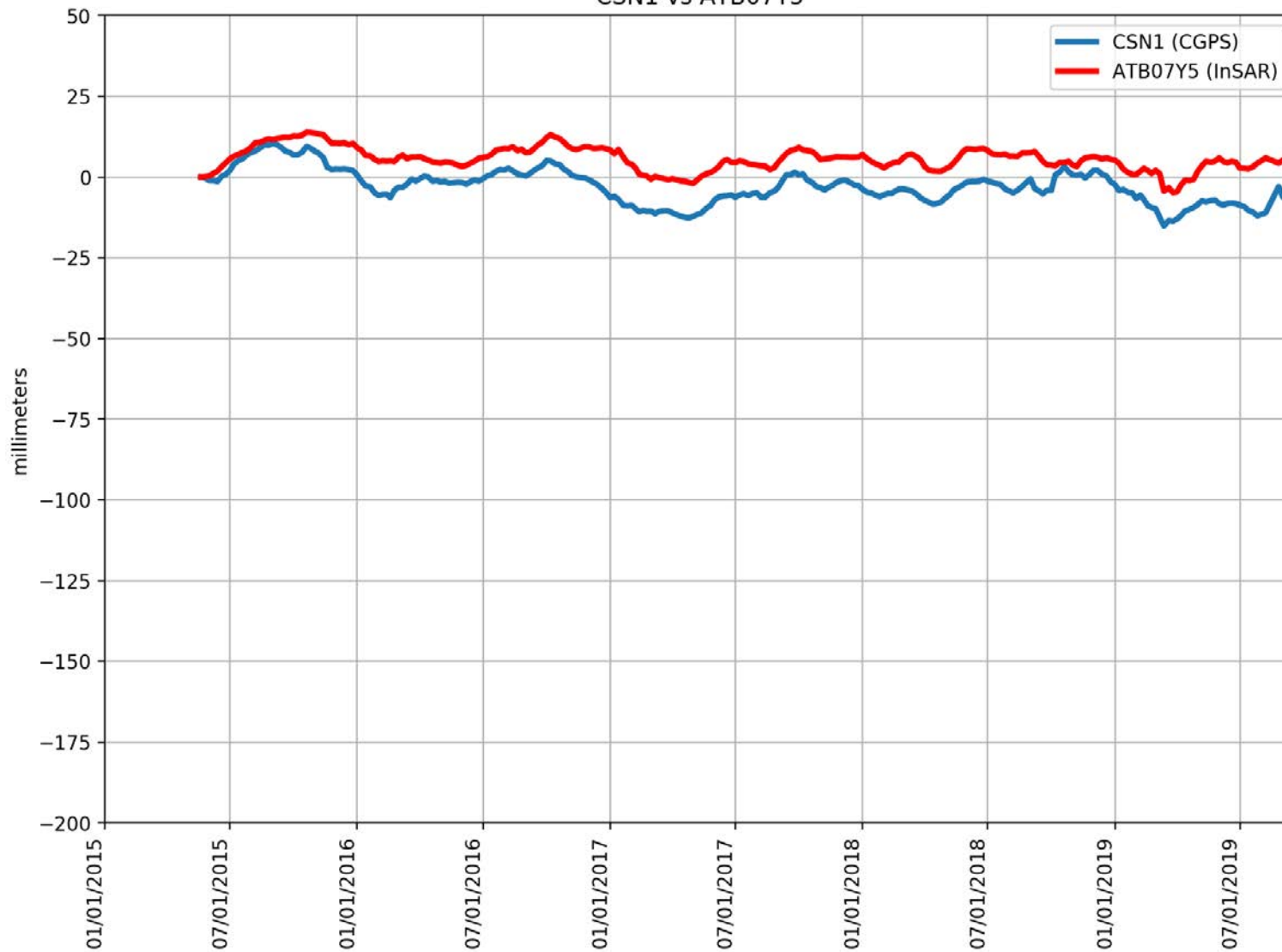
CSDH vs AM3F8DK



RMSE: 4.16 mm
Correlation: 0.83

Appendix B

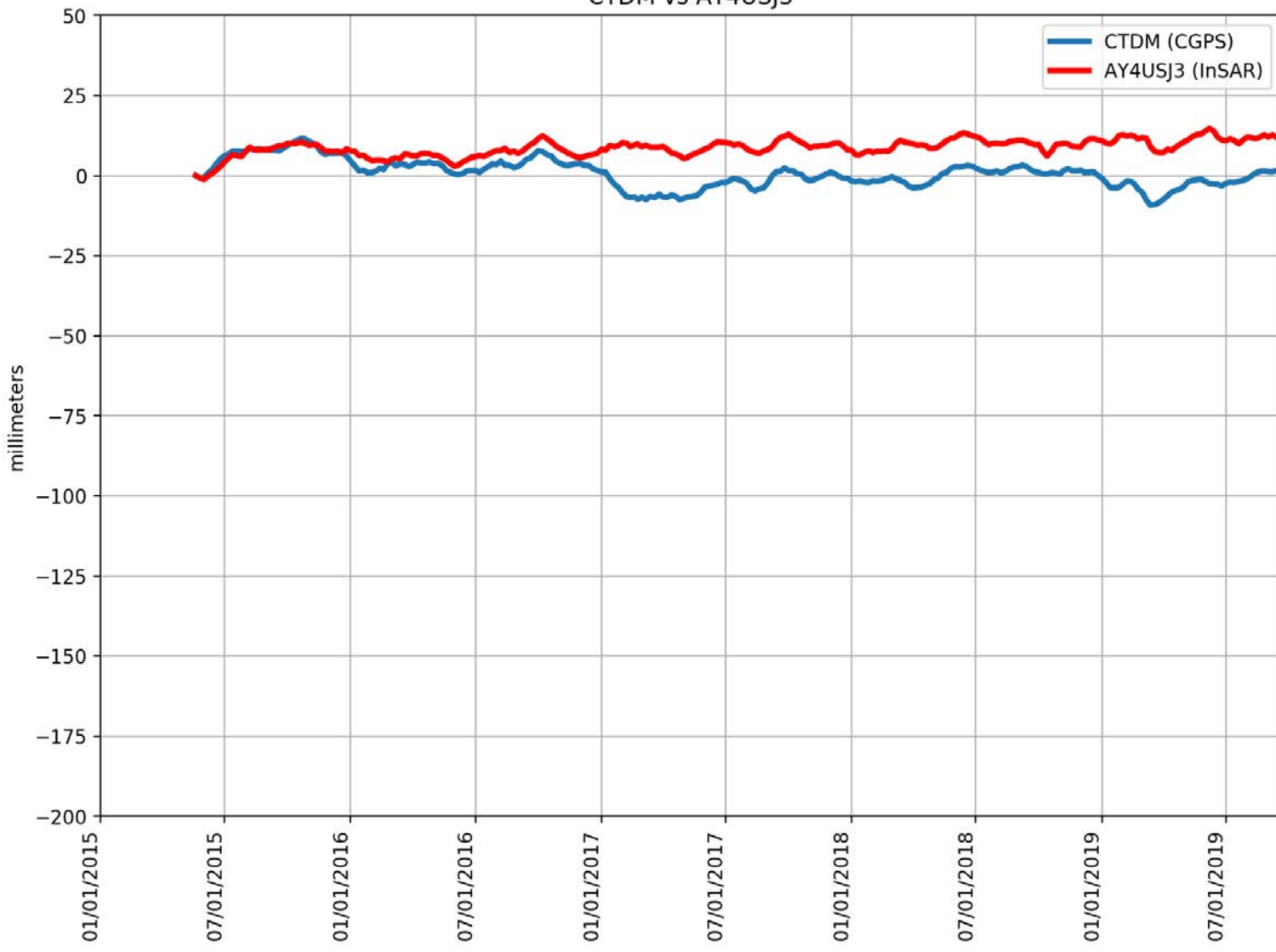
CSN1 vs ATB07Y5



RMSE: 8.97 mm
Correlation: 0.82

Appendix B

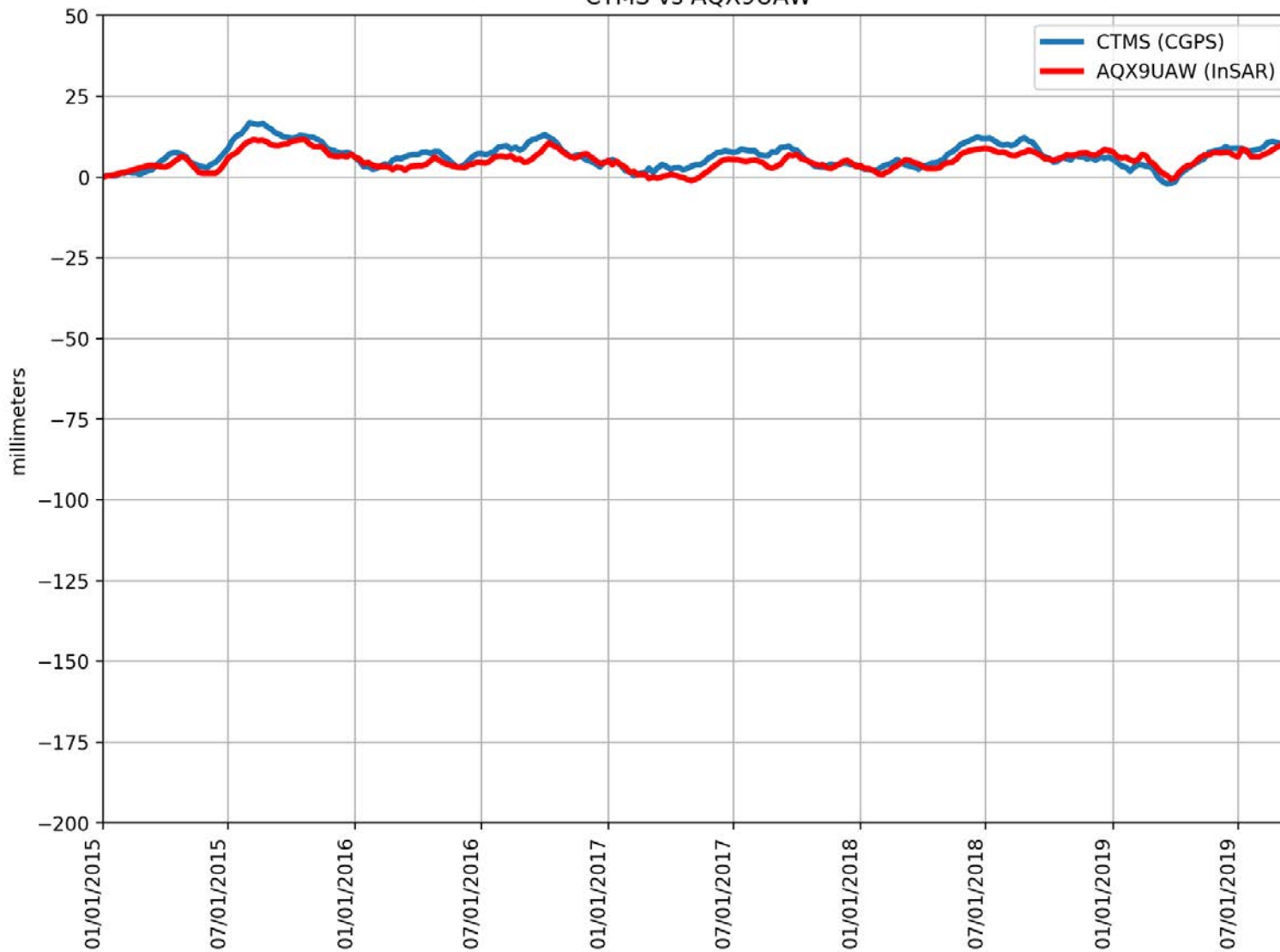
CTDM vs AY4USJ3



RMSE: 9.59 mm
Correlation: -0.09

Appendix B

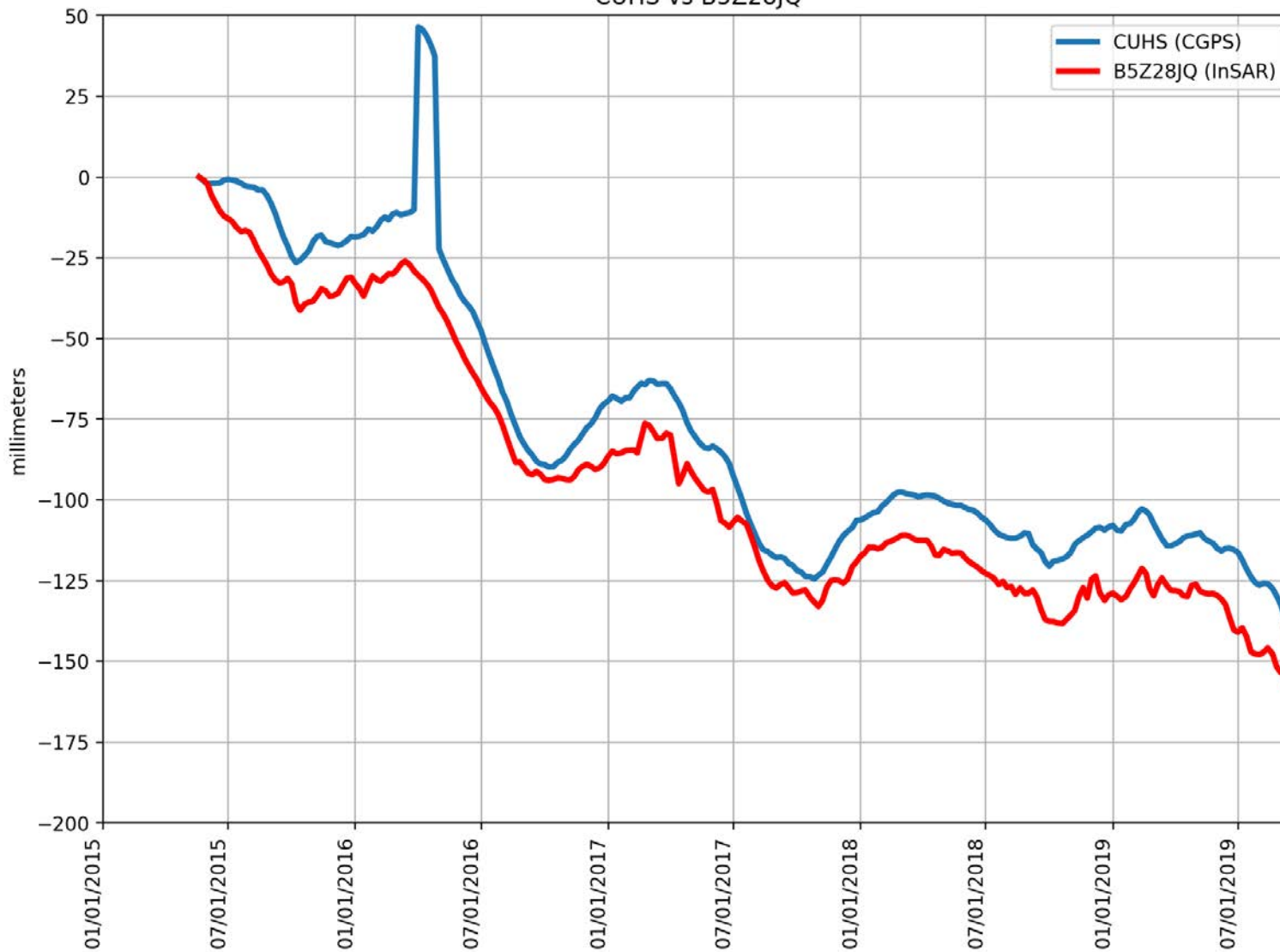
CTMS vs AQX9UAW



RMSE: 2.43 mm
Correlation: 0.84

Appendix B

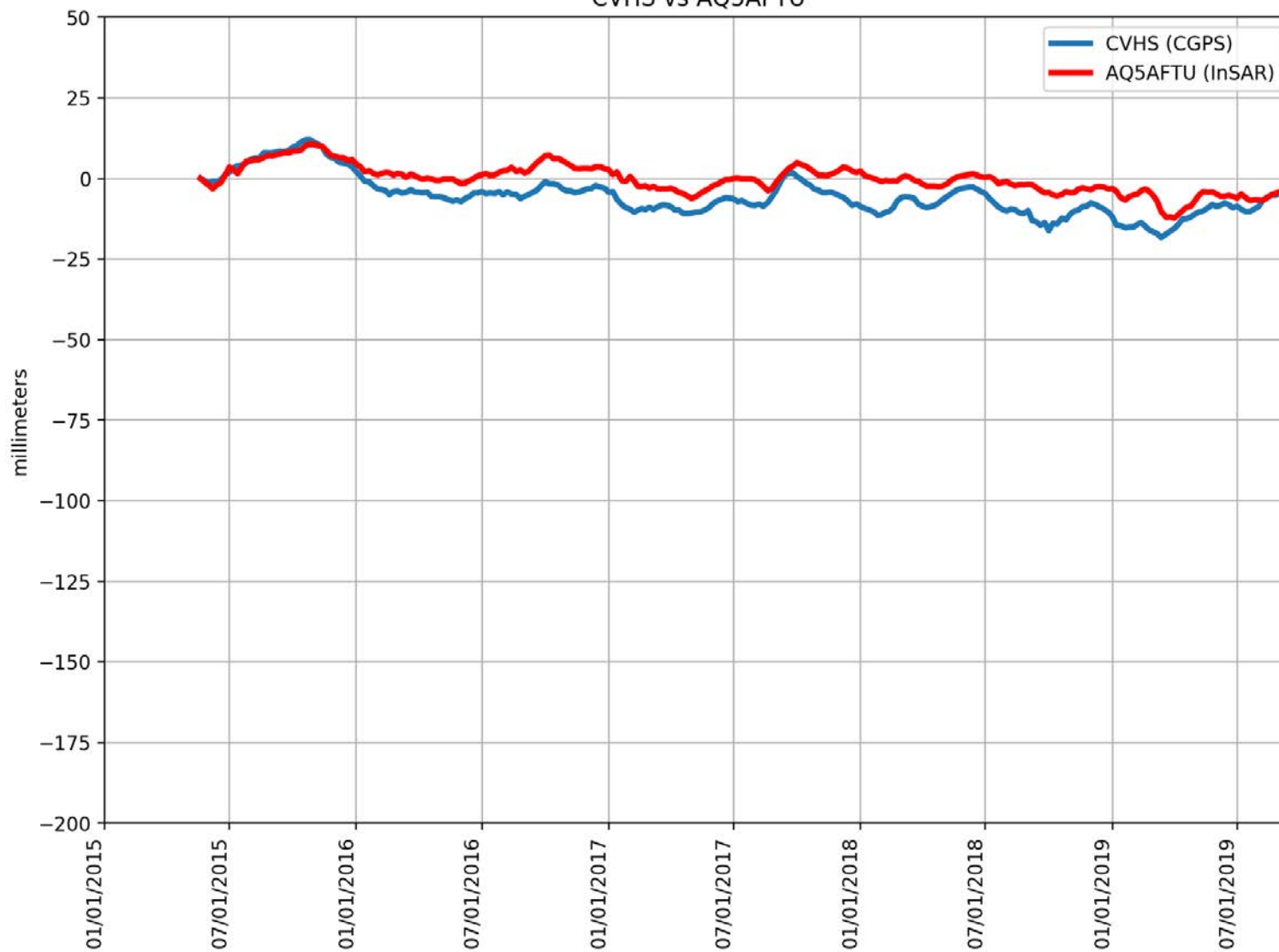
CUHS vs B5Z28JQ



RMSE: 18.56 mm
Correlation: 0.97

Appendix B

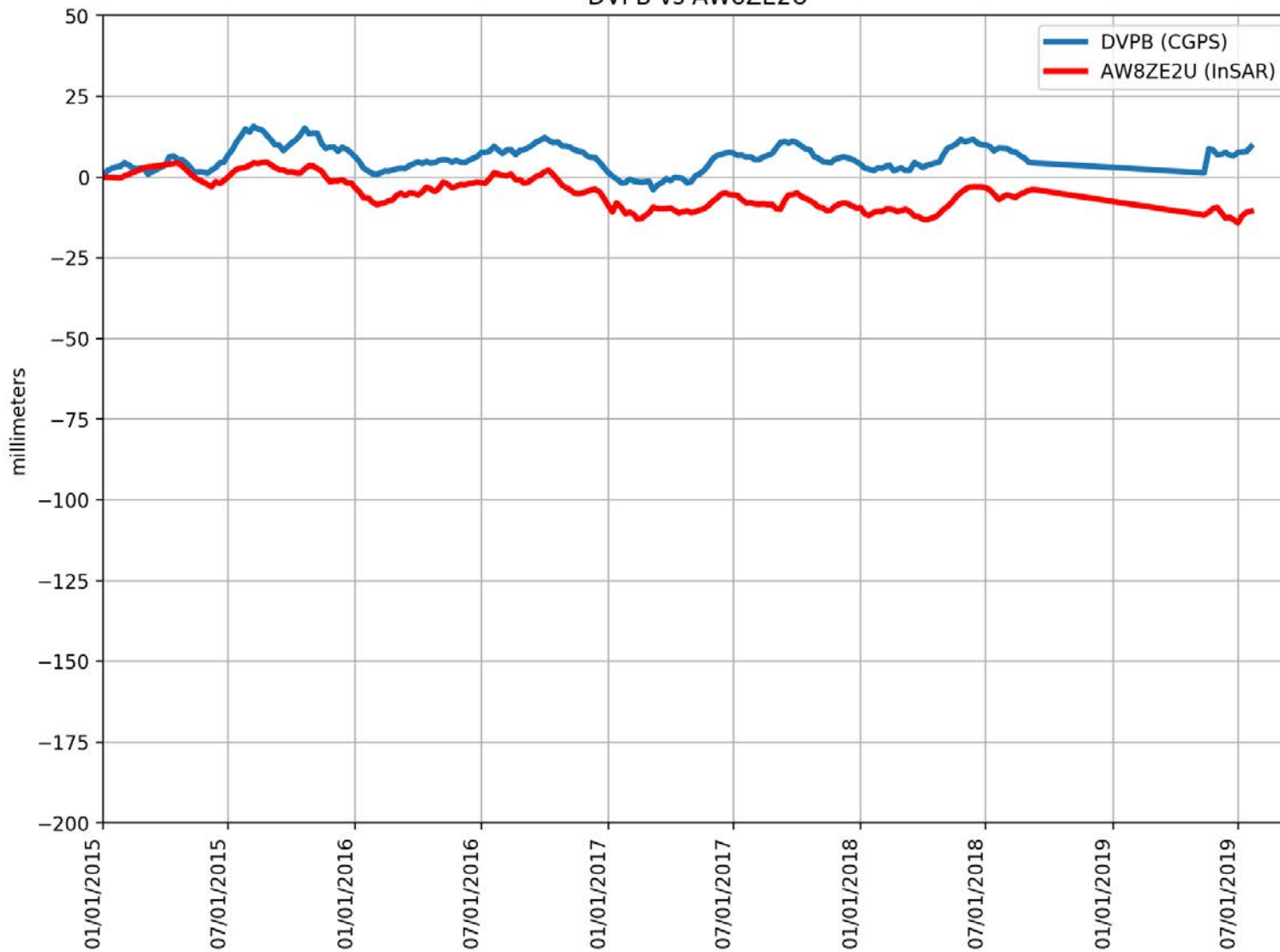
CVHS vs AQ5AFTU



RMSE: 6.15 mm
Correlation: 0.85

Appendix B

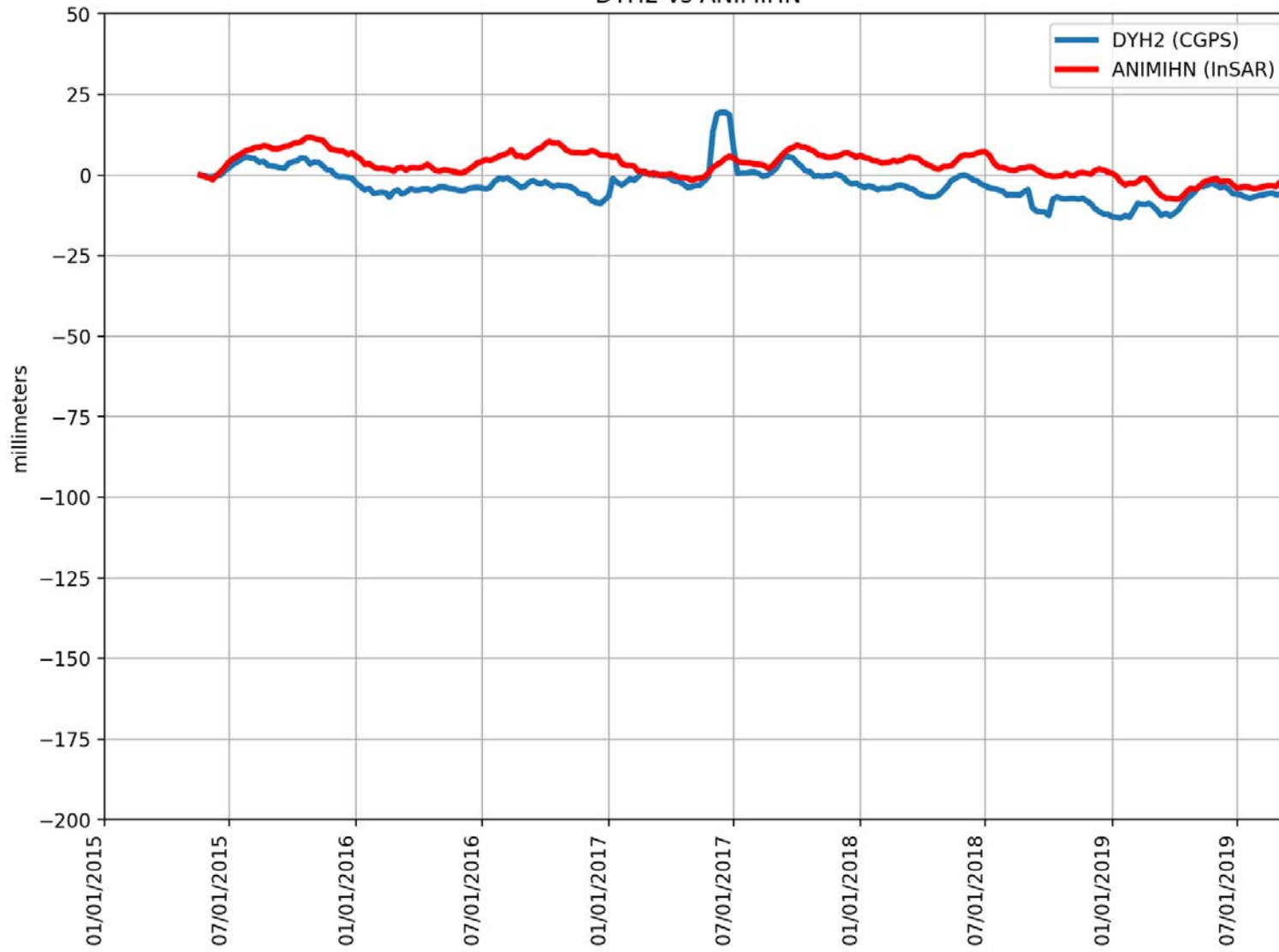
DVPB vs AW8ZE2U



RMSE: 11.56 mm
Correlation: 0.48

Appendix B

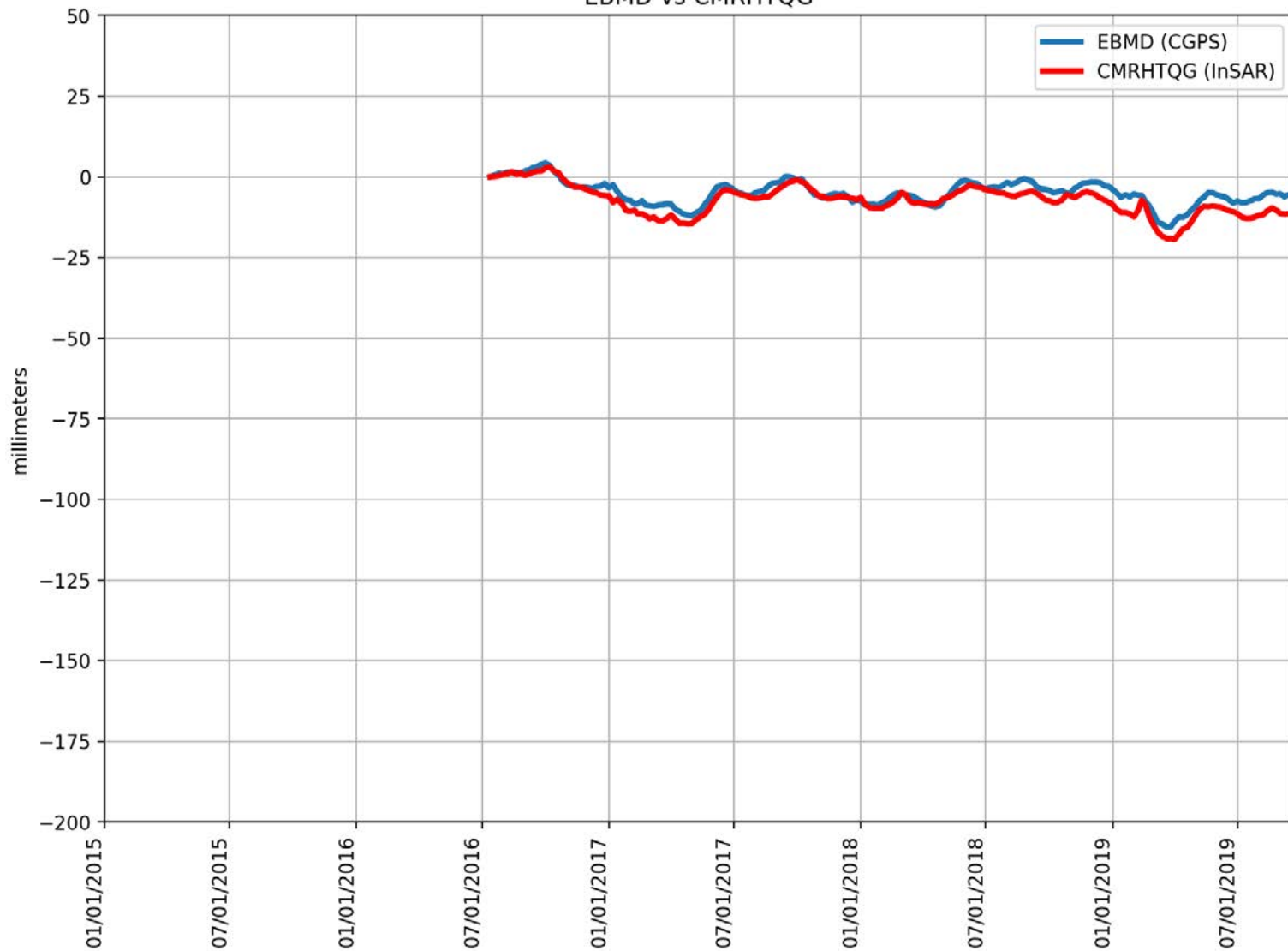
DYH2 vs ANIMIHN



RMSE: 7.46 mm
Correlation: 0.55

Appendix B

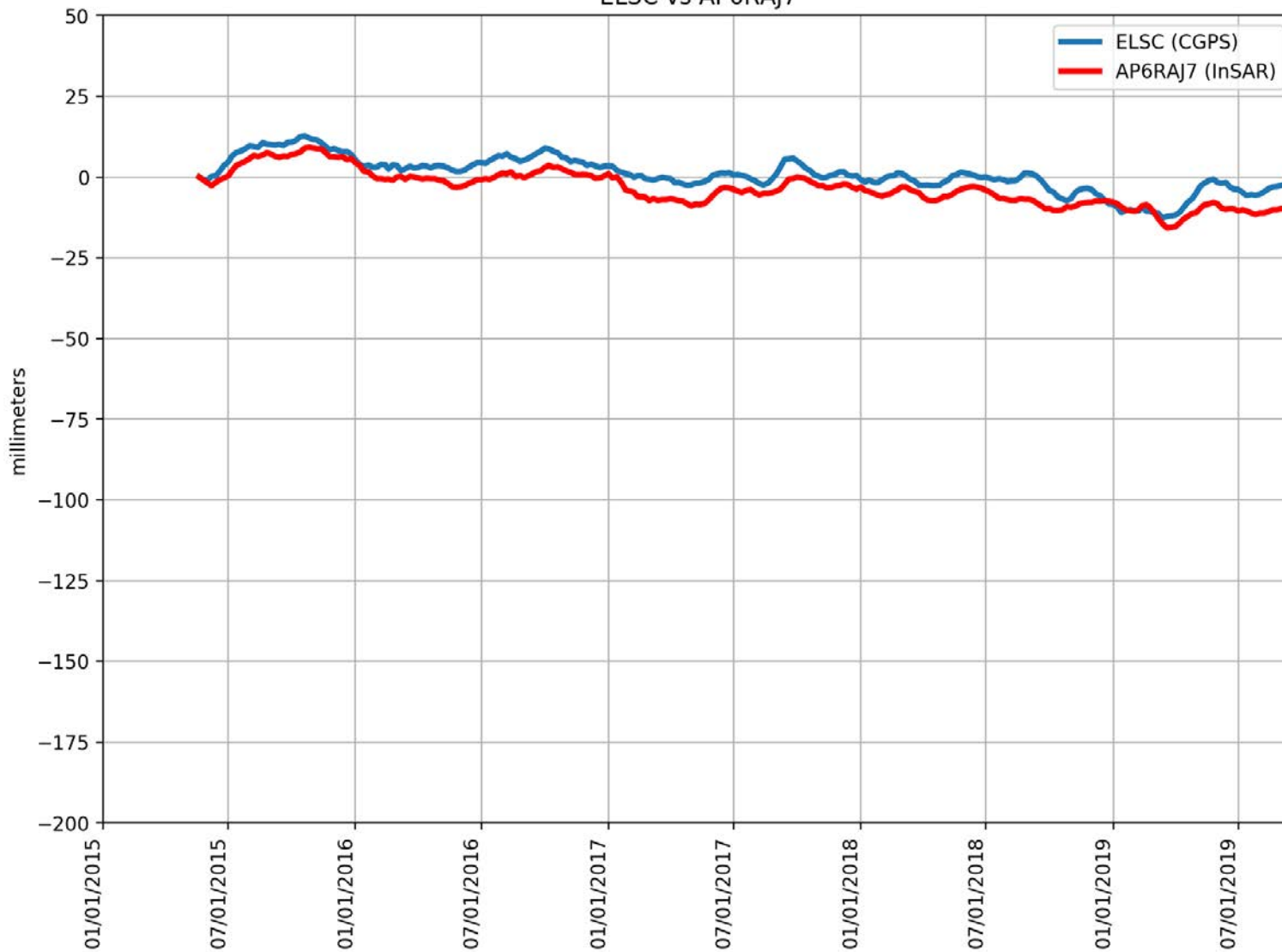
EBMD vs CMRHTQG



RMSE: 2.96 mm
Correlation: 0.92

Appendix B

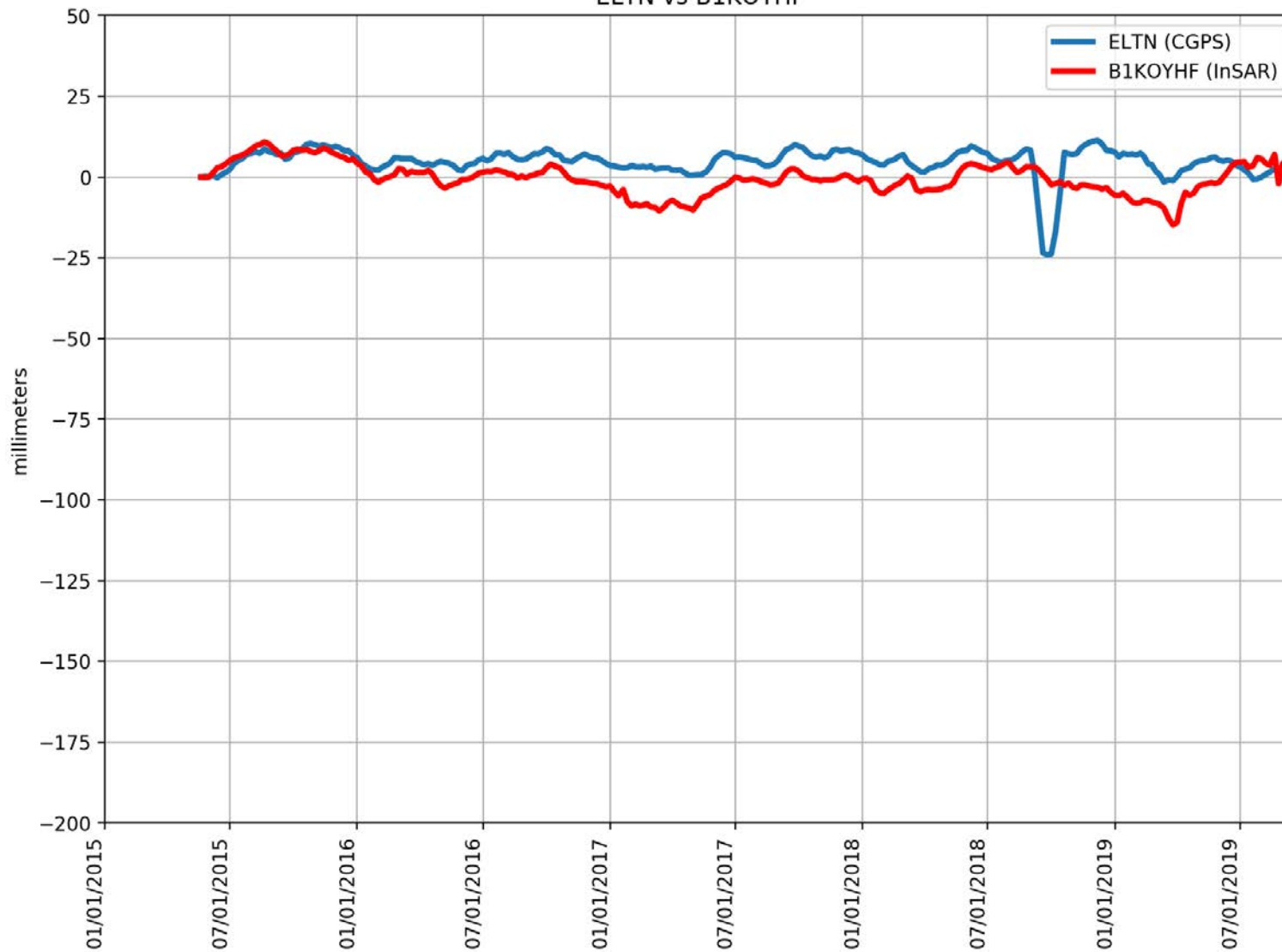
ELSC vs AP6RAJ7



RMSE: 4.66 mm
Correlation: 0.93

Appendix B

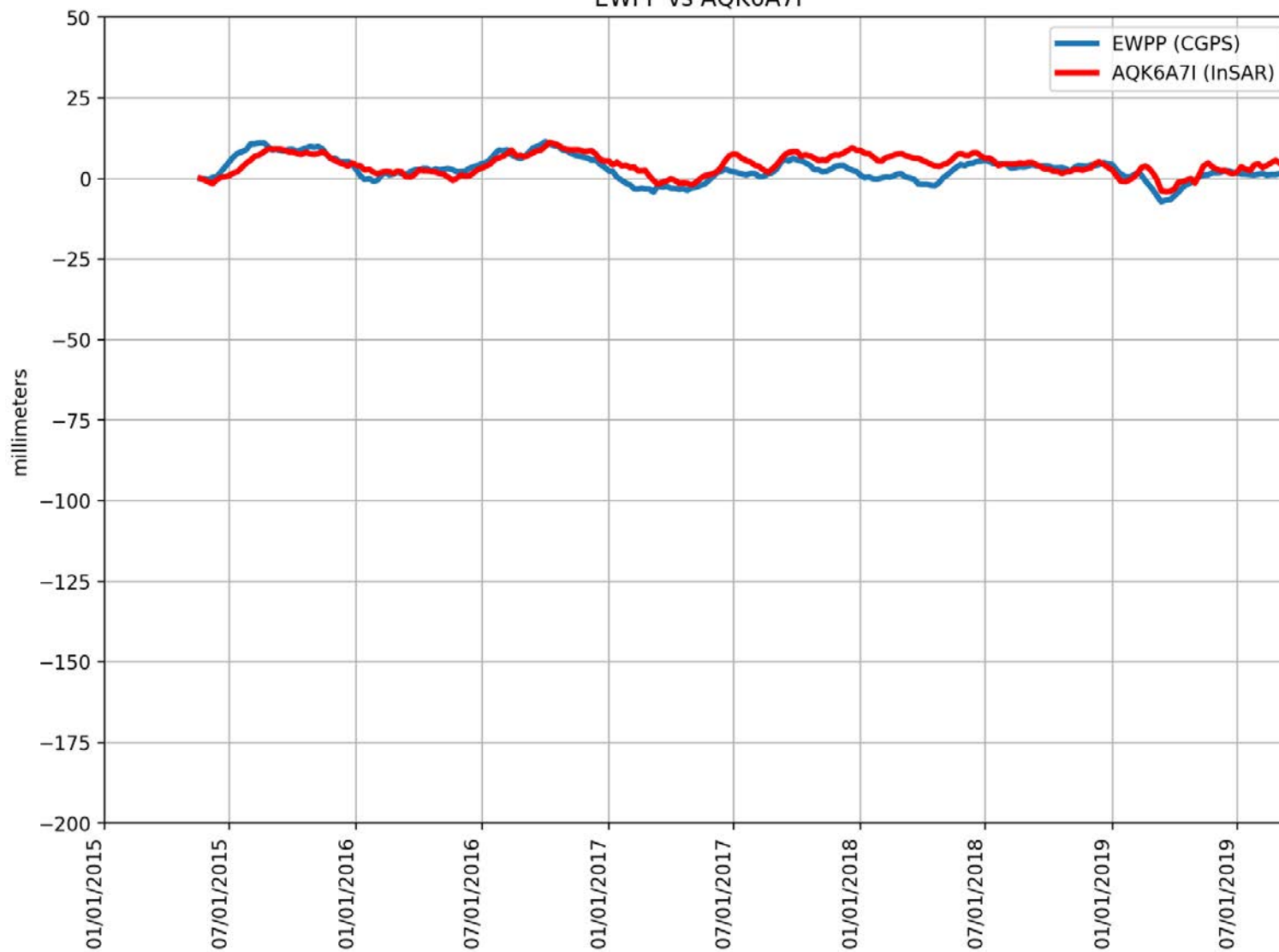
ELTN vs B1KOYHF



RMSE: 7.65 mm
Correlation: 0.25

Appendix B

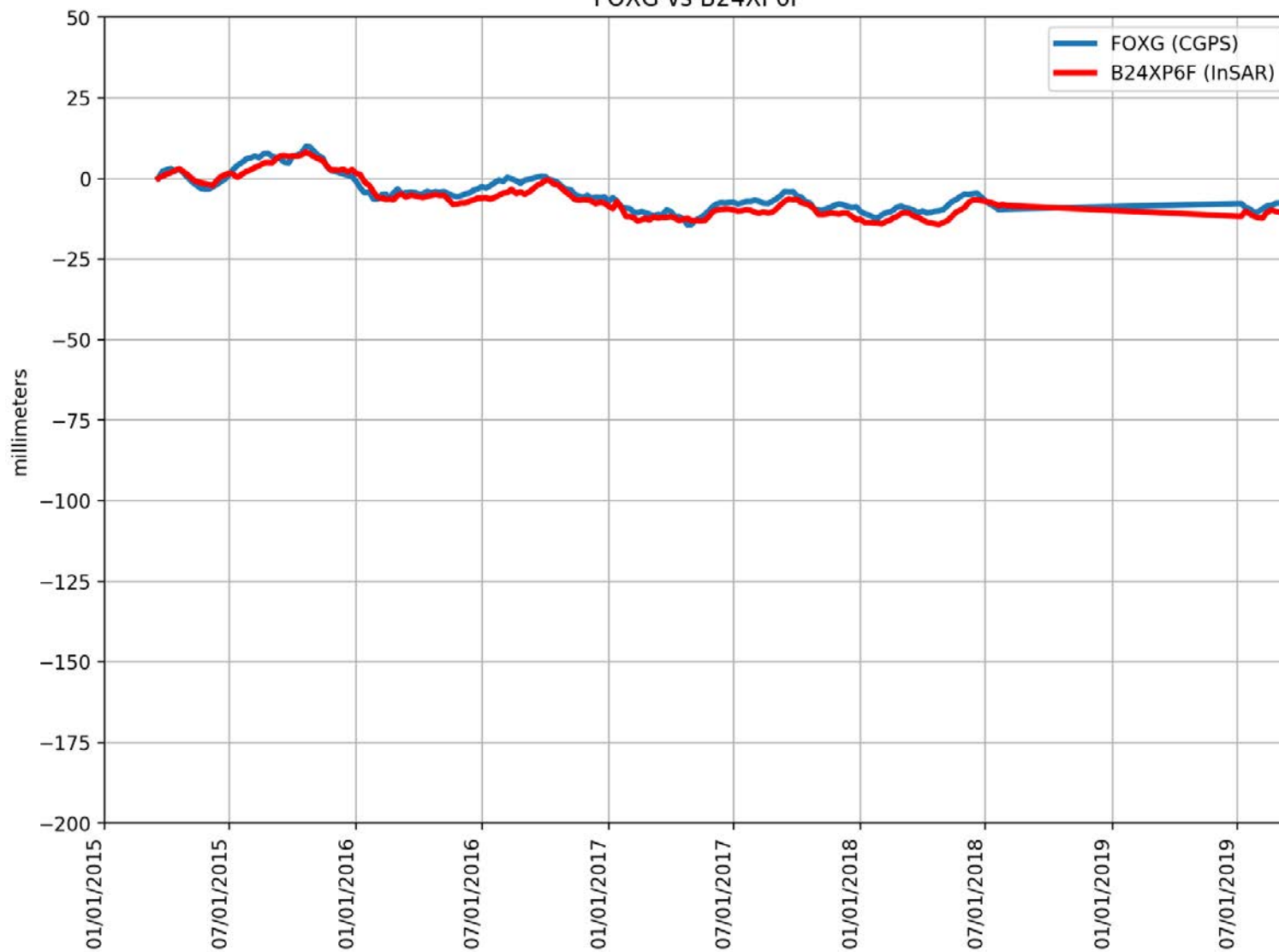
EWPP vs AQK6A7I



RMSE: 3.06 mm
Correlation: 0.70

Appendix B

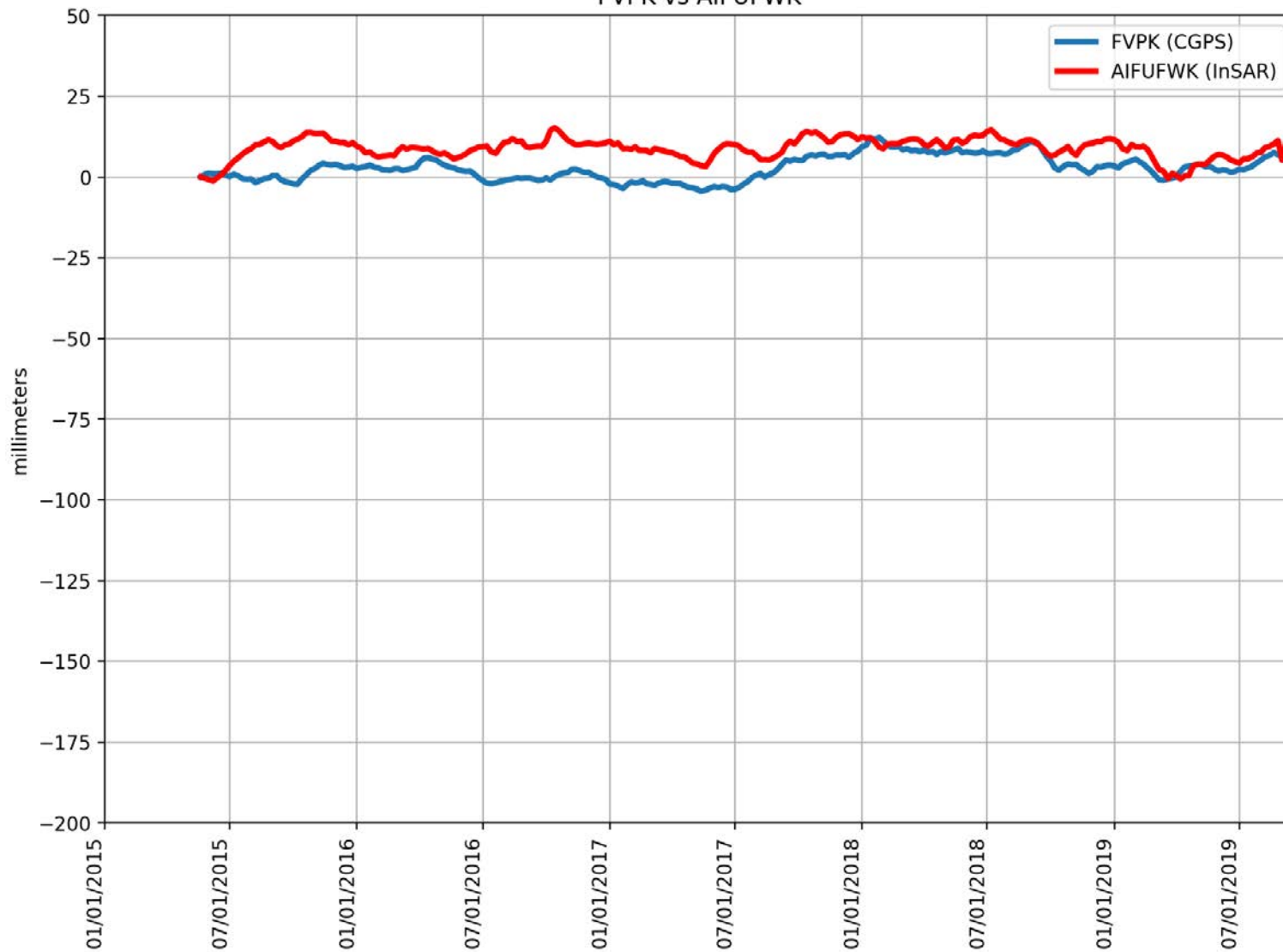
FOXG vs B24XP6F



RMSE: 2.30 mm
Correlation: 0.96

Appendix B

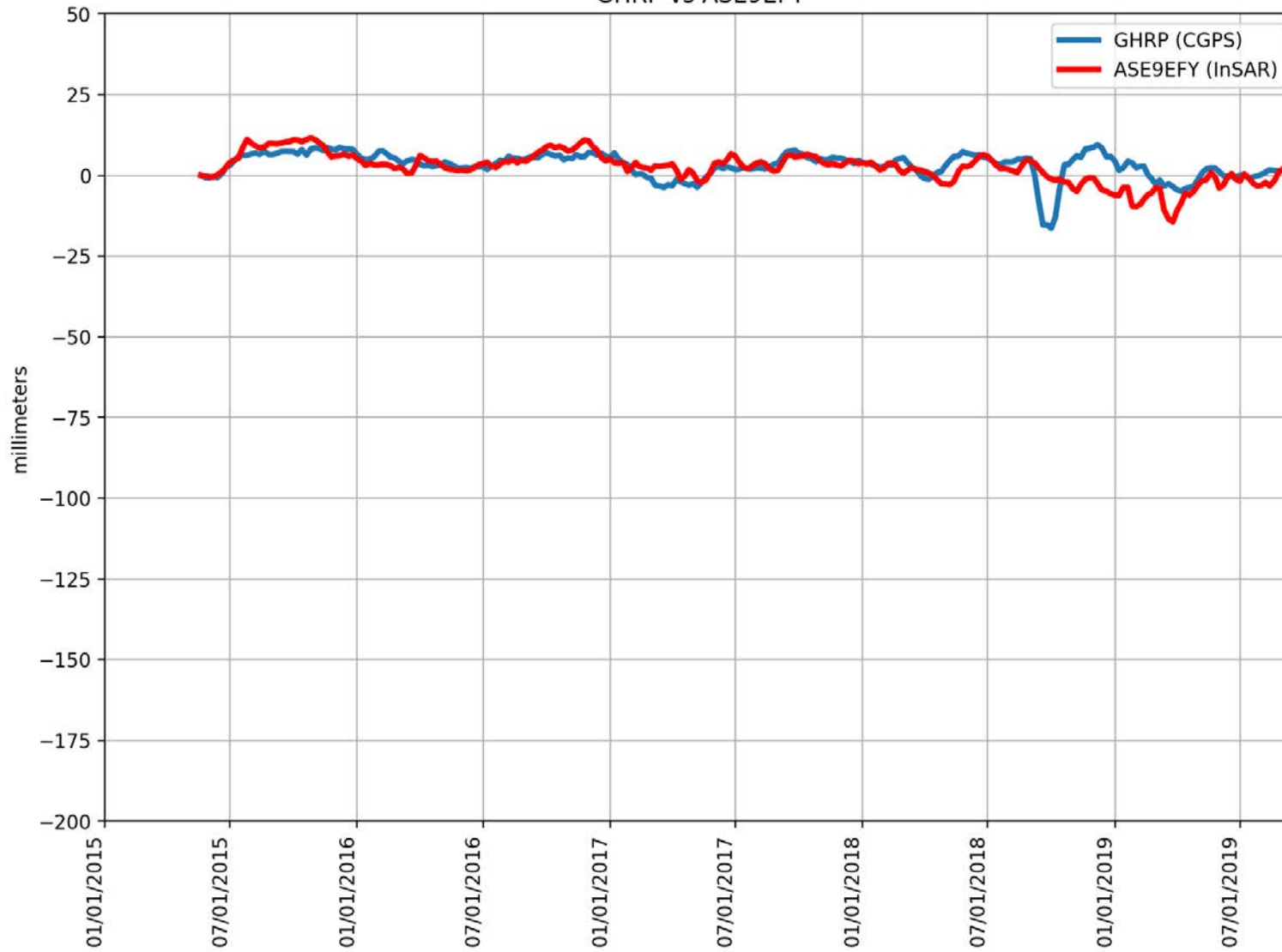
FVPK vs AIFUFWK



RMSE: 7.25 mm
Correlation: 0.36

Appendix B

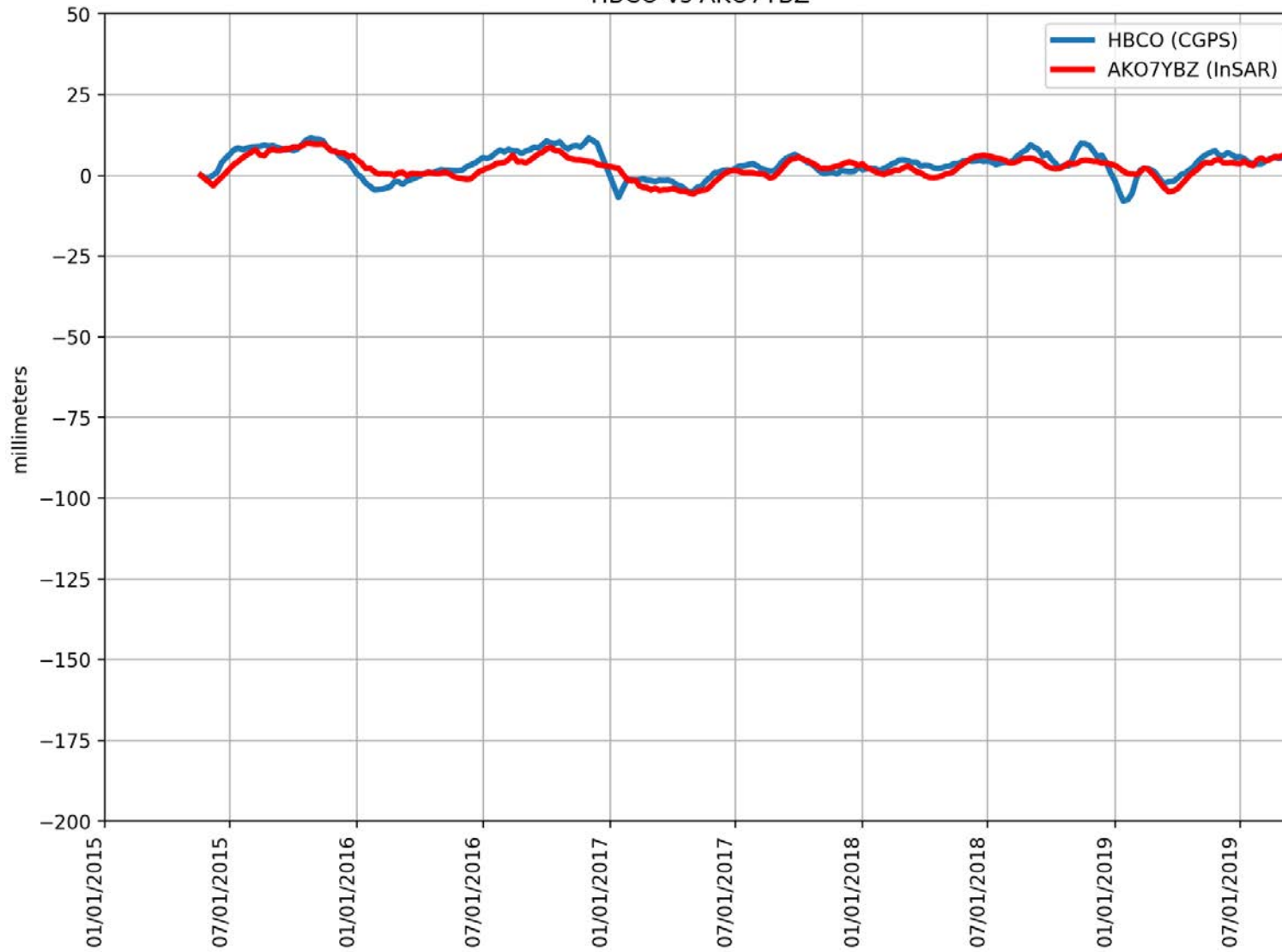
GHRP vs ASE9EFY



RMSE: 4.29 mm
Correlation: 0.52

Appendix B

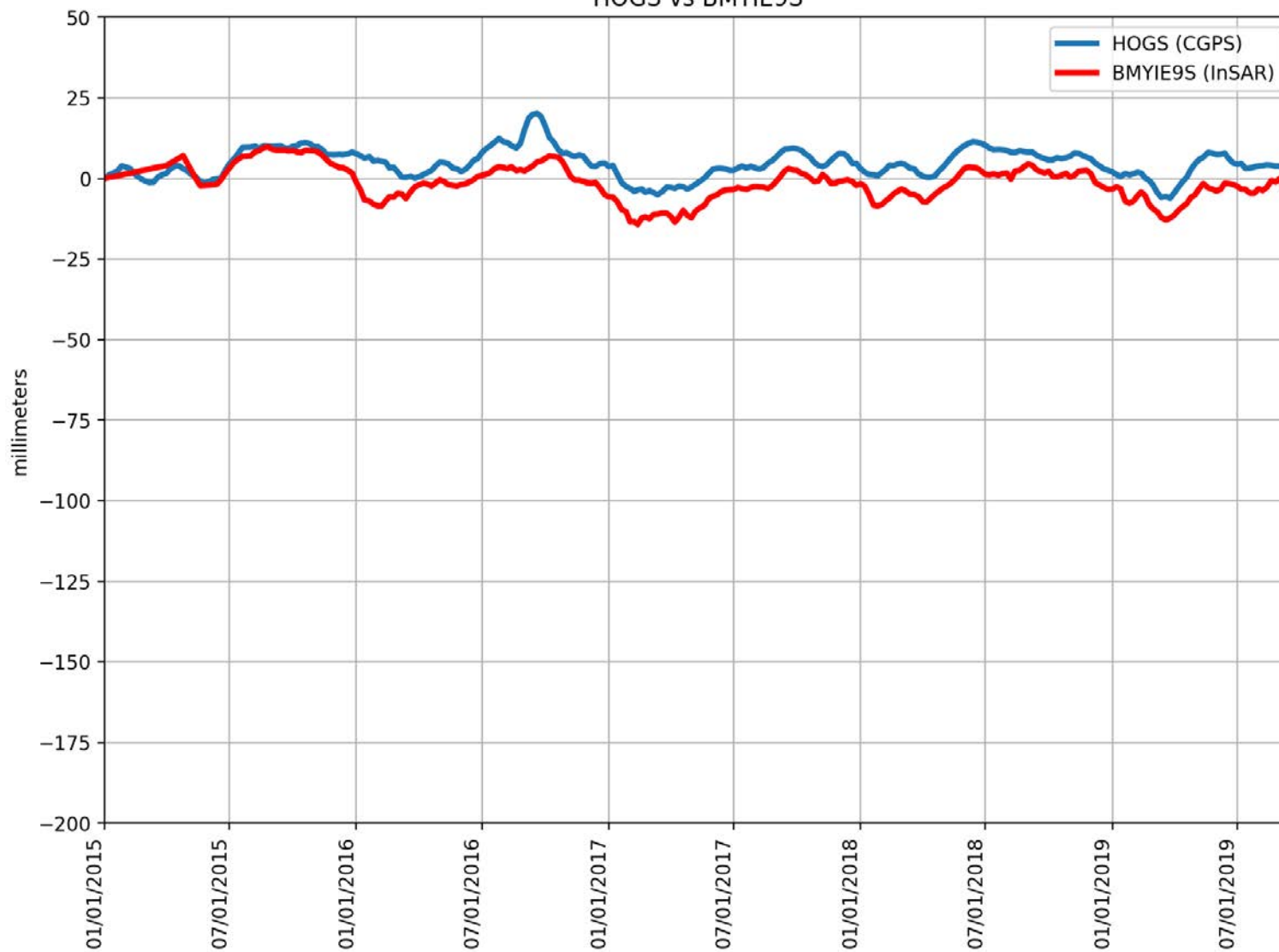
HBCO vs AKO7YBZ



RMSE: 2.75 mm
Correlation: 0.78

Appendix B

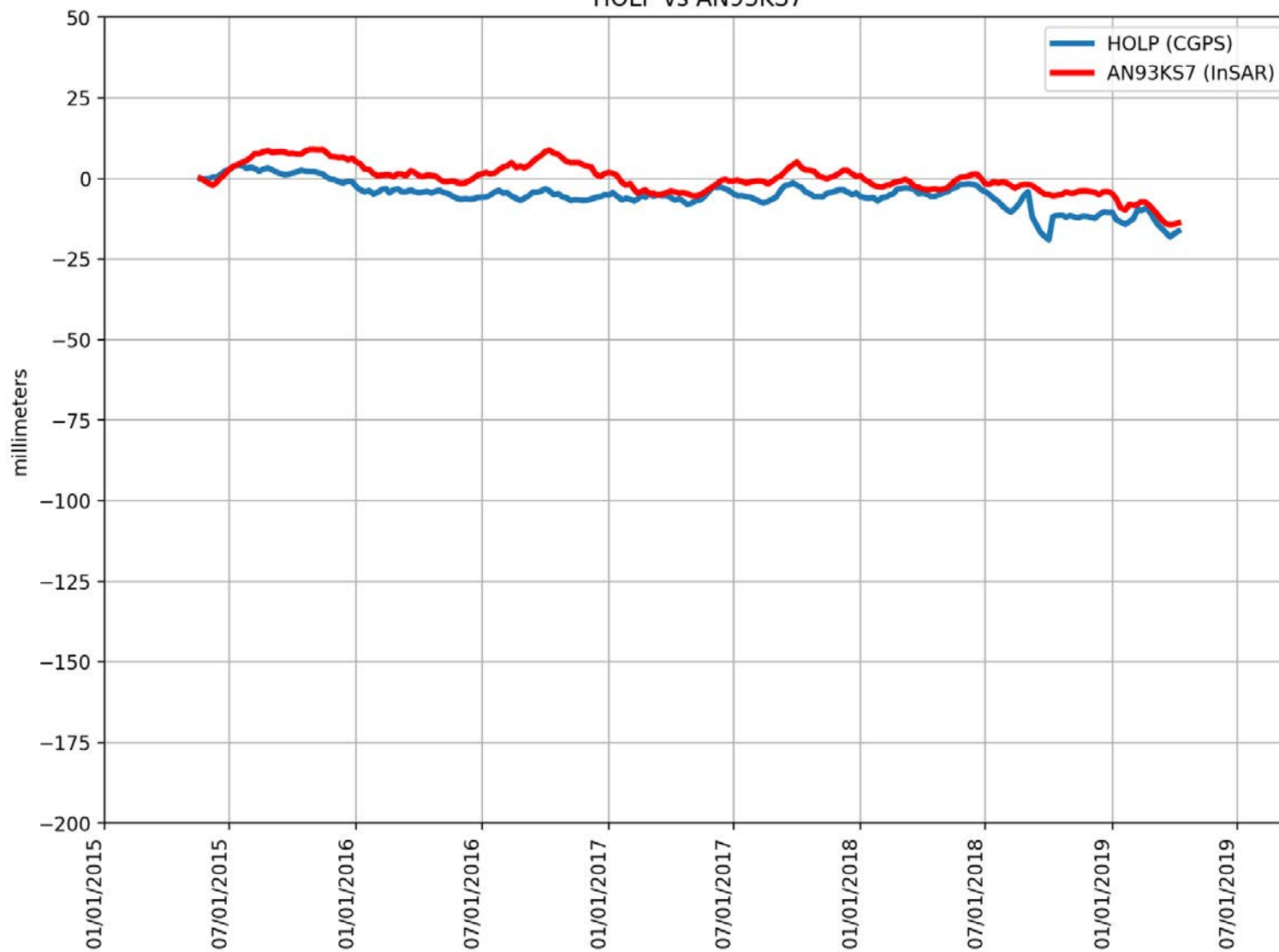
HOGS vs BMYIE9S



RMSE: 6.89 mm
Correlation: 0.75

Appendix B

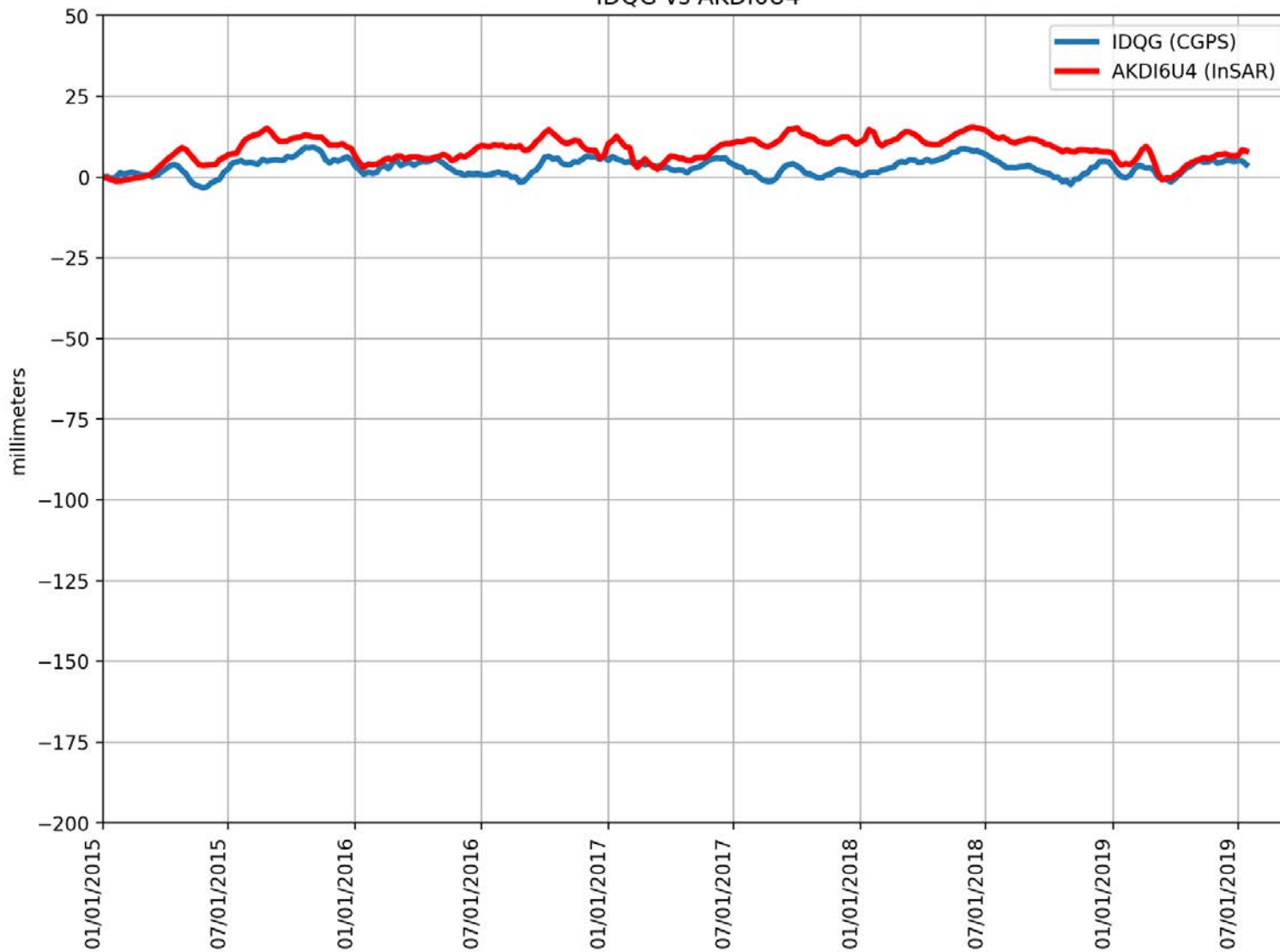
HOLP vs AN93KS7



RMSE: 6.03 mm
Correlation: 0.77

Appendix B

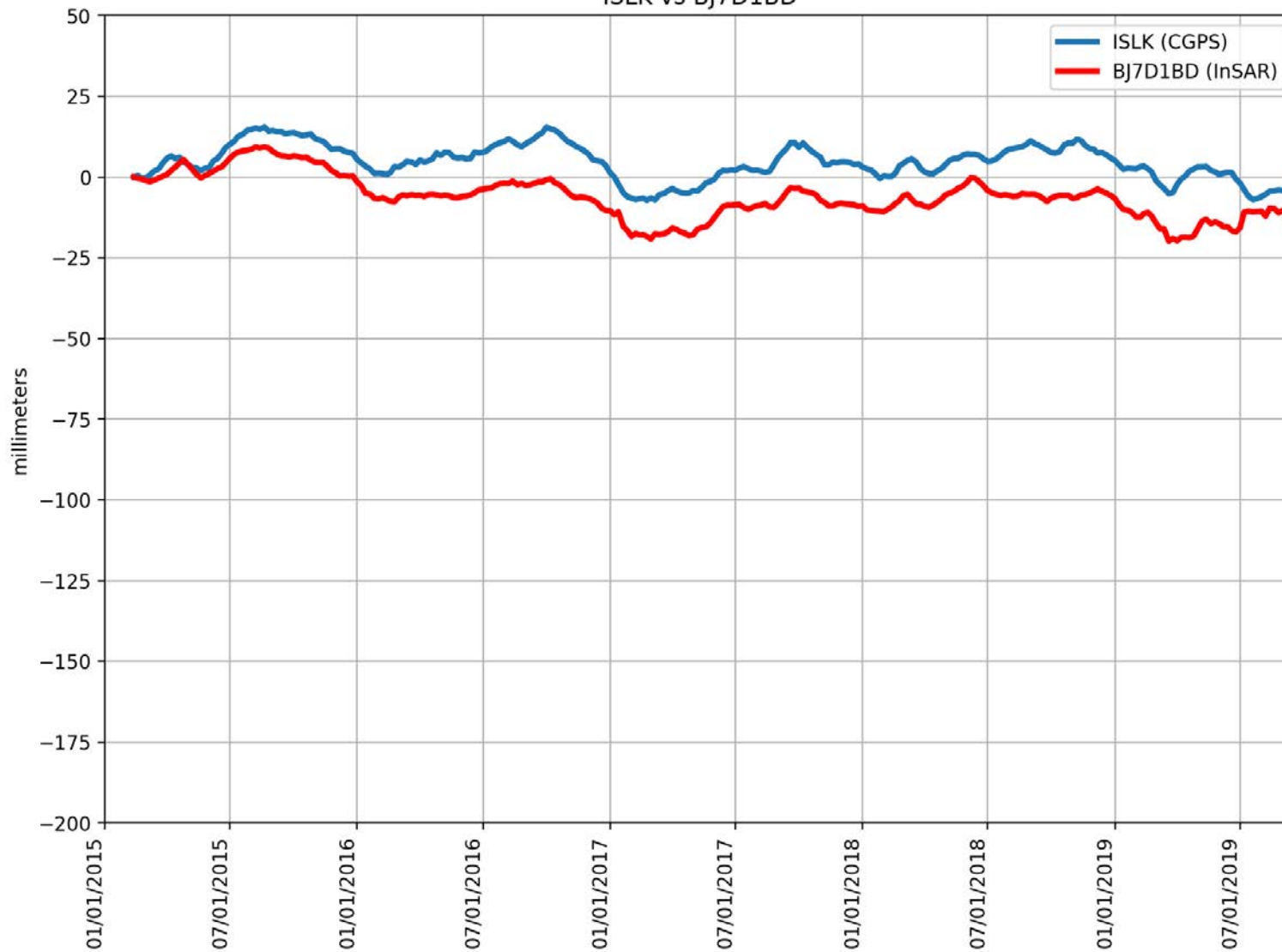
IDQG vs AKDI6U4



RMSE: 6.39 mm
Correlation: 0.46

Appendix B

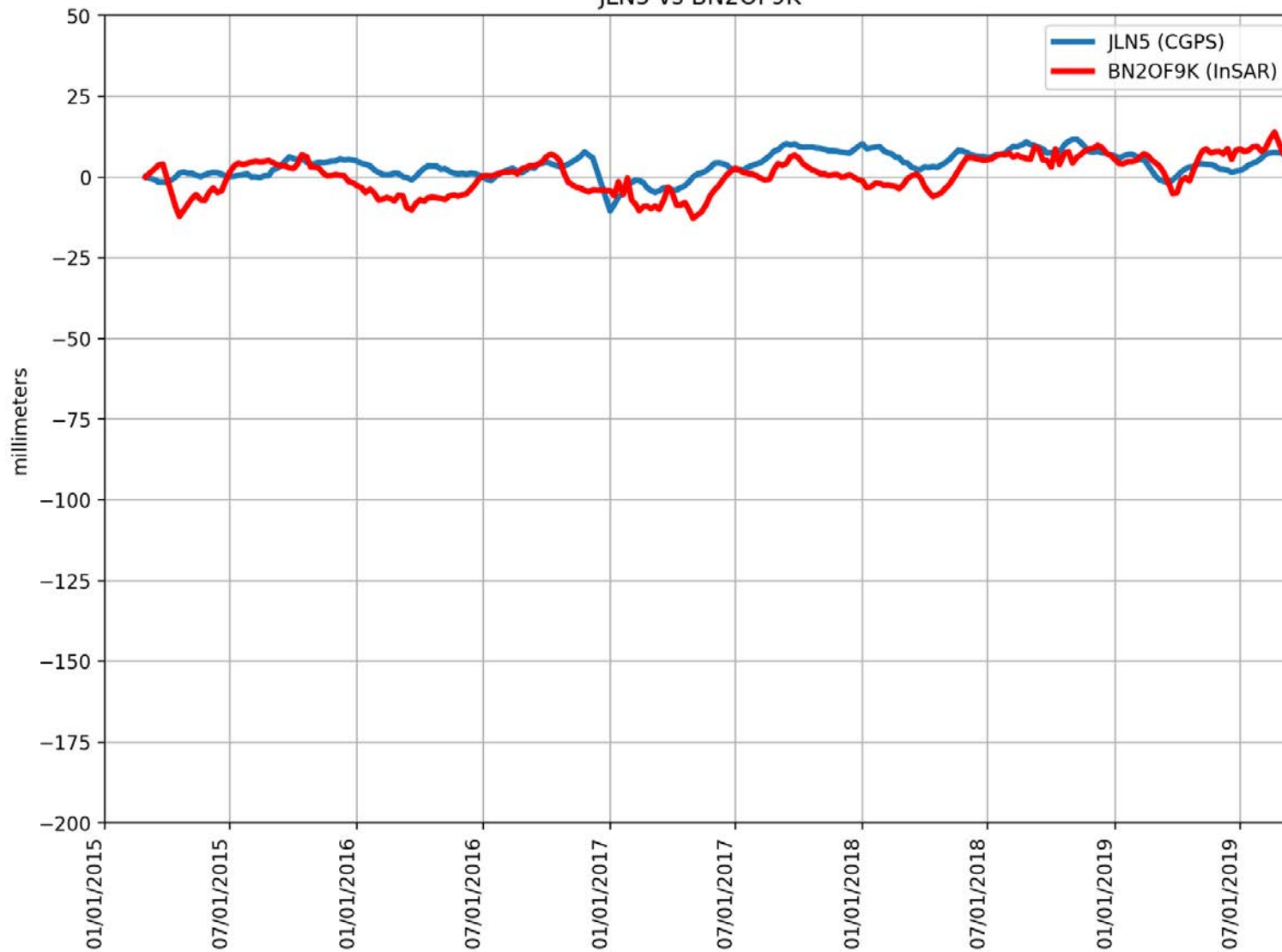
ISLK vs BJ7D1BD



RMSE: 11.59 mm
Correlation: 0.79

Appendix B

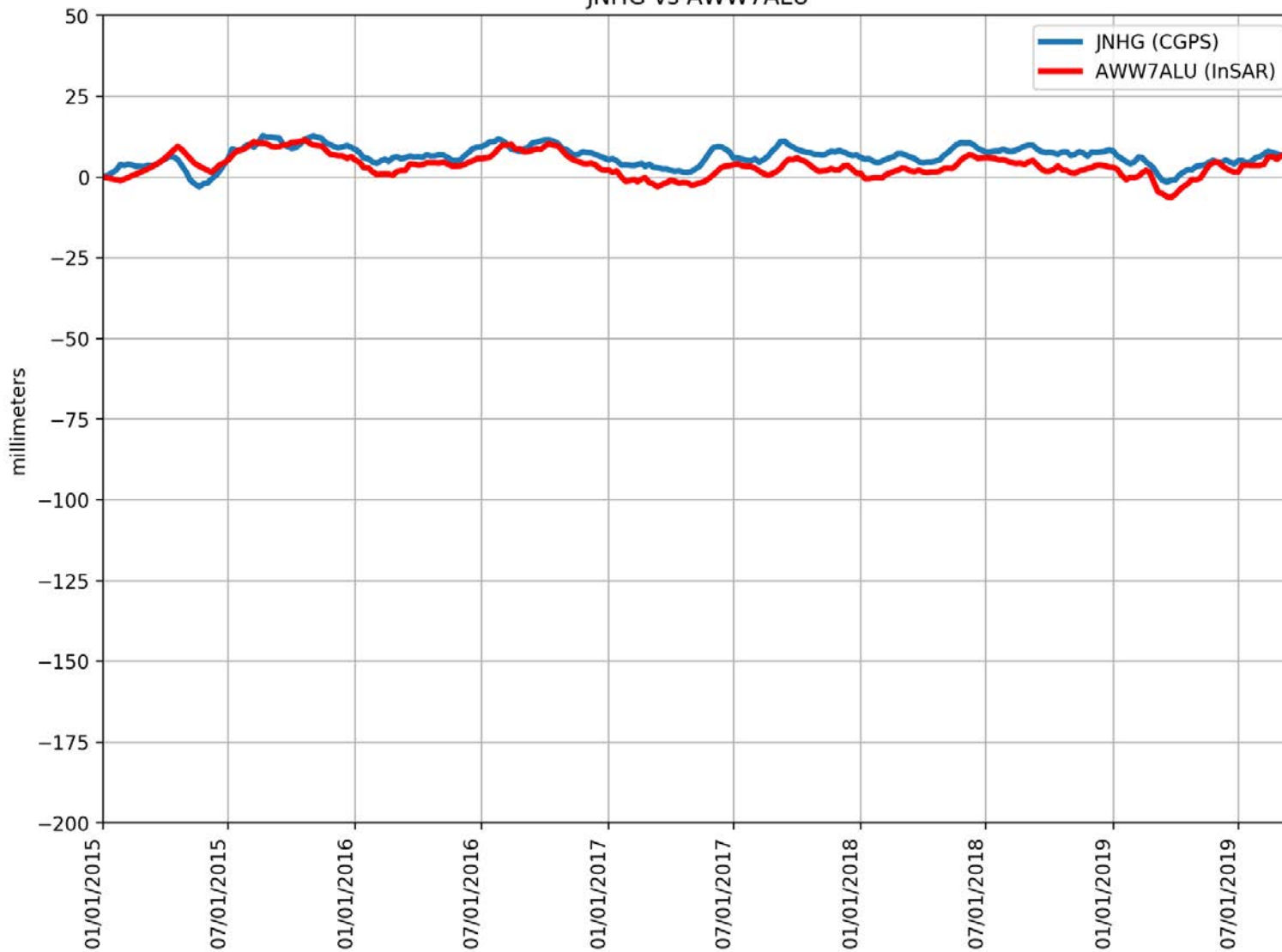
JLN5 vs BN2OF9K



RMSE: 5.77 mm
Correlation: 0.52

Appendix B

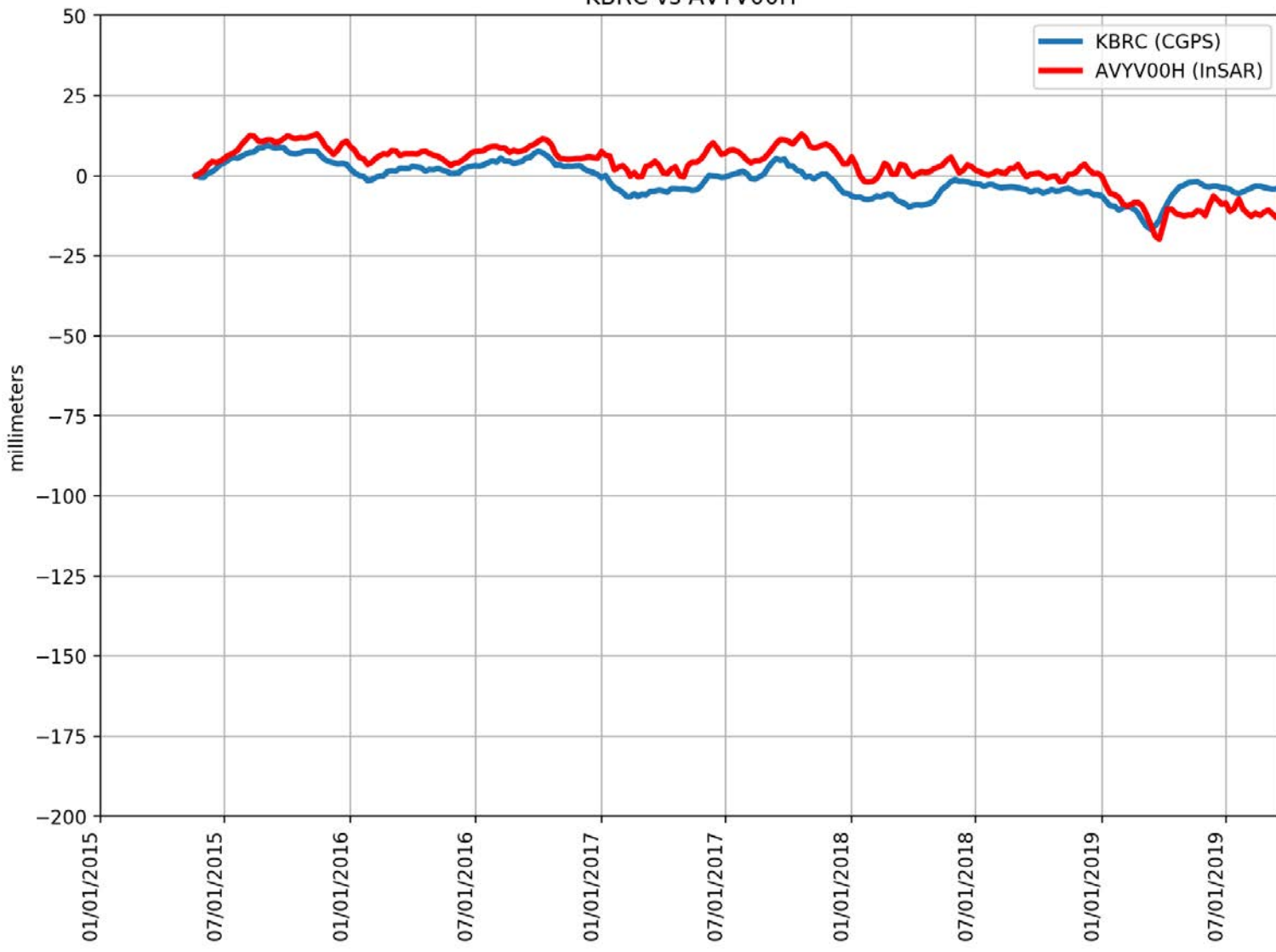
JNHG vs AWW7ALU



RMSE: 3.82 mm
Correlation: 0.74

Appendix B

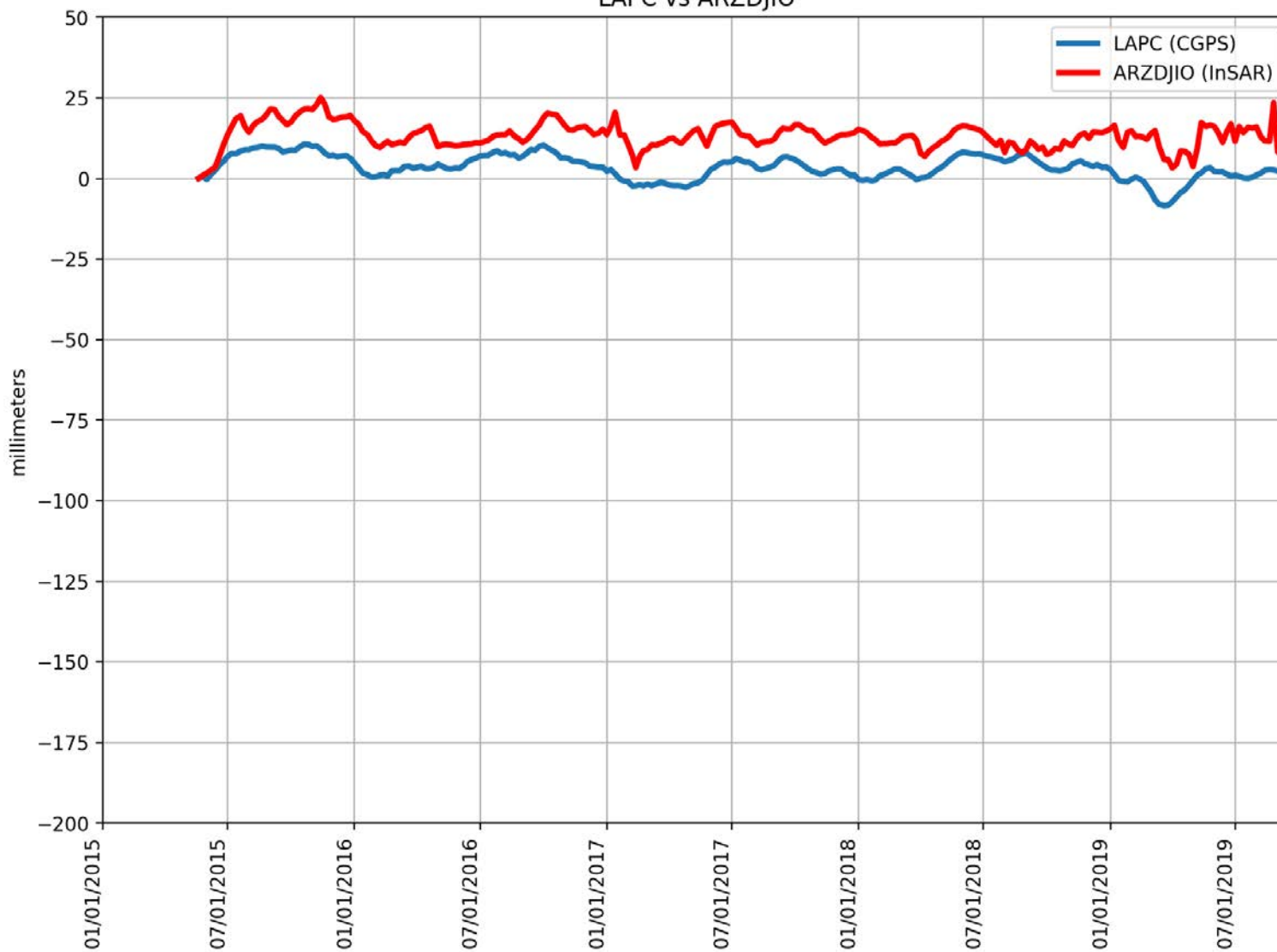
KBRC vs AVYV00H



RMSE: 6.14 mm
Correlation: 0.75

Appendix B

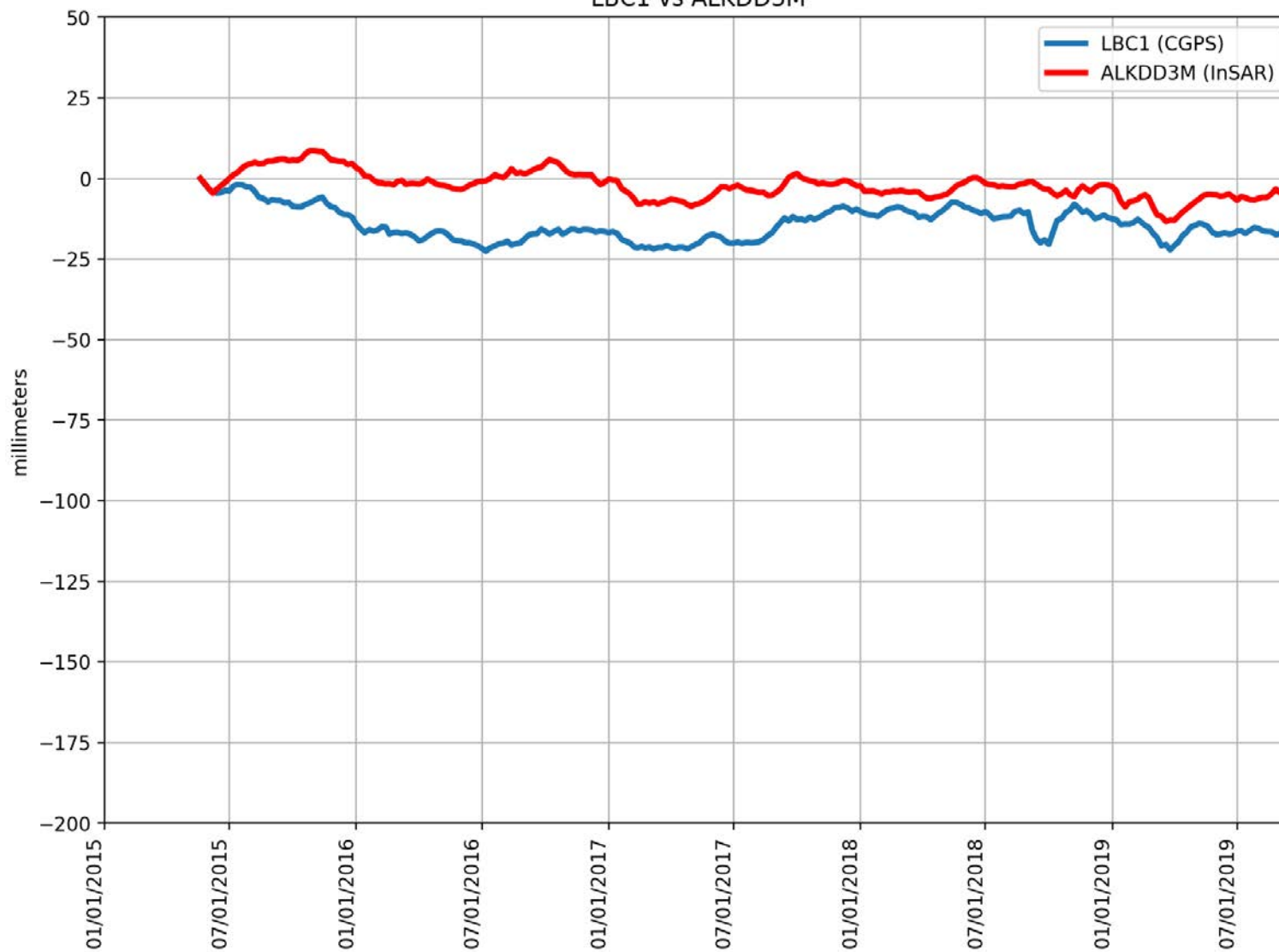
LAPC vs ARZDJIO



RMSE: 10.49 mm
Correlation: 0.55

Appendix B

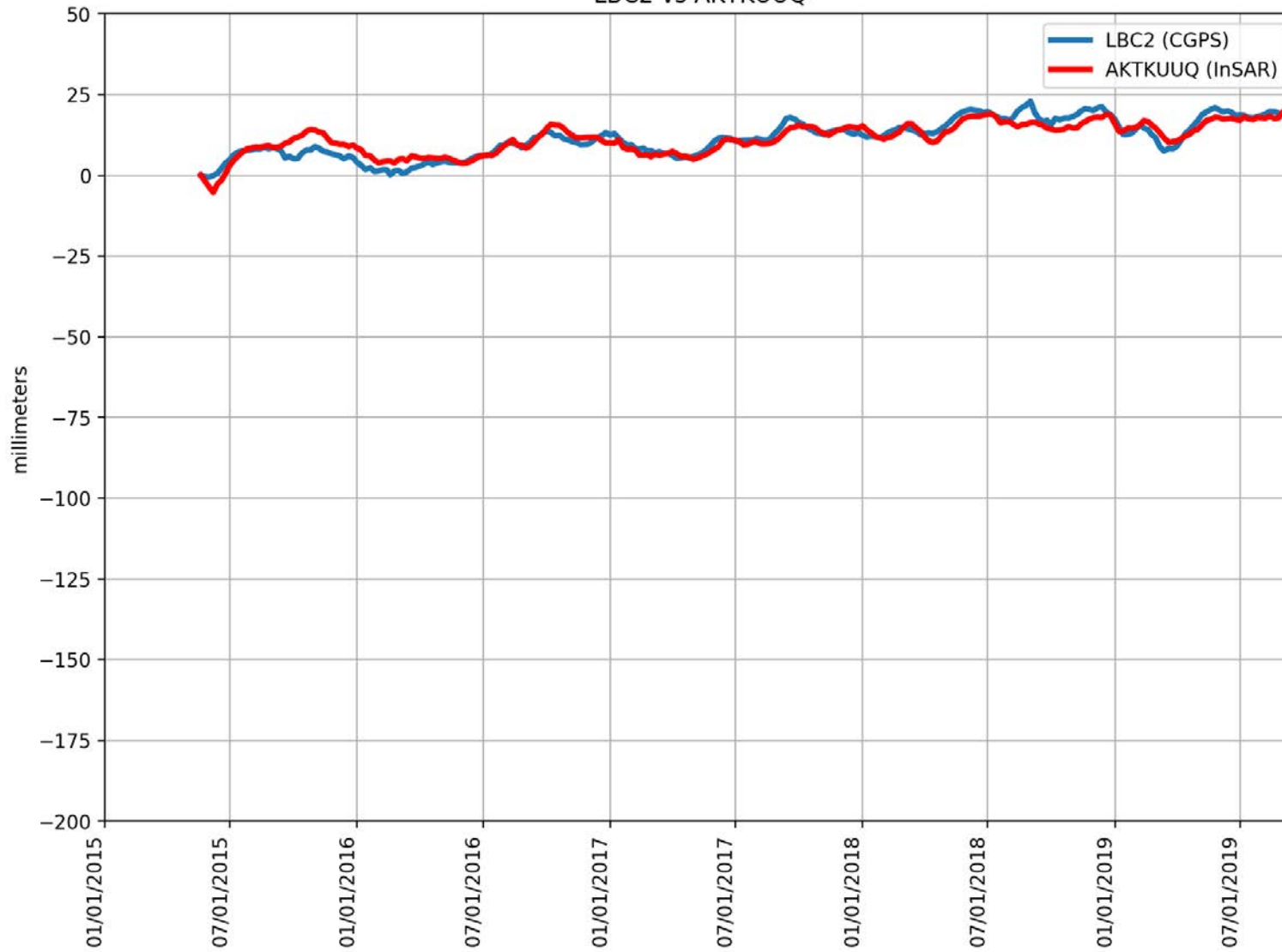
LBC1 vs ALKDD3M



RMSE: 13.02 mm
Correlation: 0.43

Appendix B

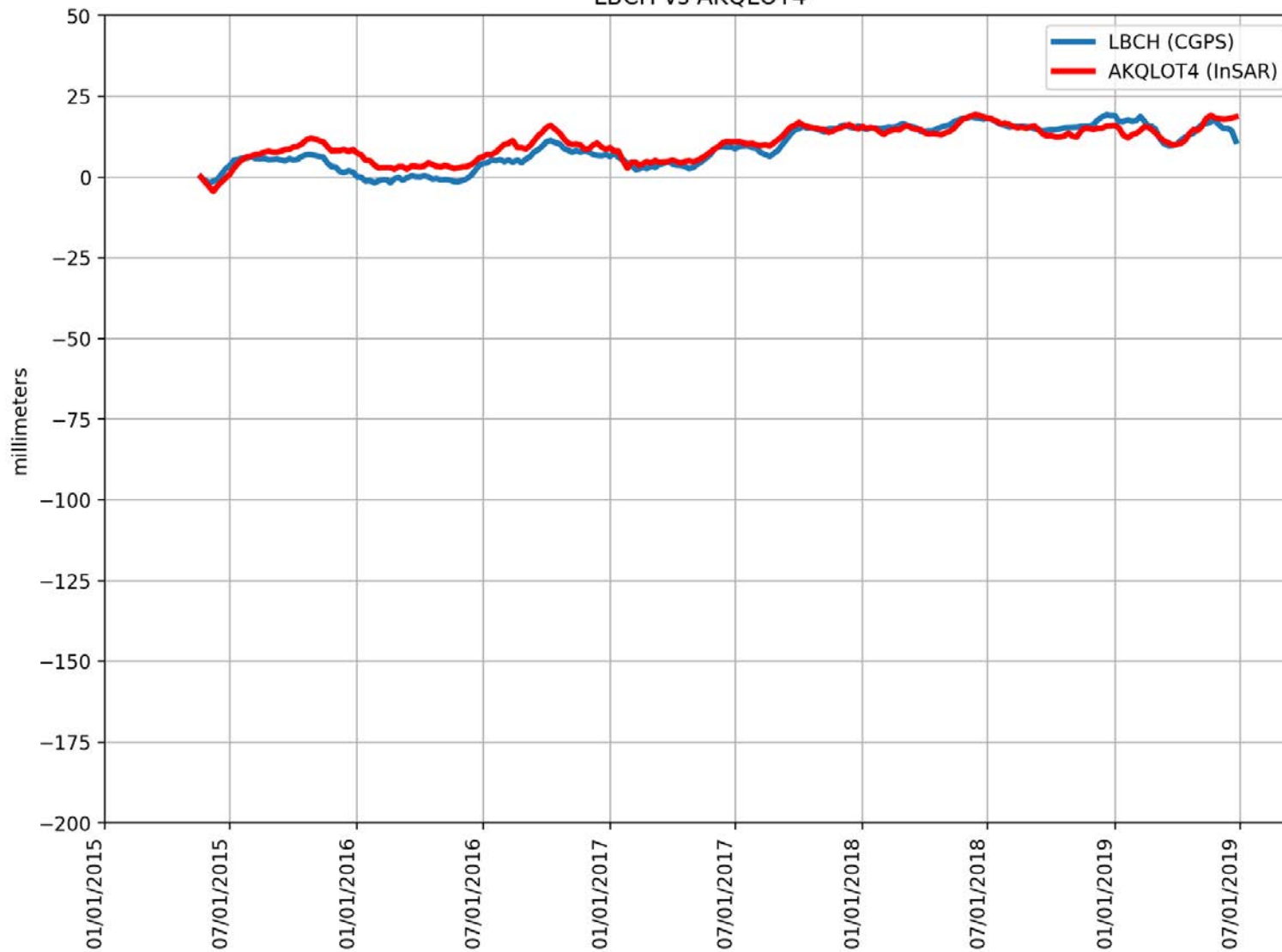
LBC2 vs AKTKUUQ



RMSE: 2.45 mm
Correlation: 0.90

Appendix B

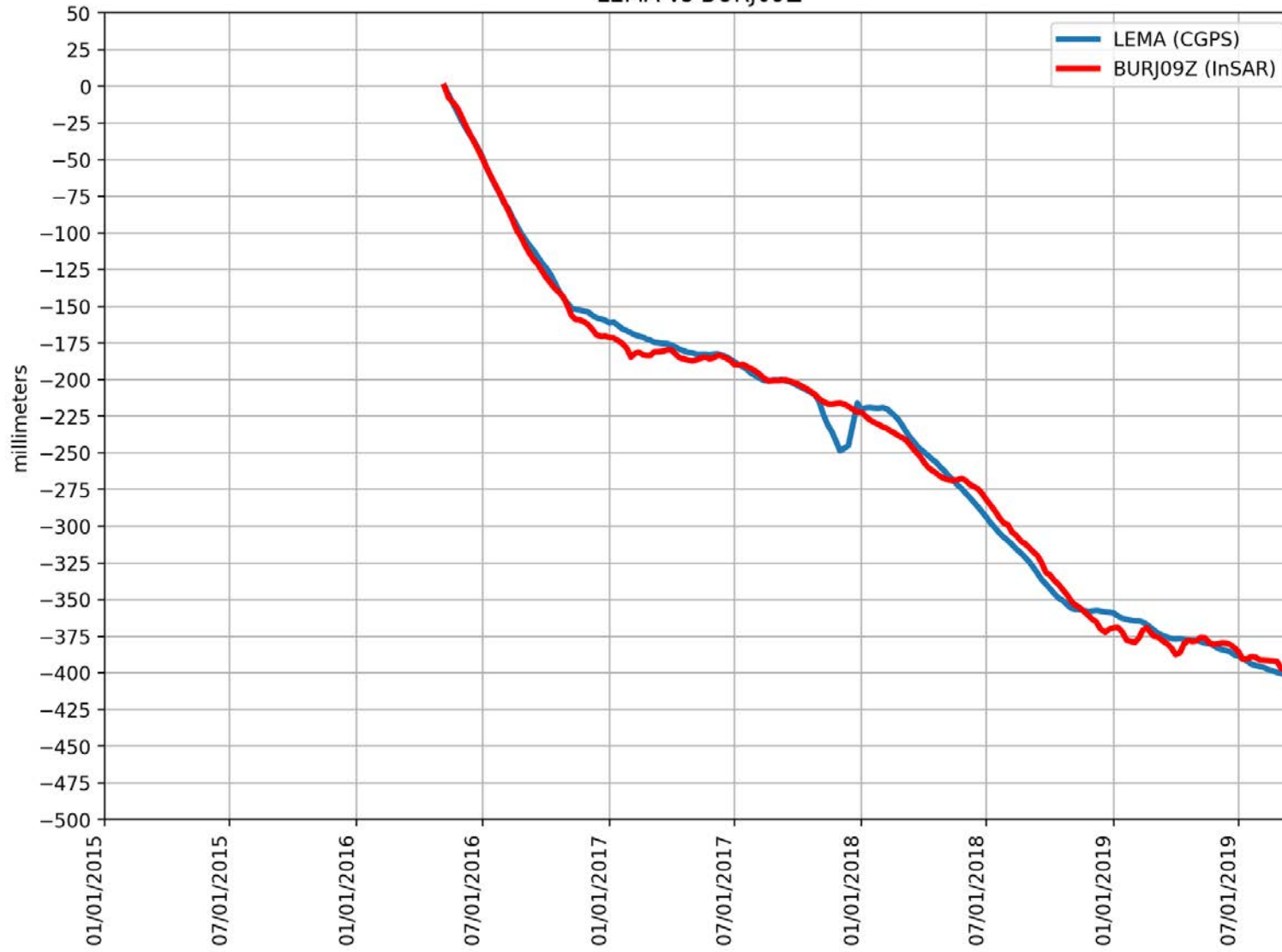
LBCH vs AKQLOT4



RMSE: 2.81 mm
Correlation: 0.92

Appendix B

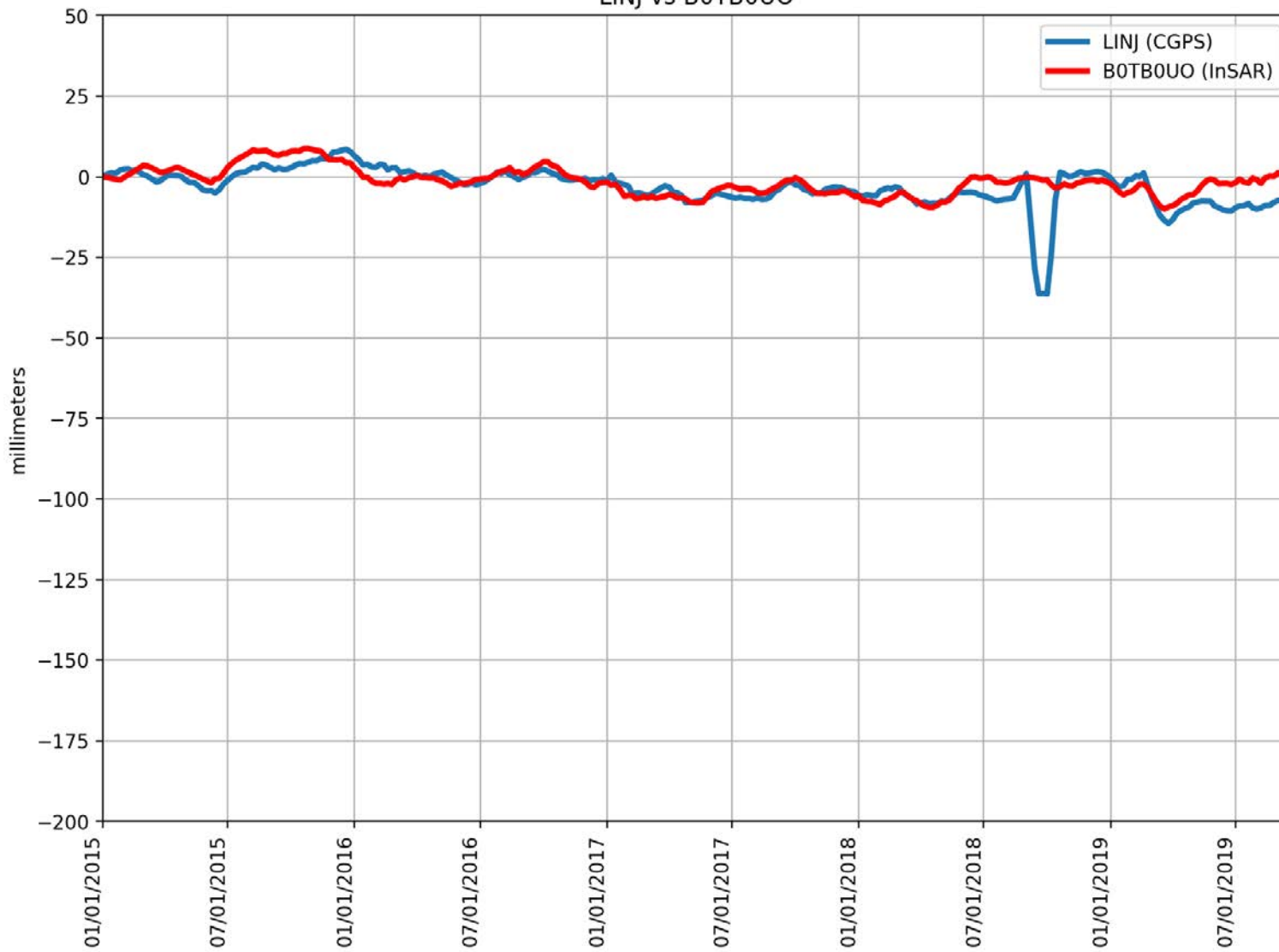
LEMA vs BURJ09Z



RMSE: 8.16 mm
Correlation: 1.00

Appendix B

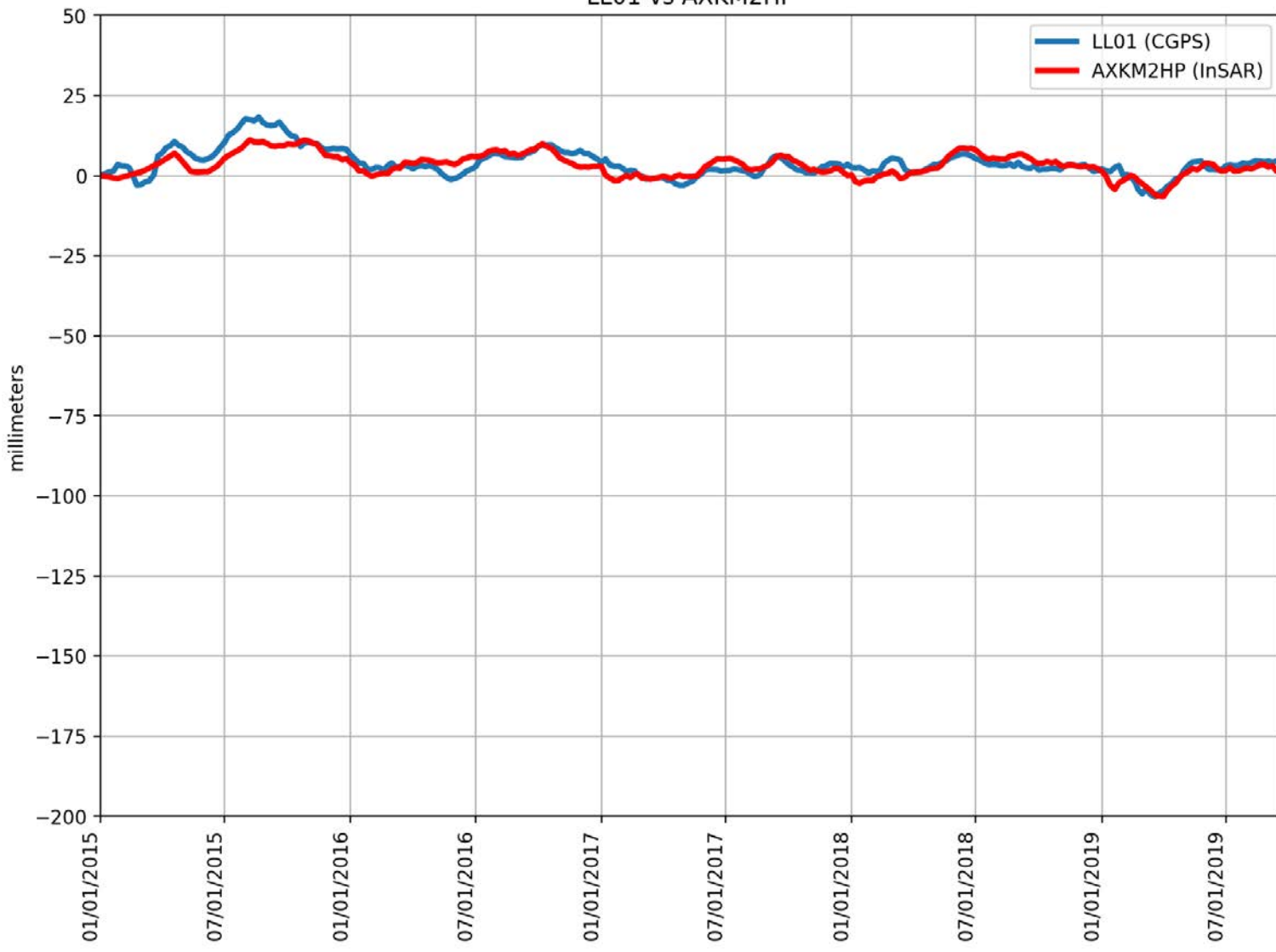
LINJ vs B0TB0UO



RMSE: 5.50 mm
Correlation: 0.51

Appendix B

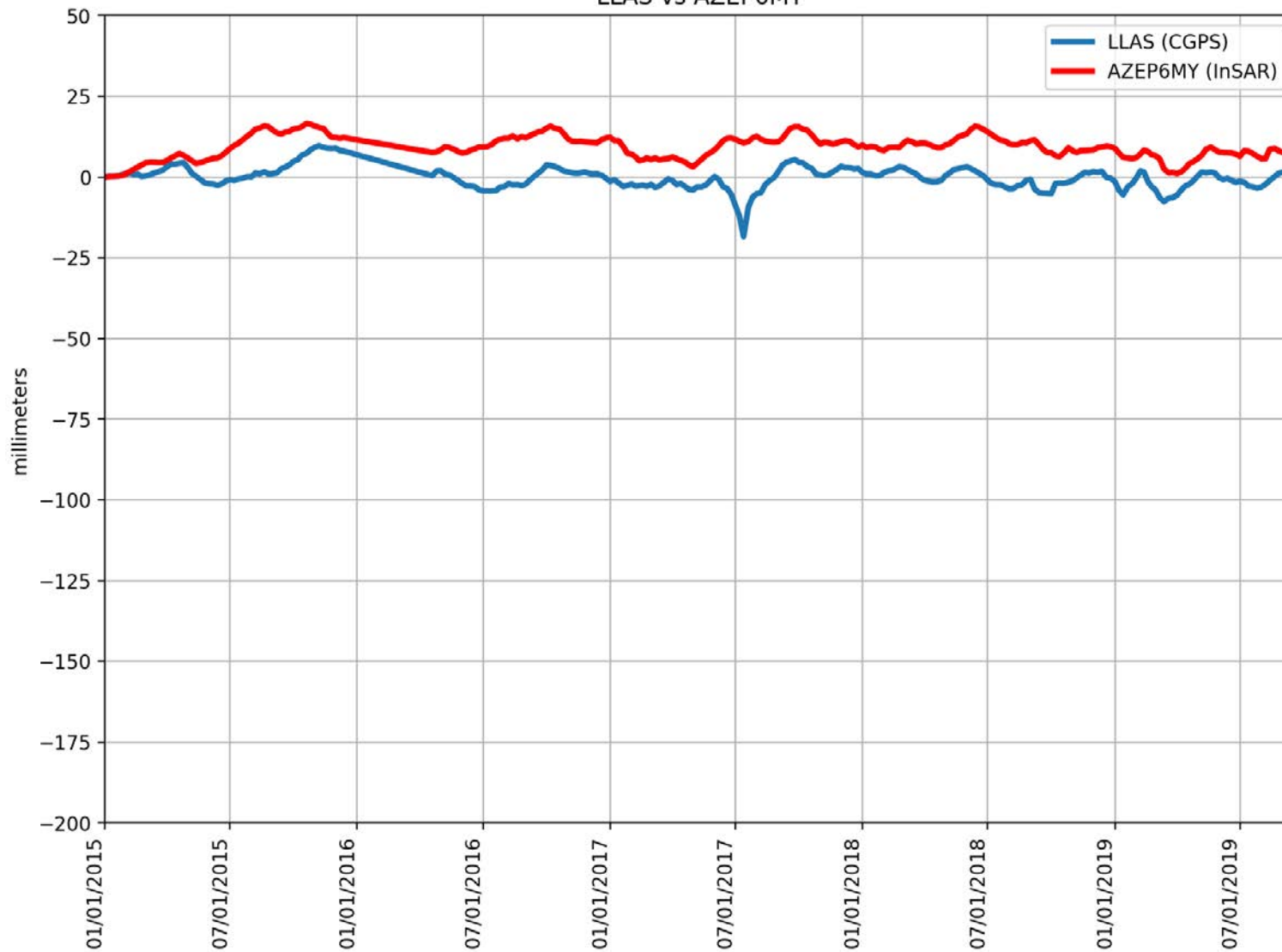
LL01 vs AXKM2HP



RMSE: 2.85 mm
Correlation: 0.77

Appendix B

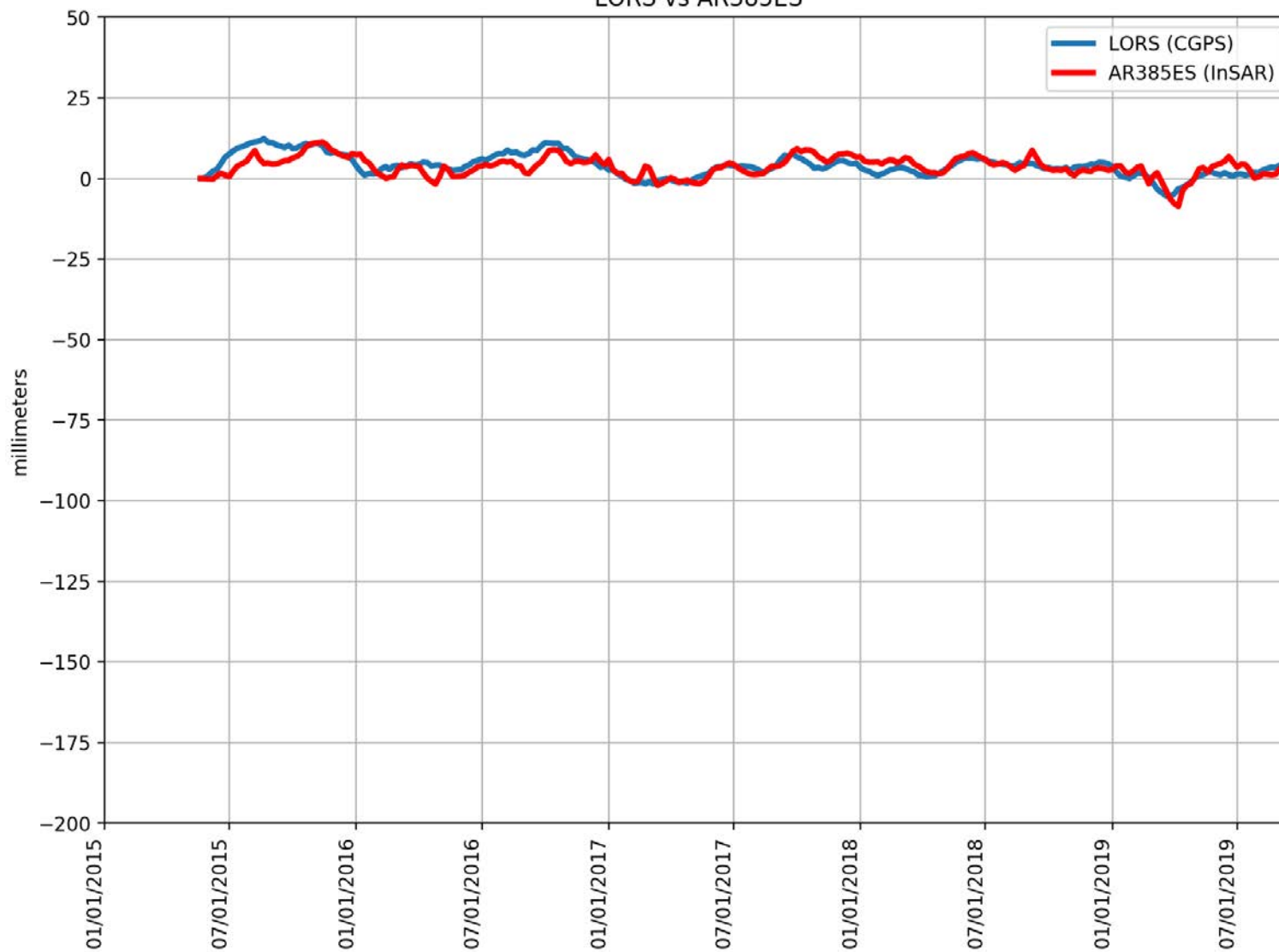
LLAS vs AZEP6MY



RMSE: 10.20 mm
Correlation: 0.37

Appendix B

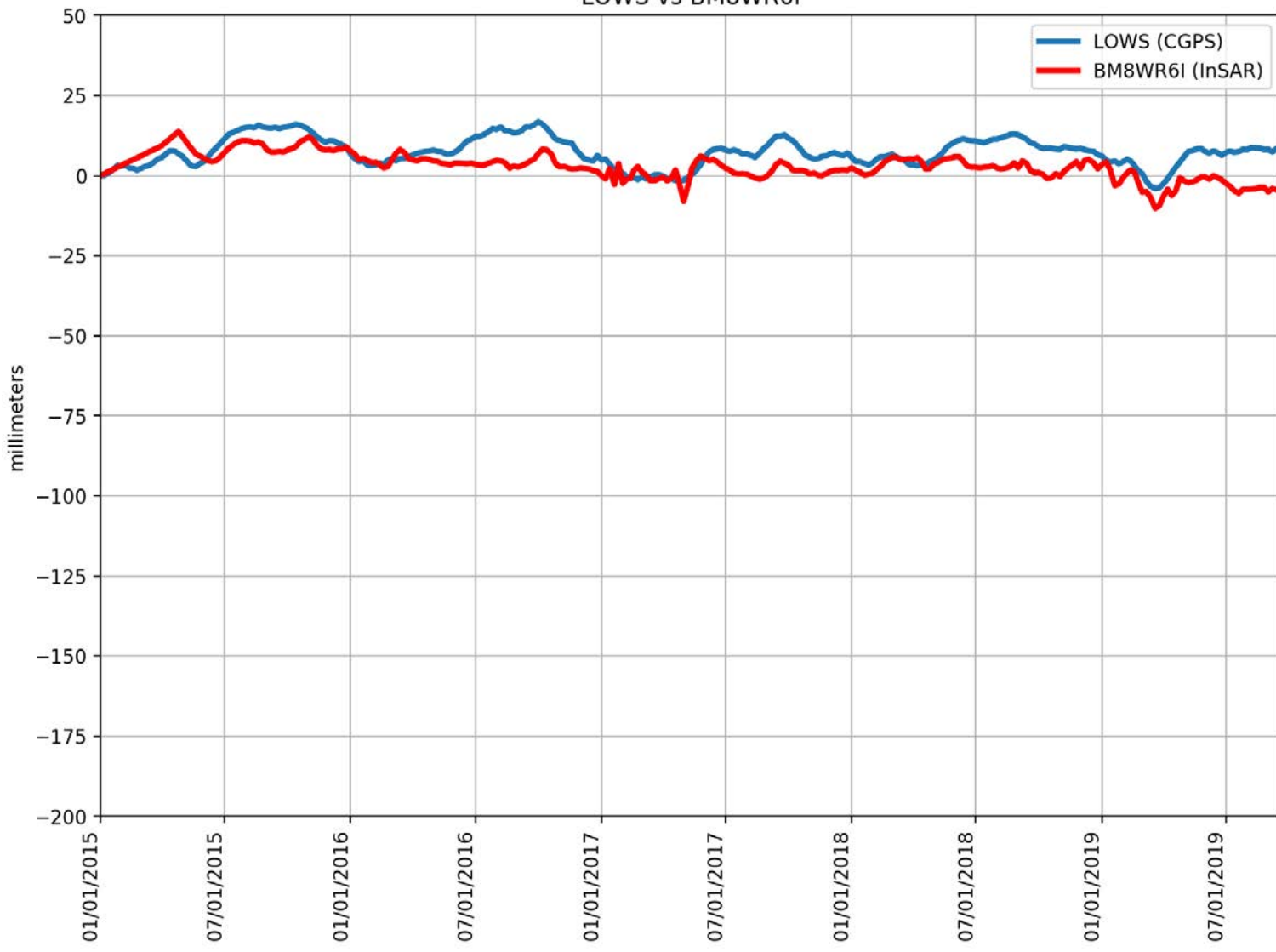
LORS vs AR385ES



RMSE: 2.67 mm
Correlation: 0.68

Appendix B

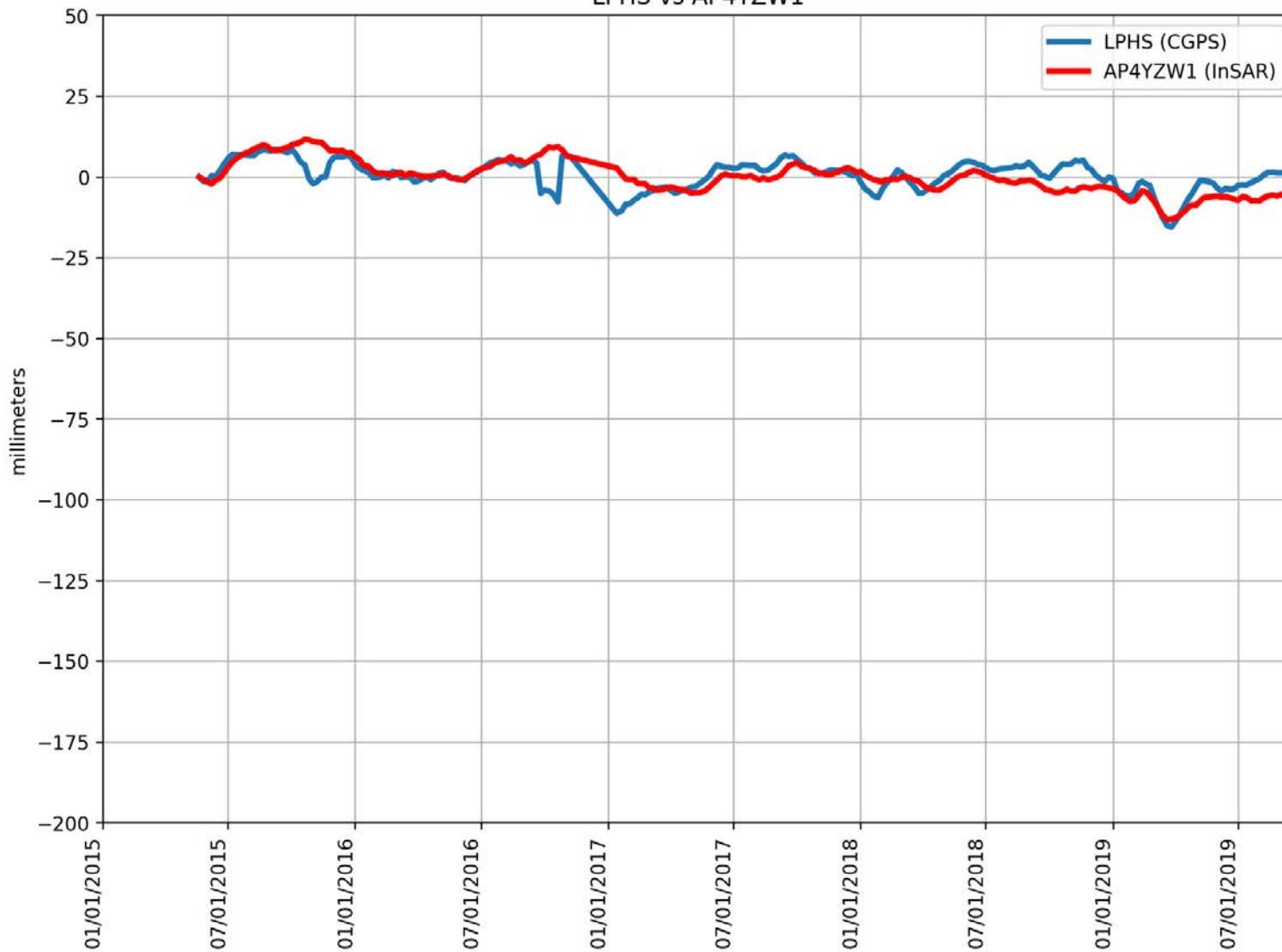
LOWS vs BM8WR6I



RMSE: 6.17 mm
Correlation: 0.49

Appendix B

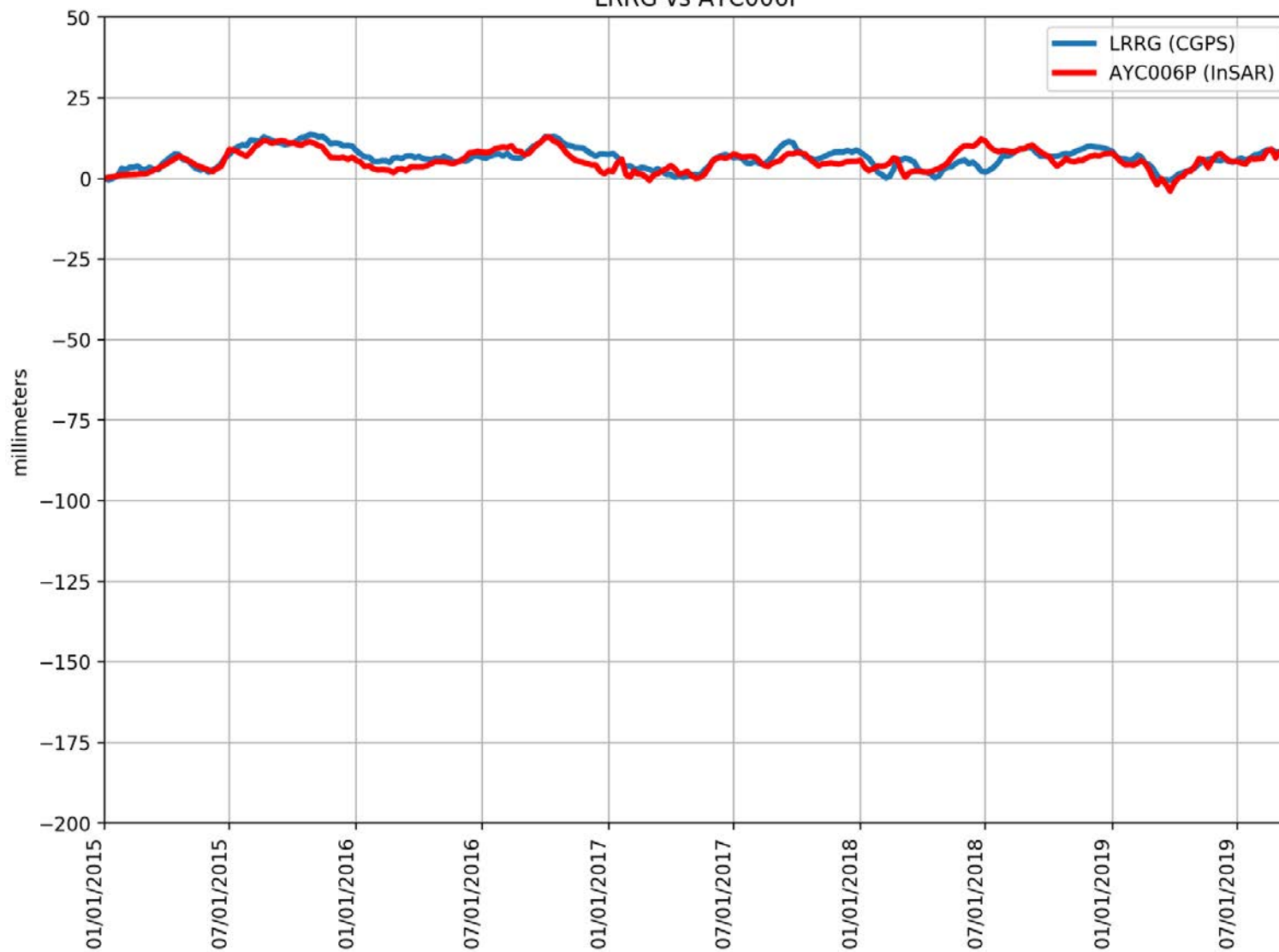
LPHS vs AP4YZW1



RMSE: 4.34 mm
Correlation: 0.61

Appendix B

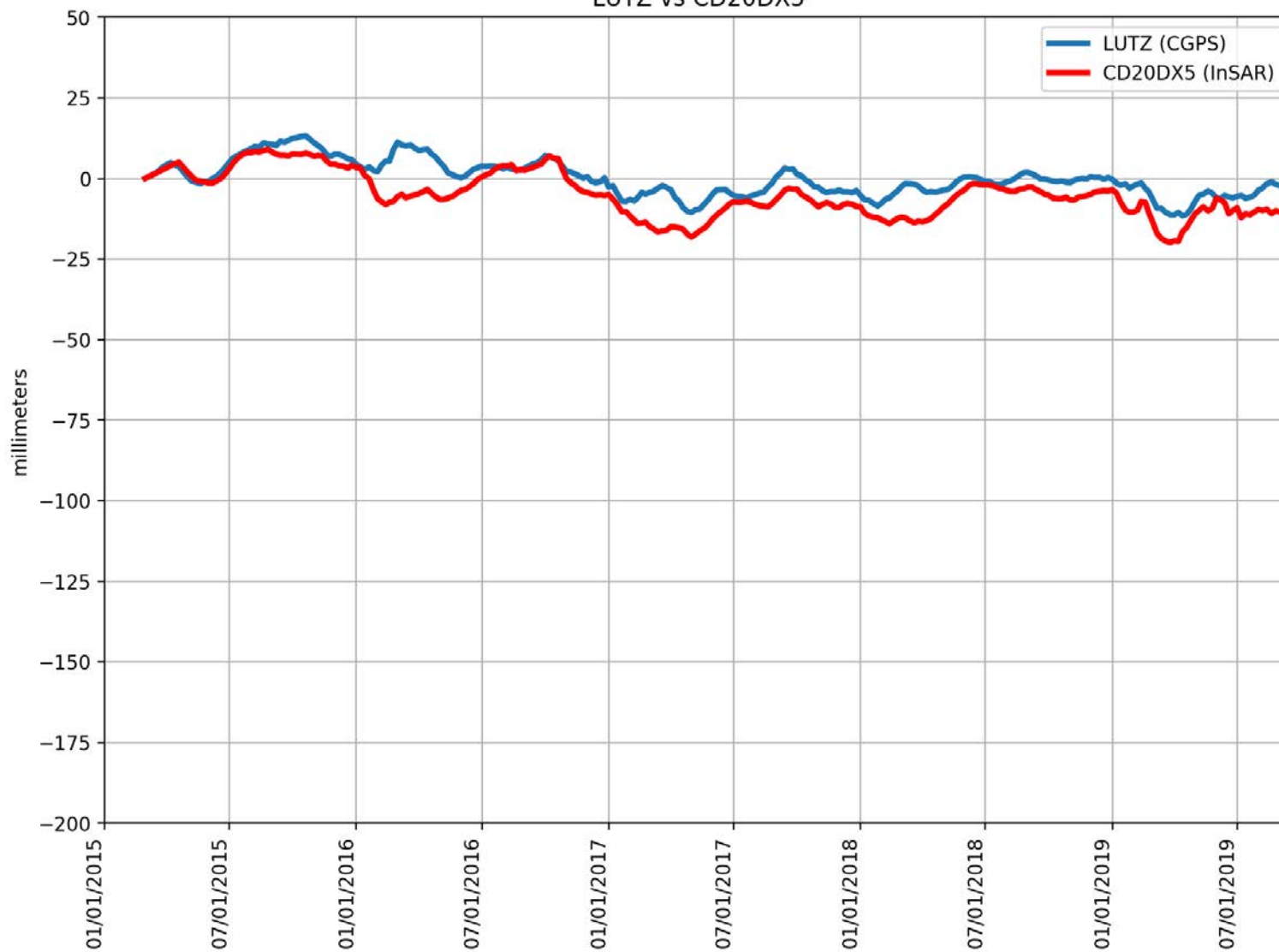
LRRG vs AYC006P



RMSE: 2.52 mm
Correlation: 0.72

Appendix B

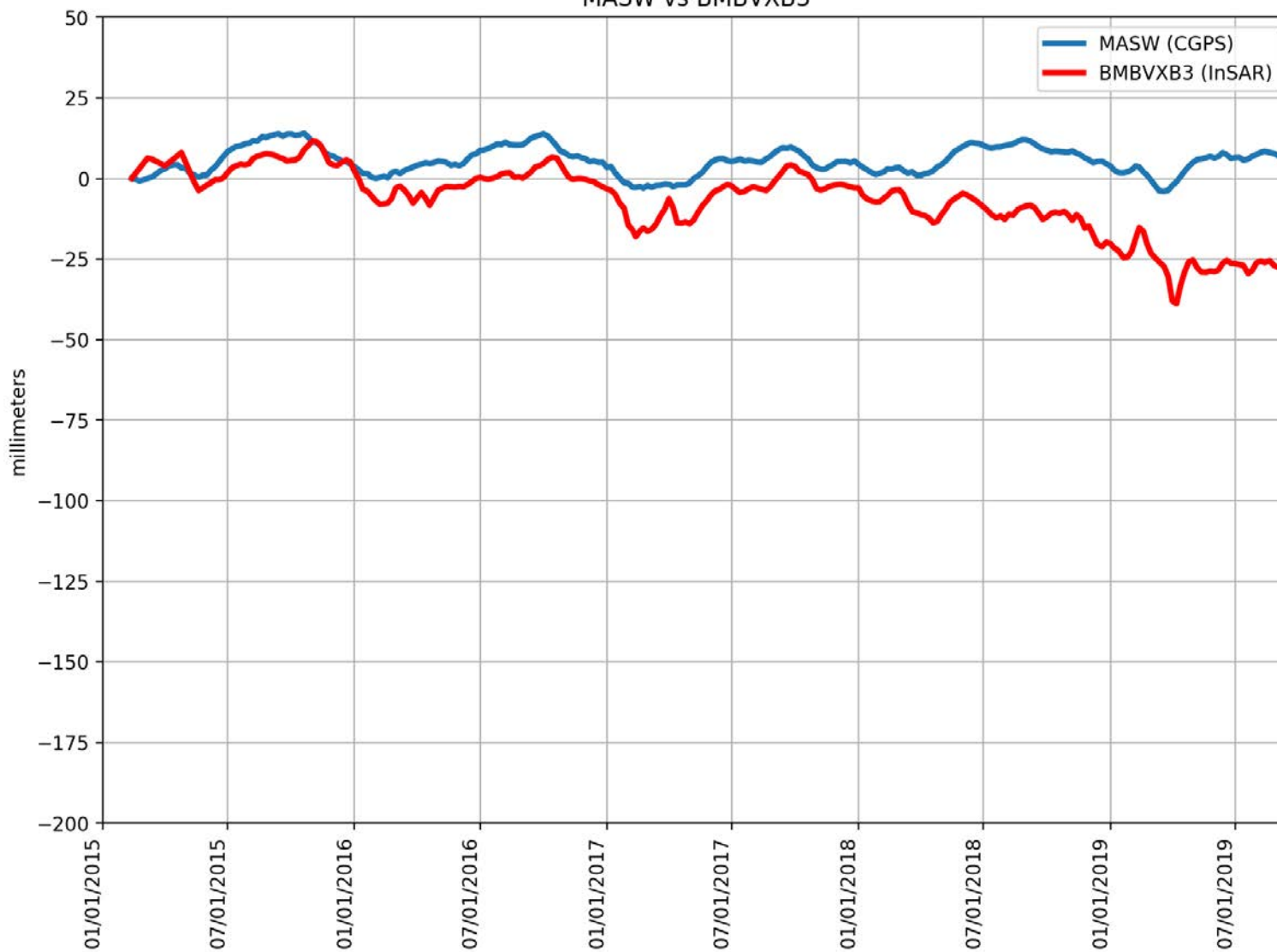
LUTZ vs CD20DX5



RMSE: 6.18 mm
Correlation: 0.85

Appendix B

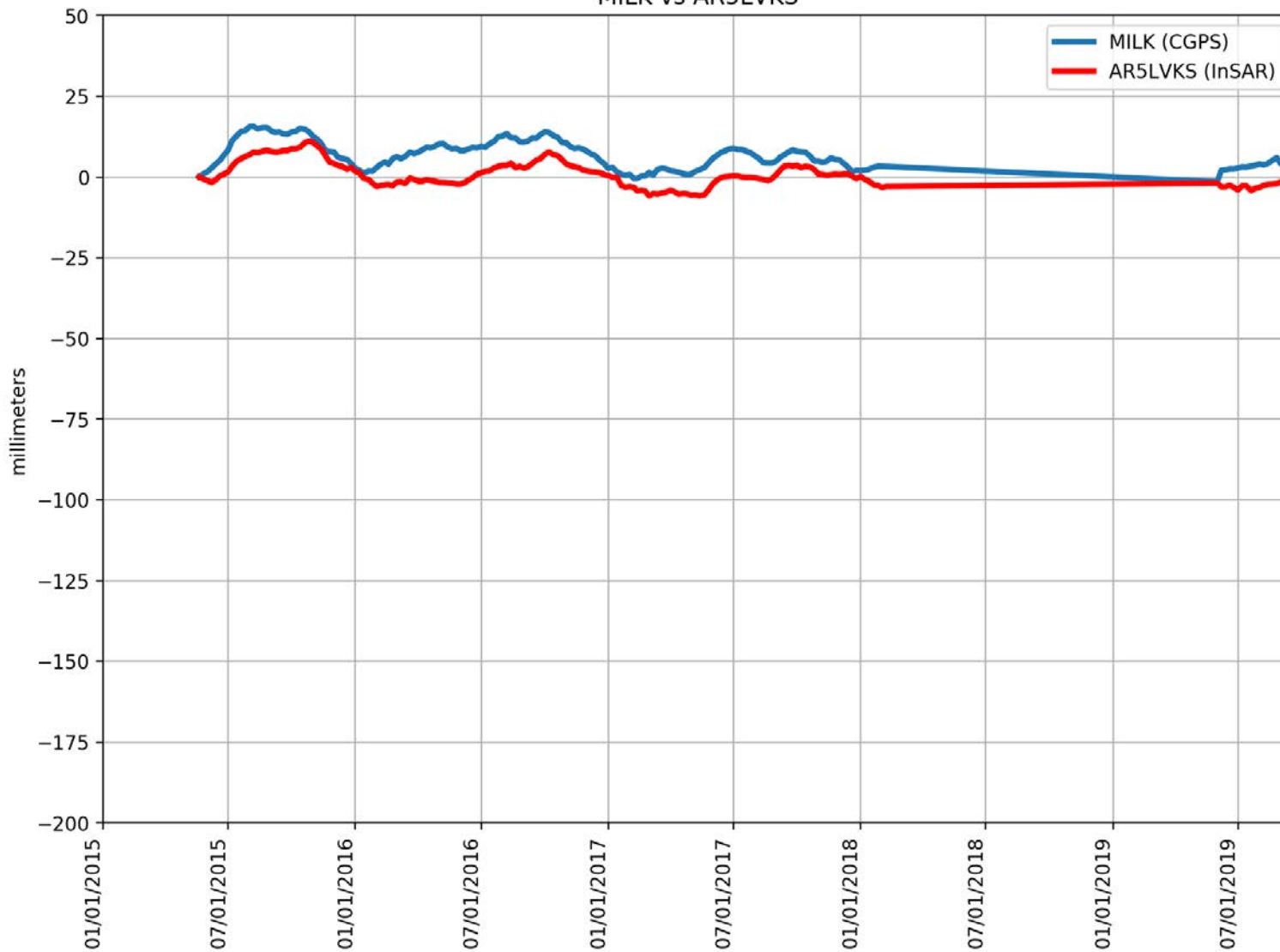
MASW vs BMBVXB3



RMSE: 15.87 mm
Correlation: 0.36

Appendix B

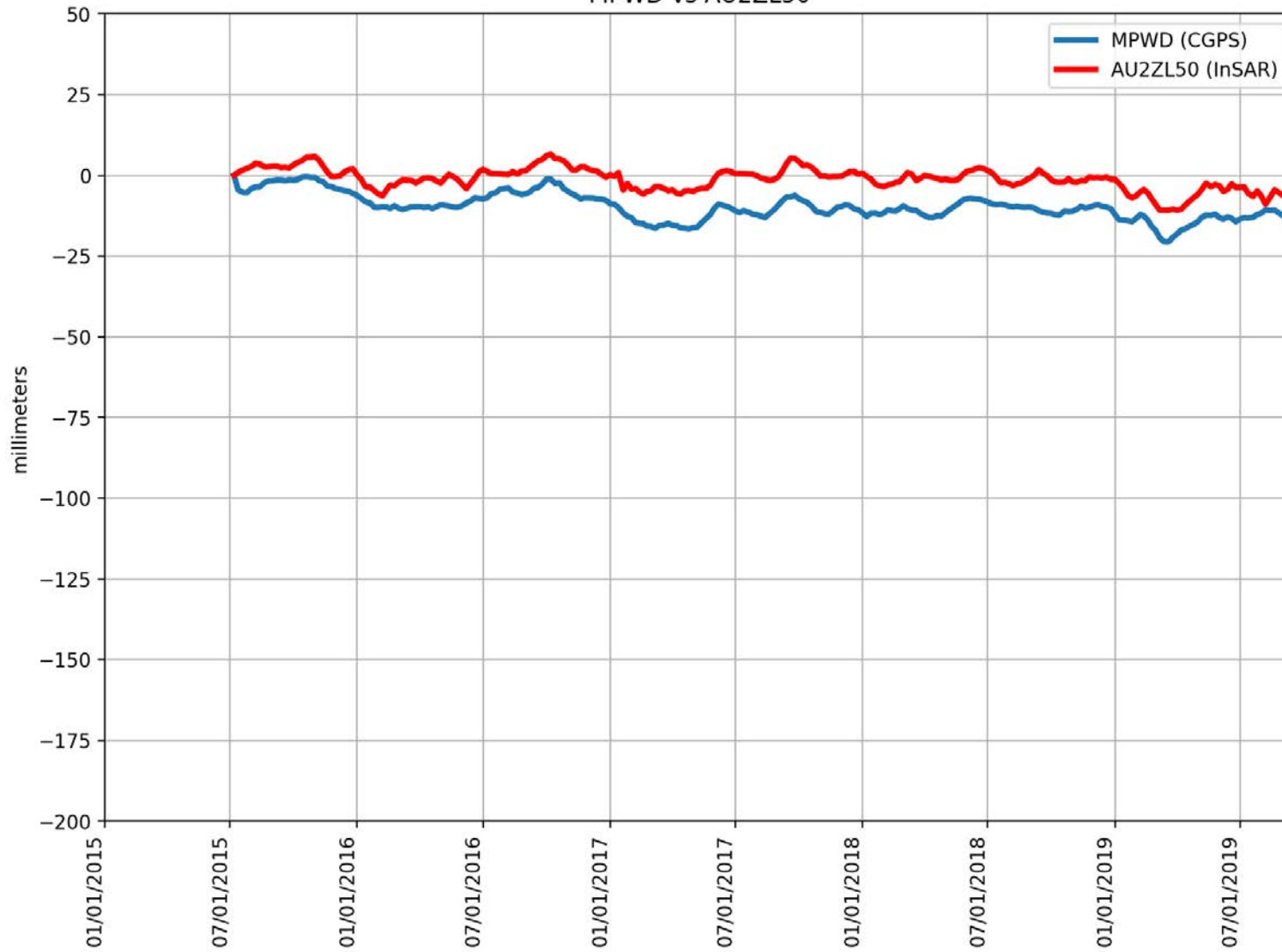
MILK vs AR5LVKS



RMSE: 6.45 mm
Correlation: 0.82

Appendix B

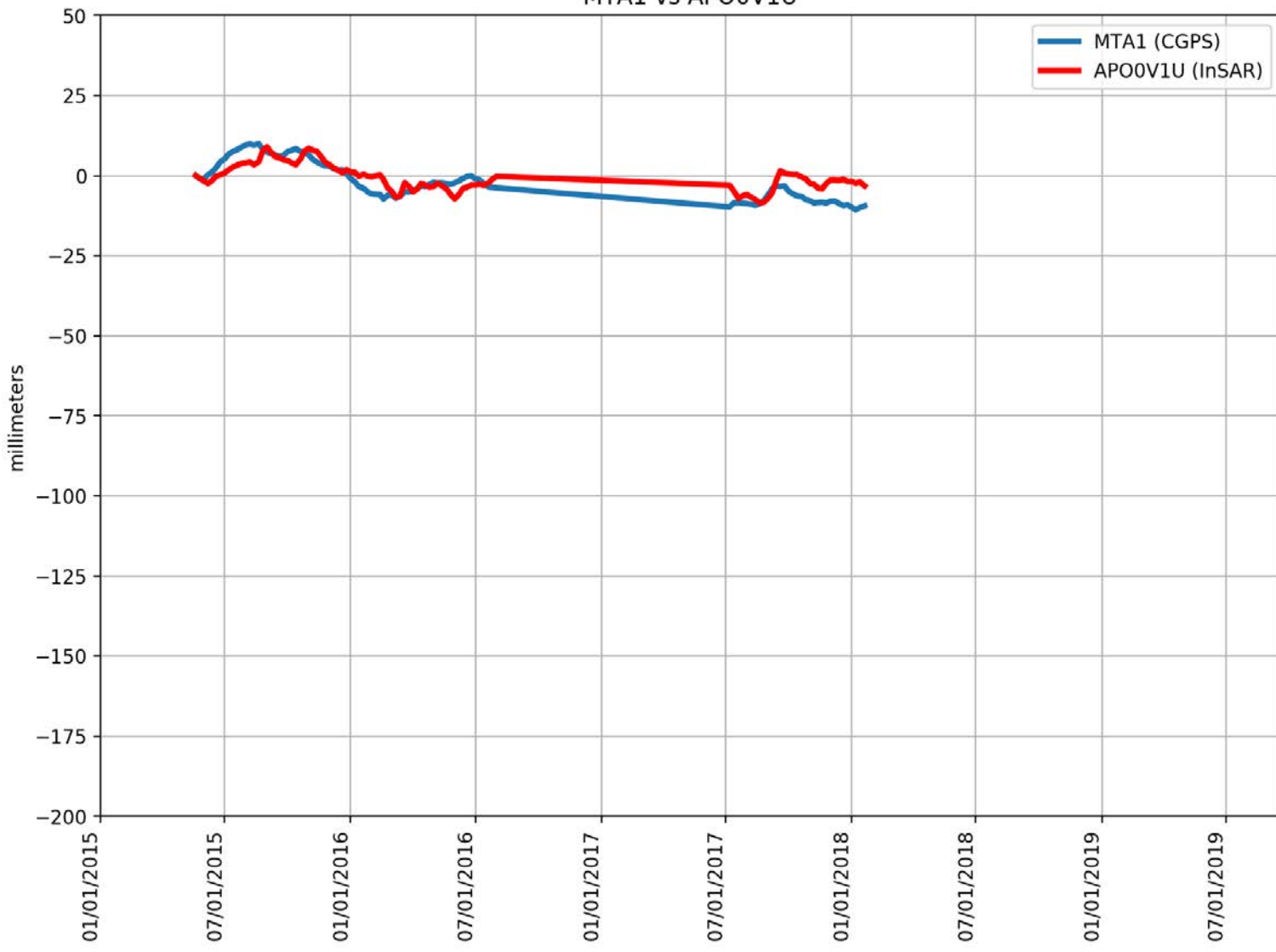
MPWD vs AU2ZL50



RMSE: 8.80 mm
Correlation: 0.82

Appendix B

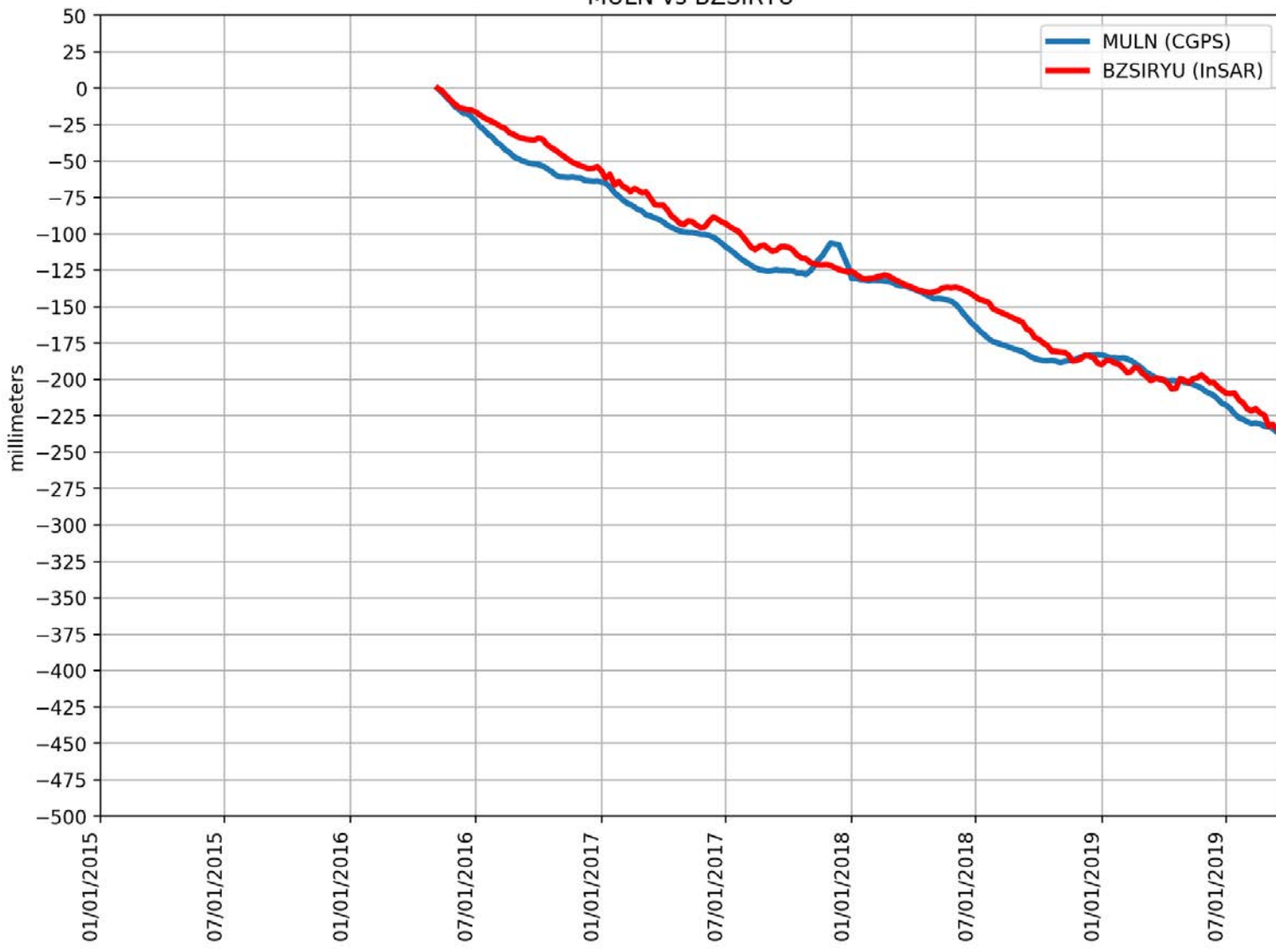
MTA1 vs APO0V1U



RMSE: 3.96 mm
Correlation: 0.77

Appendix B

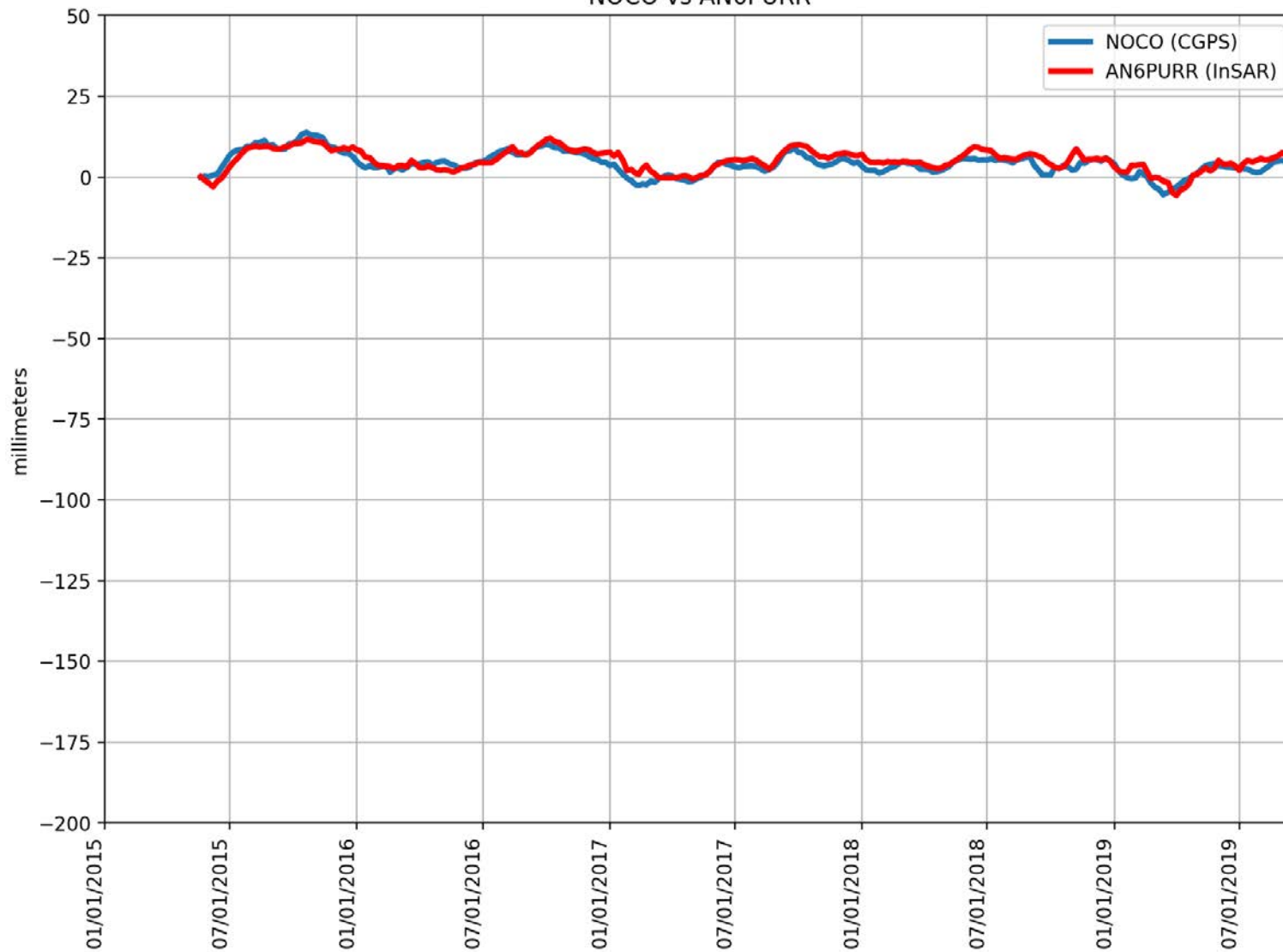
MULN vs BZSIRYU



RMSE: 10.54 mm
Correlation: 0.99

Appendix B

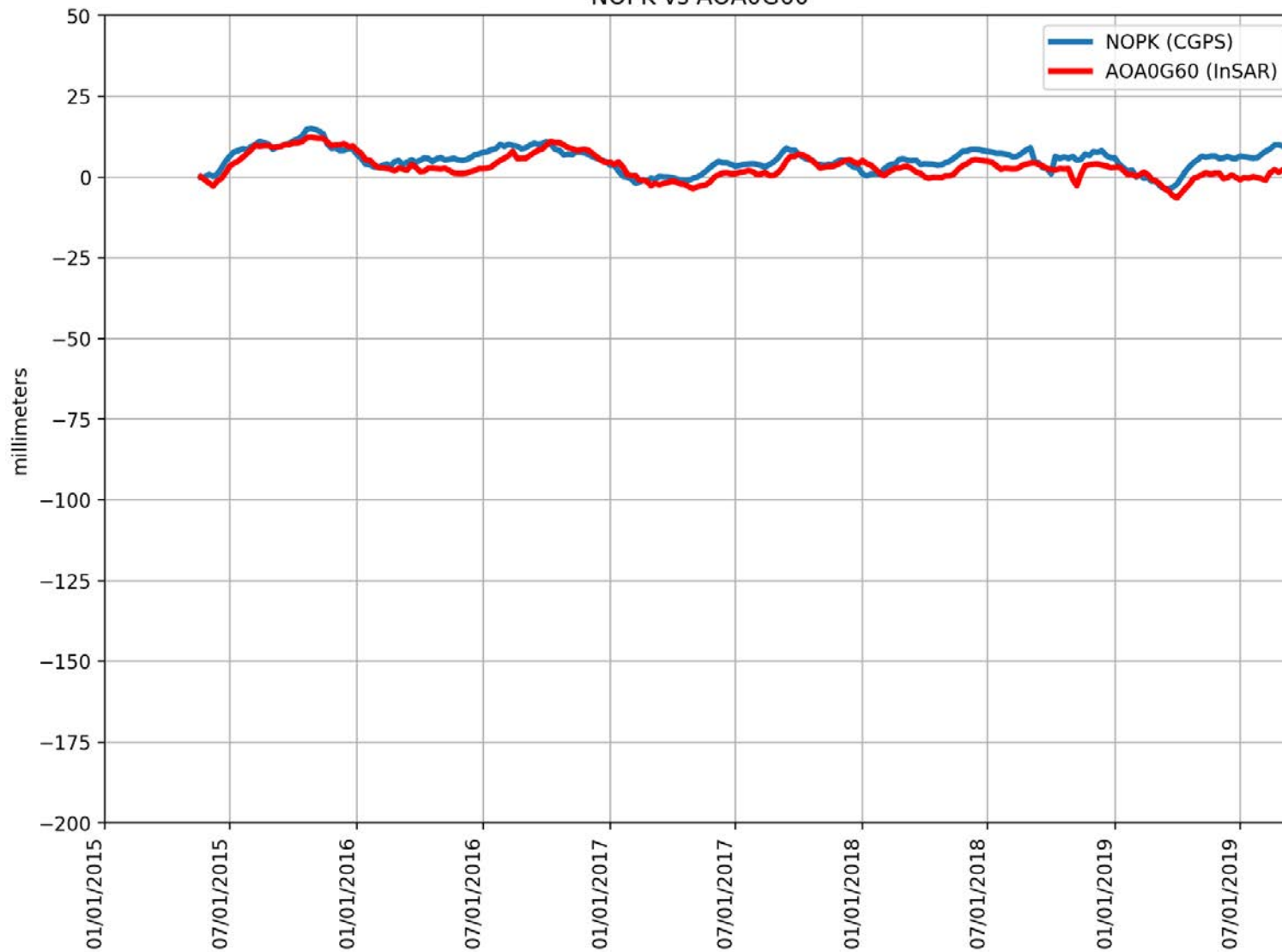
NOCO vs AN6PURR



RMSE: 2.09 mm
Correlation: 0.85

Appendix B

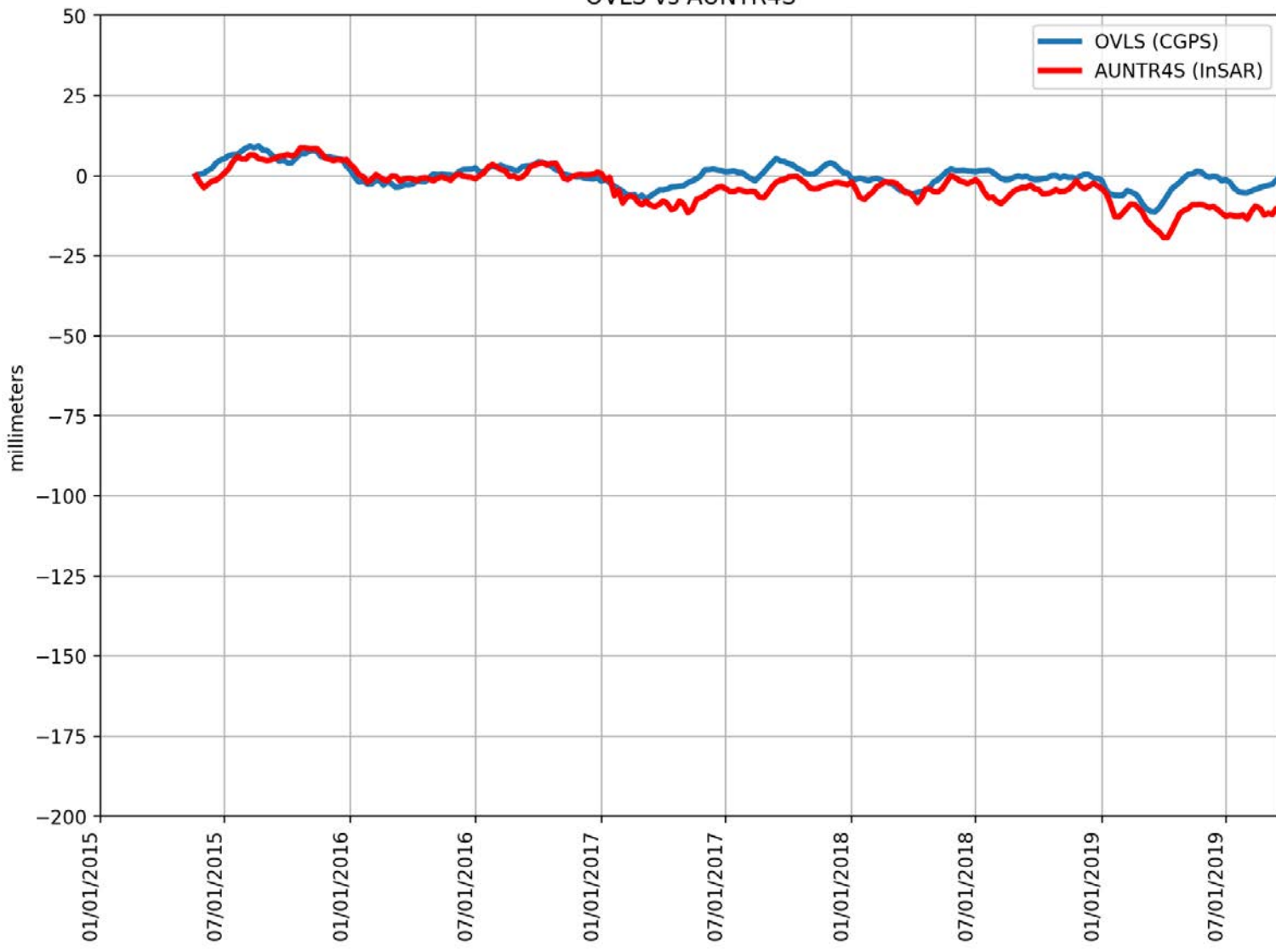
NOPK vs AOA0G60



RMSE: 3.35 mm
Correlation: 0.77

Appendix B

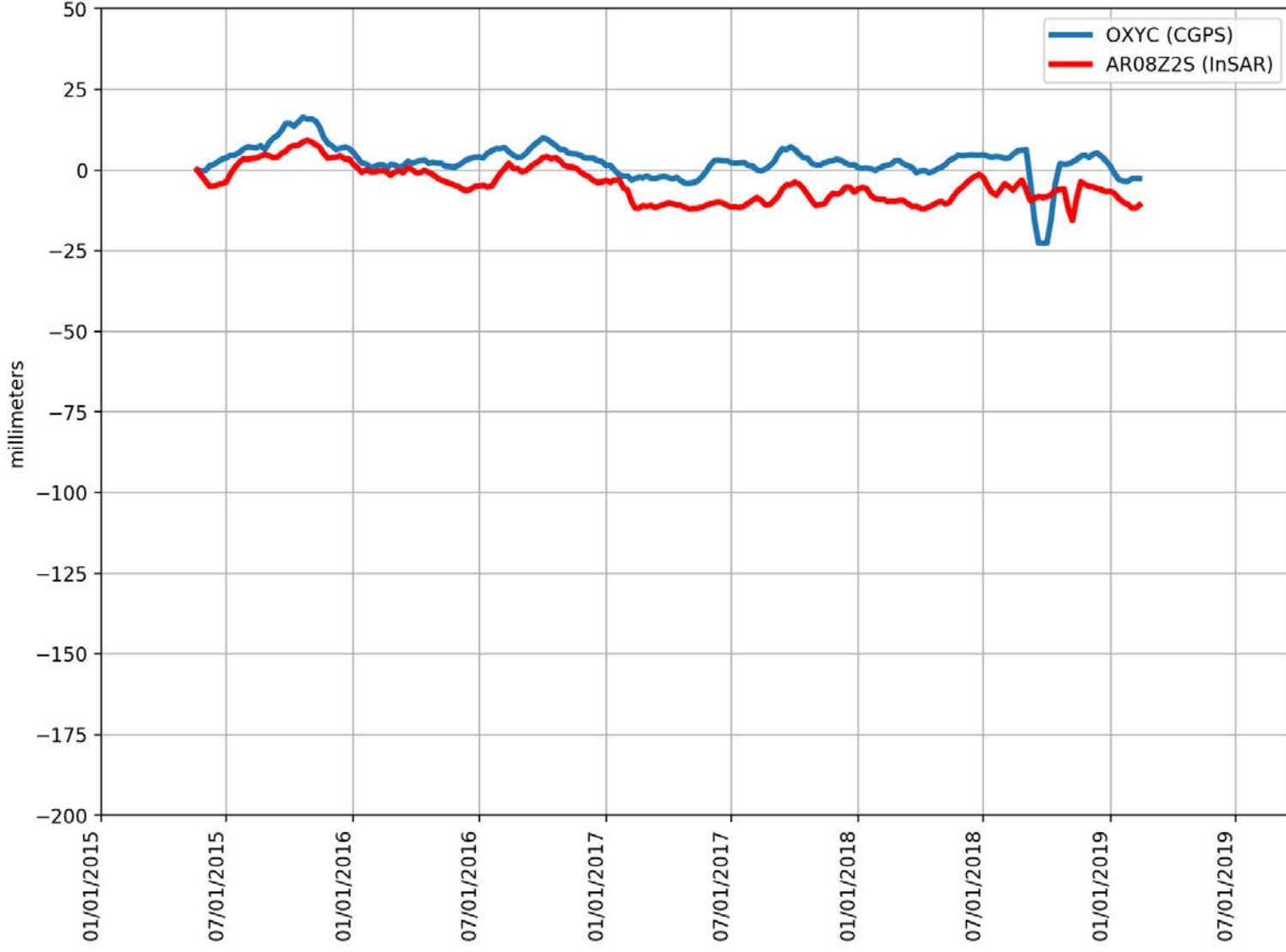
OVLS vs AUNTR4S



RMSE: 4.81 mm
Correlation: 0.78

Appendix B

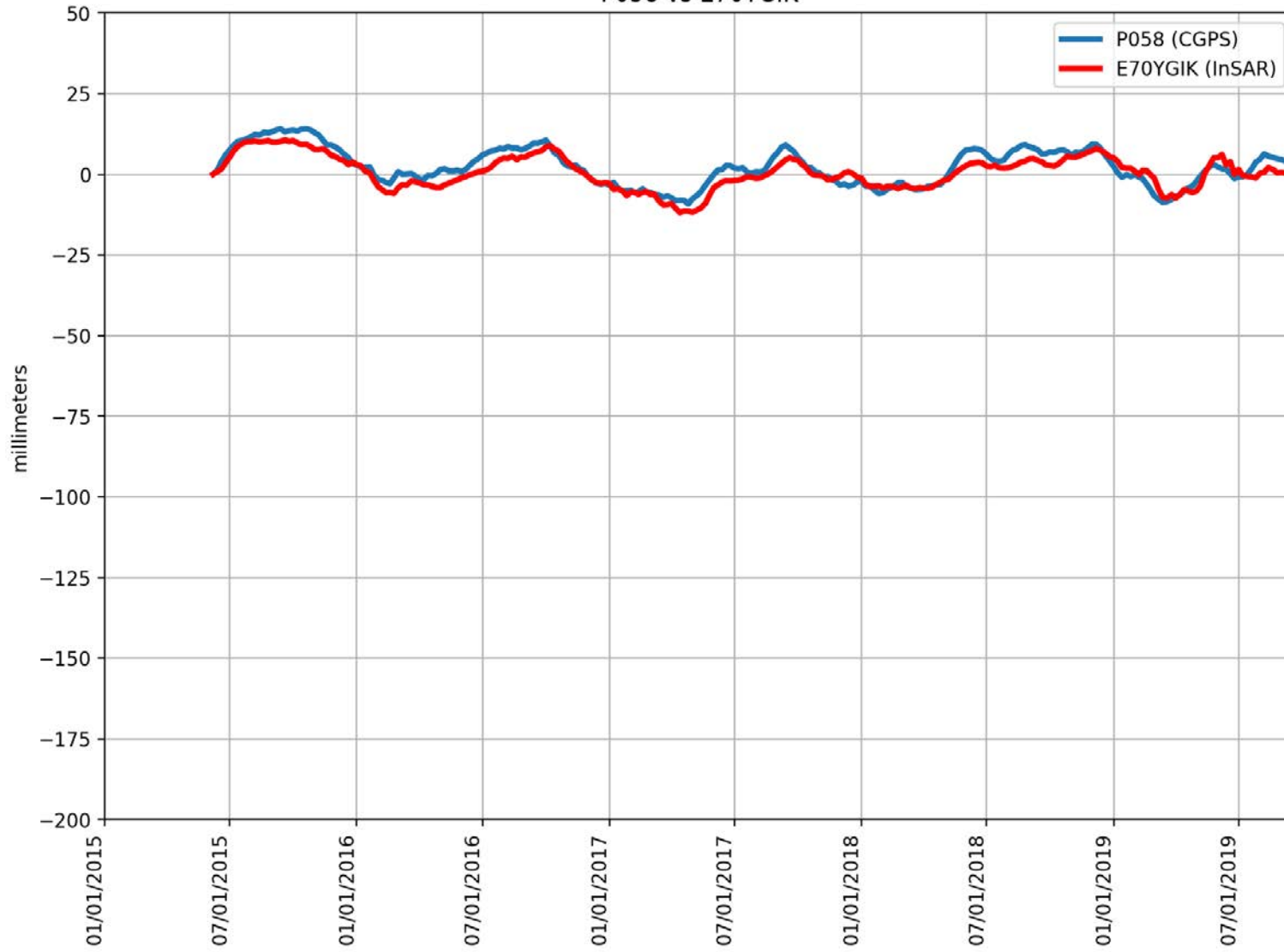
OXYC vs AR08Z2S



RMSE: 8.42 mm
Correlation: 0.66

Appendix B

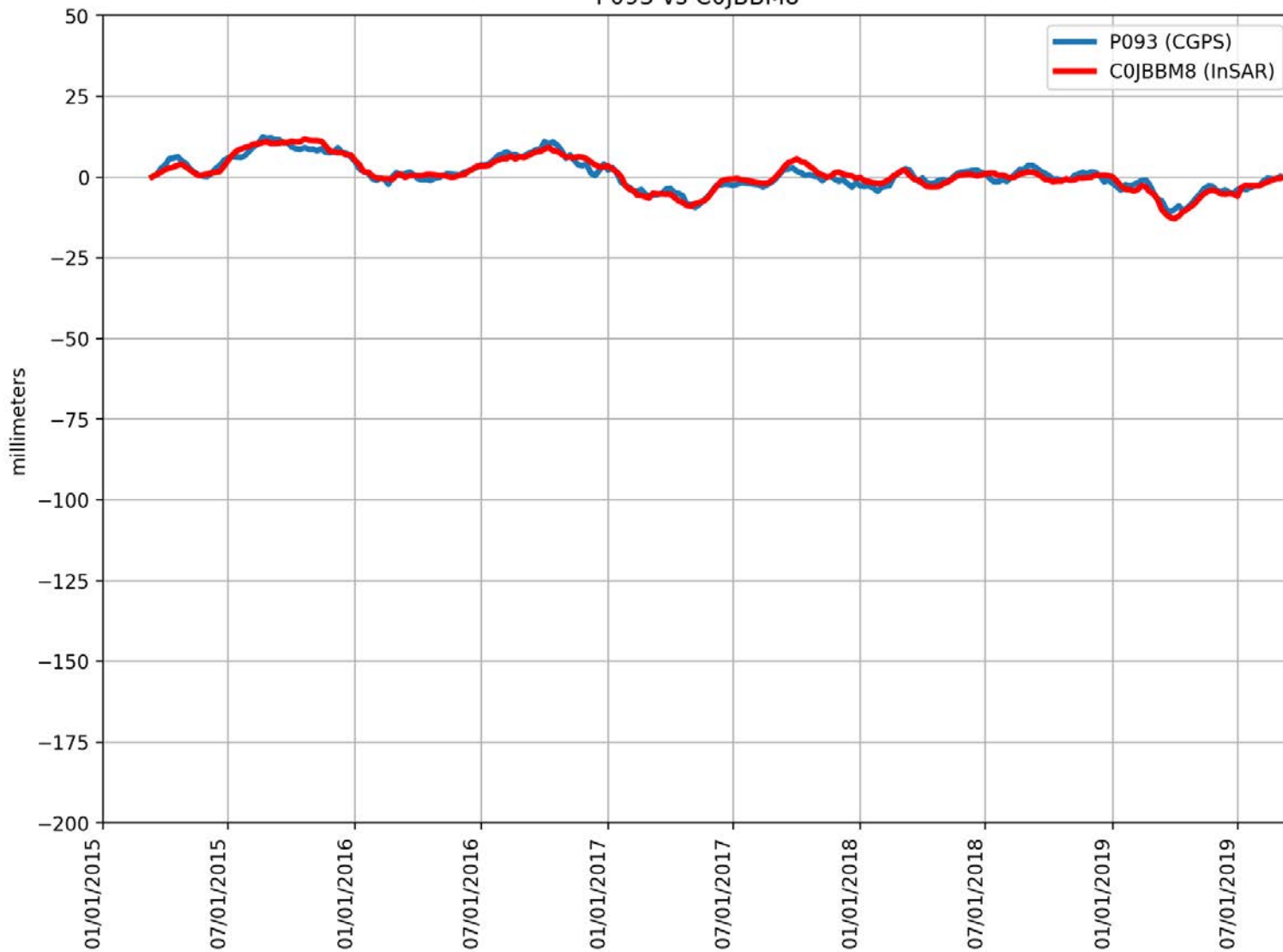
P058 vs E70YGIK



RMSE: 2.88 mm
Correlation: 0.91

Appendix B

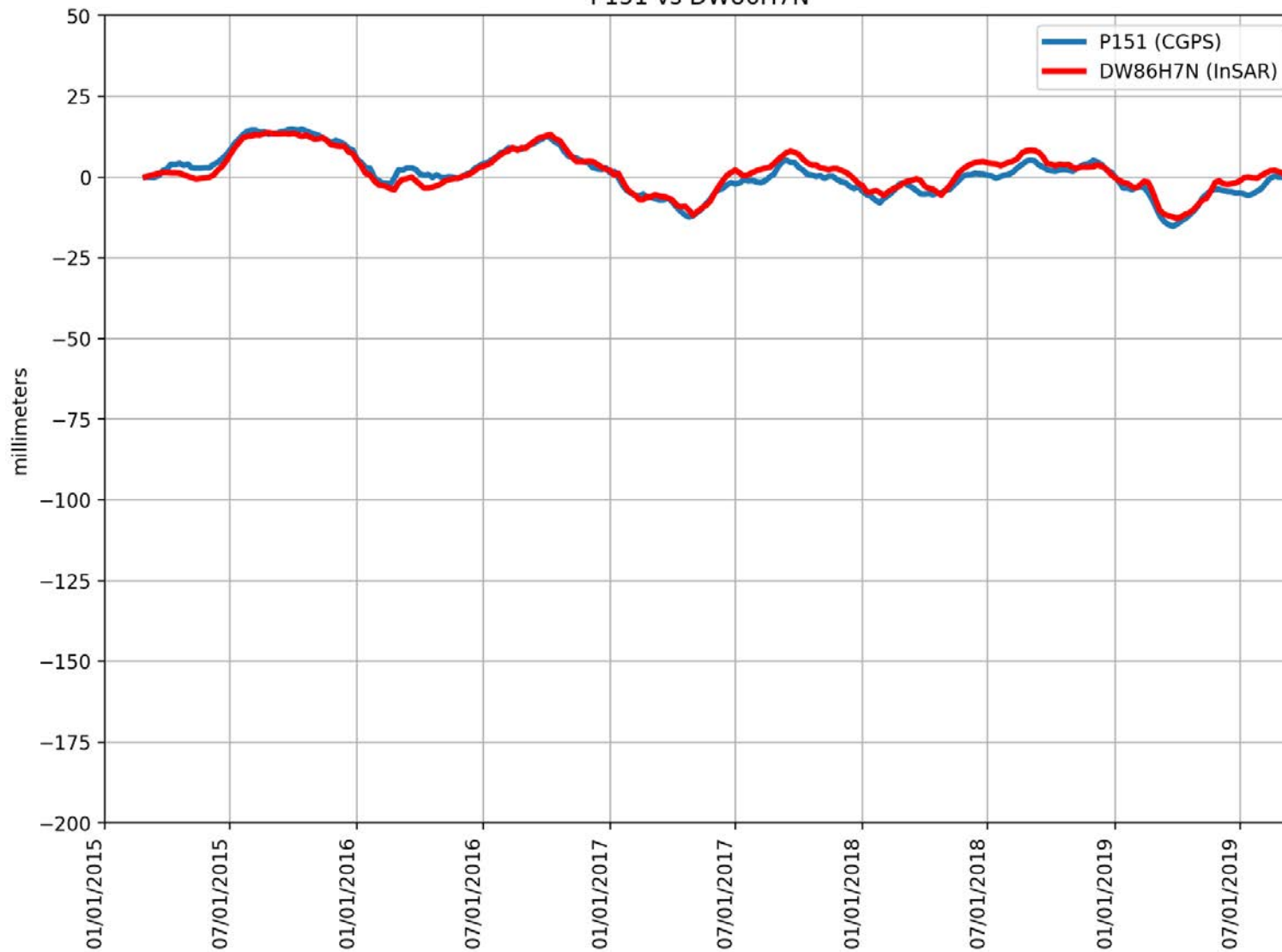
P093 vs C0JBBM8



RMSE: 1.45 mm
Correlation: 0.96

Appendix B

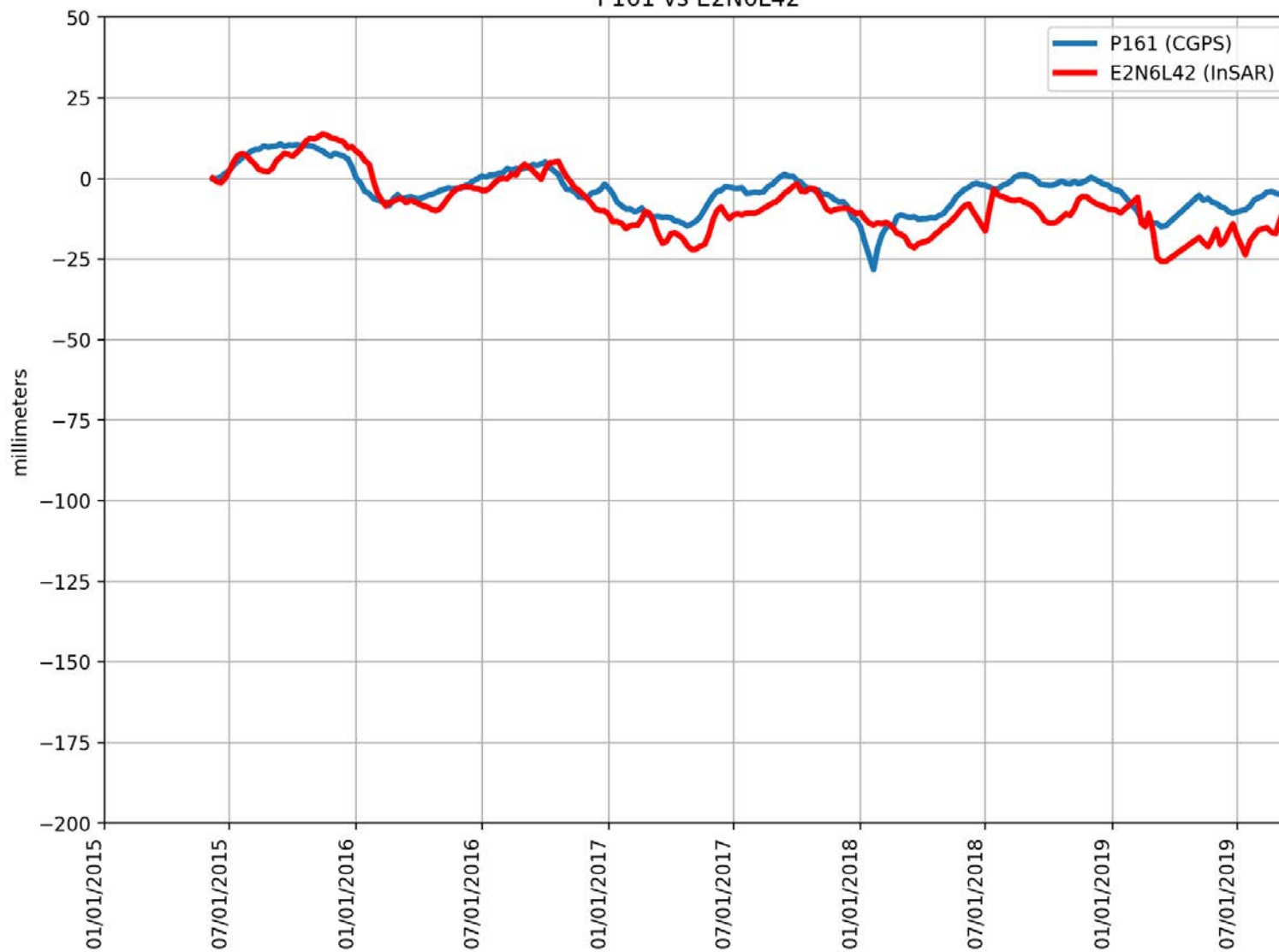
P151 vs DW86H7N



RMSE: 2.17 mm
Correlation: 0.95

Appendix B

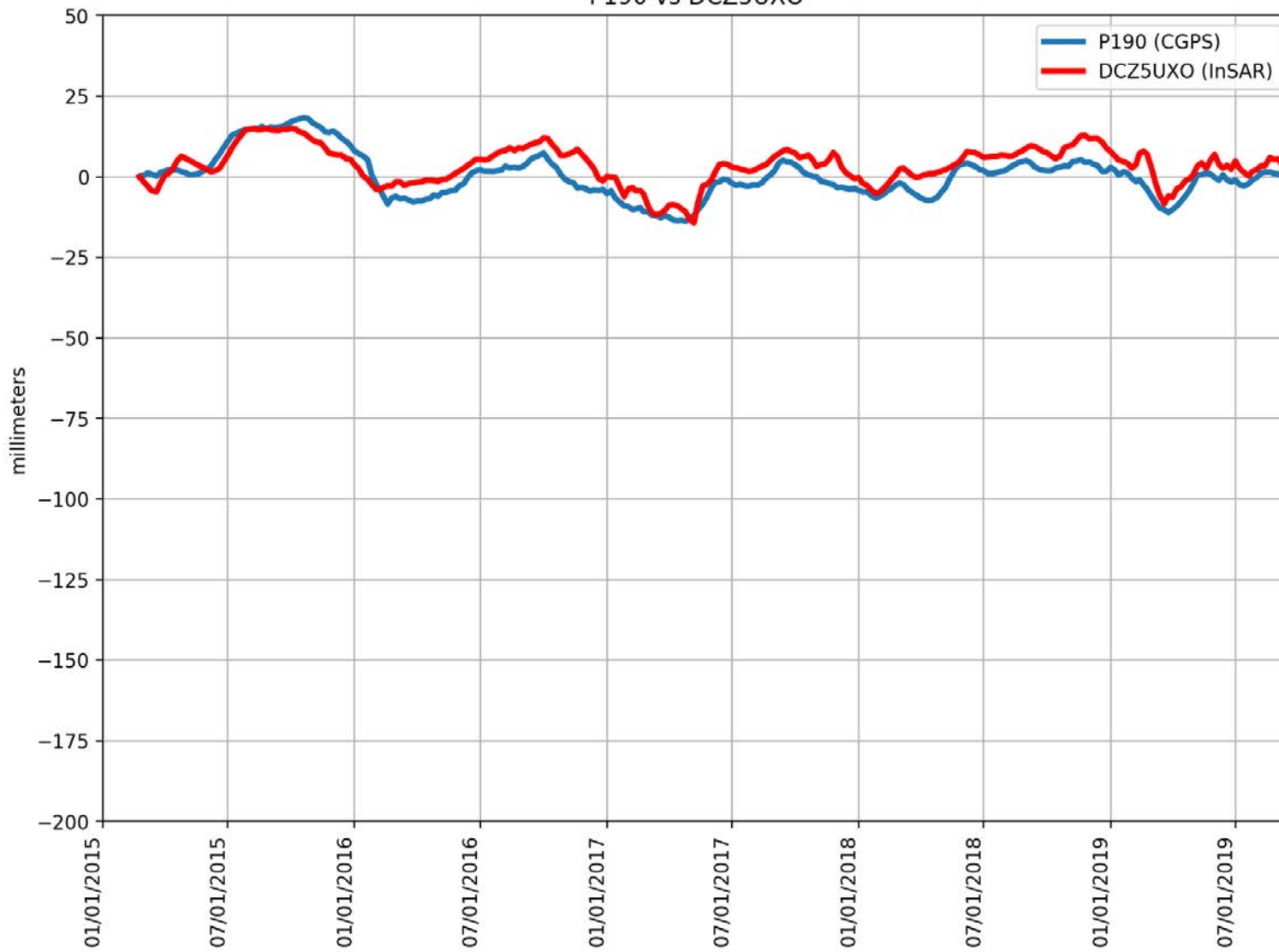
P161 vs E2N6L42



RMSE: 6.35 mm
Correlation: 0.82

Appendix B

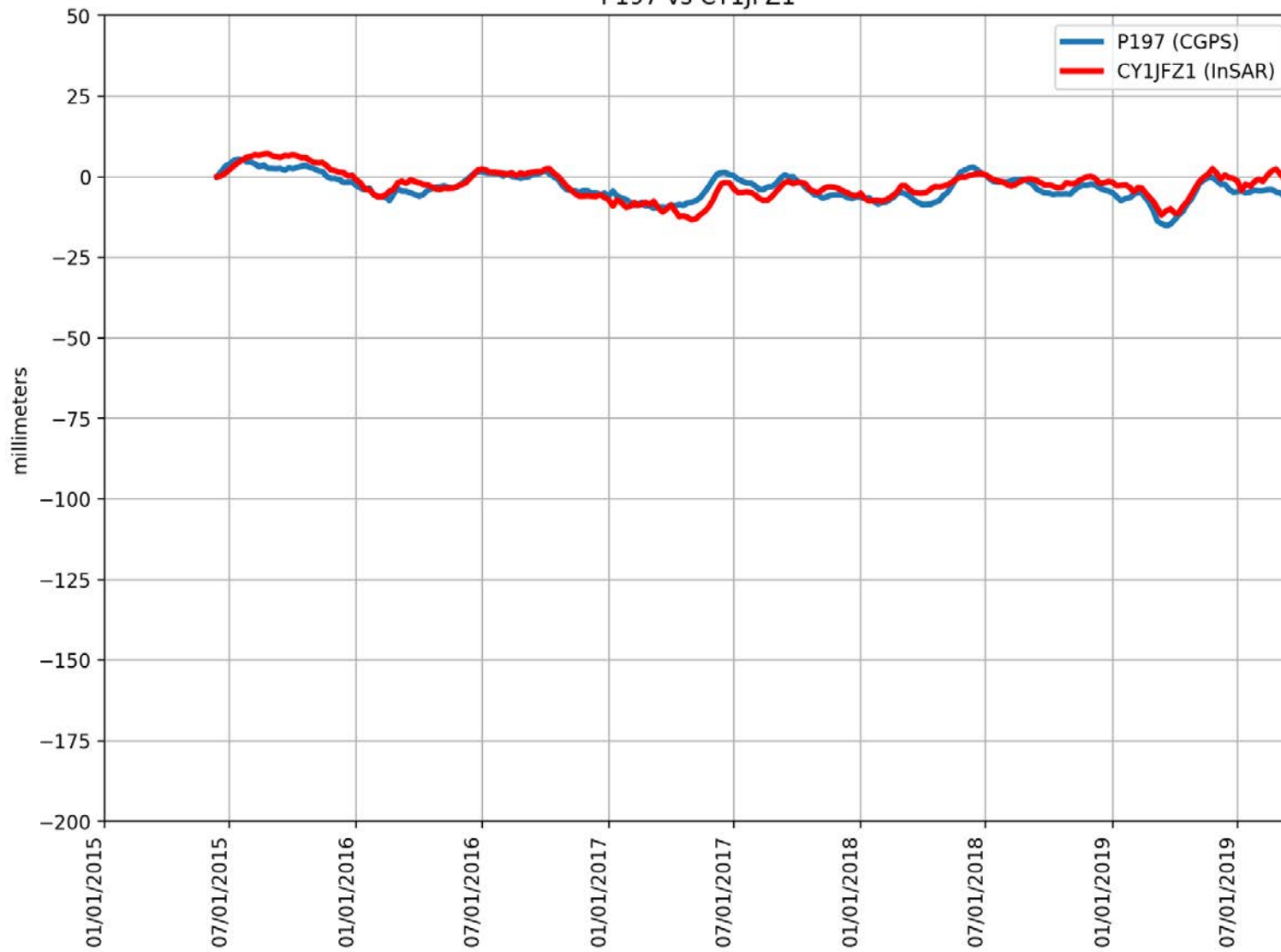
P190 vs DCZ5UXO



RMSE: 4.89 mm
Correlation: 0.85

Appendix B

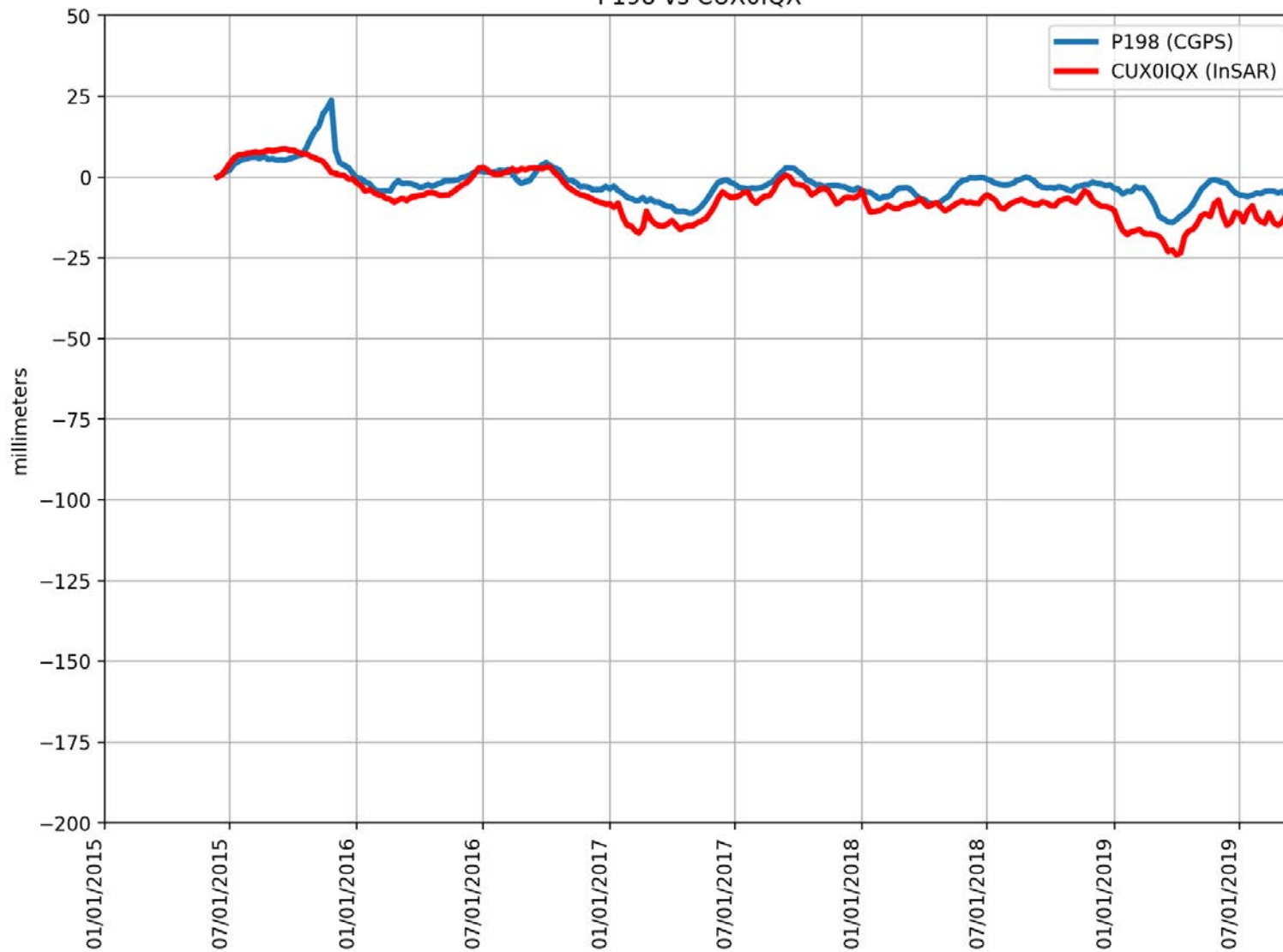
P197 vs CY1JFZ1



RMSE: 2.59 mm
Correlation: 0.83

Appendix B

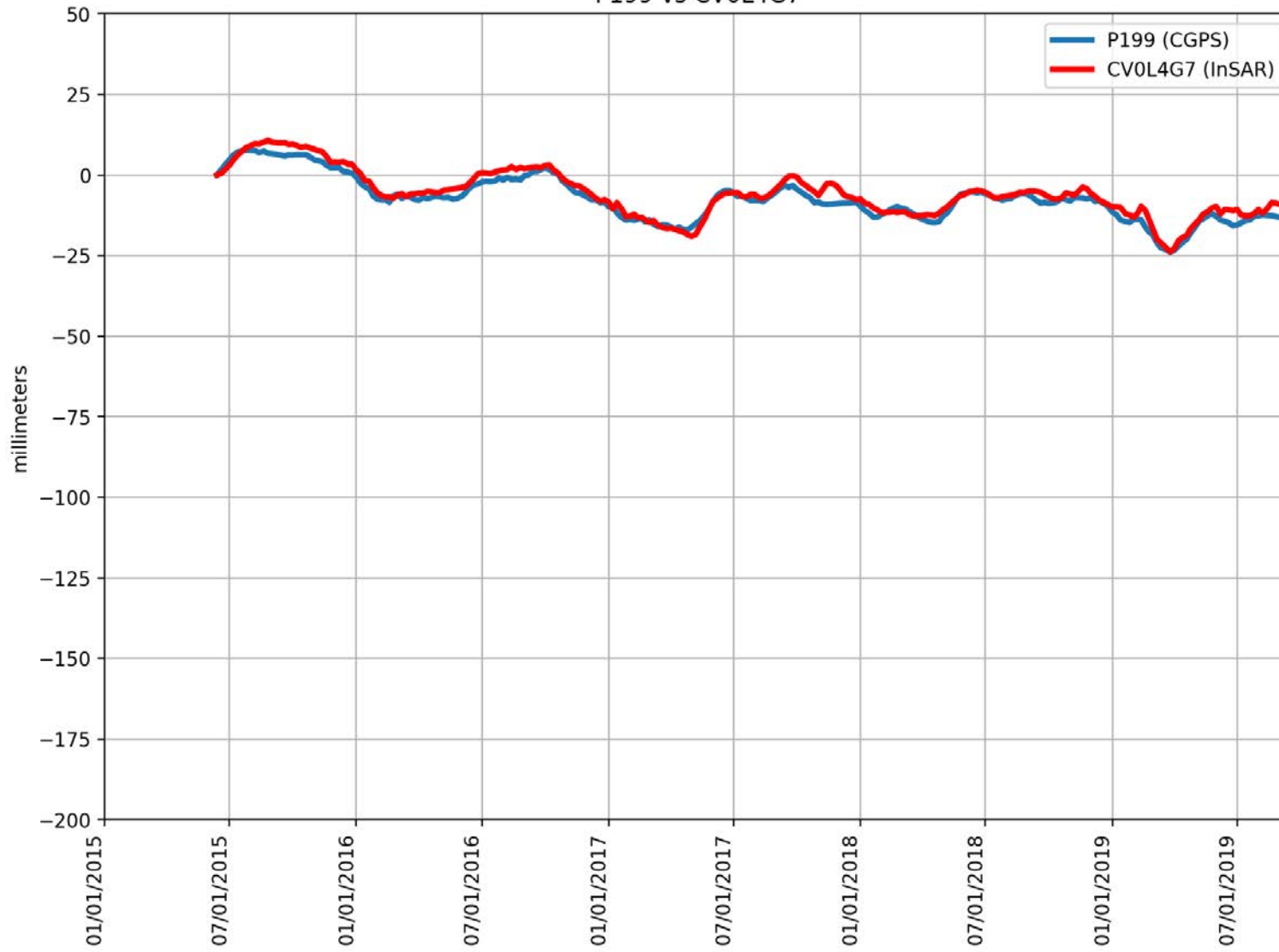
P198 vs CUX0IQX



RMSE: 5.85 mm
Correlation: 0.83

Appendix B

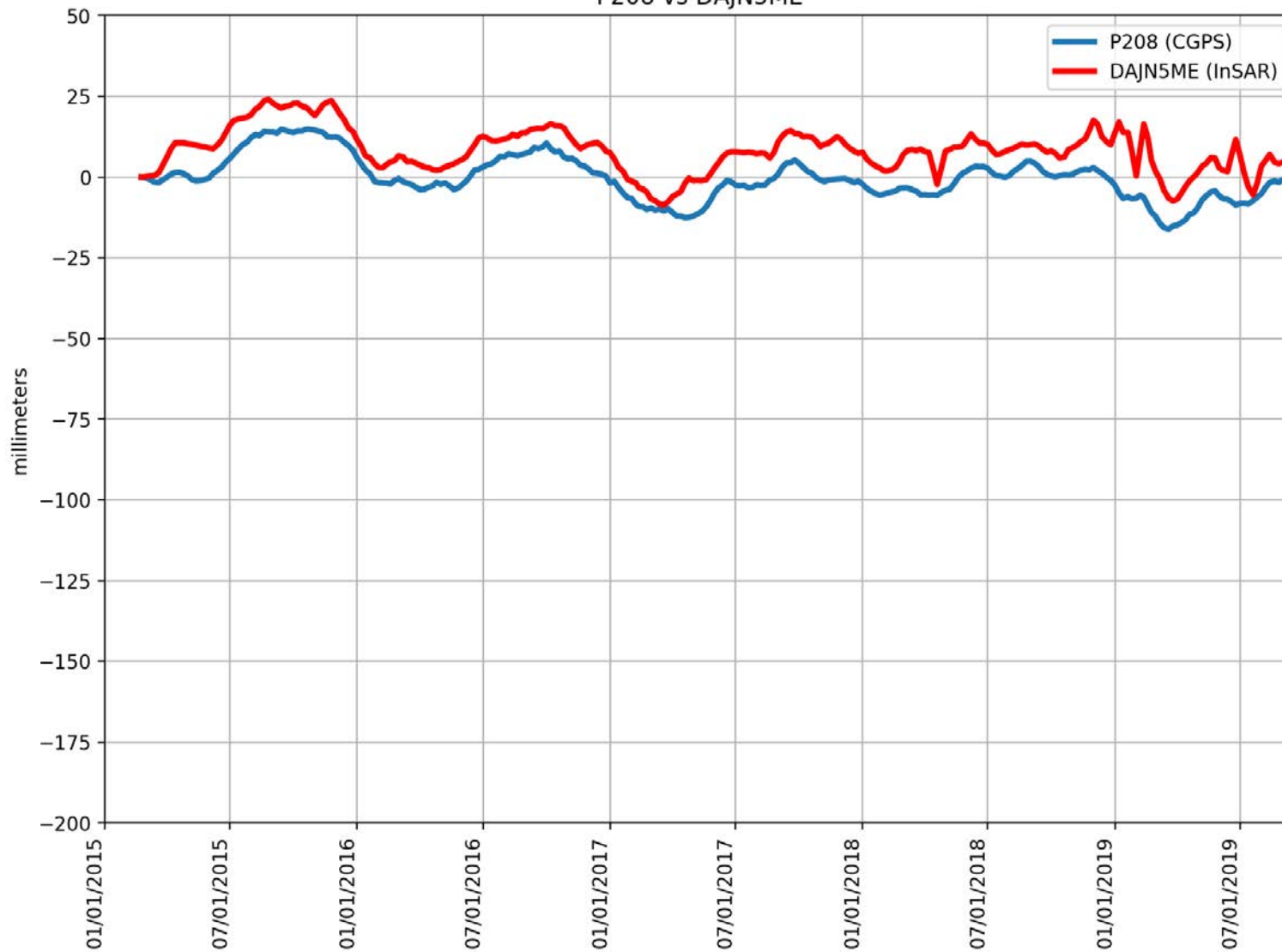
P199 vs CV0L4G7



RMSE: 2.23 mm
Correlation: 0.98

Appendix B

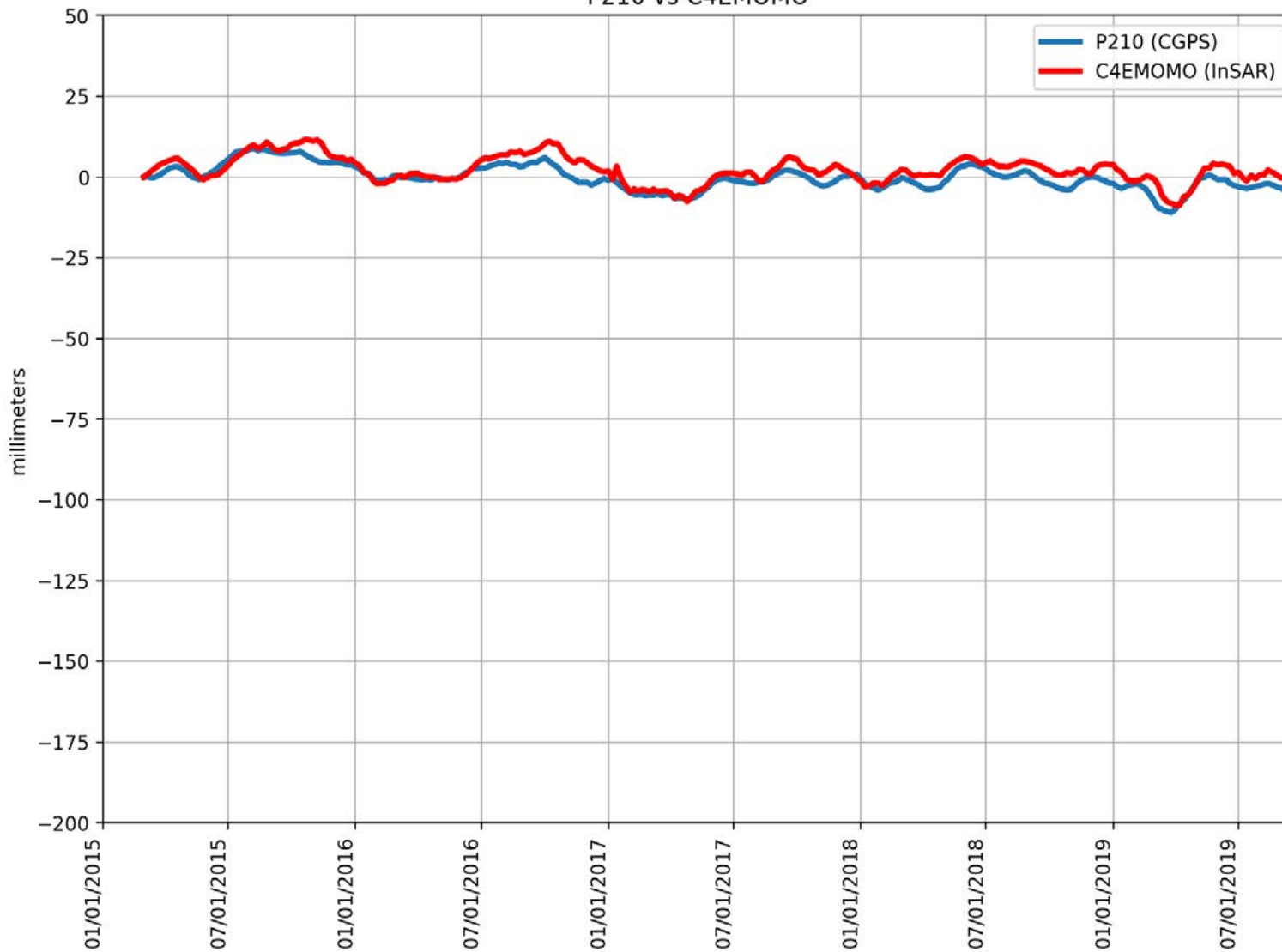
P208 vs DAJN5ME



RMSE: 9.05 mm
Correlation: 0.88

Appendix B

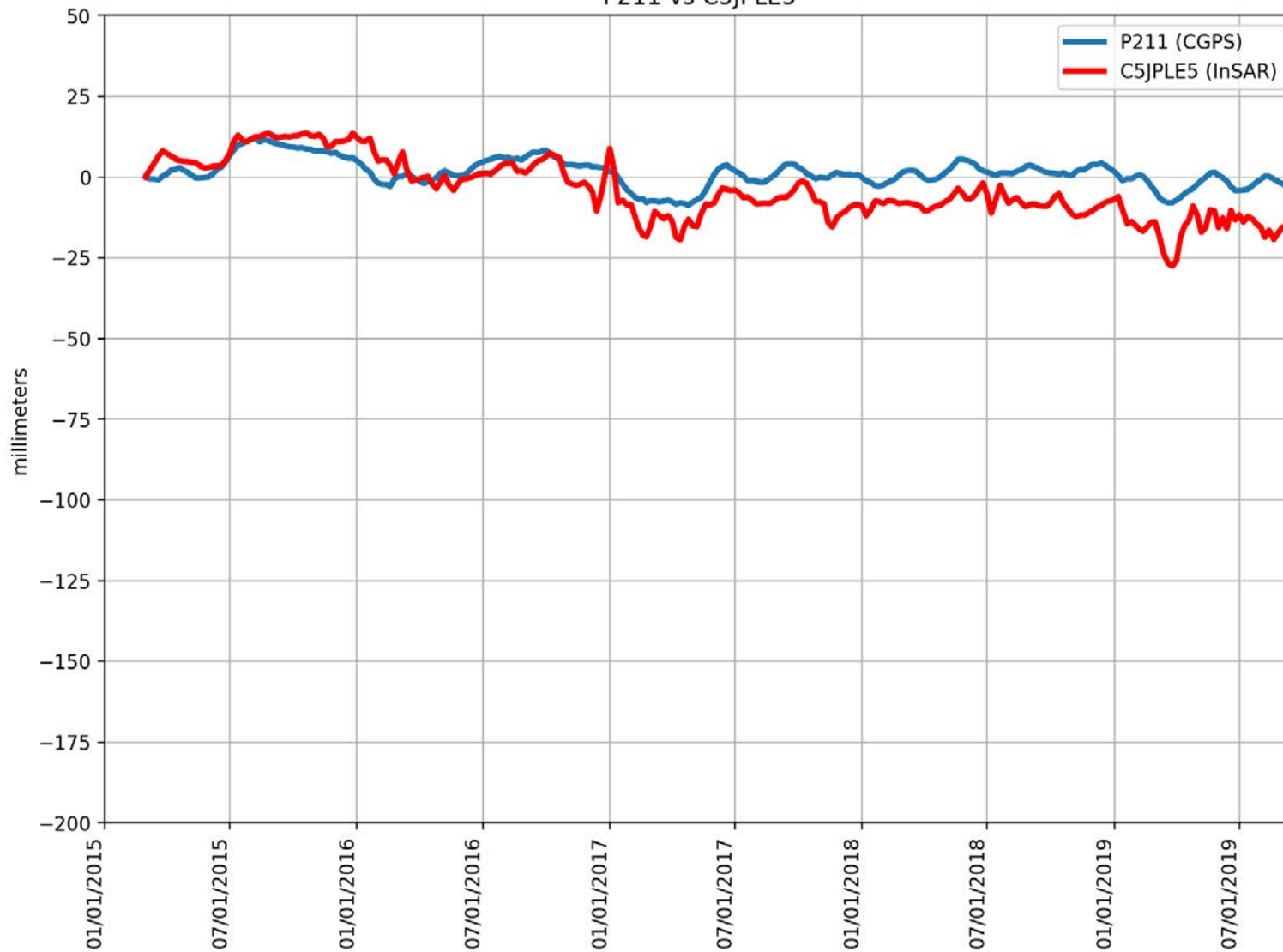
P210 vs C4EMOMO



RMSE: 3.08 mm
Correlation: 0.88

Appendix B

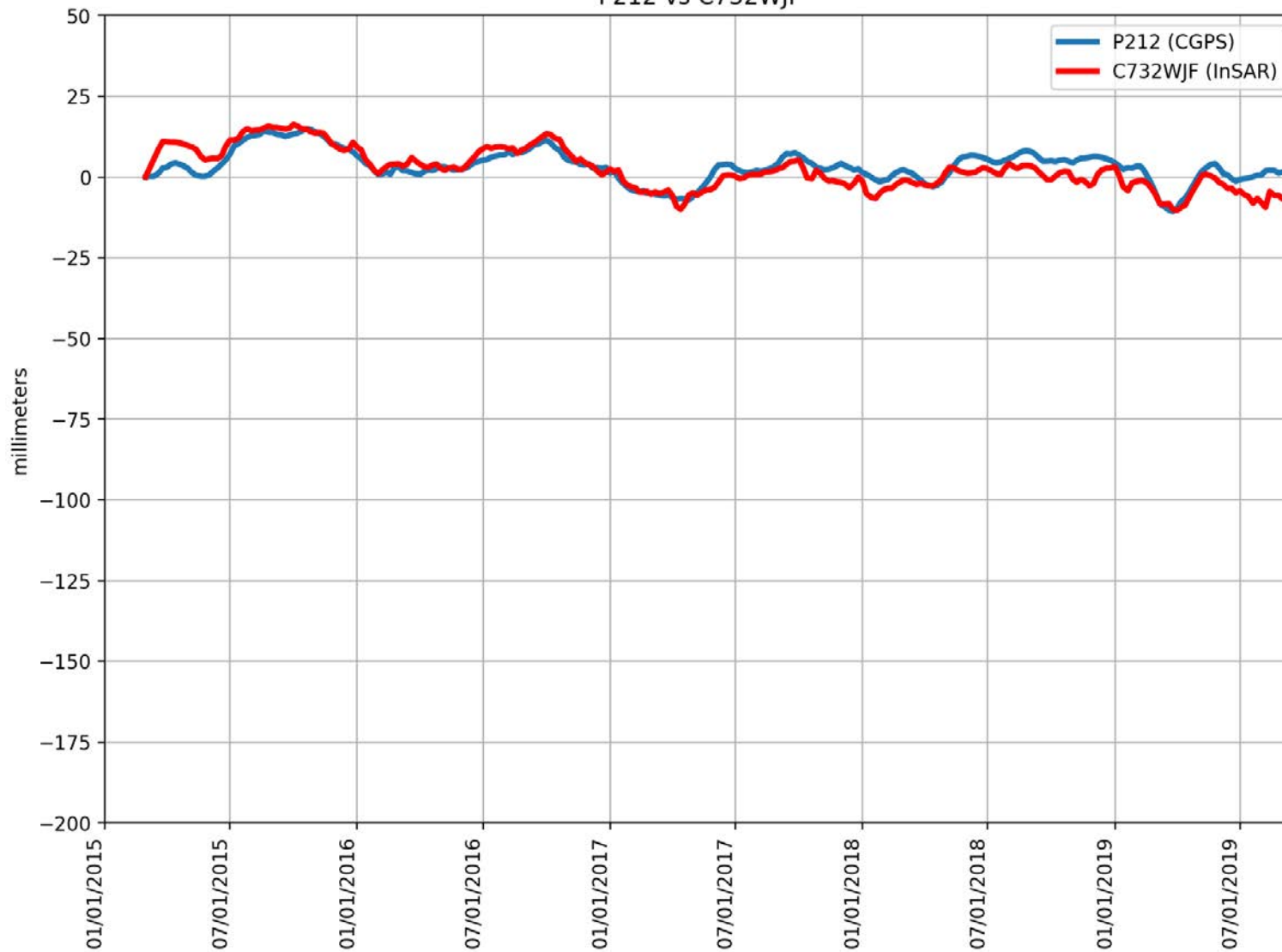
P211 vs C5JPLE5



RMSE: 8.53 mm
Correlation: 0.75

Appendix B

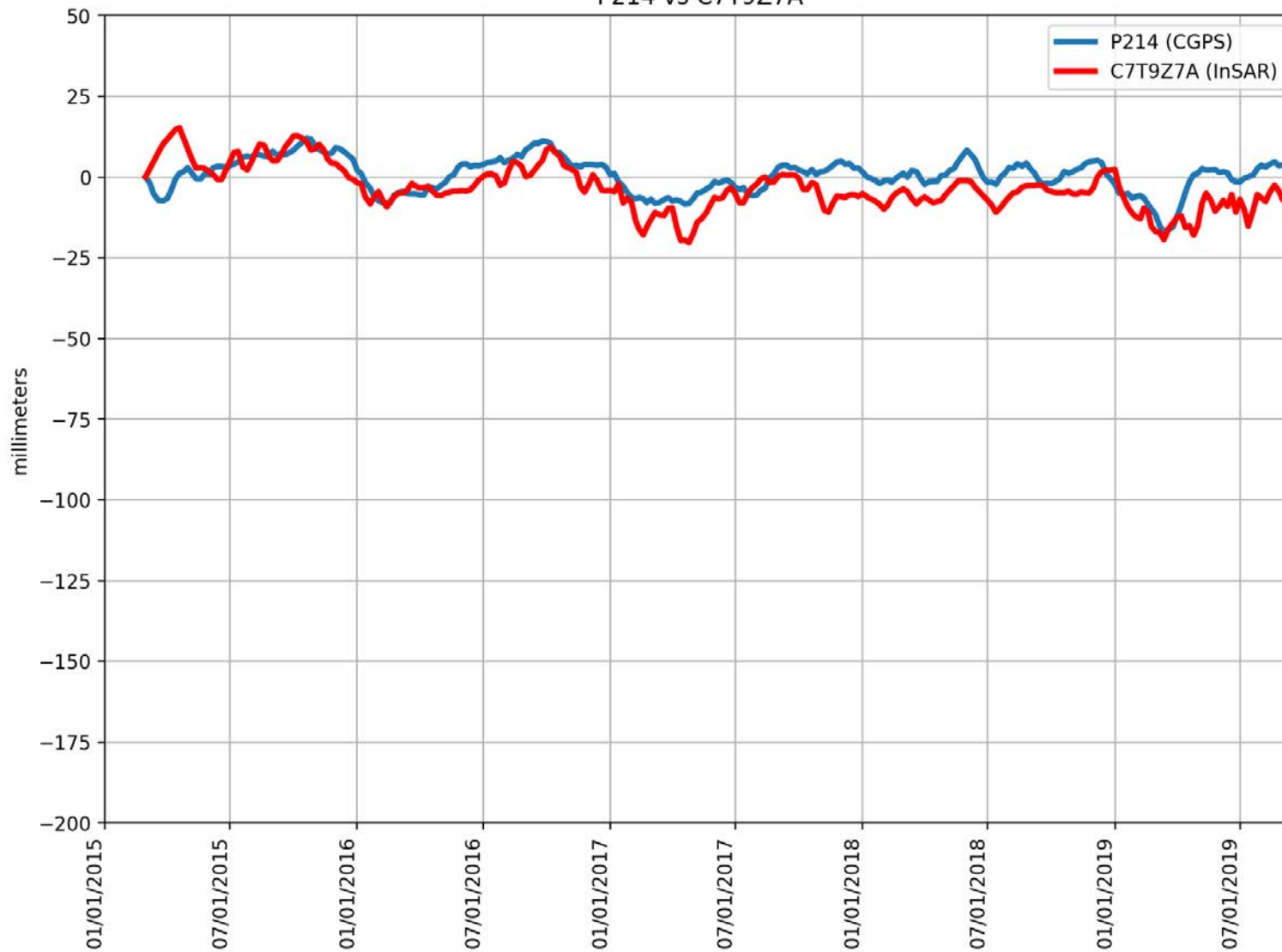
P212 vs C732WJF



RMSE: 3.66 mm
Correlation: 0.83

Appendix B

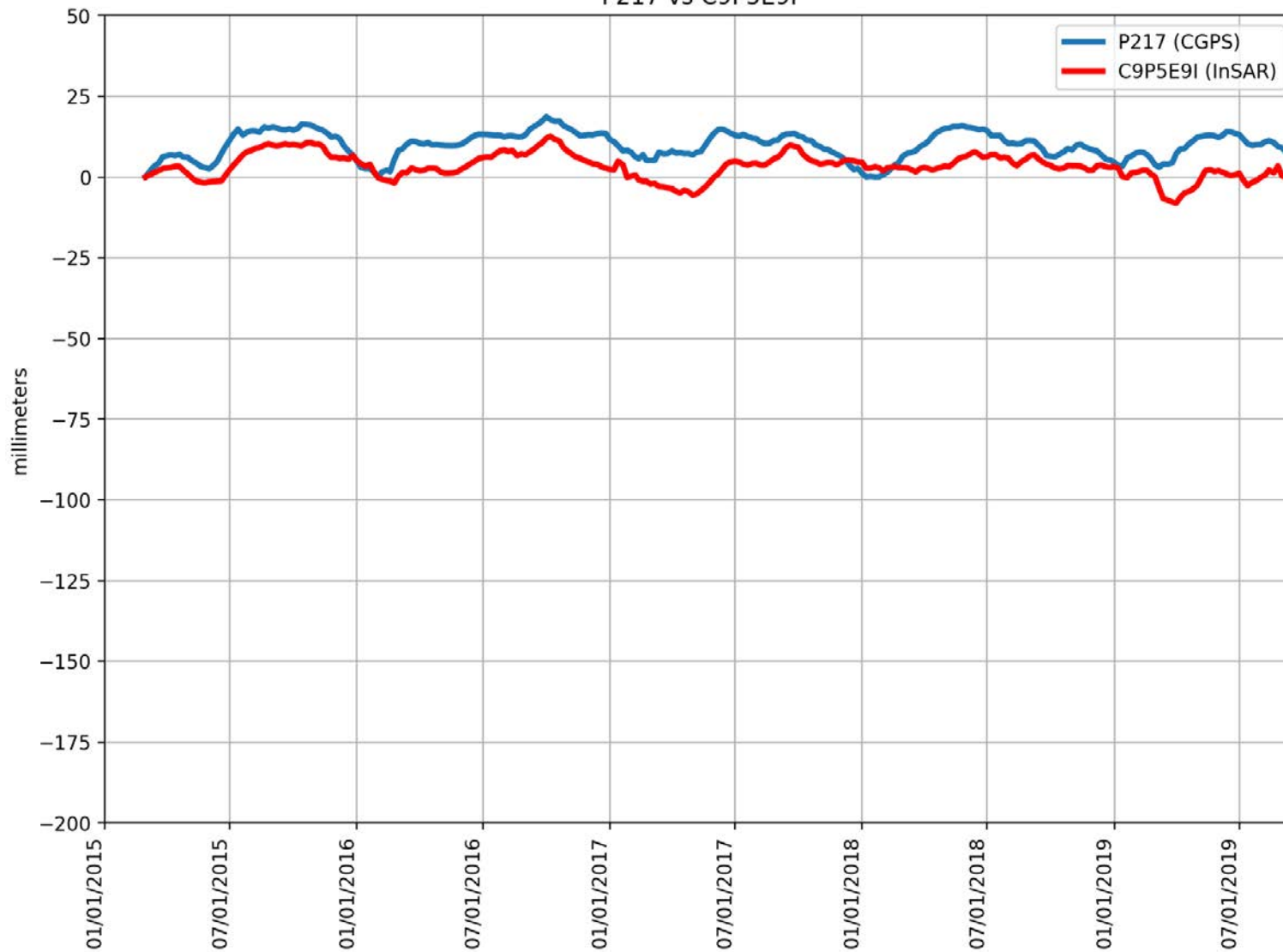
P214 vs C7T9Z7A



RMSE: 6.71 mm
Correlation: 0.64

Appendix B

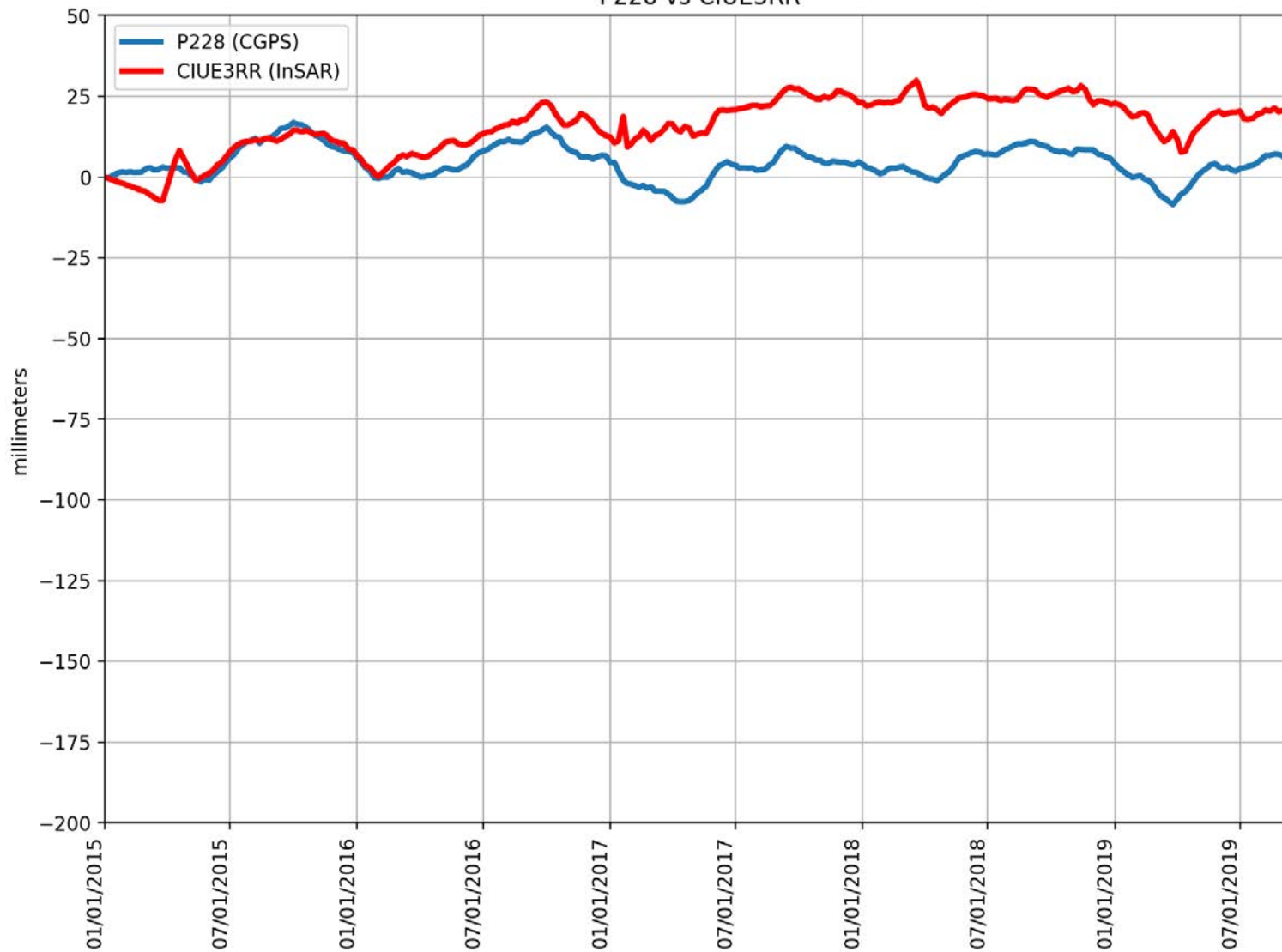
P217 vs C9P5E9I



RMSE: 7.53 mm
Correlation: 0.59

Appendix B

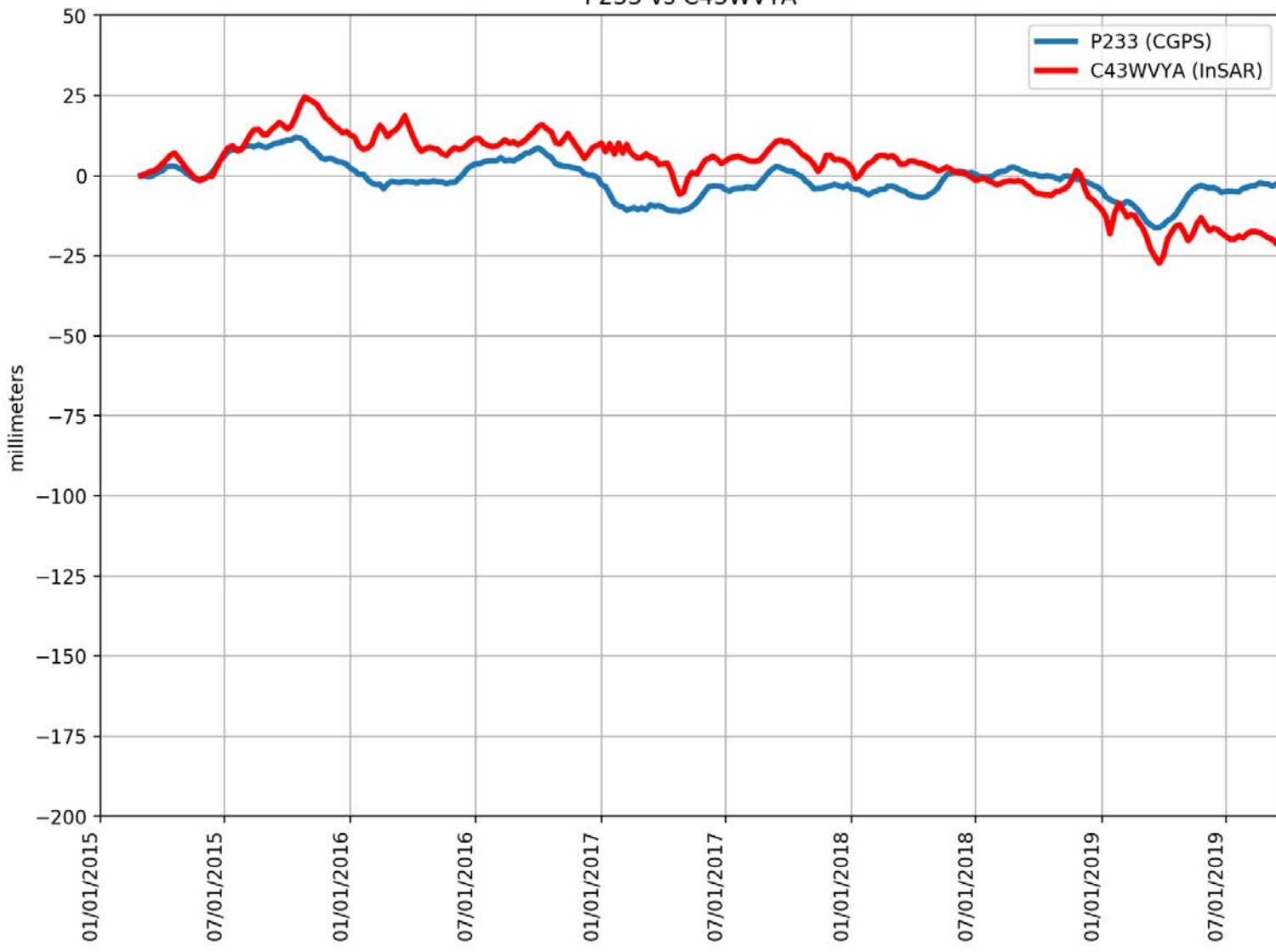
P228 vs CIUE3RR



RMSE: 14.28 mm
Correlation: 0.29

Appendix B

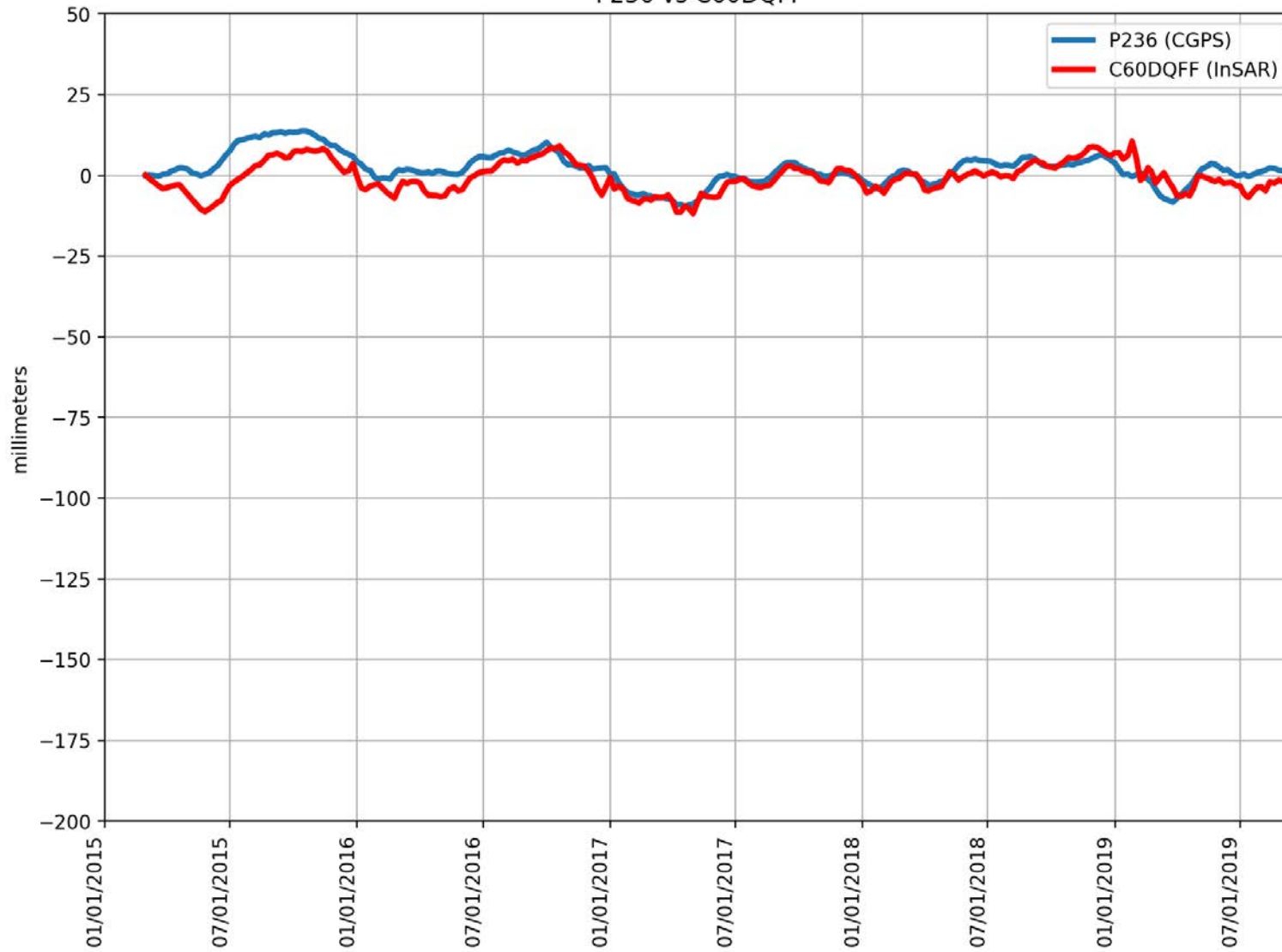
P233 vs C43WVYA



RMSE: 9.30 mm
Correlation: 0.61

Appendix B

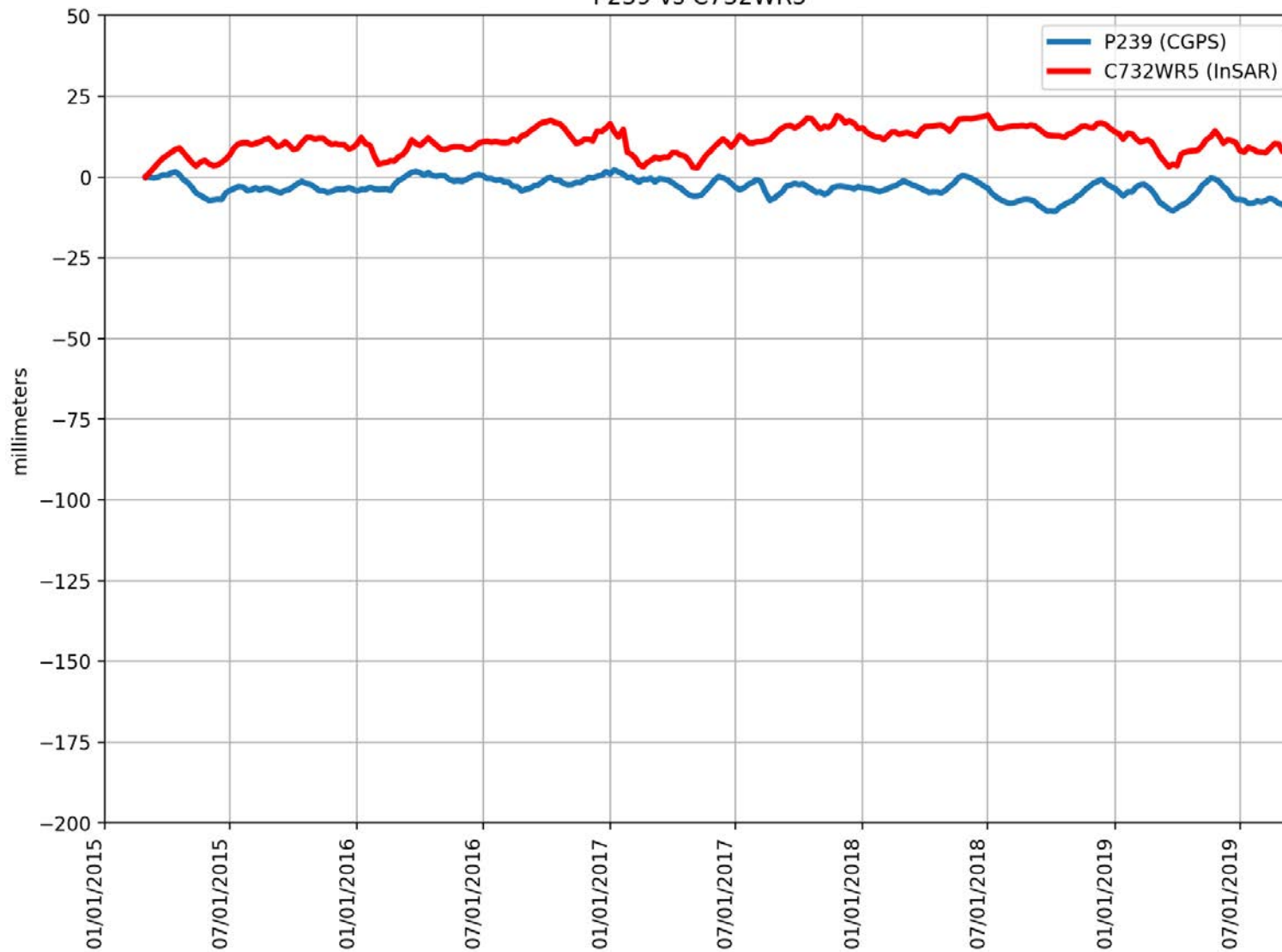
P236 vs C60DQFF



RMSE: 4.50 mm
Correlation: 0.72

Appendix B

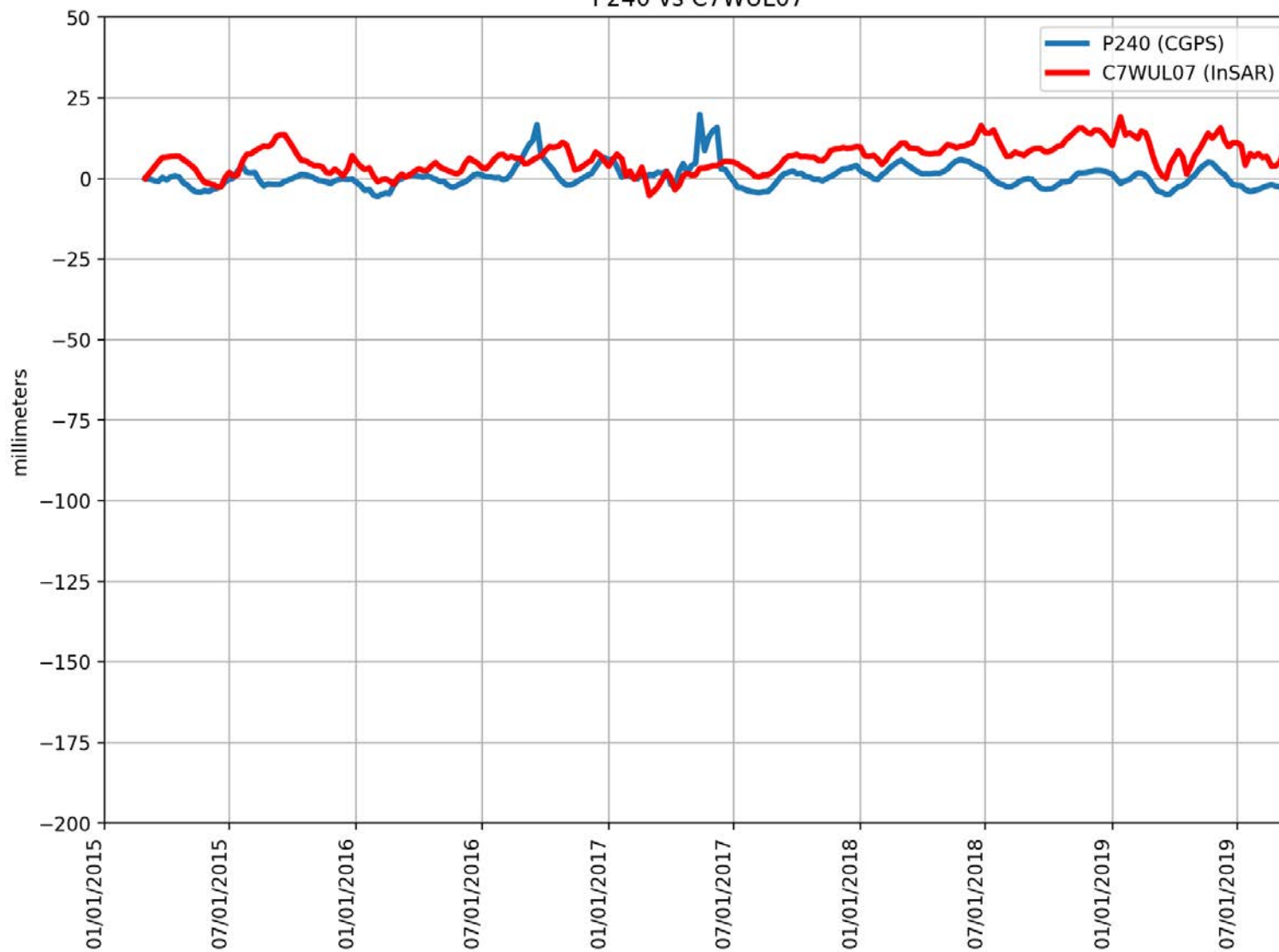
P239 vs C732WR5



RMSE: 15.28 mm
Correlation: 0.07

Appendix B

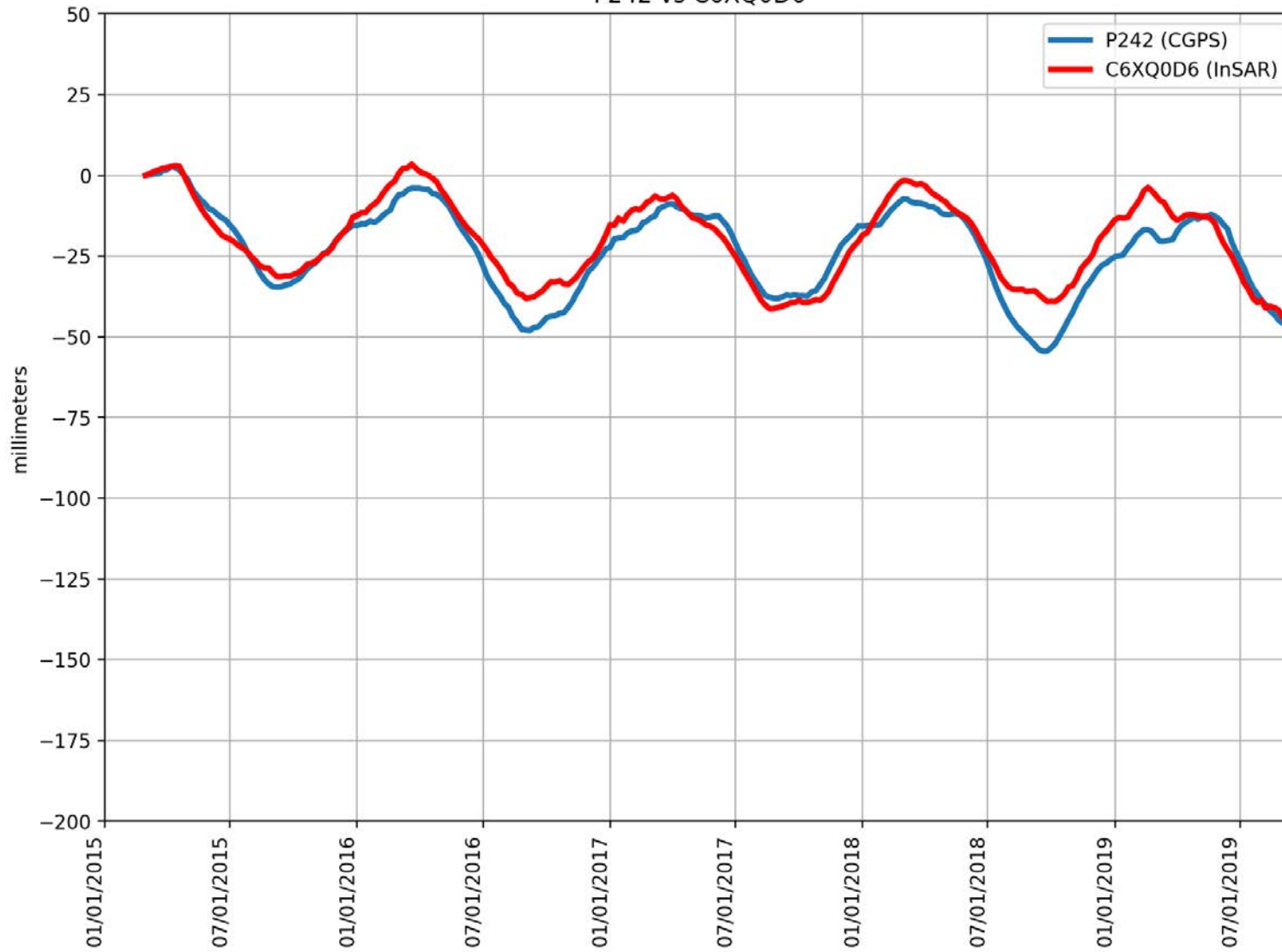
P240 vs C7WUL07



RMSE: 7.68 mm
Correlation: 0.20

Appendix B

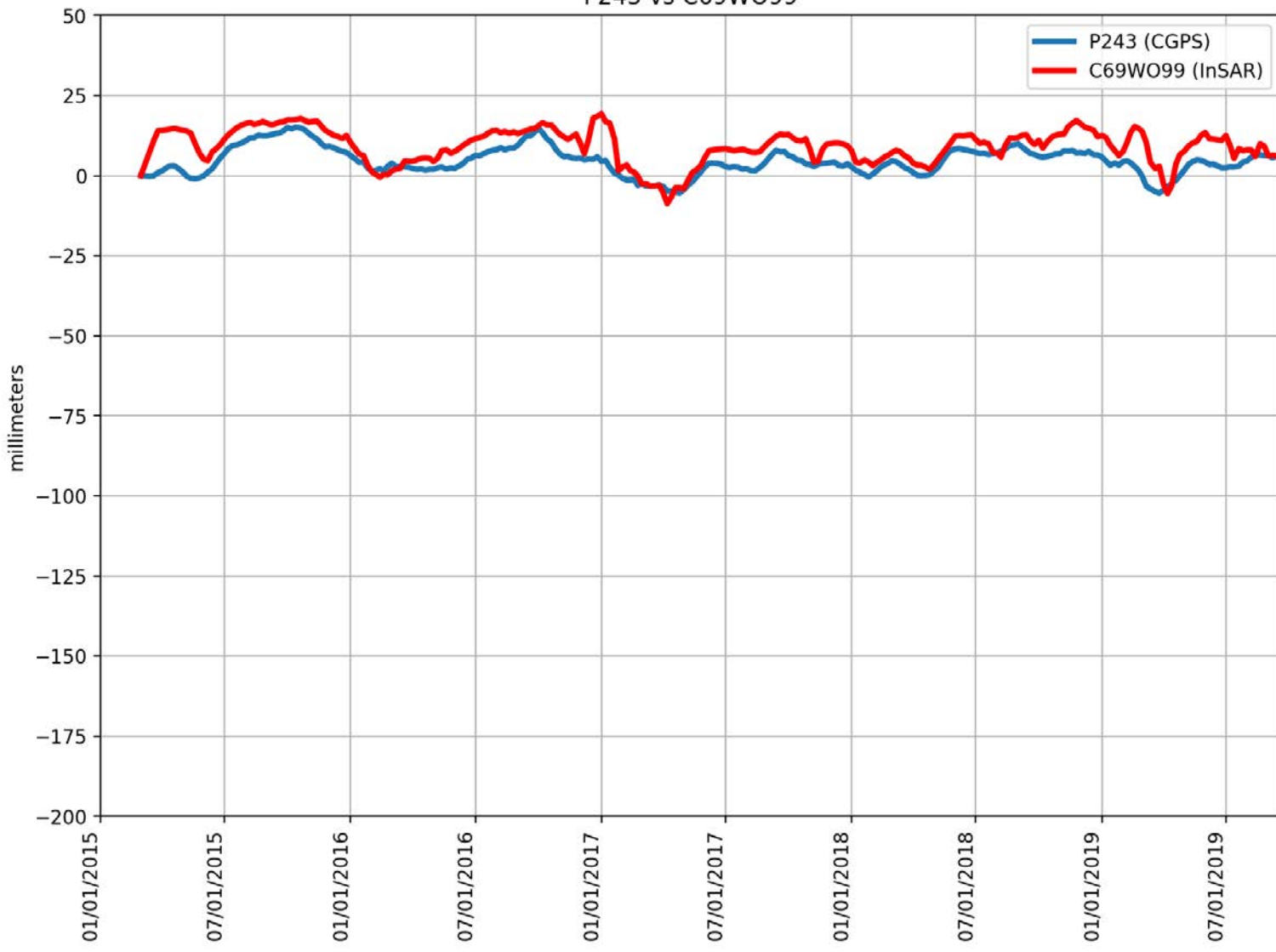
P242 vs C6XQ0D6



RMSE: 6.15 mm
Correlation: 0.92

Appendix B

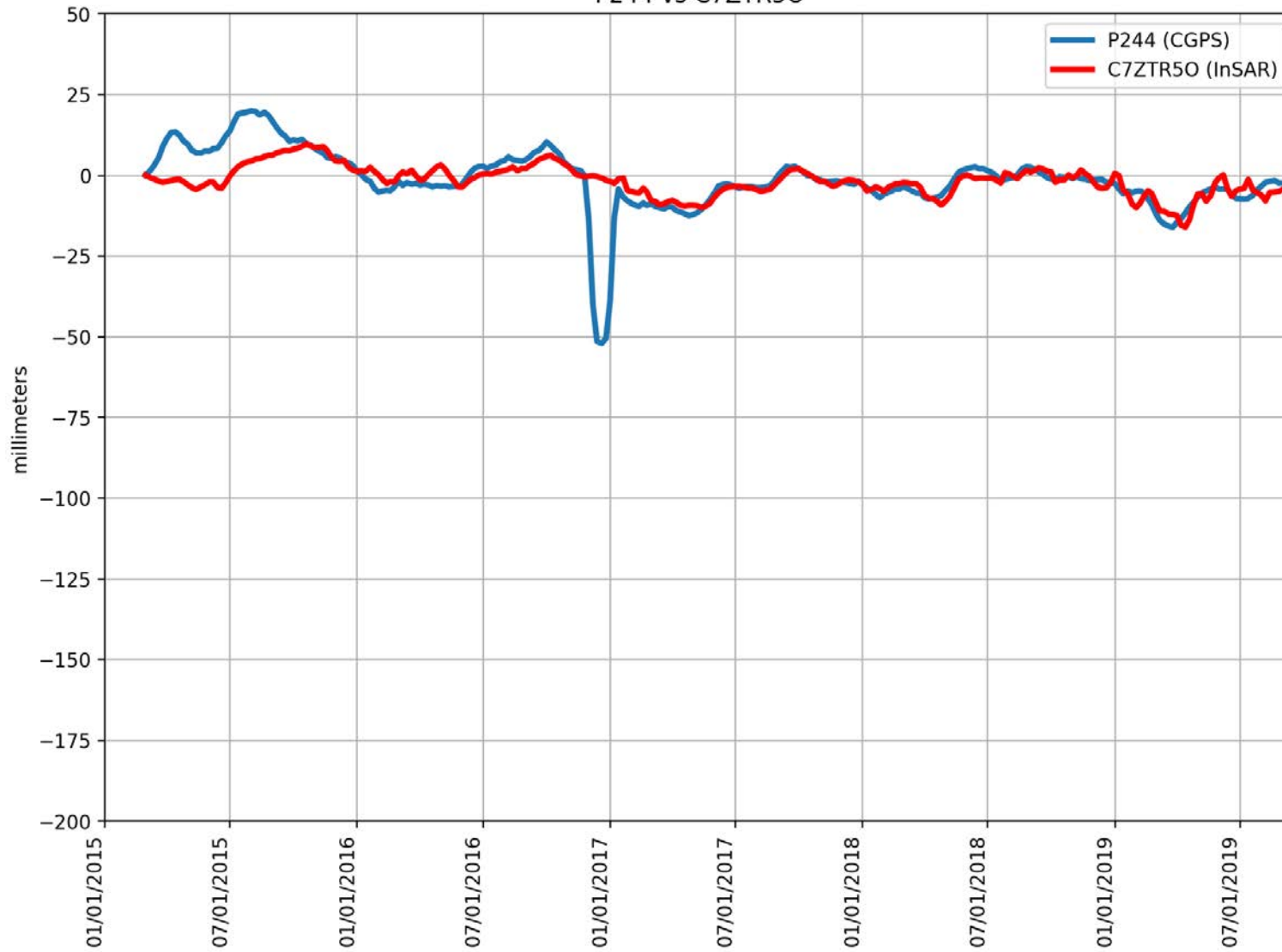
P243 vs C69WO99



RMSE: 5.68 mm
Correlation: 0.79

Appendix B

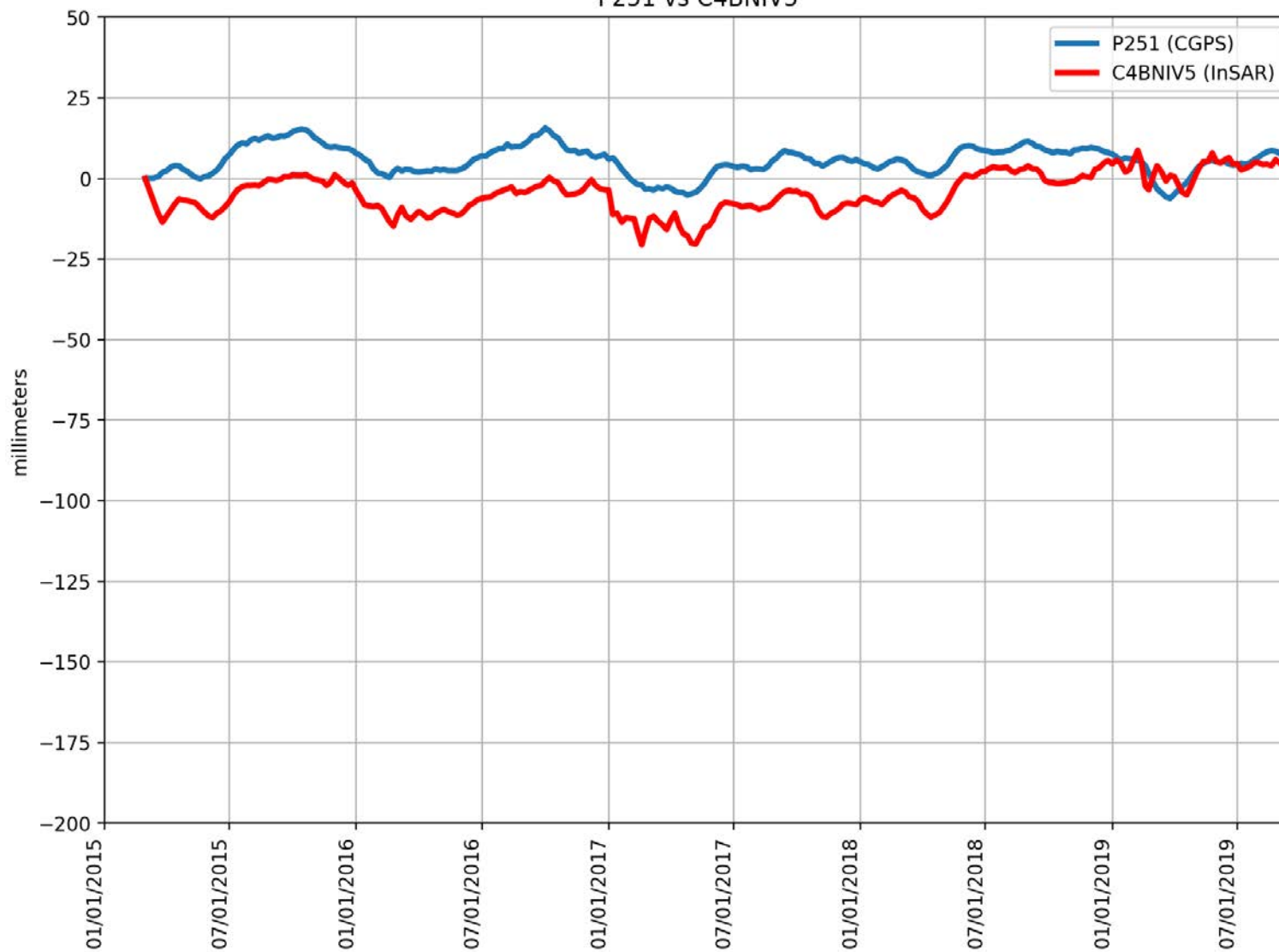
P244 vs C7ZTR50



RMSE: 7.92 mm
Correlation: 0.55

Appendix B

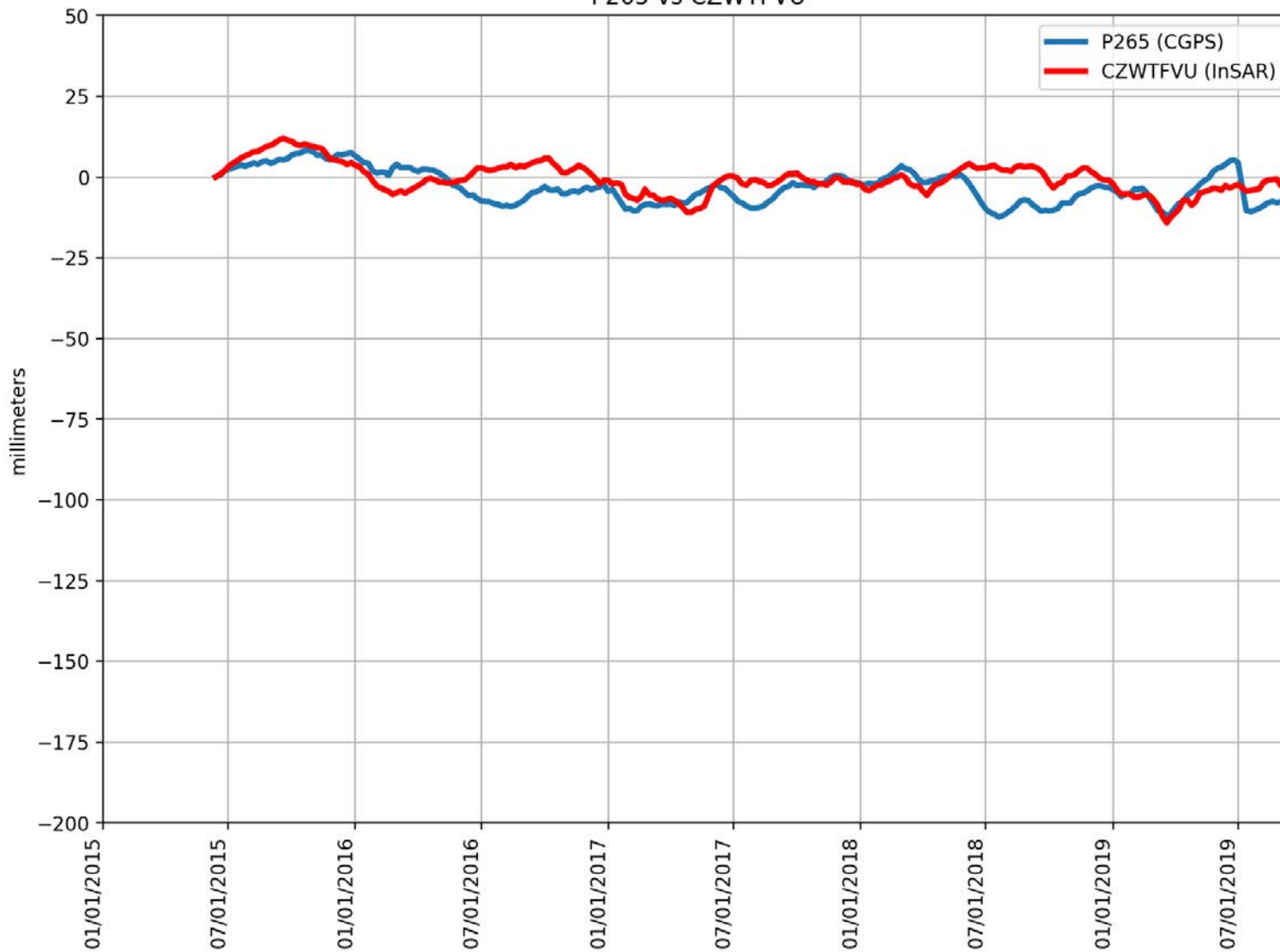
P251 vs C4BNIV5



RMSE: 11.17 mm
Correlation: 0.58

Appendix B

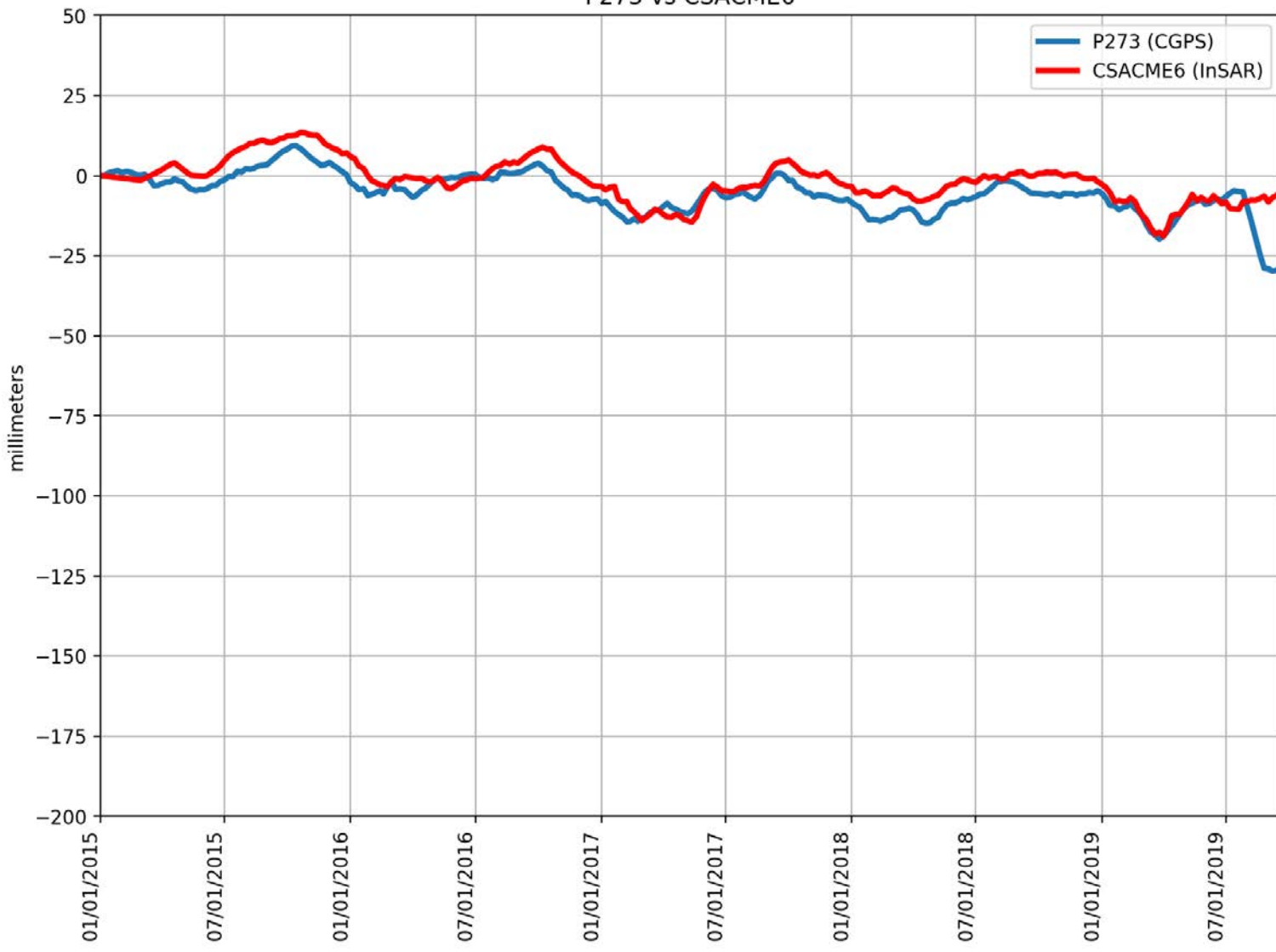
P265 vs CZWTFVU



RMSE: 5.82 mm
Correlation: 0.45

Appendix B

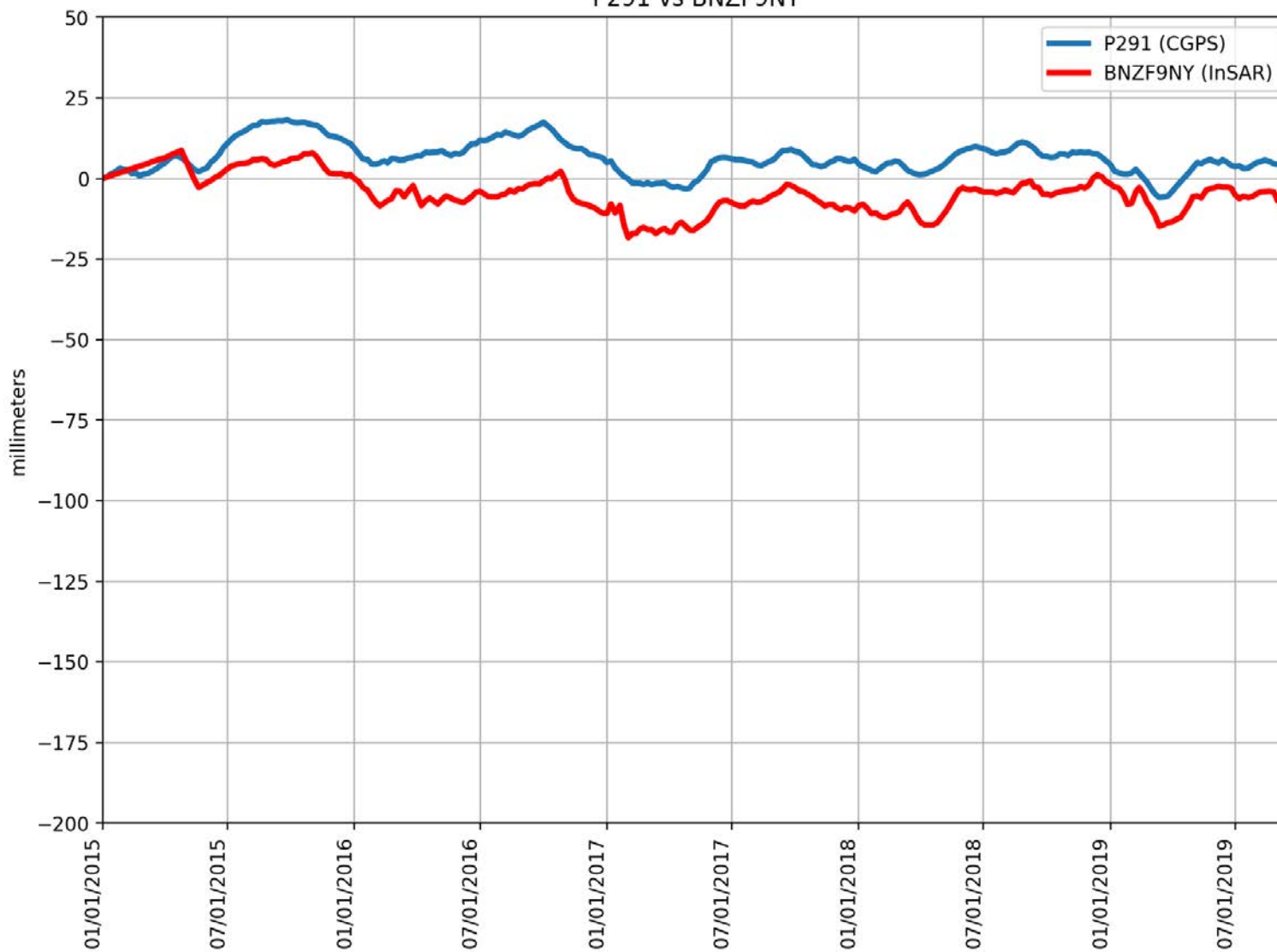
P273 vs CSACME6



RMSE: 5.65 mm
Correlation: 0.80

Appendix B

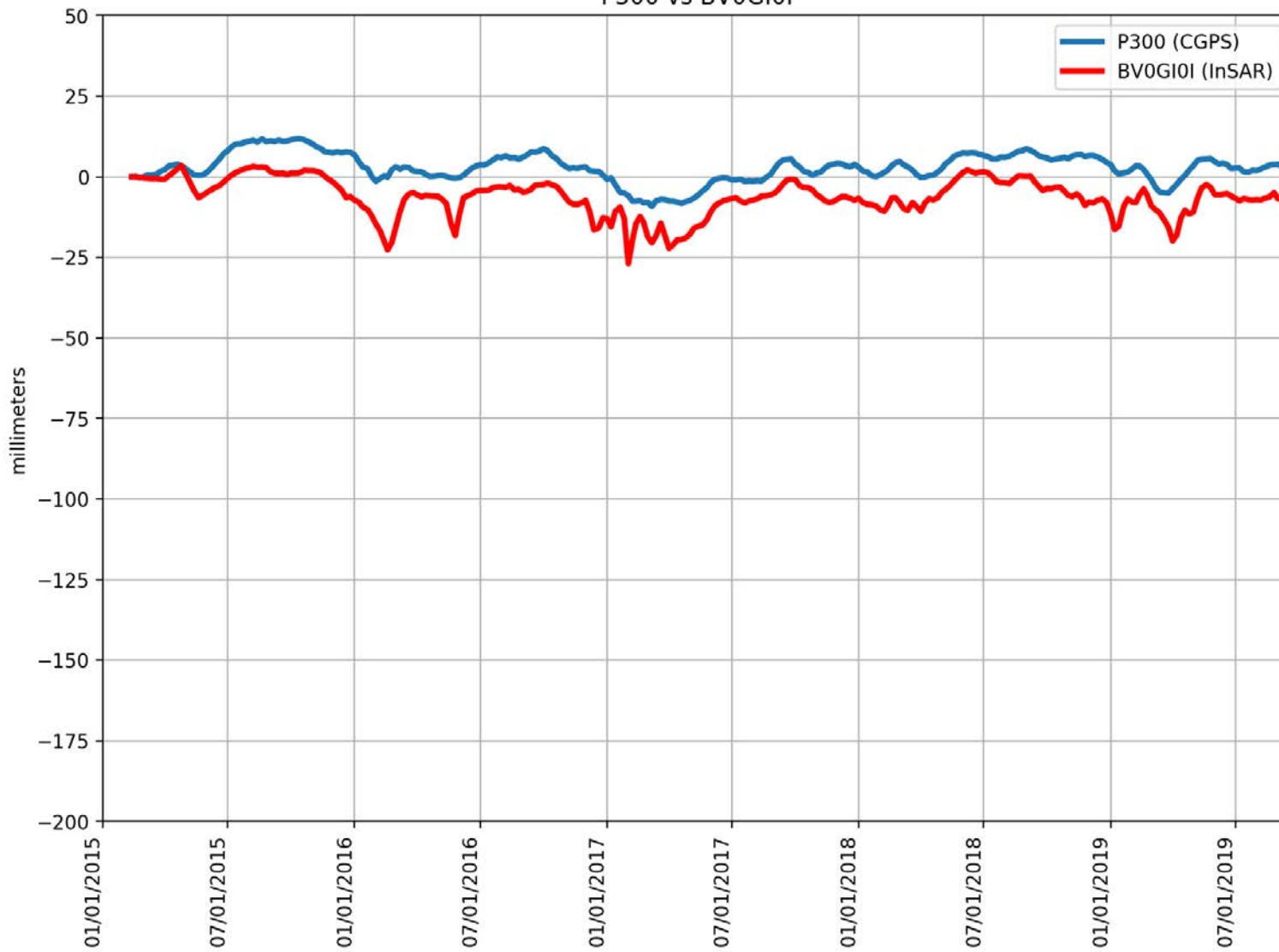
P291 vs BNZF9NY



RMSE: 12.06 mm
Correlation: 0.65

Appendix B

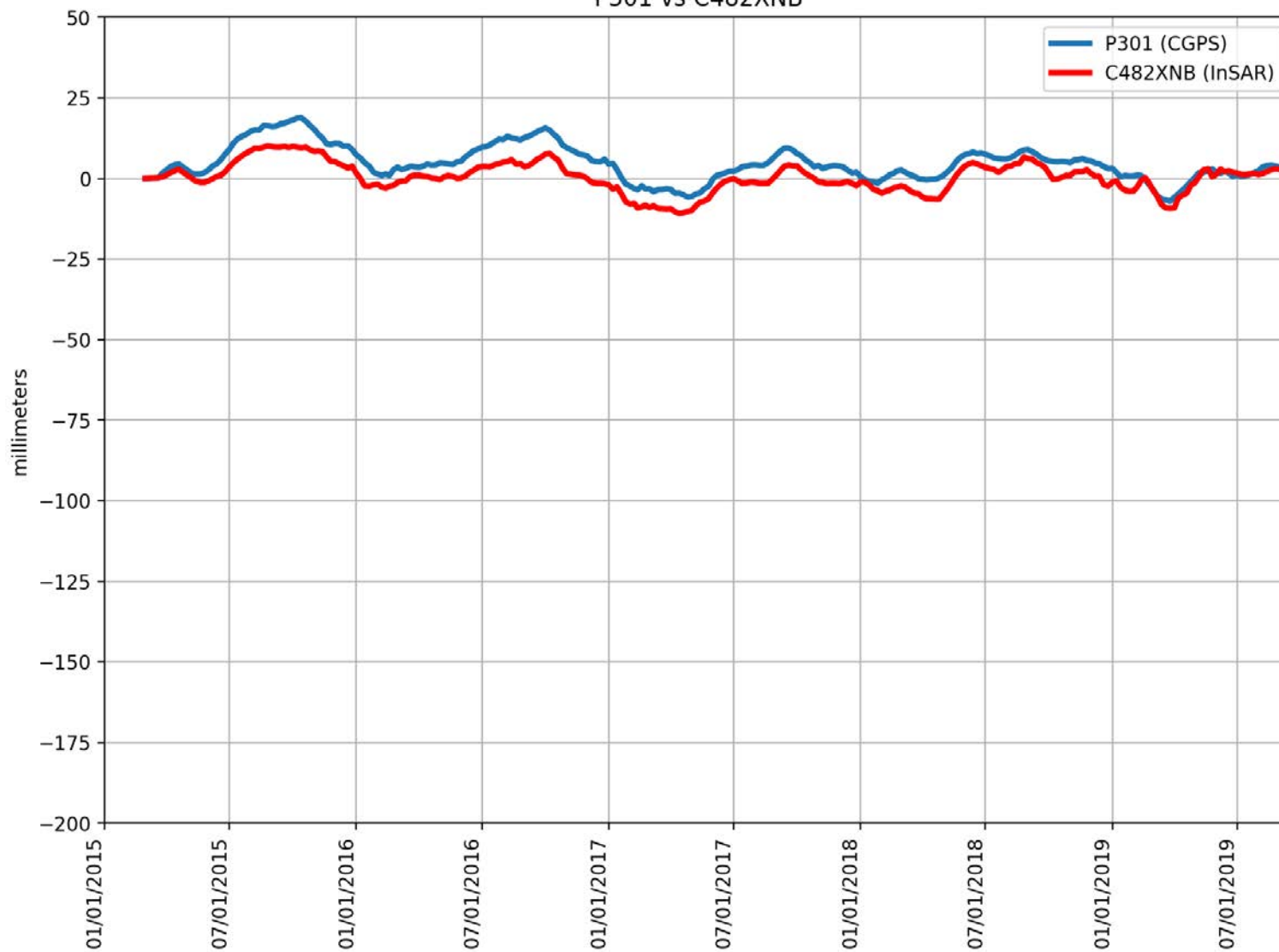
P300 vs BV0GI0I



RMSE: 9.91 mm
Correlation: 0.78

Appendix B

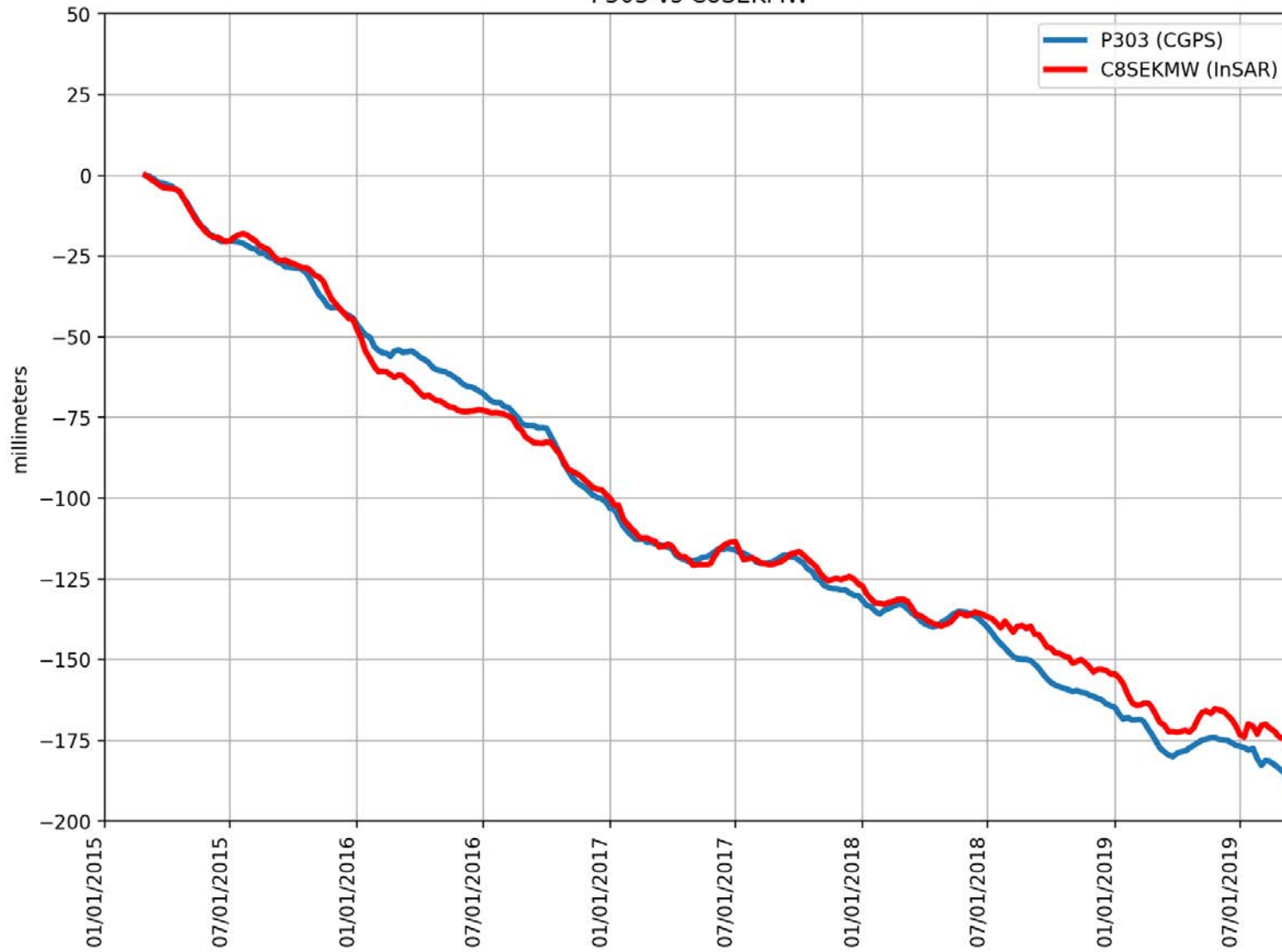
P301 vs C482XNB



RMSE: 4.86 mm
Correlation: 0.91

Appendix B

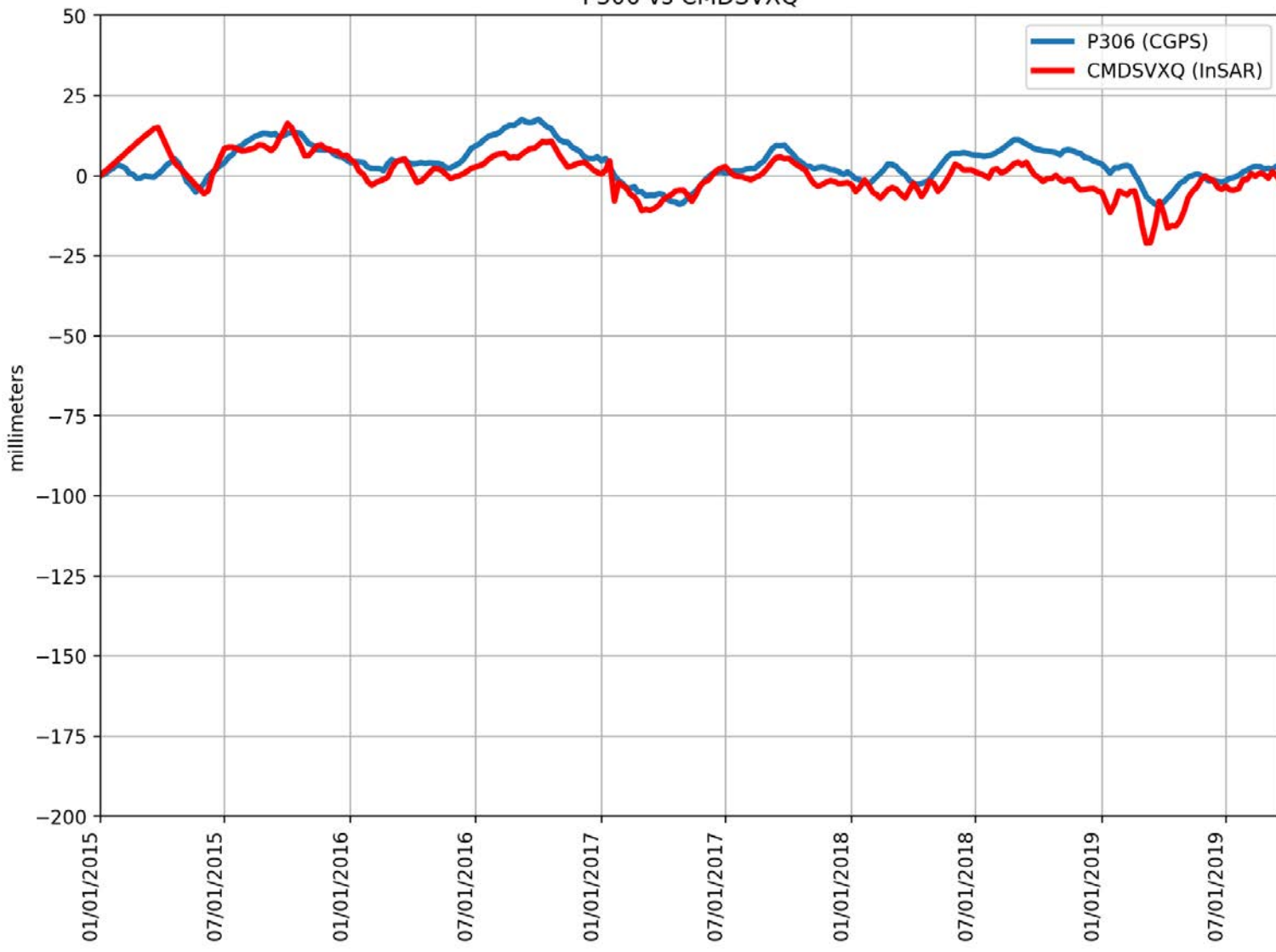
P303 vs C8SEKMW



RMSE: 5.53 mm
Correlation: 1.00

Appendix B

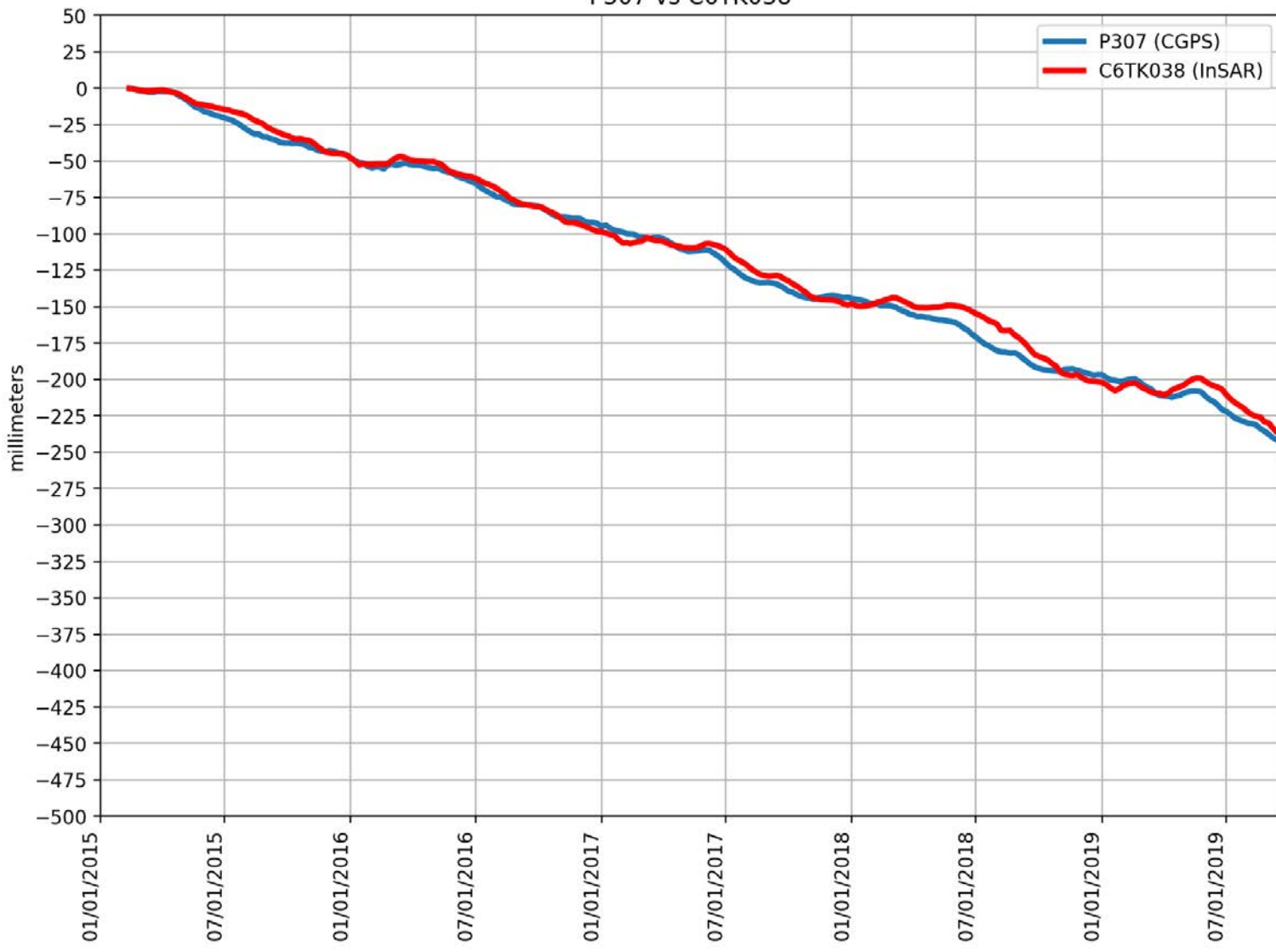
P306 vs CMDSVXQ



RMSE: 5.64 mm
Correlation: 0.71

Appendix B

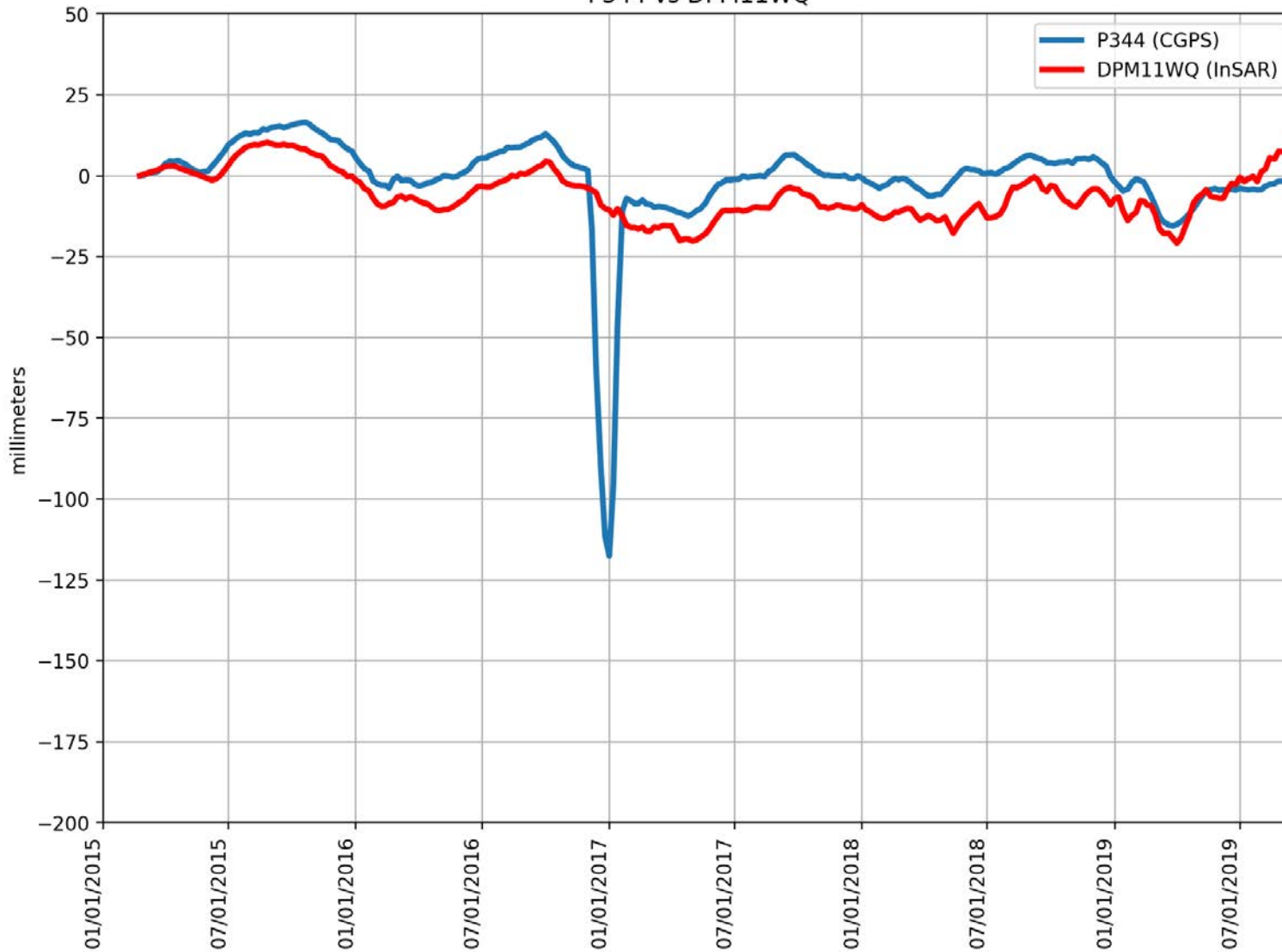
P307 vs C6TK038



RMSE: 6.32 mm
Correlation: 1.00

Appendix B

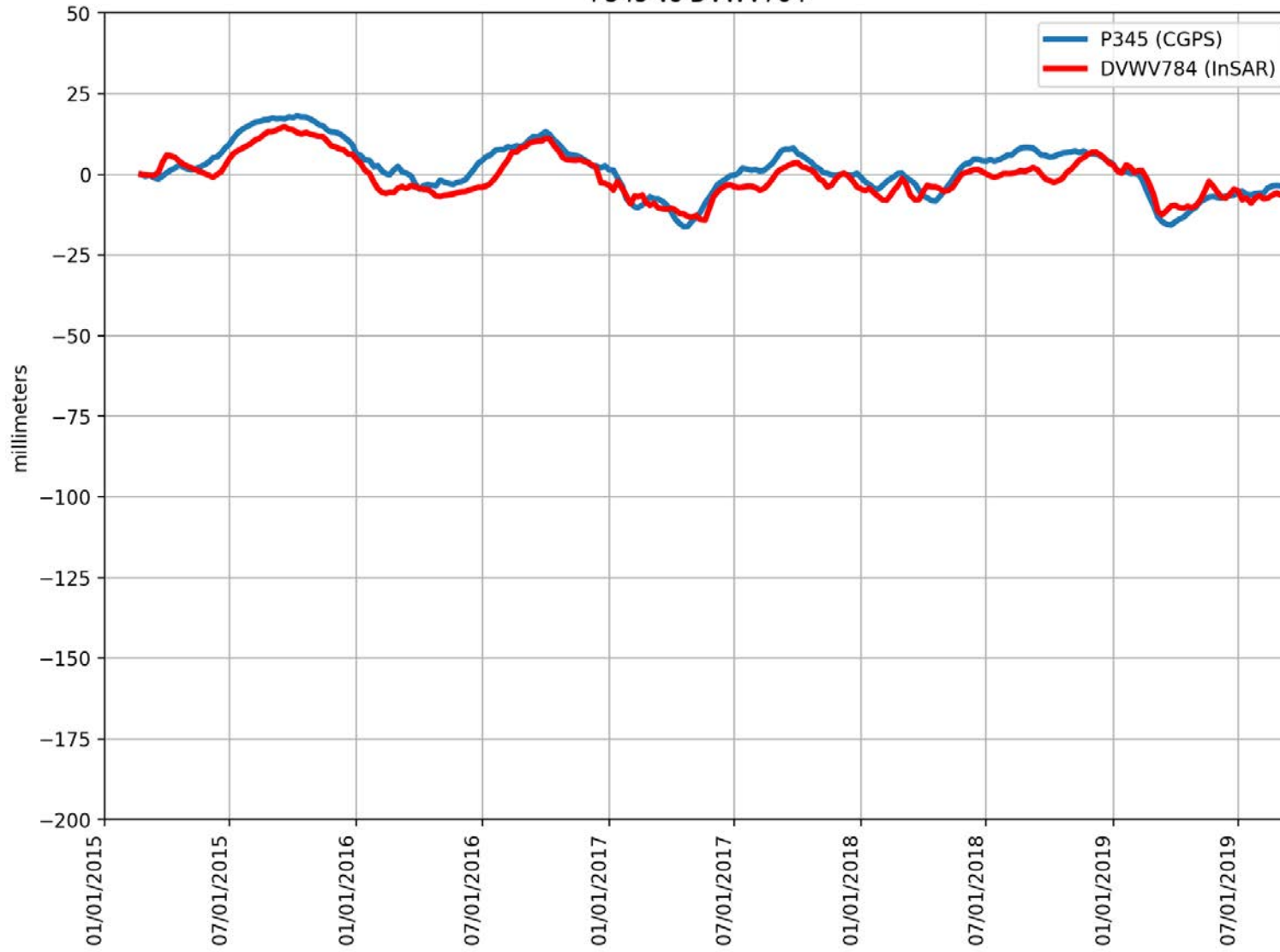
P344 vs DPM11WQ



RMSE: 14.41 mm
Correlation: 0.43

Appendix B

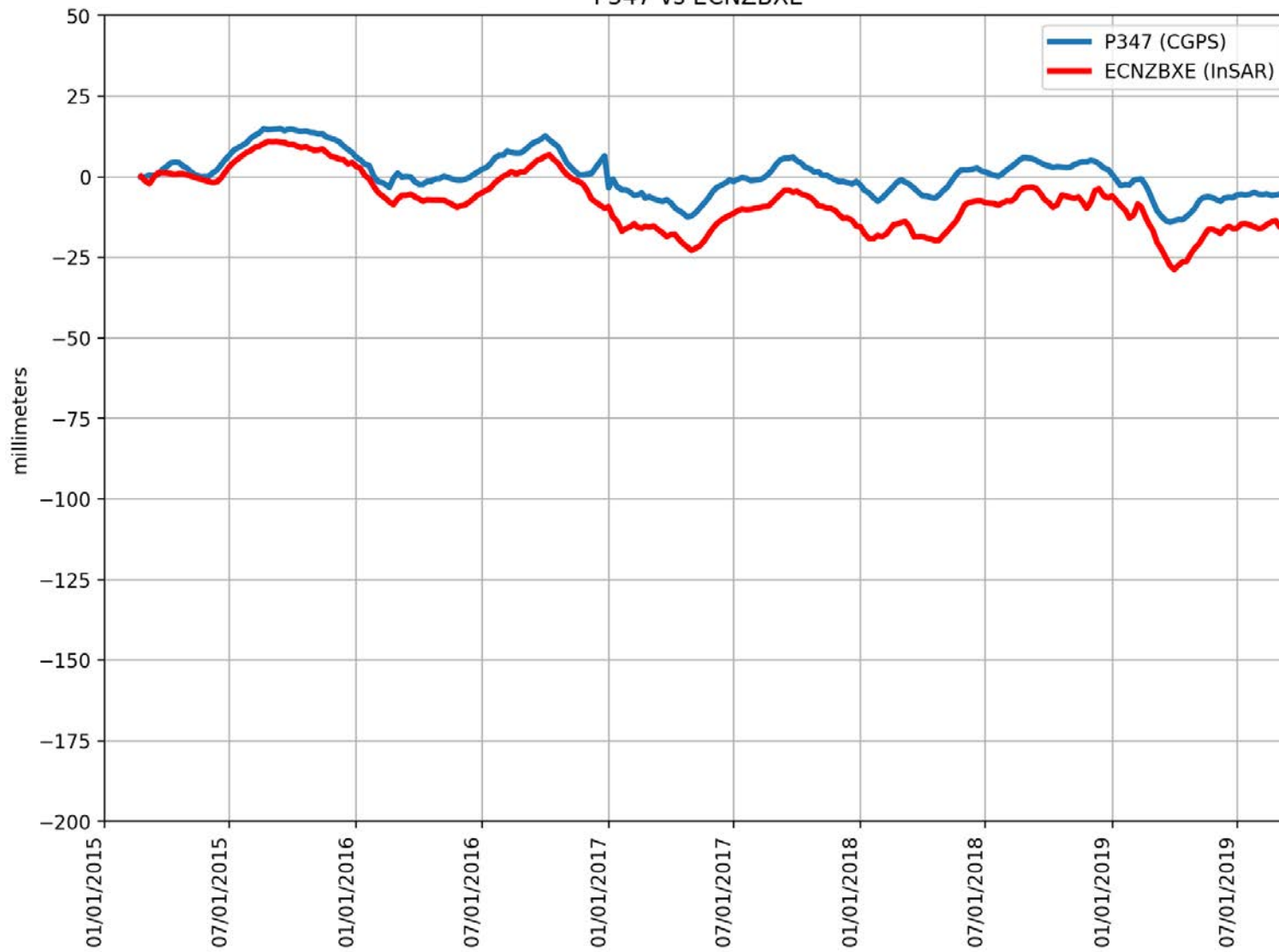
P345 vs DVWV784



RMSE: 3.89 mm
Correlation: 0.92

Appendix B

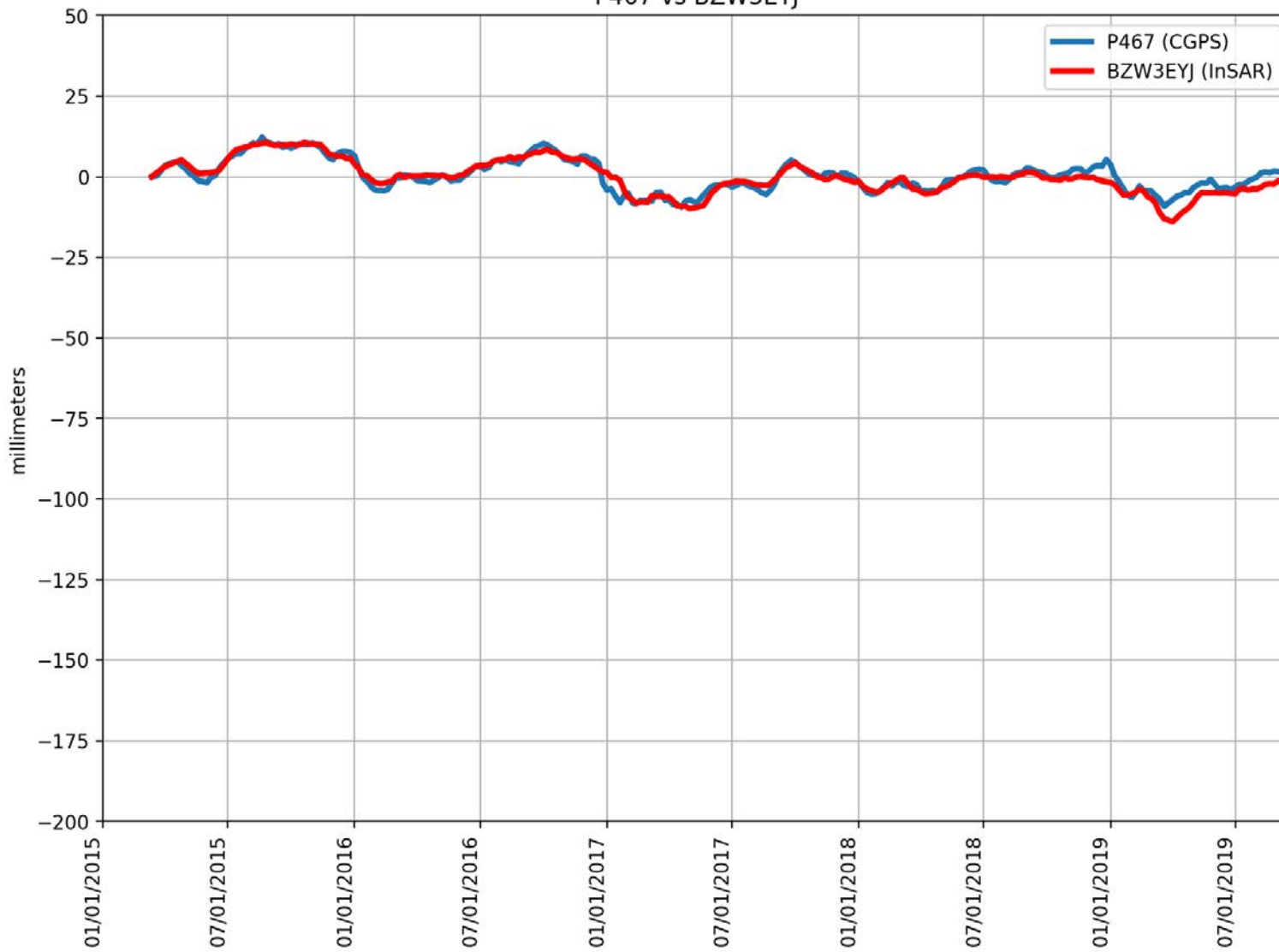
P347 vs ECNZBXE



RMSE: 8.96 mm
Correlation: 0.94

Appendix B

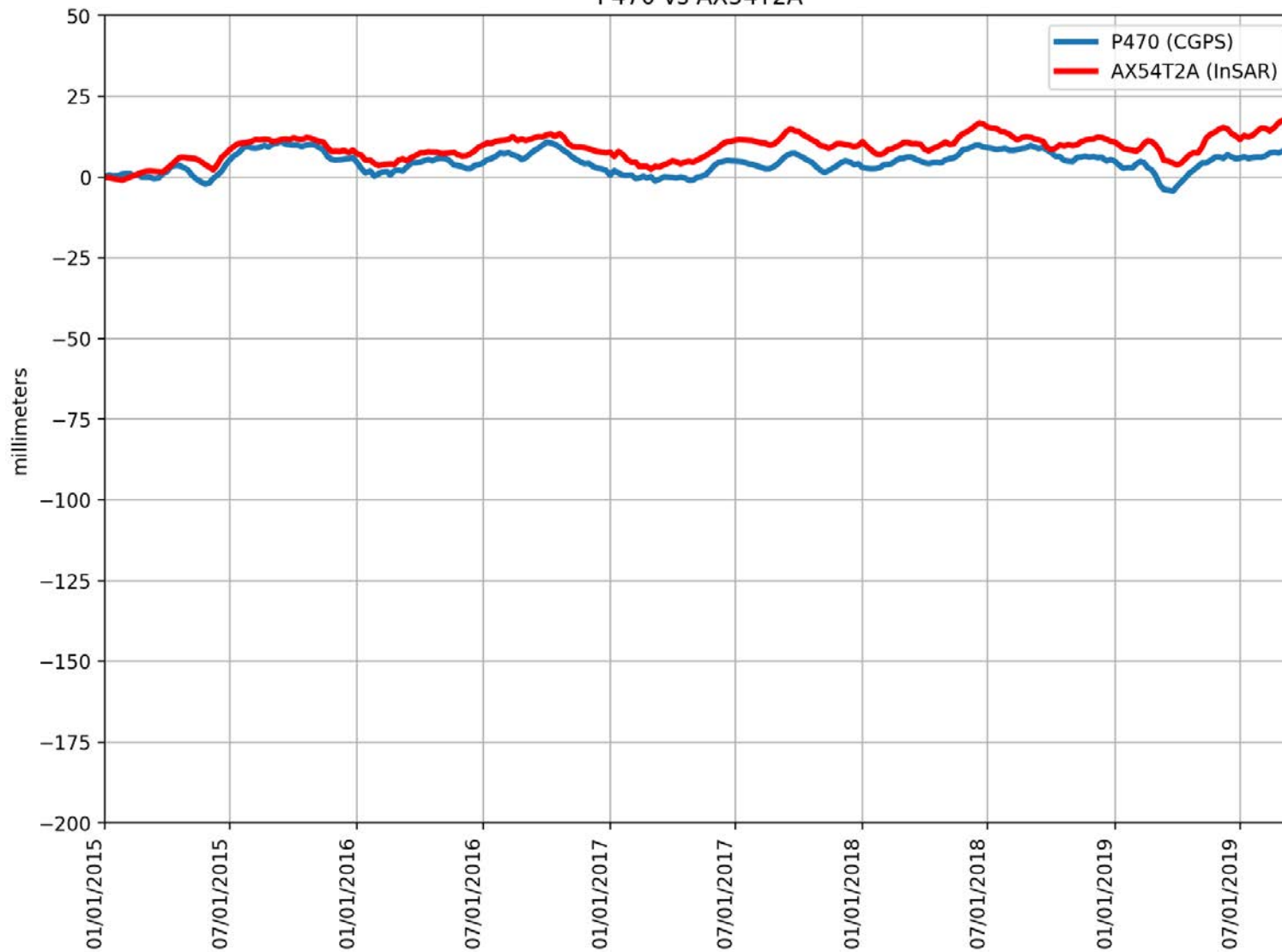
P467 vs BZW3EYJ



RMSE: 2.06 mm
Correlation: 0.92

Appendix B

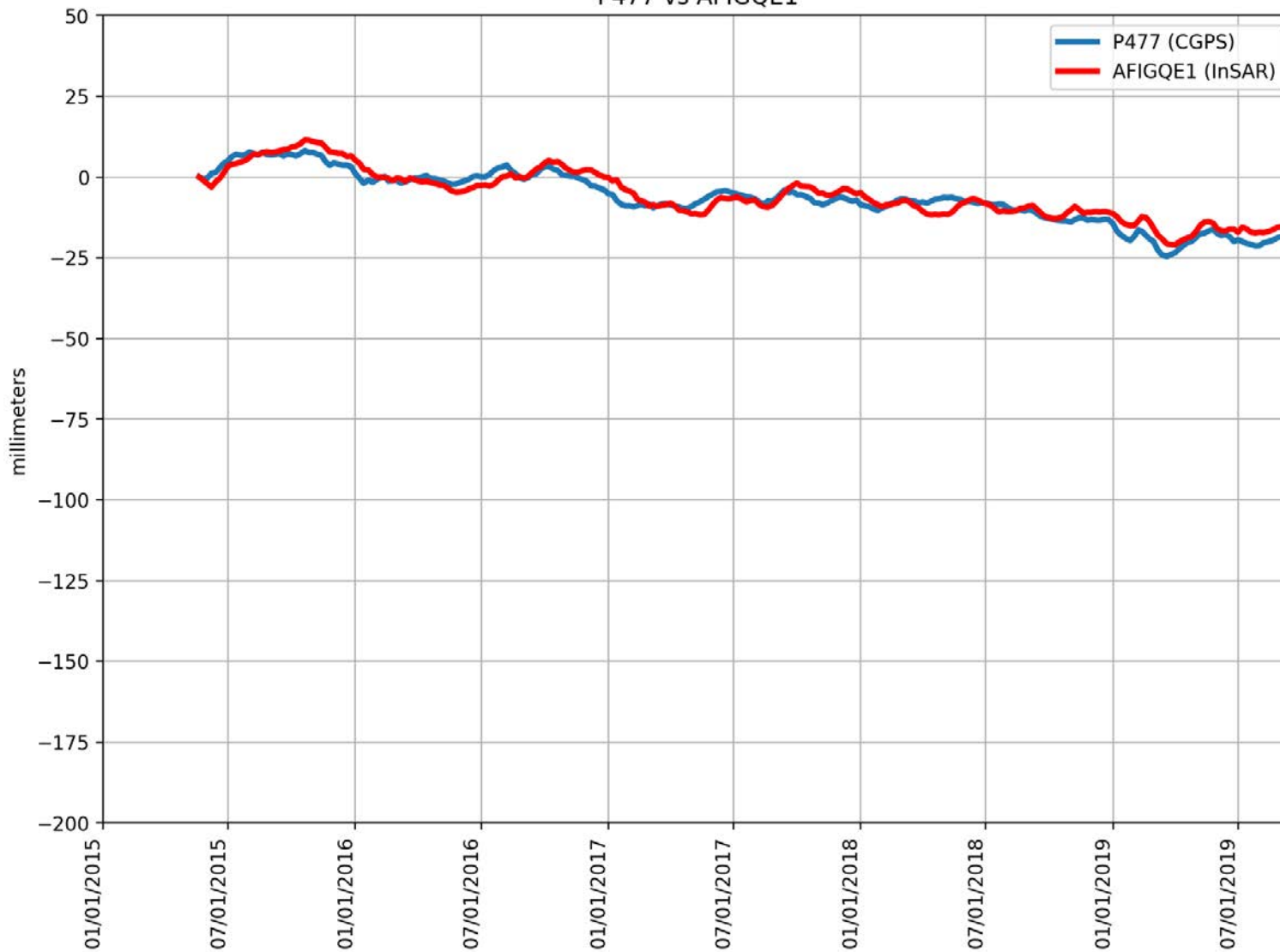
P470 vs AX54T2A



RMSE: 5.12 mm
Correlation: 0.80

Appendix B

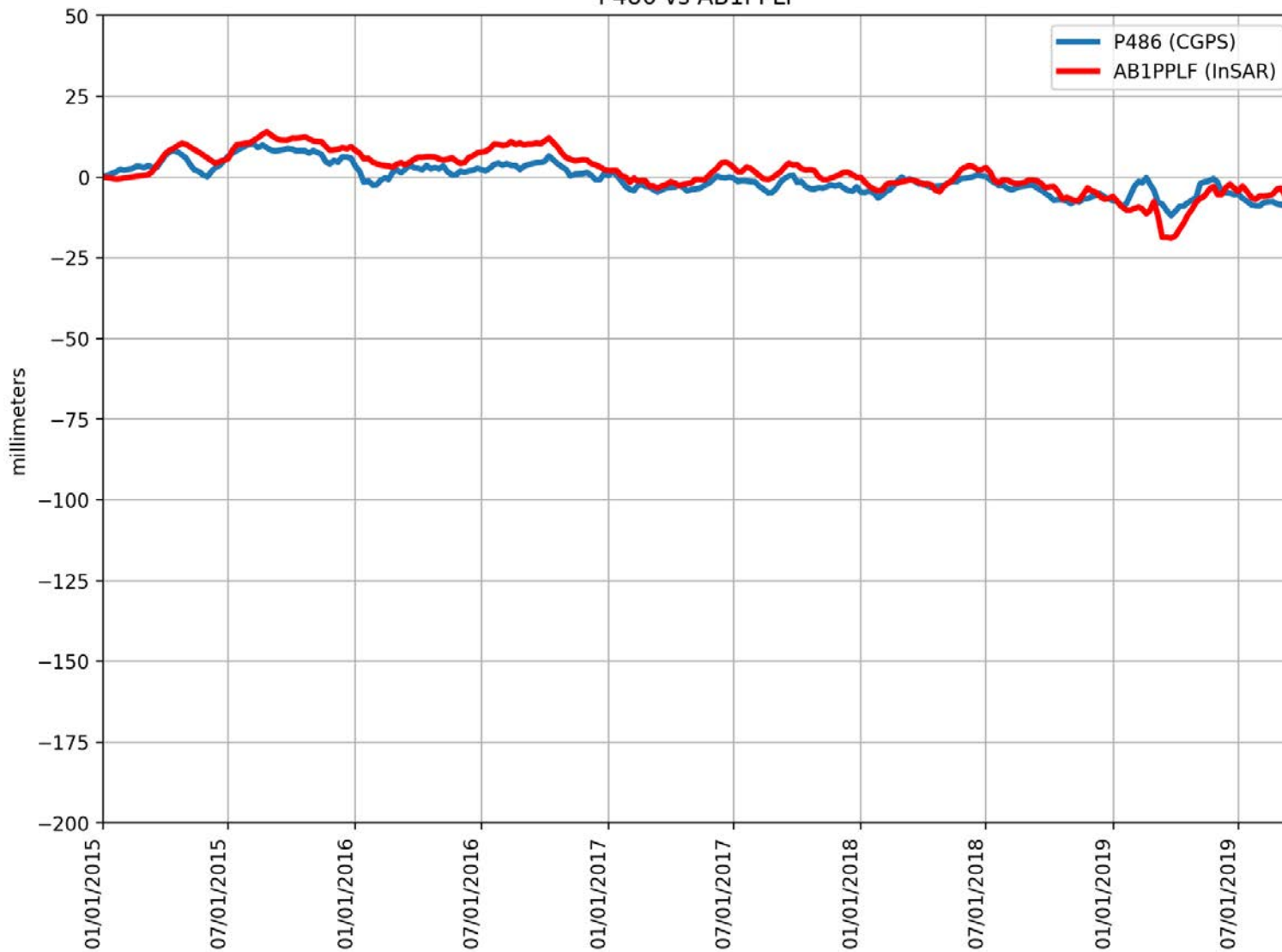
P477 vs AFIGQE1



RMSE: 2.71 mm
Correlation: 0.95

Appendix B

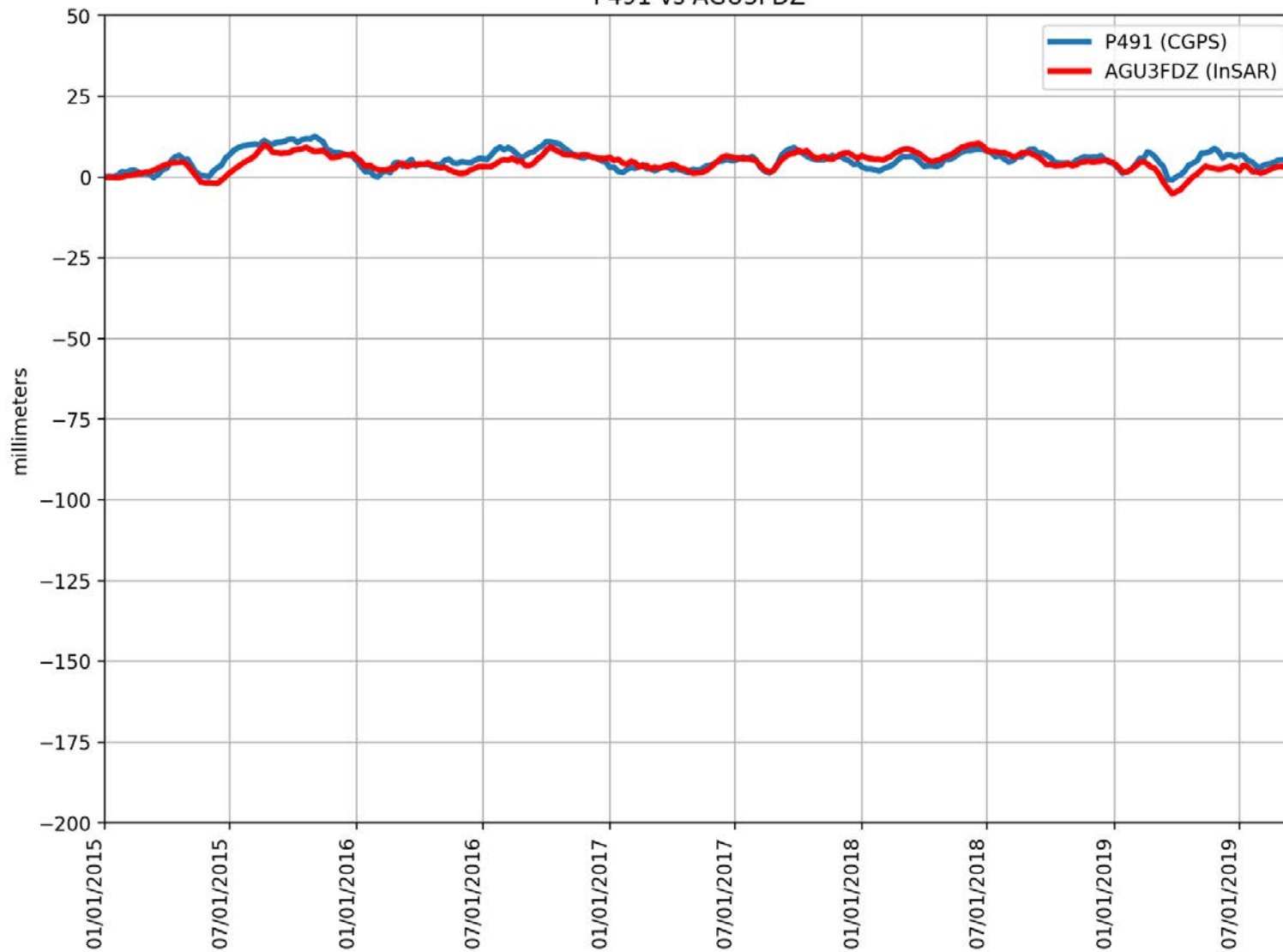
P486 vs AB1PPLF



RMSE: 3.72 mm
Correlation: 0.88

Appendix B

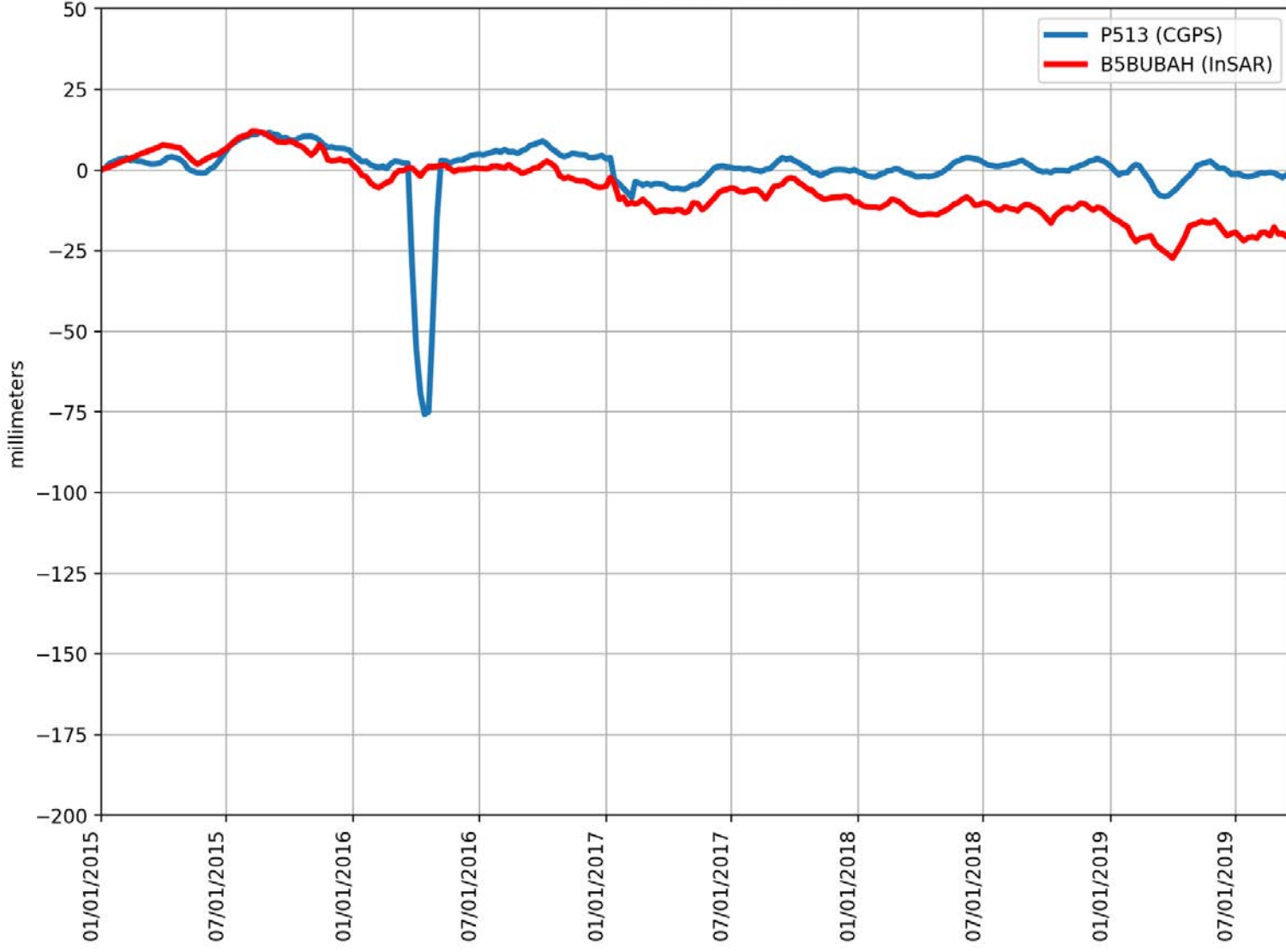
P491 vs AGU3FDZ



RMSE: 2.39 mm
Correlation: 0.69

Appendix B

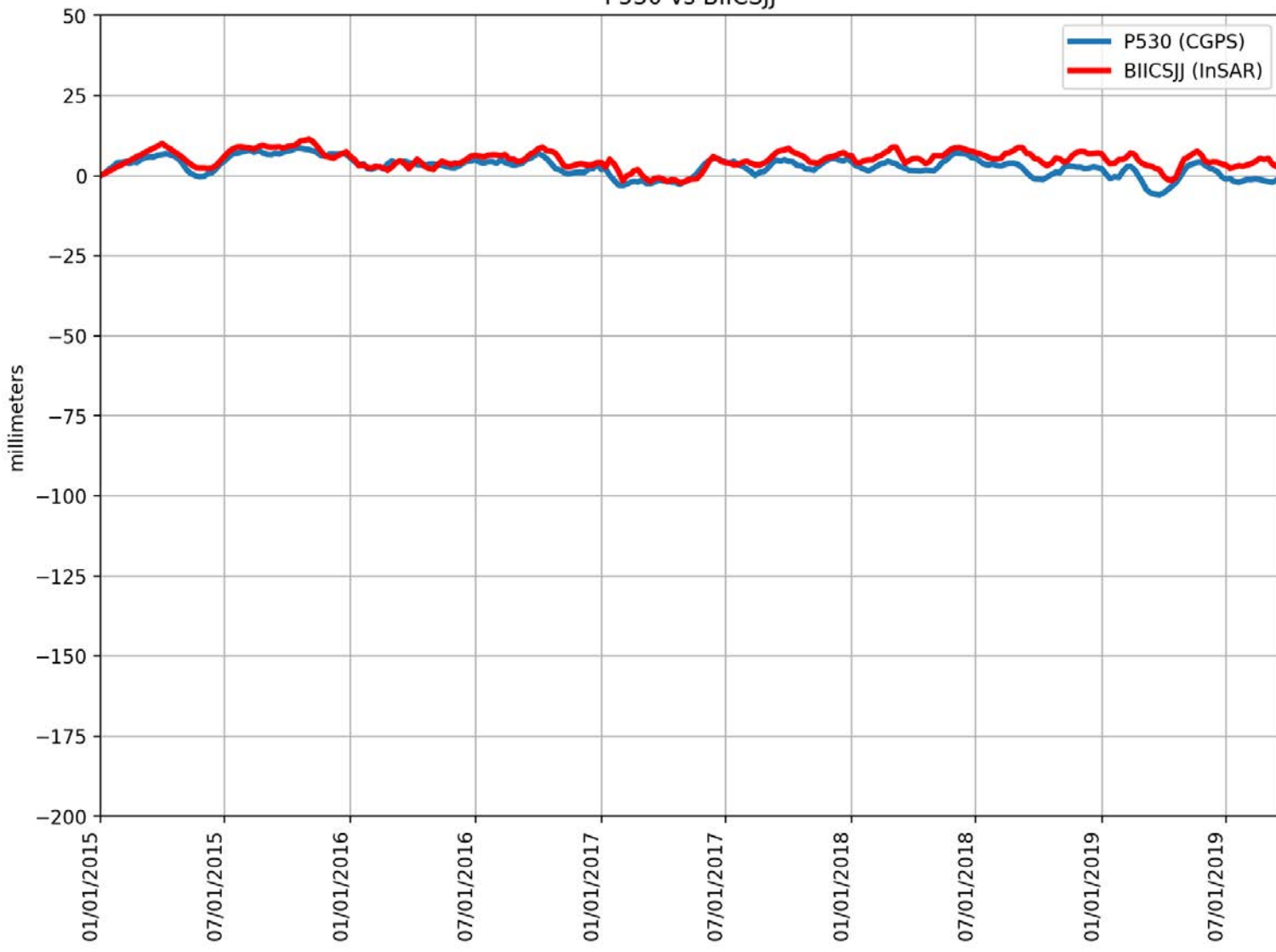
P513 vs B5BUBAH



RMSE: 13.50 mm
Correlation: 0.22

Appendix B

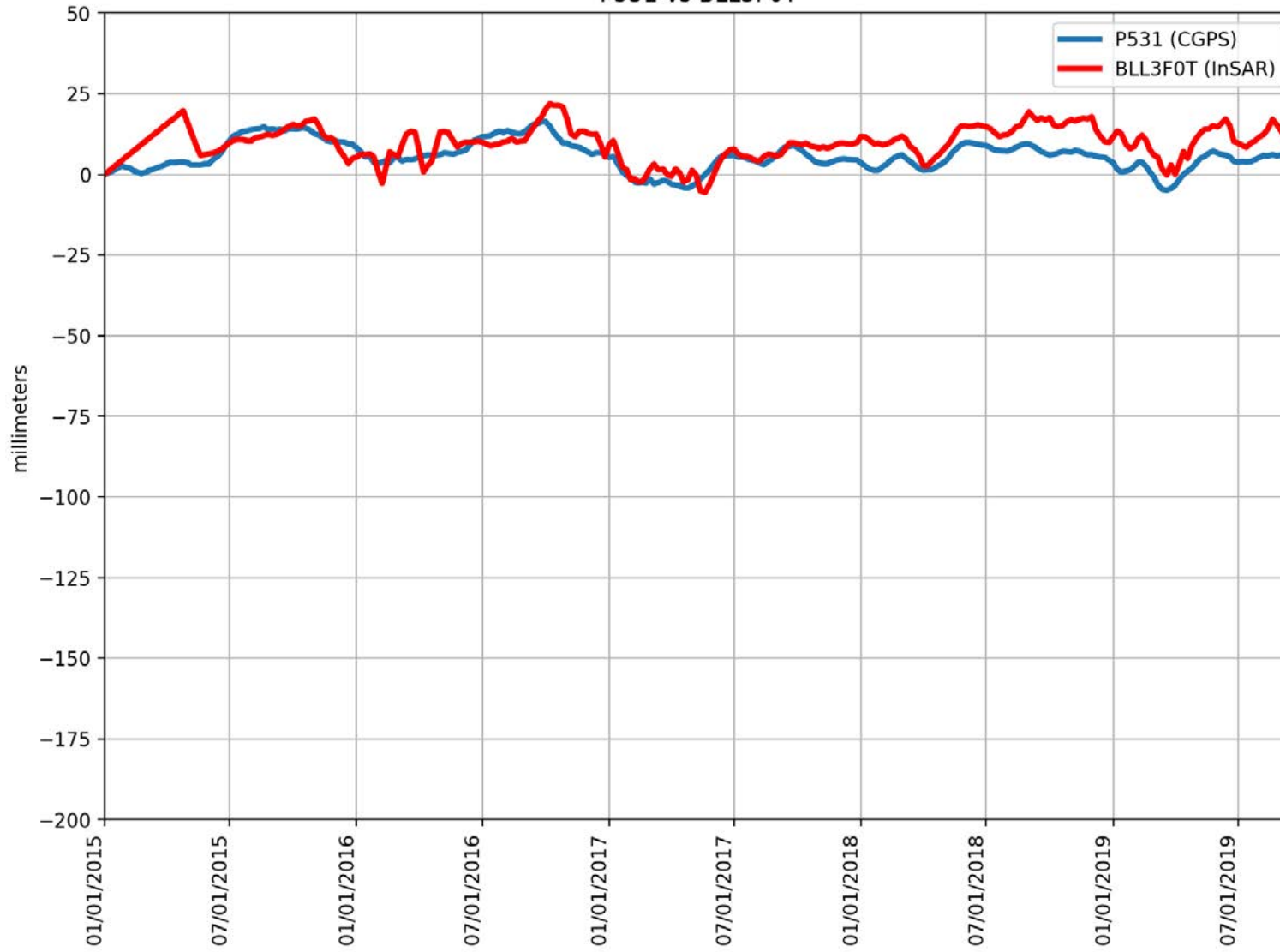
P530 vs BIICSJJ



RMSE: 2.96 mm
Correlation: 0.77

Appendix B

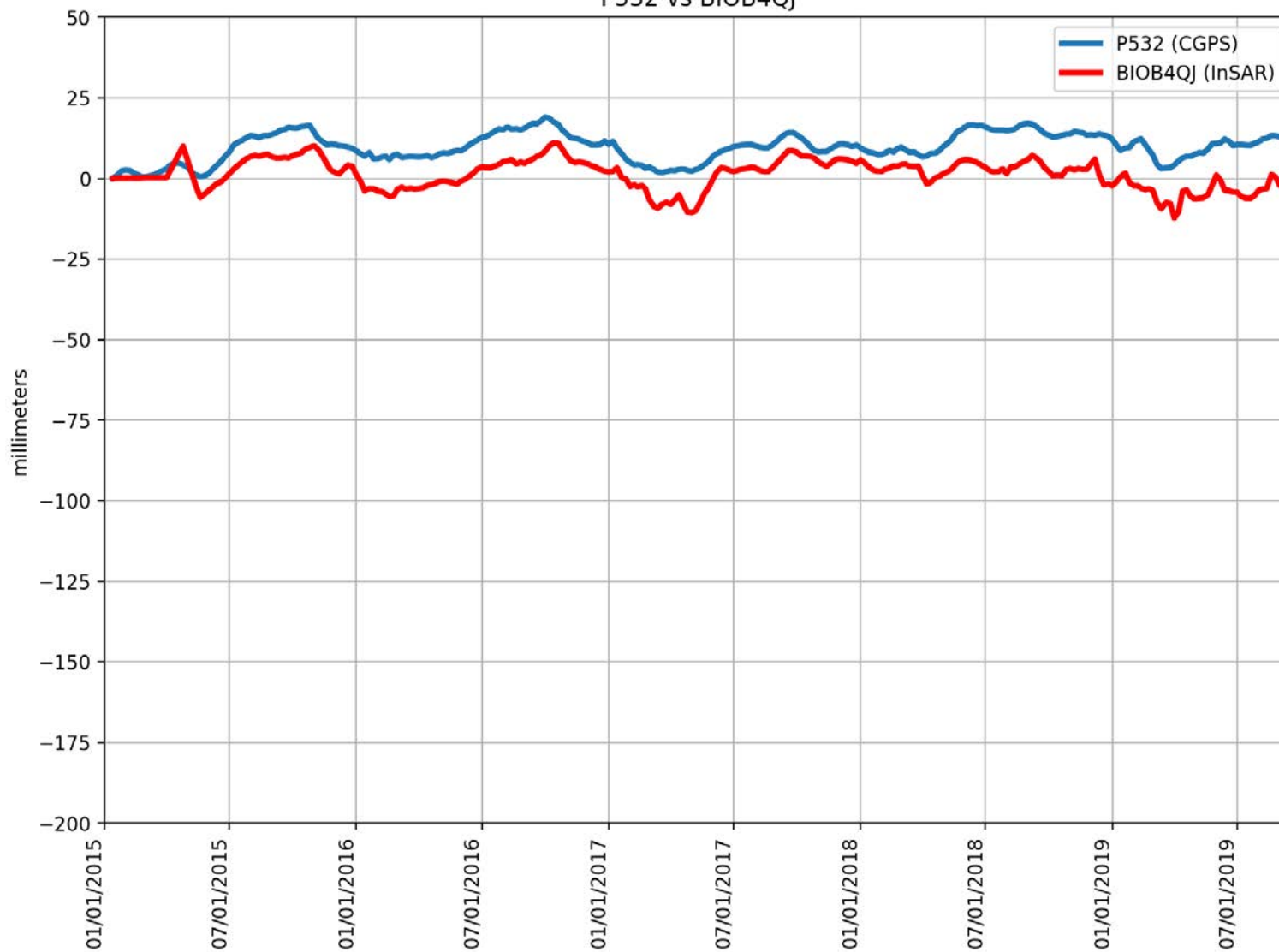
P531 vs BLL3F0T



RMSE: 5.85 mm
Correlation: 0.62

Appendix B

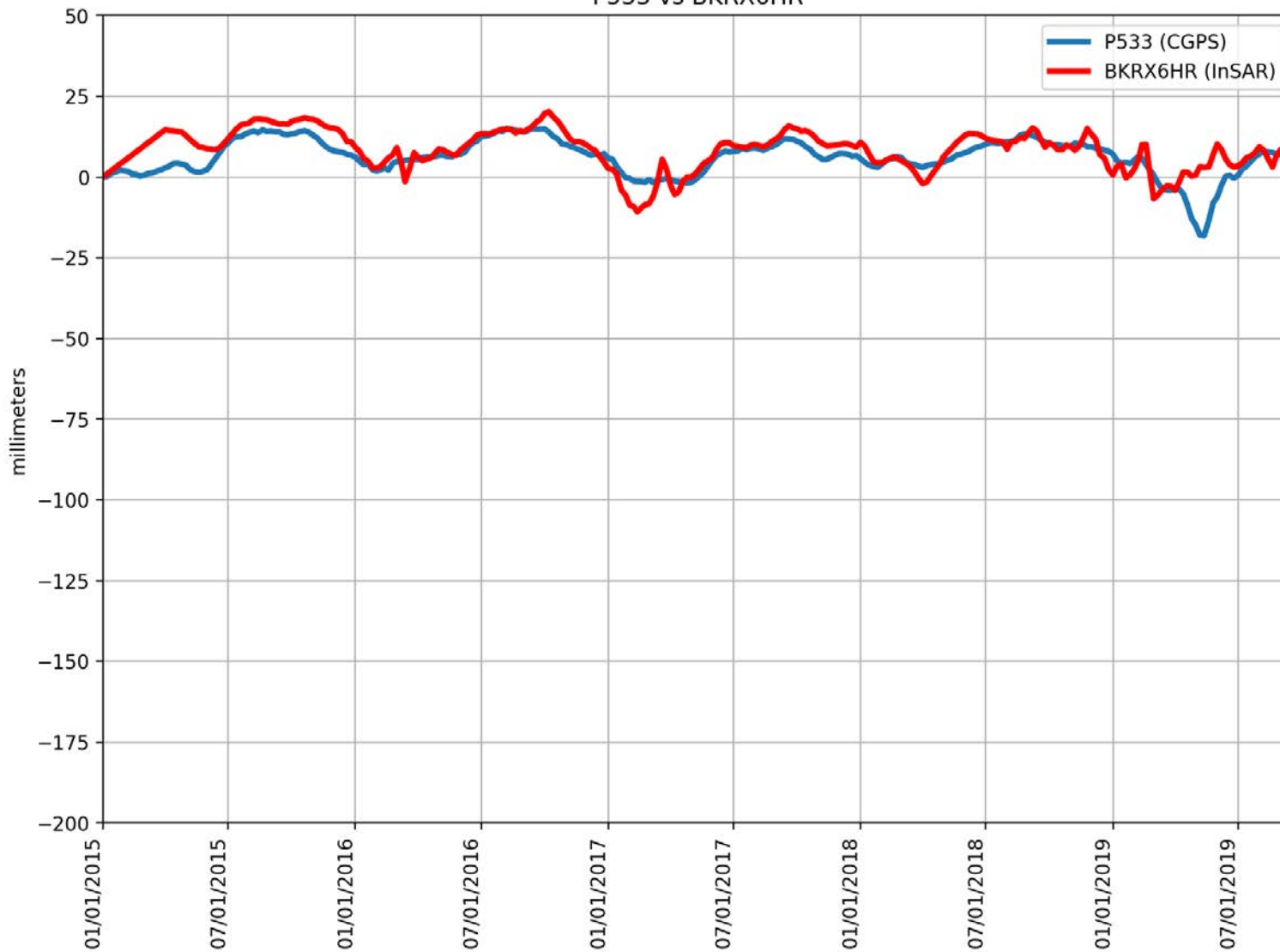
P532 vs BIOB4QJ



RMSE: 9.32 mm
Correlation: 0.65

Appendix B

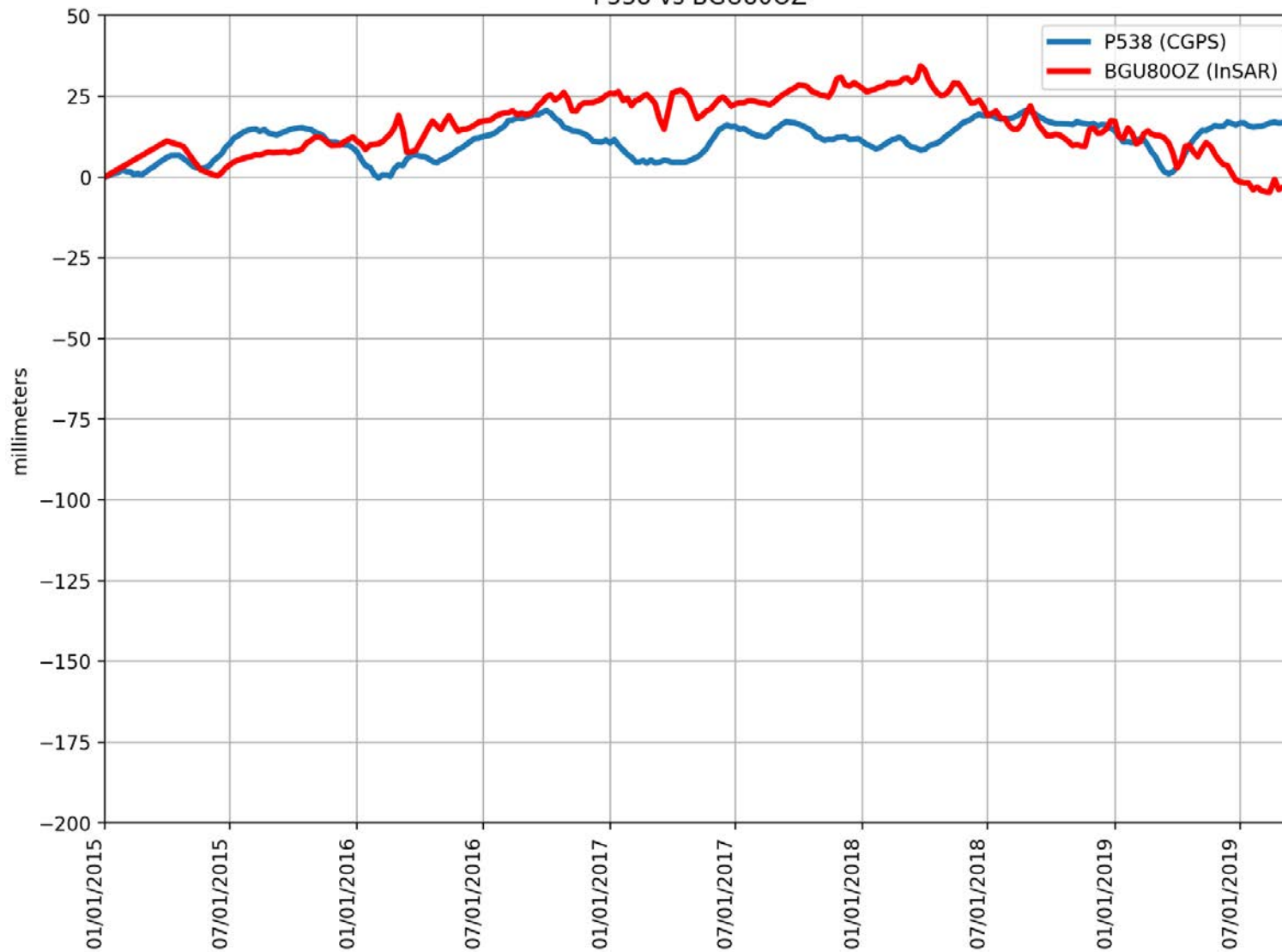
P533 vs BKRX6HR



RMSE: 4.86 mm
Correlation: 0.73

Appendix B

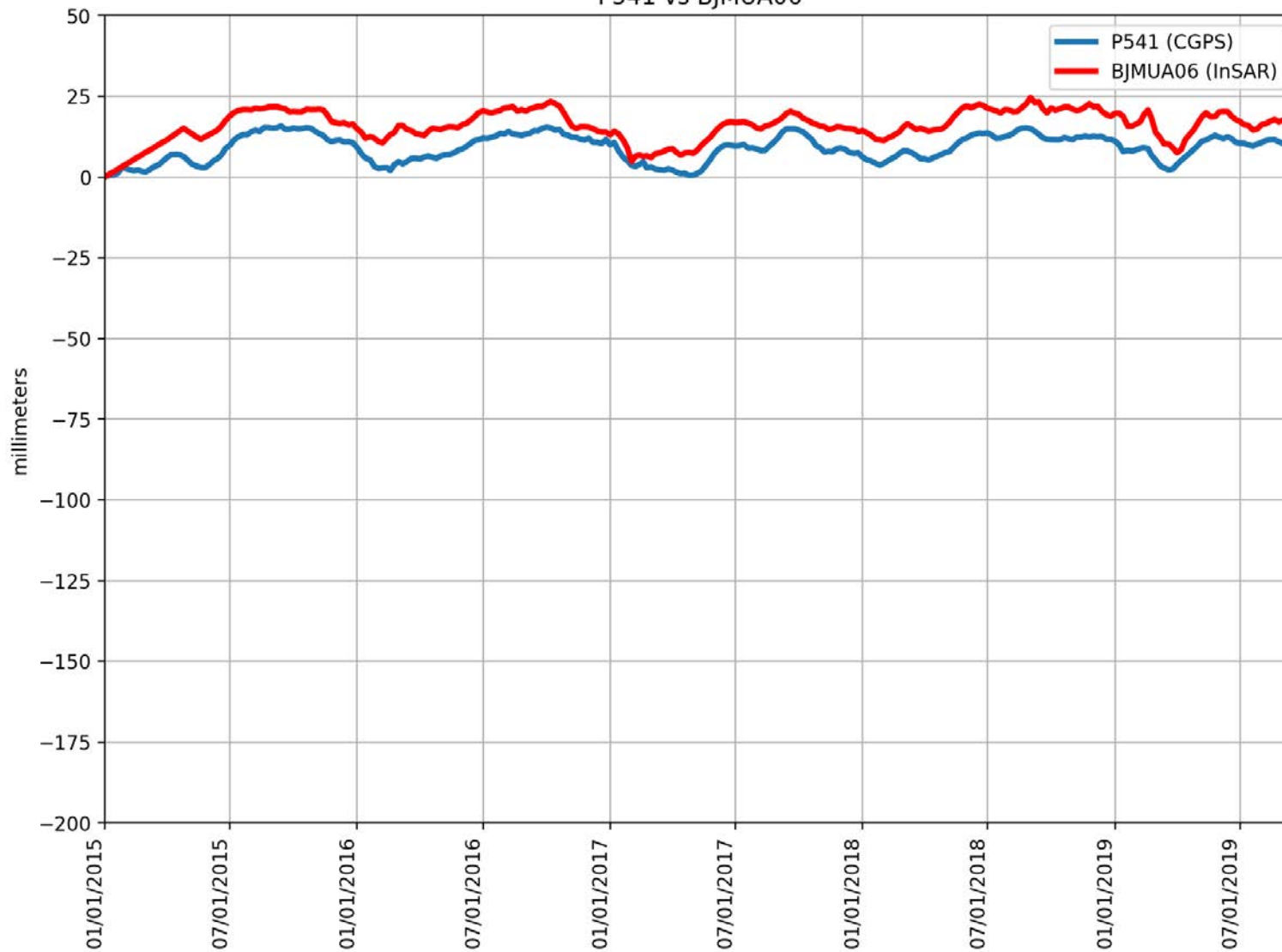
P538 vs BGU800Z



RMSE: 10.81 mm
Correlation: 0.15

Appendix B

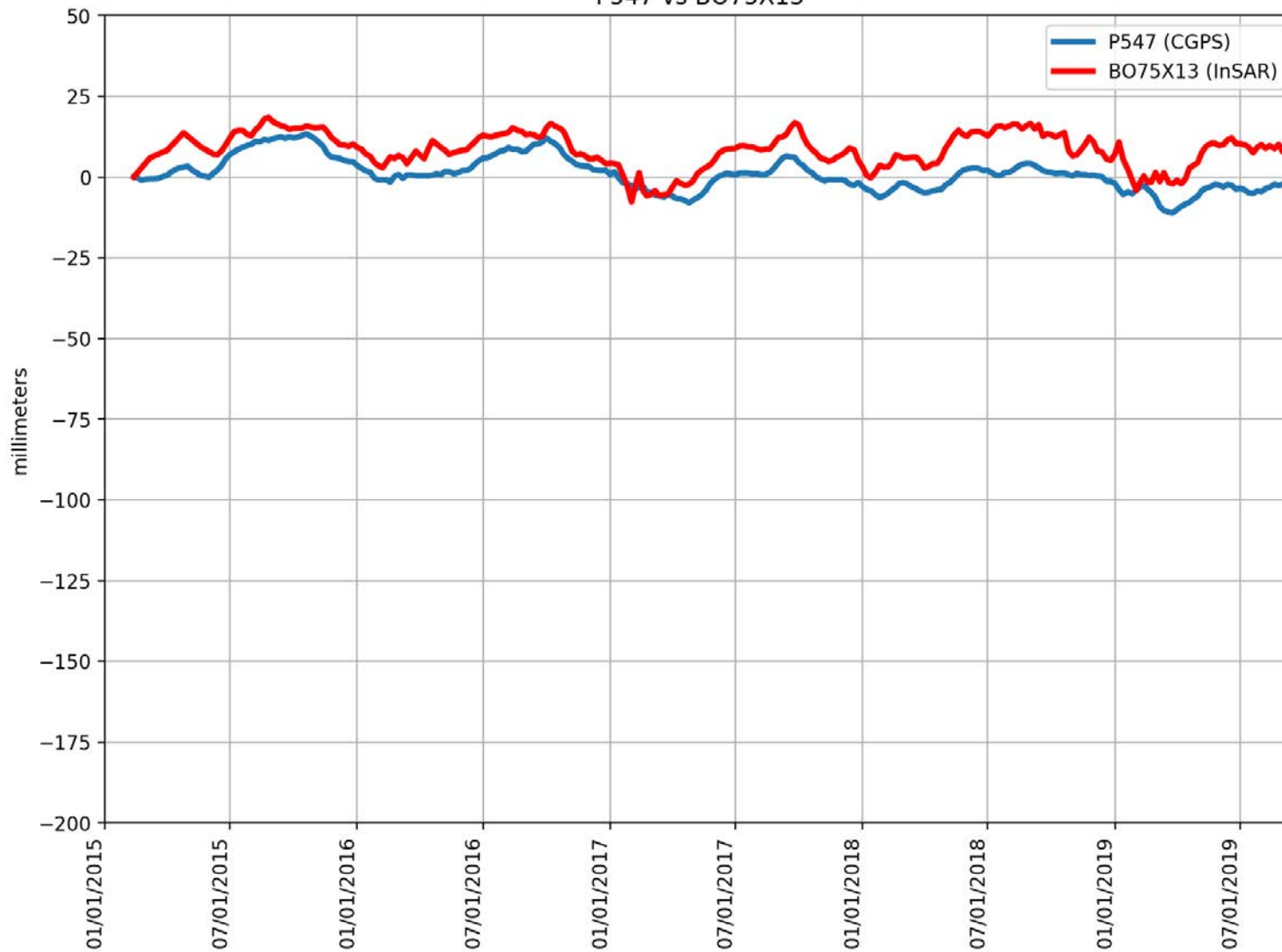
P541 vs BJMUA06



RMSE: 7.24 mm
Correlation: 0.91

Appendix B

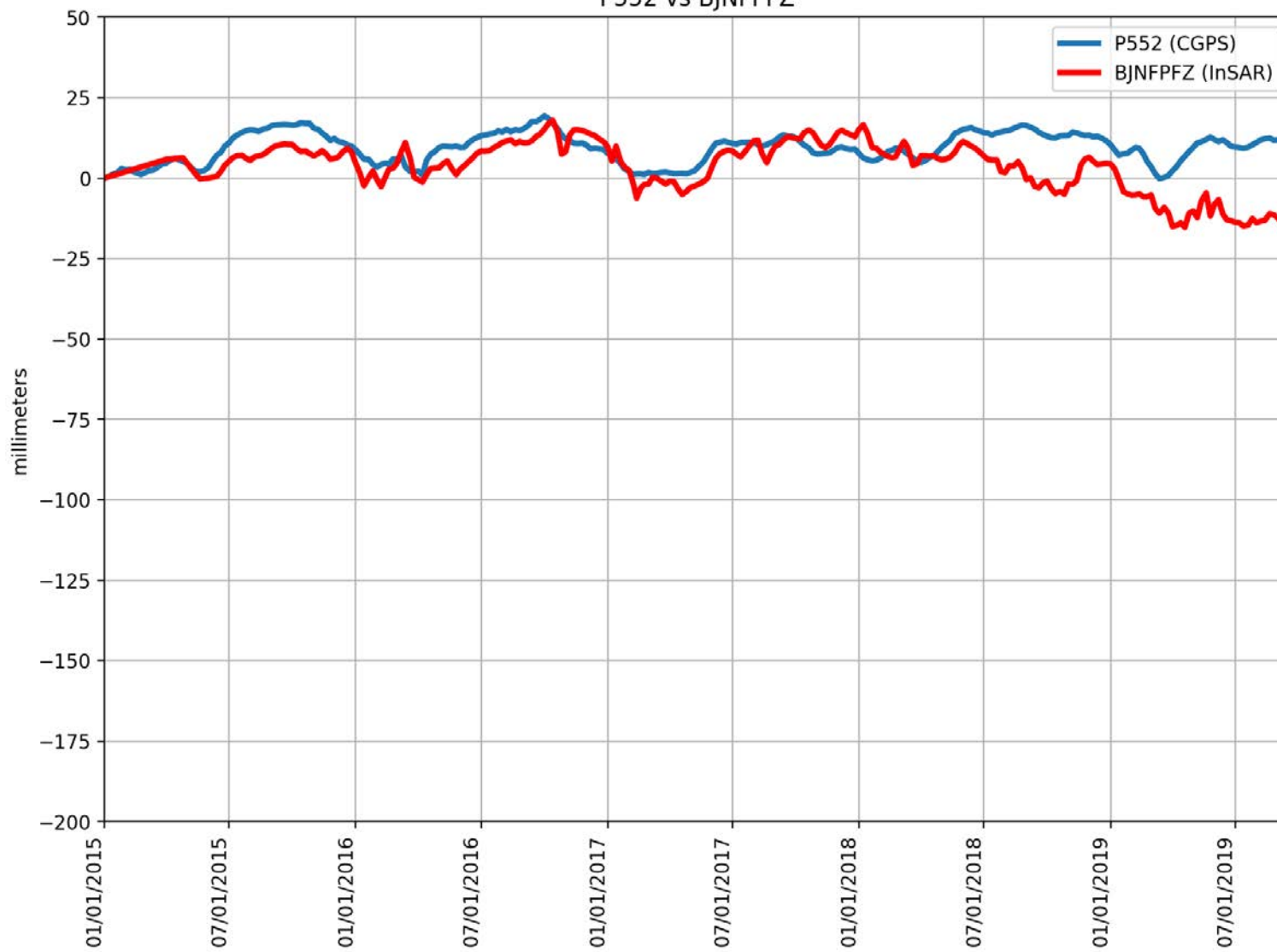
P547 vs BO75X13



RMSE: 8.13 mm
Correlation: 0.77

Appendix B

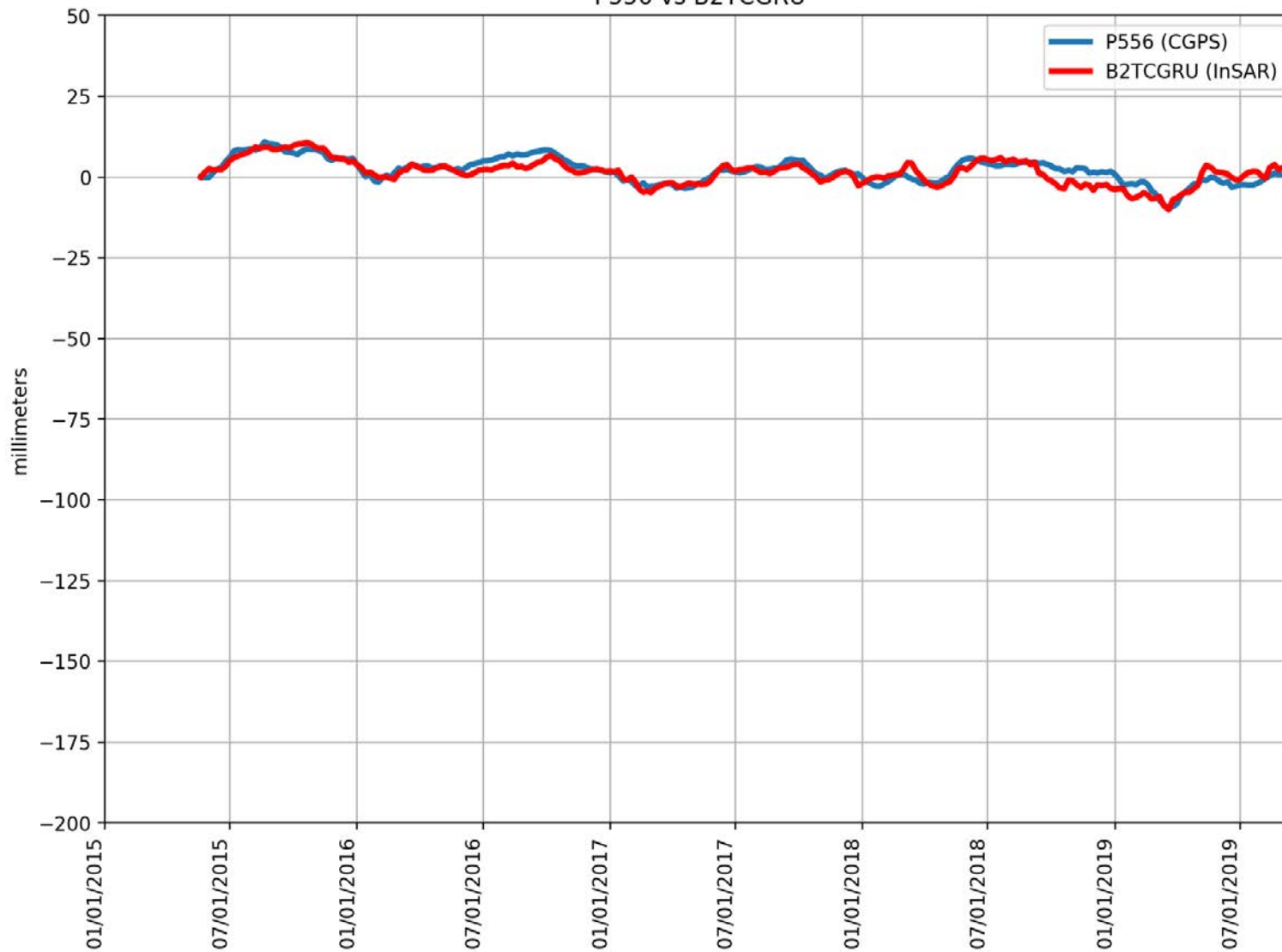
P552 vs BJNFPFZ



RMSE: 9.51 mm
Correlation: 0.32

Appendix B

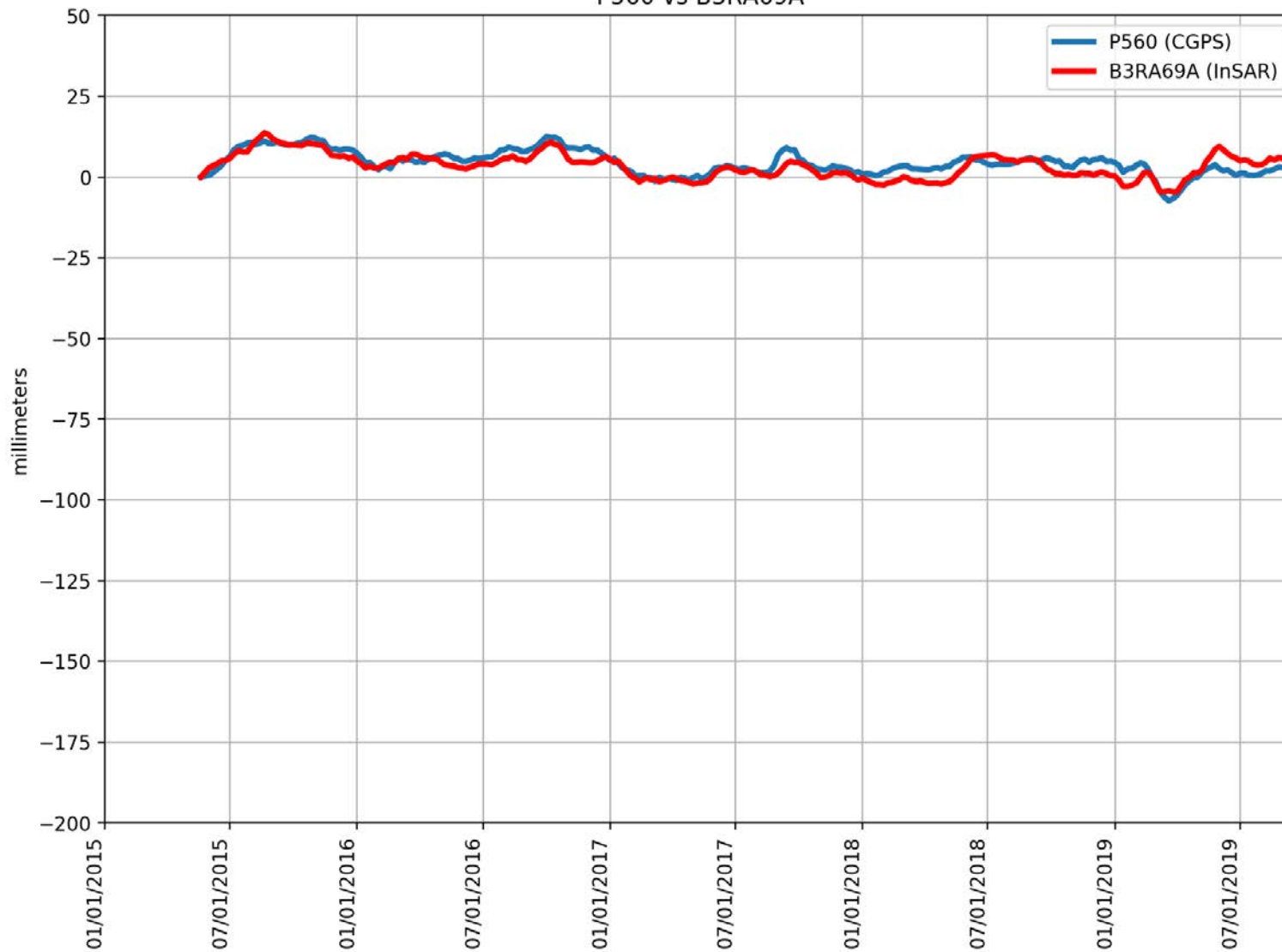
P556 vs B2TCGRU



RMSE: 2.20 mm
Correlation: 0.84

Appendix B

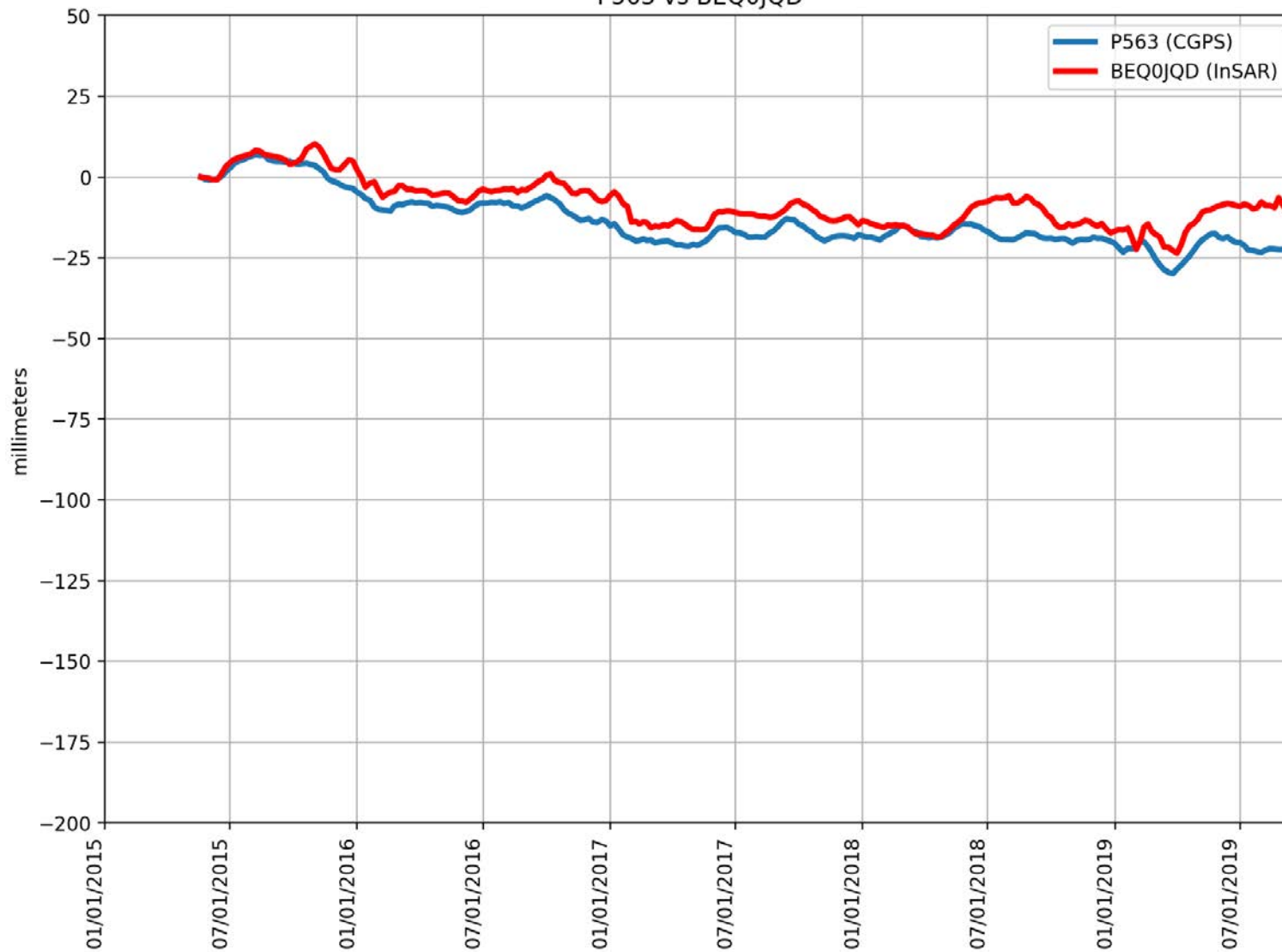
P560 vs B3RA69A



RMSE: 2.70 mm
Correlation: 0.78

Appendix B

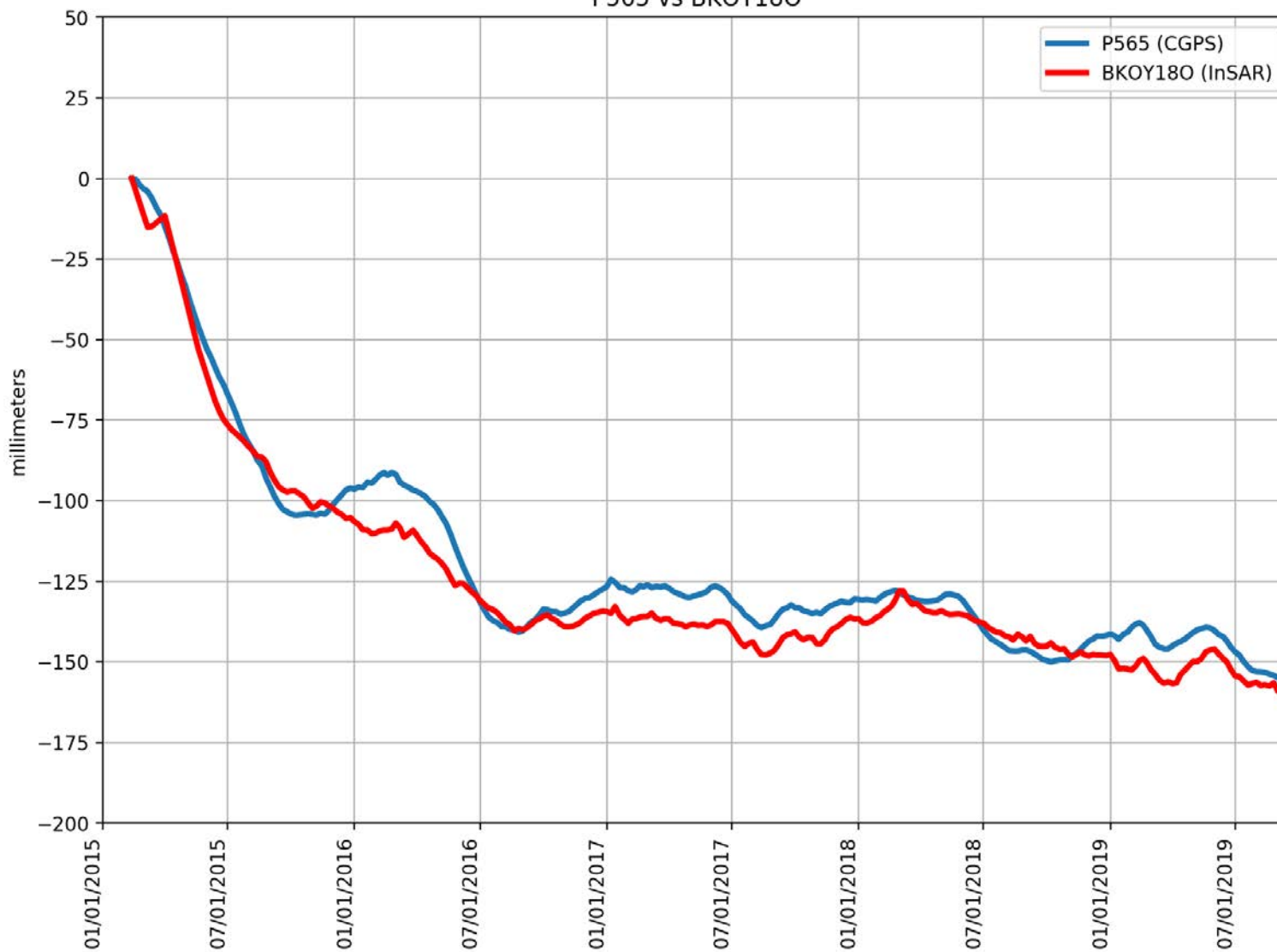
P563 vs BEQ0JQD



RMSE: 6.54 mm
Correlation: 0.91

Appendix B

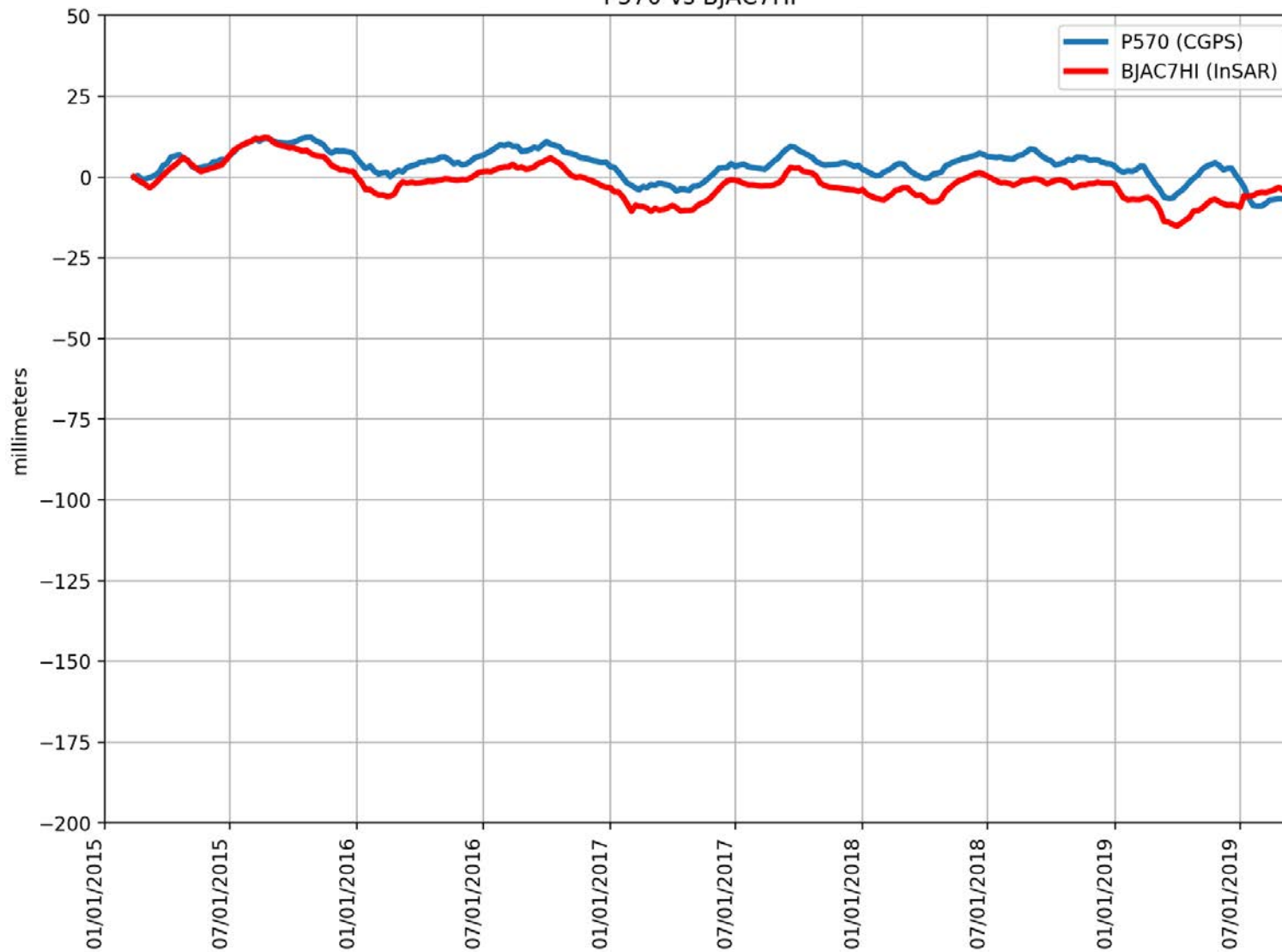
P565 vs BKOY180



RMSE: 7.80 mm
Correlation: 0.99

Appendix B

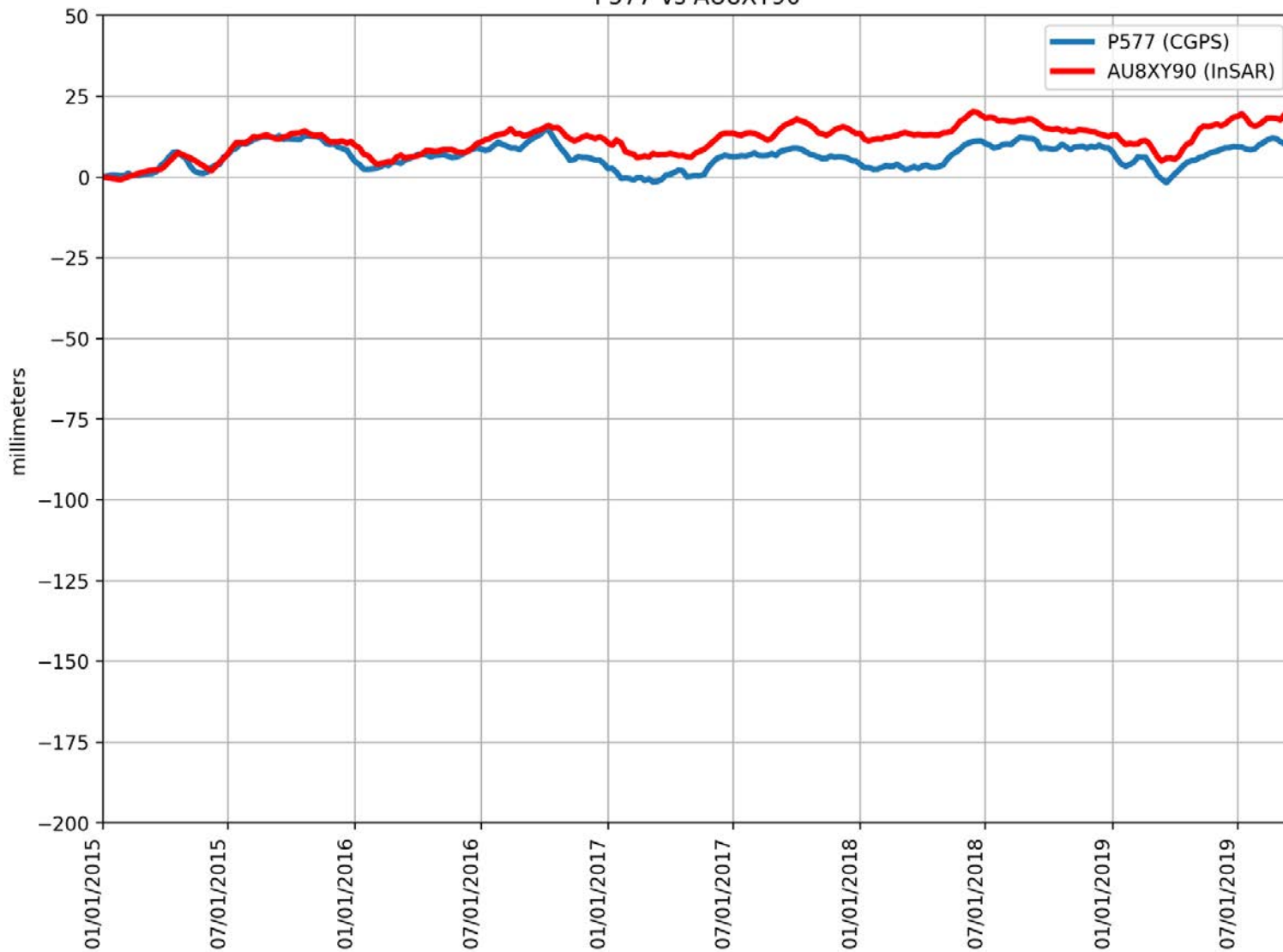
P570 vs BJAC7HI



RMSE: 6.34 mm
Correlation: 0.81

Appendix B

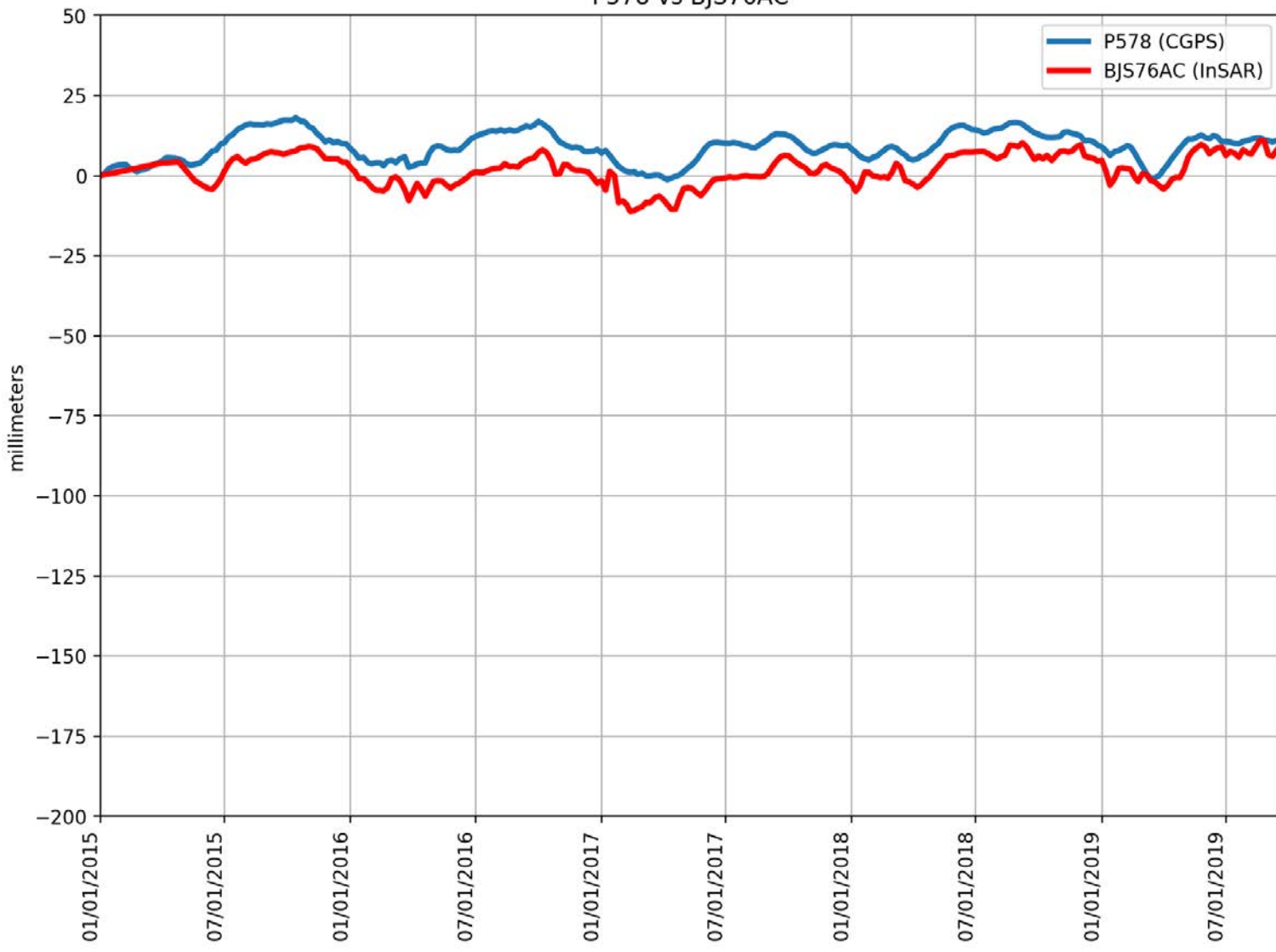
P577 vs AU8XY90



RMSE: 5.98 mm
Correlation: 0.71

Appendix B

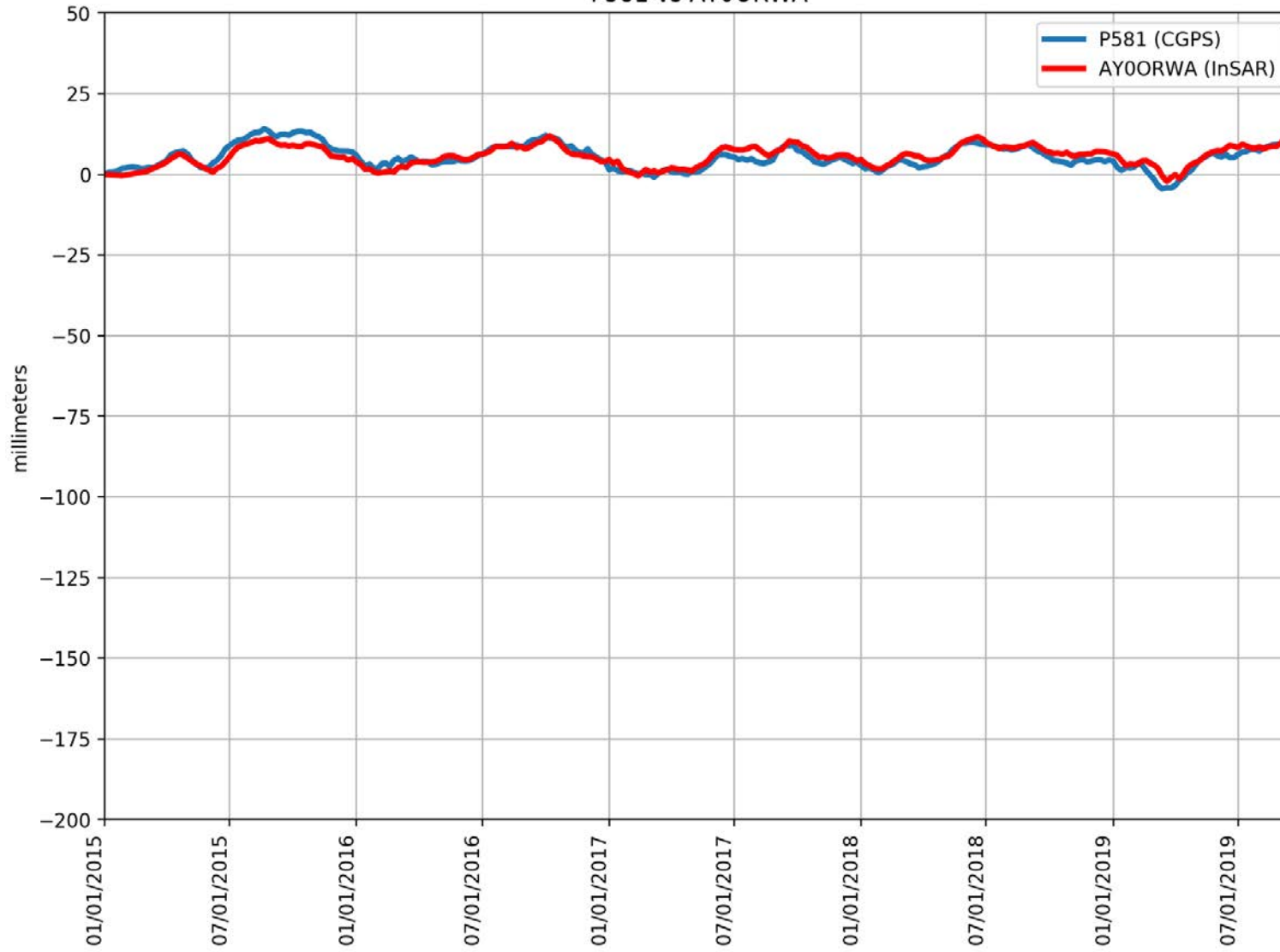
P578 vs BJS76AC



RMSE: 7.84 mm
Correlation: 0.77

Appendix B

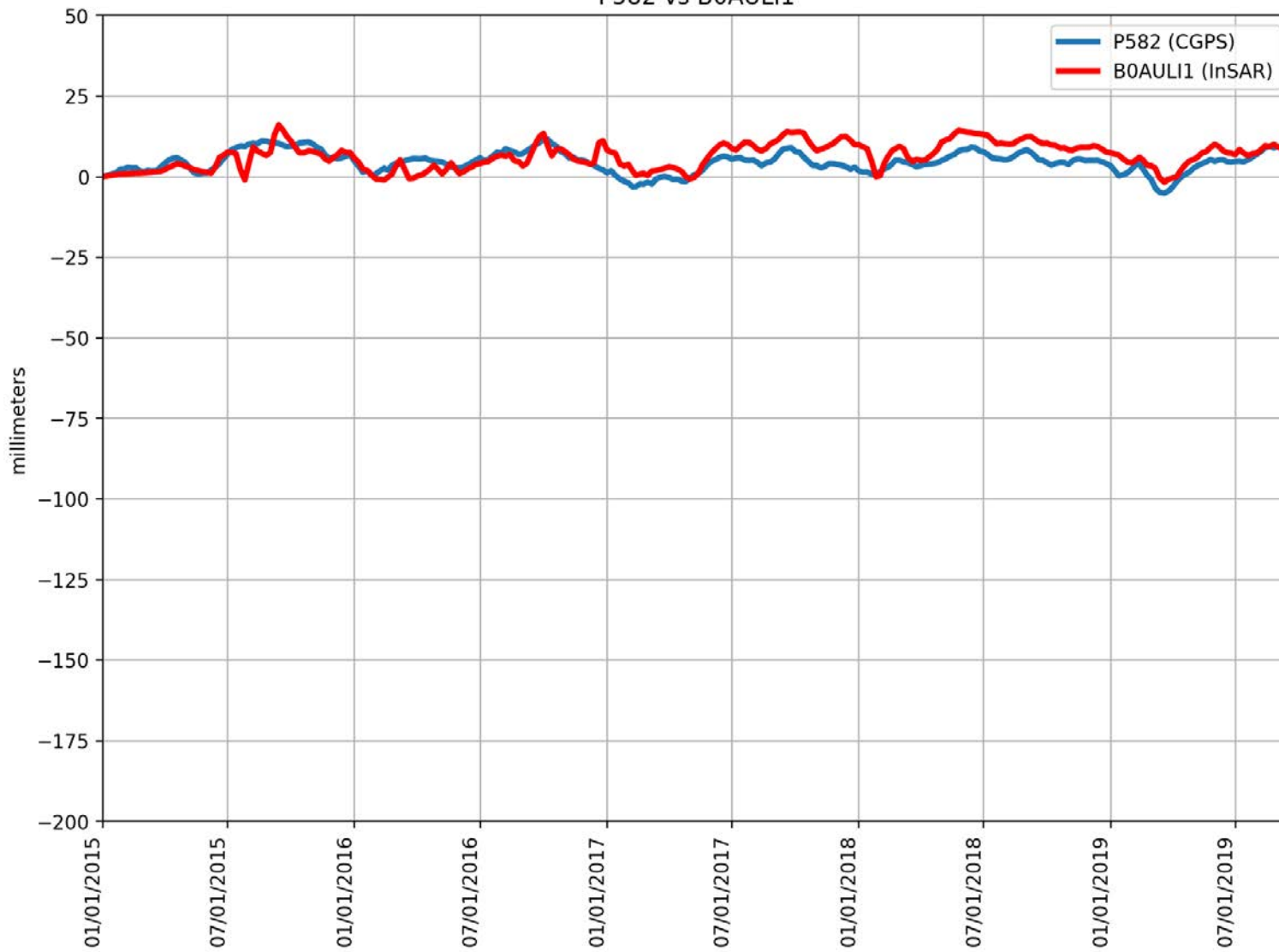
P581 vs AY0ORWA



RMSE: 1.91 mm
Correlation: 0.86

Appendix B

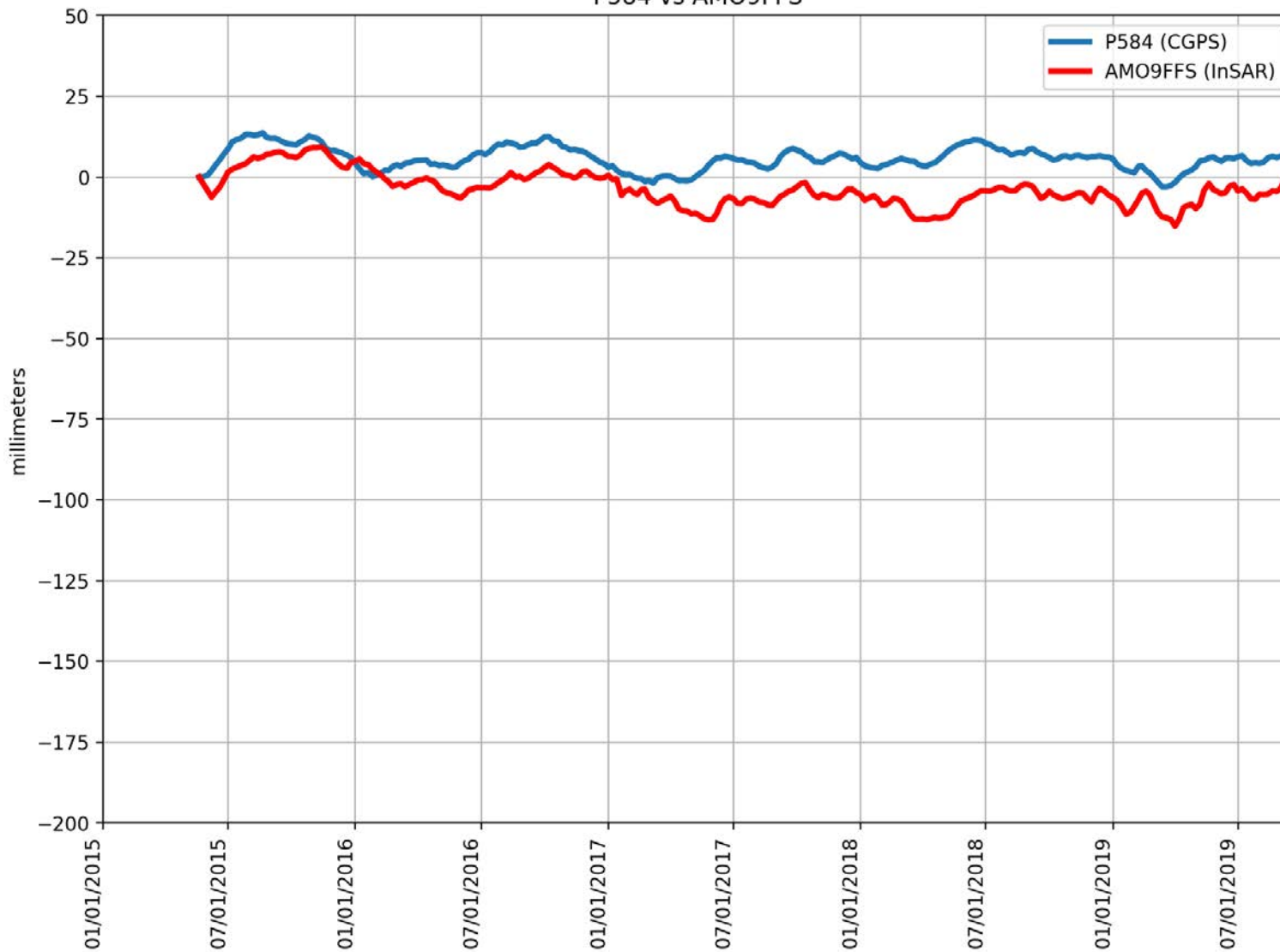
P582 vs B0AULI1



RMSE: 3.79 mm
Correlation: 0.62

Appendix B

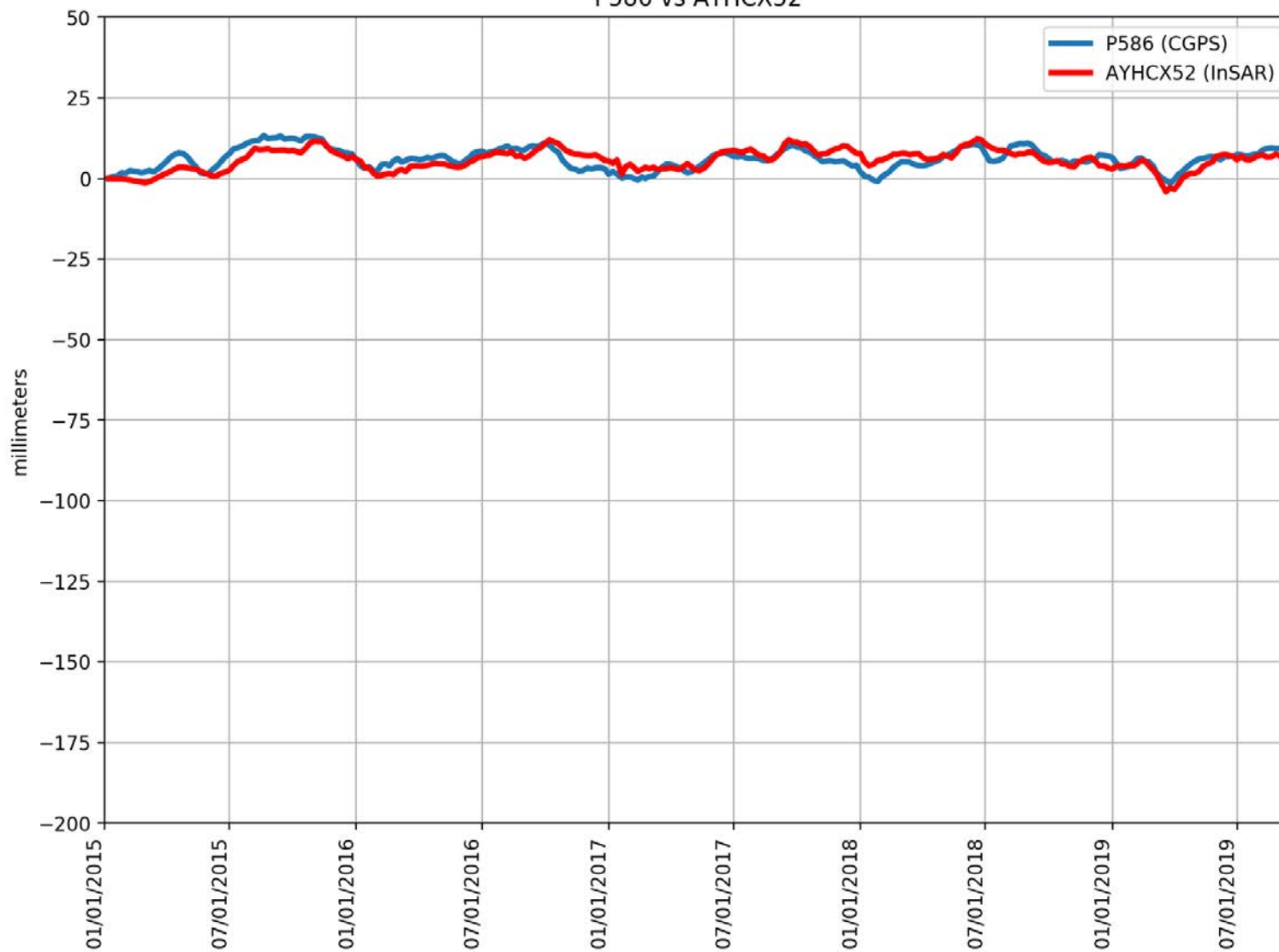
P584 vs AMO9FFS



RMSE: 10.35 mm
Correlation: 0.59

Appendix B

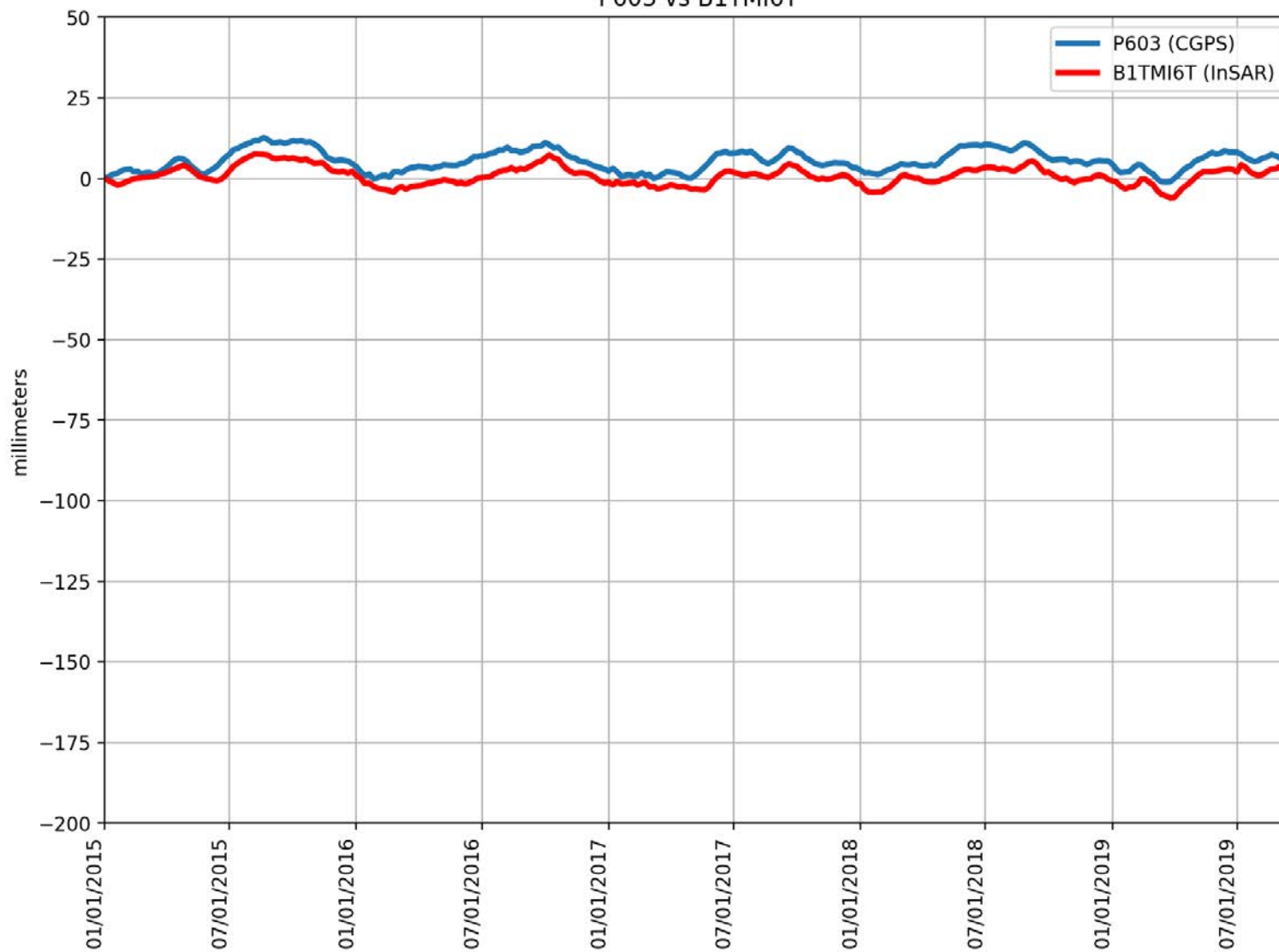
P586 vs AYHCX52



RMSE: 2.61 mm
Correlation: 0.68

Appendix B

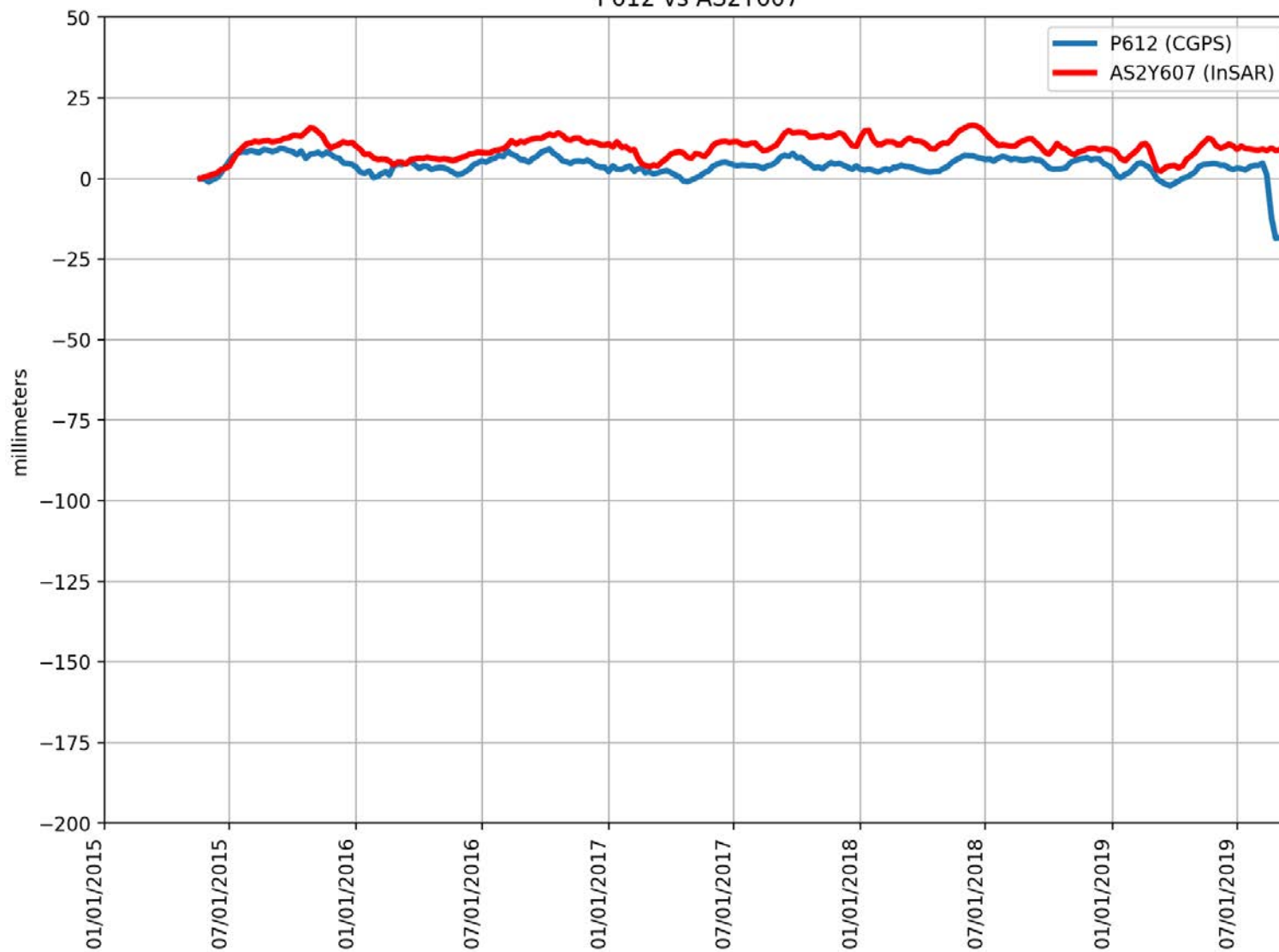
P603 vs B1TMI6T



RMSE: 4.88 mm
Correlation: 0.88

Appendix B

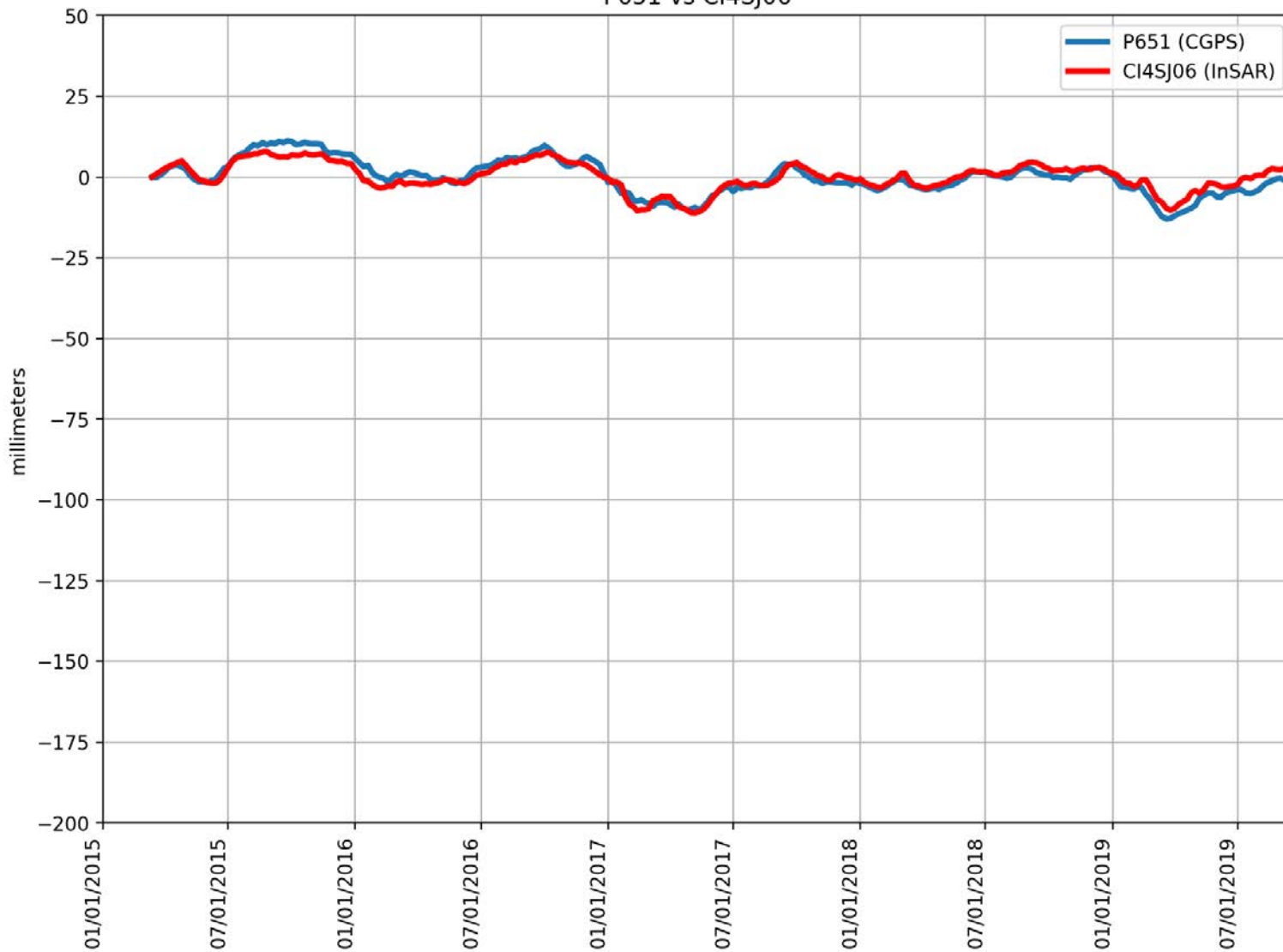
P612 vs AS2Y607



RMSE: 6.94 mm
Correlation: 0.43

Appendix B

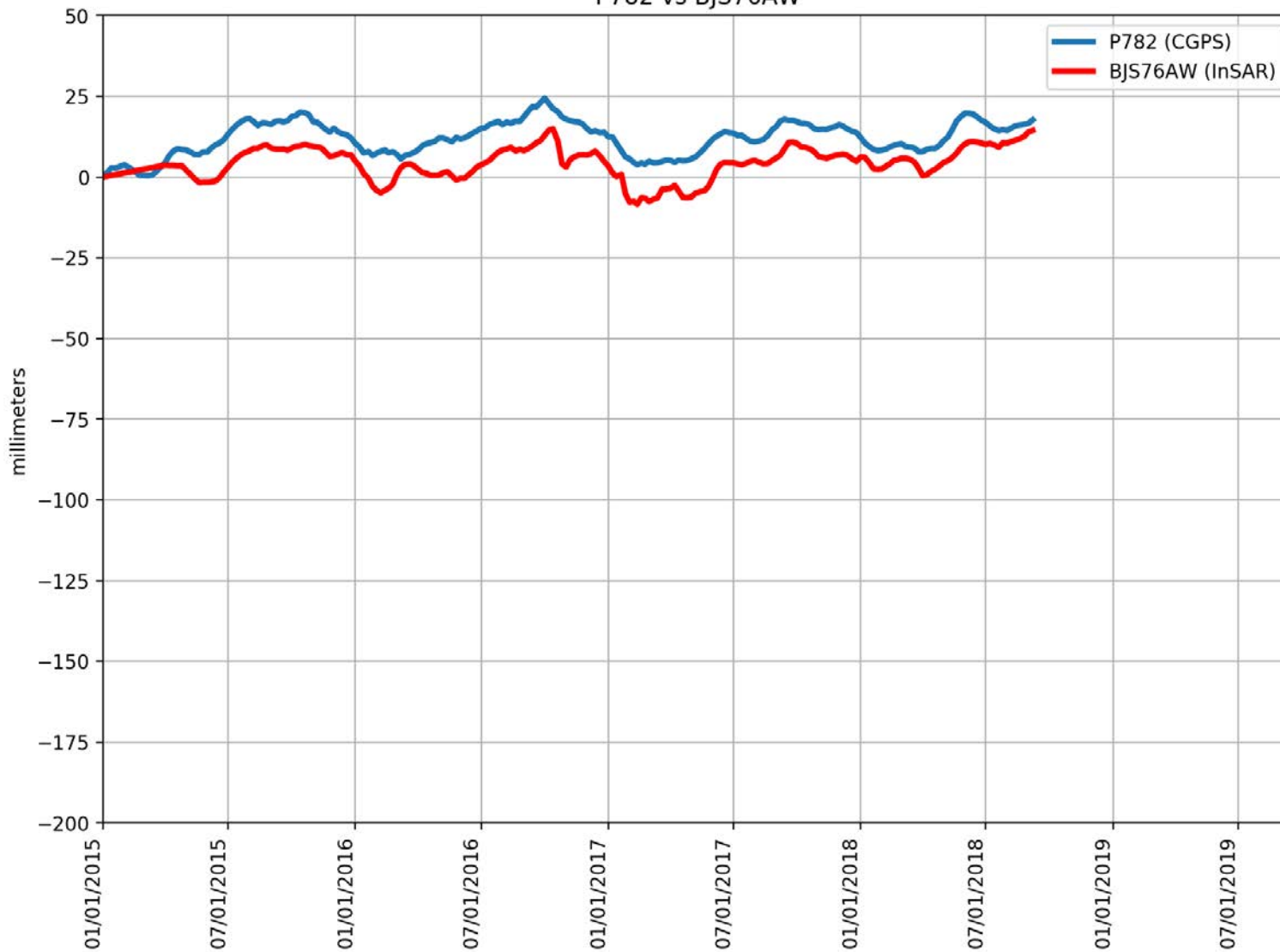
P651 vs CI4SJ06



RMSE: 2.19 mm
Correlation: 0.92

Appendix B

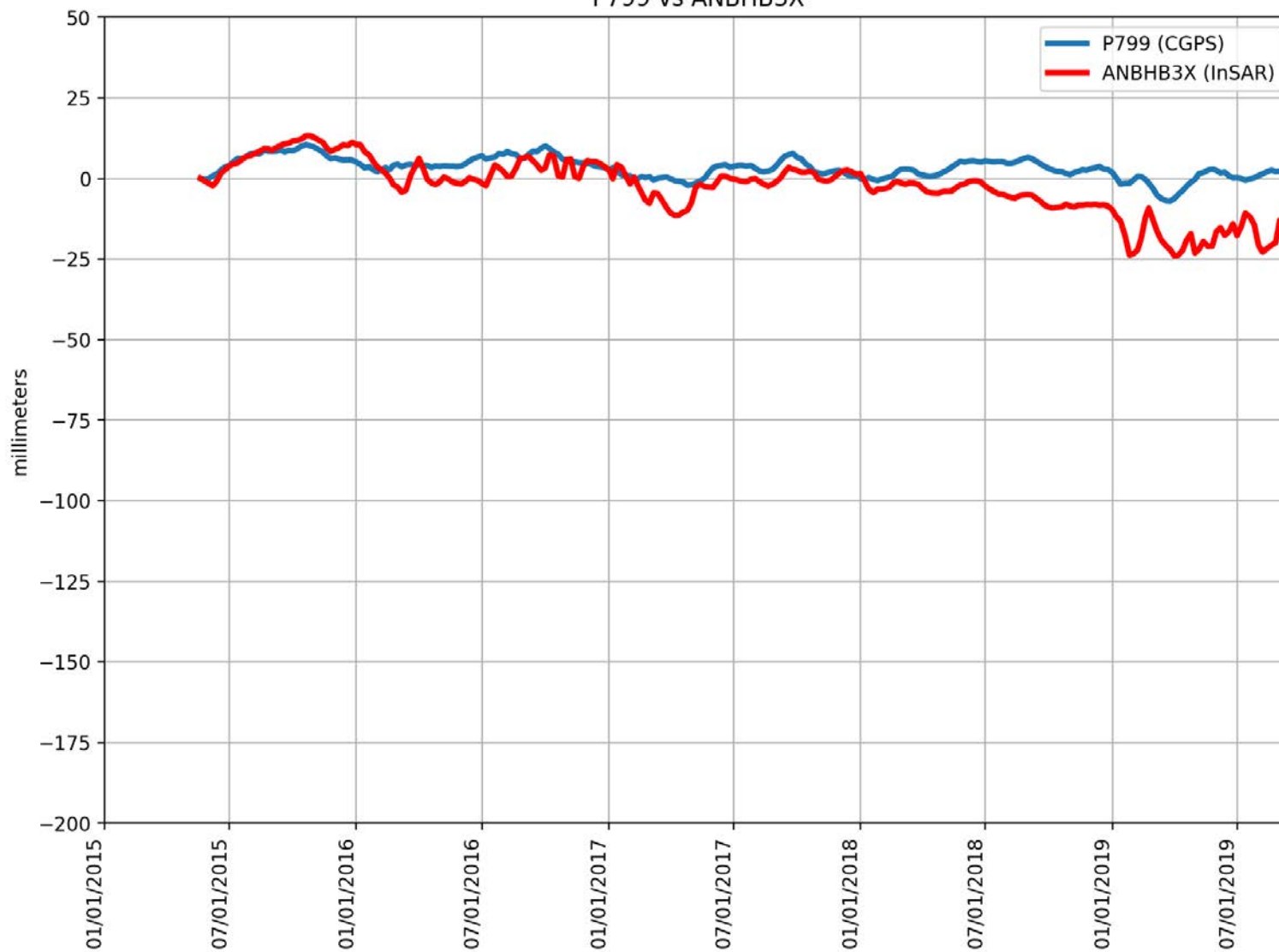
P782 vs BJS76AW



RMSE: 8.52 mm
Correlation: 0.79

Appendix B

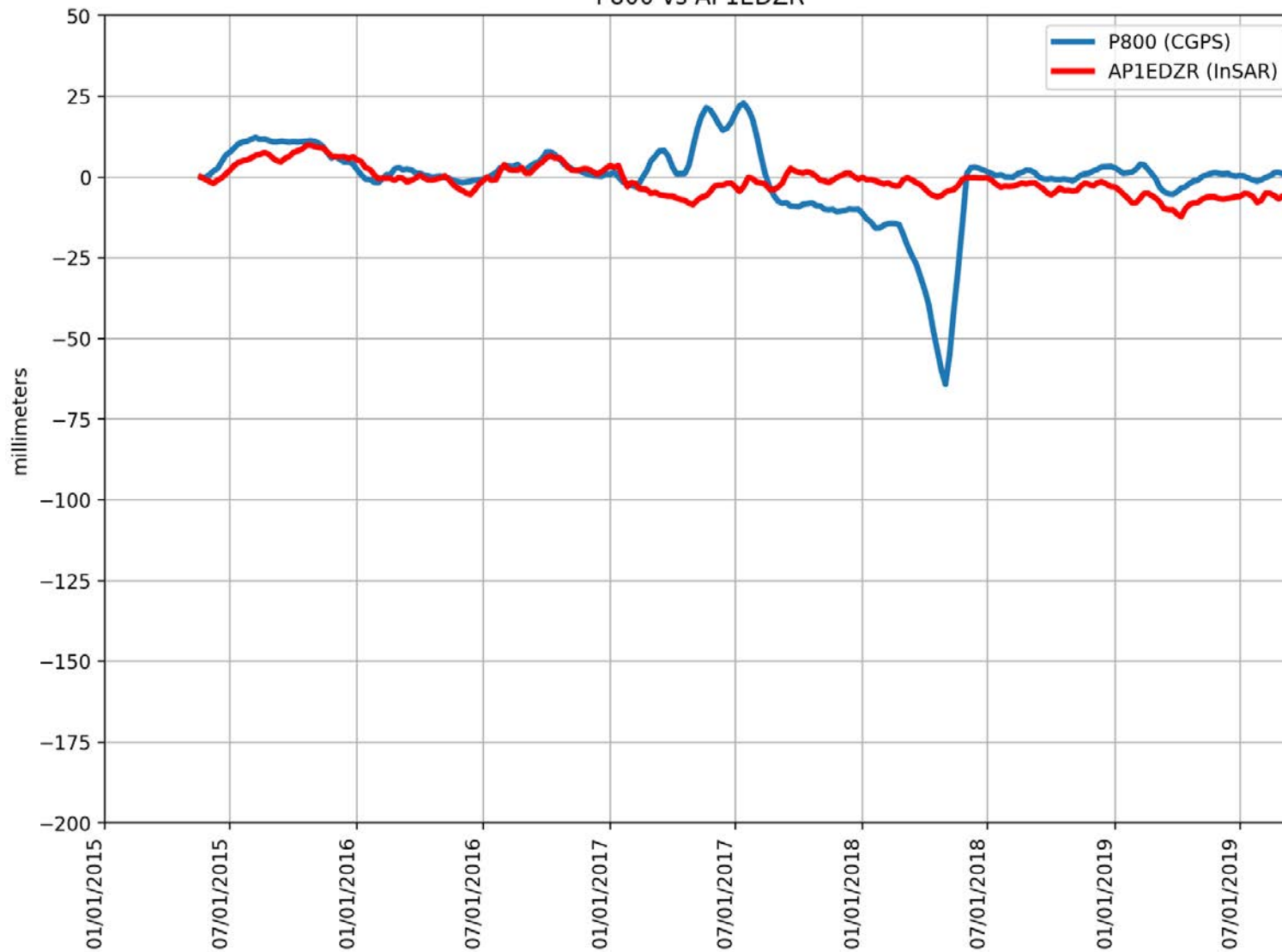
P799 vs ANBHB3X



RMSE: 9.14 mm
Correlation: 0.71

Appendix B

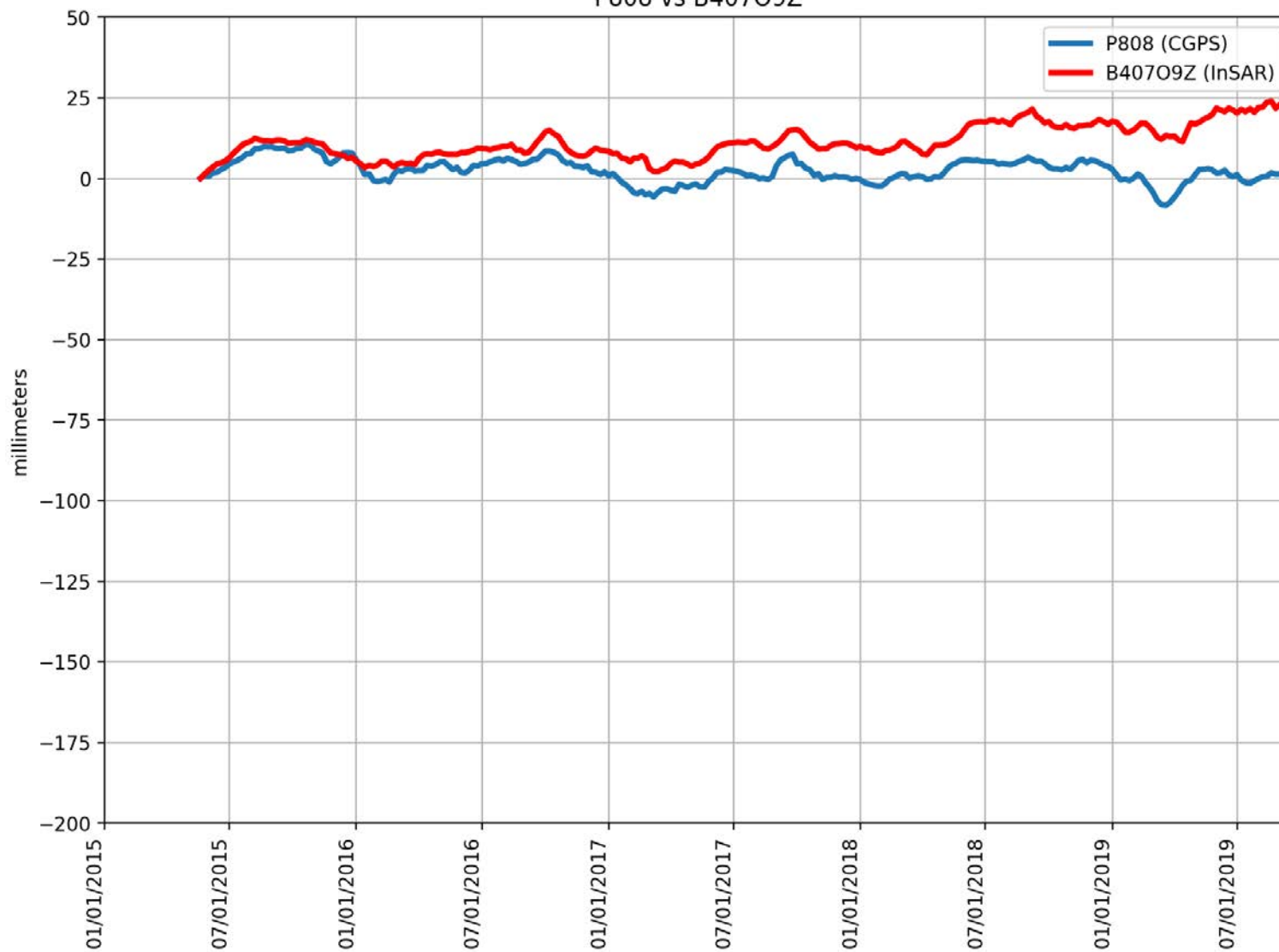
P800 vs AP1EDZR



RMSE: 11.69 mm
Correlation: 0.25

Appendix B

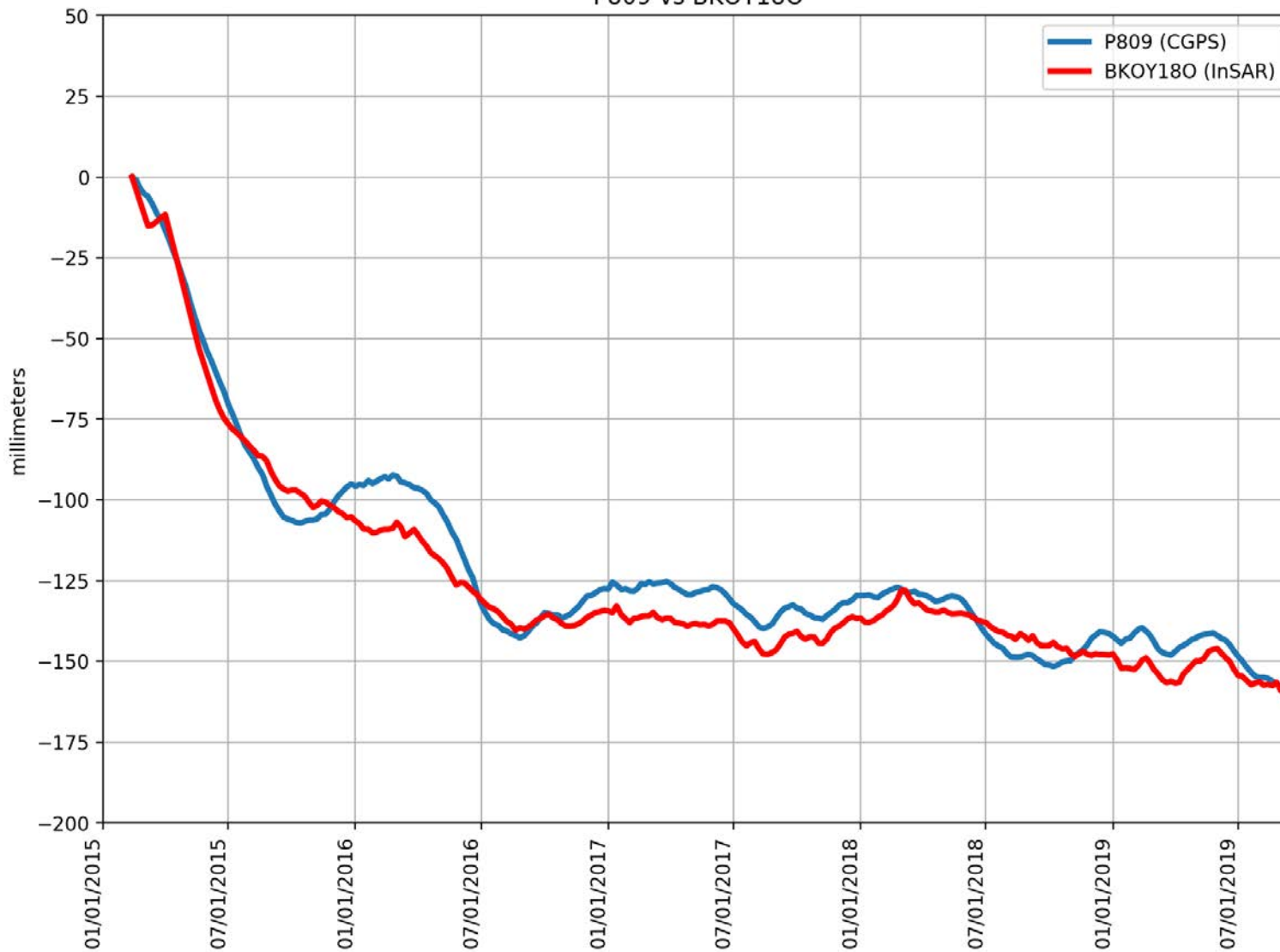
P808 vs B40709Z



RMSE: 10.65 mm
Correlation: 0.20

Appendix B

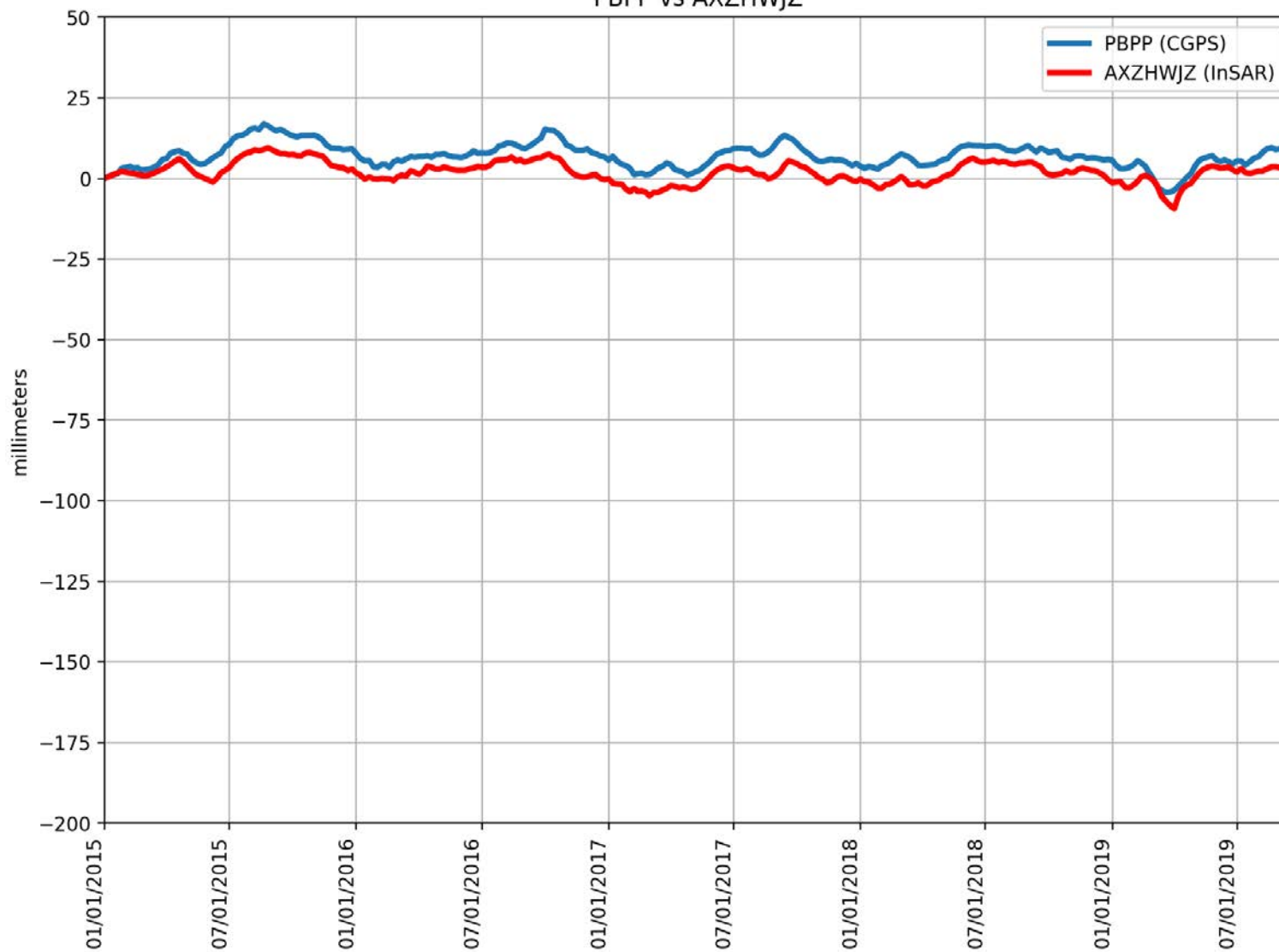
P809 vs BKOY180



RMSE: 7.67 mm
Correlation: 0.98

Appendix B

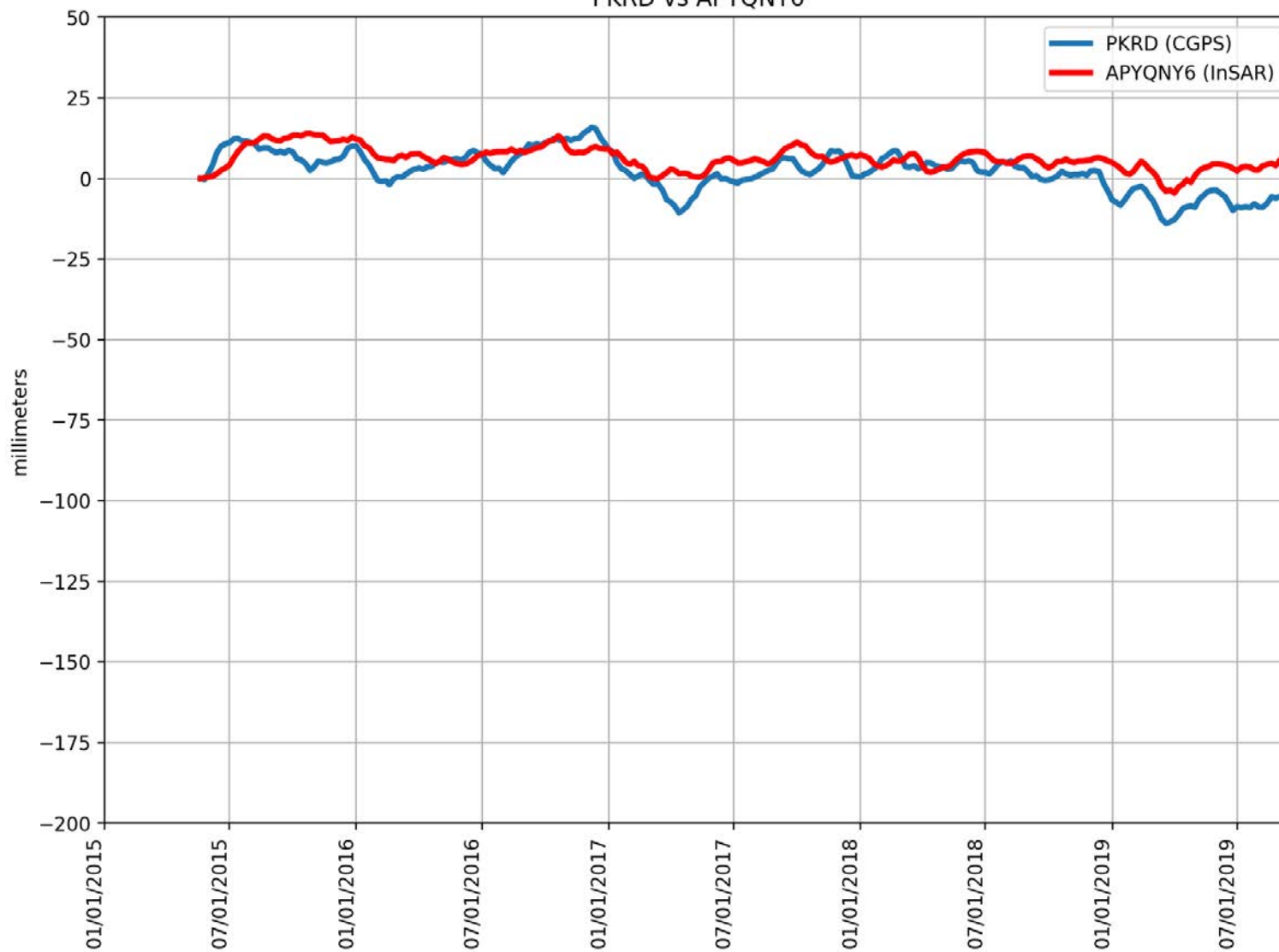
PBPP vs AXZHWJZ



RMSE: 5.40 mm
Correlation: 0.88

Appendix B

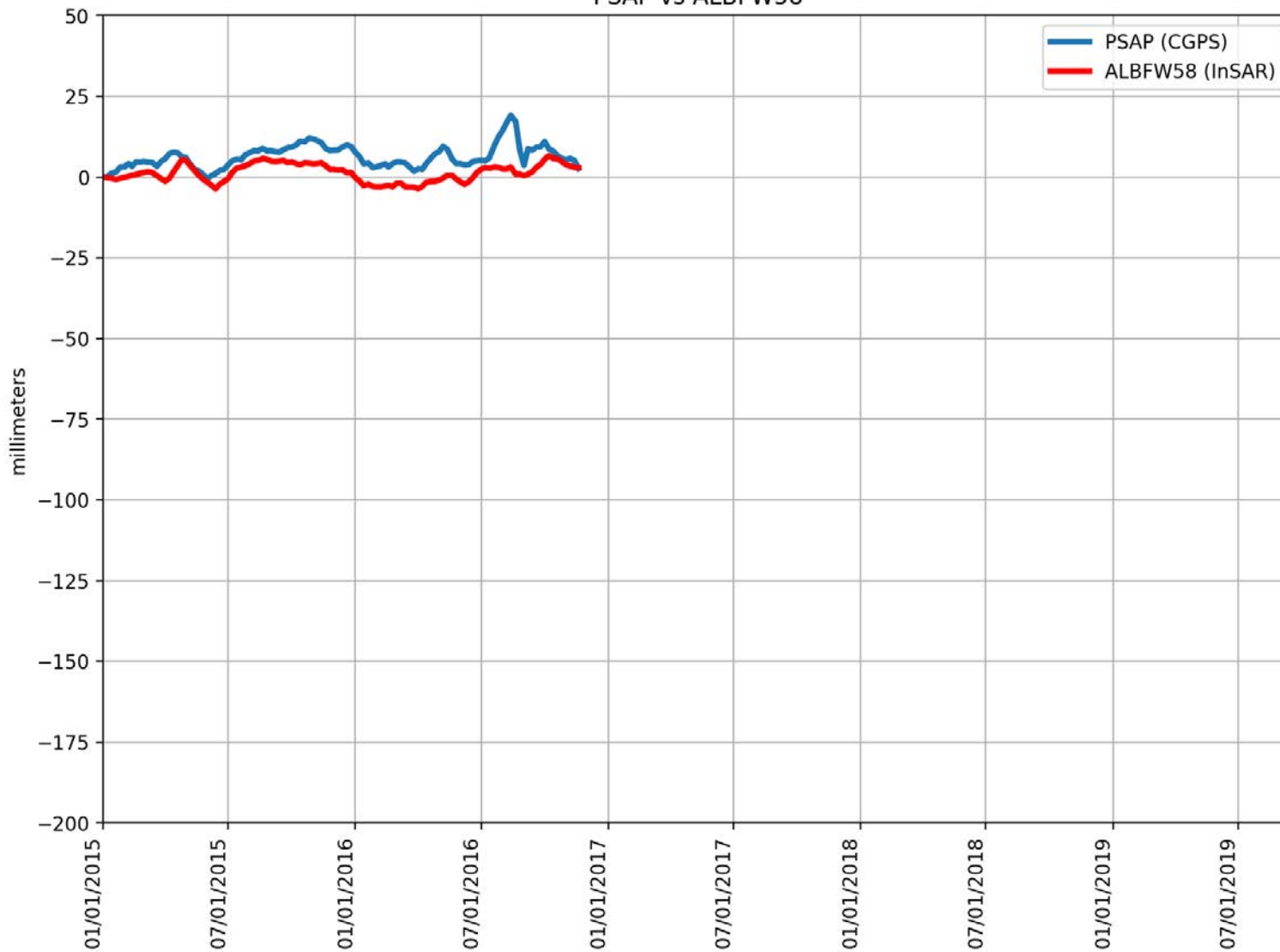
PKRD vs APYQNY6



RMSE: 5.93 mm
Correlation: 0.69

Appendix B

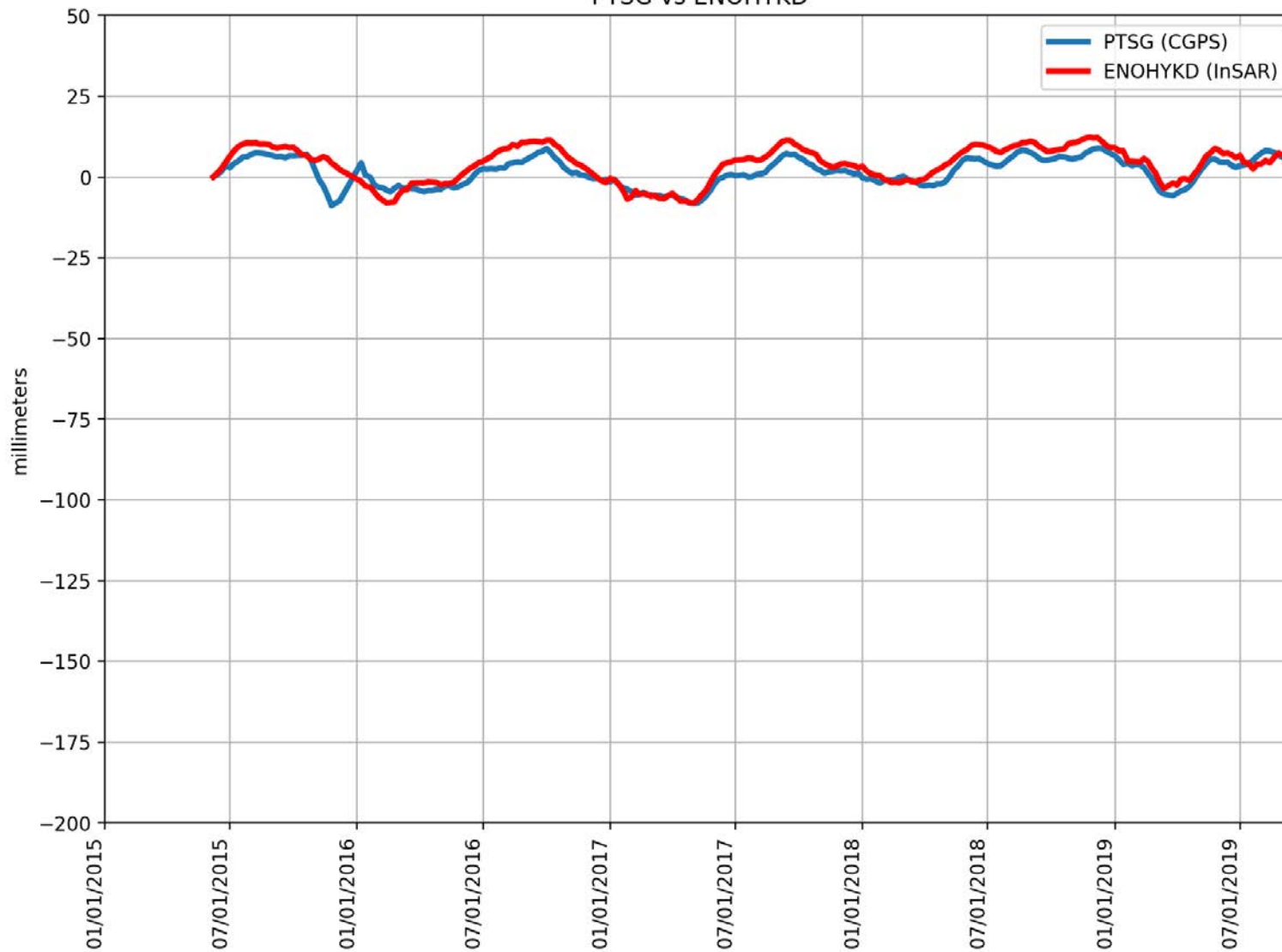
PSAP vs ALBFW58



RMSE: 5.81 mm
Correlation: 0.58

Appendix B

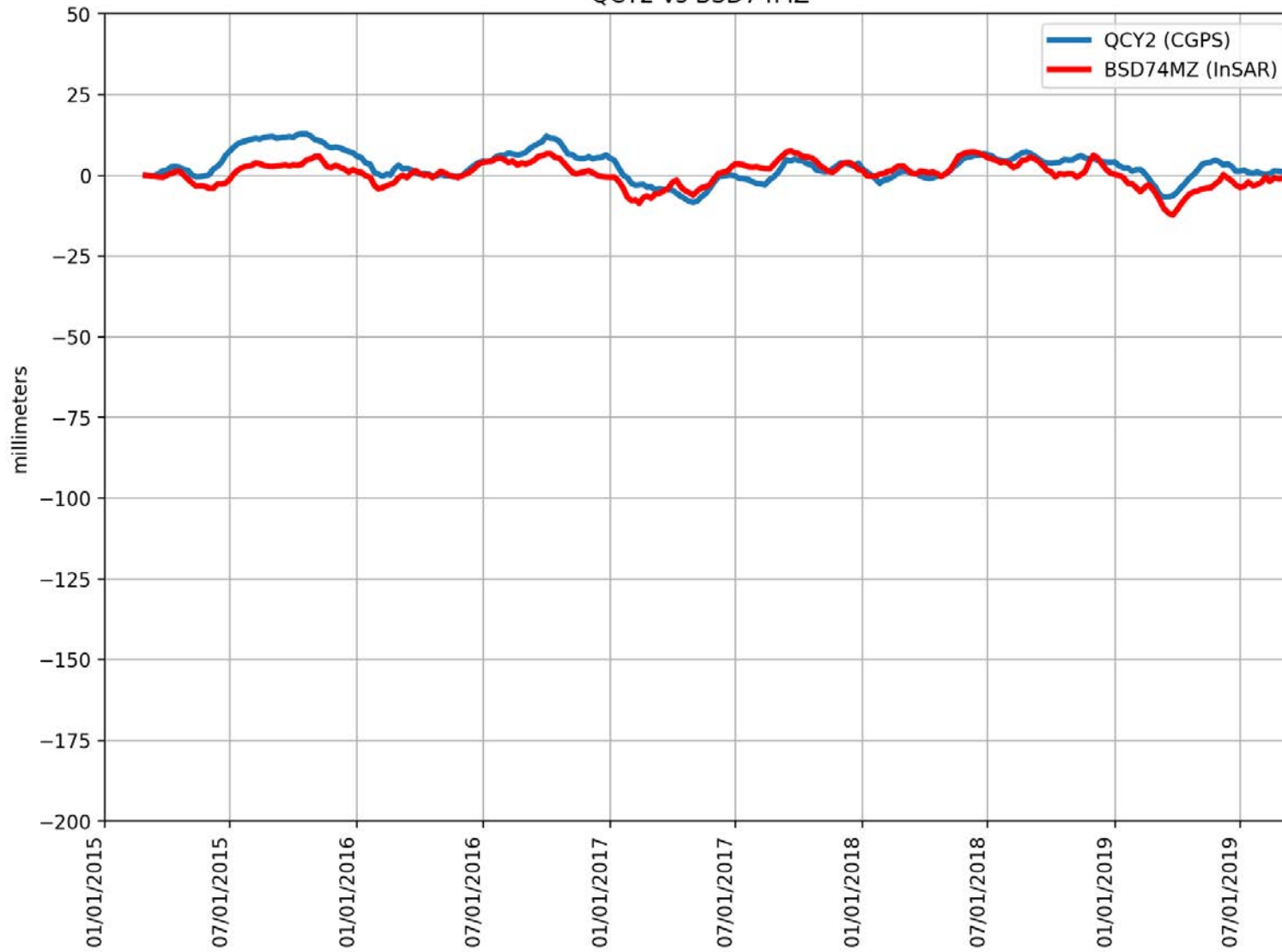
PTSG vs ENOHYKD



RMSE: 3.46 mm
Correlation: 0.89

Appendix B

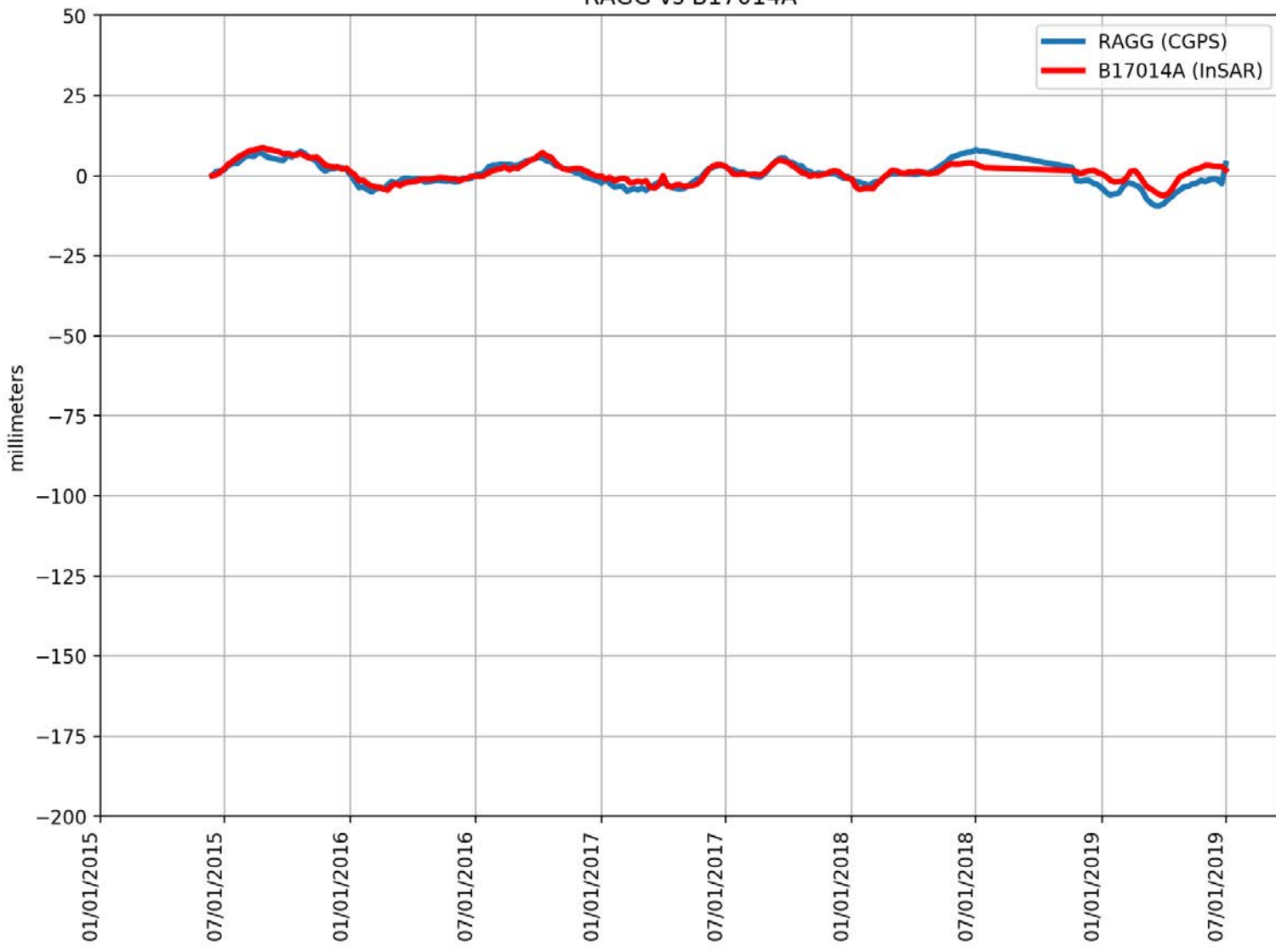
QCY2 vs BSD74MZ



RMSE: 4.09 mm
Correlation: 0.67

Appendix B

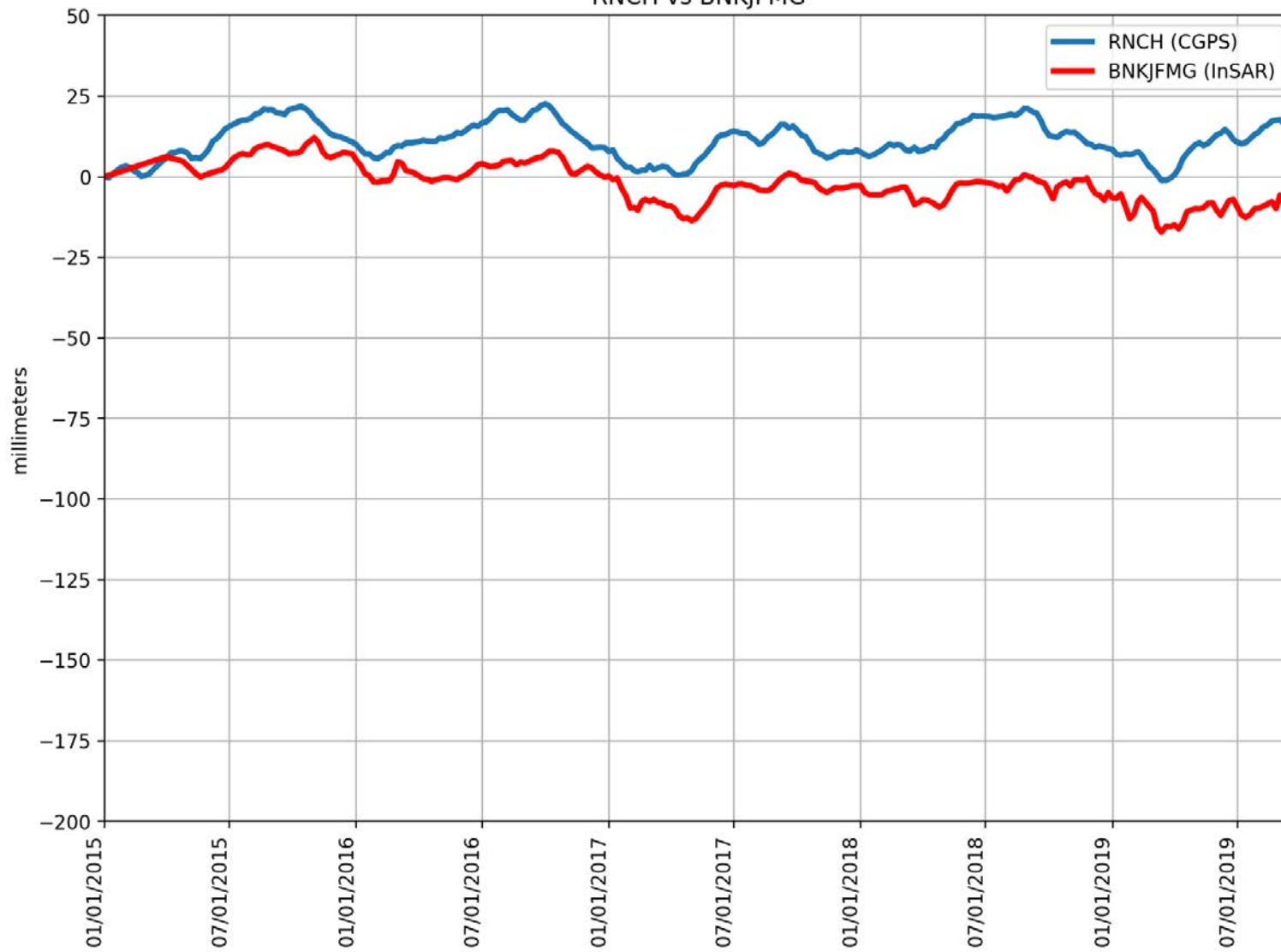
RAGG vs B17014A



RMSE: 2.01 mm
Correlation: 0.86

Appendix B

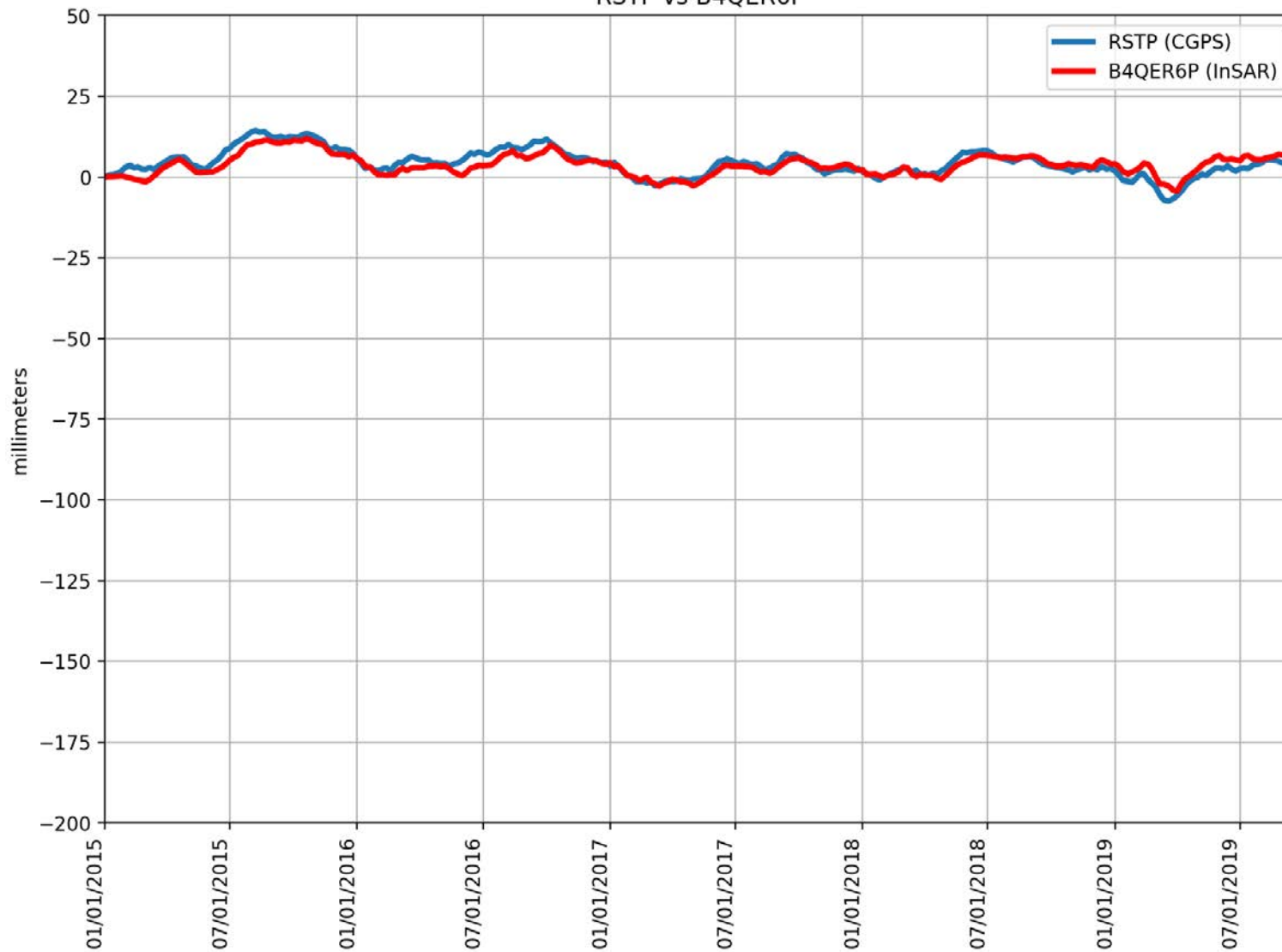
RNCH vs BNKJFMG



RMSE: 14.32 mm
Correlation: 0.50

Appendix B

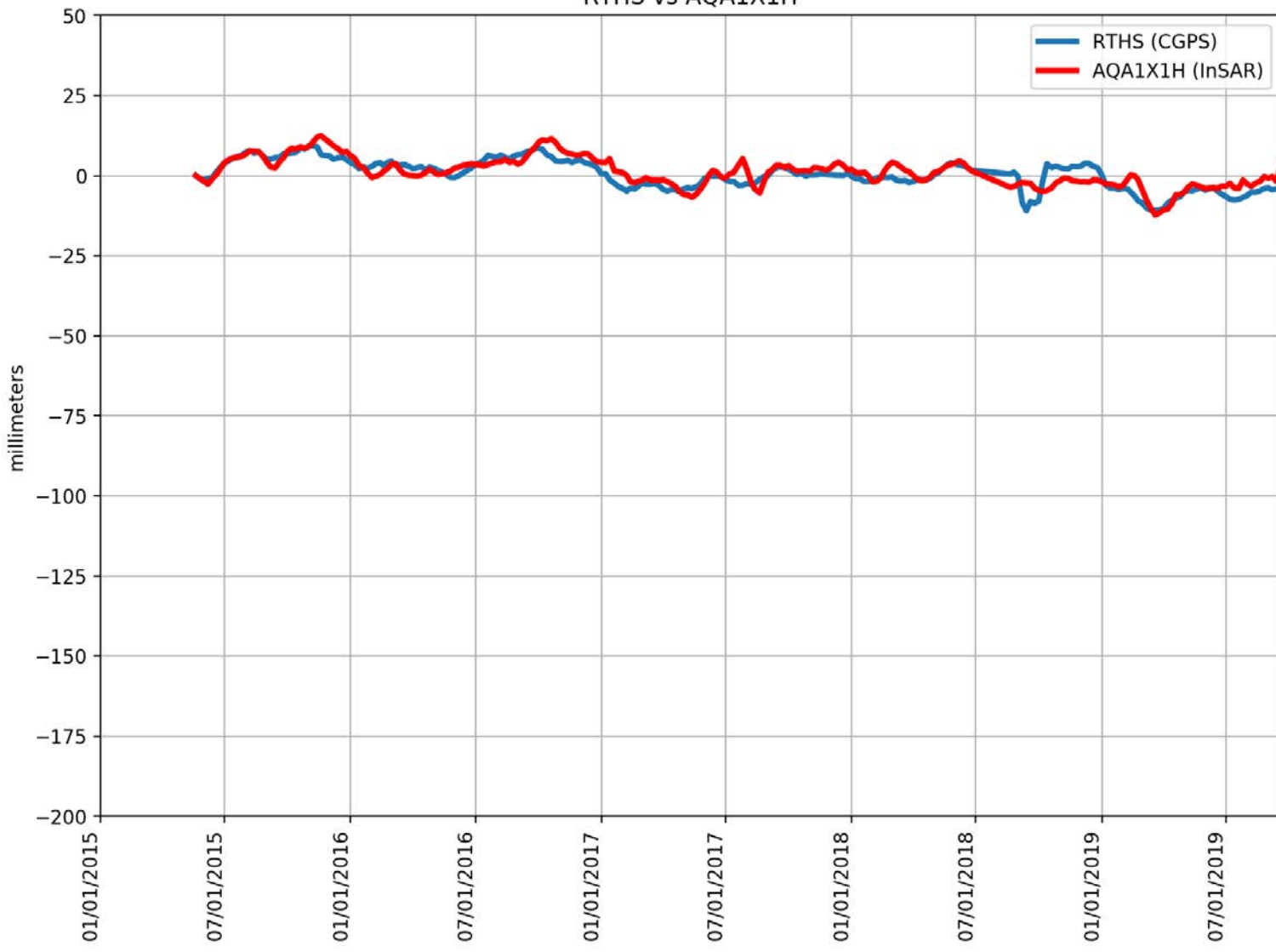
RSTP vs B4QER6P



RMSE: 2.15 mm
Correlation: 0.86

Appendix B

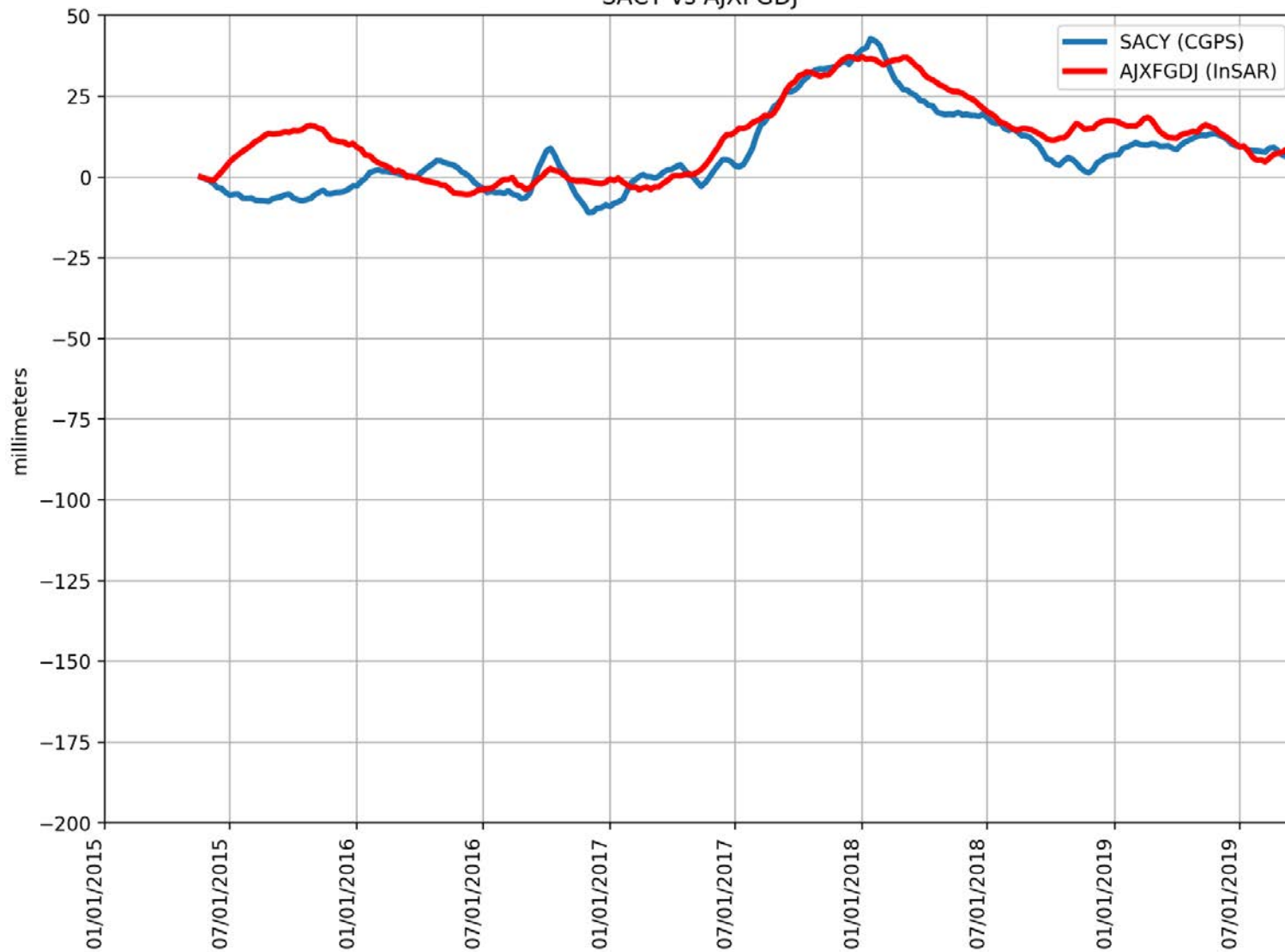
RTHS vs AQA1X1H



RMSE: 2.85 mm
Correlation: 0.82

Appendix B

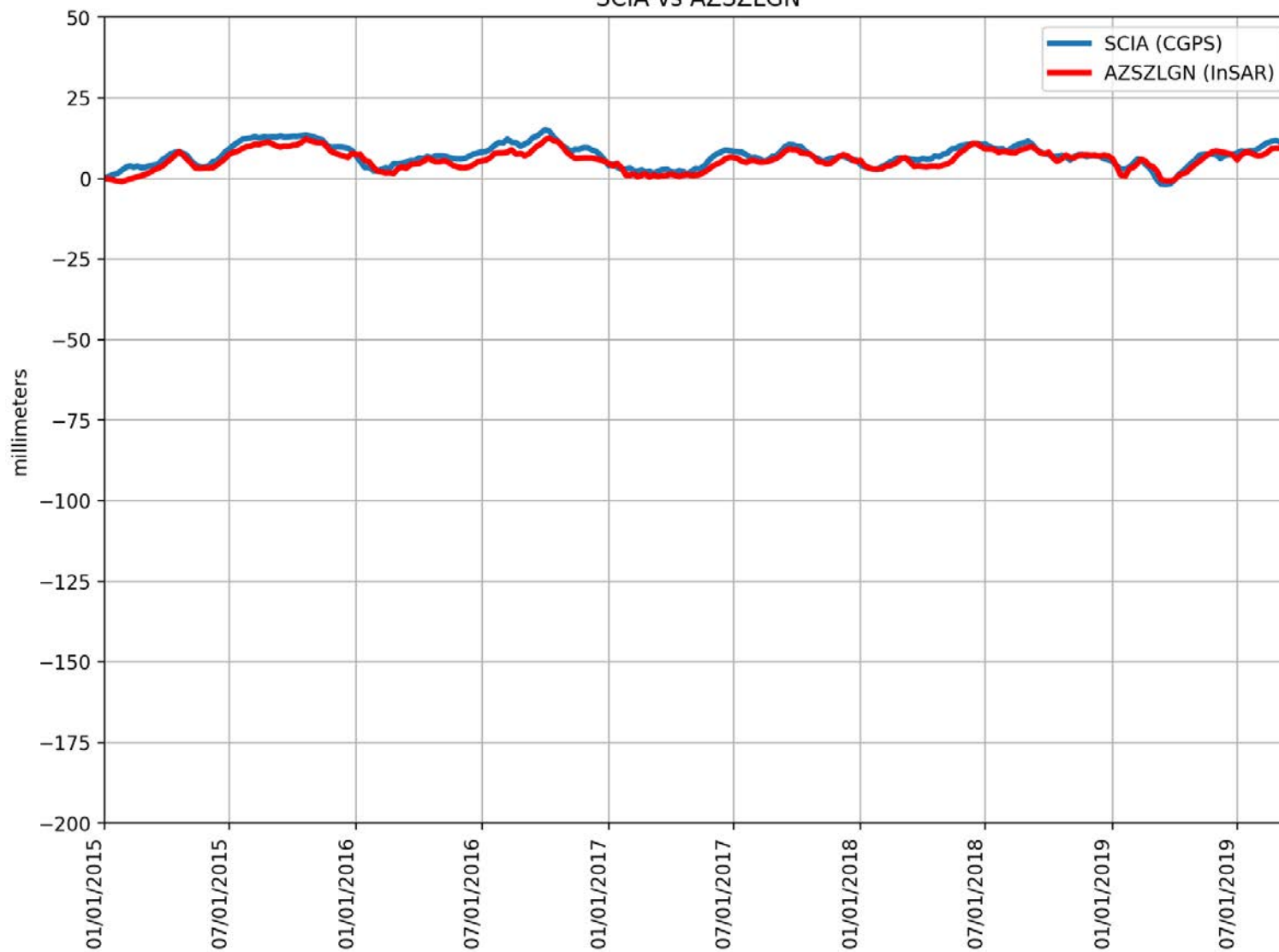
SACY vs AJXFGDJ



RMSE: 8.06 mm
Correlation: 0.85

Appendix B

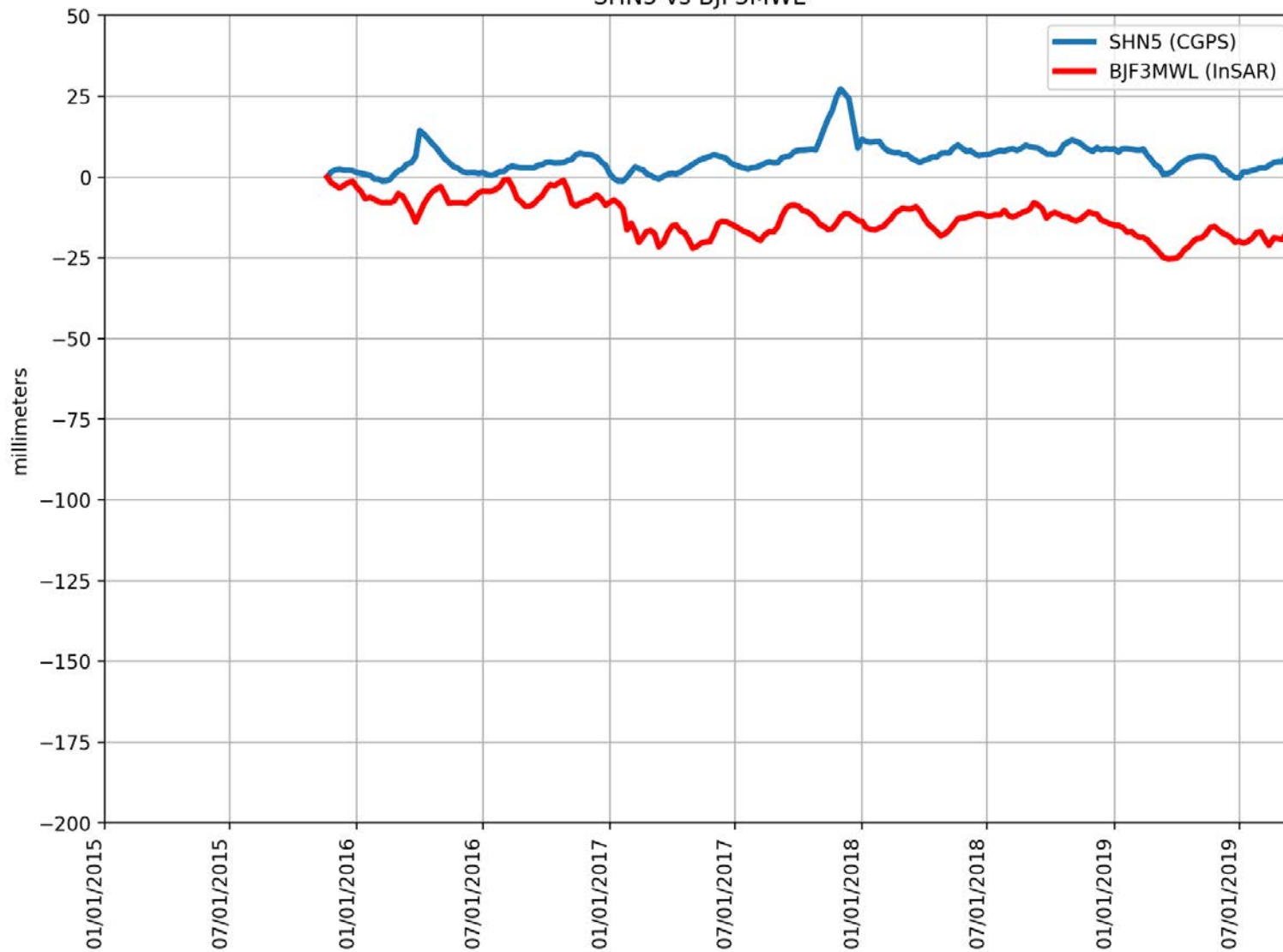
SCIA vs AZSZLGN



RMSE: 1.85 mm
Correlation: 0.92

Appendix B

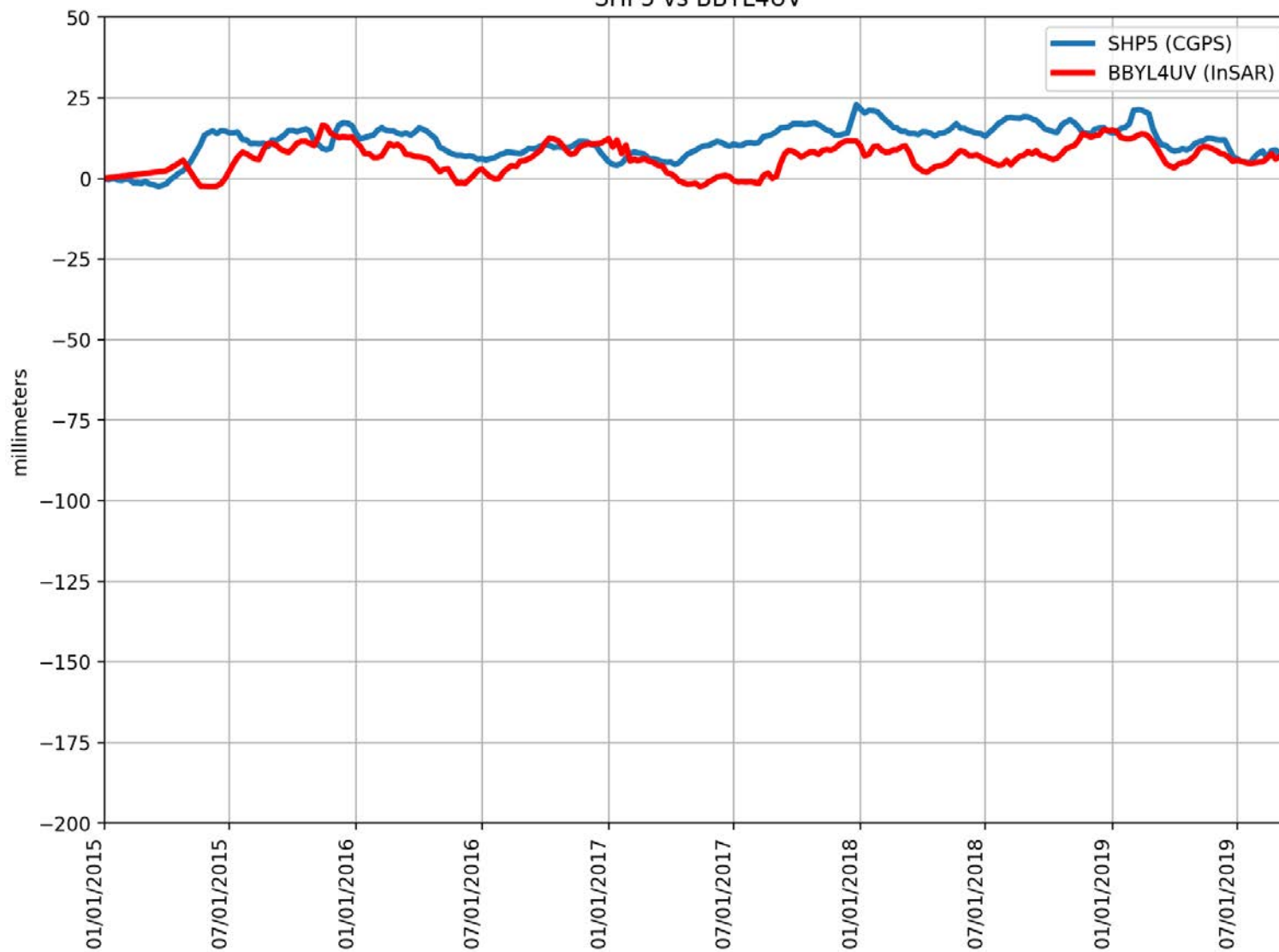
SHN5 vs BJF3MWL



RMSE: 19.68 mm
Correlation: -0.06

Appendix B

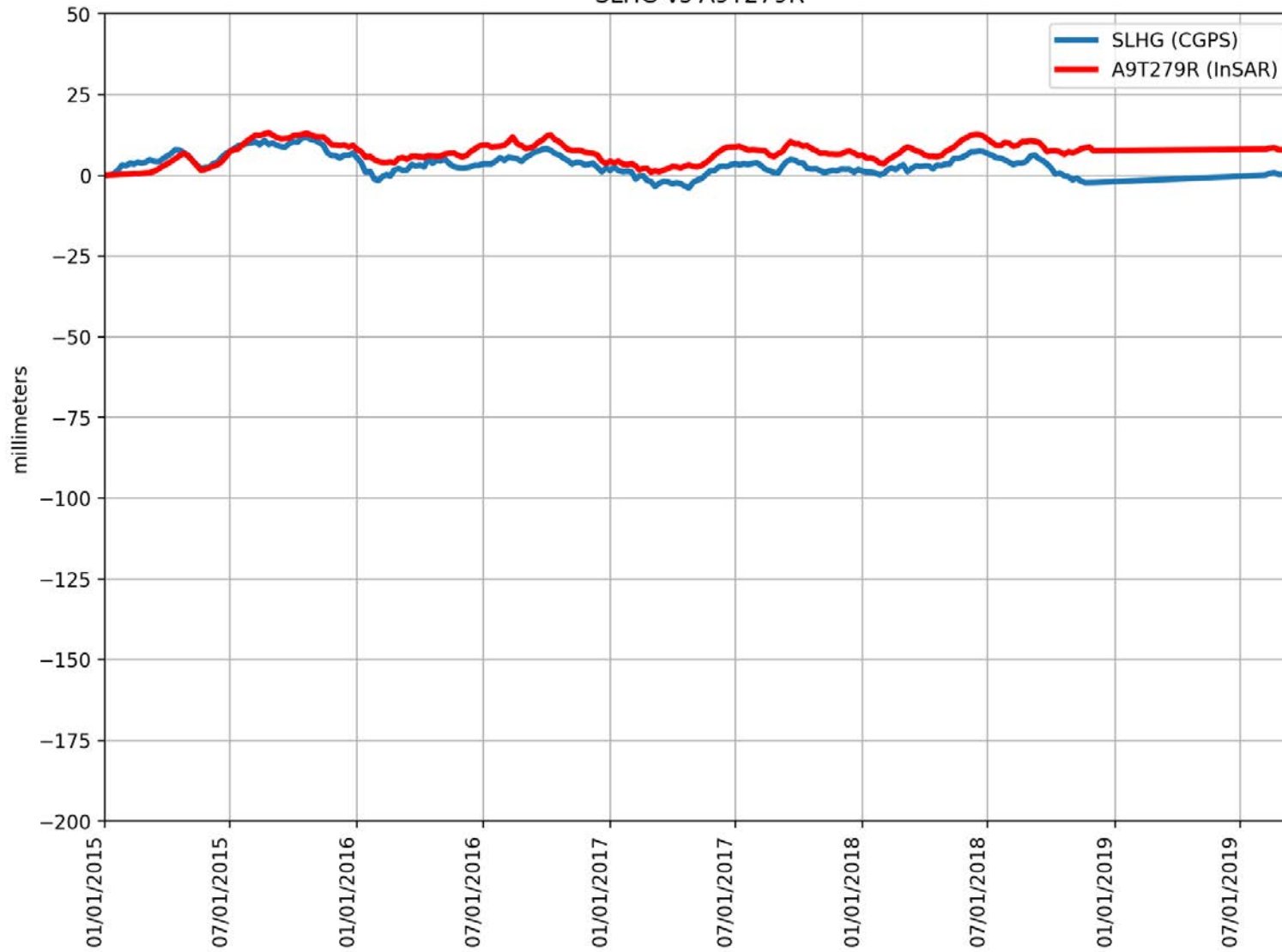
SHP5 vs BBYL4UV



RMSE: 7.19 mm
Correlation: 0.46

Appendix B

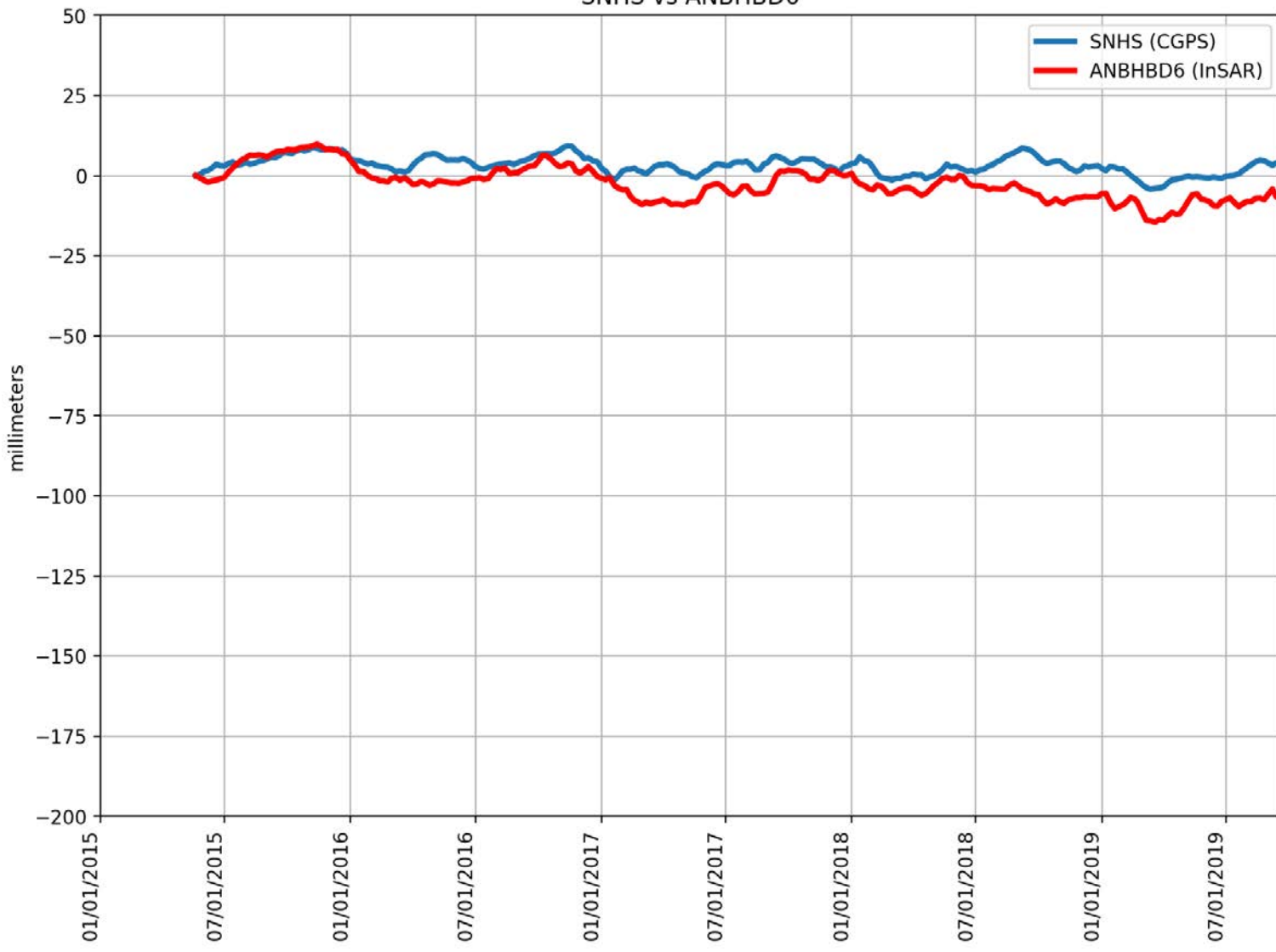
SLHG vs A9T279R



RMSE: 4.44 mm
Correlation: 0.65

Appendix B

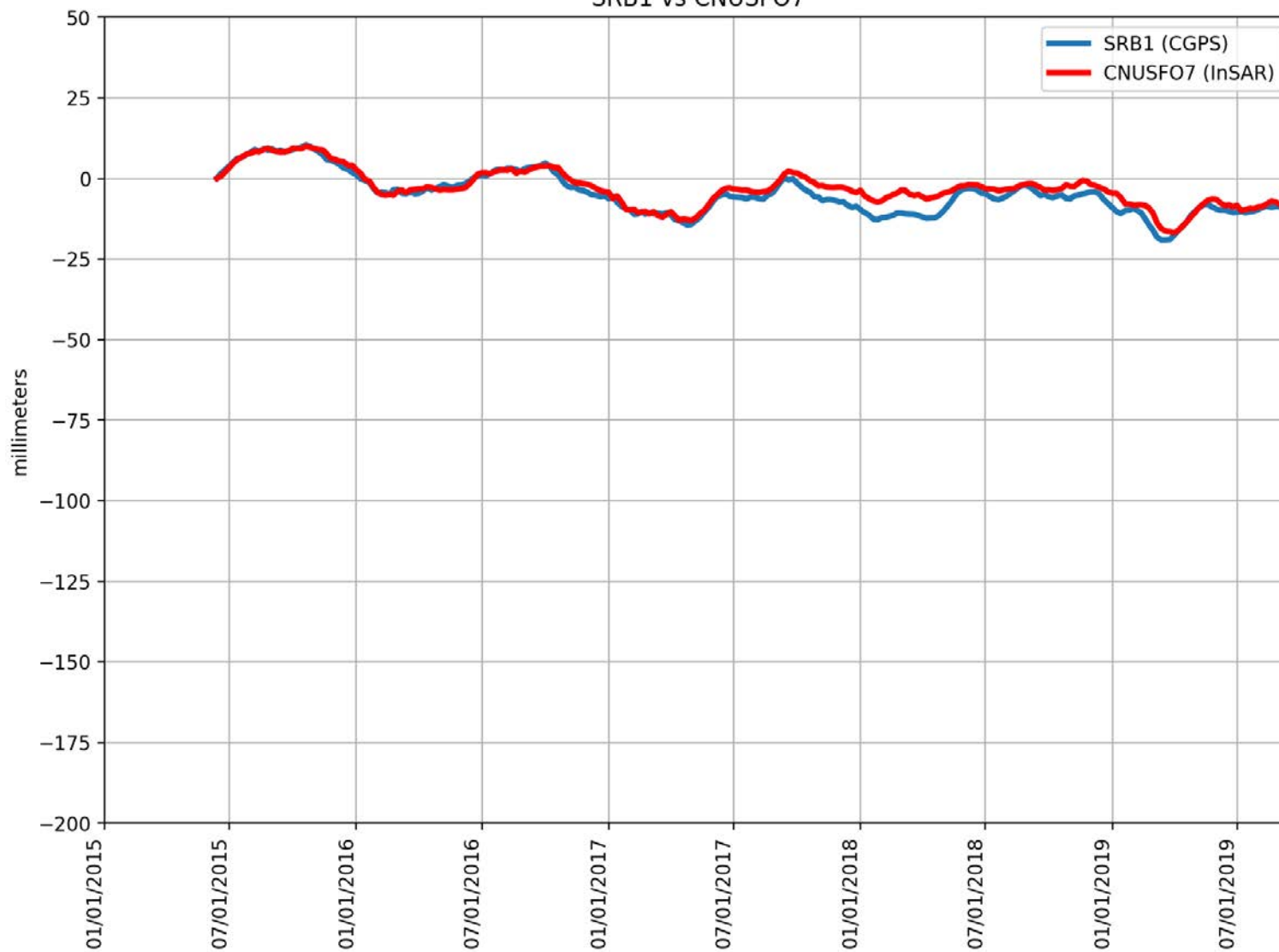
SNHS vs ANBHBD6



RMSE: 6.90 mm
Correlation: 0.69

Appendix B

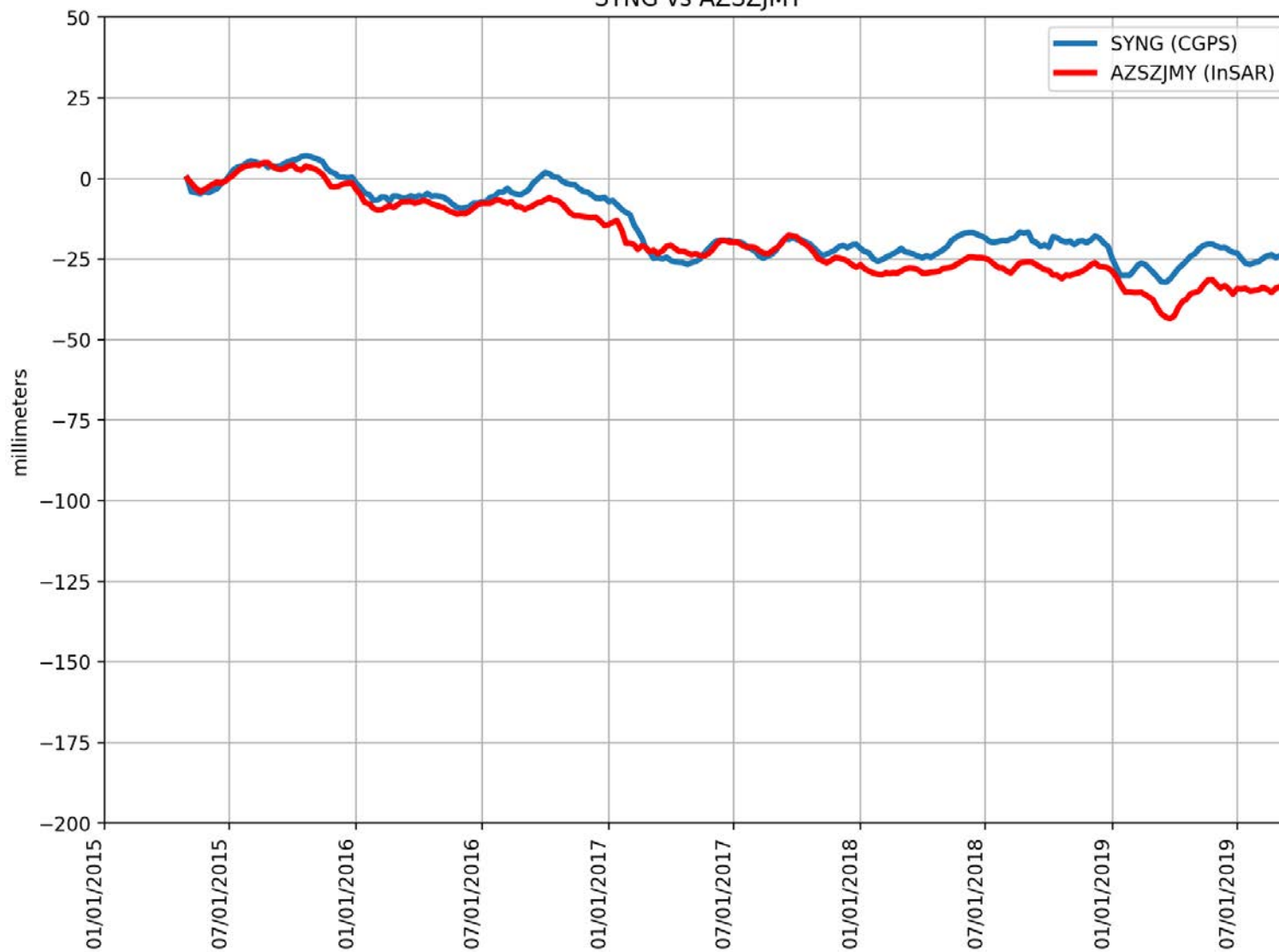
SRB1 vs CNUSFO7



RMSE: 2.61 mm
Correlation: 0.95

Appendix B

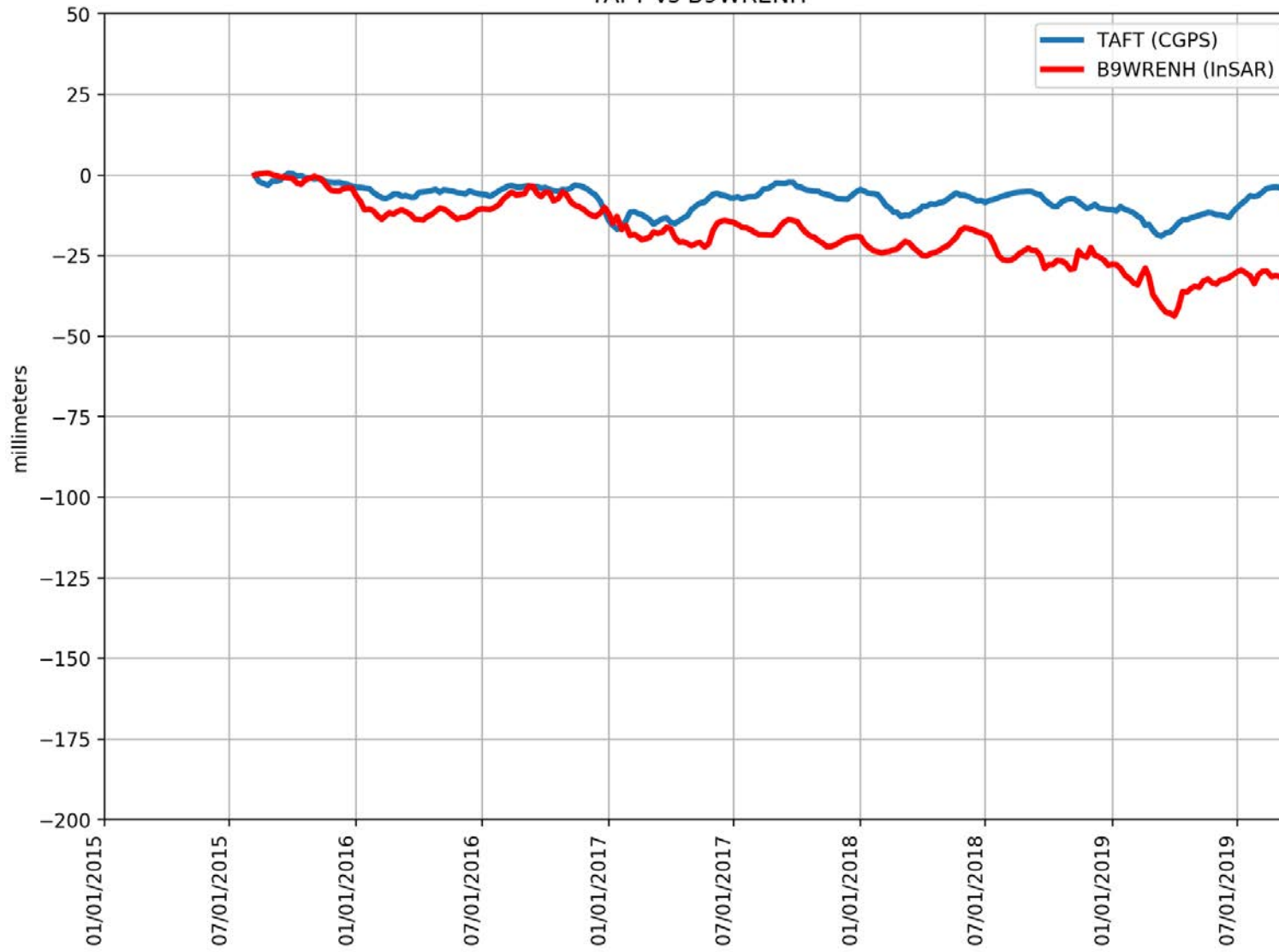
SYNG vs AZSZJMY



RMSE: 6.23 mm
Correlation: 0.95

Appendix B

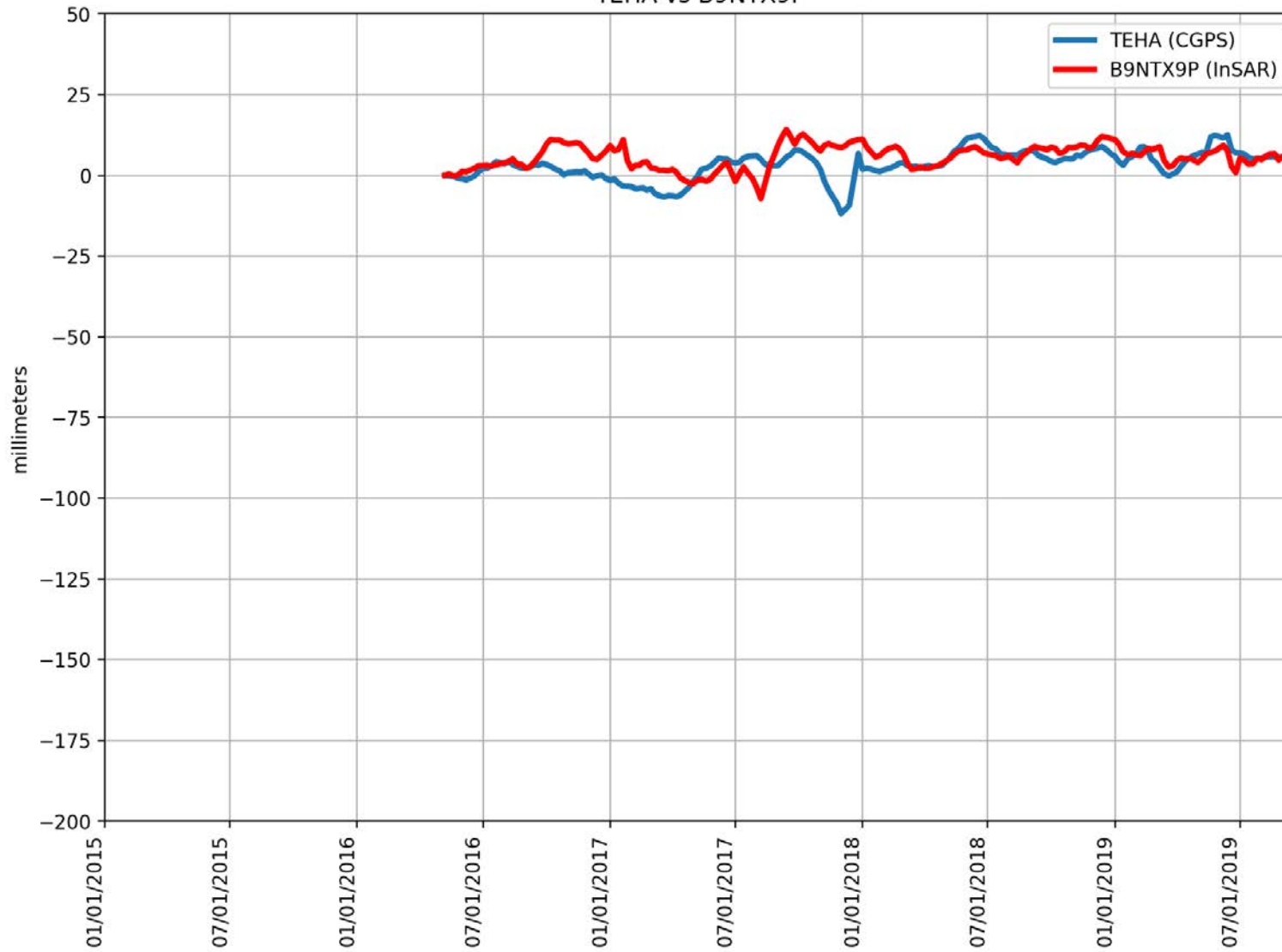
TAFT vs B9WRENH



RMSE: 13.54 mm
Correlation: 0.69

Appendix B

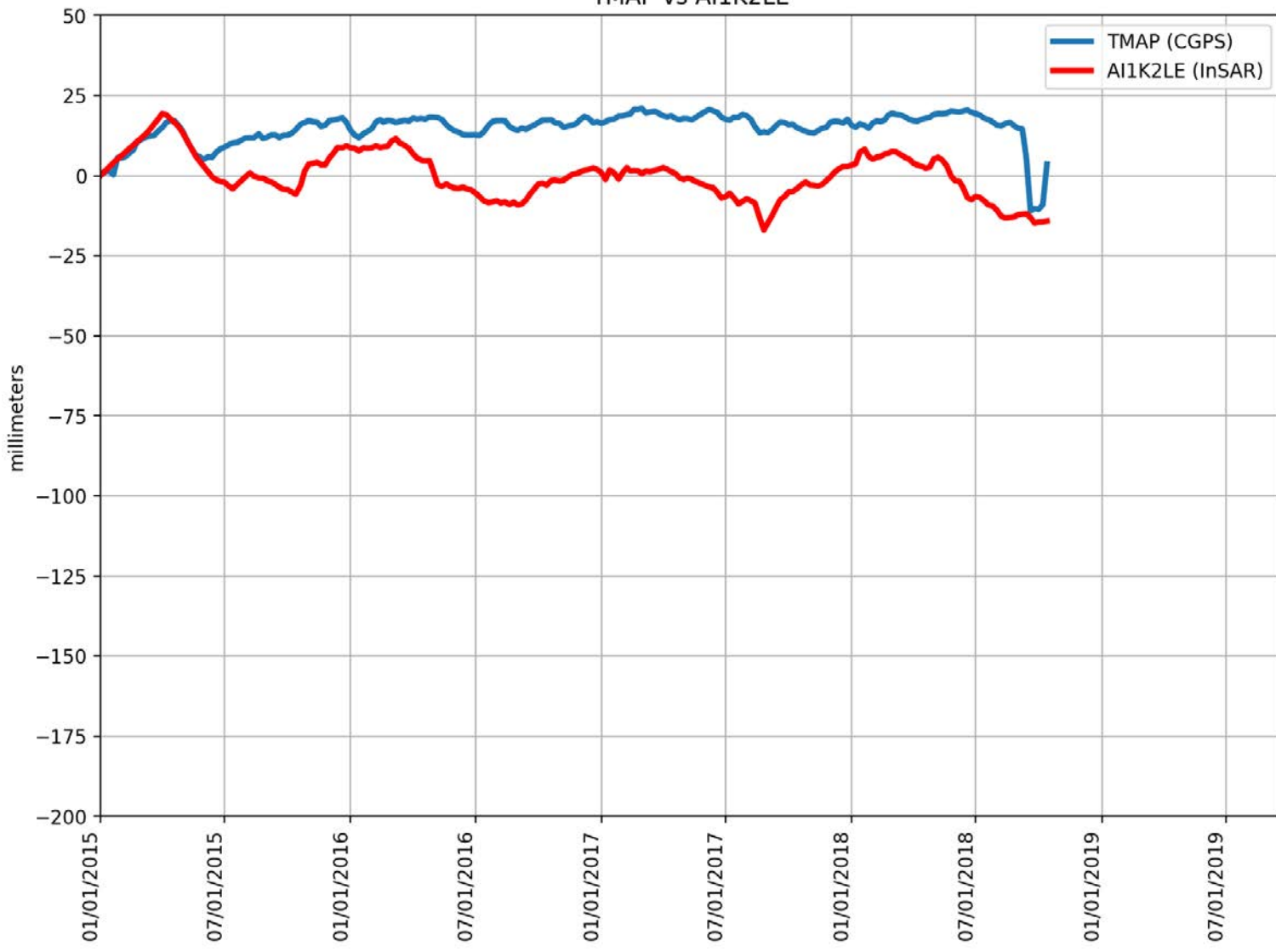
TEHA vs B9NTX9P



RMSE: 5.60 mm
Correlation: 0.26

Appendix B

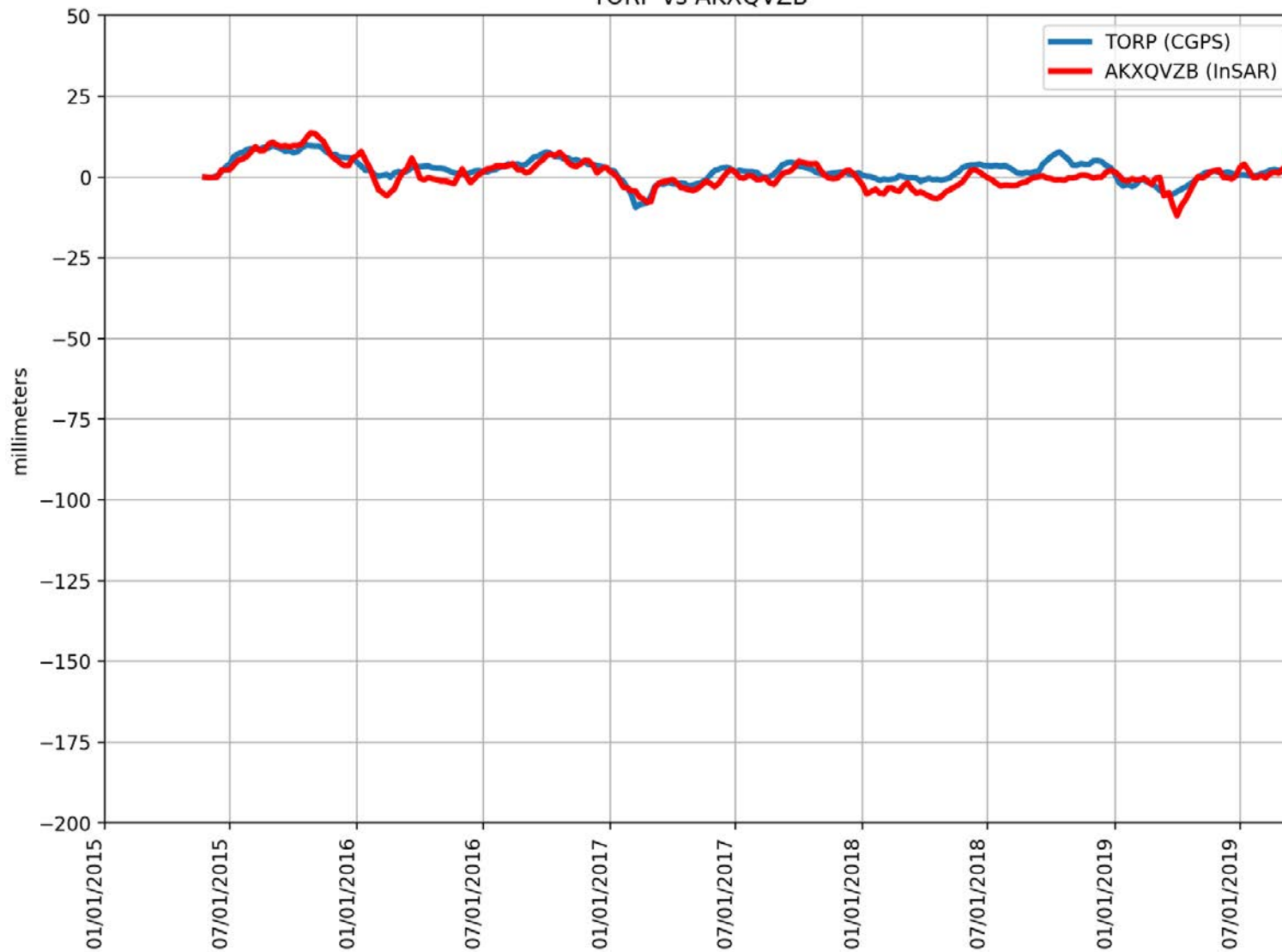
TMAP vs A11K2LE



RMSE: 16.93 mm
Correlation: 0.15

Appendix B

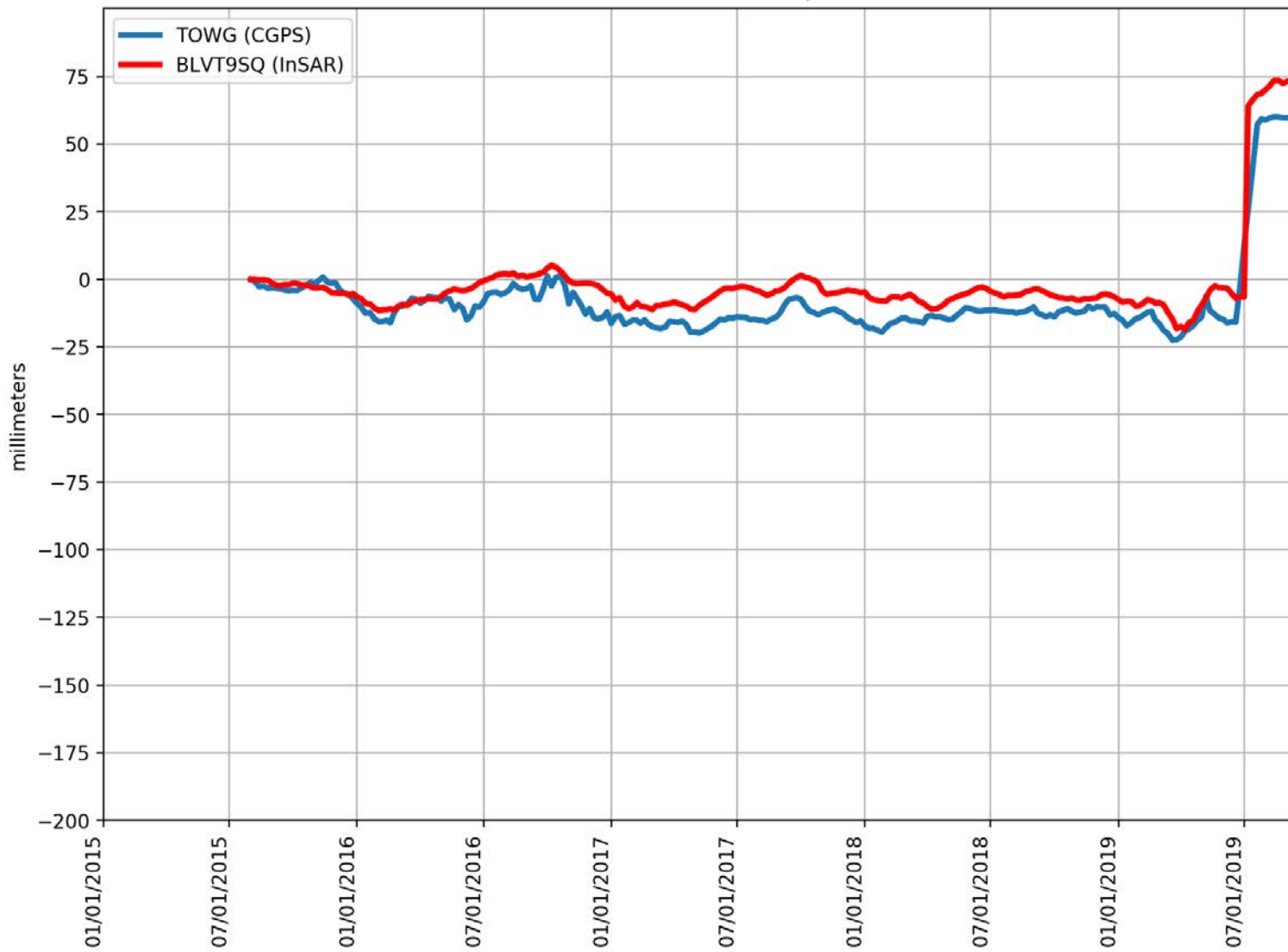
TORP vs AKXQVZB



RMSE: 2.84 mm
Correlation: 0.81

Appendix B

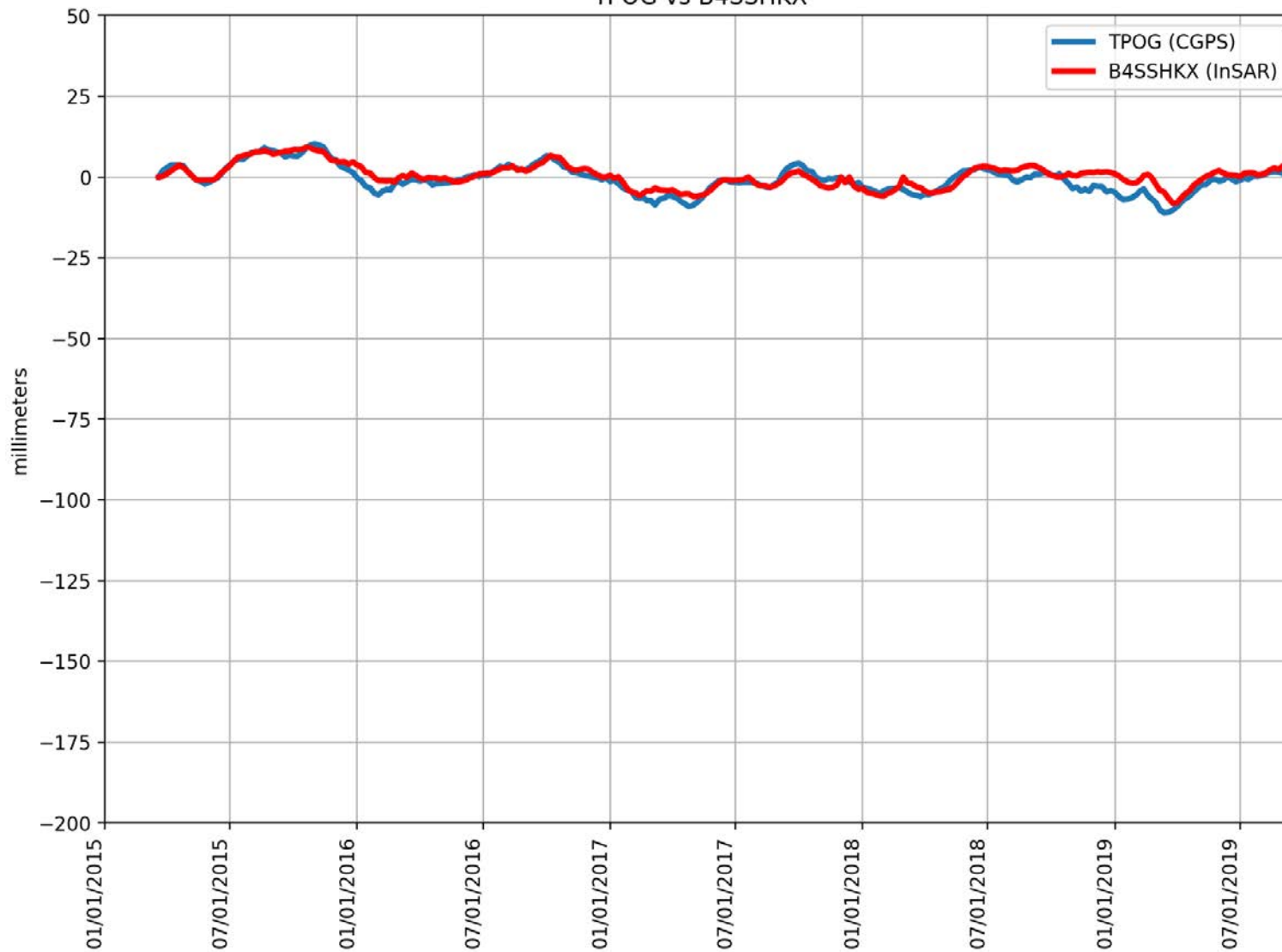
TOWG vs BLVT9SQ



RMSE: 8.04 mm
Correlation: 0.96

Appendix B

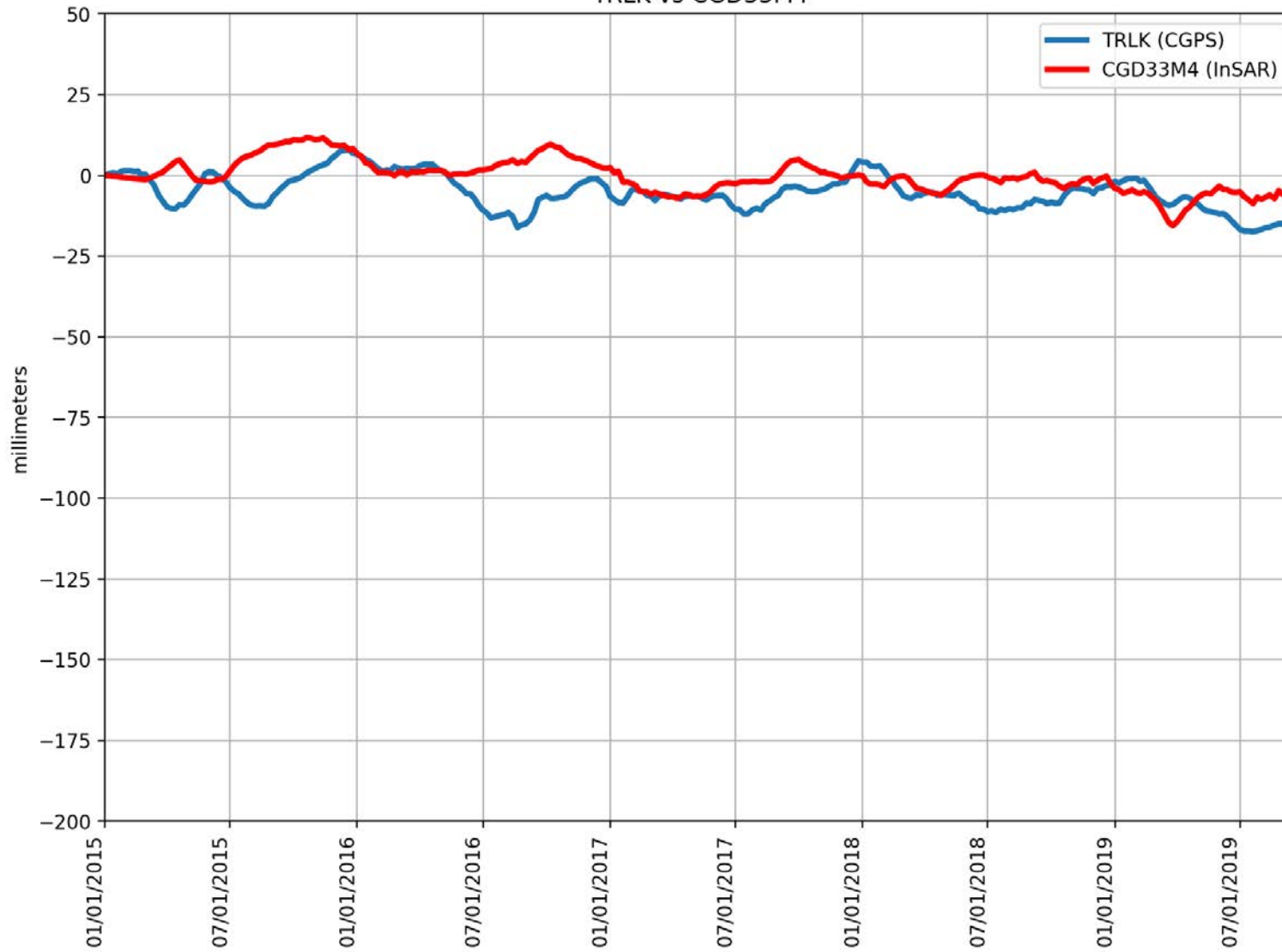
TPOG vs B4SSHKX



RMSE: 2.28 mm
Correlation: 0.88

Appendix B

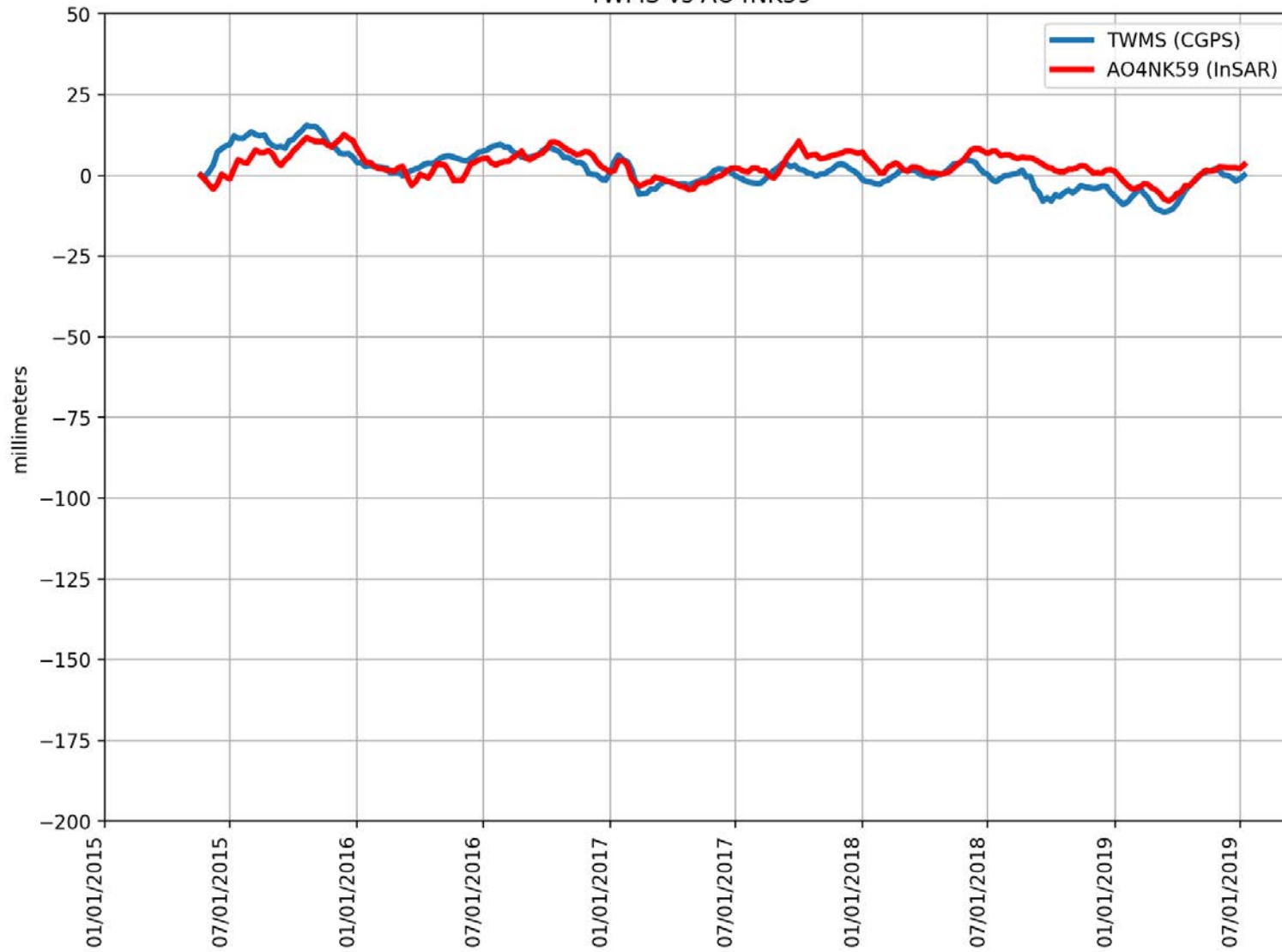
TRLK vs CGD33M4



RMSE: 7.88 mm
Correlation: 0.34

Appendix B

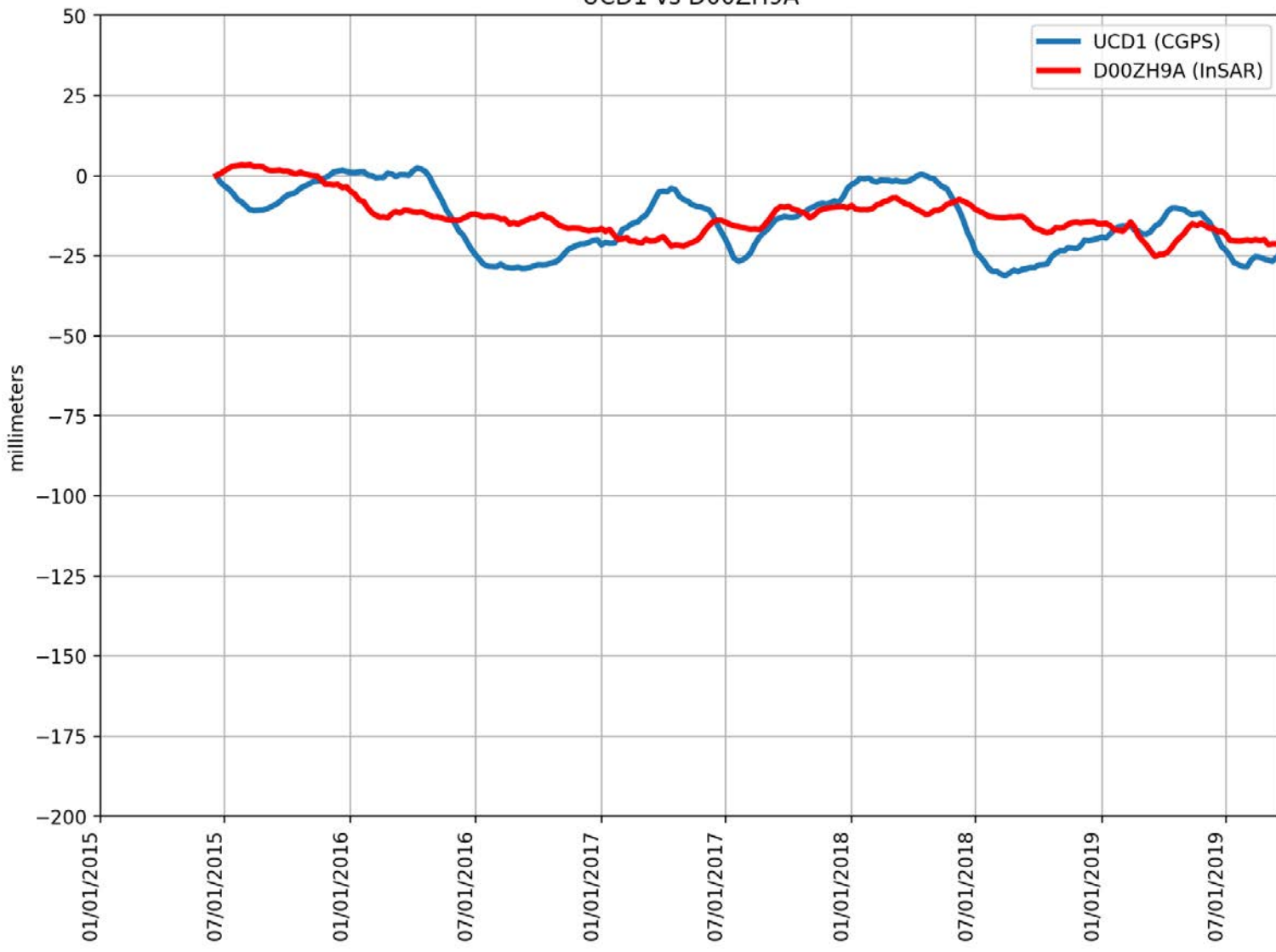
TWMS vs AO4NK59



RMSE: 4.42 mm
Correlation: 0.64

Appendix B

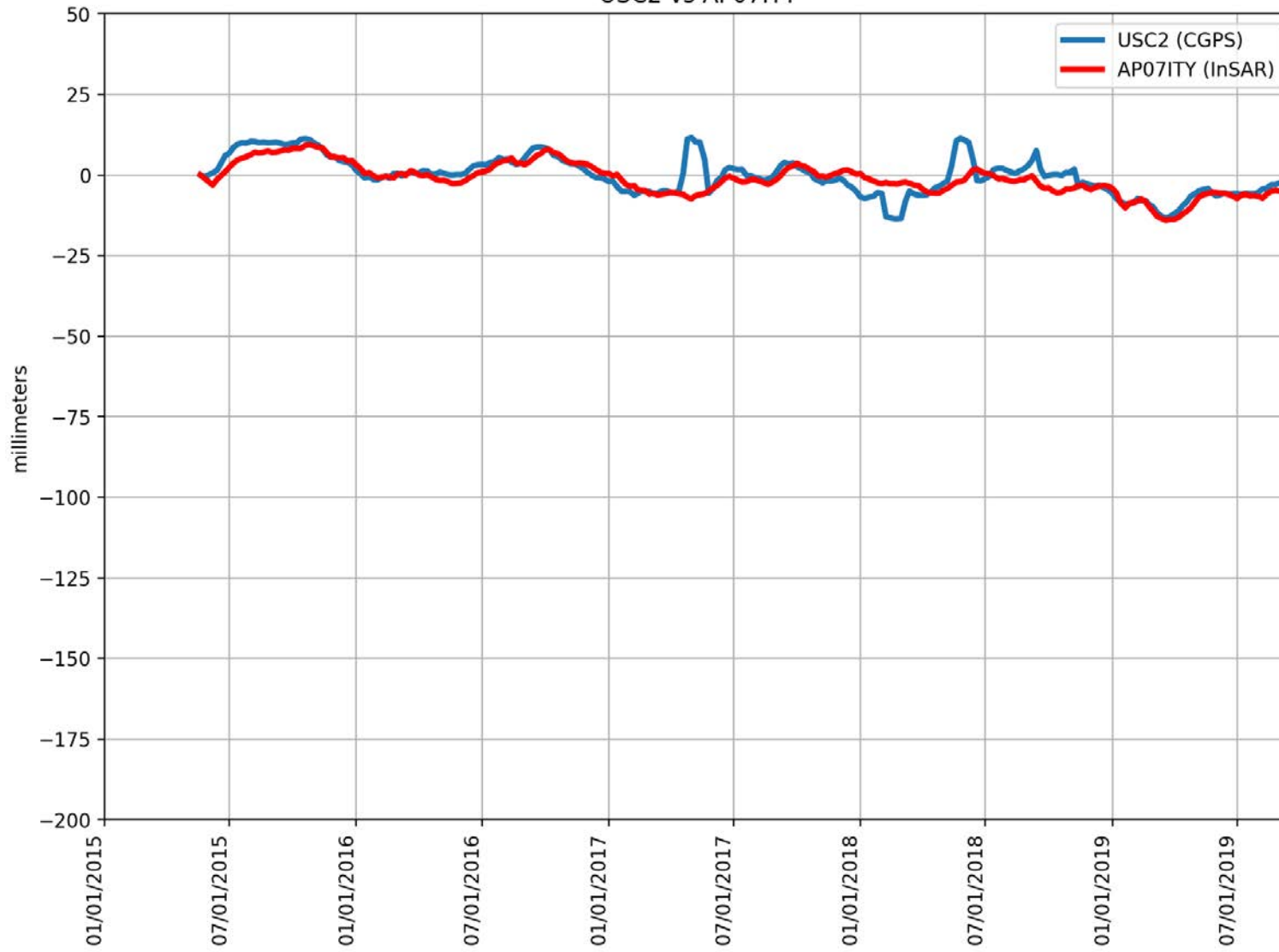
UCD1 vs D00ZH9A



RMSE: 9.19 mm
Correlation: 0.46

Appendix B

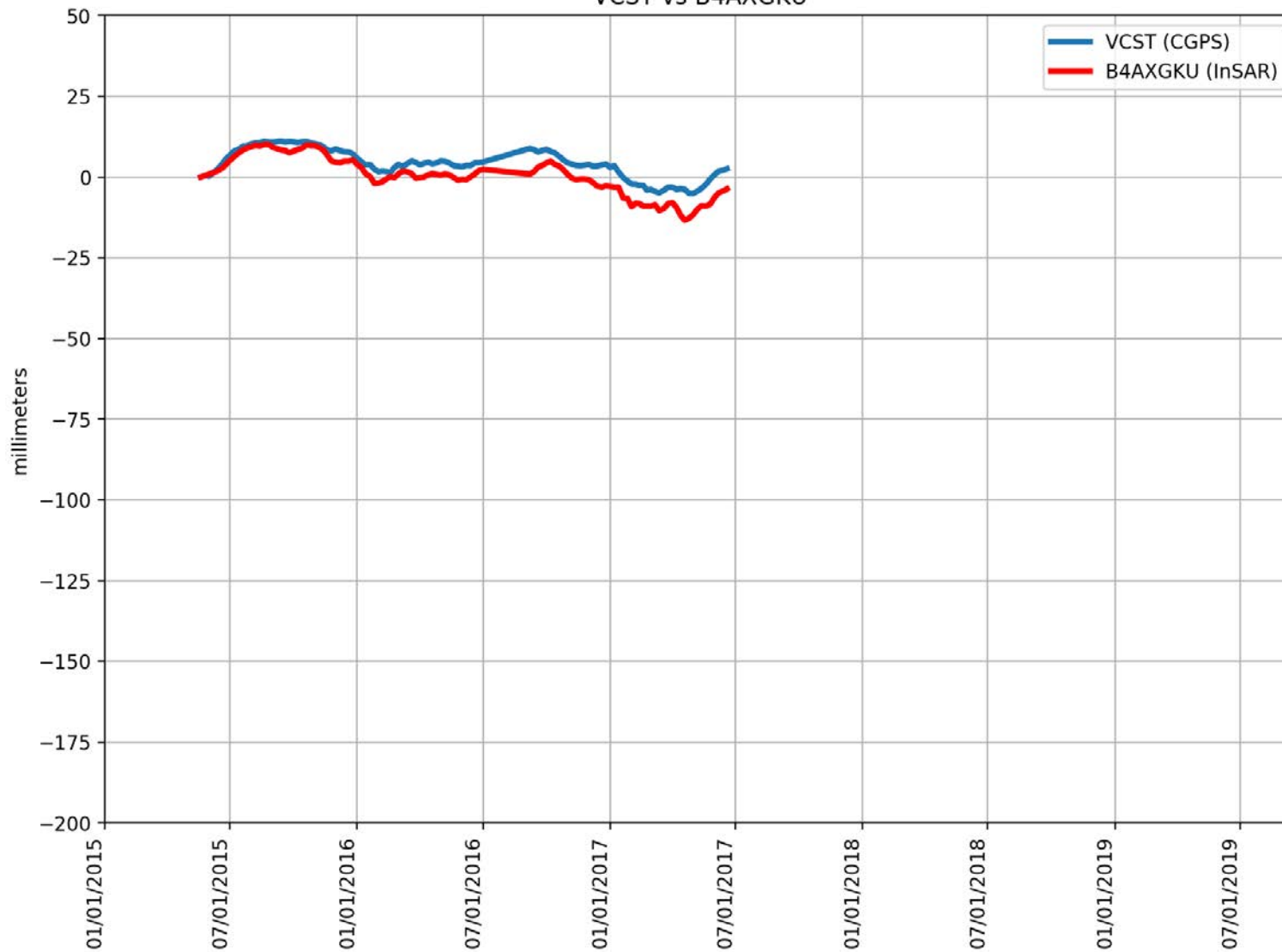
USC2 vs AP07ITY



RMSE: 3.98 mm
Correlation: 0.76

Appendix B

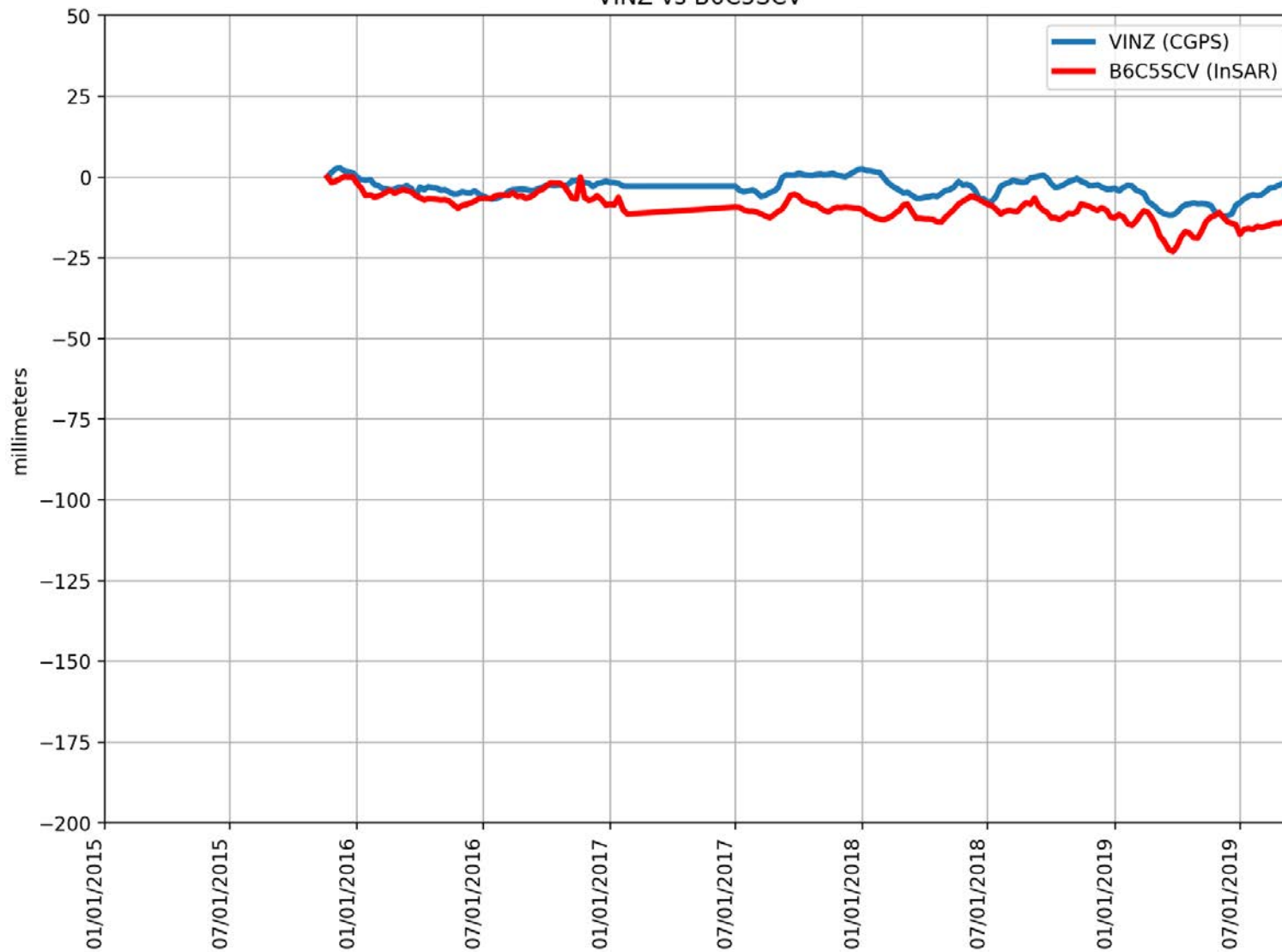
VCST vs B4AXGKU



RMSE: 4.27 mm
Correlation: 0.96

Appendix B

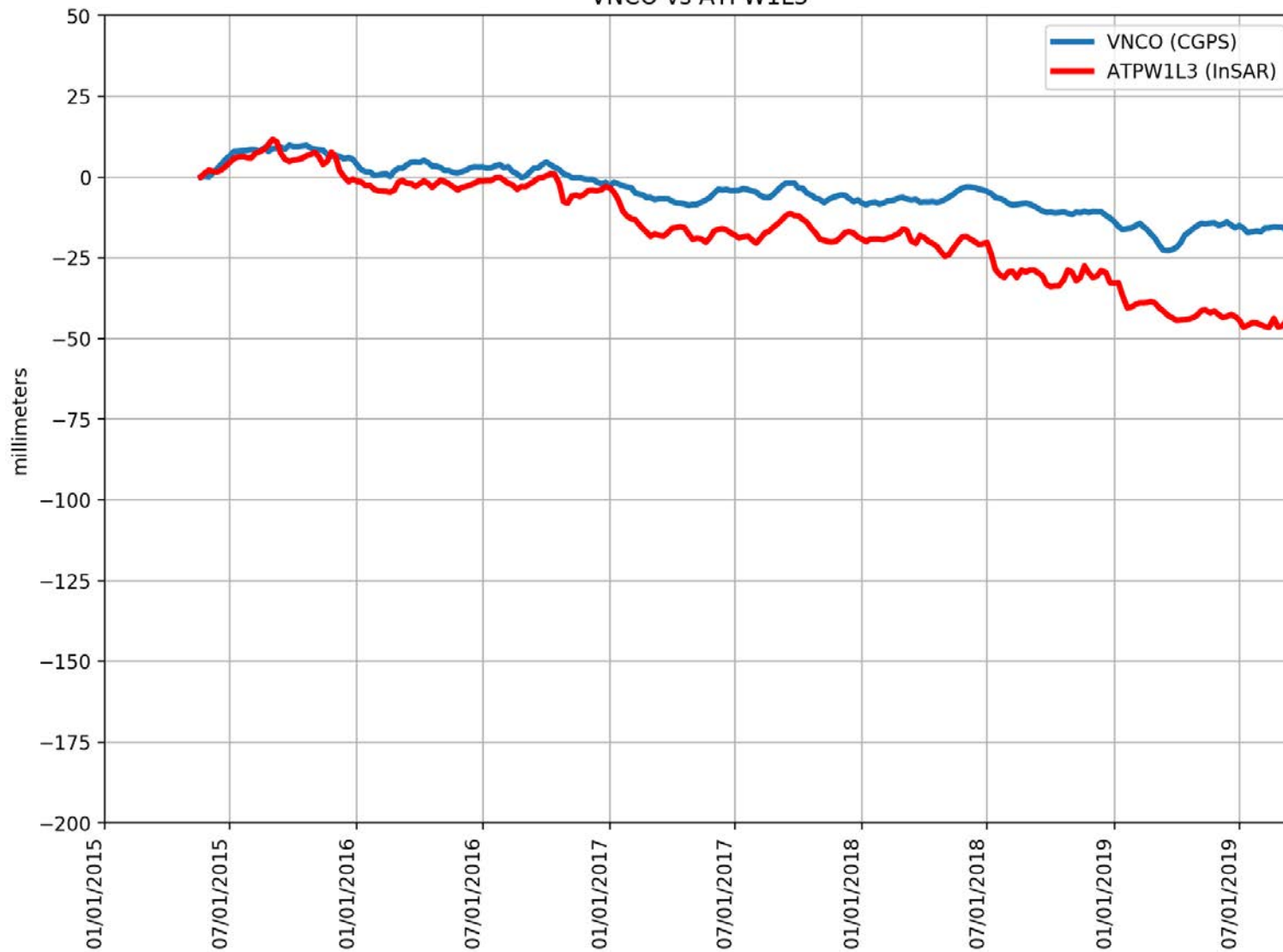
VINZ vs B6C5SCV



RMSE: 7.14 mm
Correlation: 0.53

Appendix B

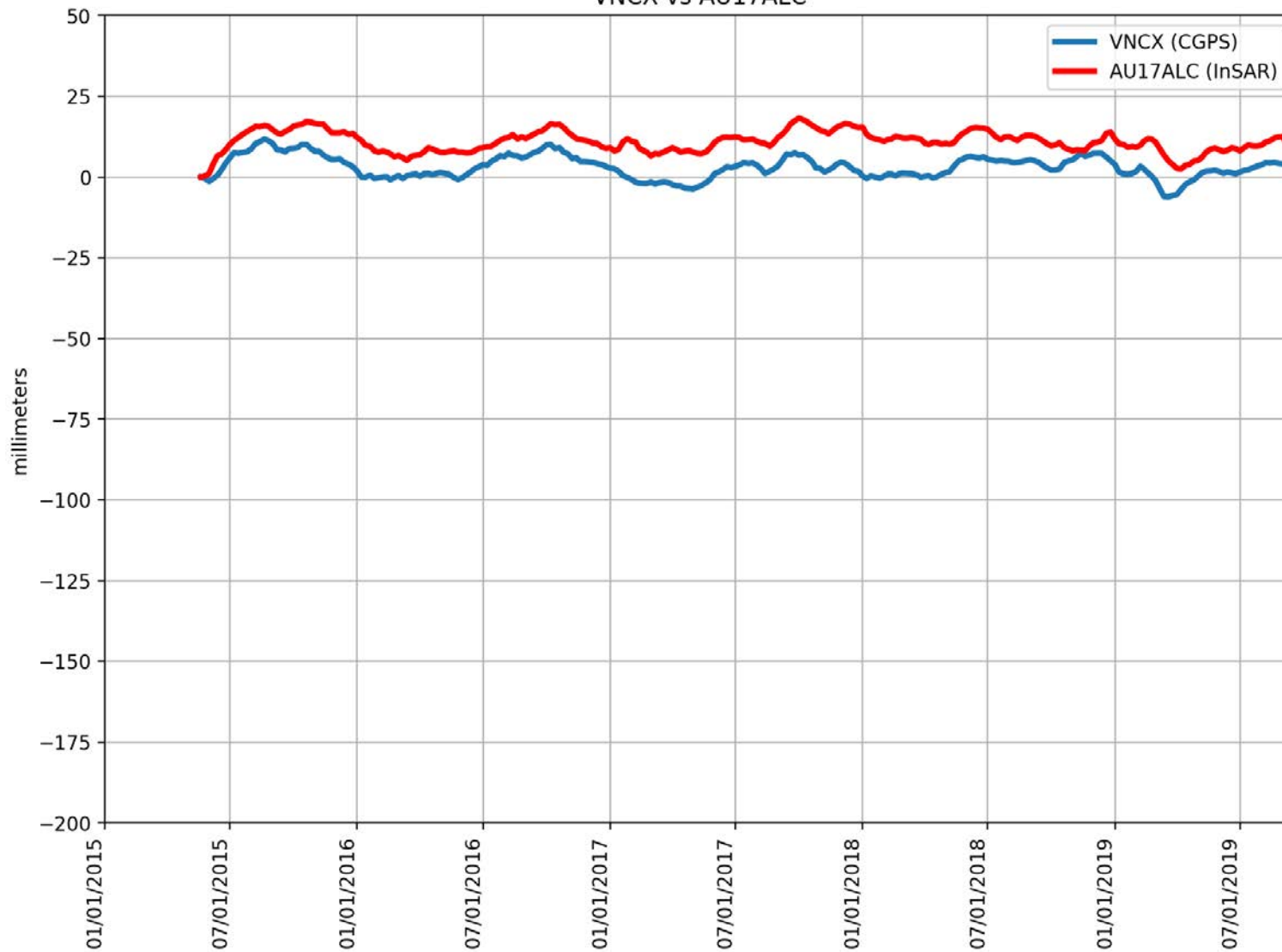
VNCO vs ATPW1L3



RMSE: 14.85 mm
Correlation: 0.97

Appendix B

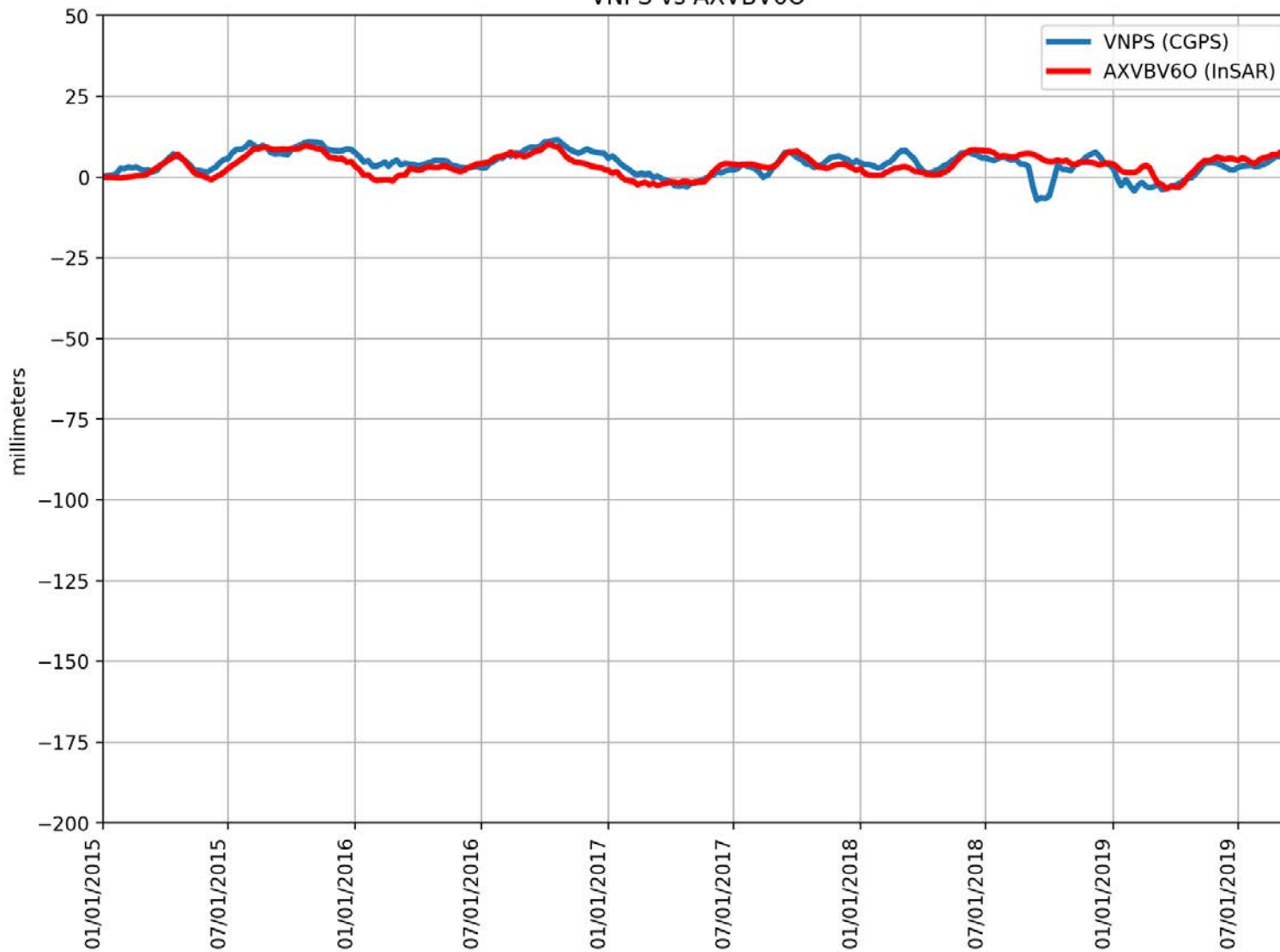
VNCX vs AU17ALC



RMSE: 8.30 mm
Correlation: 0.72

Appendix B

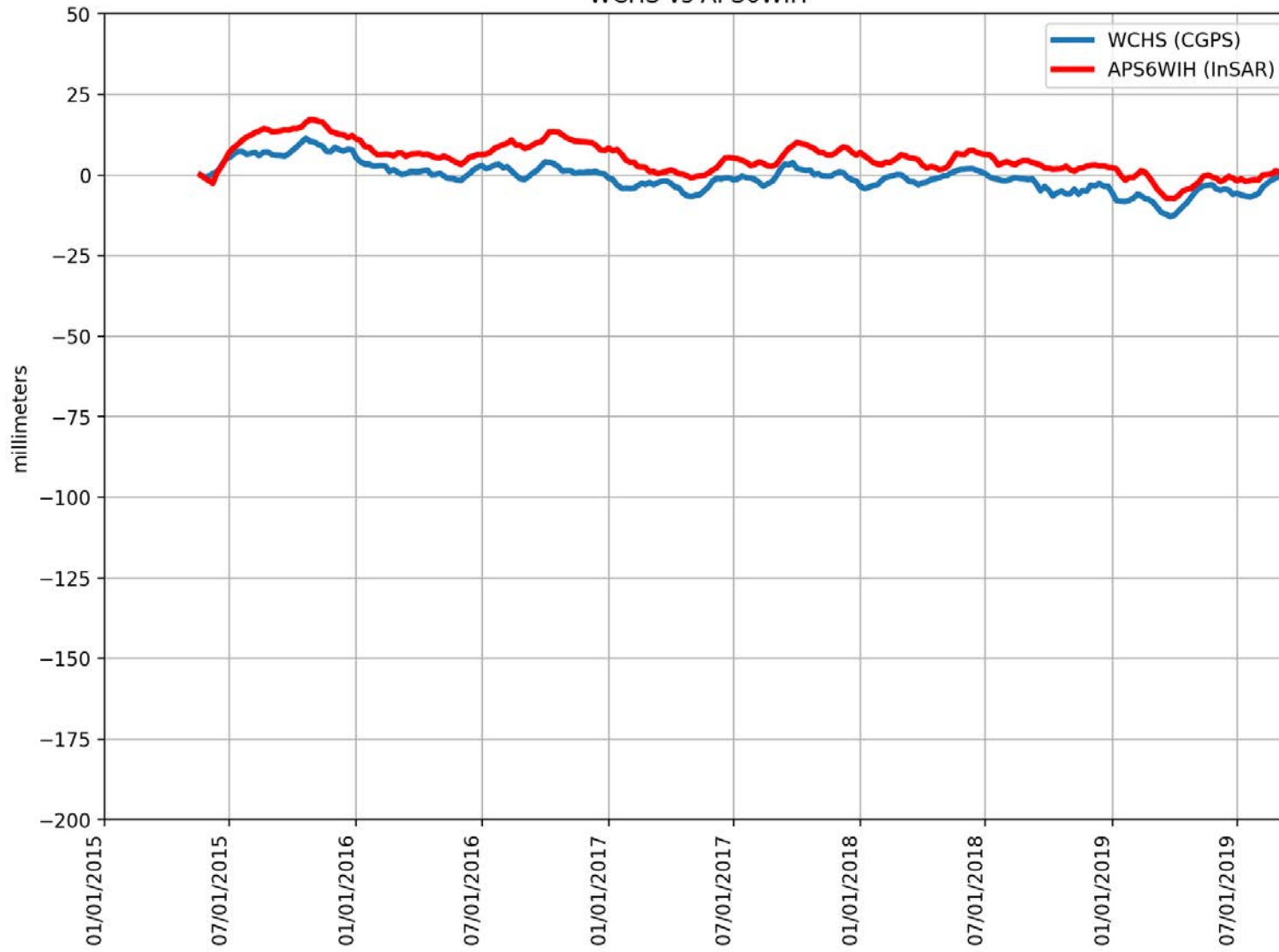
VNPS vs AXVBV60



RMSE: 2.88 mm
Correlation: 0.66

Appendix B

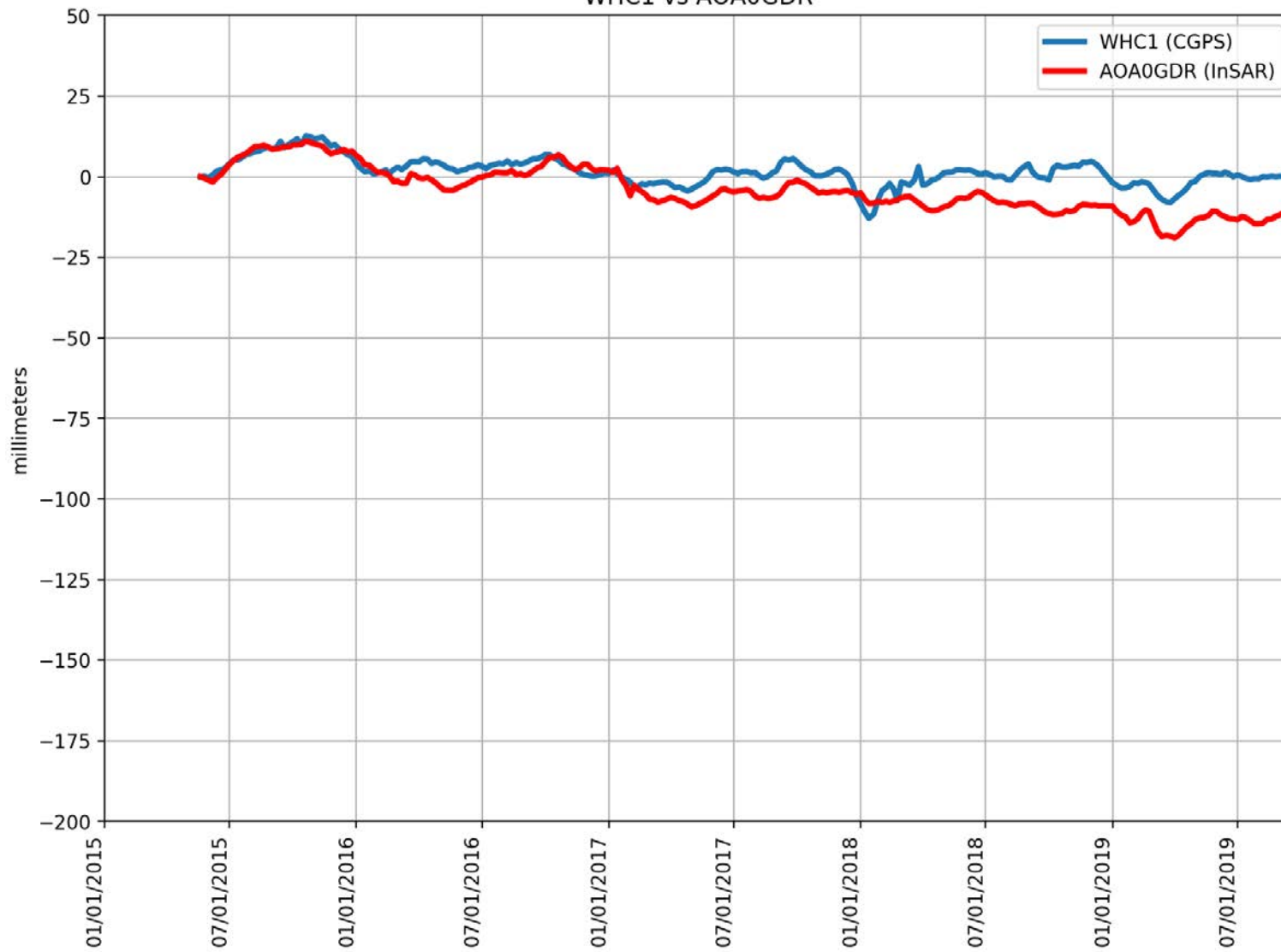
WCHS vs APS6WIH



RMSE: 6.16 mm
Correlation: 0.88

Appendix B

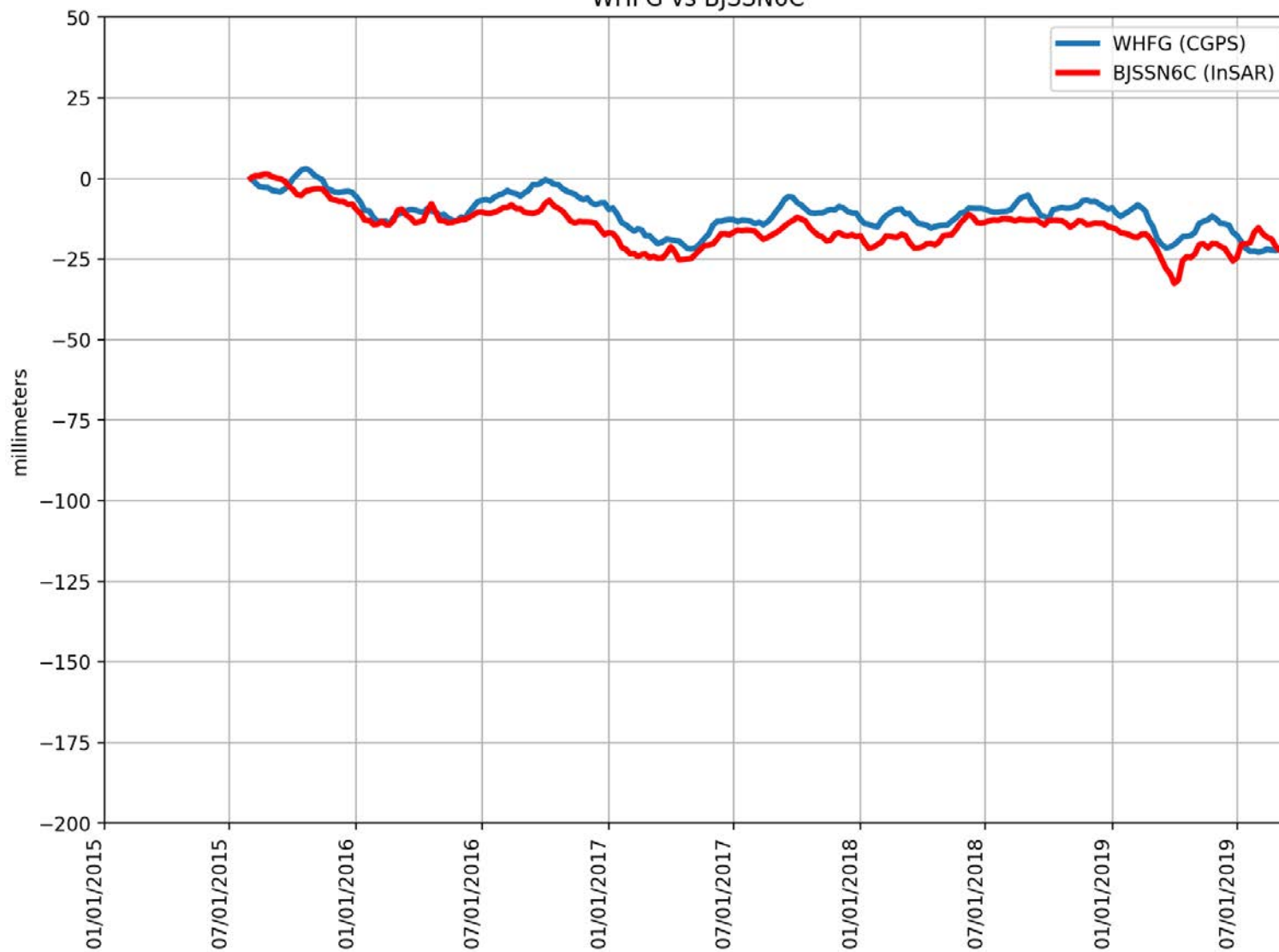
WHC1 vs AOA0GDR



RMSE: 7.37 mm
Correlation: 0.74

Appendix B

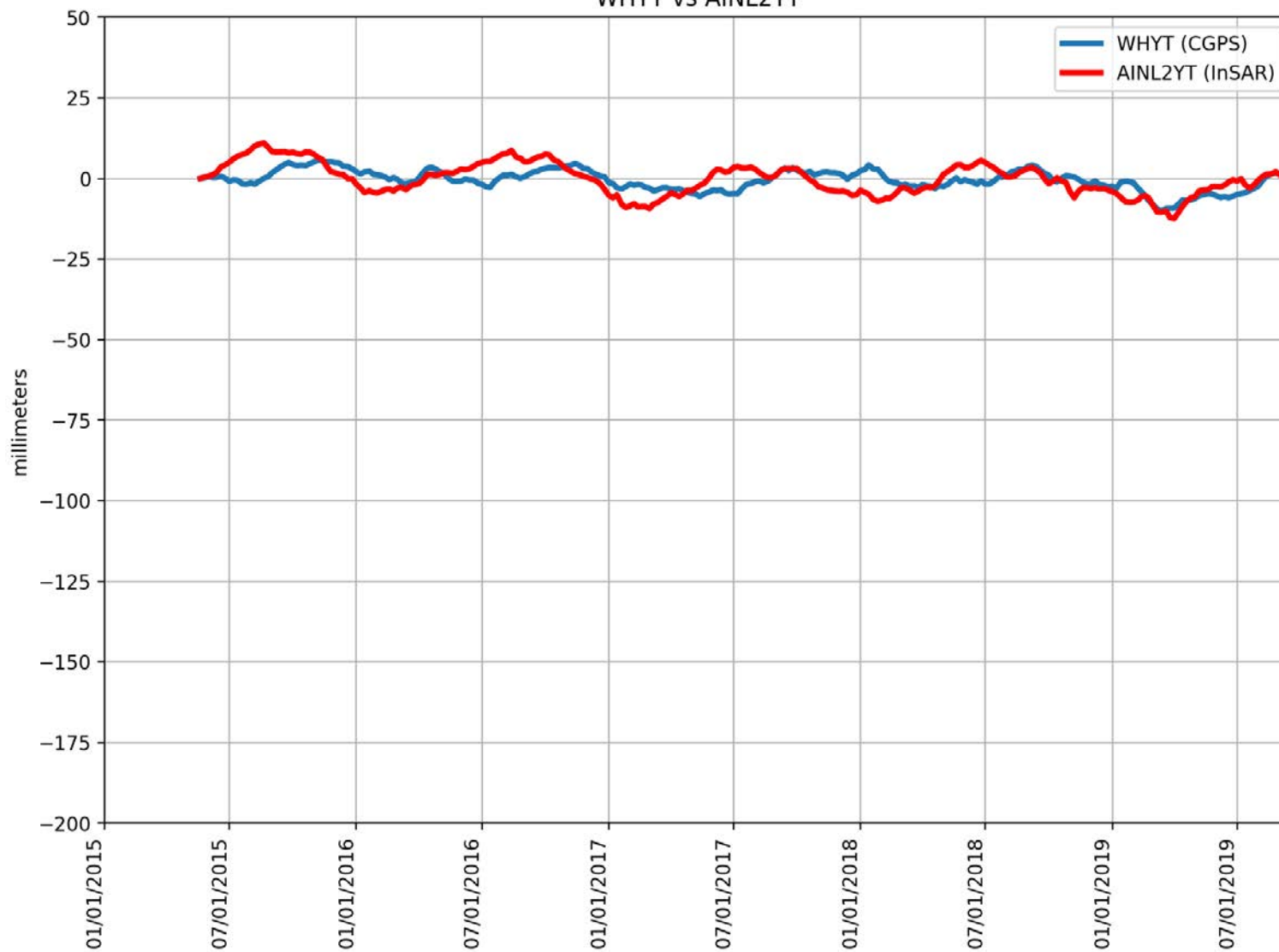
WHFG vs BJSSN6C



RMSE: 5.57 mm
Correlation: 0.84

Appendix B

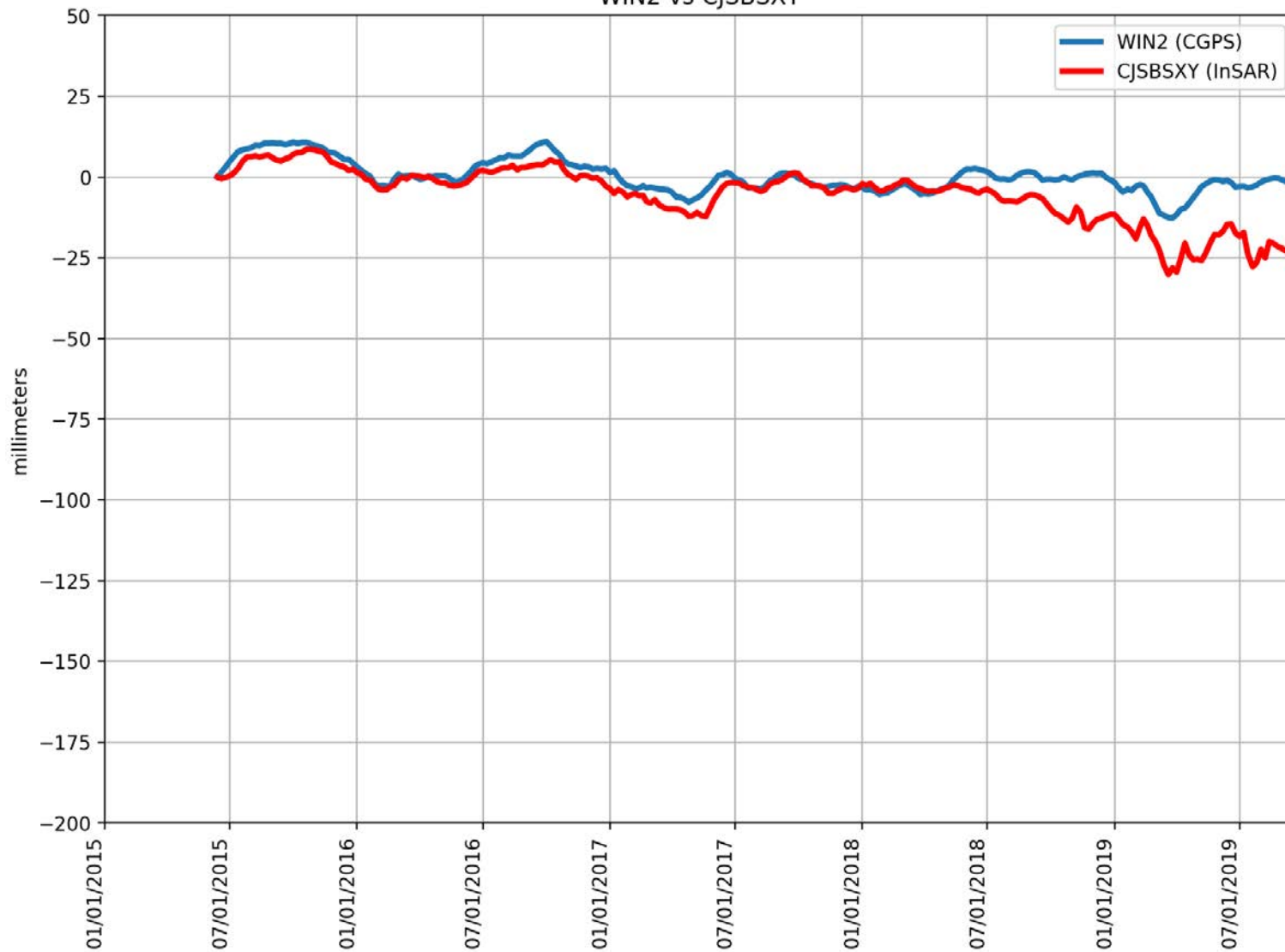
WHYT vs AINL2YT



RMSE: 4.29 mm
Correlation: 0.51

Appendix B

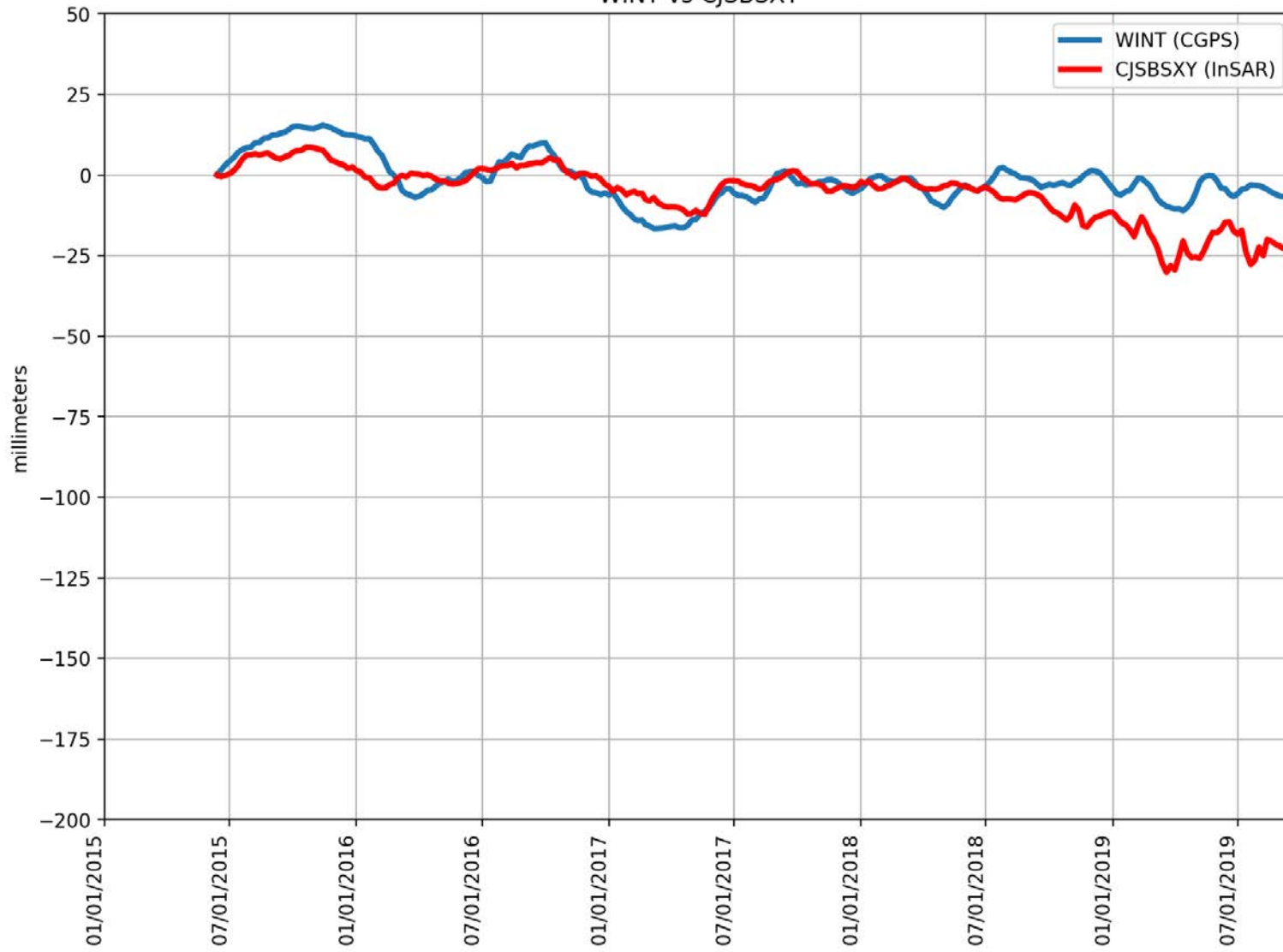
WIN2 vs CJSBSXY



RMSE: 8.42 mm
Correlation: 0.71

Appendix B

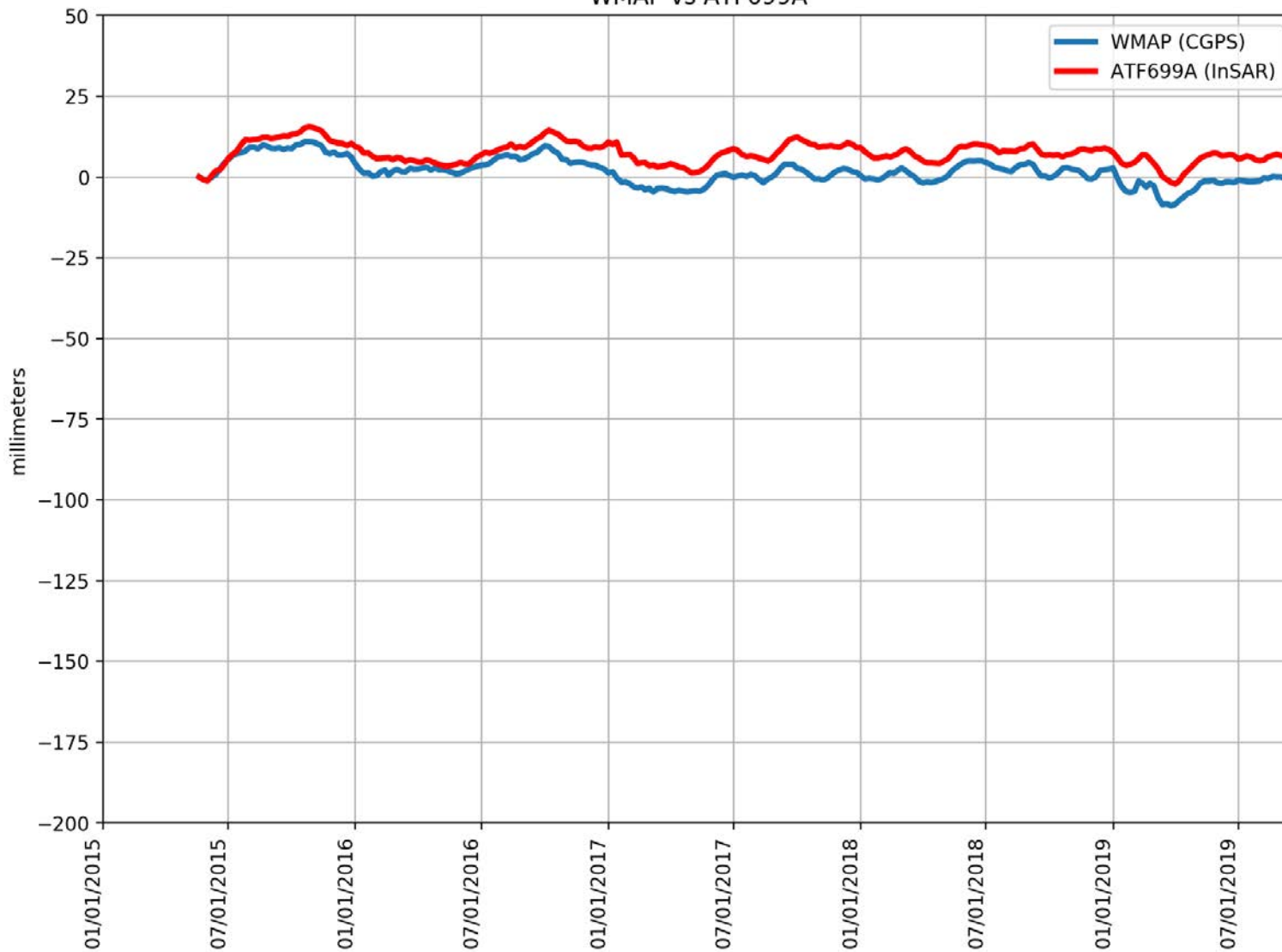
WINT vs CJSBSXY



RMSE: 8.51 mm
Correlation: 0.57

Appendix B

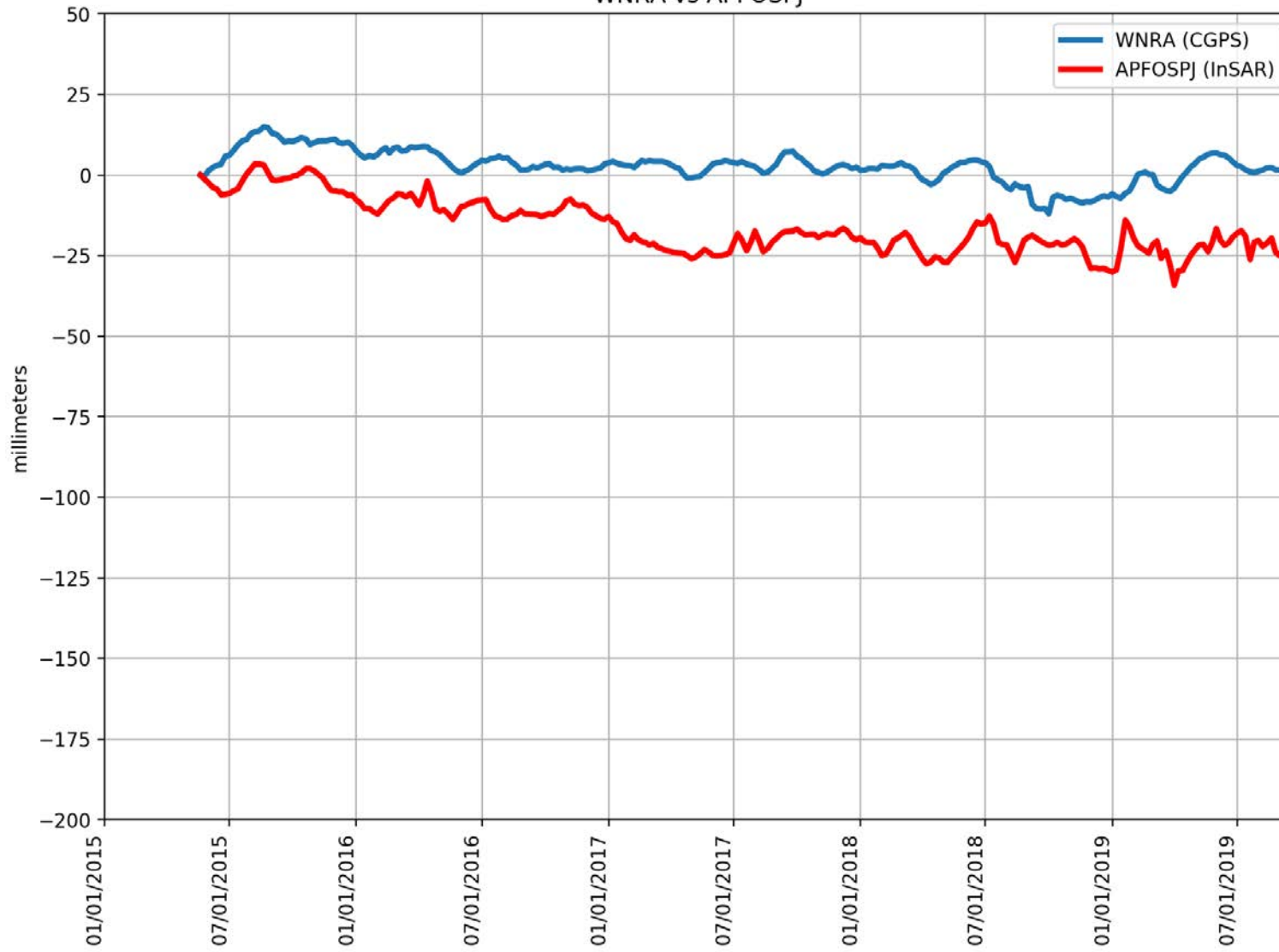
WMAP vs ATF699A



RMSE: 6.16 mm
Correlation: 0.81

Appendix B

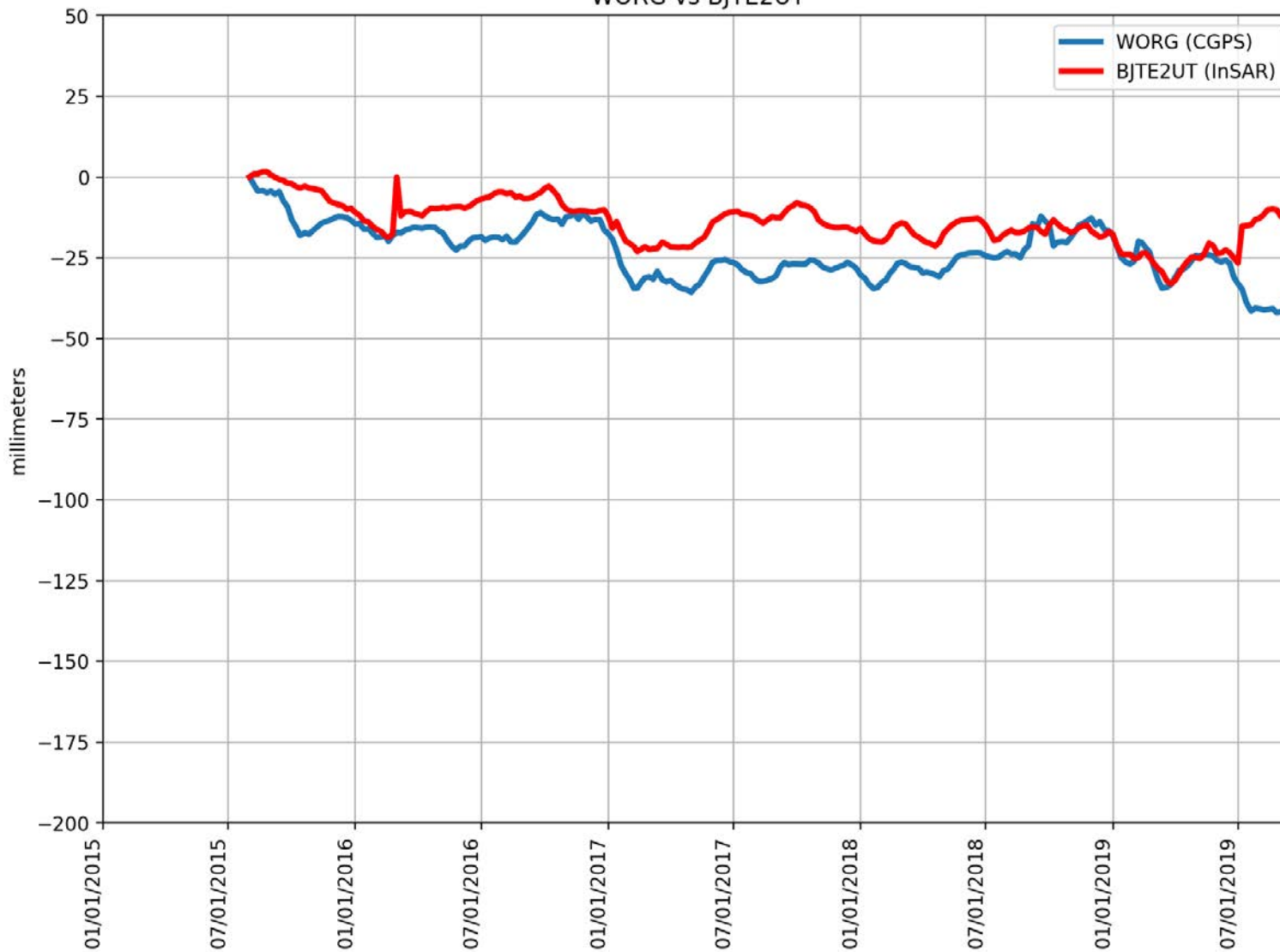
WNRA vs APFOSPJ



RMSE: 19.81 mm
Correlation: 0.69

Appendix B

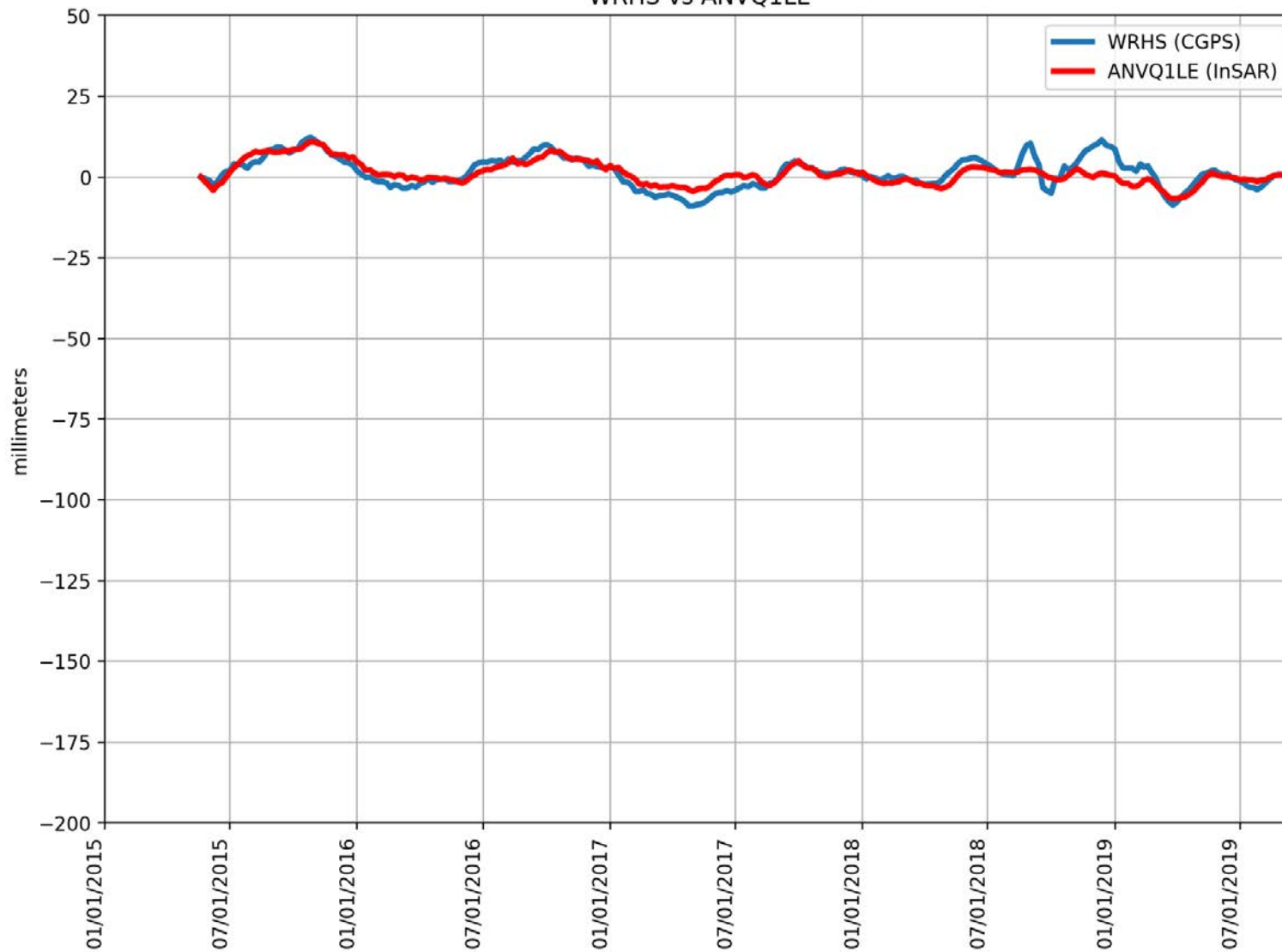
WORG vs BJTE2UT



RMSE: 11.54 mm
Correlation: 0.57

Appendix B

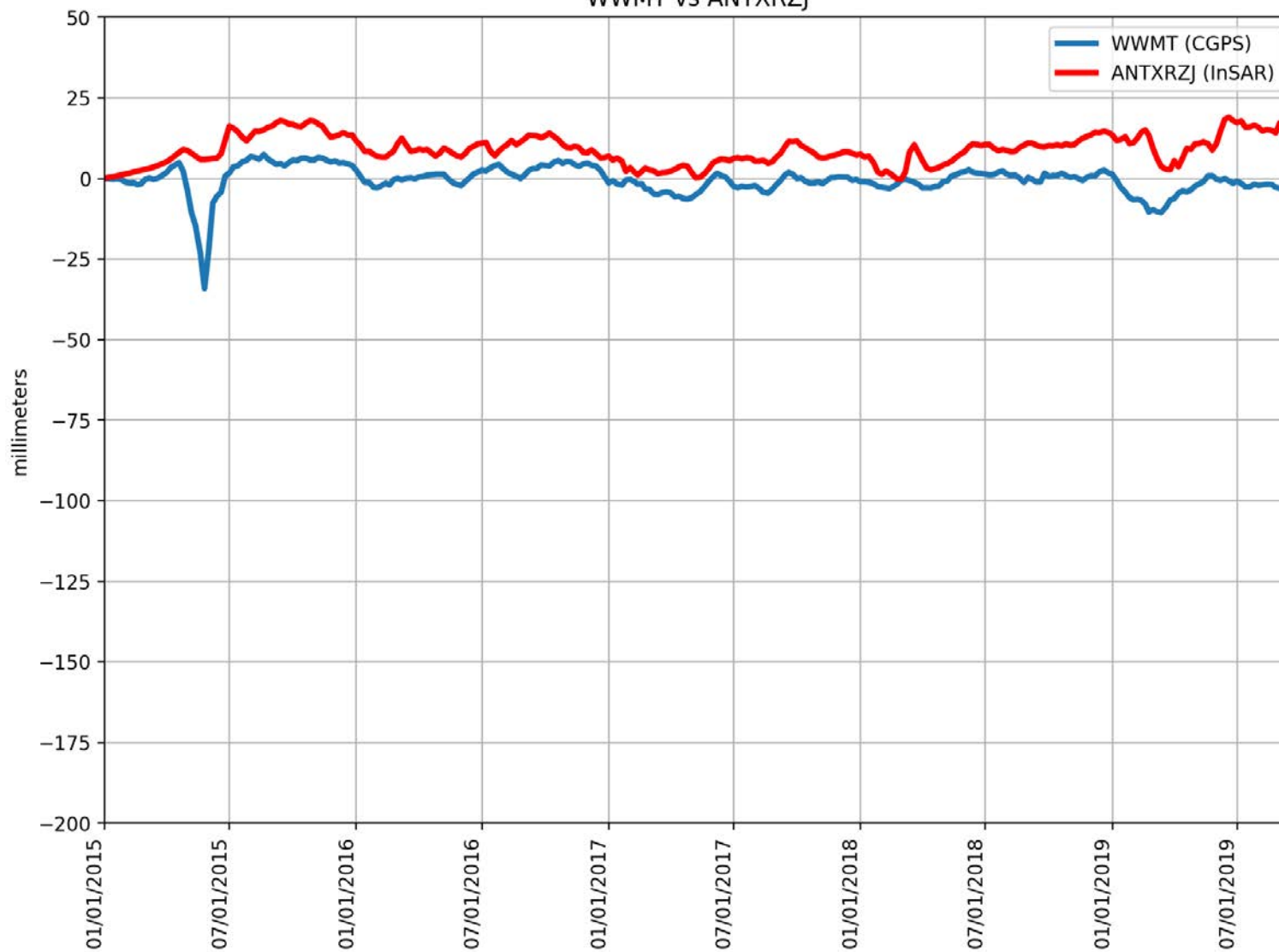
WRHS vs ANVQ1LE



RMSE: 2.85 mm
Correlation: 0.79

Appendix B

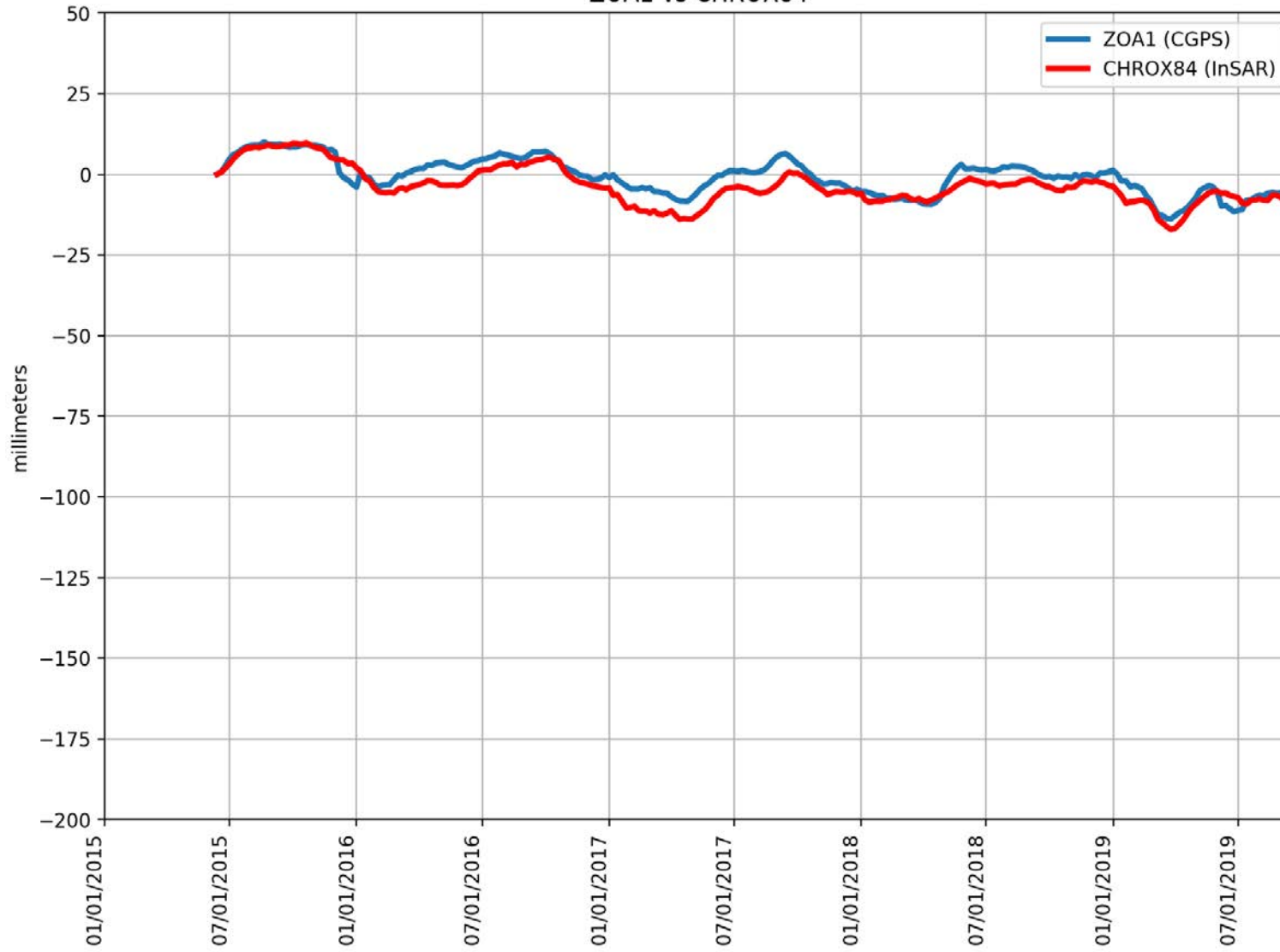
WWMT vs ANTXRZJ



RMSE: 10.61 mm
Correlation: 0.39

Appendix B

ZOA1 vs CHROX84



RMSE: 3.85 mm
Correlation: 0.89

APPENDIX C

Contract No. 4600011239
Task Order No. 26
Towill, Inc.

Final Report

CGPS Data Acquisition and Analysis

February 2019

Prepared for

California Department of Water Resources

Prepared by



Towill Project Number:
14750-0126

CONTENTS

| | |
|---|-----------|
| 1. INTRODUCTION | 6 |
| 1.1 SUMMARY OF SCOPE OF WORK AND PURPOSE | 6 |
| 1.2 POINTS OF CONTACT | 6 |
| 2. GEODETIC REFERENCE FRAMES AND DATUMS | 6 |
| 2.1 THE INTERNATIONAL EARTH ROTATION AND REFERENCE SYSTEMS SERVICE (IERS) | 6 |
| 2.2 THE INTERNATIONAL TERRESTRIAL REFERENCE FRAME (ITRF) | 7 |
| 2.2.1 ITRF Realizations | 9 |
| 2.3 THE INTERNATIONAL GNSS SERVICE (IGS) | 9 |
| 2.3.1 IGS14 Realization | 9 |
| 2.3.2 Mid-Study Epoch ITRF2014 Reference Positions | 11 |
| 3. UNAVCO AND SOPAC GNSS PROCESSING | 11 |
| 3.1 GAMIT AND GLOBK | 11 |
| 3.2 GIPSY-OASIS | 12 |
| 3.3 UNAVCO GAGE WORKFLOW AND TIME SERIES PRODUCTS | 12 |
| 3.3.1 UNAVCO Data Source | 15 |
| 3.4 SOPAC GNSS PROCESSING | 16 |
| 4. TIME SERIES DATA SOURCES AND SMOOTHING | 20 |
| 4.1 UNAVCO AND SOPAC DATA SOURCES | 20 |
| SOPAC: | 20 |
| UNAVCO: | 20 |
| 4.2 DATA TRANSFORMATION AND REFORMATTING | 20 |
| 4.3 TIME SERIES SMOOTHING | 20 |
| 4.4 INSAR CALIBRATION POINTS | 21 |
| 4.5 GRAPHICAL REVIEW AND STATISTICAL ANALYSIS OF TYPICAL RESULTS | 22 |
| 5. TEN PERCENT POSITIONAL DATA VALIDATION | 25 |
| 5.1 NRCAN PPP SPARK PROCESSING | 25 |
| 5.2 POSITIONAL COMPARISONS AND ANALYSIS OF RESULTS | 27 |
| 6. DELIVERABLES | 30 |
| 7. REFERENCES | 30 |

LIST OF FIGURES

| | |
|---|----|
| FIGURE 1. ITRF2014 NETWORK MAP | 7 |
| FIGURE 2. ITRF – FOUR TECHNIQUES CO-LOCATED | 8 |
| FIGURE 3. THE IGS TRACKING NETWORK OCT. 2015 | 11 |
| FIGURE 4. UNAVCO GNSS DATA PROCESSING AND GAGE WORKFLOW | 16 |
| FIGURE 5. GLOBAL DISTRIBUTION OF STATIONS PROCESSED INDEPENDENTLY BY SOPAC AND THE JPL (REPRODUCED AFTER BOCK ET AL., 2016) | 17 |
| FIGURE 6. WNAM GNSS PRODUCT COVERAGE | 18 |
| FIGURE 7. BASIC SOPAC/JPL PROCESS AND PRODUCT WORKFLOW | 19 |
| FIGURE 8. CGPS STATIONS PROCESSED FOR THE STUDY | 21 |
| FIGURE 9. CGPS STATIONS SELECTED FOR CALIBRATION AND VALIDATION OF INSAR DATA | 22 |
| FIGURE 10. GRAPH AND STATISTICS FOR PBO STATION P810 | 23 |

FIGURE 11. GRAPH AND STATISTICS FOR PBO STATION P54624
FIGURE 12. VALIDATION CGPS STATIONS SELECTED FOR TESTING POSITIONAL ACCURACY.....26
FIGURE 13. EXPLANATION OF THE OUTLIER FOR STATION 'TEHA'28
FIGURE 14. DISTRIBUTION OF 81 SAMPLES29

LIST OF TABLES

TABLE 1. TRANSFORMATION PARAMETERS FROM ITRF2014 TO PAST ITRFS.....10
TABLE 2. COMPARISON OF A NRCAN PPP SOLUTION WITH THOSE OF OTHER ON-LINE SERVICES28
TABLE 3. DESCRIPTIVE STATISTICS FOR THE DISCREPANCIES29

APPENDIX A: SESES ESDR PROCESSES AND PRODUCTS32
APPENDIX B: CGPS TIME-SERIES VALIDATION33

ACKNOWLEDGEMENTS

- We acknowledge Yehuda Bock, Sharon Kedar and Angelyn Moore. MEaSURES Enhanced Solid Earth Science ESDR System. La Jolla, California and Pasadena, California USA.
- We acknowledge David A. Phillips, Project Manager at UNAVCO¹ for his prompt and insightful responses to our numerous questions.
- We acknowledge Simon Banville and Brian Donahue of NRCan² Earth Sciences, Geomatics Group for assistance and programming support for the use of the new multi-GNSS 'SPARK' precise point positioning (PPP) software.
- We also acknowledge the scientific community who make available the CGPS/CGNSS time-series data and processing resources used in this study:

UNAVCO, a non-profit university-governed consortium, facilitating geoscience research and education using geodesy. UNAVCO CGPS data were downloaded on July 17, 2018 from:

<ftp://data-out.unavco.org/pub/products/position/>.

Towill downloaded the time series files 'SSSS.pbo.igs08.csv' where 'SSSS' is the four-character alphanumeric station code.

The data used span the date interval 2014.12.14 to 2018.07.15.

SOPAC³, an organization devoted to researching, analyzing and archiving high-precision geodetic and seismic data. CGPS data were downloaded from the SOPAC archive on September 9, 2018 from:

<ftp://garner.ucsd.edu/pub/timeseries/measures/ats/WesternNorthAmerica/>.

The time series file downloaded and used by Towill is:

WNAM_Clean_TrendNeuTimeSeries_sopac_20180911.tar.gz. This contains all of the station time series processed by SOPAC for stations in the Western North American (WNAM) polygon. The data used span the date interval 2014.12.14 to 2018.07.15.

NRCan Earth Sciences, Geomatics Group. This group provides useful on line tools for tools for ITRF reference frame transformations and the new online 'SPARK' PPP processor.

¹ Formerly, the University NAVSTAR Consortium.

² Natural Resources Canada.

³ The Scripps Orbit and Permanent Array Center.

EXECUTIVE SUMMARY

This report and accompanying certification describe activities and results of the CGPS Data Acquisition and Analysis activities which were performed as part of Task Order No. 26, issued to Towill, Inc. under DWR contract 4600011239. These activities are described below.

Continuous Global Positioning System (CGPS) time-series data were downloaded from UNAVCO and SOPAC archives and evaluated for use in a SGMA study which uses satellite based InSAR data to measure land subsidence. Geographic location (latitude and longitude) and ellipsoidal height were recorded each day for more than 800 CGPS stations dispersed across California. The geographic position of all CGPS stations used in this study was transformed to the ITRF2014 reference frame. Time-series data were clipped to the study period beginning January 1, 2015 and ending June 30, 2018 and smoothed using a 31-day moving average filter. The time-series data present differential movement in latitude, longitude, and height of the CGPS station relative to the start of the study period (January 1, 2015). The time-series data files are included in the electronic deliverables.

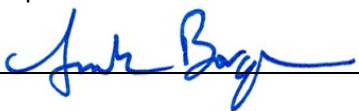
A subset of the CGPS time-series data were supplied to TRE Altamira enabling calibration of the InSAR dataset. Towill provided TRE with the geographic location of more than 800 CGPS points along with documentation of the temporal extent of the time-series data for each CGPS station. TRE selected 203 CGPS stations for use in the InSAR data calibration process. Actual ellipsoidal height values were provided to TRE following their selection of calibration points. CGPS points not selected for calibration are candidate for use as validation points. Validation points and their heights were not disclosed to TRE.

As an independent accuracy test of the online CGPS time-series data, Towill randomly selected 10% of the CGPS points residing within SGMA basins and downloaded raw 24-hour RINEX files on two dates for each CGPS station; the first date was January 1, 2015 and the second date was randomly selected within the study period. The RINEX files were processed independently using a Precision Point Positioning (PPP) processor and the change in height values between the two dates were calculated. Height differences between these two dates were also calculated from the CGPS time-series data (pre-31 day smoothing) and a comparison was made. We determined there is excellent agreement between the two data sets, yielding an RMSE of 4.3 mm for the ellipsoidal height discrepancies and 3.7 mm and 2.5 mm in the case of the Northing and Easting differences.

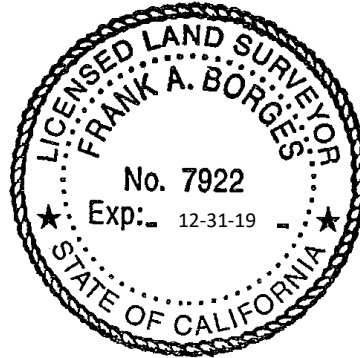
SURVEYOR'S CERTIFICATION STATEMENT

I hereby certify that this report was prepared by me or under my direction, and its contents represent an accurate assessment of the results shown.

Frank Borges, PLS, CA, No. 7922
Associate Principal

Signature: 

Date: 02/01/2019



1. Introduction

1.1 Summary of Scope of Work and Purpose

CGPS Data Acquisition and Analysis activities required researching technical details of publicly available CGPS datasets, downloading CGPS time-series datasets from online archives, performing a quality assurance test on 10% of the CGPS points, transforming the datasets onto a common reference frame, calculating a 31-day moving average on the CGPS time-series data, and reformmating the datasets to a structure supplied by TRE Altamira. These CGPS time-series datasets provided TRE Altamira with data for use in calibrating the InSAR dataset and provide Towill with validation points for use in assessing the accuracy of the InSAR derived surface height measurements.

1.2 Points of Contact

Questions regarding this report should be addressed to:

| Contractor's Project Manager | Contractor's Contract Manager |
|---|---|
| Frank Borges, PLS 2300 Clayton Road, Suite 1200 Concord, California 94520-2176 Phone: (925) 682-6976 ext. 1036 Frank.Borges@towill.com | Brian Young 2300 Clayton Road, Suite 1200 Concord, California 94520-2176 Phone: (925) 682-6976 ext. 1041 Brian.Young@towill.com |

2. Geodetic Reference Frames and Datums

2.1 The International Earth Rotation and Reference Systems Service (IERS)

The IERS was established in 1987 as the Earth Rotation Service by the International Astronomical Union (IAU) and the International Union of Geodesy and Geophysics (IUGG). In 2003 it was renamed as the International Earth Rotation and Reference Systems Service. The Service's website is at www.iers.org.

As identified by the Service's mandate, its primary objectives, quoted verbatim below, are to serve the astronomical, geodetic and geophysical communities by providing the following:

- The International Celestial Reference System (ICRS) and its realization, the International Celestial Reference Frame (ICRF).
- The International Terrestrial Reference System (ITRS) and its realization, the International Terrestrial Reference Frame (ITRF).
- Earth orientation parameters required to study earth orientation variations and to transform between the ICRF and the ITRF.
- Geophysical data to interpret time/space variations in the ICRF, ITRF or earth orientation parameters, and model such variations.

- Standards, constants and models (i.e., conventions) encouraging international adherence.

From a geodetic surveying point-of-view, the key focus is the realization (ITRF) of the ITRS.

2.2 The International Terrestrial Reference Frame (ITRF)

The ITRS is ultimately realized as the ITRF by a combination of data from four so-called 'Techniques', namely:

- VLBI (Very Long Baseline Interferometry) – IVS
- GNSS (Global Navigation Satellite System) – IGS
- DORIS (The French acronym for a high precision Doppler orbit determination and positioning system) – IDS
- SLR (Satellite Laser Ranging) – ILRS

Figure 1 below shows the network of IERS technique stations used for the realization of ITRF2014.

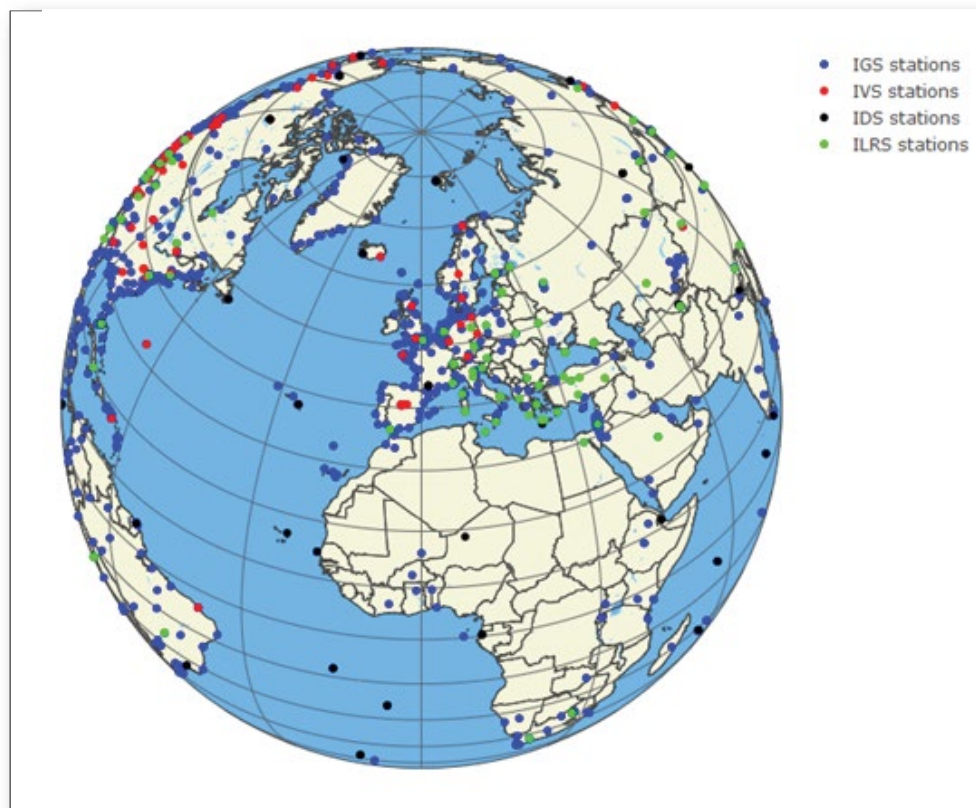


Figure 1. ITRF2014 Network Map

Figure 2 shows the co-location of the four technique instruments at the Hartebeesthoek Radio Astronomy Observatory in South Africa. Each of the techniques contributes in different ways to the realization of the ITRS in terms of its spatial orientation, location of the origin, scale and the time evolution of these parameters.

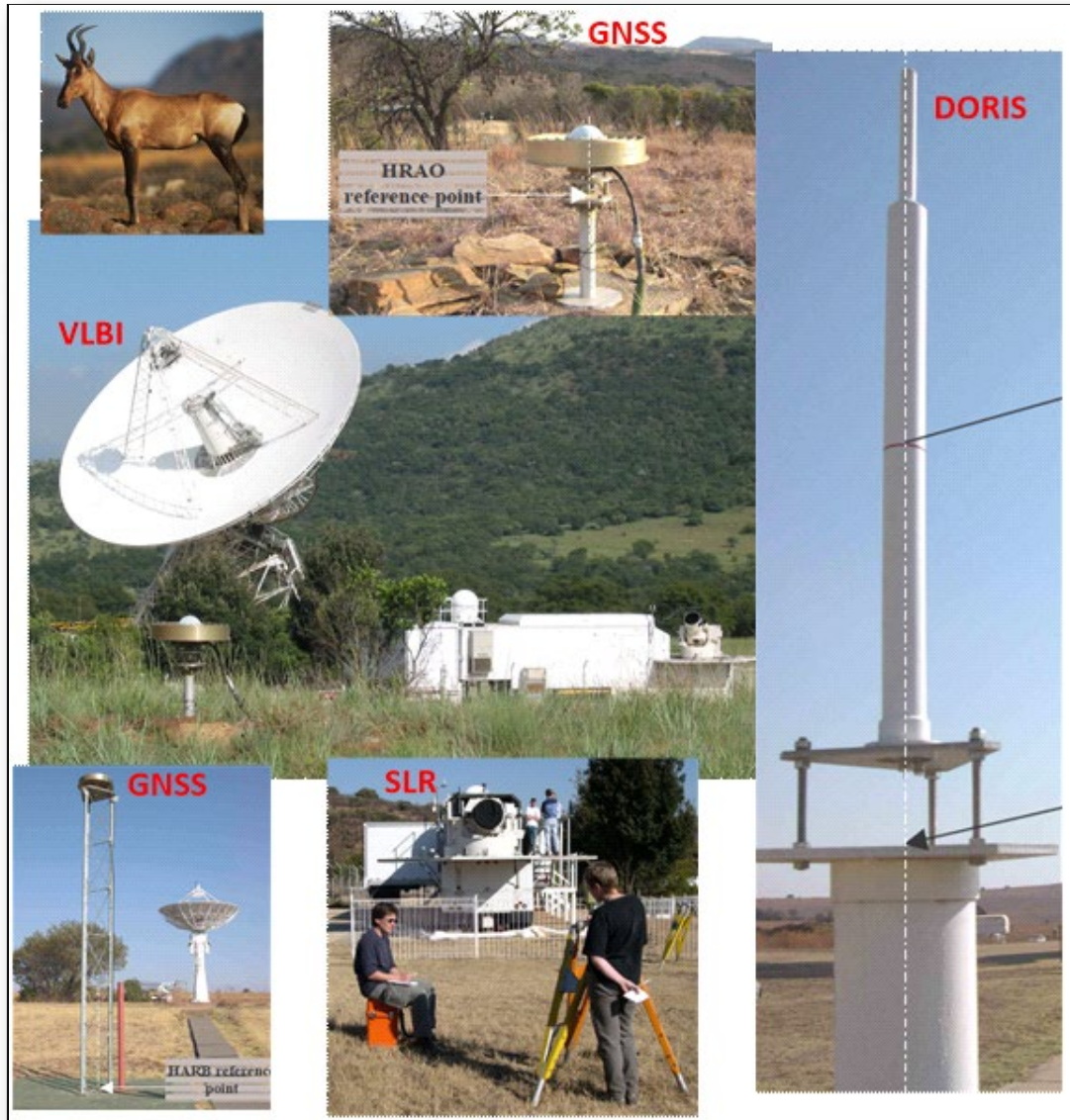


Figure 2. ITRF – Four Techniques Co-located⁴

⁴ Note the surveyors (bottom center) performing a high-precision co-location survey tying together the reference points of the various sensors.

2.2.1 ITRF Realizations

The latest realization is ITRF2014. Previous realizations of the ITRF include ITRF89, ITRF90, ITRF91, ITRF92, ITRF93, ITRF94, ITRF95, ITRF96, ITRF97, ITRF2000, ITRF2005, ITRF2008, ITRF2014; with the magnitudes of the incremental differences generally becoming smaller with each realization.

Details of the development and realization of ITRF2008 may be found in Altamimi, et al. (2012), while the description of the realization of ITRF2014 is provided in Altamimi, et al. (2016, 2017). Table 1 contains the data for the fourteen (14) parameter transformations from ITRF2014 to the superseded realizations. Note that there are 7 constant parameters valid at epoch 2010.0 and 7 annualized time varying components which must be evaluated at the desired epoch by computing the time interval (in years) from 2010.0. Note that for most purposes, ITRF2008 and ITRF2014 are practically congruent.

2.3 The International GNSS Service (IGS)

Once the IERS produces a new ITRF realization, the IGS usually produces a matching GNSS-only solution based on a subset of the ITRF points. The current IGS reference frame is IGS14 which is aligned to ITRF2014. The IGS is one of the four Technique Centers (Services) which provides GNSS data for the ITRF realizations if the ITRS.

Figure 3 shows the IGS network, reproduced after Johnston, et al. (2017). This publication also provides an excellent description of the IGS mission, structure operations, services and products, while Kouba (2015) delivers a useful end-user guide to IGS products (e.g., precise orbits, clocks, EOPs⁵, etc).

2.3.1 IGS14 Realization

IGS Technical Report 2017 (see Villiger, A., Dach, R. Eds. 2018) includes numerous ‘sub-reports’ from the IGS and a multitude of contributors, including Rebischung, et al. (2017) who review the status of the new IGS14 realization.

On January 29th, 2017 (GPS week 1934), the new reference frame, IGS14, was adopted by the IGS together with an associated set of ground and satellite antenna calibrations, `igs14_www.atx`, where ‘www’ represents the GPS week number of the latest .atx release. The new IGS14/igs14.atx framework replaces the previous IGS08/igs08.atx realization that had been used since GPS week 1632 (April 17, 2011). As stated by Rebischung, et al. (2017), “... the switch to IGS14 on week 1934 is marked by a clear increase in the number of available reference frame stations and a clear decrease of the transformation residuals, indicating an improvement in the precision of the alignment of the IGS daily solutions to the reference frame. Since then, both the number of available reference frame stations and the transformation residuals have remained at fairly stable levels. An update of the IGS14 reference frame does thus not seem necessary for now”.

⁵ Earth Orientation Parameters, such as Polar Motion (PM), Length of Day (LOD), UT1 – UTC, etc.

Table 1. Transformation Parameters from ITRF2014 to past ITRFs⁶

| SOLUTION | Tx | Ty | Tz | D | Rx | Ry | Rz | EPOCH |
|-------------|-------|------|--------|-------|---------|---------|---------|--------|
| UNITS-----> | mm | mm | mm | ppb | .001" | .001" | .001" | |
| | . | . | . | . | . | . | . | |
| RATES | Tx | Ty | Tz | D | Rx | Ry | Rz | |
| UNITS-----> | mm/y | mm/y | mm/y | ppb/y | .001"/y | .001"/y | .001"/y | |
| ITRF2008 | 1.6 | 1.9 | 2.4 | -0.02 | 0.00 | 0.00 | 0.00 | 2010.0 |
| rates | 0.0 | 0.0 | -0.1 | 0.03 | 0.00 | 0.00 | 0.00 | |
| ITRF2005 | 2.6 | 1.0 | -2.3 | 0.92 | 0.00 | 0.00 | 0.00 | 2010.0 |
| rates | 0.3 | 0.0 | -0.1 | 0.03 | 0.00 | 0.00 | 0.00 | |
| ITRF2000 | 0.7 | 1.2 | -26.1 | 2.12 | 0.00 | 0.00 | 0.00 | 2010.0 |
| rates | 0.1 | 0.1 | -1.9 | 0.11 | 0.00 | 0.00 | 0.00 | |
| ITRF97 | 7.4 | -0.5 | -62.8 | 3.80 | 0.00 | 0.00 | 0.26 | 2010.0 |
| rates | 0.1 | -0.5 | -3.3 | 0.12 | 0.00 | 0.00 | 0.02 | |
| ITRF96 | 7.4 | -0.5 | -62.8 | 3.80 | 0.00 | 0.00 | 0.26 | 2010.0 |
| rates | 0.1 | -0.5 | -3.3 | 0.12 | 0.00 | 0.00 | 0.02 | |
| ITRF94 | 7.4 | -0.5 | -62.8 | 3.80 | 0.00 | 0.00 | 0.26 | 2010.0 |
| rates | 0.1 | -0.5 | -3.3 | 0.12 | 0.00 | 0.00 | 0.02 | |
| ITRF93 | -50.4 | 3.3 | -60.2 | 4.29 | -2.81 | -3.38 | 0.40 | 2010.0 |
| rates | -2.8 | -0.1 | -2.5 | 0.12 | -0.11 | -0.19 | 0.07 | |
| ITRF92 | 15.4 | 1.5 | -70.8 | 3.09 | 0.00 | 0.00 | 0.26 | 2010.0 |
| rates | 0.1 | -0.5 | -3.3 | 0.12 | 0.00 | 0.00 | 0.02 | |
| ITRF91 | 27.4 | 15.5 | -76.8 | 4.49 | 0.00 | 0.00 | 0.26 | 2010.0 |
| rates | 0.1 | -0.5 | -3.3 | 0.12 | 0.00 | 0.00 | 0.02 | |
| ITRF90 | 25.4 | 11.5 | -92.8 | 4.79 | 0.00 | 0.00 | 0.26 | 2010.0 |
| rates | 0.1 | -0.5 | -3.3 | 0.12 | 0.00 | 0.00 | 0.02 | |
| ITRF89 | 30.4 | 35.5 | -130.8 | 8.19 | 0.00 | 0.00 | 0.26 | 2010.0 |
| rates | 0.1 | -0.5 | -3.3 | 0.12 | 0.00 | 0.00 | 0.02 | |
| ITRF88 | 25.4 | -0.5 | -154.8 | 11.29 | 0.10 | 0.00 | 0.26 | 2010.0 |
| rates | 0.1 | -0.5 | -3.3 | 0.12 | 0.00 | 0.00 | 0.02 | |

Note : These parameters are derived from those already published in the IERS Technical Notes and Annual Reports. The transformation parameters should be used with the standard model (1) given below and are valid at the indicated epoch.

$$\begin{matrix}
 : XS : & : X : & : Tx : & : D & -Rz & Ry : & : X : \\
 : & : & : & : & : & : & : \\
 : YS : & = : Y : & + : Ty : & + : Rz & D & -Rx : & : Y : \\
 : & : & : & : & : & : & : \\
 : ZS : & : Z : & : Tz : & : -Ry & Rx & D : & : Z :
 \end{matrix}
 \tag{1}$$

Where X,Y,Z are the coordinates in ITRF2014 and XS,YS,ZS are the coordinates in the other frames.

On the other hand, for a given parameter P, its value at any epoch t is obtained by using equation (2).

$$P(t) = P(\text{EPOCH}) + \dot{P} * (t - \text{EPOCH})
 \tag{2}$$

where EPOCH is the epoch indicated in the above table (currently 2010.0) and \dot{P} is the rate of that parameter.

⁶ Reproduced from http://itrf.ign.fr/doc_ITRF/Transfo-ITRF2014_ITRFs.txt.

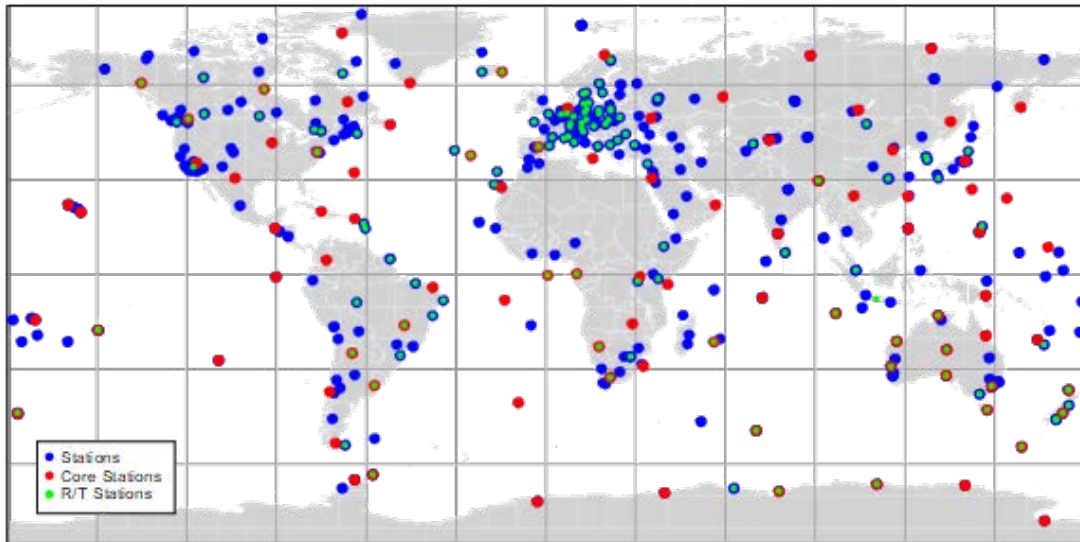


Figure 3. The IGS Tracking Network Oct. 2015

2.3.2 Mid-Study Epoch ITRF2014 Reference Positions

Since the geodetic position is not static for many of the CGPS stations, we elected to set and hold the horizontal position of each station to its location at the mid-study period epoch (09-30-2016). The process used in this study for transforming IGS08 (ITRF2008) to ITRF2014 and adding seismic delta to position CGPS to 09-30-2016 (mid-study period epoch) is outlined below:

1. Started with ListVf.csv and extracted Lat, Lon, and h into a separate file
2. Used NRCAN and converted ITRF2008 to ITRF2014
3. Used NRCAN to convert ITRF2014 to UTM Zone 10 and 11
4. Added dN and dE (based on change between January 1, 2015 and September 30, 2016) to UTM northing and easting to calculate final UTM coordinates for each CGPS
5. Used ArcGIS to convert UTM to WGS84 ("WGS84_ITRF2014_09-30-2018.xls")

3. UNAVCO and SOPAC GNSS Processing

Both UNAVCO and SOPAC employ similar software and processing strategies for the GNSS processing. In both cases, the strategy involves a pair of Analysis Centers (ACs)

3.1 GAMIT and GLOBK

Useful descriptions of the GAMIT/GLOBK suite of software may be found in Herring, et al. (2018) and in Bock and Melgar (2016). This package has been developed over a number of years and by numerous individuals at a range of universities and research institutions.

Additional and more extensive details may be found in the GAMIT and GLOBK Reference Manuals via MIT's 'GeoWeb' site: <http://www-gpsg.mit.edu> . The current release of the software suite is version 10.7 (June 2018).

GAMIT⁷ is a suite of programs used for the analysis of GPS data. It uses the GPS carrier phase and pseudorange observables to estimate three-dimensional relative positions of ground stations, precise satellite orbits, atmospheric zenith delays, and earth orientation parameters (EOPS).

GLOBK⁸ is a Kalman filter whose primary purpose is to combine various geodetic solutions such as GPS, VLBI, and SLR. It accepts as data, or "quasi-observations" the estimates and covariance matrices for station coordinates, EOPS, orbits, and positions generated from the analysis of the primary observations. The input solutions are generally performed with loose a priori constraint uncertainties assigned to all global parameters, so that constraints can be consistently applied during the processing of the combined solution.

3.2 GIPSY-OASIS

GIPSY-OASIS, or **GIPSY**, is the **GNSS-Inferred Positioning System and Orbit Analysis Simulation Software** package. GIPSY is developed by the Jet Propulsion Laboratory (JPL), and maintained by the Near Earth Tracking Applications and Systems groups. GIPSY uses JPL's precise orbit and clock products and provides GNSS (GPS and GLONASS) solutions incorporating DORS and SLR data. Note that GIPSY was replaced in 2018 by GIPSYx which adds numerous new features including models of geometric effects, support for Galileo and BeiDou and a variety of new force models such as solar and terrestrial radiation pressure⁹.

3.3 UNAVCO GAGE Workflow and Time Series Products

Figure 4, below, is reproduced after Herring, et al. (2016). UNAVCO downloads the raw GNSS/GPS data translates it to Level 1 (e.g., RINEX files), performs QC checks, stores and archives the datasets and posts it to servers for access by the public, the scientific community and the Geodesy Advancing Geosciences and EarthScope (GAGE) Facility Analysis Centers (ACs). This part of the workflow is highlighted in pink on the left-hand side of the diagram. The right-hand side of the diagram (colored blue) shows the two ACs which process the data to generate the Level 2a products. Finally, the Analysis Center Coordinator (ACC) merges the two Level 2a datasets and produces the combined Level 2b solution.

⁷ GNSS at MIT (Massachusetts Institute of Technology).

⁸ Global Kalman filter.

⁹ Details of the extensive GIPSYx upgrades can be found at <https://gipsy-oasis.jpl.nasa.gov/index.php?page=software>.

The rationale behind this tactic is to use dissimilar algorithms and software so as to identify potential processing errors and to evaluate any differences which might be attributed to modeling variations and other disparate algorithmic approaches.

The two GAGE Facility ACs are:

- Central Washington University (CWU) which uses the GPS Inferred Positioning System, Orbit Analysis and Simulation Software (GIPSY/OASIS).
- New Mexico Tech (NMT) using the GPS At MIT (GAMIT) and GLOBK (Kalman filtering) software packages.

The past few years have witnessed a transition from ITRF2008, and IGB08 to ITRF2014 and IGS14. The year 2018 has been particularly active in terms of this transition. For this reason, and since the study-period extends half-way through the year, Towill compiled a list of questions for UNAVCO staff. These were answered promptly and fully in an email response (David A. Phillips¹⁰, personal communication, Nov 21, 2018). For the sake of brevity, Towill's questions are not repeated in toto here; however the full context can be inferred by the italicized responses below:

- **Towill:** We are using SSSS.pbo.igs08.csv files for the UNAVCO time series.
UNAVCO: *These are good files to use for solutions up through 2018-09-15. As discussed further below in response to another question though, please use the "cwu" named files (SSSS.cwu.igs08.csv or *.pos) instead of the "pbo" named files for solutions after 2018-09-15.*
- **Towill:** Is the reference frame IGS08 as stated in the header metadata or is it IGB08?
UNAVCO: *IGB08.*
- **Towill:** During 'repro' were the data processed using IGS14 products including IGS14 antenna models, orbits and clocks?
UNAVCO: *No, the repro solutions in the currently available files were not produced using IGS14 models. However, the good news is that we just completed another repro run using IGS14 products and these should be released soon, hopefully before the end of December <2018>. IGS14 based products will then be available from 1996 up through summer 2018. Please note that, like other analysis centers, we have been in a transition to IGS14 over the past year and our recent final and rapid solutions have been generated using IGS14 models, orbits and clocks even though the solutions are still provided in the IGS08 (IGB08) frame until we release our IGS14 frame files. Details about the IGS14 transition are described in this document:*

¹⁰ Project Manager at UNAVCO.

http://www.unavco.org/data/gps-gnss/derived-products/docs/GAGE_IGS14_transition_update_20180626.pdf

- **Towill:** The following response relates to a question regarding metadata.
UNAVCO: *This is a good suggestion. We have tried to find the right balance between essential information and not overloading the headers by providing the details in separate documentation, especially for the combination solutions since multiple sets of parameters would need to be included and the headers would be very long. Details regarding the analysis methods including tropospheric models and other parameters used are provided in two main sources:*

The Reviews of Geophysics publication that you mention below:

http://www.unavco.org/data/gps-gnss/derived-products/docs/Herring_et_al_2016_RevGeophys.pdf

And a summary including file descriptions as an “analysis plan” white paper:

http://www.unavco.org/data/gps-gnss/derived-products/docs/GAGE_GPS_Analysis_Plan_20170912.pdf

- **Towill:** Are the details highlighted in blue still valid? (The reader is referred to Figure 4.)

UNAVCO: *... yes there are recent changes. Specifically, the NMT Analysis Center ceased operations last month <October 2018>, leaving the CWU Analysis Center as the ONLY UNAVCO/GAGE analysis center at the present time. And because we lost one of the two AC’s this means that we can no longer generate the PBO “combination” solutions that we did previously.*

So the ... flow chart is valid for UNAVCO products up through September 2018. More specifically, the “final” final NMT and PBO combination solutions were for 2018-09-15.

Since you are using the CSV files, please note that you may see “finac” solutions for PBO files from 2018-09-15 through about 2018-10-27. These are actually CWU solutions appended to the last true combined “final” solutions. These “finac” solutions will be purged from these files when we next update them.

*For solutions after 2018-09-15 please use the CWU files: SSSS.cwu.igs08.csv or *.pos.*

We do plan (hope) to provide new types of combination solutions in the future, possibly including UNR solution, but details are unknown at present. If/when we do develop new combination products, they won’t be available until some time next year <2019>.

- **Towill:** What is your preferred citation for use of your products?
UNAVCO: *Thank you very much for asking! We really appreciate this! Our preference would be to include a reference to the Herring et al. 2016 Reviews of Geophysics paper via the citation you used above.*

Also, it would be nice to include the DOIs related to the specific data products you are using. For example, the most recent DOI describing the PBO combination products would be:

<https://doi.org/10.7283/P2HT0Z>

We update product DOIs annually, so the most recent one describes products through 2017-12-02. A new product DOI will be released early next year for data up through 2018-12. The the DOI above is the most current.

3.3.1 UNAVCO Data Source

The UNAVCO time series data can be downloaded anonymously from the following ftp site:

<ftp://data-out.unavco.org/pub/products/position/>.

In this case, the data are stored in subdirectories, one for each station; e.g., SSSS.pbo.igs08.csv, where 'SSSS' is the alphanumeric station code. The release date for these data is 2018.07.17.

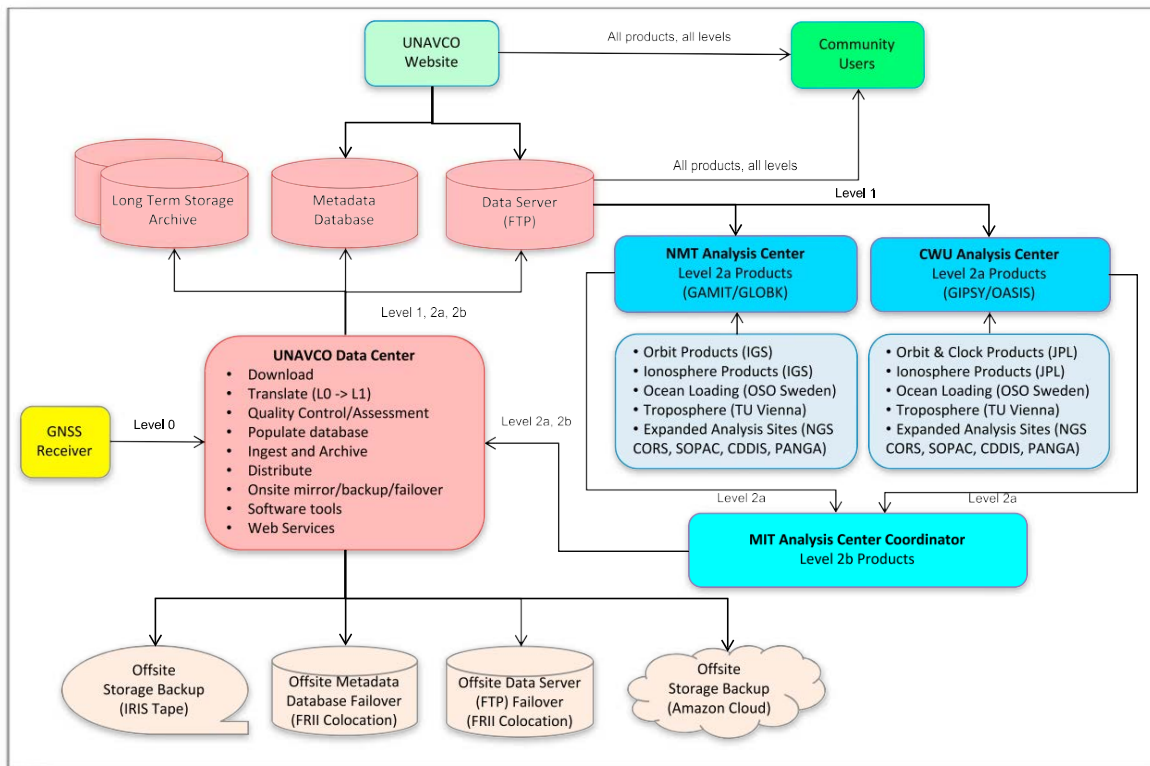


Figure 4. UNAVCO GNSS Data Processing and GAGE Workflow.

3.4 SOPAC GNSS Processing

Like UNAVCO, GAMIT/GLOBK paired with the JPL’s GIPSY(x) software is used to complete two processing streams, one network based (GIPSY), the other PPP (JPL), the solutions of which which are then combined using spatio-temporal filtering (*st_filter*) to produce the combined calibrated and validated geodetic time series (station positions).

Appendix A includes a flowchart (see Bock et al., 2016) outlining the the generation of the SESES¹¹ ESDR¹² data products as part of NASA’s MEaSURES¹³ project. SESES is an ongoing collaborative effort by JPL and SOPAC. The archived products are time series of geodetic station positions, velocity fields, strain and strain rate, and time series offsets. Weekly updates are issued by the project. In addition, the project has developed the GPS Explorer data portal (available at <http://geoapp03.ucsd.edu/gridsphere/gridsphere>), which provides tools to access and explore these data products. Note that the plots shown in Figure 9 were generated using GPS Explorer.

¹¹ Solid Earth Science ESDR System.

¹² Earth Science Data Records.

¹³ Making Earth Science Data Records for Use in Research Environments. (<https://earthdata.nasa.gov/our-community/community-data-system-programs/measures-projects>).

The left-hand side of the flowcart in Appendix A presents the workflow for the GPS timeseries products co-produced by SOPAC and the JPL. A simplified view is included in Figure 7. At the time of Towill's processing effort, it is believed that JPL's PPP software was being upgraded to support multi-GNSS solutions¹⁴ and the JPL solutions may not have been available. For this reason, only the SOPAC network solution was used by Towill. The global network of processed points is shown in

Figure 5. We downloaded (see Section 4.1) and used the the WNAM¹⁵ time series for the SOPAC points involved in this study (refer to Figure 6).

For the updating of the California Spatial Reference System's (CSRS) most recent realization of NAD83 at epoch 2017.50, SOPAC also did not use the JPL product. A clear and thorough step-by-step description of the process is included in the project report (Bock, et al., 2018).

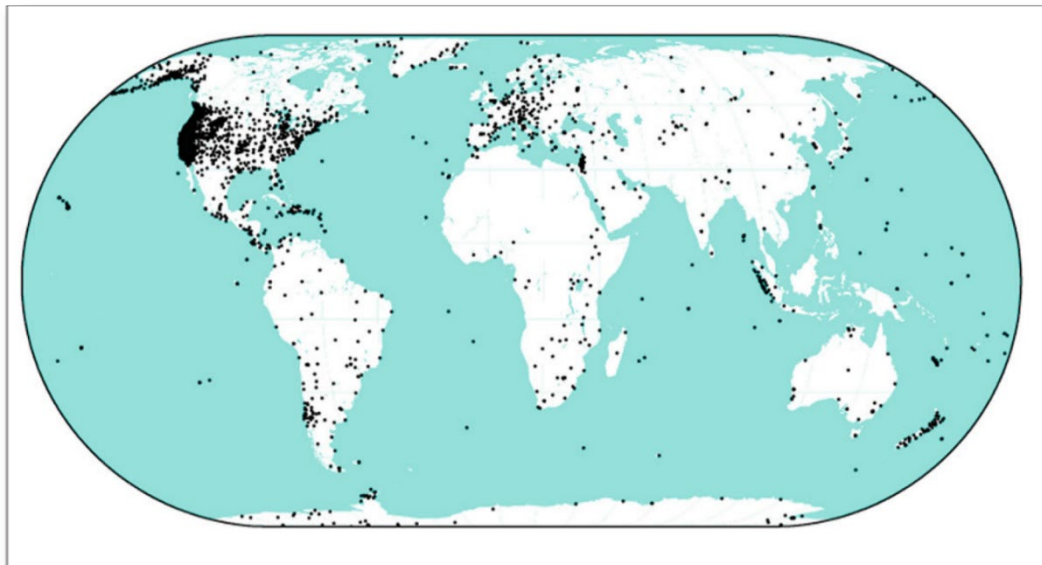


Figure 5. Global Distribution of Stations Processed Independently by SOPAC and the JPL (reproduced after Bock et al., 2016)

¹⁴ Multiple GNSS satellite constellations: GPS, GLONASS, Galileo and BeiDou.

¹⁵ Western North America.

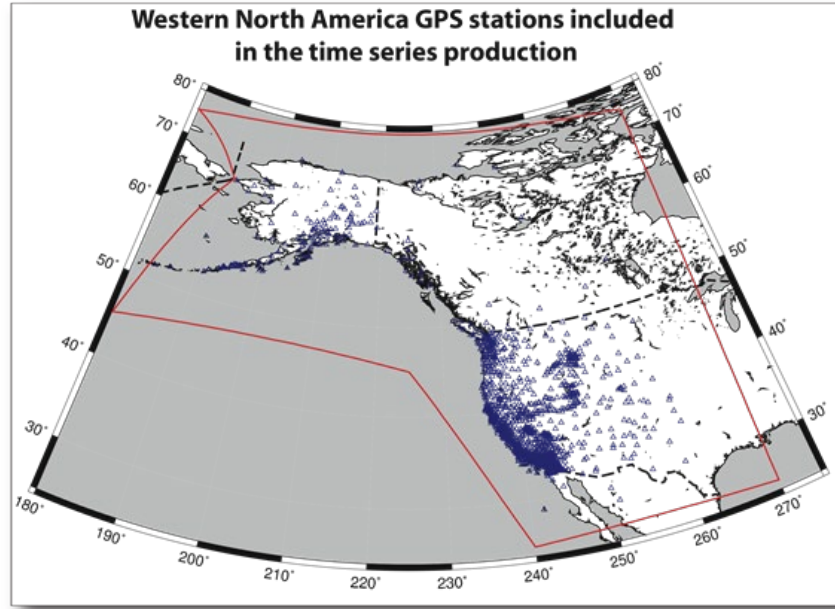


Figure 6. WNAM GNSS Product Coverage

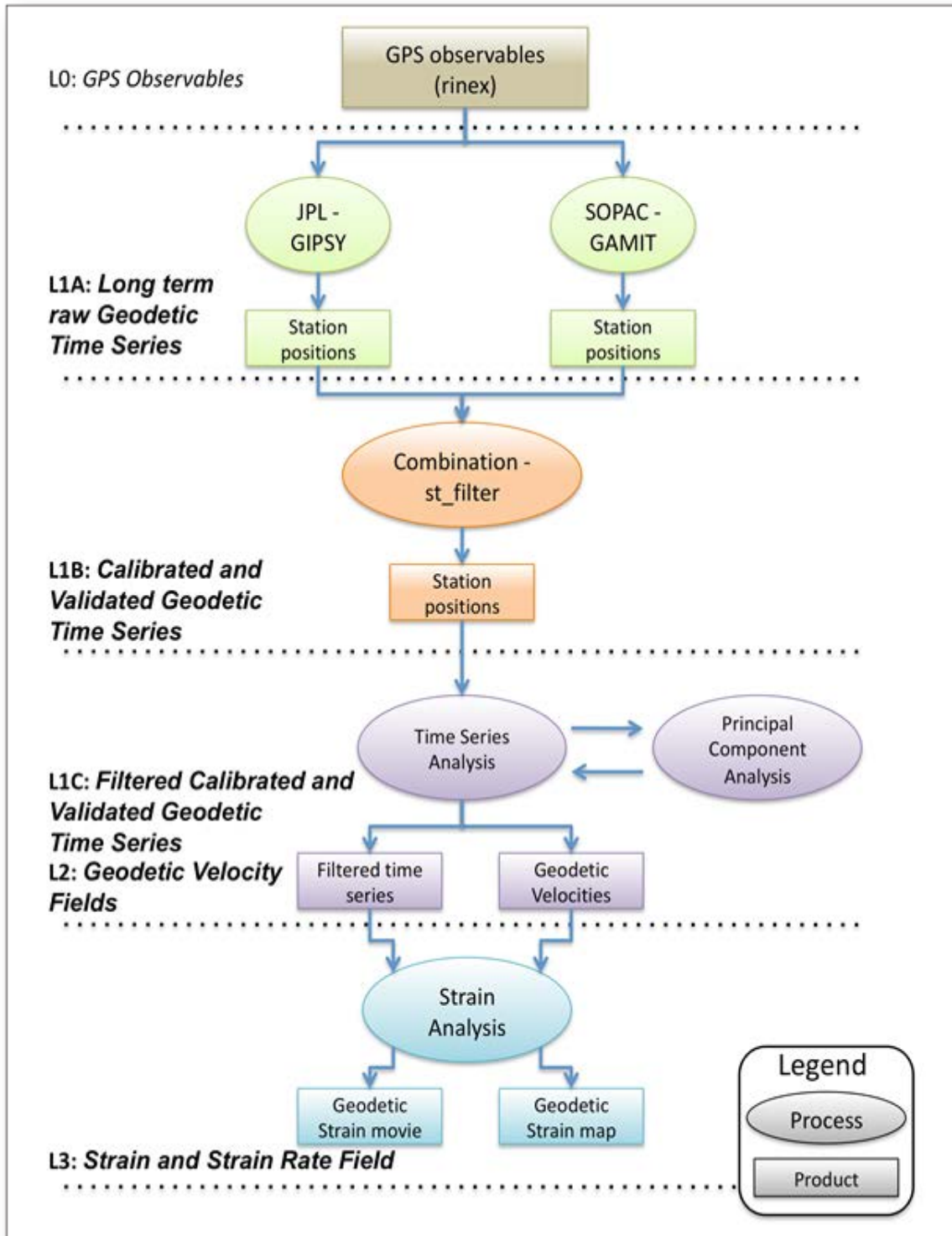


Figure 7. Basic SOPAC/JPL Process and Product Workflow

4. Time Series Data Sources and Smoothing

4.1 UNAVCO and SOPAC Data Sources

CGPS time series data were acquired within the overall study area spatial extents and spanning the study period. These data were drawn from a variety of suitable CGPS networks including the PBO (UNAVCO), CORS (NGS), and the Caltrans and SOPAC Real-time network stations. RTNs. Ultimately these time series were obtained from two ftp data archives, namely SOPAC and UNAVCO:

SOPAC: <ftp://garner.ucsd.edu/pub/timeseries/measures/ats/WesternNorthAmerica/>.

The time series file downloaded and used by Towill is:

WNAM_Clean_TrendNeuTimeSeries_sopac_20180911.tar.gz. This contains all of the station time series processed by SOPAC for stations in the WNAM polygon shown in Figure 6.

The data span the timeframe 2014.12.17 to 2018.07.15 (see Bock and Webb, 2012).

Note: in this case, only the SOPAC geodetic time series data were employed. The combined solution incorporating the JPL GIPSY solution was not used.

UNAVCO: <ftp://data-out.unavco.org/pub/products/position/>.

In this case, the data are stored in subdirectories, one for each station; e.g., SSSS.pbo.igs08.csv, where 'SSSS' is the alphanumeric station code. The release date for these data is 2018.07.17.

4.2 Data Transformation and Reformatting

CGPS time-series data were downloaded from the online archives identified above. Computer scripts and VBA macros were developed and applied to reorganize the data into a format requested by TRE Altimara.

Horizontal positions used for the CGPS stations were calculated based on the date of September 30, 2016 (mid-study epoch).

Horizontal position and ellipsoid height for CGPS stations were transformed to the ITRF2014 reference frame.

4.3 Time Series Smoothing

A 31-day moving average was used for smoothing the time series data. A similar method and window span was employed on a similar project (see Sneed et al., 2013), and was also requested by Ben Brezing (personal communication, 2018).

After selecting the 31-day moving average, the time series data were extracted from the source files identified in Section 4.1 above. To facilitate the smoothing process, the data were extended by fifteen (15) days beyond each end of the study-period. After completing the smoothing, the time series data, both smoothed and original were

'normalized' to the study start date and time, namely 2015.01.01 at 1200 UTC by resetting each time series component to zero at that time and date. The 15-day excess data at each end of the time series (study period) were discarded.

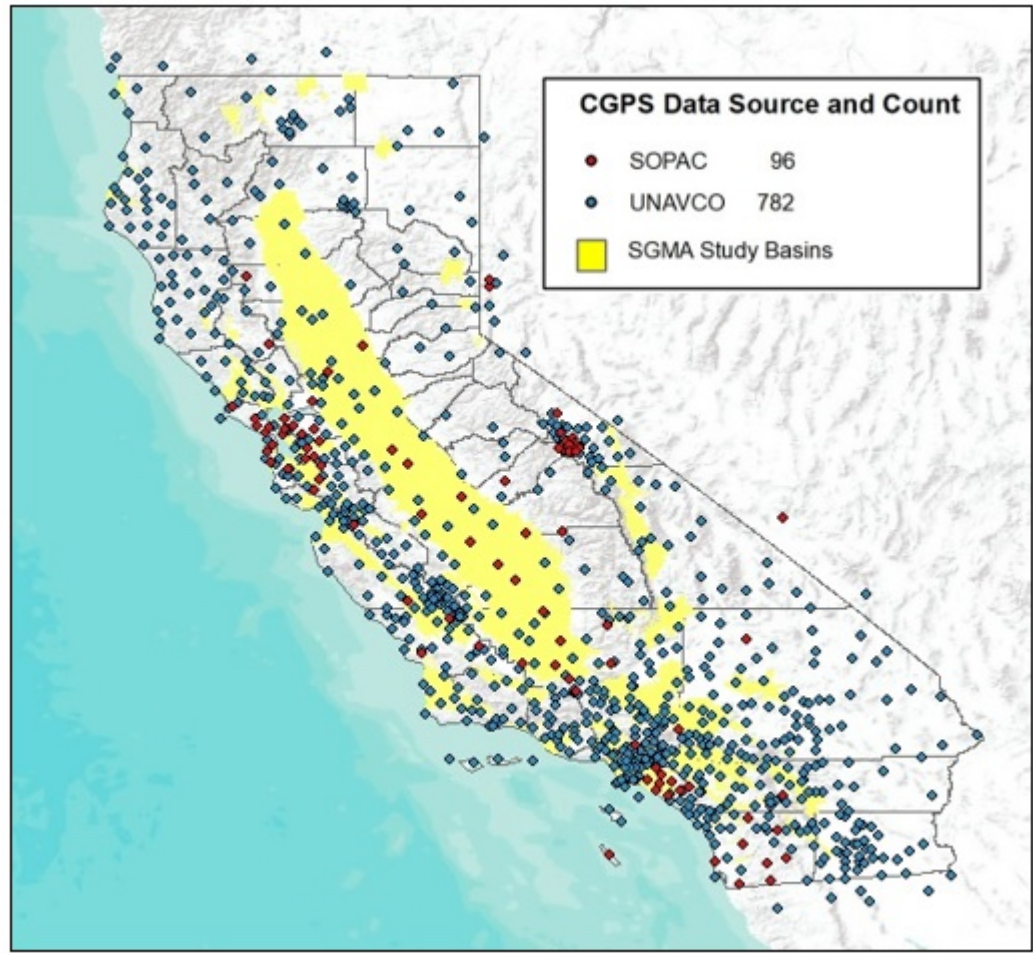


Figure 8. CGPS Stations Processed for the Study

4.4 InSAR Calibration Points

A subset of the CGPS time-series data were supplied to TRE Altamira enabling calibration of the InSAR dataset. Towill provided TRE with the geographic location of more than 800 CGPS points along with documentation of the temporal extent of the time-series data for each CGPS station. TRE selected 203 CGPS stations for use in the InSAR data calibration process. Actual ellipsoidal height values were provided to TRE following the selection of calibration points. CGPS points not selected for calibration are candidate for use as validation points. Validation points and their heights were not disclosed to TRE.

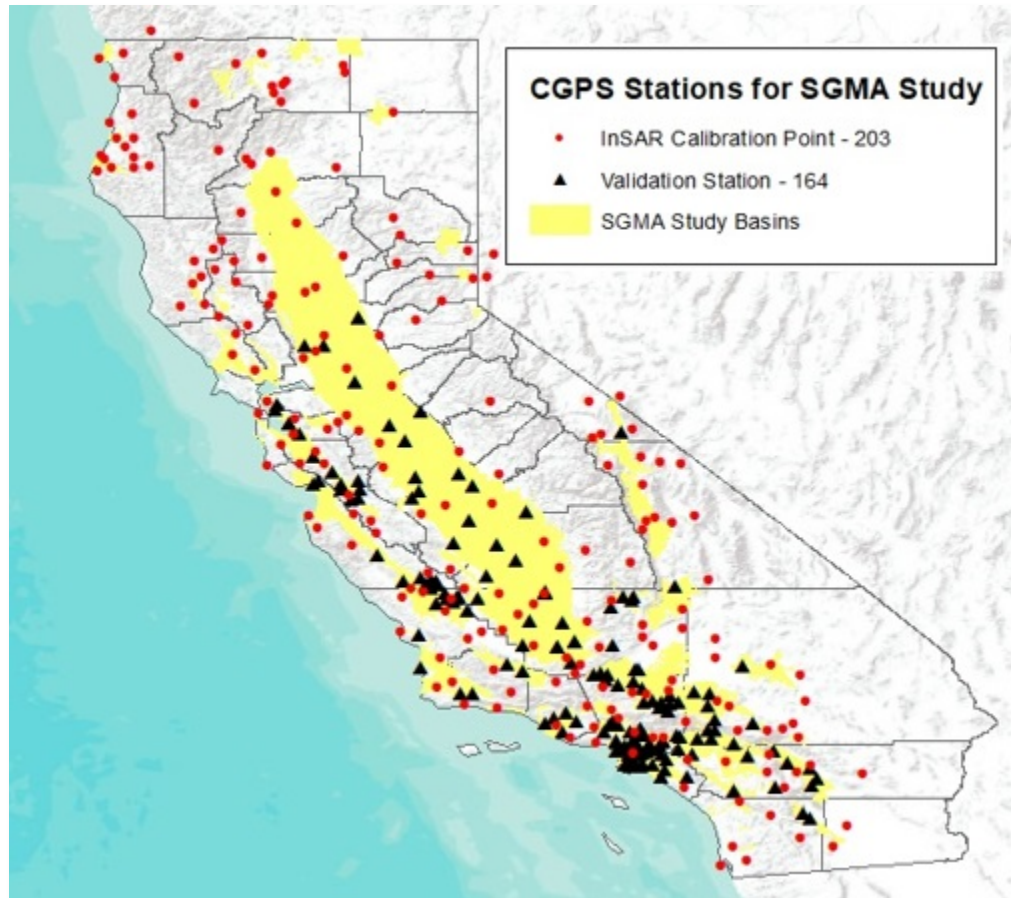


Figure 9. CGPS Stations Selected for Calibration and Validation of InSAR Data

4.5 Graphical Review and Statistical Analysis of Typical Results

At two randomly selected stations, the smoothed time series results were reviewed graphically and the residuals analyzed using Microsoft™ Excel's Descriptive Statistics and Histogram add-on utilities. For PBO station P810 the results are presented in Figure 10 while for PBO station P546 they are shown in Figure 11. A review of these two samples suggests that the smoothed time series should meet project requirements.

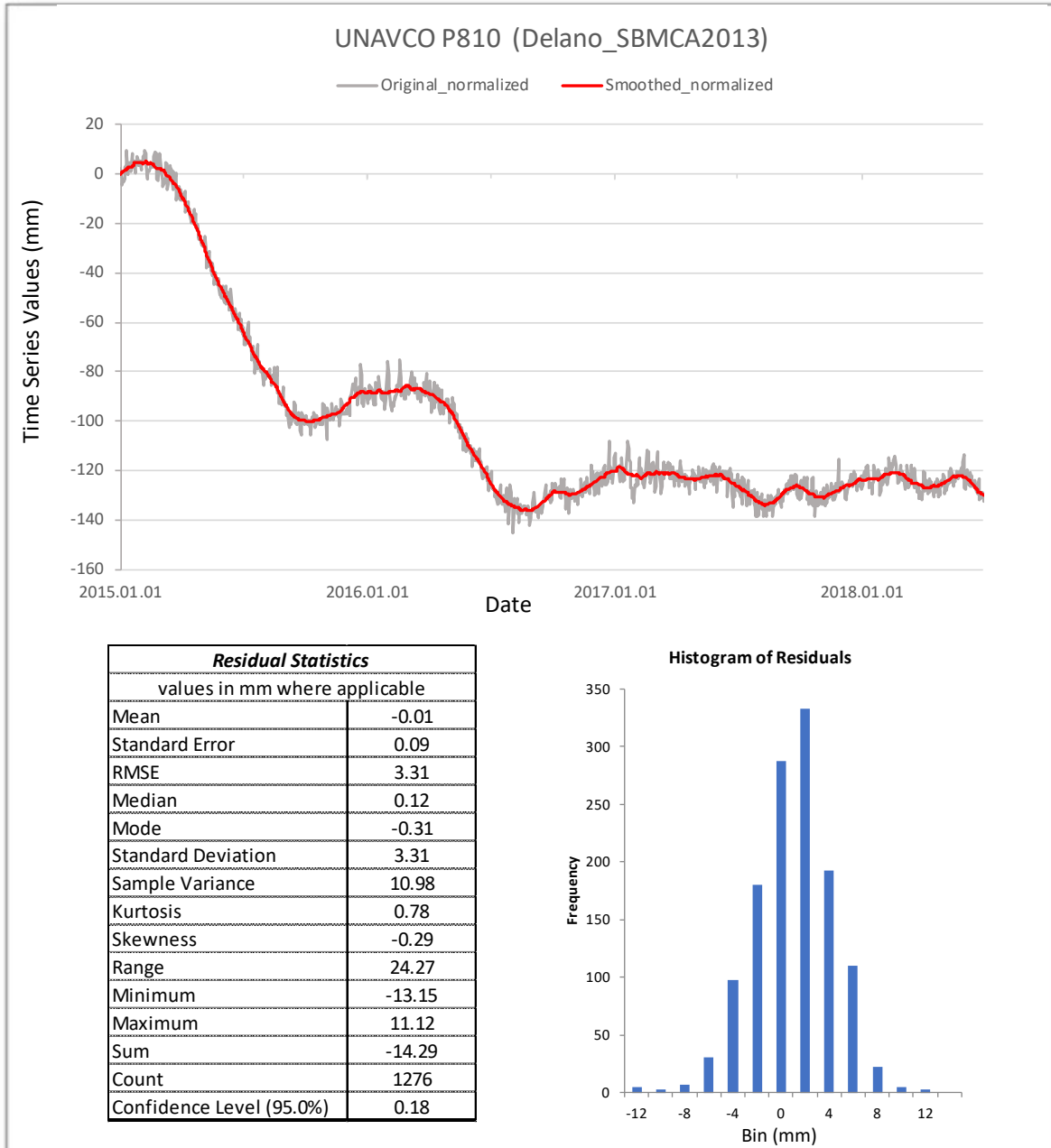


Figure 10. Graph and Statistics for PBO Station P810

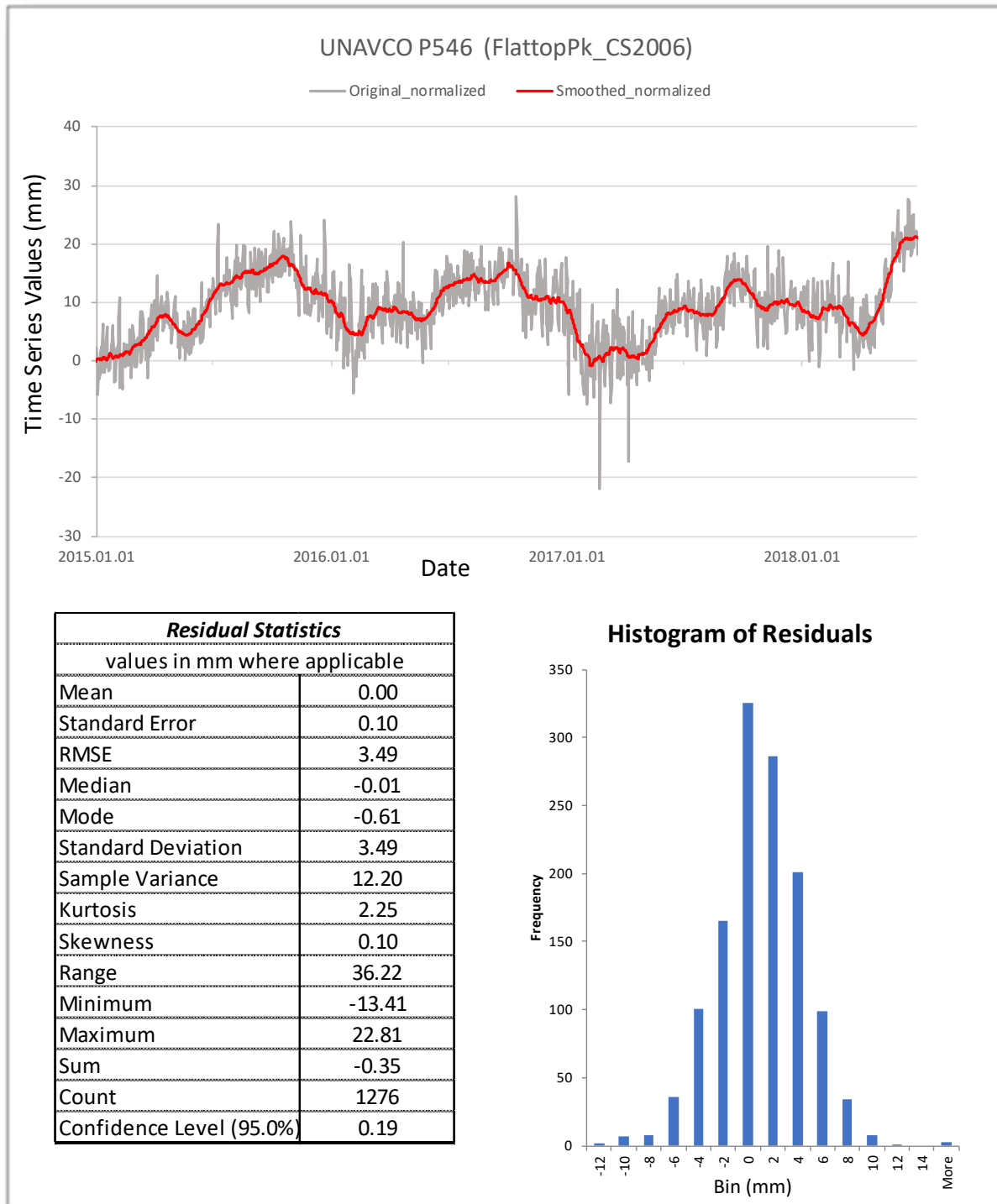


Figure 11. Graph and Statistics for PBO Station P546

5. Ten Percent Positional Data Validation

The Scope of Work (SOW) for the Task Order recommended that ~10 percent of the time series used should be independently validated to provide a measure of quality control. To this end, a random geographically dispersed sample of UNAVCO and SOPAC points were selected. A handful of these points were visually selected so as to provide project area coverage.

For each station, a time span starting at 2015.01.01 and ending at a randomly selected date within the study period was identified. Since the reference positions in the original time series are approximate and cannot be used to compute positions, Towill elected to check time series differences by comparing the 'normalized' time series data with independently processed position differences between the start and end dates. Raw RINEX data were down loaded for the SOPAC and UNAVCO stations. Data (24-hour files) were downloaded from the following locations:

- SOPAC: <ftp://garner.ucsd.edu/pub/rinex/>.
- UNAVCO: <ftp://data-out.unavco.org/pub/rinex/obs/>.

5.1 NRCan PPP SPARK Processing

The Natural Resources Canada (NRCan) Precise Point Positioning (PPP) 'SPARK' processor was used for processing the sampled RINEX files. 'SPARK' is a new modernized Multi-constellation GNSS processing engine made available for public use in August 2018. It is particularly useful in that a selection of RINEX files can simply be dragged and dropped onto a small applications which will upload the data for processing and then return the results in an email or to a specified directory on the user's computer. The primary author¹⁶ of the SPARK software referred Towill to an excellent paper written by a colleague (see Kouba, 2015). This provides a thorough explanation as to how IGS products are used for high accuracy positioning.

Prior to processing the random set of station data files, the NRCan SPARK algorithm performance was compared with a number of other online geodetic positioning services. A comparison of the results may be found in Table 2. All of the results are in extremely good agreement as indicated from the residuals from the mean of all determinations. The three PPP processing engines are all believed to have been upgraded in 2018 to accommodate the IGS move to multi-constellation GNSS processing. However, it should be noted that most algorithms use the same recommended IERS conventions and the raw data and physical conditions were identical. Hence, the solutions are not fully independent. Current conventions may be located here:

<https://www.iers.org/iers/en/Publications/TechnicalNotes/tn36.html>,

¹⁶ Simon Banville, PhD. Senior Geodetic Engineer, Surveyor General Branch, Natural Resources Canada/Government of Canada

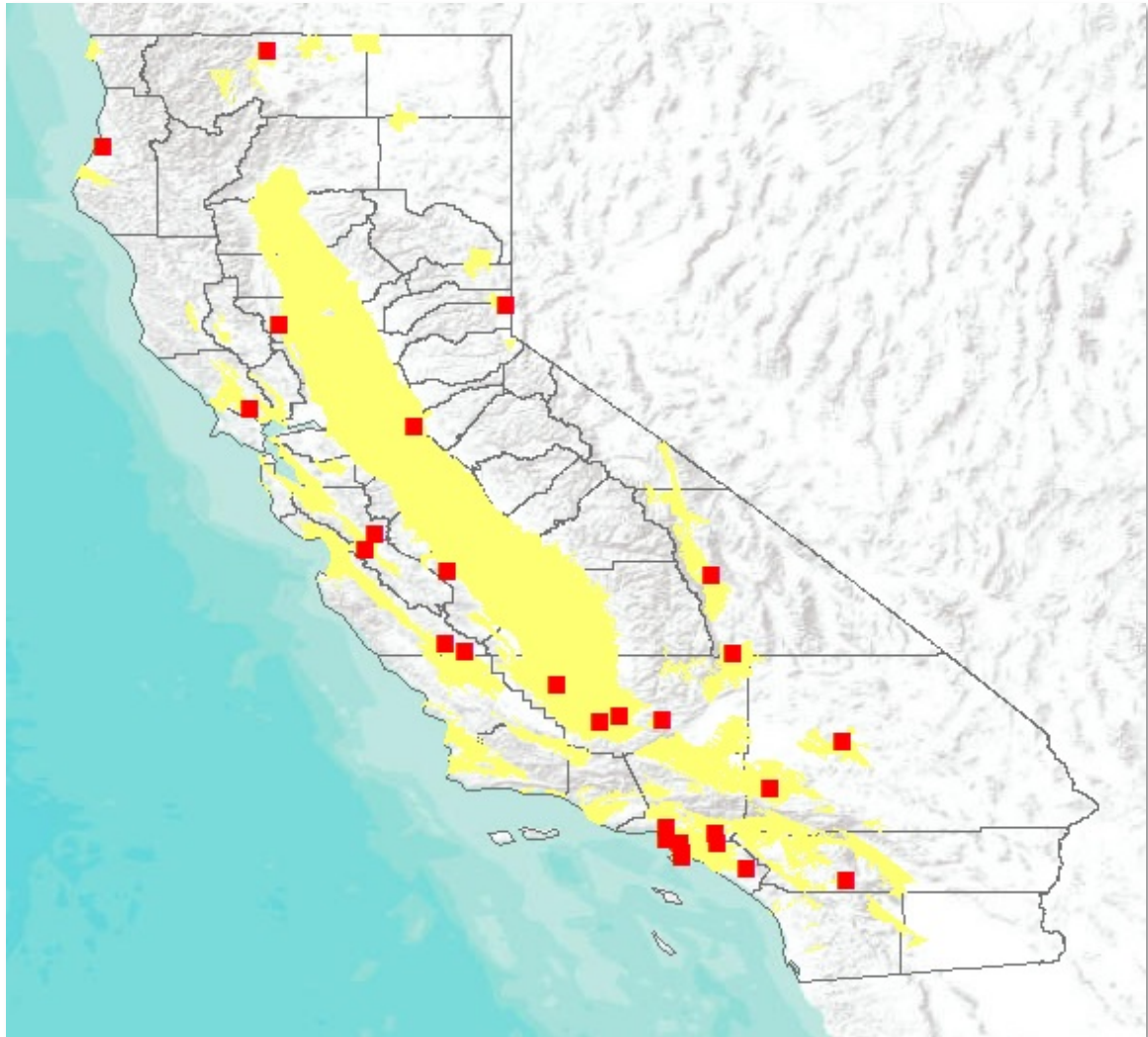


Figure 12. Validation CGPS Stations Selected for Testing Positional Accuracy

5.2 Positional Comparisons and Analysis of Results

Appendix B contains the results of the time series validation. The analysis for each CGPS station comprises two lines in the table. The columns are identified by the numbers 1 through 9. To aid in the interpretation, they are summarized as follows:

1. Four-character alphanumeric CGPS station code.
2. Time series data source (SOPAC/UNAVCO).
3. For each station, the top line is either the start date of the study period, or the station operation commencement date, if after the study period start date. The second date was randomly selected from within the study period.
4. The processing code assigned by UNAVCO. This identifies the processed solution type.
5. Extracted time series data at each of the two dates identified in item 3., above.
6. NRCan PPP solutions at each date (ITRF2014/IGS14, UTM Zone 10 or 11 North).
7. NRCan coordinate differences.
8. Time series differences.
9. Discrepancies between columns 8 and 7.

Note the apparent outlier for station 'TEHA', which is identified by pink shading. The time series discontinuity is clearly evident in Figure 9. Descriptive statistics for each of the remaining 27 stations are presented in Table 3. Figure 10 shows the distribution of all 81 discrepancies. A χ^2 – Goodness of fit test for normality (Gaussian distribution) was not performed. Considering the disparate data sources and the differencing of results at two dates, the discrepancies may be considered to be 'as expected'.

Table 2. Comparison of a NRCAN PPP Solution with Those of Other On-line Services

| ID | Epoch | Results | | | Residuals | | | Processed By | Solution Type | Frame Realizations |
|------|-------------|------------------------|-------------|--------------------------|----------------|----------------|----------------|-----------------------------------|---------------------------------------|--------------------|
| | | Northing (N) | Easting (E) | Ellips. Hgt (h) WGS84 | V _N | V _E | V _h | | | |
| | | (All values in meters) | | | | | | | | |
| P208 | 12:00:00 PM | 4329136.622 | 560186.411 | 74.291 | 0.005 | -0.001 | 0.004 | JPL GIPSY v. 6.4 | PPP | ITRF2014* |
| | 4/13/2018 | 4329136.627 | 560186.412 | 74.290 | 0.000 | -0.002 | 0.005 | NRCAN SPARK (2.18.0) | PPP | IGS14/ITRF2014 |
| | 2014.647945 | 4329136.631 | 560186.407 | 74.302 | -0.004 | 0.003 | -0.007 | UNB GAPS (6.0.1)** | PPP | IGS14/ITRF2014 |
| | | 4329136.623 | 560186.407 | 74.297 | 0.004 | 0.003 | -0.002 | AUSPOS v. 2.3*** | Network: Relative Carrier Phase | IGS14/ITRF2014 |
| | | 4329136.633 | 560186.413 | 74.296 | -0.006 | -0.003 | -0.001 | NGS OPUS (page5 v. 1603.24) | Network: Relative Carrier Phase | IGS08/ITRF2008 |

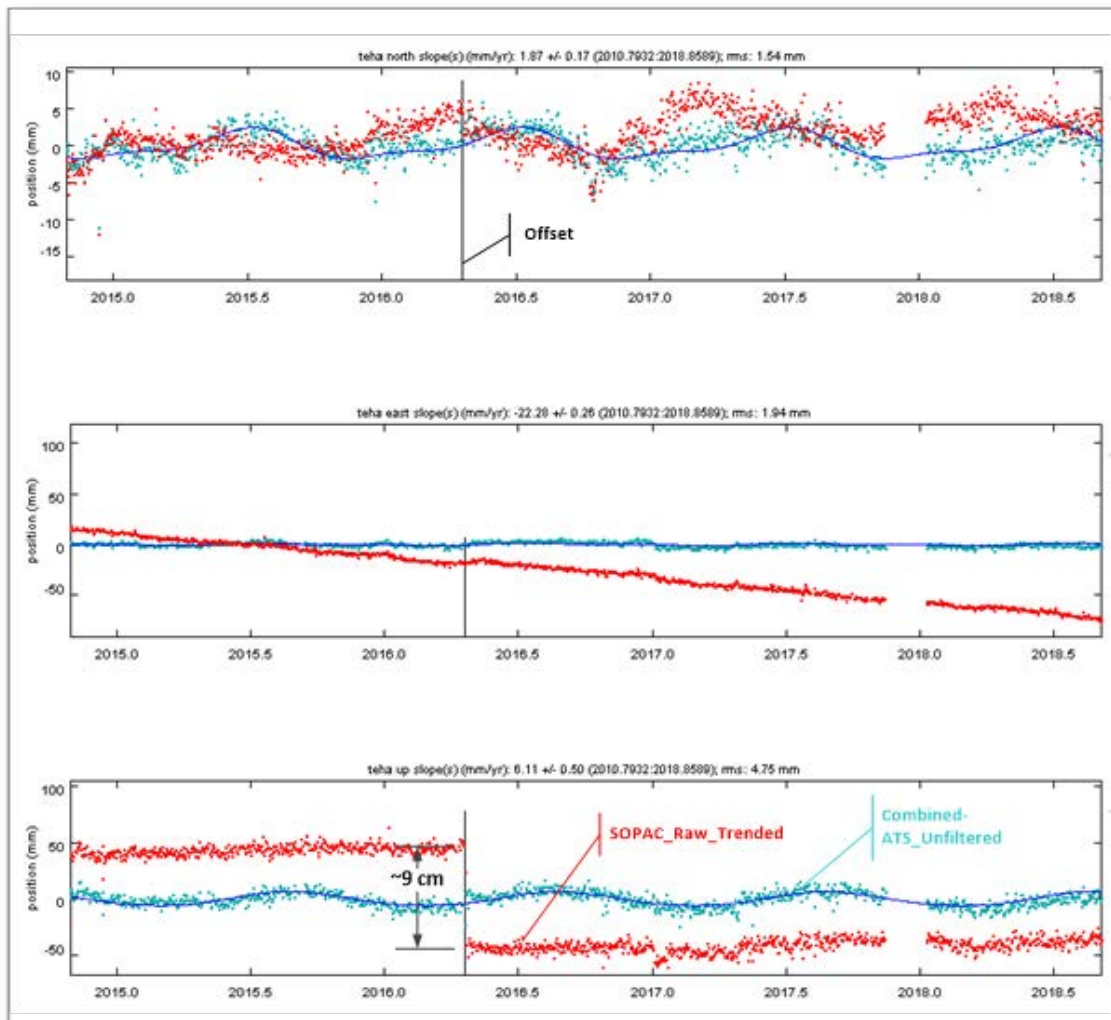


Figure 13. Explanation of the Outlier for Station 'TEHA'

Table 3. Descriptive Statistics for the Discrepancies

| Descriptive Statistics - Discrepancies | | | |
|--|----------|---------|---------------|
| (values in mm where applicable) | | | |
| | Northing | Easting | Ellps. Height |
| Mean | 0.9 | 0.4 | -0.2 |
| Standard Error | 0.7 | 0.5 | 0.8 |
| Median | 0.0 | -0.2 | 0.1 |
| Standard Deviation | 3.6 | 2.5 | 4.4 |
| RMSE | 3.7 | 2.5 | 4.3 |
| Sample Variance | 13.1 | 6.2 | 19.5 |
| Excess Kurtosis | -0.4 | 0.8 | -0.8 |
| Skewness | 0.6 | 0.8 | -0.3 |
| Range | 13.4 | 10.4 | 15.8 |
| Minimum | -4.9 | -4.1 | -9.1 |
| Maximum | 8.5 | 6.4 | 6.7 |
| Sum | 25.4 | 10.7 | -6.3 |
| Count | 27 | 27 | 27 |
| Confidence Level of Mean (95.0%) | 1.4 | 1.0 | 1.7 |

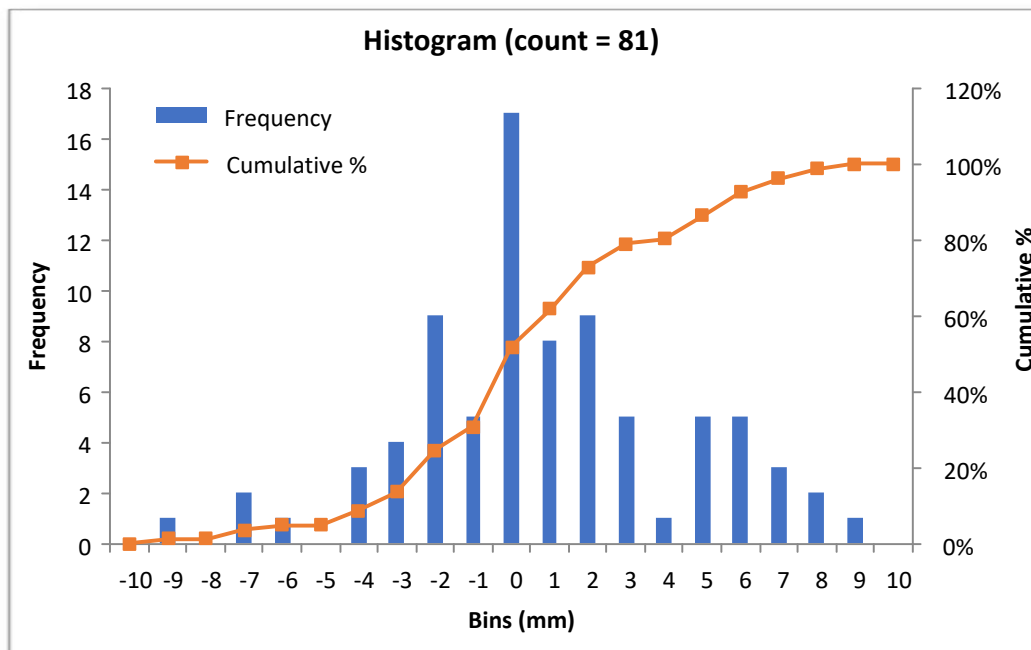


Figure 14. Distribution of 81 Samples

6. Deliverables

This task includes the following deliverables:

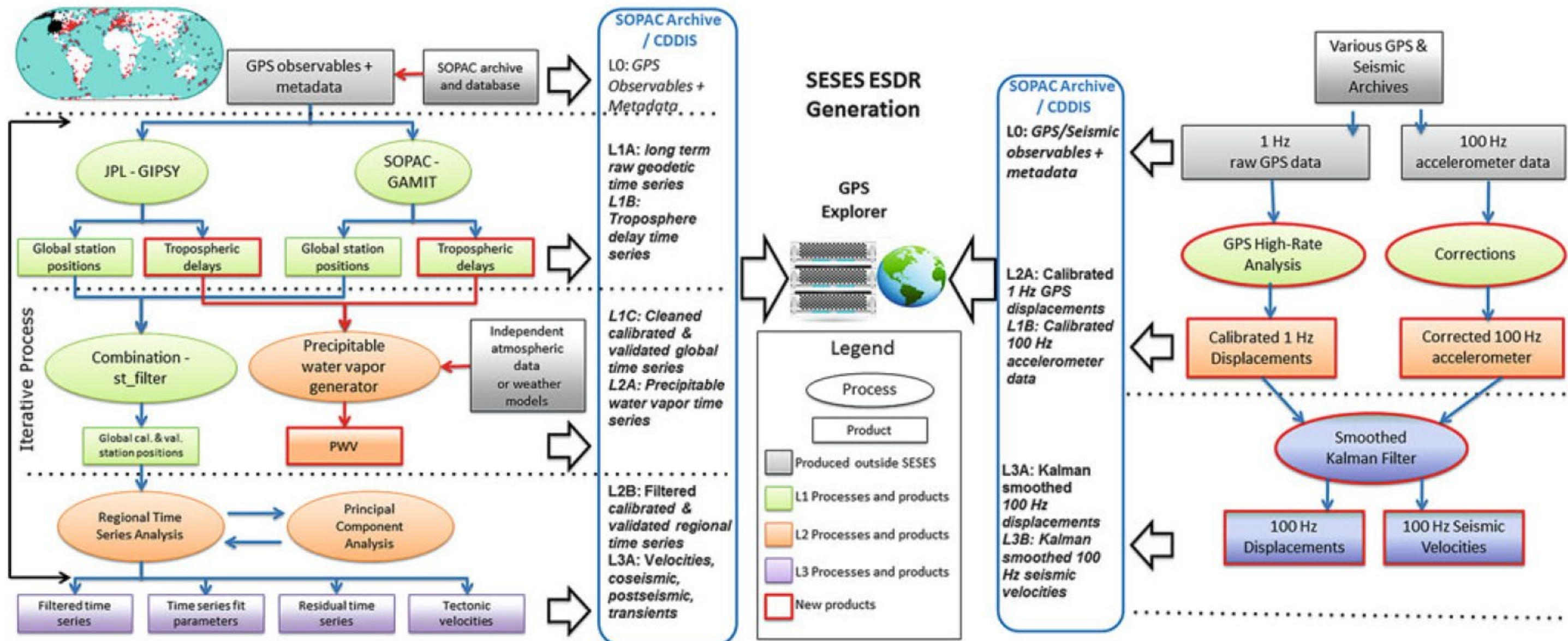
- CGPS time-series files supplied in CSV format.
- Shapefile showing CGPS stations through California; identified are which points are selected for calibration and validation of the InSAR dataset.
- This report in digital (PDF) format.

7. References

- Altamimi, Z., P. Rebischung, L. Métivier, X. Collilieux (2017). Analysis and results of ITRF2014. IERS Technical Note ; 38, Frankfurt am Main: Verlag des Bundesamts für Kartographie und Geodäsie, 76 pp., ISBN 978-3-86482-088-5
- Altamimi, Z., P. Rebischung, L. Métivier, and X. Collilieux (2016). ITRF2014: A new release of the International Terrestrial Reference Frame modeling nonlinear station motions, *J. Geophys. Res. Solid Earth*, 121, 6109–6131, doi:10.1002/2016JB013098.
- Altamimi, Z., L. Métivier, and X. Collilieux (2012). Analysis and results of ITRF2008, IERS Technical Note ; No. 37. Frankfurt am Main: Verlag des Bundesamts für Kartographie und Geodäsie, 54 pp., ISBN 978-3-86482-046-5.
- Bock, Y., P. Fang and G. R. Helmer (2018). California Spatial Reference System: CSRS Epoch 2017.50 (NAD83), Final report to California Department of Transportation (Caltrans), January 4.
- Bock, Y., S. Kedar, A. W. Moore, P. Fang, J. Geng, Z. Liu, D. Melgar, S. E. Owen, M. B. Squibb, F. Webb (2016). Twenty-Two Years of Combined GPS Products for Geophysical Applications and a Decade of Seismogeodesy, International Association of Geodesy Symposia, Springer International Publishing, doi:10.1007/1345_2016_220.
- Bock, Y. and F.H. Webb (2012). MEaSURES Solid Earth Science ESDR System. La Jolla, California and Pasadena, California USA: WNAM_Clean_TrendNeuTimeSeries_sopac_20180910.tar.gz, 2014.12.17 to 2018.06.30. Digital media.
- Herring, T. A., R. W. King, M. A. Floyd, S. C. McClusky¹⁷ (2018). Introduction to GAMIT/GLOBK. Department of Earth, Atmospheric, and Planetary Sciences Massachusetts Institute of Technology, Release 10.7, 2 June.
- Herring, T. A., T. I. Melbourne, M. H. Murray, M. A. Floyd, W. M. Szeliga, R. W. King, D. A. Phillips, C. M. Puskas, M. Santillan, and L. Wang (2016). Plate Boundary Observatory and related networks: GPS data analysis methods and geodetic products, *Rev. Geophys.*, 54 , 759 - 808, doi:10.1002/2016RG000529.

¹⁷ Now at the Australian National University.

- Johnston, G., Riddell, A., Hausler, G. (2017). The International GNSS Service. In Teunissen, Peter J.G., & Montenbruck, O. (Eds.), Springer Handbook of Global Navigation Satellite Systems (1st ed., pp. 967-982). Cham, Switzerland: Springer International Publishing, DOI: 10.1007/978-3-319-42928-1.
- Kouba, J. (2015). A Guide to Using International GNSS Service (IGS) Products. Geodetic Survey Division, Natural Resources, Canada
- Rebischung, P., Garayt, B and Z. Itamimi (2018). IGS Reference Frame Working Group Technical Report 2017. In Villiger, A., and R.Dach (eds.), International GNSS Service Technical Report 2017 (IGS Annual Report). (pp. 188-192). IGS Central Bureau and University of Bern; Bern Open Publishing DOI 10.7892/boris.116377.
- Sneed, M, Brandt, J, and M. Solt (2013). Land Subsidence along the Delta-Mendota Canal in the Northern Part of the San Joaquin Valley, California, 2003–10. Scientific Investigations Report 2013-5142. U.S. Department of the Interior, U.S. Geological Survey, Reston, Virginia.
- Villiger, A., and R.Dach (eds.) (2018). International GNSS Service Technical Report 2017 (IGS Annual Report). IGS Central Bureau and University of Bern; Bern Open Publishing DOI 10.7892/boris.116377.

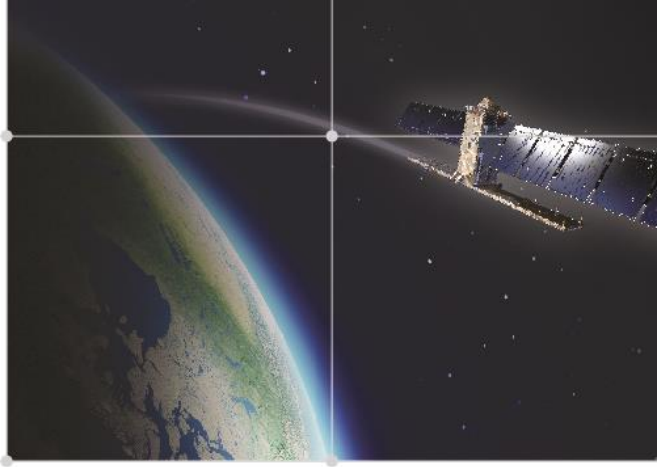


| 1 Station ID | 2 Source | 3 Date mm/dd/yyyy | 4 Processing Code | 5 Time Series Values at Date | | | UTM Zone | 6 NRCan PPP Solution at Date | | | 7 NRCan PPP Solution Differences | | | 8 Time Series Differences | | | 9 Discrepancies | | |
|-----------------|-------------|-------------------------|-------------------------|---------------------------------|------------|------------|-------------|---------------------------------|------------|----------|-------------------------------------|------------|------------|------------------------------|--------------------|--------------------|--------------------|--------|--------|
| | | | | ΔN | ΔE | Δh | | Northing | Easting | h | ΔN | ΔE | Δh | $\Delta(\Delta N)$ | $\Delta(\Delta E)$ | $\Delta(\Delta h)$ | 8 | minus | 7 |
| | | | | (mm) | | | (meters) | | | (meters) | | | (meters) | | | (meters) | | | |
| BKR1 | SOPAC | 1/1/2015 | N/A | 16.12 | -273.01 | -280.01 | 11 | 3889761.116 | 307802.183 | 56.613 | | | | | | | | | |
| BKR1 | SOPAC | 5/11/2015 | N/A | 17.42 | -287.41 | -301.31 | 11 | 3889761.121 | 307802.169 | 56.594 | 0.005 | -0.014 | -0.019 | 0.001 | -0.014 | -0.021 | -0.004 | 0.000 | -0.002 |
| SNHS | SOPAC | 1/1/2015 | N/A | 254.49 | -584.13 | 8.52 | 11 | 3754487.667 | 414168.614 | 66.421 | | | | | | | | | |
| SNHS | SOPAC | 2/17/2015 | N/A | 255.79 | -590.13 | 8.02 | 11 | 3754487.671 | 414168.602 | 66.423 | 0.004 | -0.012 | 0.002 | 0.001 | -0.006 | -0.001 | -0.003 | 0.006 | -0.002 |
| TEHA | SOPAC | 1/1/2015 | N/A | 10.47 | -93.67 | 33.40 | 11 | 3889896.658 | 366107.617 | 1174.689 | | | | | | | | | |
| TEHA | SOPAC | 6/20/2017 | N/A | 14.98 | -146.56 | 54.52 | 11 | 3889896.655 | 366107.565 | 1174.619 | -0.003 | -0.052 | -0.070 | 0.005 | -0.053 | 0.021 | 0.008 | -0.001 | 0.091 |
| WHYT | SOPAC | 1/1/2015 | N/A | 252.37 | -502.76 | -0.97 | 11 | 3726250.935 | 440351.668 | 265.406 | | | | | | | | | |
| WHYT | SOPAC | 3/30/2018 | N/A | 302.57 | -621.16 | -6.27 | 11 | 3726250.986 | 440351.551 | 265.394 | 0.051 | -0.117 | -0.012 | 0.050 | -0.118 | -0.005 | -0.001 | -0.001 | 0.007 |
| ARM1 | UNAVCO | 1/1/2015 | suppf | -8.90 | -389.77 | -261.33 | 11 | 3897033.216 | 326087.531 | 76.585 | | | | | | | | | |
| ARM1 | UNAVCO | 1/25/2016 | suppf | -8.36 | -417.37 | -310.04 | 11 | 3897033.219 | 326087.507 | 76.534 | 0.003 | -0.024 | -0.051 | 0.001 | -0.028 | -0.049 | -0.002 | -0.004 | 0.002 |
| AZRY | UNAVCO | 1/1/2015 | suppf | 231.47 | -486.44 | -15.59 | 11 | 3711223.498 | 534379.718 | 1265.695 | | | | | | | | | |
| AZRY | UNAVCO | 6/11/2017 | suppf | 260.02 | -563.98 | 1.05 | 11 | 3711223.518 | 534379.638 | 1265.707 | 0.020 | -0.080 | 0.012 | 0.029 | -0.078 | 0.017 | 0.009 | 0.002 | 0.005 |
| CRHS | UNAVCO | 1/1/2015 | suppf | 287.02 | -615.72 | 11.96 | 11 | 3743315.141 | 382216.301 | -23.554 | | | | | | | | | |
| CRHS | UNAVCO | 12/19/2015 | suppf | 303.45 | -652.23 | 21.92 | 11 | 3743315.158 | 382216.265 | -23.546 | 0.017 | -0.036 | 0.008 | 0.016 | -0.037 | 0.010 | -0.001 | -0.001 | 0.002 |
| HBCO | UNAVCO | 1/1/2015 | suppf | 277.37 | -551.47 | -16.44 | 11 | 3738910.449 | 380955.354 | -26.896 | | | | | | | | | |
| HBCO | UNAVCO | 10/22/2016 | suppf | 309.93 | -621.86 | -9.88 | 11 | 3738910.482 | 380955.283 | -26.887 | 0.033 | -0.071 | 0.009 | 0.033 | -0.070 | 0.007 | 0.000 | 0.001 | -0.002 |
| LPHS | UNAVCO | 1/1/2015 | suppf | 251.03 | -637.65 | -13.05 | 11 | 3765536.895 | 411674.879 | 68.476 | | | | | | | | | |
| LPHS | UNAVCO | 4/26/2015 | suppf | 251.51 | -649.38 | -11.18 | 11 | 3765536.896 | 411674.865 | 68.485 | 0.001 | -0.014 | 0.009 | 0.000 | -0.012 | 0.002 | -0.001 | 0.002 | -0.007 |
| MASW | UNAVCO | 1/1/2015 | suppf | 316.57 | -531.19 | 15.43 | 10 | 3968399.585 | 730961.071 | 713.732 | | | | | | | | | |
| MASW | UNAVCO | 4/25/2017 | suppf | 358.66 | -611.60 | 10.35 | 10 | 3968399.621 | 730960.990 | 713.736 | 0.036 | -0.081 | 0.004 | 0.042 | -0.080 | -0.005 | 0.006 | 0.001 | -0.009 |
| P058 | UNAVCO | 1/1/2015 | suppf | 41.17 | -87.28 | 0.58 | 10 | 4525582.510 | 409390.049 | 21.409 | | | | | | | | | |
| P058 | UNAVCO | 1/29/2016 | suppf | 44.32 | -98.04 | 6.20 | 10 | 4525582.518 | 409390.037 | 21.413 | 0.008 | -0.012 | 0.004 | 0.003 | -0.011 | 0.006 | -0.005 | 0.001 | 0.002 |
| P093 | UNAVCO | 1/1/2015 | suppf | -31.41 | -147.97 | 3.33 | 11 | 4051628.868 | 411089.219 | 1339.057 | | | | | | | | | |
| P093 | UNAVCO | 8/26/2015 | suppf | -35.00 | -162.16 | 11.57 | 11 | 4051628.864 | 411089.203 | 1339.062 | -0.004 | -0.016 | 0.005 | -0.004 | -0.014 | 0.008 | 0.000 | 0.002 | 0.003 |
| P150 | UNAVCO | 1/1/2015 | suppf | -27.44 | -136.88 | -4.11 | 10 | 4353418.391 | 755806.119 | 2619.079 | | | | | | | | | |
| P150 | UNAVCO | 9/8/2017 | suppf | -39.93 | -194.89 | -4.94 | 10 | 4353418.371 | 755806.060 | 2619.077 | -0.020 | -0.059 | -0.002 | -0.012 | -0.058 | -0.001 | 0.008 | 0.001 | 0.001 |
| P198 | UNAVCO | 1/1/2015 | suppf | 123.19 | -305.56 | -4.59 | 10 | 4234722.167 | 534342.696 | -4.623 | | | | | | | | | |
| P198 | UNAVCO | 1/1/2018 | suppf | 159.43 | -391.65 | -21.07 | 10 | 4234722.199 | 534342.610 | -4.633 | 0.032 | -0.086 | -0.010 | 0.036 | -0.086 | -0.016 | 0.004 | 0.000 | -0.006 |
| P208 | UNAVCO | 1/1/2015 | suppf | -38.42 | -200.06 | 13.68 | 10 | 4329136.643 | 560186.483 | 74.295 | | | | | | | | | |
| P208 | UNAVCO | 4/13/2018 | suppf | -52.70 | -272.05 | 6.11 | 10 | 4329136.627 | 560186.412 | 74.290 | -0.016 | -0.071 | -0.005 | -0.014 | -0.072 | -0.008 | 0.002 | -0.001 | -0.003 |
| P238 | UNAVCO | 1/1/2015 | suppf | 114.74 | -265.07 | 19.86 | 10 | 4079247.677 | 637942.744 | 44.899 | | | | | | | | | |
| P238 | UNAVCO | 6/6/2017 | suppf | 146.00 | -330.29 | 12.06 | 10 | 4079247.704 | 637942.680 | 44.896 | 0.027 | -0.064 | -0.003 | 0.031 | -0.065 | -0.008 | 0.004 | -0.001 | -0.005 |

| ① Station ID | ② Source | ③ Date mm/dd/yyyy | ④ Processing Code | ⑤ Time Series Values at Date | | | ⑥ UTM Zone | ⑥ NRCan PPP Solution at Date | | | ⑦ NRCan PPP Solution Differences | | | ⑧ Time Series Differences | | | ⑨ Discrepancies | | |
|-----------------|-------------|-------------------------|-------------------------|---------------------------------|---------|--------|------------------|---------------------------------|------------|----------|-------------------------------------|--------|----------|------------------------------|--------|--------|--------------------|--------|--------|
| | | | | ΔN | ΔE | Δh | | Northing | Easting | h | ΔN | ΔE | Δh | Δ(ΔN) | Δ(ΔE) | Δ(Δh) | ⑧ minus ⑦ | ⑦ | |
| | | | | (mm) | | | (meters) | | | (meters) | | | (meters) | | | | | | |
| P244 | UNAVCO | 1/1/2015 | suppf | -11.37 | -227.97 | 16.09 | 10 | 4097338.659 | 646393.246 | 58.712 | | | | | | | | | |
| P244 | UNAVCO | 11/26/2016 | suppf | -12.00 | -281.49 | 16.74 | 10 | 4097338.656 | 646393.193 | 58.720 | -0.003 | -0.053 | 0.008 | -0.001 | -0.054 | 0.001 | 0.002 | -0.001 | -0.007 |
| P291 | UNAVCO | 1/1/2015 | suppf | 159.80 | -281.43 | -10.33 | 10 | 3977946.685 | 712496.546 | 661.360 | | | | | | | | | |
| P291 | UNAVCO | 5/31/2018 | final | 233.26 | -407.89 | -2.21 | 10 | 3977946.751 | 712496.415 | 661.363 | 0.066 | -0.131 | 0.003 | 0.073 | -0.126 | 0.008 | 0.007 | 0.005 | 0.005 |
| P302 | UNAVCO | 1/1/2015 | suppf | -10.24 | -202.57 | 1.64 | 10 | 4056993.933 | 712916.705 | 122.647 | | | | | | | | | |
| P302 | UNAVCO | 11/1/2016 | suppf | -10.29 | -232.37 | 3.35 | 10 | 4056993.932 | 712916.677 | 122.648 | -0.001 | -0.028 | 0.001 | 0.000 | -0.030 | 0.002 | 0.001 | -0.002 | 0.001 |
| P309 | UNAVCO | 1/1/2015 | suppf | -27.30 | -204.96 | 10.56 | 10 | 4217781.757 | 679664.920 | 41.410 | | | | | | | | | |
| P309 | UNAVCO | 3/16/2018 | suppf | -29.06 | -280.53 | -3.89 | 10 | 4217781.751 | 679664.846 | 41.399 | -0.006 | -0.074 | -0.011 | -0.002 | -0.076 | -0.014 | 0.004 | -0.002 | -0.003 |
| P470 | UNAVCO | 1/1/2015 | suppf | 48.72 | -253.19 | 20.60 | 11 | 3813498.806 | 463823.213 | 991.377 | | | | | | | | | |
| P470 | UNAVCO | 9/6/2015 | suppf | 50.98 | -270.80 | 22.76 | 11 | 3813498.807 | 463823.189 | 991.374 | 0.001 | -0.024 | -0.003 | 0.002 | -0.018 | 0.002 | 0.001 | 0.006 | 0.005 |
| P545 | UNAVCO | 1/1/2015 | suppf | 16.98 | -172.20 | -50.04 | 11 | 3931432.734 | 269994.520 | 50.706 | | | | | | | | | |
| P545 | UNAVCO | 1/15/2016 | suppf | 17.28 | -195.61 | -59.81 | 11 | 3931432.737 | 269994.497 | 50.691 | 0.003 | -0.023 | -0.015 | 0.000 | -0.023 | -0.010 | -0.003 | 0.000 | 0.005 |
| P604 | UNAVCO | 1/1/2015 | suppf | -33.12 | -131.25 | 22.17 | 11 | 3866086.792 | 530003.348 | 588.427 | | | | | | | | | |
| P604 | UNAVCO | 1/11/2015 | suppf | -33.10 | -132.07 | 25.14 | 11 | 3866086.793 | 530003.347 | 588.424 | 0.001 | -0.001 | -0.003 | 0.000 | -0.001 | 0.003 | -0.001 | 0.000 | 0.006 |
| P784 | UNAVCO | 1/1/2015 | suppf | -36.90 | -103.93 | -3.15 | 10 | 4631154.452 | 548123.356 | 802.242 | | | | | | | | | |
| P784 | UNAVCO | 6/1/2018 | final | -57.21 | -154.23 | -1.30 | 10 | 4631154.430 | 548123.306 | 802.244 | -0.022 | -0.050 | 0.002 | -0.020 | -0.050 | 0.002 | 0.002 | 0.000 | 0.000 |
| P799 | UNAVCO | 2/1/2015 | suppf | 68.70 | -154.05 | 6.40 | 11 | 3754902.185 | 379255.118 | 24.832 | | | | | | | | | |
| P799 | UNAVCO | 1/12/2016 | suppf | 89.05 | -185.26 | 9.25 | 11 | 3754902.208 | 379255.087 | 24.833 | 0.023 | -0.031 | 0.001 | 0.020 | -0.031 | 0.003 | -0.003 | 0.000 | 0.002 |
| TOWG | UNAVCO | 9/1/2015 | suppf | -3.47 | -0.52 | -1.07 | 11 | 3962985.600 | 430894.981 | 657.080 | | | | | | | | | |
| TOWG | UNAVCO | 2/20/2016 | suppf | -3.10 | -9.58 | -10.10 | 11 | 3962985.603 | 430894.976 | 657.074 | 0.003 | -0.005 | -0.006 | 0.000 | -0.009 | -0.009 | -0.003 | -0.004 | -0.003 |
| UCLP | UNAVCO | 1/1/2015 | suppf | 316.54 | -725.61 | 11.96 | 11 | 3770758.156 | 366945.161 | 111.536 | | | | | | | | | |
| UCLP | UNAVCO | 3/12/2017 | suppf | 349.18 | -809.44 | 2.17 | 11 | 3770758.189 | 366945.079 | 111.527 | 0.033 | -0.082 | -0.009 | 0.033 | -0.084 | -0.010 | 0.000 | -0.002 | -0.001 |
| WRHS | UNAVCO | 1/1/2015 | suppf | 276.24 | -597.64 | 17.16 | 11 | 3758434.138 | 368093.546 | 7.870 | | | | | | | | | |
| WRHS | UNAVCO | 11/14/2016 | suppf | 309.23 | -667.06 | 15.28 | 11 | 3758434.171 | 368093.474 | 7.868 | 0.033 | -0.072 | -0.002 | 0.033 | -0.069 | -0.002 | 0.000 | 0.003 | 0.000 |

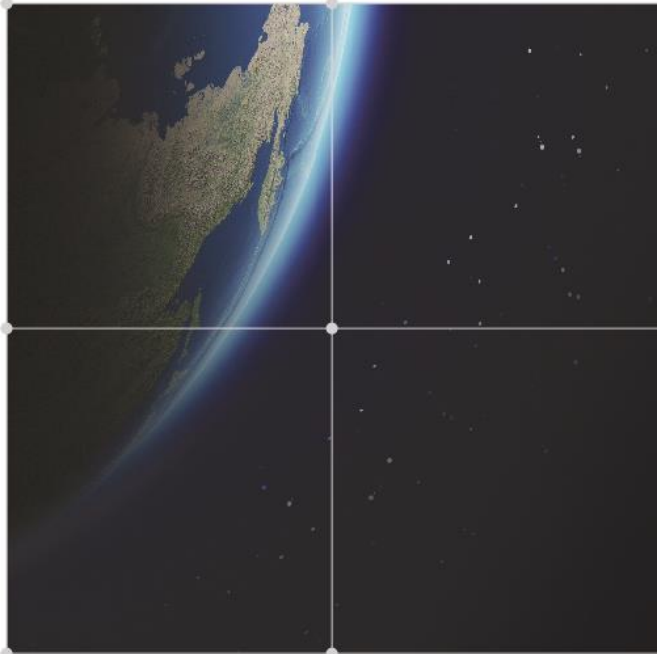
- Four-character alphanumeric CGPS station code.
- Time series data source (SOPAC/UNAVCO).
- For each station, the top line is either the start date of the study period, or the station operation commencement date, if after the study period start date. The second date was randomly selected from within the study period.
- The processing code assigned by UNAVCO. This identifies the processed solution type.
- Extracted time series data at each of the two dates identified in item 3., above.
- NRCan PPP solutions at each date (ITRF2014/IGS14, UTM Zone 10 or 11 North).
- NRCan coordinate differences.
- Time series differences.
- Discrepancies between columns 8 and 7.

APPENDIX D



InSAR land surveying and mapping services in support of the DWR SGMA program

Technical Report - March 2020



TRE
ALTAMIRA
A CLS Group Company



Report prepared by

TRE ALTAMIRA Inc.

Address:

#410 – 475 West Georgia Street
Vancouver, BC, V6B 4M9

Date:

16 March 2020

Executive Summary

TRE Altamira Inc. (TRE) has been contracted by Towill, Inc (Towill) to provide InSAR ground deformation measurements over groundwater basins in California (Task Order No. 37 – Contract No. 4600011239, *supporting the Sustainable Groundwater Management Act (SGMA) of the California Department of Water Resources*).

The objective of the work is to update the 2018 ground deformation measurements (Task Order No. 26 – Contract No. 4600011239) up to September 2019. The output consists of continuous uninterrupted vertical deformation time series from 01 January 2015 to Sept 2019, obtained by stitching the 2019 results to the 2018 historical data.

TRE's SqueeSAR algorithm is used to generate the ground deformation measurements and the results are calibrated and validated using ground-based, continuously operating Global Positioning System (GPS) stations located throughout the state of California.

This **Milestone 4 Report** represents the final deliverable and provides a description of all tasks and milestones.

- **Task 1 - Study Area:** The study area defined by DWR covers 101,210 km² (39,000 mi²) in California. It has increased by 6,737 km² (2,600 mi²) compared to the 2018 study as it now includes additional basins located in the north and in the south of California.
- **Task 2.1 - Imagery procurement:** All available (2,235) Sentinel images were downloaded. The new imagery covers the period 01 June 2018 - 30 September 2019 for the areas in common with the 2018 analysis and the full 01 January 2015 – 30 September 2019 period for the new areas.
- **Task 2.2 - Processing polygons definition:** The downloaded imagery was analyzed and 35 polygons defined for the data processing. To maintain maximum consistency with the 2018 results, the 27 processing polygons over the 2018 areas have remained unchanged while 8 new processing polygons were defined for the new basins.
- **Task 2.3 – SqueeSAR Processing:** The SqueeSAR data processing for the 27 previous processing polygons produced LOS measurements that cover 01 January 2018 - 30 September 2019, which includes an overlap of 15-20 images with the previous analysis. These results were then integrated with the 01 January 2015 – 01 June 2018 measurements to generate uninterrupted deformation time series from January 2015 to September 2019. Over the new areas, the SqueeSAR processing was carried out from scratch, using the entire image archive available from January 2015 to September 2019.

- **Task 2.4 – Data calibration:** 231 GPS stations were selected from the UNAVCO network to calibrate the LOS measurements. The calibration was performed using the methodology defined in the 2018 analysis.
- **Task 2.5 – Vertical measurements:** The vertical measurements were derived from the LOS calibrated time series using the same methodology of the 2018 analysis. To maintain the maximum consistency with the previous results, the same spatial grid and temporal sampling were used.
- **Task 2.6 – Draft deliverables:** The draft deliverables were generated for both the common period and the variable start date results, using the same format defined in the 2018 analysis and made available on the TREmaps web platform and a dedicated SFTP.
- **Task 2.7 – Final deliverables:** TRE received and addressed the modification requests from DWR and Towill to produce the final deliverables, including the high-resolution LOS data. All deliverables were provided to Towill and DWR through TREmaps and SFTP.



Contents

| | |
|---|-----------|
| Executive Summary | 2 |
| Acronyms and Abbreviations..... | 5 |
| 1. Introduction..... | 6 |
| 2. Task 1: Study Area | 7 |
| 3. Task 2.1: Imagery procurement | 8 |
| 4. Task 2.2: Processing polygons definition | 9 |
| 5. Task 2.3: SqueeSAR processing | 10 |
| 6. Task 2.4: Data Calibration | 11 |
| 6.1. Methodology..... | 12 |
| 7. Task 2.5: Vertical measurements | 14 |
| 8. Task 2.6: Draft deliverables | 15 |
| 9. Task 2.7: Final Deliverables..... | 16 |
| 9.1. Common start date: | 16 |
| 9.2. Cumulative raster maps..... | 17 |
| 9.3. Variable start date:..... | 17 |
| 9.4. Annual raster maps | 18 |
| 9.5. LOS measurements..... | 19 |
| 9.5.1. LOS measurements characteristics | 19 |
| 9.5.2. Notes for the comparison of LOS data with other 3-D data | 24 |
| 10. Data delivery | 27 |
| 11. Summary | 28 |

Acronyms and Abbreviations

| | |
|-----------|---|
| AOI | Area of Interest (study area) |
| ASC/A | Ascending orbit |
| DESC/D | Descending orbit |
| GNSS | Global Navigation Satellite System |
| InSAR | Interferometric Synthetic Aperture Radar |
| LOS | Line of Sight |
| MP | Measurement Point |
| SNT | Sentinel Satellite |
| TS | Time series |
| SqueeSAR® | Advanced InSAR algorithm patented by TRE Altamira |

Confidentiality disclaimer

This document contains confidential proprietary information and is intended solely for the recipient. The contents of this document, including information related to TRE ALTAMIRA methodology and know-how, may not be disclosed in whole or in part to any third party by any means or used for any other purpose without the express written permission of TRE ALTAMIRA

1. Introduction

TRE has been contracted by Towill under Task Order No. 37 - Contract No. 4600011239 to provide InSAR ground deformation monitoring data over groundwater basins in California, in support of land surveying and mapping services for the Department of Water Resources (DWR) and its mission to enact the Sustainable Groundwater Management Act (SGMA).

The project consists of four Tasks (Table 1), with TRE responsible for Task 2 - *InSAR data Acquisition and Analysis*, whose objective is to update the ground deformation measurements provided in 2018 (Task Order No. 26 – Contract No. 4600011239) to September 2019. Task 2 comprised seven sub-tasks and four milestones (Table 2) and this Milestone 4 report constitutes the final document.

| Project Task | Description | Appointed |
|--------------|-------------------------------------|-----------|
| 1 | Study Area definition | DWR |
| 2 | InSAR data Acquisition and Analysis | TRE |
| 3 | CGPS Data Acquisition and Analysis | Towill |
| 4 | InSAR-CGPS Comparative Analysis | Towill |

Table 1: Project Tasks

| Task 2 | Description | Milestone (report) | Expected Delivery | Delivery date |
|--------|----------------------------------|--------------------|-------------------|---------------|
| 2.1 | Imagery procurement | M1 | 25 Oct 2019 | 28 Oct 2019 |
| 2.2 | Processing polygons definition | M2 | 16 Dec 2019 | 23 Dec 2019 |
| 2.3 | SqueeSAR processing (LOS data) | | | |
| 2.4 | Data calibration (LOS data) | M3 | 14 Feb 2020 | 20 Feb 2020 |
| 2.5 | Vertical measurements generation | | | |
| 2.6 | Draft deliverables | | | |
| 2.7 | Final deliverable | M4 | 16 Mar 2020 | 16 Mar 2020 |

Table 2: Task 2 subtasks and schedule.

2. Task 1: Study Area

The study area covers 101,210 km² (39,000 mi²) and includes the groundwater basins of interest to DWR. The area has increased by 6,737 km² (2,600 mi²) compared to the 2018 study as it now includes additional basins located in the north and in the south of California (Figure 1).

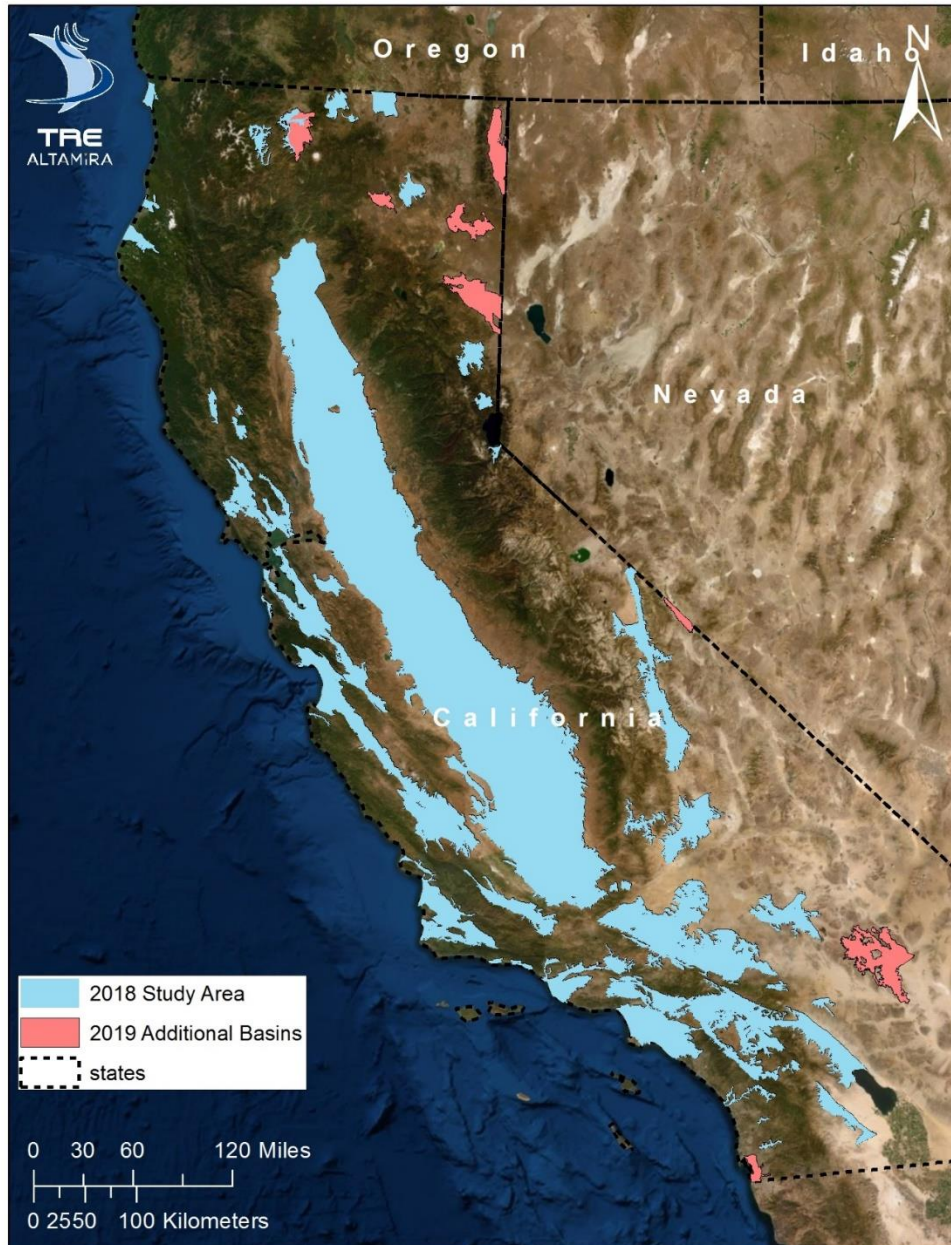


Figure 1: The 2019 study area covers the groundwater basins of the 2018 analysis (light blue) and also includes new basins (light red).

3. Task 2.1: Imagery procurement

The 2019 update included new satellite radar imagery acquired over the study area by the Sentinel-1 (SNT) mission since the end of the 2018 analysis (01 June 2018).

The SNT mission is part of the European Radar Observatory for the Copernicus joint initiative of the European Commission and the European Space Agency and comprises two satellites that share the same orbit, with each satellite acquiring data in the C-band wavelength (5.9 cm), with a 5x20 meter ground resolution. SNT has been collecting radar imagery over California since late 2014 from both ascending and descending orbits (Figure 2), initially with a 24-day revisit frequency and, since early 2017, with a nominal 12-day revisit frequency. The acquisition orbits are denominated ascending (south to north) or descending (north to south) according to the flight direction of the sensor.

The ascending and descending imagery acquired between 1 June 2018 and 30 September 2019 over the previous study area, and from 1 January 2015 and 01 June 2018 over the new basins (Figure 1) consisted of 2,235 images.

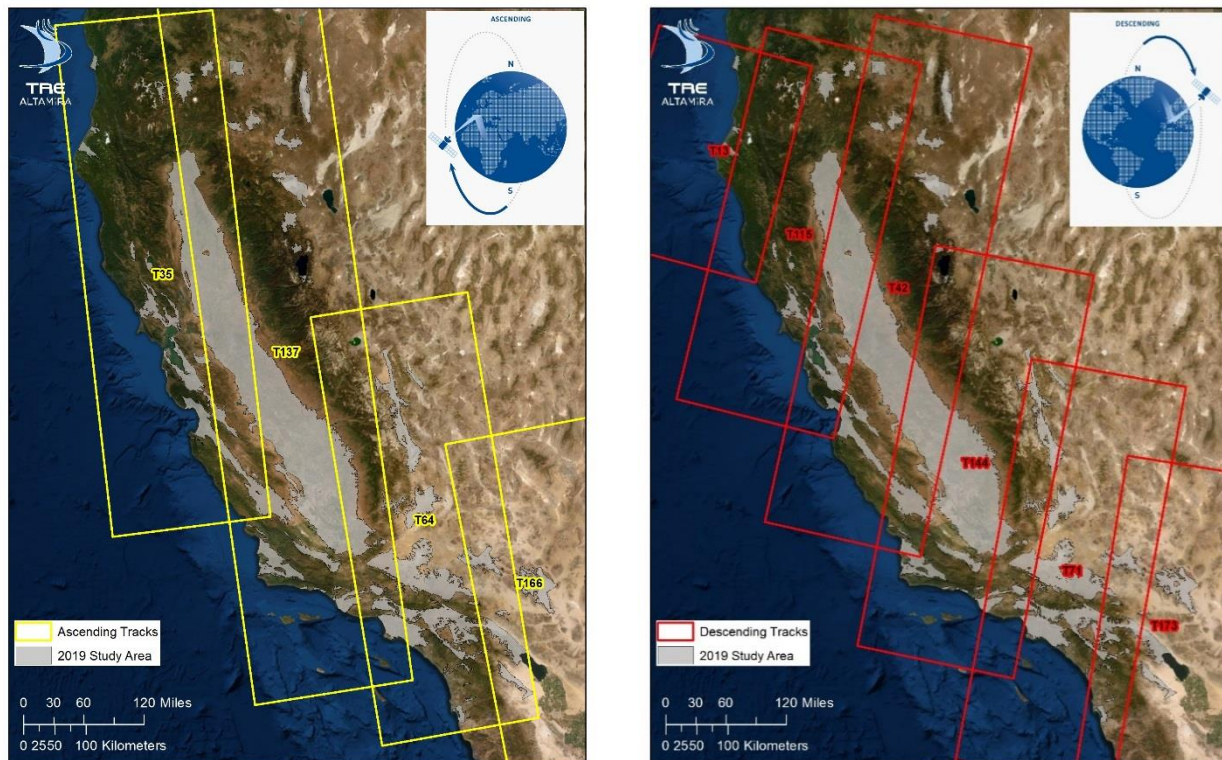


Figure 2: Ascending and Descending SNT acquisition tracks over California.

4. Task 2.2: Processing polygons definition

The downloaded imagery was analyzed to define the number of processing polygons. To maintain maximum consistency with the 2018 results, the 27 processing polygons over the 2018 areas have remained unchanged while 8 new processing polygons were defined for the new 2019 basins, based on their extent, the maximization of the temporal coverage and the optimization of GPS station coverage.

The final data processing includes 18 descending and 17 ascending polygons (Figure 2).

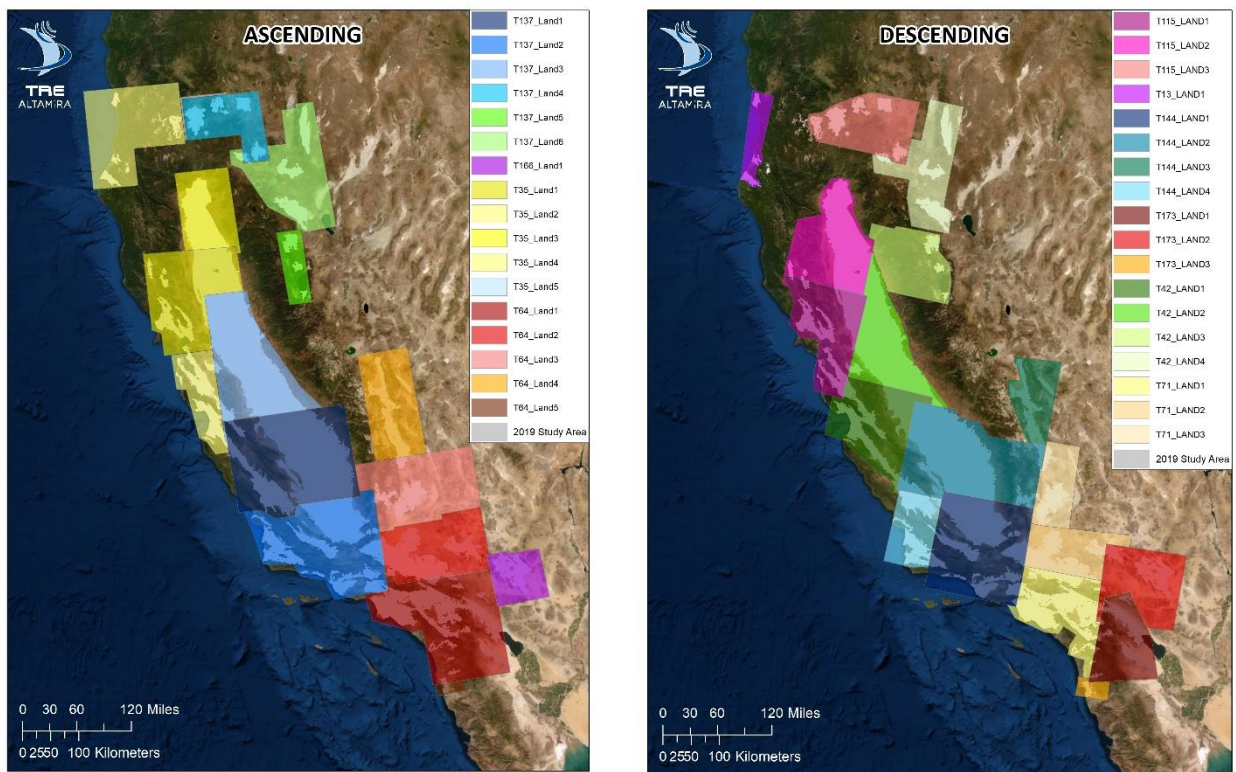


Figure 3: Ascending and Descending processing polygons.

5. Task 2.3: SqueeSAR processing

The SqueeSAR processing for the 27 previous processing polygons produced LOS measurements that cover 01 January 2018 - 30 September 2019, which includes an overlap of 15-20 images with the previous analysis (Figure 4). The overlap was applied in order to maximize the robustness of the integration with the 2018 measurements and minimize the impact of isolated noisy measurements in the time series.

The integration of the new LOS measurements with the 2018 measurements generated uninterrupted deformation time series spanning the period January 2015 – September 2019. Over the new 2019 areas, the SqueeSAR processing was carried out ex novo, using the entire image archive available from January 2015.

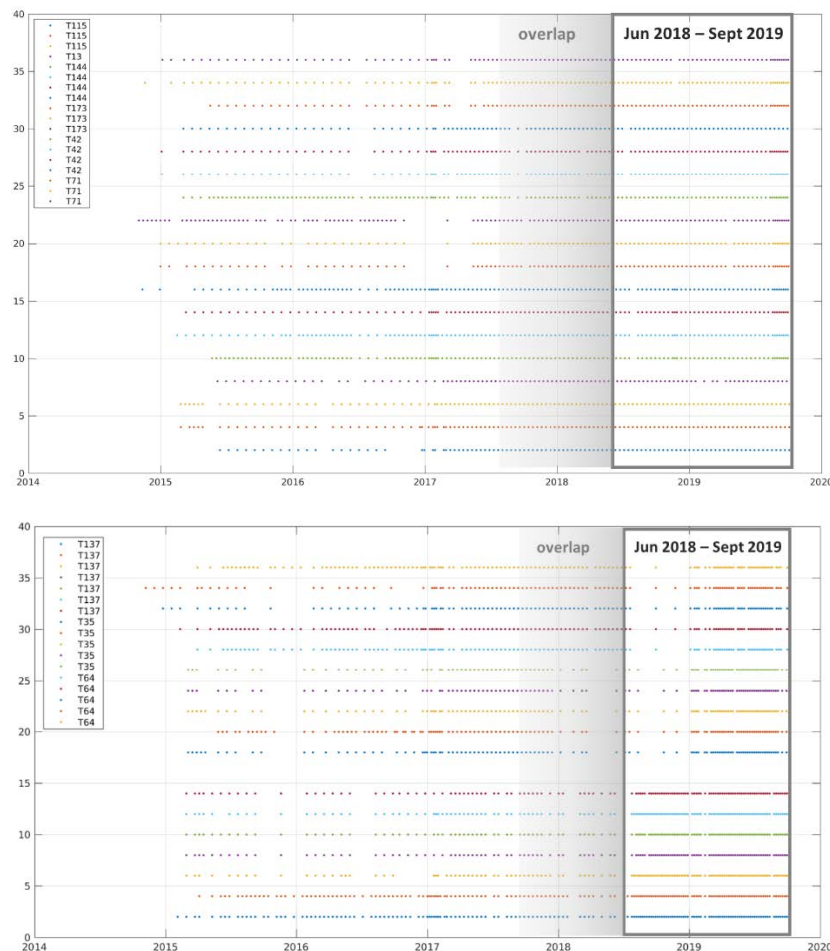


Figure 4: Temporal distribution of the imagery for all ascending and descending processing polygons. The current 2019 analysis used the imagery collected between June 2018 and September 2019 plus an overlap of approximately 15-20 images with the historical imagery.

6. Task 2.4: Data Calibration

A total of 231 GPS stations was selected from the UNAVCO network to perform the calibration of the 2019 measurements. This network included the 200 stations used in the 2018 analysis as well as 31 additional stations to cover the new 2019 areas (Figure 5). The selection criteria for the calibration stations were the same as for the 2018 project: at least 10 stations (when available) with a homogeneous spatial distribution within each processing polygon and absence of long temporal gaps in the time series.

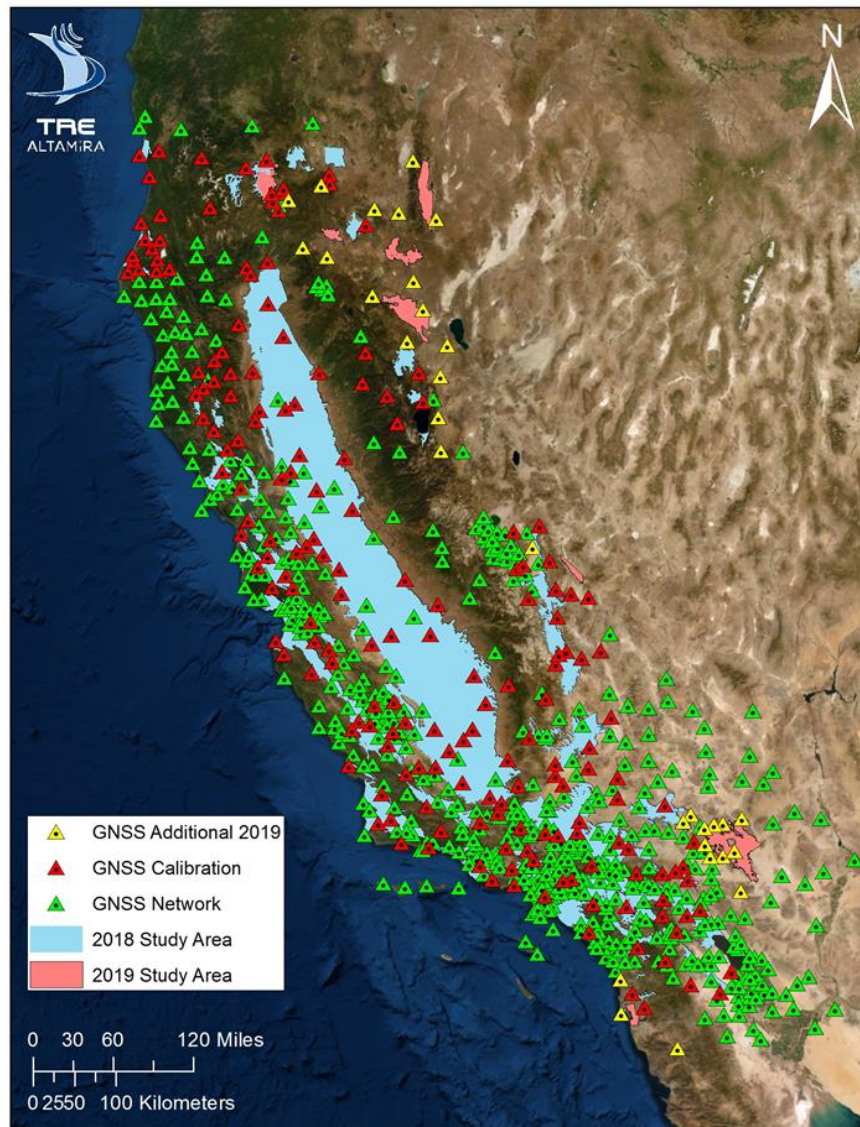


Figure 5: GNSS network over California. The same stations (red) used for the 2018 calibration will be used for the 2019 update, with the addition of 31 stations (yellow) to cover the new areas

The GPS time series have minor differences with the data used for the 2018 analysis within the overlap period (1/1/2015 to 6/30/2018), due to the use of a different file format starting from September 2018 and the removal of NULL values through linear interpolation prior to applying the 31-day moving average (Towill communication).

An analysis of the updated GPS time series by TRE confirmed slight differences with an overall improvement of the quality of the time series (Figure 6). The average differences in rate are within $\pm 2\text{mm}$ for all three motion components (N, E and Vertical) and had a minimal impact on the consistency of the calibration results with the historical data.

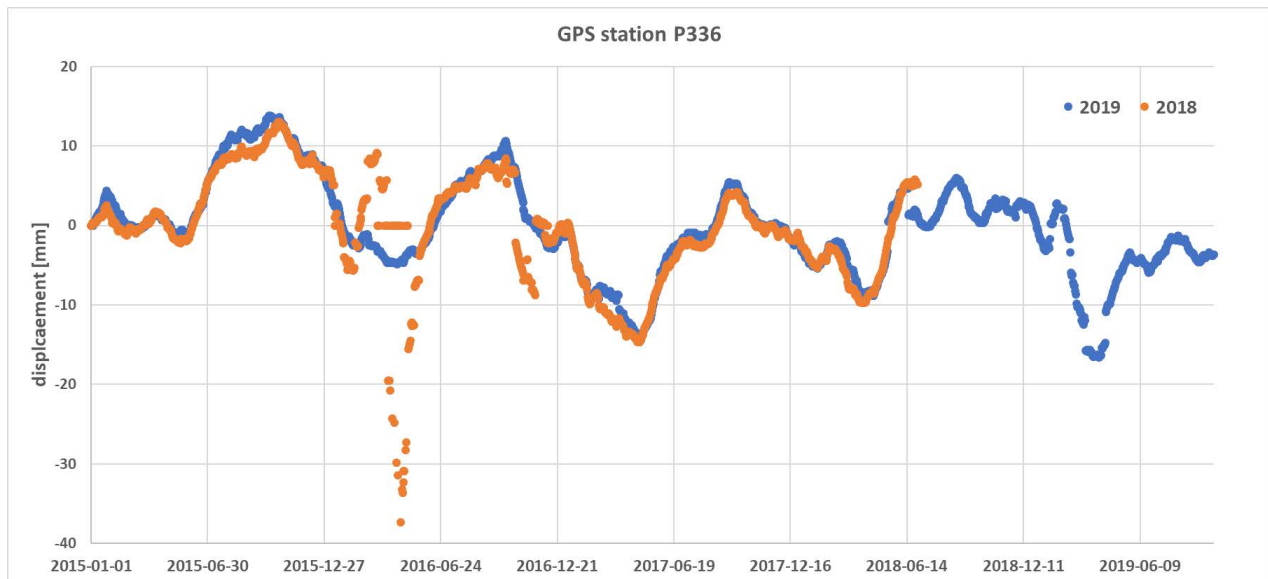


Figure 6: Comparison between the time series of the GPS P336 used for the 2018 analysis (in orange) and the 2019 analysis (in blue).

6.1. Methodology

The calibration of the LOS data was performed using the methodology defined in 2018, which is reiterated below (Figure 7):

- Time series filtering and projection to the satellite LOS:
 - The GNSS 3-D measurements provided by Towill were projected to the satellite 1-D LOS to create a GNSS LOS time series (LTS). This step allows a direct comparison of the two independent measurements (InSAR and GPS).
 - All InSAR measurement points (MP) within a 100-meter radius of each GNSS were selected and used to calculate an average time series (ATS) for the overlapping period with the GNSS

time series (one InSAR ATS for each GNSS). This step allows the comparison of data collected at a same location over a corresponding period of time.

- Plane removal: to remove possible linear errors related to potential satellite orbital inaccuracies, a difference in average velocity (linear trend) was calculated for each ATS and corresponding LTS. The average velocity differences calculated for each ATS and LTS pair were then used to estimate and remove a first order surface (plane) from all InSAR MP. The plane is statistically estimated at regional scale by minimizing the residuals of the differences between the ATS and corresponding LTS.
- Absolute calibration: to tie the two measurement techniques together and convert the relative InSAR measurements to the absolute reference system of the GNSS network, it was necessary to calibrate the local InSAR reference points to the same absolute reference. The procedure involved the generation of an average time series of residuals by comparing the ATS to the corresponding LTS for each GNSS location. All the time series of residuals obtained were then averaged to define a unique common time series of residuals (cRTS) at regional scale. This cRTS represents the movement of the local InSAR reference points with respect to the absolute GNSS reference frame. The cRTS was then removed from every InSAR MP time series.

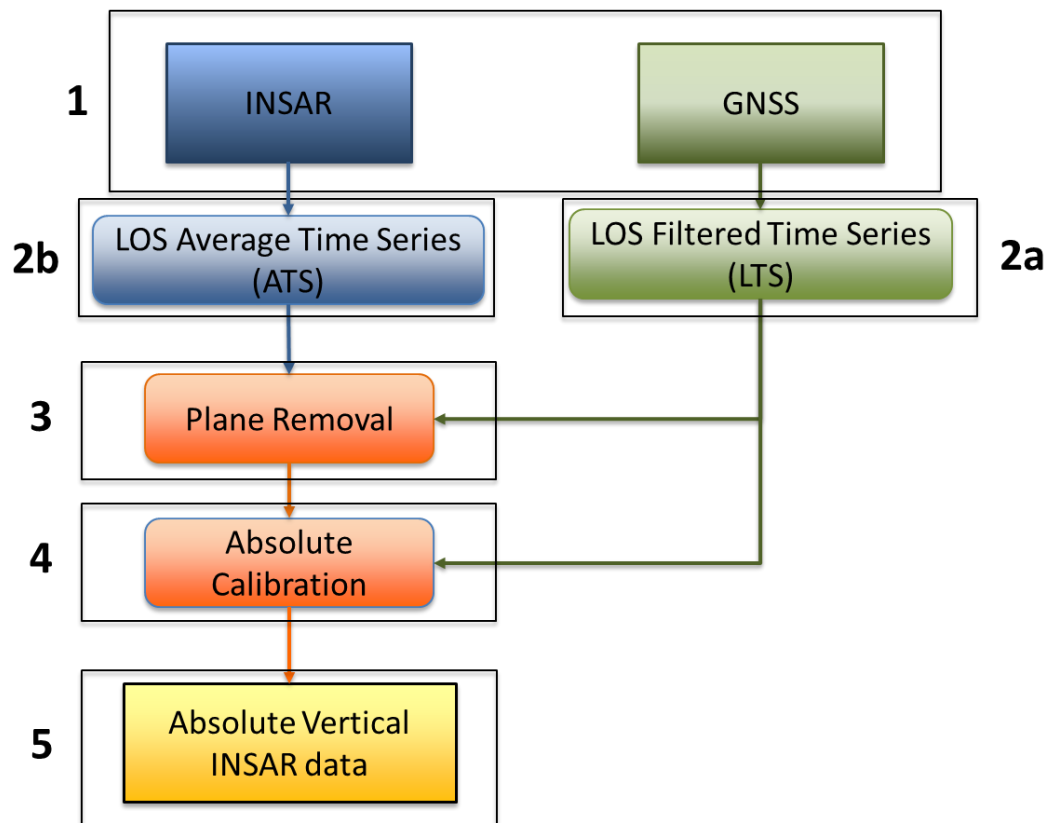


Figure 7: Diagram of the calibration methodology.

7. Task 2.5: Vertical measurements

The ascending and descending calibrated LOS InSAR time series covering the period January 2015 – September 2019, constitute the input for the absolute vertical time series estimation. The vertical measurements are produced using the same assumptions and methodology of the 2018 analysis:

- Satellites from different orbits and tracks identify different objects on the ground. For this reason, the data combination procedure requires the use of a common spatial grid to subsample the full resolution LOS results. The entire area was divided into a lattice of cells, using the same grid of the 2018 analysis (100x100 m square cells with the same code of the 2018 analysis), with the assumption that MPs belonging to the same cell are affected by the same motion.
- The average of all measurements within a same cell are referred to as synthetic measurement points (SMP). Both ascending and descending SMP are calculated for each cell. The resolution of the SMP, and thus of the resulting vertical data, as consequence of the use of the previously mentioned grid, is 100 m. SMP do not correspond to specific radar targets on the ground but instead represent synthetic points positioned at the centre of the cells.
- Since acquisition dates differ for each processing polygon, the LOS displacement time series of each SMP must be interpolated and re-sampled on a common temporal grid. The temporal grid was defined with the same criteria used for the 2018 analysis: one sample at the 1st day of each month and a frequency of approximately 7 days within the same month.
- The vertical time series of deformation for each SMP was calculated by combining all available ascending and descending LOS time series for the period in common to all LOS data (13 June 2015 – 19 September 2019). The data combination is only performed for cells that contain SMP from both ascending and descending orbits.
- Following the same procedure as in 2018, for those areas where either the ascending or descending orbit data were unavailable, the vertical time series were calculated by projecting the available LOS results to the vertical direction. Descending results were selected by default as they are generally less affected by atmospheric noise compared to the ascending data.

This methodology maintains the maximum consistency with the 2018 vertical results. Minimal differences in the point coverage were observed with respect to the 2015-2018 analysis (due to the loss of a few cells stemming from changes to the ground surface) as well as in the time series (due to the changes in the input GNSS time series), with an overall further improvement of the results.

8. Task 2.6: Draft deliverables

The draft deliverables were generated for both the common period and the variable start date results, as for the 2018 results, and made available on the TREmaps web platform and the dedicated SFTP.

Following the delivery of the draft data sets (Milestone 3), TRE received and addressed the following requests from DWR and Towill:

- Include within the final vertical measurements the points that have lost coherence in the 2018-2019 period by padding them with Null values in the database.
- Include an additional cumulative displacement raster map for the last image of the vertical dataset, 19 September 2019, even if it covers a period shorter than 1 month.

9. Task 2.7: Final Deliverables

The following are the final deliverables:

- Common start date measurements
- Cumulative deformation raster maps
- Variable start date measurements
- Annual deformation raster maps
- LOS (ascending and descending) measurements

9.1. Common start date:

- Start date: 13 June 2015
- Period covered: 13 June 2015 - 19 September 2019
- Vertical measurement point database is provided in shapefile format, subdivided into 9 shapefiles to not exceed the file size limitations of current GIS software. Database contents are reported in Figure 8.
- The temporal sampling consists of one measurement every ~7 days with a sample fixed at the first day of each month.
- The reference system is WGS84 and the measurements are in metric units (mm).

| Field | Description |
|------------|---|
| CODE | Synthetic Measurement Point (sMP) identification code |
| VEL_V | sMP average vertical displacement rate in the common period 13 June 2015 - June 2018. Positive values correspond to uplift; negative values correspond to subsidence. Values are expressed in [mm/year] |
| V_STDEV | Vertical displacement rate standard deviation [mm/year] |
| ACC | Acceleration [mm/year ²] |
| SEASON_AMP | Average seasonal amplitude [mm] |
| Dyyyymmdd | Each field contains the cumulative displacement with respect to the first acquisition. Displacement values are expressed in [mm] |

Figure 8: Database contents of the common start date shapefiles.

9.2. Cumulative raster maps

- Cumulative raster maps are generated using the common start date database
- Each map covers an increasing window with monthly increments, starting from 13 June 2015, using the measurement value at the 1st of each month. As required, a final raster map covering the period 13 June 2015-19 September 2019 was added.
- Raster maps are generated using an interpolation radius of 500m, have a geotiff format, are 32-bit and have 100-meter resolution.
- The maps are in WGS84 reference system and measurement unit is U.S. Survey feet.

9.3. Variable start date:

- Variable start date for each point. The temporal coverage of each measurement point depends on the available satellite imagery in that area.
- Period covered: 01 January 2015 - 19 September 2019.
- Vertical measurement point database is provided in
 - shapefile format, subdivided into 10 shapefiles to not exceed the file size limitations of GIS software. Database contents are reported in Figure 9.
 - table format (.csv), subdivided into 10 files to not exceed file size limitations. *Null* values assigned for dates where there is no satellite data or loss of interferometric coherence (i.e. for points that are no longer radar reflectors because of the surface changes occurred with respect to the 2018 analysis). Zero value corresponds to the start date. Database contents are reported in Figure 10.
- The temporal sampling consists of one measurement every ~7 days with a sample mandated to the first day of each month.
- The reference system is WGS84 and the measurements are in metric units (mm).

| Field | Description |
|------------|--|
| CODE | Synthetic Measurement Point (sMP) identification code |
| VEL_V | sMP average vertical displacement rate in the specific period. Positive values correspond to uplift; negative values correspond to subsidence. Values are expressed in [mm/year] |
| V_STDEV | Vertical displacement rate standard deviation [mm/year] |
| ACC | Acceleration [mm/year ²] |
| SEASON_AMP | Average seasonal amplitude [mm] |
| Dyyyymmdd | Each field contains the cumulative displacement with respect to a variable start date. Zero value assigned for dates where there is no satellite data. Displacement values are expressed in [mm] |

Figure 9: Database contents of the variable start date shapefiles.

| | A | B | C | D | E | F | G | H | I | J | K | L | M | N | O |
|----|---------|----------|----------|-----------|-----------|-----------|-----------|-----------|-----------|-----------|-----------|-----------|-----------|-----------|-----------|
| 1 | CODE | X | Y | D20150101 | D20150107 | D20150113 | D20150120 | D20150126 | D20150201 | D20150207 | D20150212 | D20150218 | D20150223 | D20150301 | D20150307 |
| 2 | ERSS159 | -121.97 | 42.00544 | NULL | 0 | -1.9 | -2.8 |
| 3 | ERSS15A | -121.969 | 42.00544 | NULL | 0 | -3.2 | -5.4 |
| 4 | ERSS15C | -121.966 | 42.00544 | NULL | 0 | 1 | 1.6 |
| 5 | ERSS15D | -121.965 | 42.00544 | NULL | 0 | 2.1 | 4.2 |
| 6 | ERSS15E | -121.964 | 42.00544 | NULL | 0 | -0.1 | -0.3 |
| 7 | ERSS15F | -121.963 | 42.00544 | NULL | 0 | 0.3 | 0.7 |
| 8 | ERSS15G | -121.962 | 42.00544 | NULL | 0 | -0.6 | -0.9 |
| 9 | ERSS15H | -121.961 | 42.00544 | NULL | 0 | 0.2 | 0.6 |
| 10 | ERRK2JM | -121.964 | 42.00454 | NULL | 0 | -0.6 | -1.3 |
| 11 | ERRK2JN | -121.963 | 42.00454 | NULL | 0 | -0.2 | -0.2 |
| 12 | ERRK2JO | -121.962 | 42.00454 | NULL | 0 | 2.2 | 3.5 |
| 13 | ERRK2JP | -121.961 | 42.00454 | NULL | 0 | 2 | 4.2 |
| 14 | ERRK2JQ | -121.96 | 42.00454 | NULL | 0 | 2 | 3.8 |
| 15 | ERQYMXV | -121.963 | 42.00364 | NULL | 0 | -2 | -4.2 |
| 16 | ERQYMXW | -121.962 | 42.00364 | NULL | 0 | 1.4 | 2.5 |

Figure 10: Example of the table contents.

9.4. Annual raster maps

- Annual raster maps are generated using the variable start date database
- Each raster map covers a moving one-year period, produced at monthly intervals starting from 01 Jan 2015, using the measurement value at the 1st of each month. The maps contain values for those areas where measurements exist for the full annual interval (other cells have No Data values). As requested, a final raster map covering the period 01 Oct 2018 - 19 September 2019 was added.
- Raster maps are generated using an interpolation radius of 500m, have a geotiff format, are 32-bit and have 100-meter resolution.
- The maps are in WGS84 reference system and measurement unit is U.S. Survey feet.

9.5. LOS measurements

- The full resolution LOS data consist of 40 shapefiles, 20 ascending (Figure 11) and 20 descending (Figure 12), divided into two main groups:
 - OLD AREAS: 30 shapefiles including the 2018-2019 LOS measurements obtained by the 2019 processing of the areas covered in the 2018 analysis.
 - NEW AREAS: 10 shapefiles including the 2015- 2019 LOS measurements over the new basins covered by the 2019 analysis.
- Table 3 describes the parameters included in the database of each LOS shapefile.
- The reference system is WGS84 and the measurements are in metric units (mm).

9.5.1. LOS measurements characteristics

Every measurement point (MP) identified by SqueeSAR corresponds to a radar target on the ground that displays stable reflectivity and coherent phase throughout every image of the processed imagery. The MPs belong to two different families (indicated by the parameter EFF_AREA in Table 3):

- Permanent Scatterers (PS): point-wise radar targets characterized by high stable radar signal return (e.g. buildings, rocky outcrops, linear structures, etc.), with EFF_AREA = 0 in the attribute table.
- Distributed Scatterers (DS): patches of ground exhibiting a lower but homogenous radar signal return (e.g. uncultivated land, debris, deserted areas, etc.), with EFF_AREA > 0 in the attribute table.

The density and distribution of the MPs depends on the land cover. In general, MP density increases with the presence of man-made structures and decreases with the presence of vegetation. The highest density is reached over urban areas and arid ground, while it is lower over vegetated or agricultural areas, which are affected by reflectivity changes over time.

For each MP identified, SqueeSAR provides the ground target's position and the displacement time series (Dyyyymmdd fields in Table 3), representing the evolution of the MP's displacement for each acquisition date measured along the LOS direction.

SqueeSAR displacement measurements are provided with two precision indices:

- Displacement rate standard deviation (V_STDEV in Table 3), which provides an indication of the error bar associated with the annual displacement rate measurements.
- Time series standard deviation (STD_DEF in Table 3), which provides an indication of the error bar associated with the displacement time series.

The displacement rate standard deviation characterizes the error associated with rate measurements. Given the standard deviation (σ), and assuming that the errors are normally distributed (or Gaussian), 95% of the values tend to be included in a $\pm 2\sigma$ range

The standard deviation of the deformation time series indicates how well an analytical model fits the deformation time series. The model is selected individually for each measurement point with an advanced Model Order Selection technique that also considers the quality of the image archive (number of processed images, time span covered by the archive and possible gaps in the acquisitions). The lower the standard deviation, the lower the average residual with respect to the analytical model. (i.e. the smaller the error bar of the time series).

In order to facilitate the analysis of non-linear movements, acceleration (ACC in Table 3) and seasonal amplitude (SEASON_AMP in Table 3) parameters are provided within the database of each shapefile.

The acceleration [mm/year^2] is calculated by fitting a displacement polynomial model to the time series:

$$d(t) = a + bt + ct^2$$

The seasonal amplitude [mm] is calculated by fitting a displacement polynomial model with a seasonal component to the time series:

$$d(t) = a + bt + ct^2 + A \cos\left(\frac{2\pi T}{365} + \varphi\right)$$

Where A = semi-amplitude, T = time [day] and φ = phase (seasonal amplitude maximum value with respect to the first image acquisition)

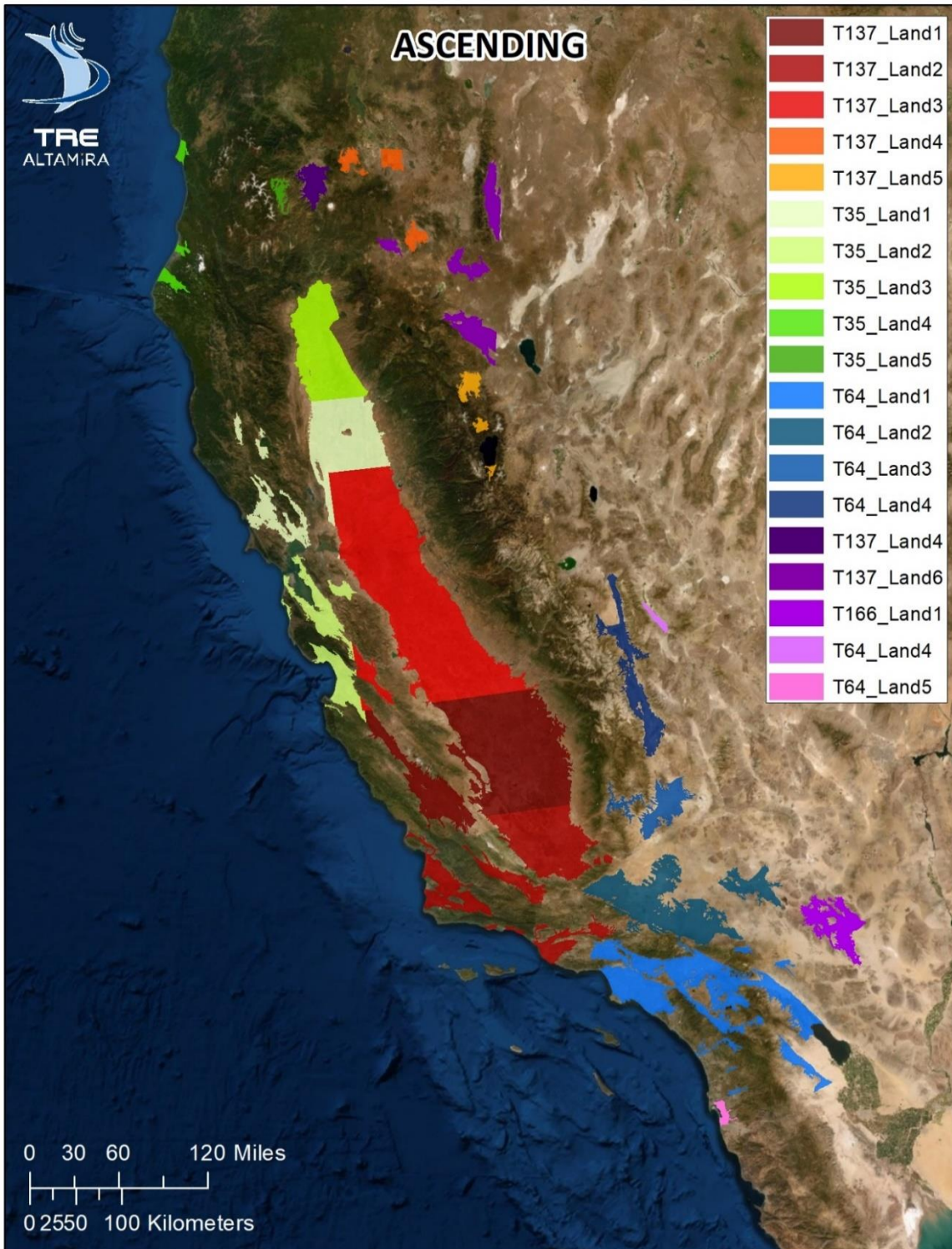


Figure 11: Coverage of the 20 LOS ascending shapefiles.

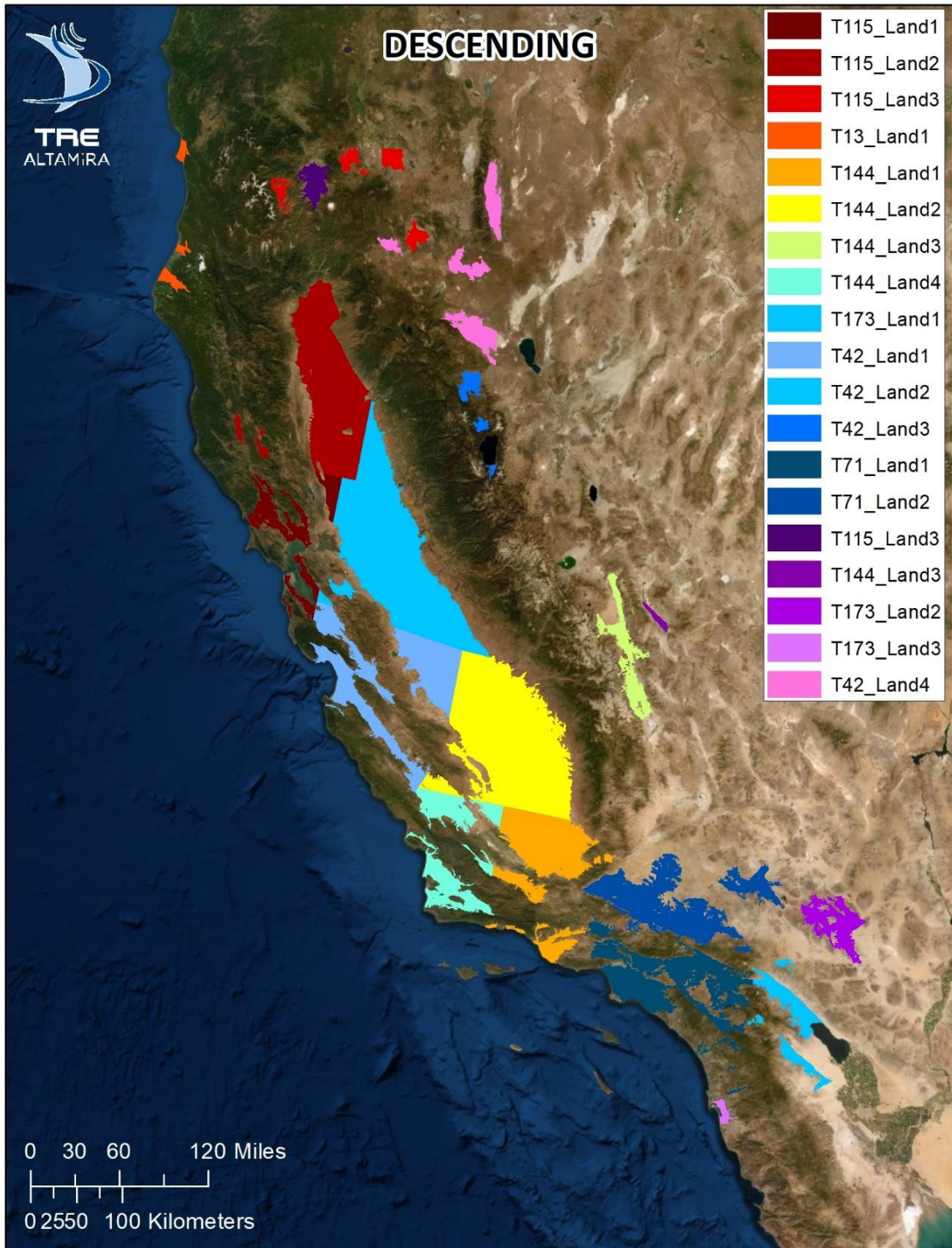


Figure 12: Coverage of the 20 LOS descending shapefiles.

| Field | Description |
|-------------------|--|
| CODE | Measurement Point (MP) identification code |
| HEIGHT | Topographic Elevation [m] referred to WGS84 ellipsoid |
| H_STDEV | Height standard deviation [m] |
| VEL | MP displacement rate. Positive values correspond to motion <i>toward the satellite</i> ; negative values correspond to motion <i>away from the satellite</i> [mm/year] |
| V_STDEV | Displacement rate standard deviation [mm/year] |
| ACC | Acceleration [mm/year ²] |
| SEASON_AMP | Average seasonal amplitude [mm] |
| COHERENCE | Index varying between 0 and 1, related to the MP phase noise and to the capability of the motion model adopted to cope with the actual MP behaviour |
| STD_DEF | Average standard deviation of the displacement time series |
| EFF_AREA | This parameter represents the effective extension of the area [m ²] covered by Distributed Scatterers (DS). For Permanent Scatterers (PS), its value is set to 0 |
| Dyyyymmdd | Fields containing the displacement values of successive acquisitions relative to the first acquisition available. Displacement values are expressed in [mm] |

Table 3: Description of the fields contained in the database of a LOS shapefile

9.5.2. Notes for the comparison of LOS data with other 3-D data

InSAR measurements are originally 1-D, corresponding to the projection of real movement onto the satellite Line of Sight (LOS). The schematic of ascending and descending acquisition geometries is reported in Figure 13. θ is the angle between the LOS and the vertical direction. δ is the angle between the LOS and the NS direction.

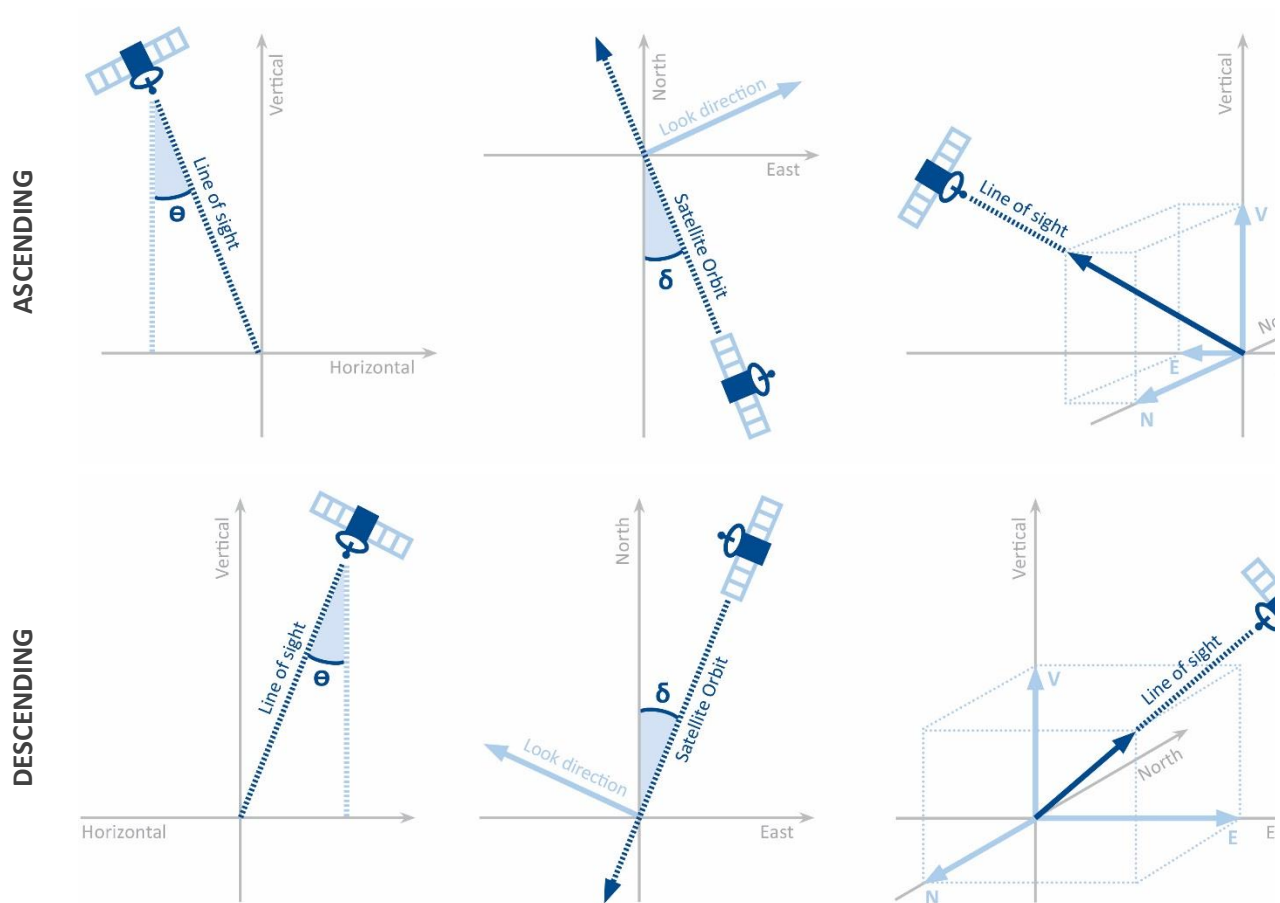


Figure 13: Schematic of the LOS orientation for ascending and descending orbits.

To compare 3-D measurements obtained by other technique such a GNSS network with InSAR LOS data, it is necessary to project the 3-D measurement to the specific LOS according to:

$$D_{LOS} = D_{VERT} * H_{LOS} + D_{EW} * E_{LOS} + D_{NS} * N_{LOS}$$

D_{VERT} , D_{EW} e D_{NS} are the measurements provided by the GNSS along the three directions. H_{LOS} , E_{LOS} e N_{LOS} are the cosine versors of the LOS along the three directions, which are specific for each LOS processing

polygon and are reported in the metadata files (xml) attached to the shapefile. D_{LOS} is the GNSS measurement projected to the LOS direction. The cosine versors of each LOS shapefiles are summarized in Table 4.

| Orbit | Processing polygon | N_{LOS} | E_{LOS} | H_{LOS} | new/old |
|-----------|-----------------------------|-----------|-----------|-----------|-------------|
| ASCENDING | CALIFORNIA_SNT_A_T35_LAND1 | -0.117 | -0.646 | 0.753 | old |
| | CALIFORNIA_SNT_A_T35_LAND2 | -0.121 | -0.649 | 0.750 | old |
| | CALIFORNIA_SNT_A_T35_LAND3 | -0.119 | -0.671 | 0.731 | old |
| | CALIFORNIA_SNT_A_T35_LAND4 | -0.102 | -0.589 | 0.801 | old |
| | CALIFORNIA_SNT_A_T35_LAND5 | -0.116 | -0.669 | 0.733 | old |
| | CALIFORNIA_SNT_A_T64_LAND1 | -0.111 | -0.632 | 0.766 | old |
| | CALIFORNIA_SNT_A_T64_LAND2 | -0.109 | -0.631 | 0.767 | old |
| | CALIFORNIA_SNT_A_T64_LAND3 | -0.101 | -0.593 | 0.798 | old |
| | CALIFORNIA_SNT_A_T64_LAND4 | -0.102 | -0.617 | 0.780 | old and new |
| | CALIFORNIA_SNT_A_T64_LAND5 | -0.113 | -0.631 | 0.767 | new |
| | CALIFORNIA_SNT_A_T166_LAND1 | -0.118 | -0.603 | 0.788 | new |
| | CALIFORNIA_SNT_A_T137_LAND1 | -0.129 | -0.611 | 0.780 | old |
| | CALIFORNIA_SNT_A_T137_LAND2 | -0.096 | -0.634 | 0.766 | old |
| | CALIFORNIA_SNT_A_T137_LAND3 | -0.125 | -0.603 | 0.787 | old |
| | CALIFORNIA_SNT_A_T137_LAND4 | -0.114 | -0.577 | 0.808 | old and new |
| | CALIFORNIA_SNT_A_T137_LAND5 | -0.132 | -0.647 | 0.750 | old |
| | CALIFORNIA_SNT_A_T137_LAND6 | -0.129 | -0.645 | 0.753 | new |
| | CALIFORNIA_SNT_A_T166_LAND1 | -0.604 | -0.118 | 0.789 | new |

Table 4: Cosine versors of the LOS ascending data.

| Orbit | Processing polygon | N _{LOS} | E _{LOS} | H _{LOS} | new/old |
|-------------------|-----------------------------|------------------|------------------|------------------|-------------|
| DESCENDING | CALIFORNIA_SNT_D_T13_LAND1 | -0.115 | 0.594 | 0.795 | old |
| | CALIFORNIA_SNT_D_T42_LAND1 | -0.100 | 0.625 | 0.774 | old |
| | CALIFORNIA_SNT_D_T42_LAND2 | -0.095 | 0.615 | 0.782 | old |
| | CALIFORNIA_SNT_D_T42_LAND3 | -0.095 | 0.627 | 0.772 | old |
| | CALIFORNIA_SNT_D_T42_LAND4 | -0.094 | 0.646 | 0.757 | new |
| | CALIFORNIA_SNT_D_T71_LAND1 | -0.115 | 0.613 | 0.781 | old |
| | CALIFORNIA_SNT_D_T71_LAND2 | -0.115 | 0.622 | 0.773 | old |
| | CALIFORNIA_SNT_D_T71_LAND3 | -0.121 | 0.661 | 0.740 | old |
| | CALIFORNIA_SNT_D_T115_LAND1 | -0.105 | 0.593 | 0.798 | old |
| | CALIFORNIA_SNT_D_T115_LAND2 | -0.103 | 0.597 | 0.795 | old |
| | CALIFORNIA_SNT_D_T115_LAND3 | -0.101 | 0.602 | 0.792 | old and new |
| | CALIFORNIA_SNT_D_T144_LAND1 | -0.121 | 0.587 | 0.799 | old |
| | CALIFORNIA_SNT_D_T144_LAND2 | -0.127 | 0.624 | 0.770 | old |
| | CALIFORNIA_SNT_D_T144_LAND3 | -0.112 | 0.558 | 0.821 | old and new |
| | CALIFORNIA_SNT_D_T144_LAND4 | -0.096 | 0.670 | 0.735 | old |
| | CALIFORNIA_SNT_D_T173_LAND1 | -0.110 | 0.653 | 0.748 | old |
| | CALIFORNIA_SNT_D_T173_LAND2 | -0.108 | 0.652 | 0.750 | new |
| | CALIFORNIA_SNT_D_T173_LAND3 | -0.117 | 0.687 | 0.717 | new |

Table 5: Cosine versors of the LOS descending data

10. Data delivery

All deliverables are provided to Towill and DWR through the [TREmaps](#) web platform and a dedicated SFTP site (login credentials provided by email).

For ease of use, the deliverables are organized into four different groups: 1) Common start date; 2) Cumulative raster maps; 3) Variable start date; 4) Annual raster maps; 5) LOS data

Cumulative and annual maps are visualized on TREmaps starting from the last map of the 2018 analysis but all the raster files for the entire period 01 January 2015-01 September 2019 can be downloaded.

LOS results are provided only through the SFTP site because of the big size of the files.

11. Summary

Ground deformation measurements over the basins indicated by DWR were updated using the SqueeSAR data processing algorithm for the period June 2018 - September 2019. The results were integrated with the previous 2018 study results to generate uninterrupted vertical deformation time series for the period January 2015 - September 2019. New basins indicated by DWR were processed separately and then included in the final database.

The processing strategy had the aim of providing the most accurate measurements over the entire extent of the area of interest while maintaining the maximum consistency with the results obtained in 2018. This was achieved in several steps that included the minimization of possible sources of noise (e.g. atmospheric variations, satellite orbital errors) and calibrating the InSAR data to the regional GNSS network.

The calibration phase followed the regional scale methodology defined in the 2018 study, using 231 GNSS stations out of 782 available from the UNAVCO network, to remove orbital inaccuracies and to fix the local InSAR reference points to the absolute GNSS network reference system. The results will be validated by Towill in the project Task 4.



**TRE
ALTAMIRA**
A CLS Group Company



MILAN

Ripa di Porta Ticinese, 79
20143 Milano - Italy
Tel. +39.02.4343.121
Fax +39.02.4343.1230

tre-altamira.com

BARCELONA

C/ Corsega, 381-387
E-08037 Barcelona Spain
Tel.: +34 93 183 57 50
Fax: +34 93 183 57 59

VANCOUVER

410 - 475 West Georgia Street
Vancouver, BC V6B 4M9 - Canada
Tel. +1.604.331.2512
Fax +1.604.331.2513